frontiers | Research Topics

Hepatocellular carcinoma: from diagnostic approaches to surgical and systemic therapies

Edited by
Liliana Chemello, Pradeep Kumar Shukla and Marcello Dallio

Published in
Frontiers in Medicine
Frontiers in Pharmacology

ISSN 1664-8714
ISBN 978-2-8325-7034-0
DOI 10.3389/978-2-8325-7034-0

Generative AI statement
Any alternative text (Alt text) provided alongside figures in the articles in this ebook has been generated by Frontiers with the support of artificial intelligence and reasonable efforts have been made to ensure accuracy, including review by the authors wherever possible. If you identify any issues, please contact us.

About Frontiers

Frontiers is more than just an open access publisher of scholarly articles: it is a pioneering approach to the world of academia, radically improving the way scholarly research is managed. The grand vision of Frontiers is a world where all people have an equal opportunity to seek, share and generate knowledge. Frontiers provides immediate and permanent online open access to all its publications, but this alone is not enough to realize our grand goals.

Frontiers journal series

The Frontiers journal series is a multi-tier and interdisciplinary set of open-access, online journals, promising a paradigm shift from the current review, selection and dissemination processes in academic publishing. All Frontiers journals are driven by researchers for researchers; therefore, they constitute a service to the scholarly community. At the same time, the *Frontiers journal series* operates on a revolutionary invention, the tiered publishing system, initially addressing specific communities of scholars, and gradually climbing up to broader public understanding, thus serving the interests of the lay society, too.

Dedication to quality

Each Frontiers article is a landmark of the highest quality, thanks to genuinely collaborative interactions between authors and review editors, who include some of the world's best academicians. Research must be certified by peers before entering a stream of knowledge that may eventually reach the public - and shape society; therefore, Frontiers only applies the most rigorous and unbiased reviews. Frontiers revolutionizes research publishing by freely delivering the most outstanding research, evaluated with no bias from both the academic and social point of view. By applying the most advanced information technologies, Frontiers is catapulting scholarly publishing into a new generation.

What are Frontiers Research Topics?

Frontiers Research Topics are very popular trademarks of the *Frontiers journals series*: they are collections of at least ten articles, all centered on a particular subject. With their unique mix of varied contributions from Original Research to Review Articles, Frontiers Research Topics unify the most influential researchers, the latest key findings and historical advances in a hot research area.

Find out more on how to host your own Frontiers Research Topic or contribute to one as an author by contacting the Frontiers editorial office: frontiersin.org/about/contact

Hepatocellular carcinoma: from diagnostic approaches to surgical and systemic therapies

Topic editors

Liliana Chemello — University of Padua, Italy

Pradeep Kumar Shukla — University of Tennessee Health Science Center (UTHSC), United States

Marcello Dallio — University of Campania Luigi Vanvitelli, Italy

Citation

Chemello, L., Shukla, P. K., Dallio, M., eds. (2025). *Hepatocellular carcinoma: from diagnostic approaches to surgical and systemic therapies*.

Lausanne: Frontiers Media SA. doi: 10.3389/978-2-8325-7034-0

Table of contents

frontiers | Frontiers in Medicine

TYPE Editorial
PUBLISHED 26 June 2025
DOI 10.3389/fmed.2025.1633587

OPEN ACCESS

EDITED AND REVIEWED BY
Pedro M. Baptista,
Health Research Institute of Aragon (IIS Aragon), Spain

*CORRESPONDENCE
Liliana Chemello
✉ liliana.chemello@unipd.it

RECEIVED 22 May 2025
ACCEPTED 03 June 2025
PUBLISHED 26 June 2025

CITATION
Shukla PK, Dallio M and Chemello L (2025) Editorial: Hepatocellular carcinoma: from diagnostic approaches to surgical and systemic therapies. *Front. Med.* 12:1633587. doi: 10.3389/fmed.2025.1633587

Editorial: Hepatocellular carcinoma: from diagnostic approaches to surgical and systemic therapies

Pradeep Kumar Shukla[1], Marcello Dallio[2] and Liliana Chemello[3]*

[1]Department of Pathology, St. Jude Children's Research Hospital, Memphis, TN, United States, [2]Department of Precision Medicine, Hepatology and Digestive Endoscopy, University of Campania "Luigi Vanvitelli, " Naples, Italy, [3]Department of Medicine-DIMED, University-Hospital of Padova, Padua, Italy

KEYWORDS

HCC, primary liver cancer, cirrhosis, radiomics, liver diseases

Editorial on the Research Topic
Hepatocellular carcinoma: from diagnostic approaches to surgical and systemic therapies

Hepatocellular carcinoma (HCC) represents a significant global health challenge, being one of the most common primary liver tumors worldwide. Its complex pathogenesis and often late presentation pose significant obstacles to effective management. The variability of HCC burden, its biological behavior, and often the underlying liver dysfunction require a multifaceted research approach, spanning computational modeling, biomarker identification, and novel therapeutic strategies, which are the emerging trends and future prospects in this rapidly evolving field. This Research Topic offers a window into the latest efforts to improve the clinical management of HCC patients by combining data science, interventional medicine, and molecular oncology.

Recent research in HCC has provided valuable insights into biomarkers and the role of inflammation in disease progression, paving the way for improving diagnostic tools and prediction algorithms. Li et al. constructed a prognostic model for HCC based on inflammation-related genes. This bioinformatics-based approach offers a promising tool for predicting patient outcomes and personalizing treatment strategies, underlining the important role of inflammation in HCC progression and the value of integrating molecular data into clinical practice. Equally important is the integration of biologically meaningful clinical variables into predictive frameworks. The platelet count to spleen diameter ratio (PSL), a non-invasive surrogate for portal hypertension, has emerged as a powerful predictor of survival in cirrhosis-associated HCC as presented by Yan et al. Its incorporation into LASSO-derived nomograms has yielded models that surpass traditional tools in discriminative power and calibration. This approach underscores a growing recognition that variables reflecting the liver's functional status and hemodynamics are as crucial to prognosis as tumor-specific metrics. A new recent terminology proposed for definition of fatty liver disease or "metabolic disfunction-associated steatotic liver disease (MASLD)" was introduced being close associated with presence of cardiometabolic indexes. Therefore, the cross-sectional study by Bai et al., who explored the link between albumin-corrected anion gap (ACAG), which reflects the body's acid-base balance, and hepatic metabolic syndrome using 2017–2018 NHANES data, reveals a positive correlation

between elevated ACAG and—NAFLD or MASLD—, positioning ACAG as a potential early biomarker for metabolic liver disease. Further research is needed to confirm these findings and explore the underlying mechanisms, laying the foundation for new diagnostic strategies in MASLD, which affects approximately 30% of the adult population worldwide and is closely linked to the risk of HCC. At the molecular level, a deeper understanding of HCC biology is beginning to clarify why certain patients progress more aggressively or respond differently to therapy. The protein KEAP1, a regulator of oxidative stress response, has been identified in the study of Wei et al. as a marker of poor prognosis, associated with immune dysregulation and altered liver function. High KEAP1 expression correlates with shifts in immune infiltration—specifically increased Th2 cell presence and diminished cytotoxic cell activity—suggesting a role in immune evasion. Such molecular insights not only deepen our biological understanding of HCC, but also suggest new avenues for targeted therapy and immunomodulation.

While systemic strategies are expanding, refinement of curative-intent local therapies remains equally critical. For early-stage HCC, particularly single tumors $\leq$5 cm, image-guided radiofrequency ablation (RFA) remains a mainstay. However, its efficacy can be compromised by incomplete ablation or recurrence. A novel approach presented by Xie et al. which combined transarterial chemoembolization (TACE) with multi-image guidance during RFA has shown promising results, achieving high technical success and long-term survival with minimal complications. Furthermore, the debate is also on the use of adjuvant systemic treatment, as already used in other cancer types, even in early HCC. A meta-analysis by Tuersun et al. evaluates the efficacy of neoadjuvant immune checkpoint inhibitors (ICIs) in cases with resectable HCC. This study shows improved pathological responses without significantly increasing adverse events, suggesting a promising new direction for perioperative cancer care, and supporting further investigation into the use of immunotherapy also in early-HCC stage management, at least for the patients with the more invasive histotypes.

Also therapeutically, the landscape is evolving. Patients with advanced HCC and high tumor burden—long considered to have limited treatment options—are now benefiting from strategic combinations of locoregional and systemic therapies. Evidence from a multicenter analysis by Zhao Z. et al. suggests that hepatic arterial infusion chemotherapy (HAIC), when combined with Lenvatinib and Tislelizumab, significantly improves both overall and progression-free survival, with manageable toxicity. This multimodal approach leverages the cytotoxic precision of HAIC with the systemic control of immunotherapy and targeted agents, offering a new avenue for patients traditionally underserved by monotherapies. A similar study in patients staged Barcelona Clinic Liver Cancer B (intermediate-stage) or unresectable HCC, proposed the TACE associated to a systemic regimen with Atezolizumab plus Bevacizumab, to offer the possibility for downstaging to meet the criteria for curative surgery and the possible restitution of patient life expectancy, as reported in the article of Ai et al.. These new multimodal approach on interventional oncology propose a greater effectiveness, by improving both the precision and duration of local treatments, particularly for advanced HCC.

However, resistance to Regorafenib in advanced HCC continues to pose challenges. A study by Hu, Shi et al. reveals that bypass activation of the epidermal growth factor receptor (EGFR) pathway mediates acquired resistance. This suggests that combination therapies targeting EGFR could restore treatment efficacy, providing new strategies to overcome drug resistance and improve patient outcomes.

In the context of hepatitis B virus-related HCC, Hu, Yang et al. also compare the effects of tenofovir (TDF) and entecavir (ETV) in patients undergoing liver resection. TDF was found to offer superior benefits in reducing recurrence and improving survival post-surgery, highlighting its potential for guiding antiviral therapy selection. Further prospective trials are needed to validate these findings and refine guidelines for HBV-HCC management.

Another important aspect certainly concerns the desirable application of shared protocols in the study of images obtained with CT/MR. The standardized technique, implemented using an appropriate tracer concentration, improves image quality to facilitate HCC reconstruction and can be decisive for studying the tumor vasculature, especially to reveal microvascular invasion in cases with advanced HCC, as demonstrated in the study of Peng et al.. This can allow us to obtain the best quality for the most accurate study of the tumor stage, avoiding additional sessions. In the article by Huang et al., also quantification of intra-tumoral fat, which is commonly detected during MRI, serves as an important ancillary feature for the diagnosis of HCC, and furthermore it allows distinguishing the low-proliferative tumor pattern with better prognostic prediction, effectively influencing the therapeutic choice.

Finally, a note of caution is reiterated in the systematic review and meta-analysis of Yan et al., which highlight the clinical relevance of the rare arc of Bühler, particularly in abdominal surgery and interventional radiology. The study emphasizes also the utility of computed tomography angiography (CTA) and digital subtraction angiography (DSA) for preoperative diagnosis, which helps reduce intraoperative risks by increasing awareness of vascular anomalies, which can produce severe complications in treated patients.

Nowadays the diagnostic techniques and therapeutic strategies, especially by integration of machine learning and artificial intelligence to clinical practice, drastically improved early detection, personalize treatment plans, and ultimately achieve better outcomes for patients with HCC. A common thread across these contributions is the pressing need for more accurate prognostic tools. As current staging systems such as AJCC-TNM fall short in capturing the true clinical diversity of HCC—particularly in advanced or multifocal disease—researchers are increasingly turning to data-driven approaches. Recent work by Shen et al. harnessing large-scale registry data has demonstrated that machine learning algorithms, especially gradient boosted models, can outperform traditional statistical methods in stratifying risk and predicting survival. These models not only show high accuracy in validation cohorts but also offer interpretability through techniques like SHAP, supporting their integration into clinical workflows. This evolution in prognostic

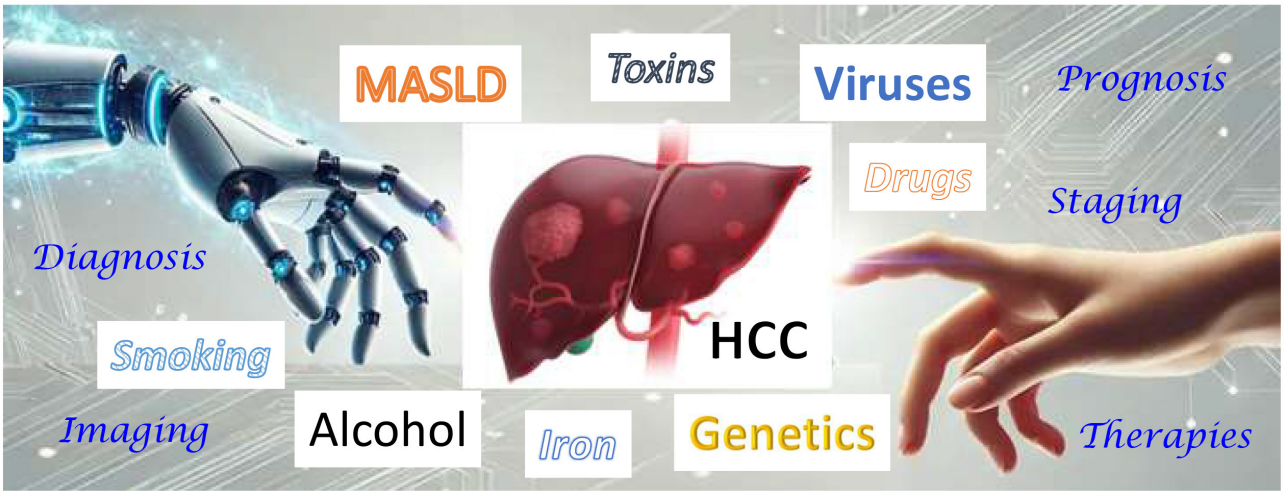

FIGURE 1
Ethiologies of hepatocellular carcinoma (HCC) and clinical interventional processes.

modeling signals a shift toward personalized risk assessment in HCC, where prediction is tailored to the individual rather than to broad disease categories.

Early recurrence of HCC after surgical resection occurs in more than 50% of cases. This suggests the need to improve prediction accuracy compared to traditional methods. The radiomics-deep learning integrated model approach presented by Zhao Y. et al. showed an AUC of 0.917, with diagnostic accuracy of 88.6%, largely outperforming traditional clinical models in predicting early HCC recurrence and could significantly improve risk stratification and prognosis for HCC patients undergoing previous curative resection. A similar integrated model was also proposed in the study by Zhang M. et al., who applied a clinical selection of patient characteristics (age at DGN, TNM stage, and metastasis) and tested various machine learning algorithms, confirming enhanced power for outcomes prediction in patients treated with TACE for HCC by the model XGBoost. The knowledge and application of these models is fundamental to improve the diagnosis and prognosis in HCC cases. The gadoxetic acid-enhacement MRI for pre-operative evaluating of vessels encapsulating tumor clusters (VETC) patterns in HCC results of crucial importance, as the VECT phenotype, showing intra-tumoral blood vessels enveloped sections, exerts an impact on early recurrence and overall survival of HCC and proved higher sensitivity to angiopoietin-2 inhibitors therapy. A nomogram presented by Zhang J. et al. visualizing the integrated model, composed of selected traditional imaging features (i.e., necrosis or ischemia, wash-out and lesion-to-liver ratio) and radiomics application on arterial, portal and hepato-biliary phase, showed a significant (AUC 0.873; 95%CI 0.821–0.925) accuracy in predicting VETC patterns by preoperative MRI analysis. Thus, VECT profile may provide guidance for prevention and treatment of patients with HCC-recurrence.

At the end, we must not give up, because HCC appears to be an indolent but progressive liver tumor, with a remaining patient life expectancy of 5–8 years from diagnosis. Over the last decade, local and minimally invasive treatments and complex-combined strategies of surgery and systemic immunotherapy have been tested with the aim of proposing, in the majority of cases, a curative therapy or, when possible, a liver transplant. The studies presented in Research Topic point toward these new frontiers, even if much remains to be discovered on the mechanisms of carcinogenesis, which often develop through variable forms of liver damage (Figure 1), and do not yet reveal a common biological and molecular pathway.

Author contributions

PS: Conceptualization, Data curation, Supervision, Validation, Visualization, Writing – original draft, Writing – review & editing. MD: Conceptualization, Data curation, Supervision, Validation, Visualization, Writing – original draft, Writing – review & editing. LC: Conceptualization, Data curation, Methodology, Supervision, Validation, Visualization, Writing – original draft, Writing – review & editing.

Conflict of interest

The authors declare that the research was conducted in the absence of any commercial or financial relationships that could be construed as a potential conflict of interest.

The author(s) declared that they were an editorial board member of Frontiers, at the time of submission. This had no impact on the peer review process and the final decision.

Publisher's note

frontiers | Frontiers in Oncology

TYPE Original Research
PUBLISHED 05 April 2024
DOI 10.3389/fonc.2024.1347675

OPEN ACCESS

EDITED BY
Marcello Dallio,
University of Campania Luigi Vanvitelli, Italy

REVIEWED BY
Mengxuan Zuo,
Sun Yat-sen University Cancer Center (SYSUCC), China
Liliana Chemello,
University of Padua, Italy
Vishal G. Shelat,
Tan Tock Seng Hospital, Singapore

*CORRESPONDENCE
Jian Wang
yinghzou@139.com
Yinghua Zou
yinghzou_doctor@139.com

†These authors have contributed equally to this work and share first authorship

RECEIVED 01 December 2023
ACCEPTED 25 March 2024
PUBLISHED 05 April 2024

CITATION
Xie Y, Lyu T, Song L, Tong X, Wang J and Zou Y (2024) TACE-assisted multi-image guided radiofrequency ablation for the treatment of single hepatocellular carcinoma ≤ 5 cm: a retrospective study. *Front. Oncol.* 14:1347675. doi: 10.3389/fonc.2024.1347675

TACE-assisted multi-image guided radiofrequency ablation for the treatment of single hepatocellular carcinoma ≤ 5 cm: a retrospective study

Yong Xie†, Tianshi Lyu†, Li Song, Xiaoqiang Tong, Jian Wang* and Yinghua Zou*

Department of Interventional Radiology and Vascular Surgery, Peking University First Hospital, Beijing, China

Background/Objective: Treatment of hepatocellular carcinoma (HCC) with ablation alone often results in high rates of recurrence and metastasis, reaching up to 25.9% within two years. Therefore, this study aimed to examine the efficacy and safety of transarterial chemoembolization (TACE)-assisted multi-image guided radiofrequency ablation (RFA) for the treatment of stage Ia HCC according to the China liver cancer staging (CNLC).

Methods: This study enrolled and analyzed a total of 118 patients diagnosed with HCC, each with a single nodular lesion no larger than 5 cm, who received TACE-RFA as first-line therapy between February 1, 2014, and December 31, 2021. The median/mean follow-up period was 29.0 months [95% confidence interval (CI): 21.8-36.2 months] and 31.8 months (95% CI: 27.5-36.0 months), respectively. We assessed the treatment's effectiveness, potential complications, and survival rate.

Results: The technical success rate was 100% (118/118) after the initial treatment. Out of the total, 3 out of 118 patients (2.5%) developed local tumor progression (LTP) during the follow-up period. The median time for LTP was 29.0 months (95%CI: 21.9-36.1 months; mean: 31.5 months; range 1-92 months). At 1, 3, 5, and 7 years after treatment, the cumulative LTP rates were 0%, 4.6%, 4.6%, and 4.6%, respectively. The overall survival rates at 1, 3, 5, and 7 years were 100%, 95.2%, 95.2%, and 95.2%, respectively. In total, 28 patients experienced minor Grade B complications, and no major complications or treatment-related mortality occurred.

Conclusion: The treatment of CNLC stage Ia HCC using TACE-assisted multi-image-guided RFA was found to be both safe and feasible.

KEYWORDS

hepatocellular carcinoma (HCC), transarterial chemoembolization (TACE), radiofrequency ablation (RFA), local tumor progression (LTP), overall survival (OS), complication

Introduction

Hepatocellular carcinoma (HCC) is one of the most common malignancies worldwide (1). According to recent research (2), an estimated 905,700 new liver cancer diagnoses are expected globally in 2020, leading to 830,200 deaths from the disease. China accounts for half of the world's new cases and deaths from liver cancer.

HCC accounts for approximately 75-85% of liver cancer cases. The differences in pathogenesis, biological behavior, histopathology, treatment, and prognosis of different types of liver cancer contribute significantly to the global healthcare burden. HCC is a prevalent subtype of liver cancer and a malignant tumor of the digestive tract, characterized by a high degree of malignancy, disease progression, mortality rate, and poor efficacy. In most cases, HCC presents with no typical clinical signs in its early stages, and nearly 70-80% of patients are diagnosed at advanced stages, resulting in a missed opportunity for optimal surgical intervention (3).

Radiofrequency ablation (RFA) remains the primary treatment for minimally invasive management of unresectable early-stage HCC. Transarterial chemoembolization (TACE) is recommended as the first-line treatment for intermediate-stage HCC. However, despite its widespread use, the long-term efficacy of RFA is unsatisfactory due to suboptimal ablation boundaries (4). This results in estimated 3- and 5-year survival rates of 60-84% and 40-68%, respectively (5). Additionally, conventional ultrasound (US)-guided RFA is associated with a high rate of tumor recurrence, particularly when ablating poorly developed lesions or difficult-to-locate tumors, such as those located near the diaphragm (6, 7). Recent studies using iodide oil (4, 6) to label tumor lesions through the arterial route have shown significant improvement in long-term survival prognosis and satisfactory, clear, safe ablation boundaries. However, the safety and efficacy of TACE-assisted multi-image-guided RFA for the treatment of stage Ia HCC (i.e., performance status score 0~2, Child-Pugh grade A/B liver function, single tumor ≤5cm, no vascular invasion and extrahepatic metastasis) based on the China liver cancer staging (CNLC) (8) is unclear.

Therefore, we aimed to investigate the clinical safety and efficacy of TACE-assisted multi-image-guided RFA for the treatment of stage Ia HCC in patients with CNLC using ultrasound, computed tomography (CT), or cone beam CT to leverage their respective strengths and advantages, minimize the risk of local recurrence, and enhance the safety zones of ablation.

Abbreviations: ALBI, albumin bilirubin; CNLC, China liver cancer staging; CI, confidence interval; CBCT, cone beam computed tomography; DSA, digital subtraction angiography; ECOG PS, Eastern Cooperative Oncology Group performance status; HR, hazard ratio; HBV, hepatitis B virus; HCV, hepatitis C virus; HCC, hepatocellular carcinoma; IDR, intrahepatic distant recurrence; LTP, local tumor progression; MRI, magnetic resonance imaging; OS, overall survival; PVTT, portal vein tumor thrombus; RFA, radiofrequency ablation; RFS, recurrence-free survival; TACE, transarterial chemoembolization; TBS, tumor burden score; US, ultrasound.

Materials and methods

Patients

A retrospective cohort study was carried out on patients diagnosed with HCC who underwent TACE-RFA as their initial treatment at our institution from February 1, 2014, to December 31, 2021. The study was approved by the institutional review board, and written informed consent was waived due to the retrospective nature of the analysis.

The study's inclusion criteria comprised patients with the following characteristics: (a) histopathologically confirmed diagnosis of HCC or diagnoses compliant with the guidelines of the European Association for the Study of Liver/American Association for the Study of Liver Disease (9); (b) diagnosed with stage Ia HCC; (c) aged 18 years or older; (d) classified as Child-Pugh Grade A or B; (e) Eastern Cooperative Oncology Group performance status (ECOG PS) of 0-1; (f) patients who had declined surgery. Exclusion criteria encompassed: (a) pregnancy, lactation, or of childbearing age; (b) acute infection or acute onset of chronic infection; (c) patients with hepatitis B virus (HBV) or hepatitis C virus (HCV) without regular antiviral therapy; (d) presence of malignant tumors in sites other than the liver; (e) prior radiotherapy, chemotherapy, molecular targeting, or immunotherapy; (f) loss to follow-up; (g) incomplete imaging data; (h) microwave or cryoablation following TACE; (i) TACE or RFA as monotherapy; (j) RFA followed by TACE. Patients meeting the inclusion criteria were enrolled and analyzed.

TACE procedure

Under the guidance of digital subtraction angiography (DSA), the 5-Fr Rosch hepatic catheter (Cook, Bloomington, IN, USA) was routinely chosen for intubating the hepatic artery or superior mesenteric artery to assess the tumor blood supply. Subsequently, a 1.9-French microcatheter (Asahi Intecc Co., Ltd., Japan) was employed to super selectively access the tumor's feeding arteries. Cone beam computed tomography (CBCT) with dynamic contrast and three-dimensional reconstruction was performed using the microcatheter, and the blood supply to the lesion was identified at the post-processing station. Additionally, careful attention was given to detecting any abnormal tumor-stained nodules, and microcatheters were utilized for embolization whenever possible. A mixture of 5-10 mL of iodide oil (Guerbet, Villepinte, Seine-Saint-Denis, France) and 10-30 mg of epirubicin was emulsified in specific proportions and used to embolize the feeding arteries. Lesions with abundant blood supply were embolized with gelatin sponge granules or embolic microspheres in the interim, and the embolization was ceased when blood flow was essentially stagnant. Finally, the iodized oil deposition of the tumor was checked through

three-dimensional reconstruction of CBCT, and embolization was performed as needed until satisfactory embolization was achieved.

RFA procedure

We conducted RFA procedures within 4 weeks following TACE. The median time interval between TACE and RFA was 4 days, with a range of 0-30 days. The RFA procedure was guided by a combination of imaging equipment, including ultrasound combined with CT or ultrasound combined with CBCT, and DSA if needed. Ultrasound was primarily used for real-time monitoring of tumor puncture and ablation processes, while CT/CBCT was used to assess ablation areas and safety boundaries. DSA was utilized for fluoroscopic adjustment of multipolar ablation needles in cases of obvious lesions with iodide oil deposits (Figure 1). Depending on the manufacturer's power settings, we employed the Boston Medical Device (RF 3000TM, Boston Scientific Way, Marlborough, MA 01752, US). The choice of electrode needle (LeVeenTMSuperSlimTM, Needle Electrode System, Boston Scientific) often depended on the size of the tumor and the location of the lesion.

First, the positioning of ultrasound is combined with preoperative CT and magnetic resonance imaging (MRI) to select the appropriate puncture point and needle angle. After administering local anesthesia with 1% lidocaine, the patient was instructed to hold their breath, and the multipole needle was inserted subcutaneously close to the liver envelope. Then, the patient was again instructed to hold their breath, and the multipole needle was inserted into the target lesion. The direction of the puncture needle was fine-tuned under ultrasound scan until the multipole needle fully covered the lesion. Real-time ultrasound was used to monitor tumor ablation progression. This was followed by multiple CT/CBCT scans to determine if there was a sufficient ablation area (greater than 5-10 mm). If not, the position of the needle tip was adjusted several times. Finally, the puncture channel was ablated during electrode retraction to prevent bleeding or tumor cell seeding.

All patients underwent repeat abdominal contrast MRI or CT within 1 month after initial RFA to assess for residual lesions after ablation. Immediate remedial RFA was conducted if the lesion was still viable. All procedures are performed by the same team at our center, with more than 10 years of experience in interventional therapy.

Variable collection and follow-up strategies

The general information collected includes age, sex, alcohol consumption, smoking status, presence of cirrhosis of the liver, tumor location, tumor maximum diameter, tumor burden score (TBS) (10), Child-Pugh score, type of liver disease, ECOG PS, relevant laboratory tests within 7 days before treatment, and so on. The primary endpoints were local tumor progression (LTP), and the secondary endpoints were technical success, overall survival (OS), and postoperative complications. LTP is defined as the presence of a newly enhanced tumor within the original ablation zone. Technical success rate is defined as a repeat abdominal contrast MRI or CT within 1 month after RFA to assess the absence of tumor remnants in the ablation area. OS is defined as the time from the start of RFA treatment to death from any cause. Complications include local hematoma, bleeding, local skin infection, pain, gastrointestinal reactions (e.g., nausea and vomiting), and so on, classified with reference to the Society Guidelines for Interventional Radiology (11), and major complications are defined as any adverse event leading to

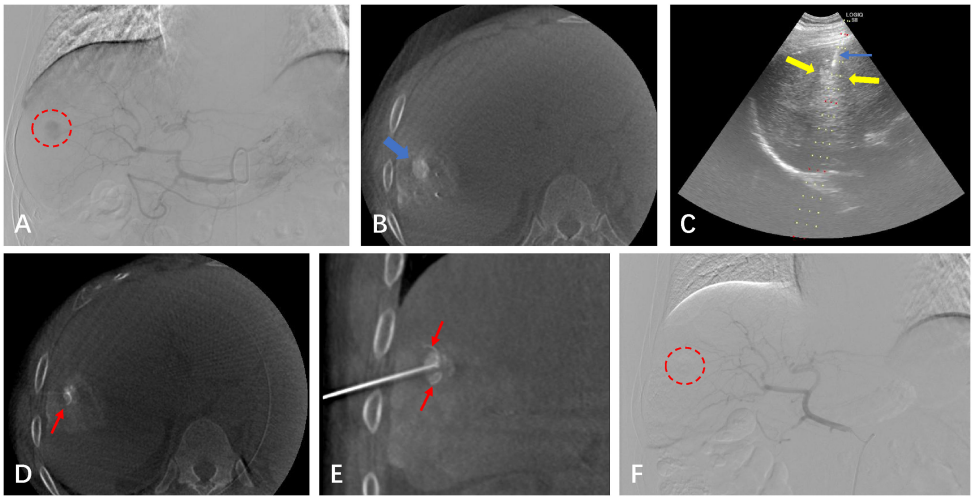

FIGURE 1
A 64-year-old male with a small HCC of 1.8 cm in the right hepatic lobe. **(A)** CBCT-guided angiography shows the HCC lesion (red circle). **(B)** After undergoing the TACE procedure, the CBCT scan shows dense iodinated oil deposits in the lesion (blue arrow). **(C)** Real-time puncture under fluoroscopy with US guidance. **(D, E)** CBCT image confirming the position of the RFA needle (red arrow). **(F)** After the lesion underwent simultaneous TACE-RFA, CBCT-guided selective angiography does not show the original abnormal staining of the small HCC.

additional treatment, such as an increased level of care, prolonged hospital stay, fatality, or disability. Intrahepatic distant recurrence (IDR) was defined as any new emerging tumor that occurred in the liver separate from the ablated zone. Extrahepatic recurrence was defined as the appearance of new lesions outside the liver postoperatively. Portal vein tumor thrombus (PVTT) is defined as a lesion in the portal vein, observable in all stages of CT/MRI, with partial enhancement in the arterial phase and a filling defect in the portal vein phase. Liver tumor progression, including LTP, PVTT, IDR, and extrahepatic recurrence, was measured from the time of the RFA procedure to either local or distant progression or death, whichever came first. Patients were followed up with outpatient or inpatient visits every 3 months for the first year after treatment and every 3-6 months thereafter to assess clinical symptoms, conduct relevant laboratory tests, and undergo contrast-enhanced CT scans or MRI examinations. Follow-up time, tumor progression, and patient survival were recorded. If tumor progression is found during follow-up, the best treatment strategy will be carried out according to the latest liver cancer diagnosis and treatment guidelines based on individual conditions (including ablation, surgical resection, liver transplantation, TACE, systemic therapy, radiation therapy, or combination therapy).

Statistical analysis

Data analysis was performed using R statistical software (version 3.6.1). Measurement data with a normal distribution were reported as mean ± standard deviation. Pairwise t-tests or ANOVA were utilized for group comparisons. Counting data was presented as a percentage, and group comparisons were assessed using the chi-square test. The Kaplan-Meier method was employed to calculate LTP and OS, and group differences were evaluated using the Log-rank test. A P-value of less than 0.05 (two-sided) was considered statistically significant.

Results

Baseline characteristics of the patients

A total of 118 patients were included in this study, of whom 92 (77.97%) were male and 26 (22.03%) were female, with a mean age of 59.47 ± 11.82 (range, 29.00-89.00) years. The maximum tumor diameter was 2.32 ± 1.03 (range, 0.70-5.00) cm, and the tumor burden score was 2.56 ± 0.95 (range, 1.22-5.10). Among the included patients, 31 (26.27%) had tumors located in the left lobe of the liver, while 87 (73.73%) had tumors located in the right lobe of the liver. Twenty-one (17.80%) cases had diabetes, 32 (27.12%) had hypertension, 52 (44.07%) were smokers, and 4 (3.39%) were alcohol consumers. With respect to hepatitis, 93 (78.81%) cases involved hepatitis B or C, 4 (3.39%) involved alcoholic or autoimmune hepatitis, and 21 (17.80%) were normal. Furthermore, 109 (92.37%) cases had an ECOG PS of 0, while 9 (7.63%) had an ECOG PS of 1. The incidence of liver cirrhosis was 75 (63.56%), and 54 (46.15%) were in albumin bilirubin (ALBI) grade 1, while 63 (53.85%) were in ALBI grade 2. Additionally, 102 (88.70%) were in Child-Pugh grade A, while 13 (11.30%) were in grade B (Table 1).

Local tumor control rate

LTP was identified in 3 out of 118 (2.5%) patients during the follow-up period. The median time to LTP was 29.0 months (95% CI: 21.9-36.1 months; range 1-92 months; mean: 31.5 months). The cumulative 1-, 3-, 5-, and 7-year LTP rates were 0%, 4.6%, 4.6%, and 4.6%, respectively (Figure 2). In terms of recurrence patterns, 42 cases (35.6%) had IDR, while 3 and 4 cases showed extrahepatic recurrence and PVTT, respectively. Finally, a total of 66 (55.9%) patients did not experience disease progression or recurrence during follow-up (Table 2). For disease progression or recurrent lesions, second-line therapy was received, including TACE-RFA (n=23), TACE/TAI (n=15), RFA (n=2), TACE-RFA+systemic therapy (lenvatinib) (n=1), systemic therapy (sorafenib) (n=1), optimal supportive therapy (n=4), and unknown (n=4).

Overall survival

The median follow-up period was 29.0 months (95%CI: 21.8-36.2 months; range 1–92 months; mean: 31.8 months). The cumulative 1-, 3-, 5-, and 7-year OS rates were 100%, 95.2%, 95.2%, and 95.2% (Figure 3).

Technical success and complications

After the initial treatment, the technical success rate was 100% (118 out of 118). Twenty-eight patients (23.7%) developed minor grade B complications, which included twenty-six cases of pain in the liver area, one case of fever, and one case of vomiting (Table 2). All complications were successfully treated. The major complication rate was 0%. Overall, there were no treatment-related deaths during hospitalization.

Discussion

Despite constant updates and revisions to the guidelines for diagnosing and treating HCC, the recommended radical treatment strategy for patients with CNLC stage Ia or BCLC stage 0-A HCC has remained unchanged. The challenge, however, is that the survival prognosis for patients at this stage has essentially plateaued, making further improvement difficult. One primary limitation of thermal ablation, a radical treatment method, is that when the tumor diameter exceeds 3 cm, local tumor control diminishes rapidly. Achieving a sufficient range of safe ablation boundary is necessary to control the *in-situ* progression of the local tumor (12). The "heat sink effect," which results in the dissipation of heat energy, is a key factor affecting the safety boundary. To address this issue, the combination of TACE and thermal ablation has been

10.3389/fonc.2024.1347675

TABLE 1 Basic characteristics of 118 patients who received TACE-RFA as the first-line treatment for HCC.

Variables	Value
Age, years[§]	59.47 (11.82)/57.00 (29.00-89.00)
Sex, n (%)	
Female	26 (22.03)
Male	92 (77.97)
TBS[§]	2.56 (0.95)/2.24 (1.22-5.10)
Maximum tumor diameter, cm[§]	2.32 (1.03)/2.00 (0.70-5.00)
Maximum tumor diameter, n (%)	
<3	89 (75.42)
≥3, ≤5	29 (24.58)
ALBI score [†§]	-2.53 (-0.45)/-2.57 (-1.43–3.48)
ALBI, n (%) [†§]	
Grade 1	54 (46.15)
Grade 2	63 (53.85)
Hypertension, n (%)	
No	86 (72.88)
Yes	32 (27.12)
Diabetes, n (%)	
No	97 (82.20)
Yes	21 (17.80)
Smoking, n (%)	
No	66 (55.93)
Yes	52 (44.07)
Alcohol abuse, n (%)	
No	84 (71.19)
Yes	34 (28.81)
Is TACE performed concurrently with RFA, n (%)	
No	96 (81.36)
Yes	22 (18.64)
Location of the tumor, n (%)	
Left	31 (26.27)
Right	87 (73.73)
BCLC stage, n (%)	
0	61 (51.69)
A	57 (48.31)
Child-Pugh class, n (%)†	
A	102 (88.70)
B	13 (11.30)
Cirrhosis, n (%)	
No	43 (36.44)
Yes	75 (63.56)
ECOG PS, n (%)	
0	109 (92.37)
1	9 (7.63)
Liver disease type, n (%)	
Non-hepatitis	21 (17.80)
Hepatitis B/C	93 (78.81)
Other hepatitis	4 (3.39)
AFP, n (%)	
≤20 ng/ml	78 (66.10)
>20 ng/ml	40 (33.90)
Hemoglobin, g/L[§]	137.09 (17.92)/138.00 (78.00-178.00)
WBC count, 10^9/L[§]	4.98 (1.91)/4.90 (1.40-12.70)
Platelet count, 10^9/L[§]	125.70 (68.69)/120.00 (28.00-628.00)
ALT, IU/L[§]	26.45 (18.44)/21.00 (7.00-96.00)
AST, IU/L[§]	32.51 (19.55)/26.00 (12.00-131.00)
Serum albumin, g/L[§]	39.05 (4.91)/39.50 (26.80-50.80)
Total bilirubin, umol/L[§]	17.59 (8.10)/15.70 (4.50-46.00)
Alkaline phosphatase, IU/L[§]	80.32 (31.28)/74.00 (31.00-284.00)
Creatinine, mg/dL[§]	78.13 (14.05)/78.80 (46.20-117.44)
International standardized ratio[§]	1.11 (0.14)/1.09 (0.89-1.60)
Prothrombin time, s[§]	12.20 (1.48)/11.80 (9.30-16.90)

[†]Missing data.
[§]Mean (SD)/Median (range).
TBS, tumor burden score (TBS^2 = (maximum tumor diameter)^2 + (number of tumors)^2); ALBI, albumin bilirubin (ALBI score = (0.66×log10 bilirubin (μmol/L) -(0.085×albumin (g/L))); BCLC, Barcelona Clinic Liver Cancer; ECOG PS, Eastern Cooperative Oncology Group Performance Status; WBC, white blood cell; ALT, alanine transaminase; AST, aspartate aminotransferase.

widely utilized, emerging as a research hotspot in recent years. Our center has achieved a satisfactory rate of tumor local control and survival prognosis using TACE-assisted multi-image-guided RFA, and the procedure has been deemed safe.

TACE followed by RFA has become increasingly popular in recent years, and current clinical data suggest that this combination is superior to using RFA alone. Specifically, TACE in conjunction with RFA induces higher rates of complete necrosis and improves OS. Our research showed that the cumulative 1-, 3-, 5-, and 7-year OS rates were 100%, 95.2%, 95.2%, and 95.2%. Cao et al. (13) conducted several studies on single small HCC (≤ 3.0 cm), and their related studies confirmed that the 1-year, 3-year, and 5-year OS rates of the TACE-RFA and RFA groups were similar (98.7%,

10.3389/fonc.2024.1347675

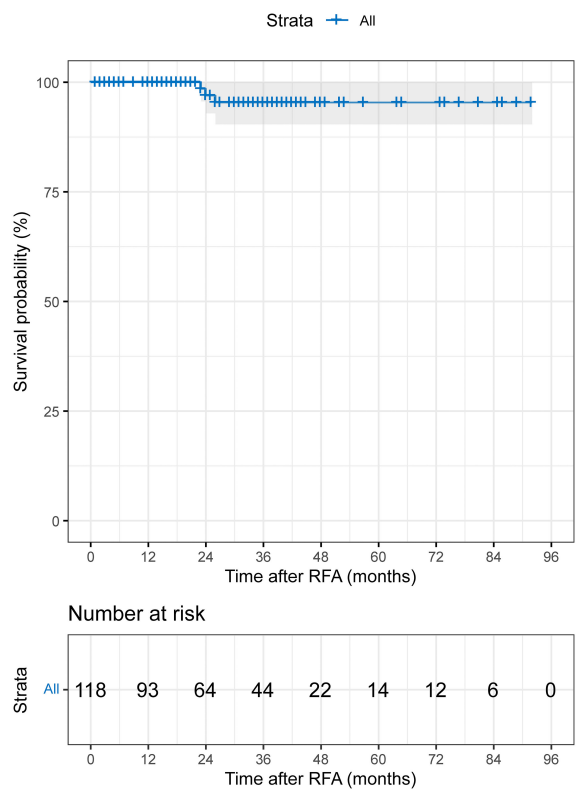

FIGURE 2
The Kaplan–Meier curve demonstrates the LTP of patients with HCC who received TACE-RFA.

TABLE 2 Events during the follow-up.

Category	Number of patients
Complications¶	
Minor complications	
Grade A	n=80
Grade B	pain (n=26), fever (n=1), vomit (n=1)
Major complications	n=0
Tumor events after RFA	
LTP	n=3
IDR	n=42
Extrahepatic recurrence	n=4
PVTT	n=3
No	n=66
Second-line treatments	
TACE-RFA	n=23
TACE/TAI	n=15
RFA	n=2
TACE-RFA+Systemic therapy	n=1
Systemic therapy	n=1
Support therapy	n=4
Unknown	n=4
No	n=68

¶ Minor complications include grade A and B. Grade A, no therapy, no consequences; Grade B, nominal therapy, no consequence, includes overnight admission for observation only. Major complications include grades C, D, E and F. Grade C, requires therapy, minor hospitalization (< 48 h); Grade D, requires major therapy, unplanned increase in level of care, prolonged hospitalization (> 48 h); Grade E, permanent adverse sequelae; Grade F: death. LTP, local tumor progression; IDR, intrahepatic distant recurrence; PVTT, portal vein tumor thrombus.

93.0%, and 75.9% *vs*. 97.4%, 88.0%, and 77.4%, P=0.444). In terms of long-term survival benefit (greater than 5 years), an article in the JAMA sub-journal, through a secondary analysis of a phase III randomized controlled clinical study, found that the 5- and 7-year OS rates in the TACE-RFA group versus the RFA group were 52.0% and 36.4% *vs*. 43.2% and 19.4%, respectively (HR=0.55, 95% CI: 0.39-0.78, P=0.001). Subgroup analysis also confirmed that the OS of the TACE-RFA group was significantly better than that of the RFA group (HR=3.20, 95% CI=1.91-5.35, P<0.001) regardless of the diameter (>3 cm *vs*. ≤3 cm) (14). Yang et al. (15) retrospectively found that the overall 1-year, 3-year, and 5-year OS of the RFA group was 73.9%, 51.1%, and 28.0%, respectively, while the TACE-RFA combined group was 88.5%, 64.6%, and 44.3%, respectively, and there were significant differences between the groups. In the latest retrospective multicenter study (16) of the First Affiliated Hospital of Sun Yat-sen University, 468 patients with single small HCC (≤3.0 cm) received RFA (322 cases) or TACE-RFA (146 cases), respectively, with 74.8% and 42.5% of the 1-year and 5-year OS rates in the combined group, and 53.5% and 28.7% in the RFA group (P<0.001), respectively. It has been determined that the combination of TACE-RFA can effectively reduce recurrence following RFA and improve the long-term survival rate of patients with small HCC. According to existing evidence-based medical literature, the cumulative 5-year survival rate of the TACE-RFA combination is superior, and the local control effect and long-term survival rate (> 5 years) are also more satisfactory. While combination therapy has effectively improved OS and prolonged recurrence-free survival (RFS), RFS was not assessed in this study due to the nature of early-stage HCC and its 'on-off-on' recurrence pattern (13). A phase III randomized controlled clinical study (14) found that the 5- and 7-year RFS of TACE-RFA and RFA groups were 41.4%, 34.5%, 27.4%, and 18.1%, respectively (HR=0.66, 95% CI: 0.49-0.89, P=0.007). A retrospective multicenter study (16) revealed that the RFS rates at 1 and 5 years were 51.7% and 24.4% in the combined group, and 36.1% and 9.3% in the RFA group (P<0.001). It is evident that the advantages of TACE-RFA over RFA monotherapy in RFS are undeniable.

In this study, 66 out of 118 patients (55.9%) showed no recurrence or metastasis, 42 patients (35.6%) developed IDR (Figure 4), and only 3 patients (2.5%) experienced LTP during the entire follow-up period (Figure 5). The study results also revealed that the LTP rates at 1, 3, 5, and 7 years following TACE-RFA therapy were 0%, 4.6%, 4.6%, and 4.6%, respectively. These findings are consistent with previous studies (13, 17, 18) which also indicated LTP occurrences within the first 3 years, followed by a gradual decrease in the incidence rate. The study suggests that patients who undergo

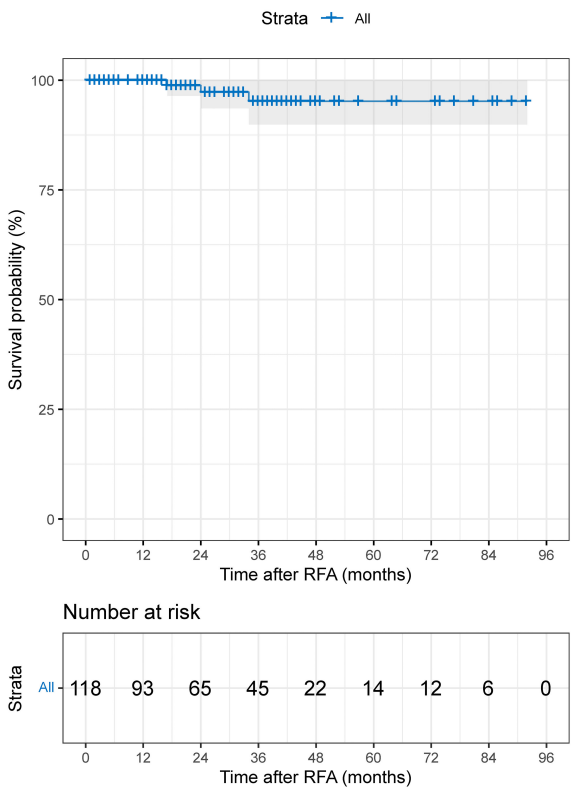

FIGURE 3
The Kaplan–Meier curve demonstrates the OS of patients with HCC who received TACE-RFA.

TACE-RFA therapy should have more frequent follow-up in the first 3 years after treatment. So, what factors are prone to LTP? A study by Huang et al. (19) recruited 249 patients into two groups (TACE group *vs* TACE-RFA group) based on diameter; they found that undergoing RFA alone and an insufficient ablative margin were independent risk factors for LTP. To minimize the adverse effects of these risk factors, we implemented a different approach compared to the study by Huang et al. (19). We directly treated single lesions ≤ 5 cm with TACE-RFA, which can reduce the problem of insufficient safety boundaries resulting from ablation alone. Additionally, conventional methods of ablation guidance such as US, CBCT, CT, and DSA can be enhanced by utilizing a multi-image guidance mode. This approach involves using US for puncture positioning and real-time monitoring of the ablation process, including observation of heat coverage and heat sink effect. CT or CBCT is used for the assessment of ablation areas and safety boundaries, with a multiple overlapping ablation strategy required for larger lesions (3-5 cm) to implement the entire ablation process. Following an ablation cycle, our center performs a CT or CBCT scan on the patient and reviews three-dimensional images in the coronal, sagittal, and axial positions using the post-processing workstation. This evaluation is done to determine if the angle, orientation, or umbrella needle should be adjusted. For lesions with obvious iodized oil deposits, DSA is also used to fluoroscopically adjust the ablation needles to ensure complete coverage of the entire tumor lesion. A previous study (20) found that imaging-invisible micrometastases may exist around HCC, and a 5-mm ablative margin is typically required to completely eradicate these microsatellite foci (12). However, in our center's practice of

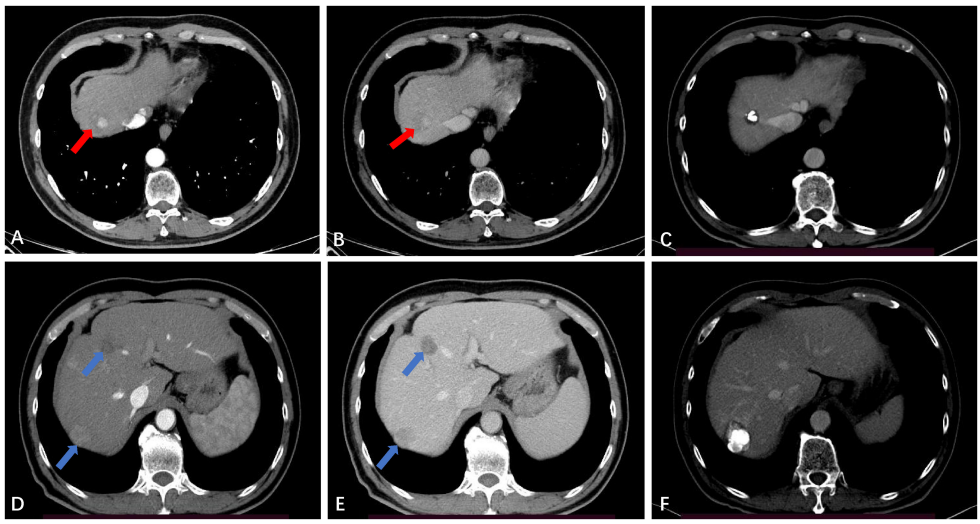

FIGURE 4
Intrahepatic distant recurrence (IDR) after TACE-RFA for HCC in a 56-year-old man. **(A, B)** Dynamic contrast-enhanced axial CT scan shows a single HCC with diameter of 2.4cm (red arrow). **(C)** Axial CT scan shows the complete ablation zone, with "intratumoral lipiodol deposition" visible in the ablation zone. **(D, E)** CT scan obtained during the hepatic arterial phase and portal venous phase 51 months after TACE-RFA shows IDR (blue arrows), with the largest lesions measuring about 2.7 cm. The two lesions received RFA and TACE-RFA, respectively. **(F)** Iodide oil deposits are visible in the largest lesion.

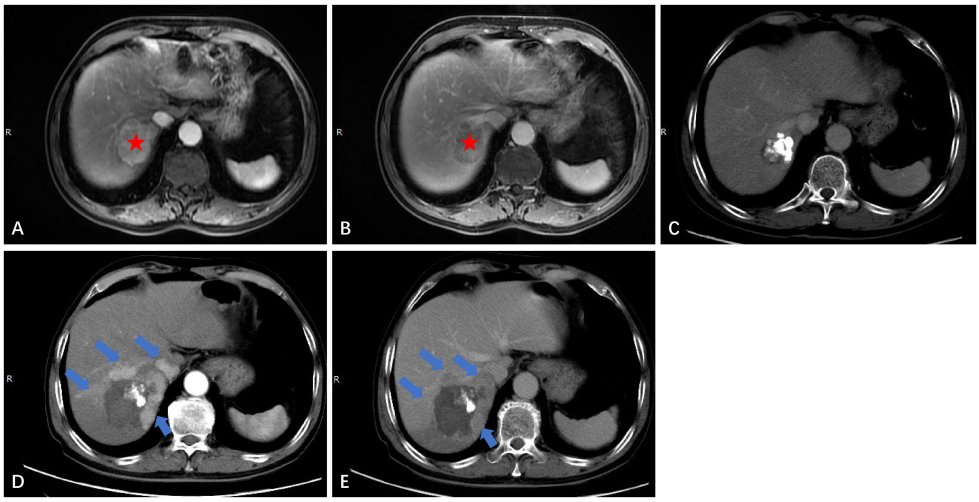

FIGURE 5
Local tumor progression (LTP) after TACE-RFA for HCC in a 72-year-old man. Finally, the patient received TACE as a second-line treatment. **(A)** Dynamic contrast-enhanced axial MRI scan shows a single 4.6cm×3.7cm×3.4cm HCC (red star). **(B)** MRI scan shows washout at the portal venous phase (red star). **(C)** CT scan obtained during the portal venous phase 1 month after TACE-RFA shows the complete ablation zone adjacent to the hepatic vein. **(D, E)** CT scan obtained during the hepatic arterial phase and portal venous phase 28 months after TACE-RFA shows the LTP, with multiple arterial enhancing nodules around the original ablation lesion and washout at the portal venous phase (blue arrows).

expanding the safety ablation boundary to 1 cm, it is encouraging to note that the LTP was only 2.5% at the follow-up cut-off time in this study. Gui et al. reported 8.7% (21), and they conclusively showed that TACE + RFA provided comparable results compared to surgical resection. As with us, the effectiveness of combination therapy has been demonstrated, although the range of tumor diameters varies. The use of TACE in combination with RFA for HCC lesions presents several potential clinical implications. Firstly, this combination therapy may provide a curative treatment option for a subset of patients with HCC lesions that are not amenable to surgery or transplantation. Secondly, it may offer a potential bridge to liver transplantation by achieving tumor downstaging and preventing tumor progression in patients on the transplant waiting list. Additionally, the combination of TACE and RFA may contribute to improved OS and reduced recurrence rates in patients with larger HCC lesions, thus impacting long-term clinical outcomes. Further research and well-designed clinical trials are warranted to better define the role of this combined approach and to validate its potential benefits in improving patient outcomes. A retrospective study by Lee et al. (22) also suggested that the combination of TACE and RFA results in low LTP (about 5%). Previous studies by Cao et al. (13) showed that tumor size [hazard ratio (HR)=1.592, 95% CI: 1.313–1.930, P<0.001] is an independent risk factor for tumor progression. We speculate that this result may be due to most of the tumors in our included population being less than 3 cm in diameter. Therefore, we suggest that TACE-RFA should be considered for HCC ≤ 5 cm, with sufficiently large ablation boundaries being equally important. In addition to studying LTP, we observed recurrence patterns in 118 patients, with 42 (35.6%) having IDR, 4 (3.4%) experiencing extrahepatic recurrence, and 3 (2.5%) developing PVTT. A meta-analysis by Gui et al. (21) found that after undergoing TACE-RFA, 227 (43.0%) developed IDR, and 23 (3.7%) had extrahepatic recurrence, which aligns with our study.

In this study, we noted minor complications, but no major complications were observed. The minor complications improved with symptomatic treatment, suggesting that the treatment strategy is relatively safe and suitable for clinical promotion.

The reason our research achieved relatively satisfactory efficacy and safety is closely linked to the continuous improvement and maturity of current TACE or RFA treatments. More importantly, we utilized the TACE-RFA joint strategy to maximize its efficacy through: (a) providing additional survival benefit from chemoembolization; (b) using TACE before ablation to mark the lesion with iodine oil or microsphere deposition, enabling clear display of the lesion's location under multi-image guidance combined with US/CT/CBCT/DSA and other imaging equipment, and assisting with positioning; (c) enhancing heat conduction through the deposition of iodine oil or microspheres in the tumor to better kill tumor cells and induce complete necrosis; (d) reducing the inherent "heat sink effect" of thermal ablation by effectively blocking the rich blood flow in and around the tumor lesion with TACE; (e) improving the prognosis of patients by detecting some microlesions as soon as possible through arteriography and early intervention; and (f) strictly adhering to safe ablation boundaries.

There were limitations to our study. Firstly, this is a retrospective, single-center study with limited sample sizes and inevitable selection bias. Secondly, this is a one-arm study that lacks head-to-head comparisons and can only compare efficacy and safety through historical controls. Thirdly, the time interval between TACE and RFA is typically within 4 weeks, so differences in the time interval between TACE and RFA may lead to biases in the evaluation of treatment efficacy and safety. However, there are few studies on the timing of treatment intervals for combination therapy, which is still in the exploratory stage, but most of them advocate ablation after TACE with an interval of 0-4 weeks (23–25). The main considerations are as follows: first, it takes

time for patients to recover liver function after TACE. Second, excessively prolonging the time interval can lead to recanalization and neoangiogenesis of the cancer nest. However, some scholars think that RFA performed on the same day as chemoembolization has the greatest efficacy in tumor ablation (23). But the optimal interval between TACE and RFA remains a topic of debate, and individualized approaches based on tumor characteristics and patient-specific factors may be necessary. Further prospective studies are needed to clarify the optimal interval selection and to develop guidelines for the combined use of TACE and RFA in the treatment of HCC. In other words, the interval selection for TACE combined with RFA in the treatment of HCC is a complex and multifaceted issue that requires careful consideration of various clinical and tumor-specific factors. As research in this area continues to evolve, a better understanding of the optimal interval and its impact on treatment outcomes will further enhance the effectiveness of this combined therapeutic approach.

Conclusion

In conclusion, our study found that TACE-assisted multi-image-guided RFA is a feasible and safe treatment option for stage Ia HCC of CNLC. The combination therapy of TACE-RFA should be considered as one of the modified ablation strategies that provide a more effective treatment for stage Ia HCC of CNLC.

Data availability statement

The original contributions presented in the study are included in the article/supplementary material. Further inquiries can be directed to the corresponding authors.

Ethics statement

The studies involving humans were approved by the Institutional Review Boards of the Peking University First Hospital. The studies were conducted in accordance with the local legislation and institutional requirements. The ethics committee/institutional review board waived the requirement of written informed consent for participation from the participants or the participants' legal guardians/next of kin because this was a retrospective study.

Author contributions

YX: Data curation, Formal analysis, Resources, Software, Writing – original draft. TL: Data curation, Formal analysis, Resources, Software, Writing – original draft. LS: Investigation, Methodology, Writing – review & editing. XT: Investigation, Methodology, Writing – review & editing. JW: Conceptualization, Supervision, Writing – review & editing. YZ: Conceptualization, Supervision, Writing – review & editing.

Funding

The author(s) declare that no financial support was received for the research, authorship, and/or publication of this article.

Conflict of interest

The authors declare that the research was conducted in the absence of any commercial or financial relationships that could be construed as a potential conflict of interest.

Publisher's note

References

1. Sung H, Ferlay J, Siegel RL, Laversanne M, Soerjomataram I, Jemal A, et al. Global cancer statistics 2020: GLOBOCAN estimates of incidence and mortality worldwide for 36 cancers in 185 countries. *CA Cancer J Clin*. (2021) 71:209–49. doi: 10.3322/caac.21660

2. Rumgay H, Arnold M, Ferlay J, Lesi O, Cabasag CJ, Vignat J, et al. Global burden of primary liver cancer in 2020 and predictions to 2040. *J Hepatol*. (2022) 77:1598–606. doi: 10.1016/j.jhep.2022.08.021

3. European Association for the Study of the Liver and Electronic address eee, European Association for the Study of the L. EASL Clinical Practice Guidelines: Management of hepatocellular carcinoma. *J Hepatol*. (2018) 69:182–236. doi: 10.1016/j.jhep.2018.03.019

4. Nishikawa H, Inuzuka T, Takeda H, Nakajima J, Sakamoto A, Henmi S, et al. Percutaneous radiofrequency ablation therapy for hepatocellular carcinoma: a proposed new grading system for the ablative margin and prediction of local tumor progression and its validation. *J Gastroenterol*. (2011) 46:1418–26. doi: 10.1007/s00535-011-0452-4

5. Nault JC, Sutter O, Nahon P, Ganne-Carrie N, Seror O. Percutaneous treatment of hepatocellular carcinoma: State of the art and innovations. *J Hepatol*. (2018) 68:783–97. doi: 10.1016/j.jhep.2017.10.004

6. Wu CH, Liang PC, Su TH, Lin MC, Chang YH, Shih TT, et al. Iodized oil computed tomography versus ultrasound-guided radiofrequency ablation for early hepatocellular carcinoma. *Hepatol Int*. (2021) 15:1247–57. doi: 10.1007/s12072-021-10236-0

7. Lee MW, Rhim H, Cha DI, Kim YJ, Choi D, Kim YS, et al. Percutaneous radiofrequency ablation of hepatocellular carcinoma: fusion imaging guidance for management of lesions with poor conspicuity at conventional sonography. *AJR Am J Roentgenol*. (2012) 198:1438–44. doi: 10.2214/AJR.11.7568

8. Xie DY, Zhu K, Ren ZG, Zhou J, Fan J, Gao Q. A review of 2022 Chinese clinical guidelines on the management of hepatocellular carcinoma: updates and insights. *Hepatobiliary Surg Nutr*. (2023) 12:216–28. doi: 10.21037/hbsn-22-469

9. Bruix J, Sherman MPractice Guidelines Committee and American Association for the Study of Liver Diseases. Management of hepatocellular carcinoma. *Hepatology*. (2005) 42:1208–36. doi: 10.1002/hep.20933

10. Ho SY, Liu PH, Hsu CY, Huang YH, Liao JI, Su CW, et al. Radiofrequency ablation versus transarterial chemoembolization for hepatocellular carcinoma within milan criteria: prognostic role of tumor burden score. *Cancers (Basel)*. (2022) 14:4207. doi: 10.3390/cancers14174207

11. Khalilzadeh O, Baerlocher MO, Shyn PB, Connolly BL, Devane AM, Morris CS, et al. Proposal of a new adverse event classification by the society of interventional radiology standards of practice committee. *J Vasc Interv Radiol*. (2017) 28:1432–7 e3. doi: 10.1016/j.jvir.2017.06.019

12. Crocetti L, de Baere T, Pereira PL, Tarantino FP. CIRSE standards of practice on thermal ablation of liver tumours. *Cardiovasc Intervent Radiol*. (2020) 43:951–62. doi: 10.1007/s00270-020-02471-z

13. Cao S, Zou Y, Lyu T, Fan Z, Guan H, Song L, et al. Long-term outcomes of combined transarterial chemoembolization and radiofrequency ablation versus RFA monotherapy for single hepatocellular carcinoma </=3 cm: emphasis on local tumor progression. *Int J Hyperthermia*. (2022) 39:1–7. doi: 10.1080/02656736.2021.1998660

14. Zhang YJ, Chen MS, Chen Y, Lau WY, Peng Z. Long-term outcomes of transcatheter arterial chemoembolization combined with radiofrequency ablation as an initial treatment for early-stage hepatocellular carcinoma. *JAMA Netw Open*. (2021) 4:e2126992. doi: 10.1001/jamanetworkopen.2021.26992

15. Yang W, Chen MH, Wang MQ, Cui M, Gao W, Wu W, et al. Combination therapy of radiofrequency ablation and transarterial chemoembolization in recurrent hepatocellular carcinoma after hepatectomy compared with single treatment. *Hepatol Res*. (2009) 39:231–40. doi: 10.1111/j.1872-034X.2008.00451.x

16. Peng Z, Wu X, Li J, Pang H, Zhang Y, Lin M, et al. The role of neoadjuvant conventional transarterial chemoembolization with radiofrequency ablation in the treatment of recurrent hepatocellular carcinoma after initial hepatectomy with microvascular invasion. *Int J Hyperthermia*. (2022) 39:688–96. doi: 10.1080/02656736.2022.2051613

17. Lee MW, Kang D, Lim HK, Cho J, Sinn DH, Kang TW, et al. Updated 10-year outcomes of percutaneous radiofrequency ablation as first-line therapy for single hepatocellular carcinoma < 3 cm: emphasis on association of local tumor progression and overall survival. *Eur Radiol*. (2020) 30:2391–400. doi: 10.1007/s00330-019-06575-0

18. Shiina S, Tateishi R, Arano T, Uchino K, Enooku K, Nakagawa H, et al. Radiofrequency ablation for hepatocellular carcinoma: 10-year outcome and prognostic factors. *Am J Gastroenterol*. (2012) 107:569–77; quiz 78. doi: 10.1038/ajg.2011.425

19. Huang J, Huang W, Guo Y, Cai M, Zhou J, Lin L, et al. Risk factors, patterns, and long-term survival of recurrence after radiofrequency ablation with or without transarterial chemoembolization for hepatocellular carcinoma. *Front Oncol*. (2021) 11:638428. doi: 10.3389/fonc.2021.638428

20. Renzulli M, Brocchi S, Cucchetti A, Mazzotti F, Mosconi C, Sportoletti C, et al. Can current preoperative imaging be used to detect microvascular invasion of hepatocellular carcinoma? *Radiology*. (2016) 279:432–42. doi: 10.1148/radiol.2015150998

21. Gui CH, Baey S, D'Cruz RT, Shelat VG. Trans-arterial chemoembolization + radiofrequency ablation versus surgical resection in hepatocellular carcinoma - A meta-analysis. *Eur J Surg Oncol*. (2020) 46:763–71. doi: 10.1016/j.ejso.2020.01.004

22. Lee HJ, Kim JW, Hur YH, Cho SB, Lee BC, Lee BK, et al. Conventional chemoembolization plus radiofrequency ablation versus surgical resection for single, medium-sized hepatocellular carcinoma: propensity-score matching analysis. *J Vasc Interv Radiol*. (2019) 30:284–92 e1. doi: 10.1016/j.jvir.2018.09.030

23. Morimoto M, Numata K, Kondou M, Nozaki A, Morita S, Tanaka K. Midterm outcomes in patients with intermediate-sized hepatocellular carcinoma: a randomized controlled trial for determining the efficacy of radiofrequency ablation combined with transcatheter arterial chemoembolization. *Cancer*. (2010) 116:5452–60. doi: 10.1002/cncr.25314

24. Kim JW, Kim JH, Won HJ, Shin YM, Yoon HK, Sung KB, et al. Hepatocellular carcinomas 2-3 cm in diameter: transarterial chemoembolization plus radiofrequency ablation vs. radiofrequency ablation alone. *Eur J Radiol*. (2012) 81:e189–93. doi: 10.1016/j.ejrad.2011.01.122

25. Zhang K, Mu L, Ren Y, Jiang T. Comparing Long-Term survival benefits of hepatocellular carcinoma between thermal ablation monotherapy and combined therapy with transarterial Chemoembolization: A propensity score matched study. *Eur J Radiol*. (2023) 167:111092. doi: 10.1016/j.ejrad.2023.111092

frontiers | Frontiers in Oncology

TYPE Original Research
PUBLISHED 11 April 2024
DOI 10.3389/fonc.2024.1367907

OPEN ACCESS

EDITED BY
Liliana Chemello,
University of Padua, Italy

REVIEWED BY
Hao Chi,
Southwest Medical University, China
Yandong Wang,
Tianjin Third Central Hospital, China

*CORRESPONDENCE
Xuemei Hu
mayjuly3720@163.com
Gen Chen
genchen@hust.edu.cn

RECEIVED 09 January 2024
ACCEPTED 26 March 2024
PUBLISHED 11 April 2024

CITATION
Huang M, Zhang F, Li Z, Luo Y, Li J, Wang Z, Ma L, Chen G and Hu X (2024) Fat fraction quantification with MRI estimates tumor proliferation of hepatocellular carcinoma. *Front. Oncol.* 14:1367907. doi: 10.3389/fonc.2024.1367907

Fat fraction quantification with MRI estimates tumor proliferation of hepatocellular carcinoma

Mengqi Huang, Fan Zhang, Zhen Li, Yan Luo, Jiali Li, Zixiong Wang, Liya Ma, Gen Chen* and Xuemei Hu*

Tongji Hospital, Tongji Medical College, Huazhong University of Science and Technology, Wuhan, Hubei, China

Purpose: To assess the utility of fat fraction quantification using quantitative multi-echo Dixon for evaluating tumor proliferation and microvascular invasion (MVI) in hepatocellular carcinoma (HCC).

Methods: A total of 66 patients with resection and histopathologic confirmed HCC were enrolled. Preoperative MRI with proton density fat fraction and R_2* mapping was analyzed. Intratumoral and peritumoral regions were delineated with manually placed regions of interest at the maximum level of intratumoral fat. Correlation analysis explored the relationship between fat fraction and Ki67. The fat fraction and R_2* were compared between high Ki67(>30%) and low Ki67 nodules, and between MVI negative and positive groups. Receiver operating characteristic (ROC) analysis was used for further analysis if statistically different.

Results: The median fat fraction of tumor (tFF) was higher than peritumor liver (5.24% vs 3.51%, P=0.012). The tFF was negatively correlated with Ki67 (r=-0.306, P=0.012), and tFF of high Ki67 nodules was lower than that of low Ki67 nodules (2.10% vs 4.90%, P=0.001). The tFF was a good estimator for low proliferation nodules (AUC 0.747, cut-off 3.39%, sensitivity 0.778, specificity 0.692). There was no significant difference in tFF and R2* between MVI positive and negative nodules (3.00% vs 2.90%, P=0.784; 55.80s-1 vs 49.15s-1, P=0.227).

Conclusion: We infer that intratumor fat can be identified in HCC and fat fraction quantification using quantitative multi-echo Dixon can distinguish low proliferative HCCs.

KEYWORDS

hepatocellular carcinoma, fat fraction, proliferation, MVI, MRI

Abbreviations: HCC, Hepatocellular carcinoma; MVI, Microvascular invasion; MRI, Magnetic Resonance Imaging; HBV, Hepatitis B Virus; HCV, Hepatitis C Virus; tFF, Fat fraction of tumor; TR, Repetition Time; TE, Echo Time; FOV, Field of View; ROI, Region of Interest; AUC, Area Under the Curve; ROC, Receiver Operating Characteristic

Highlights

- The intratumor fat on MRI is commonly detected and serves as an important ancillary feature for the diagnosis of HCC.
- The intratumor fat can be identified in HCC with chronic hepatitis and distinguish low proliferative HCCs which hold promise as a prognostic predictor.

Introduction

Tumor proliferation and microvascular invasion (MVI) in hepatocellular carcinoma (HCC) are pivotal factors leading to early recurrence following radical therapy and portend a poor prognosis (1). The immunohistochemical marker Ki-67 serves as a common indicator of cell proliferation and has been established as an independent predictor of early recurrence and poor prognosis in surgically resected HCC (2). A preoperative evaluation of proliferation and MVI may furnish additional insights for treatment strategies, such as limitation of ablation and liver transplantation, neoadjuvant and adjuvant therapeutics. However, determining proliferation and MVI is currently confined to specimens, limiting their broader clinical application.

The intra-tumoral fat is commonly identified in HCC, manifesting in various degrees of differentiation (3). Fatty change is known to be a marker of transformation from dysplastic nodule to HCC. It is more prevalent in well-differentiated HCC, with focal fatty changes observed in larger tumors. In clinical practice, poorly differentiated HCC often exhibits focal fatty change. A prevalent hypothesis for intra-tumoral fatty change involves reduced blood flow due to portal tract destruction and inadequate neovascularization (4, 5), which exposes the HCC to a hypoxic environment. Concurrently, upregulation of hypoxia-related signaling pathways promote the proliferation and migration of cancer cells (6). Therefore, quantifying fatty changes may serve as an indicator of HCC proliferation. Additionally, the invasiveness of HCC is corelated with increased tumor vascularity, and the HCC with diffuse fat tends to grow slowly and with lower risk of MVI (7), leading to favorable prognosis (8). Nevertheless, the relationship between the risk of MVI and the fat quantification in HCC with focal fat and chronic hepatitis remains unclear.

MRI with multi-echo Dixon and chemical shift encoded technique possesses a unique advantage in evaluating intracellular fat, as it can distinguish signals of water, triglyceride (9), and iron (10), which provide a non-invasive and quantitative evaluation. The quantitative multi-echo Dixon enables iron correction and accurate detection of fat, as well as MRI spectroscopy (11, 12). The intra-tumoral fat on MRI is an important ancillary feature for diagnosing HCC (13) and a potential biomarker for favorable performances after treatment (14). Thus, we hypothesize that the quantitative multi-echo Dixon may enable preoperative, non-invasive, and comprehensive assessment of cell proliferation and MVI, which may guide clinical treatment selection. Hence, this study aims to estimate the diagnostic value of fat fraction quantification based on MRI quantitative multi-echo Dixon for tumor proliferation and MVI in HCC.

Materials and methods

This retrospective study was approved by the institutional ethics committee and the requirement of informed written consent was waived.

Patients

We enrolled 203 consecutive patients who were suspected or known of hepatocellular carcinoma clinically or at previously performed ultrasonography or computed tomography underwent dynamic enhanced liver MRI and quantitative multi-echo Dixon from August 2021 to March 2023 in this study. We excluded patients who (1) had undergone non-surgical treatments (n=67); (2) has previous treated HCCs (n=18); (3) had histopathologically proven non-HCC (n=31); (4) encountered analysis difficulties due to small lesion size (n=10) or apparent artifacts in fat fraction mapping and R_2* mapping(n=11). A final cohort of 66 patients with 66 lesions were analyzed. The study flowchart of patient selection is presented in Figure 1.

Clinical information including demographics, causes of liver disease and laboratory data (total bilirubin, alanine transaminase, aspartate transaminase, albumin, serum alpha-foetoprotein) were collected.

MRI protocol

All MRI examinations were performed using the same protocol at 3.0T (MAGNETOM Skyra, Siemens, Germany) with an 18-channel phased-array coil and the spine coil with feet first and supine position. After conventional MRI sequences include the coronal T2-weighted Half-Fourier acquisition single-shot turbo spin-echo sequence (HASTE), the axial T1-weithted dual-echo sequence, the quantitative multi-echo Dixon was acquired in a single 20-second breath-hold. The detailed scanning parameters were as follows: repetition time (TR) = 9.00 msec, echo time (TE) =1.05/2.46/3.69/4.92/6.15/7.38msec, field of view (FOV) = 450 mm × 450 mm; slice thickness = 3.5mm, voxel size = 1.4 × 1.4 × 3.5mm; Flip angle= 4°; matrix size=160 ×95, bandwidth=1080Hz/Px, and an acceleration technique of CAIPIRINHA was employed with the acceleration factor was 2. A Levenberg-Marquardt nonlinear fitting was then utilized to fit the magnitude of the complex signal of the multi-echo data. Inline reconstruction was performed by addressing confounding factors that included magnetic field inhomogeneity, eddy currents, T1 bias, T2* decay, and spectral complexities.

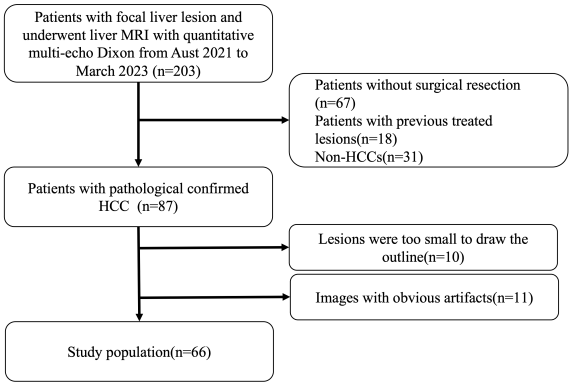

FIGURE 1
Patient selection. We enrolled 203 consecutive patients who were suspected or known of hepatocellular carcinoma clinically or at previously performed ultrasonography or computed tomography underwent dynamic enhanced liver MRI and quantitative multi-echo Dixon from August 2021 to March 2023 in this study. Patients who had undergone non-surgical treatments (n=67), had previous treated HCCs (n=18), had histopathologically proven non-HCC (n=31), encountered analysis difficulties due to small lesion size (n=10) or apparent artifacts in fat fraction mapping and R2* mapping(n=11) were excluded. And a final cohort of 66 patients with 66 lesions were enrolled.

Imaging analysis

The fat fraction mapping and R_2* mapping was automatically calculated without the need for further post-processing. The region of interest (ROI) of the tumor, peritumoral regions, and liver were manually drawn. The ROI of the tumor was delineated in the maximum plane of the intatumoral fat or the maximum plane of tumor if no significant fat was depicted in fat fraction mapping and was delineated in the T1WI and copied to the fat fraction mapping and R_2* mapping (Figure 2). The ROI of the peritumor liver was delineated in the peritumoral region of the tumor with a circle of about 1cm^2 which avoided the main vessels and bile duct. The fat fraction of liver was the average of 3 different ROIs randomly delineated in the liver with 3 circles of about 3cm^2, and avoided the main vessels and bile duct.

Histopathological analysis

Data of tumor pathologic factors including size, tumor differentiation based on Edmondson-Steiner grade, MVI, satellite nodule and expression of Ki67 were obtained from pathology reports. MVI was defined as the presence of tumor cells in the vessels of surrounding liver tissue which were lined by the endothelium that was visible only on microscopy. The positive cellular index of Ki67 was evaluated by a trained pathologist and described according to the presence of nuclear staining regardless of the intensity of staining. The percentage of Ki67 was determined by counting 1000 cells/slide at 100x magnification in five randomly selected fields.

Statistical analysis

Continuous variables were reported as means and standard deviations or medians and interquartile ranges. Categorical variables were displayed as percentages and numbers. The differences between groups were assessed using Mann-Whitney U test or Chi-squared test because data were non-normally distributed. The relationship between MRI parameters and Ki67 was assessed through nonparametric Spearman correlation coefficients. ROC analysis was performed if the MRI parameters showed statistically significant differences between the two Ki67 groups. A two-sided P-value less than 0.05 was considered statistically significant. All statistical analyses, utilizing SPSS software (version 26.0) and R statistical software (version 4.1.2), included t-tests, paired t-tests, and Mann–Whitney U tests for continuous variables, and the chi-square test for categorical variables. ROC analysis was performed using the "pROC" and "ggplot2" packages.

Results

Clinical characteristics

Of the 66 patients (mean age, 55.59 ± 8.99 years, 55(83.33%) males), 60 patients were infected with HBV, while 4 patients were infected with HCV and 2 patients have pathology proved chronic hepatitis change and no history of HBV, HCV, ASH, NASH and alcohol abuse. Furthermore, 18 (27.27%) HCCs were well-differentiated, while 17 (25.76%) patients had moderately differentiated HCCs and 31 (46.97%) HCCs were poorly differentiated. More details of patients are given in Table 1.

Fat fraction and R_2* of tumor and liver

The HCCs have a median intratumor fat fraction (tFF) of 5.24% (IQR 1.88% - 8.52%) and was higher than the median fat fraction of peritumor liver (5.24% vs 3.51%, P=0.012). Of the 66 HCCs, 42 (63.64%) had an tFF of less than 5%, 13 (19.69%) had an intratumor fat fraction of more than 5% and less than 10%, and 11 (16.67%)

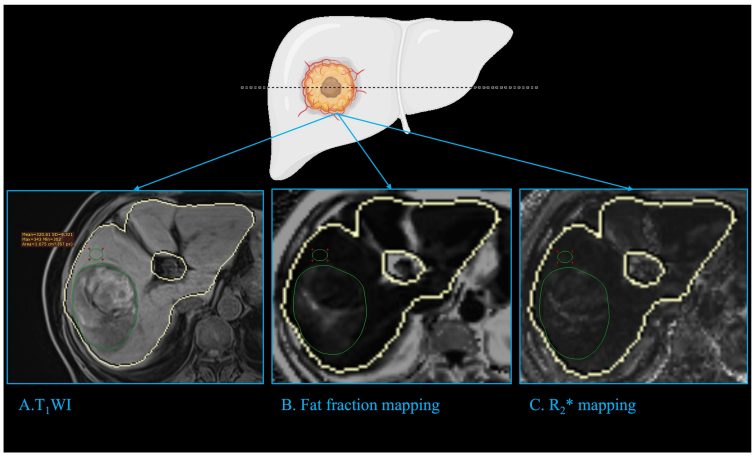

FIGURE 2
Imaging analysis. The fat fraction mapping and R_2* mapping was automatically calculated with the liver automatically delineated (closed yellow curve). The ROI of tumor (green circle) was delineated in the maximum plane of the intatumoral fat or the tumor if no significant fat was depicted in fat fraction mapping, and was delineated in the T_1WI **(A)** and copied to fat fraction mapping **(B)** and R_2* mapping **(C)**. The ROI of the peritumor liver (green circle) was delineated in the peritumoral region of the tumor with a circle of about 1cm^2, which avoided the main vessels and bile duct. ROI: region of interest.

TABLE 1 Characteristics of the study population.

	All	Ki67%<=30	Ki67>30	P
Number	66	39	27	
Age [a]	55.59(8.99)	56.23(8.56)	54.67(9.67)	0.492
Sex				0.737*
Female	11	7	4	
Male	55	32	23	
HBV	53	35	25	0.692*
HCV	4	2	2	0.703*
TB(umol/L) [b]	11.95(8.57-14.95)	12.70(8.32-15.80)	13.40(9.20-14.90)	0.514**
ALT(U/L) [b]	22.50(16.75-33.75)	22.00(18.00-30.50)	25.00(14.00-38.00)	1.000**
AST(U/L) [b]	24.50(20.00-34.50)	23.00(18.00-33.00)	26.00(21.00-37.00)	0.855**
ALB(g/L) [a]	39.24(3.08)	38.89(2.87)	39.74(3.34)	0.278
sAFP(ng/ml) [b]	80.63(6.73-661.55)	9.40(3.85-260.60)	301.80(77.70-1210.00)	0.012**
Diam(mm) [b]	43(24-83)	42.50(21.00-77.00)	46.00(25.00-96.00)	0.324**
Differentiation				0.001*
Well	18(27.27%)	16(24.24%)	2(3.03%)	
Moderately	17(25.76%)	12(18.18%)	5(7.58%)	
poorly	31(46.97%)	11(16.67%)	20(30.30%)	
MVI				<0.001*
Positive	18	3	15	
Negtive	48	36	12	
Satellite	0	0	0	

Except where indicated, data are absolute frequencies.
[a]Data are means (standard deviation).
[b]Data are medians (interquartile range).
HBV, hepatitis B virus; HCV, hepatitis C virus; TB, total bilirubin; ALT, alanine transaminase; AST, aspartate transaminase; ALB, albumin; sAFP, serum alpha-foetoprotein; Diam, diameter.
*Chi-squared test.
**Mann-Whiney U test.

had an intratumor fat fraction of more than 15%. The fat fraction of peritumor was not significantly different from fat fraction of liver (3.51% vs 3.54%, P =0.739). Of the 66 patients, 9 (13.64%) had fatty liver with a liver fat fraction of more than 5% (15). The fat fraction of tumor had no significant difference between the fatty liver patients and nonfatty liver patients (4.32% vs5.38%, P=0.502).

The median R_2* of HCC was 38.55s^{-1} (IQR 26.40-47.81 s^{-1}) while that of the peritumor liver was 51.40 s^{-1}(IQR 42.75-69.82 s^{-1}). The R_2* of the tumor was significantly lower than that of the peritumor liver (38.55s^{-1} vs 51.40s^{-1}, P<0.001).

Relationship of fat fraction and R_2* with the Ki67

The spearman's correlation analysis indicated that the tFF was negatively correlated with the expression of Ki67 (r=-0.306, P=0.012). The correlation analysis showed that the fat fraction of the liver, R_2* of the tumor and R2* of the liver were not significantly correlated with the Ki67 of the tumor (P>0.05), as shown in Table 2.

The median Ki67 of the 66 HCCs was 27.5% (IQR 10.0%-50.0%), with 39 HCCs had less than 30.0%. The tFF was higher in the Ki67<=30% group than the Ki67>30% group (4.90% vs 2.10%, P=0.001), and the R_2* of the liver was higher in the Ki67<=30% group than the Ki67>30% group (56.90 s^{-1} vs 49.60 s^{-1}, P=0.003), as shown in Table 3 and Figure 3. The ROC analysis demonstrated that the tFF could distinguish the Ki67<=30% group with an AUC was 0.747(95%CI 0.628-0.867) and a cut-off of 3.39% (sensitivity 77.8%, specificity 69.2%), as shown in Figure 4. The R_2* could not be used to distinguish the Ki67<=30% group (AUC 0.553, 95%CI 0.409-0.697, P=0.469).

Relationship of fat fraction and R_2* with the MVI

Of the 66 patients, 48 (72.73%) had no MVI in the peritumoral liver, while 18 (27.27%) had MVI in at least one vessel in the peritumoral region. The fat fraction and R_2* of the tumor in MVI negative group were not significantly different from those in the MVI positive group (4.05% vs 2.25%, P=0.087; 36.60s^{-1} vs 39.05s^{-1}, P=0.194). The fat fraction and R_2* of the liver in the MVI negative group were also not significantly different from those in the MVI positive group (3.00% vs 2.90%, P=0.784; 55.80s^{-1} vs 49.15s^{-1}, P=0.227), as shown in Table 4. The frequency of MVI was not significantly different between the high tFF HCCs and the low tFF HCCs (25.00% vs 30.00%, P=0.650).

TABLE 2 Spearman's correlation analysis of MRI and Ki67.

	r	P
tFF	-0.306	0.012
FF	0.037	0.770
tR_2*	0.132	0.290
R_2*	0.007	0.954

tFF, fat fration of tumor; FF, fat fraction of peritumoral liver; tR_2*, R_2* of tumor.

TABLE 3 Comparison of MRI between the low Ki67 and high Ki67 groups.

	Ki67%<=30	Ki67>30	P [a]
Number	39	27	
tFF (%)	4.90(2.50-10.50)	2.10(1.60-3.30)	0.001
FF (%)	3.00(1.35-4.80)	3.00(2.10-3.60)	0.634
tR_2* (s^{-1})	39.20(26.60-49.10)	38.30(25.80-47.60)	0.469
R_2* (s^{-1})	56.90(41.20-69.80)	49.60(42.90-69.90)	0.003

Data are medians (interquartile range).
[a]Mann-Whiney U test.
tFF, fat fration of tumor; FF, fat fraction of peritumoral liver; tR_2*, R_2* of tumor.

Discussion

This study estimated the relationship between the proliferation marker Ki67 of HCC and the fat fraction of the tumor, as determined by the MRI quantitative multi-echo Dixon. Furthermore, the ROC analysis highlighted the fat fraction of the tumor as a good discriminator of HCCs with Ki67<=30%. Thus, we have successfully validated the fat fraction as an accurate, noninvasive, and *in vivo* biomarker of proliferation for HCCs.

The tumor proliferation of HCC can be non-invasively evaluated with MRI. Chen at al. reported a strong relationship of Ki67 with Gd-EOB-DTPA-enhanced MRI in HCC (16). And Jing at al. indicated that the expression of Ki67 was associated with apparent diffusion coefficients (17). Gd-EOB-DTPA-enhanced MRI and apparent diffusion coefficient is an advanced MRI technique, which needs special contrast media and advanced post-operative software. And these two techniques were used to evaluate the tumor proliferation from the perspective of uptake of specific contrast agents and tissue microstructure. Furthermore, Hu et al. estimated the value of viscoelasticity measured by MRI elastography for prediction of Ki67 expression (18). Our study revealed similar result that the MRI quantitative multi-echo Dixon was a good discriminator of Ki67, which is a completely different MRI technique that mainly reflects fatty changes within the tumor. To our knowledge, it was the first to evaluate the proliferation of HCC using the fat quantification of MRI.

The intra tumoral fat is an important feature of HCC (19) and represents focal hypoxia due to the transition of blood supply from portal vein to hepatic artery with insufficient neovascularization. Intra tumoral fat was found in both early stage and progressed HCCs. Our study demonstrated that 13 (19.69%) patients had an intratumor fat fraction of more than 5% and less than 10%, and 11 (16.67%) had an intratumor fat fraction of more than 15%, with most patients having chronic HBV and HCV infection, which suggested that intra tumoral fat was not only found in patients with fatty liver. Furthermore, our study reveals a negative correlation between fat fraction and Ki67, suggesting that intra-tumoral fat serves as a marker of tumor proliferation. The most

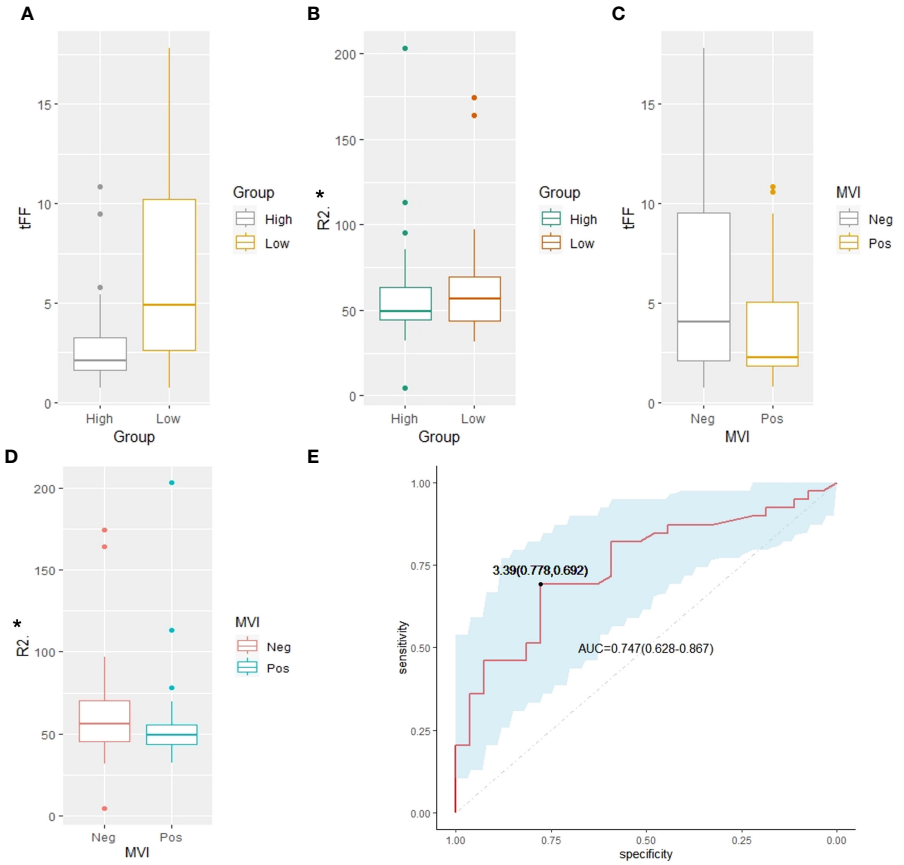

FIGURE 3
Comparison analysis. **(A)** The tFF of the high Ki67 was lower than that of the low Ki67 group (2.10% vs 4.90%, P=0.001). **(B)** The R_2* of the high Ki67 was lower than that of the low Ki67 group (49.60 s^{-1} vs56.90 s^{-1}, P=0.003). **(C)** The tFF in MVI negative group had no significant difference from that of the MVI positive group (4.05% vs 2.25%, P=0.087). **(D)** The R_2* of the tumor in MVI negative group had no significant difference from that of the MVI positive group (36.60s^{-1} vs 39.05s^{-1}, P=0.194). **(E)** The ROC analysis demonstrated that the tFF of the tumor can distinguish the Ki67<=30% group with an AUC of 0.747(95%CI 0.628-0.867) and cut-off of 3.39% (sensitivity 77.8%, specificity 69.2%). tFF, the fat fraction of the tumor; MVI, microvascular invasion; ROC, receiver operating characteristic; AUC, area under the curve.

possible hypothesis may be that the intra tumoral fat was caused by dysregulated lipogenesis that was due to clonal proliferation in proliferative HCCs (20). And the intracellular lipid droplets broke down if energy was deficient in proliferative tumors (21). Hence, the intra tumoral fat can also be found in proliferative HCCs and the fat fraction may be less than that in less proliferative HCCs. Previous studies have also suggested that poorly differentiated HCC is prone to have focal steatosis (5), which may explain the relative low-fat fraction observed in high Ki67 group in our quantitative measurement study. This study provides a quantitative method for measuring fat fraction and demonstrates its potential as an imaging marker of tumor proliferation.

TABLE 4 Comparison of MRI between the negative and positive MVI groups.

	MVI (-)	MVI (+)	P [a]
Number	48	18	
tFF (%)	4.05(2.02-9.58)	2.25(1.75-5.70)	0.087
FF (%)	3.00(1.46-4.74)	2.90(2.05-3.66)	0.784
tR_2* (s^{-1})	36.60(24.03-48.72)	39.05(31.94-47.58)	0.194
R_2* (s^{-1})	55.80(43.62-71.10)	49.15(41.02-59.82)	0.227

Data are medians (interquartile range).
[a]Mann-Whiney U test.
MVI, microvascular invasion; tFF, fat fration of tumor; FF, fat fraction of peritumoral liver; tR_2*, R_2* of tumor.

Some studies have reported that increased fat content may correlated with improved prognosis (14, 22). The mild accumulation of fat may reflect changes in the microenvironment of hepatocellular carcinoma tumors that reduce tumor aggressiveness. Tani et al. also demonstrated that the peritumoral fat content, as identified by MRI, correlates with prognosis of breast cancer (23). This study demonstrates the potential of fat fraction as an imaging marker of tumor proliferation, which is a prognostic factor in HCC. Consequently, the fat content in hepatocellular carcinoma may affect the response to treatment, such as resection, chemotherapy, or radiation therapy (22). In summary, fat content is associated with outcomes in patients with HCC and has important clinical implications. Through further research and validation, we can better use this indicator of fat fraction based on MRI to guide the treatment and management of HCC patients, and it may also have application prospects in other types of cancer.

10.3389/fonc.2024.1367907

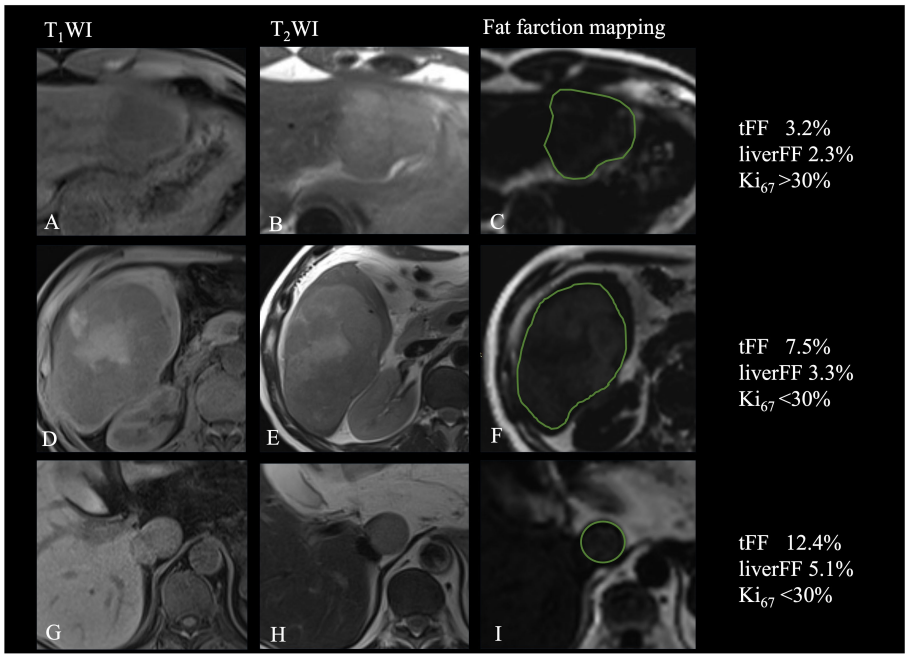

FIGURE 4
Relationship of fat fraction and R_2* with the Ki67. **(A-C)** Patient with focal fat and high expression of Ki67. **(D-F)**. Patient with diffuse fat in mass and low expression of Ki67. **(G-I)** Patient with diffuse fat in small lesion and low expression of Ki67.

Additionally, our study finds that the fat fraction of the tumor does not significantly differ between patients with fatty liver and non-fatty liver, despite a previous study indicating a higher median fat fraction in HCCs with liver steatosis (3). It's worth noting that steatotic and steatohepatitic HCCs, which often exhibit diffuse fat in the mass (24), are closely associated with underlying fatty liver disease and metabolic syndrome (25). Most of the patients with fatty liver or without fatty liver in this study were accompanied by chronic HBV or HCV infection. Chronic hepatitis is suggested to have an influence on metabolic changes (26), potentially leading to fatty liver development. Therefore, the observed fatty liver in our study may be attributed to chronic hepatitis rather than non-alcoholic fatty liver disease or metabolic syndrome, explaining the lack of significant differences in tumor fat fraction between the two groups.

Numerous studies have been devoted to the preoperative prediction of MVI and the results are still uncertain. In our present study, the fat fraction determined by MRI quantitative multi-echo Dixon did not exhibit significant difference between the MVI-negative and MVI-positive groups. Some researchers have indicated that the intra tumoral fat may suggest a lower risk of MVI (7), which was partially explained by the relationship of intra tumoral fat and lower histological grades. However, not all studies support this finding (27). Further investigations, such as subclassification analysis of MVI number and location (28), or advanced analyses of intra-tumoral fat using texture analysis or radiomics (29), may enhance our understanding of this relationship.

This study has some limitations. First, it was a retrospective, single-center research with a small number of HCC patients accompanied with HBV, HCV infection or pathology proved hepatitis. However, the present study was the first to evaluate the proliferation of HCC using the fat quantification of MRI. Therefore, it will be necessary to confirm the results through prospective, multicenter study with a larger number of patients. Second, the Ki-67 index has traditionally served as a biomarker indicating tumor proliferation, while recent studies has classified HCC proliferation through diverse molecular analyses and genomic profiling. Third, we did not assess the influence of ROI sampling strategies on measurement and reproducibility of quantitative multi-echo Dixon. Previous studies have indicated that the reproducibility and repeatability of measurements were improved as much area of the ROI (30). Therefore, the ROI of the tumor was delineated in the maximum plane of the intatumoral fat or tumor in this study. And the fat fraction based on MRI has been extensively explored in the literature and is considered a stable and non-invasive tool compared to pathology. Forth, the fat fraction in the maximum plane of the intatumoral fat or tumor was used to analyze, and the distribution of intra tumoral fat was not evaluated. As the distribution of fat is another important feature for the diagnosis of steatotic or steatohepatitic HCCs, we hypothesize that the quantification and distribution of fat could offer greater clinical insight for prognosis and treatment. Thus, we intent to investigate further how fat quantification and radiomic or machine learning features will influence patient prognosis and treatment outcomes in subsequent studies. Lastly, this study did not investigate how fat quantification affects patient outcomes due to the limited follow-up time. Previous studies have shown that fat sparing in solid mass was potential marker to evaluate the survival with favorable performance and discriminator of complete response under

TACE treatment (14). Therefore, a further validation study is needed to confirm the prognostic value of fat fraction.

Conclusion

In conclusion, fat fraction quantification based on quantitative multi-echo Dixon can effectively differentiate low-proliferation HCCs, although it may not be suitable for diagnosing MVI. Fat fraction quantification holds promise as a potential prognostic predictor of treatment option.

Data availability statement

The original contributions presented in the study are included in the article/supplementary material. Further inquiries can be directed to the corresponding author.

Ethics statement

The studies involving humans were approved by Ethics Committee of Tongji Hospital, Tongji Medical College, Huazhong University of Science and Technology. The studies were conducted in accordance with the local legislation and institutional requirements. The ethics committee/institutional review board waived the requirement of written informed consent for participation from the participants or the participants' legal guardians/next of kin because This was a retrospective study and the patient information was encrypted during the study.

Author contributions

MH: Conceptualization, Data curation, Formal analysis, Funding acquisition, Investigation, Methodology, Project administration, Resources, Software, Supervision, Validation, Visualization, Writing – original draft, Writing – review & editing. FZ: Investigation, Data curation, Formal analysis, Methodology, Project administration, Software, Validation, Writing – original draft. ZL: Data curation, Formal analysis, Investigation, Methodology, Project administration, Software, Validation, Conceptualization, Resources, Supervision, Writing – review & editing. YL: Conceptualization, Data curation, Formal analysis, Investigation, Methodology, Project administration, Writing – review & editing, Funding acquisition. JL: Conceptualization, Data curation, Formal analysis, Funding acquisition, Investigation, Methodology, Project administration, Writing – review & editing, Resources. ZW: Conceptualization, Data curation, Formal analysis, Investigation, Methodology, Project administration, Writing – original draft. LM: Investigation, Methodology, Project administration, Resources, Validation, Writing – review & editing. GC: Investigation, Methodology, Project administration, Writing – review & editing, Conceptualization, Data curation, Formal analysis, Software. XH: Conceptualization, Investigation, Writing – review & editing, Resources, Supervision.

Funding

The author(s) declare that financial support was received for the research, authorship, and/or publication of this article. This work was supported by National Natural Science Foundation of China (82202127, 82001786) and Foundation of Tongji Hospital (2022B14).

Conflict of interest

The authors declare that the research was conducted in the absence of any commercial or financial relationships that could be construed as a potential conflict of interest.

Publisher's note

References

1. Lee S, Kang TW, Song KD, Lee MW, Rhim H, Lim HK, et al. Effect of microvascular invasion risk on early recurrence of hepatocellular carcinoma after surgery and radiofrequency ablation. *Ann Surg*. (2021) 273:564–71. doi: 10.1097/SLA.0000000000003268

2. Li H-H, Qi LN, Ma L, Chen ZS, Xiang BD, Li LQ. Effect of KI-67 positive cellular index on prognosis after hepatectomy in Barcelona Clinic Liver Cancer stage A and B hepatocellular carcinoma with microvascular invasion. *OncoTargets Ther*. (2018) 11:4747–54. doi: 10.2147/OTT

3. Kupczyk PA, Kurt D, Endler C, Luetkens JA, Kukuk GM, Fronhoffs F, et al. MRI proton density fat fraction for estimation of tumor grade in steatotic hepatocellular carcinoma. *Eur Radiol*. (2023) 33(12):8974–85. doi: 10.1007/s00330-023-09864-x

4. Kutami R, Nakashima Y, Nakashima O, Shiota K, Kojiro M. Pathomorphologic study on the mechanism of fatty change in small hepatocellular carcinoma of humans. *J Hepatol*. (2000) 33:282–9. doi: 10.1016/S0168-8278(00)80369-4

5. Asayama Y, Nishie A, Ishigami K, Ushijima Y, Takayama Y, Okamoto D, et al. Fatty change in moderately and poorly differentiated hepatocellular carcinoma on MRI: a possible mechanism related to decreased arterial flow. *Clin Radiol*. (2016) 71:1277–83. doi: 10.1016/j.crad.2016.04.020

6. Li Y, Liang X, Che G, Chen Y, Luo L, Liu K, et al. Molecular classification of genes associated with hypoxic lipid metabolism in pancreatic cancer. *Biomolecules*. (2022) 12 (10):1533. doi: 10.3390/biom12101533

7. Min JH, Kim YK, Lim S, Jeong WK, Choi D, Lee WJ. Prediction of microvascular invasion of hepatocellular carcinomas with gadoxetic acid-enhanced MR imaging: Impact of intra-tumoral fat detected on chemical-shift images. *Eur J Radiol*. (2015) 84:1036–43. doi: 10.1016/j.ejrad.2015.03.002

8. An C, Kim M-J. Imaging features related with prognosis of hepatocellular carcinoma. *Abdominal Radiol (New York)*. (2019) 44:509–16. doi: 10.1007/s00261-018-1758-y

9. Yang Y, Xu K, Chen X, Ding J, Shi J, Li J. The accuracy and clinical relevance of the multi-echo dixon technique for evaluating changes to hepatic steatosis in patients with non-alcoholic fatty liver disease treated with formulated food. *Magnetic Resonance In Med Sciences: MRMS*. (2023) 22:263–71. doi: 10.2463/mrms.mp.2021-0168

10. Hu F, Yang R, Huang Z, Wang M, Yuan F, Xia C, et al. 3D Multi-Echo Dixon technique for simultaneous assessment of liver steatosis and iron overload in patients with chronic liver diseases: a feasibility study. *Quantitative Imaging In Med Surg*. (2019) 9:1014–24. doi: 10.21037/qims

11. Zhan C, Olsen S, Zhang HC, Kannengiesser S, Chandarana H, Shanbhogue KP. Detection of hepatic steatosis and iron content at 3 Tesla: comparison of two-point Dixon, quantitative multi-echo Dixon, and MR spectroscopy. *Abdominal Radiol (New York)*. (2019) 44:3040–8. doi: 10.1007/s00261-019-02118-9

12. Rajlawot K, Jiang T, Zhou J, Lin C, Kuang S, Chen J, et al. Accuracies of chemical shift in/opposed phase and chemical shift encoded magnetic resonance imaging to detect intratumoral fat in hepatocellular carcinoma. *J Magnetic Resonance Imaging: JMRI*. (2021) 53:1791–802. doi: 10.1002/jmri.27539

13. Nougaret S, Monsonis B, Molinari N, Riviere B, Piron L, Kassam Z, et al. Quantification of liver fat content in liver and primary liver lesions using triple-echo-gradient-echo MRI. *Eur Radiol*. (2020) 30:4752–61. doi: 10.1007/s00330-020-06757-1

14. Song W, Chen Q, Guo D, Jiang C. Preoperative estimation of the survival of patients with unresectable hepatocellular carcinoma achieving complete response after conventional transcatheter arterial chemoembolization: assessments of clinical and LI-RADS MR features. *La Radiologia Med*. (2022) 127:939–49. doi: 10.1007/s11547-022-01517-1

15. Starekova J, Hernando D, Pickhardt PJ, Reeder SB. Quantification of liver fat content with CT and MRI: state of the art. *Radiology*. (2021) 301:250–62. doi: 10.1148/radiol.2021204288

16. Chen Y, Qin X, Long L, Zhang L, Huang Z, Jiang Z, et al. Diagnostic value of gd-EOB-DTPA-enhanced MRI for the expression of ki67 and microvascular density in hepatocellular carcinoma. *J Magnetic Resonance Imaging: JMRI*. (2020) 51:1755–63. doi: 10.1002/jmri.26974

17. Jing M, Cao Y, Zhang P, Zhang B, Lin X, Deng L, et al. The benefit of apparent diffusion coefficient in evaluating the invasiveness of hepatocellular carcinoma. *Front In Oncol*. (2021) 11:719480. doi: 10.3389/fonc.2021.719480

18. Hu X, Zhou J, Li Y, Wang Y, Guo J, Sack I, et al. Added value of viscoelasticity for MRI-based prediction of ki-67 expression of hepatocellular carcinoma using a deep learning combined radiomics (DLCR) model. *Cancers*. (2022) 14(11):2575. doi: 10.3390/cancers14112575

19. Mulé S, Serhal A, Pregliasco AG, Nguyen J, Vendrami CL, Reizine E, et al. MRI features associated with HCC histologic subtypes: a western American and European bicenter study. *Eur Radiol*. (2023) 33:1342–52. doi: 10.1007/s00330-022-09085-8

20. Zhu Y, Weng S, Li Y, Yan C, Ye R, Wen L, et al. A radiomics nomogram based on contrast-enhanced MRI for preoperative prediction of macrotrabecular-massive hepatocellular carcinoma. *Abdominal Radiol (New York)*. (2021) 46:3139–48. doi: 10.1007/s00261-021-02989-x

21. Paul B, Lewinska M, Andersen JB. Lipid alterations in chronic liver disease and liver cancer. *JHEP Reports: Innovation In Hepatol*. (2022) 4:100479. doi: 10.1016/j.jhepr.2022.100479

22. Hermida M, Preel A, Assenat E, Piron L, Cassinotto C, Ursic-Bedoya J, et al. Small steatotic HCC: A radiological variant associated with improved outcome after ablation. *Hepatol Commun*. (2021) 5:689–700. doi: 10.1002/hep4.1661

23. Tani NH, Koreeda Y, Nawata A, Fujisaki A, Hayashida Y, Shimajiri S, et al. Peritumoral fat content identified using iterative decomposition of water and fat with echo asymmetry and least-squares estimation (IDEAL) correlates with breast cancer prognosis. *Magnetic Resonance In Med Sci*. (2024). doi: 10.2463/mrms.mp.2023-0127

24. Chen K, Xu Y, Dong Y, Han H, Mao F, Wang H, et al. Contrast-enhanced imaging features and clinicopathological investigation of steatohepatitic hepatocellular carcinoma. *Diagnostics (Basel Switzerland)*. (2023) 13(7):1337. doi: 10.3390/diagnostics13071337

25. Park JH, Park YN, Kim MJ, Park MS, Choi JY, Chung YE, et al. Steatotic hepatocellular carcinoma: Association of MRI findings to underlying liver disease and clinicopathological characteristics. *Liver Int*. (2023) 43:1332–44. doi: 10.1111/liv.15589

26. Tourkochristou E, Assimakopoulos SF, Thomopoulos K, Marangos M, Triantos C. NAFLD and HBV interplay - related mechanisms underlying liver disease progression. *Front In Immunol*. (2022) 13:965548. doi: 10.3389/fimmu.2022.965548

27. Chen J, Zhou J, Kuang S, Zhang Y, Xie S, He B, et al. Liver imaging reporting and data system category 5: MRI predictors of microvascular invasion and recurrence after hepatectomy for hepatocellular carcinoma. *AJR. Am J Roentgenol*. (2019) 213:821–30. doi: 10.2214/AJR.19.21168

28. Kang I, Jang M, Lee JG, Han DH, Joo DJ, Kim KS, et al. Subclassification of microscopic vascular invasion in hepatocellular carcinoma. *Ann Surg*. (2021) 274:e1170–8. doi: 10.1097/SLA.0000000000003781

29. Chong H-H, Yang L, Sheng RF, Yu YL, Wu DJ, Rao SX, et al. Multi-scale and multi-parametric radiomics of gadoxetate disodium-enhanced MRI predicts microvascular invasion and outcome in patients with solitary hepatocellular carcinoma ≤ 5 cm. *Eur Radiol*. (2021) 31:4824–38. doi: 10.1007/s00330-020-07601-2

30. Campo CA, Hernando D, Schubert T, Bookwalter CA, Pay AJV, Reeder SB. Standardized approach for ROI-based measurements of proton density fat fraction and R2* in the liver. *AJR. Am J Roentgenol*. (2017) 209:592–603. doi: 10.2214/AJR.17.17812

frontiers | Frontiers in Immunology

TYPE Case Report
PUBLISHED 28 May 2024
DOI 10.3389/fimmu.2024.1358602

OPEN ACCESS

EDITED BY
Liliana Chemello,
University of Padua, Italy

REVIEWED BY
Najib Ben Khaled,
LMU Munich University Hospital, Germany
Antonio Giovanni Solimando,
University of Bari Aldo Moro, Italy

*CORRESPONDENCE
Xuelin Zhao
zhaoxuelin321@126.com

RECEIVED 20 December 2023
ACCEPTED 13 May 2024
PUBLISHED 28 May 2024

CITATION
Ai H, Gong T, Ma Y, Ma G, Ding W, Ding W, Wang W and Zhao X (2024) Transarterial chemoembolization combined with atezolizumab plus bevacizumab conversion therapy for intermediate-stage hepatocellular carcinoma: a case report and literature review.
Front. Immunol. 15:1358602.
doi: 10.3389/fimmu.2024.1358602

Transarterial chemoembolization combined with atezolizumab plus bevacizumab conversion therapy for intermediate-stage hepatocellular carcinoma: a case report and literature review

Haidong Ai[1], Ting Gong[2], Yongbiao Ma[1], Guixu Ma[1], Wei Ding[1], Weibao Ding[1], Wenjuan Wang[1] and Xuelin Zhao[1]*

[1]Hepatobiliary and Pancreatic Medical Center, The First Affiliated Hospital of Weifang Medical College (Weifang People's Hospital), Weifang, China, [2]Department of Ophthalmology, The First Affiliated Hospital of Weifang Medical College (Weifang People's Hospital), Weifang, China

Hepatocellular carcinoma (HCC) ranks as the sixth most common malignancy globally, with the majority of patients presenting at the initial diagnosis with locally advanced or metastatic disease, precluding the opportunity for curative surgical intervention. With the exploration and advancement of locoregional treatments, novel molecular-targeted therapies, anti-angiogenic agents, and immunomodulatory drugs, the management of HCC has seen an increase in objective response rates and prolonged duration of response significantly enhancing the potential for conversion to resectable disease in intermediate and advanced-stage unresectable HCC. Herein, we present a case of Barcelona Clinic Liver Cancer stage B unresectable HCC, where after two courses of treatment with transarterial chemoembolization combined with atezolizumab plus bevacizumab significant tumor reduction was achieved. Per Response Evaluation Criteria in Solid Tumors 1.1, partial response culminated in successful curative surgical resection. No drug-related adverse reactions occurred during hospitalization, and there has been no recurrence during the 11-month postoperative follow-up. For patients with Barcelona Clinic Liver Cancer stage B (intermediate-stage) unresectable HCC, the transarterial chemoembolization combined with atezolizumab plus bevacizumab regimen may offer improved therapeutic outcomes leading to a higher success rate of conversion therapy and, thus, improved survival.

KEYWORDS

atezolizumab plus bevacizumab, transarterial chemoembolization, intermediate-stage unresectable hepatocellular carcinoma, conversion therapy, immunotherapy

Introduction

HCC remains one of the most prevalent malignancies globally ranking sixth in incidence and third in cancer-related mortality (1). Of patients, 60%–70% are diagnosed with unresectable HCC (2, 3). For such patients, administering systemic and/or locoregional treatment to create an opportunity for radical resection, reduce postoperative recurrence, and improve prognosis is referred to as conversion therapy for liver cancer (4). Tumor reduction or downstaging following conversion therapy is a crucial means for unresectable HCC patients to achieve curative resection and long-term survival. Historically, conversion therapy has primarily involved local treatments, with a low conversion resection rate and overall poor efficacy. However, with the emergence and advancement of various molecularly targeted drugs and immune checkpoint inhibitors (ICIs), systemic therapy has rapidly progressed, leading to a gradual increase in conversion resection rates, significantly improving the prognosis of intermediate and advanced-stage HCC patients (2, 5, 6).

The clinical guidelines from the European Association for the Study of the Liver (EASL) and the American Association for the Study of Liver Diseases (AASLD) recommend transarterial chemoembolization (TACE) and atezolizumab plus bevacizumab (Atezo/Bev) as the first-line treatment choice for Barcelona Clinic Liver Cancer (BCLC) stage B (intermediate-stage) HCC patients (7, 8). However, to date, there have been no studies reporting the survival outcomes of intermediate-stage HCC patients undergoing curative surgery following TACE combined with Atezo/Bev conversion therapy. This article reports on the detailed treatment process of a case of large unresectable HCC classified as BCLC stage B, which underwent only two sessions of TACE combined with the Atezo/Bev regimen, resulting in significant tumor volume reduction and subsequent successful radical surgical resection. By presenting this case and combining it with relevant literature, we aim to explore new treatment approaches for similar patients and provide a reference for future clinical endeavors.

Case presentation

The patient, a 53-year-old male, was admitted to the hospital on 13 March 2023 due to persistent nausea for 2 months and the discovery of a liver mass 10 days prior. He has experienced fatigue and weight loss over the past 2 months. His medical history includes a 2-year duration of hepatitis B without regular antiviral treatment. There was no history of hypertension, diabetes, or coronary artery disease, and no family history of psychological disorders or genetic conditions. Before the current visit, he had not received any treatment. Physical examination revealed tenderness in the right upper abdomen, with no other abnormalities noted. Laboratory tests revealed elevated levels of AFP (45,316.0 ng/ml, normal range 0–10 ng/ml), AFP-L3% (24.1%, normal range 0%–10%), PIVKA-II (11,278.0 ng/ml, normal range 0–40 ng/ml), HBV-DNA (2.386 × 103 IU/ml, normal range <500 IU/ml), ALT (69 U/L, normal range 0–50 U/L), AST (65 U/L, normal range 0–40 U/L), GGT (135 U/L, normal range 4–60 U/L), T-BIL (45.8 μmol/L, normal range 0–23 μmol/L). The preoperative indocyanine green (ICG) retention rate at 15 min was 12%. Routine blood examination and coagulation function showed no significant abnormalities. Enhanced CT of the upper abdomen revealed multiple liver lesions, with the largest measuring 10 cm in diameter consistent with HCC and multiple intrahepatic metastases (Figures 1A, B). Considering the medical history, serological markers, and imaging examinations, intrahepatic cholangiocarcinoma and benign liver tumors were excluded. The preoperative diagnosis was HCC, BCLC stage B, Child–Pugh class A, and Eastern Cooperative Oncology Group (ECOG) Performance Status 0. Following a multi-disciplinary discussion, we identified three tumors in the patient, with the largest lesion measuring approximately 10 cm in diameter and the combined diameter of the two largest lesions totaling approximately 18.2 cm. The lesions predominantly affected the liver S5, 6, and 7, with suspected tumor invasion into S8. If a right hepatectomy was performed, the estimated residual liver area would be 38%. Considering the patient's concurrent liver cirrhosis, which complicates extensive liver resection, we deemed the tumor non-resectable, necessitating conversion therapy to create a surgical opportunity. Hence, we devised a treatment regimen consisting of the TACE combination with Atezo/Bev for the patient. The TACE treatment was to be administered every 4 weeks, while the Atezo/Bev treatment was to be administered every 3 weeks. Concurrently, oral entecavir antiviral therapy was initiated, and the patient and their family members were thoroughly informed about the potential complications and adverse reactions of TACE combination with Atezo/Bev therapy, as well as the possibility of tumor progression despite treatment. Additionally, the necessity of surgical resection following successful conversion was conveyed. The patient's family members expressed consent and agreed to the treatment plan. The pharmaceuticals administered for the TACE procedure comprised 4 mg of raltitrexed and 20 mg of pirarubicin. The treatment process was as follows: Hepatic arterial angiography revealed tumor staining, with the catheter inserted into the hepatic artery. Initially, 4 mg of raltitrexed was administered, followed by selective insertion of a microcatheter into the tumor-feeding arteries, delivering 10 ml of iodized oil plus 20 mg of pirarubicin, effectively disrupting the tumor's blood supply. Subsequent imaging revealed satisfactory deposition of the iodized oil (Figure 2). The patient experienced mild fever on the first day after the procedure, without any other adverse reactions. Two days after receiving TACE treatment, the Atezo/Bev therapy was initiated, involving an intravenous infusion of atezolizumab (1,200 mg) and bevacizumab (15 mg/kg), with no drug-related adverse reactions observed during the treatment process.

Following two cycles of TACE combined with Atezo/Bev therapy, a subsequent examination revealed significant reductions in AFP (1,710.0 ng/ml, normal range 0–10 ng/ml), AFP-L3% (19.35%, normal range 0–10%), and PIVKA-II (261.3 ng/ml, normal range 0–40 ng/ml). Abdomen-enhanced CT displayed marked tumor shrinkage, with the maximum tumor diameter reducing to 6.9 cm, and the diameter of the two largest lesions

10.3389/fimmu.2024.1358602

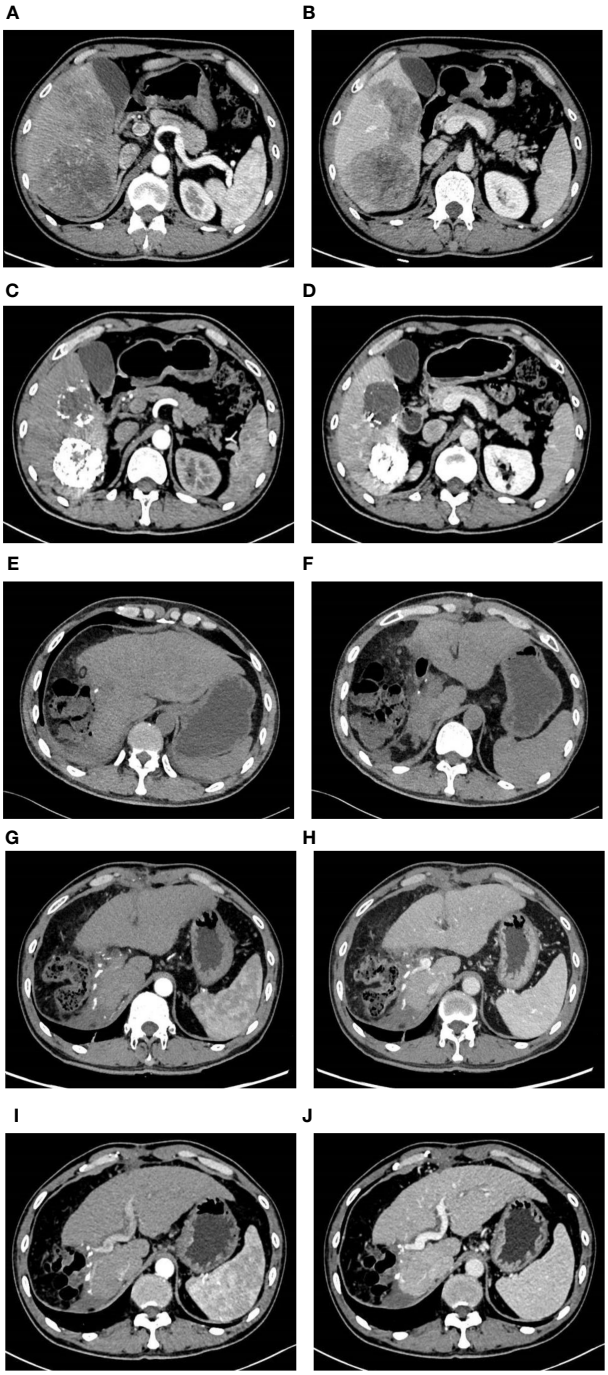

FIGURE 1
Imaging pictures. Before TACE combined with Atezo/Bev treatment, the abdomen enhanced CT revealed multiple tumors in the right liver, with the largest measuring approximately 10 cm × 7.50 cm. During the arterial phase, the tumors exhibited uneven enhancement, while during the venous phase, the degree of enhancement was relatively reduced **(A, B)**. Following two courses of TACE combined with Atezo/Bev treatment, the abdomen enhanced CT indicated a significant reduction in the size of the right liver tumors compared to before, with the largest measuring approximately 6.9 cm × 6.2 cm. Patchy high-density shadows were observed internally, considered to be iodine oil deposition after TACE treatment, with no obvious enhancement on the enhanced scan **(C, D)**. Three days after liver resection, the abdomen plain CT indicated postoperative changes in the right liver lobe, with a small amount of free gas around the liver and no significant fluid accumulation **(E, F)**. One month after liver resection, the abdomen enhanced CT revealed postoperative changes in the right liver lobe, with no abnormal enhanced lesions in the liver parenchyma and a small amount of abdominal fluid **(G, H)**. Six months after liver resection, the abdomen enhanced CT indicated the absence of the right liver lobe, with no abnormal enhanced lesions in the liver parenchyma and a small amount of abdominal fluid around the liver **(I, J)**.

FIGURE 2
During the TACE procedure, the imaging showed staining of the right liver tumors.

decreasing to 12.3 cm, demonstrating a reduction exceeding 30% compared to the initial assessment (Figures 1C, D). According to the Response Evaluation Criteria in Solid Tumors 1.1 (RECIST 1.1), the treatment response was assessed as a partial response (PR). Subsequent multi-disciplinary discussion determined that post-conversion therapy, there was a notable diminution in tumor volume facilitating the preservation of S8 hepatic tissue. At this juncture, the estimated remnant liver volume reached 58.9% allowing for safe implementation of R0 resection and with more than a 2-week interval from the last Atezo/Bev treatment. Subsequently, comprehensive communication with the patient and their family was conducted providing detailed information regarding the potential, necessity, risks, and complications of the surgical resection to which the patient and family provided informed consent. Before the procedure, a comprehensive CT three-dimensional reconstruction model (Figure 3) was perfected, and on 4 May 2023, a laparoscopic hepatic partial resection was performed.

The surgical procedure proceeded as follows: meticulous exploration of the abdominal cavity under laparoscopy revealed no evidence of tumor metastasis. Intraoperatively, ultrasonography confirmed the presence of the tumor in liver segments S5, 6, and 7. Considering the patient's hepatitis B-related cirrhosis, a decision was made to preserve liver segment S8 to protect hepatic function. The tumor and liver S5, 6, and 7 were completely excised. The duration of the surgery was 3.5 h with an estimated intraoperative blood loss of approximately 150 ml. Postoperative pathological examination revealed poorly differentiated HCC, and extensive necrosis (approximately 70%) was observed within the tumors, with three nodular tumors measuring 6.8 cm × 6.2 cm × 6 cm, 5 cm × 4 cm × 3.8 cm, and 2.2 cm × 1.8 cm × 1.8 cm (Figure 4). The tumors did not invade the capsule, and no satellite nodules, definite neural invasion, or intravascular cancer thrombi were observed. No tumor tissue was found at the resection margins; nodular cirrhosis was observed surrounding the margins (Figure 5A). Immunohistochemical staining revealed AFP (+), HepPar-1 partial (+), Ki-67 index 60% (Figures 5B–D). An upper abdomen CT conducted 3 days postoperatively revealed the postoperative appearance of the right lobe of the liver, with no significant fluid accumulation in the abdominal cavity or around the liver (Figures 1E, F). The abdominal drainage tube was removed 1 week after the surgery, and the patient was discharged uneventfully after 10 days. One month postoperatively, tumor-related markers indicated AFP (21.9 ng/ml, normal range 0–10 ng/ml), AFP-L3% (16.84%, normal range 0%–10%), and PIVKA-II (50.7 ng/ml, normal range 0–40 ng/ml), with no apparent abnormalities on upper abdomen enhanced CT (Figures 1G, H). Over the subsequent 11-month follow-up period, tumor markers remained within normal limits (Figures 6A–C), and no tumor recurrence was observed in the imaging examination after the surgery (Figures 1G–J). Relevant data and the treatment timeline are depicted in Figure 6.

Discussion

HCC is the most prevalent malignant tumor of the liver accounting for 75% to 85% of primary liver cancer cases. With over 500,000 new cases annually, approximately 80% of HCC patients are unable to undergo curative surgical treatment due to reasons such as local tumor invasion, distant metastasis, or inadequate residual liver volume (1, 3, 9, 10). In such instances, local and systemic treatments have emerged as the standard therapeutic approaches for intermediate and advanced-stage HCC. The purpose of conversion therapy is to convert unresectable HCC into resectable HCC playing a

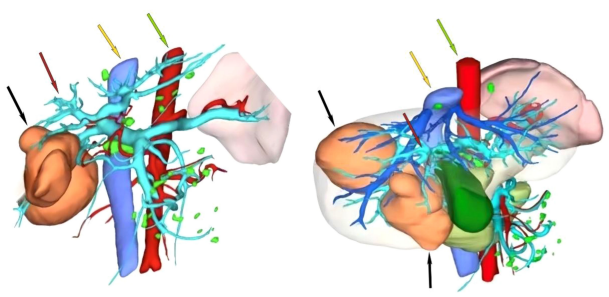

FIGURE 3
Preoperative CT three-dimensional reconstruction model. The black arrow indicates the tumor, the red arrow indicates the portal vein, the yellow arrow indicates the inferior vena cava, and the green arrow indicates the abdominal aorta.

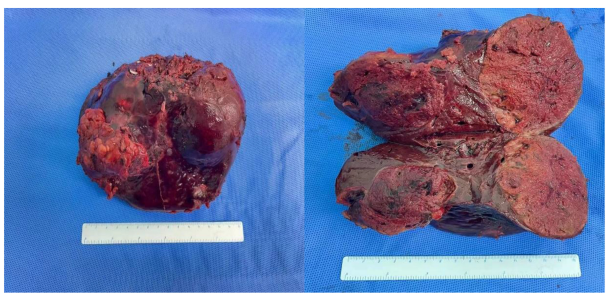

FIGURE 4
Specimen of tumor resection. Resection specimen of the tumor: there were a total of three tumors, with volumes of 6.9 cm × 6.2 cm × 6 cm, 5 cm × 4 cm × 3.8 cm, and 2.2 cm × 1.8 cm × 1.8 cm, respectively.

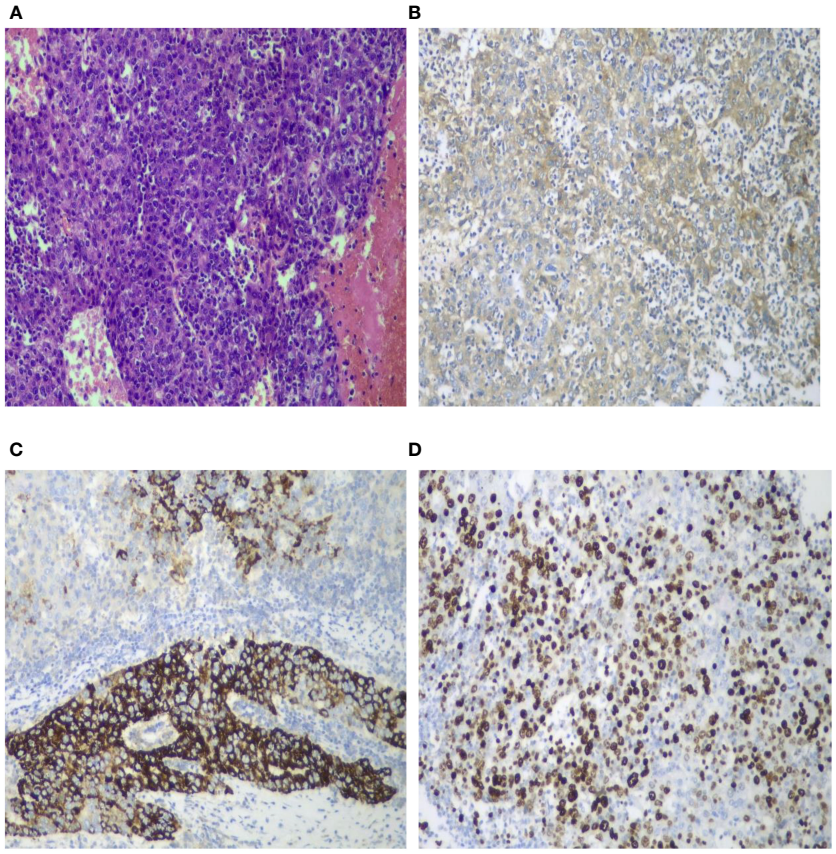

FIGURE 5
Pathological and immunohistochemical images. Histological staining of the tumor sections (HE ×100) revealed poorly differentiated hepatocellular carcinoma accompanied by extensive degeneration and necrosis. The tumor cells exhibited significant atypia, including the presence of giant cells, without satellite nodules, definite neural invasion, or intravascular tumor thrombi. Nodular cirrhosis was observed around the liver section, with partial hepatocyte cholestasis and fatty degeneration **(A)**. AFP demonstrated a positive reaction **(B** ×100**)**. HepPar-1 exhibited partial positive reaction **(C** ×100**)**. Ki-67 positivity index was 60% **(D** ×100**)**.

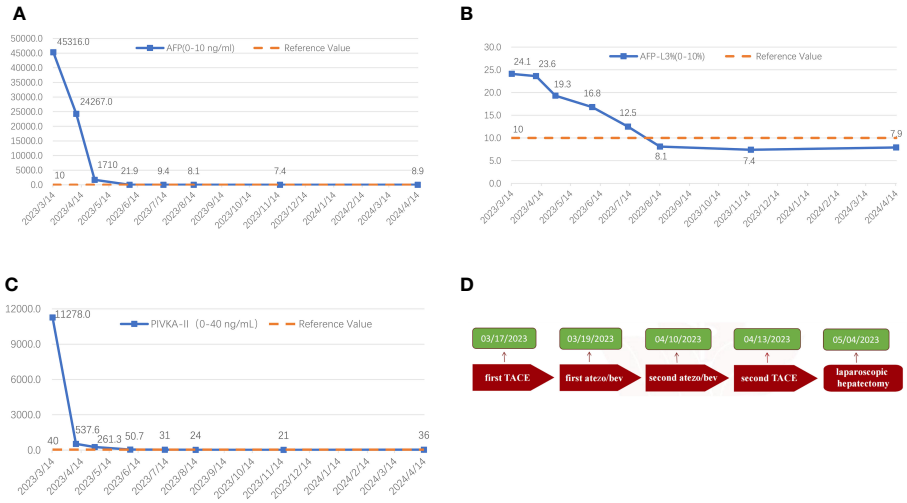

FIGURE 6
The graphical depiction of the dynamic shifts in AFP **(A)**, AFP-L3% **(B)**, and PIVKA-II **(C)** throughout the therapeutic course, along with the treatment timeline **(D)**.

crucial role in improving the prognosis of intermediate and advanced-stage HCC (11–14).

In recent years, groundbreaking progress has been made in researching novel anti-angiogenic agents and ICIs. These two combined applications can enhance host immune activity and tumor immunogenicity synergistically exerting antitumor effects and achieving favorable therapeutic efficacy in patients with intermediate and advanced-stage HCC. Bevacizumab is an anti-angiogenic agent that selectively binds to vascular endothelial growth factor (VEGF) blocking its bioactivity and inhibiting the binding of VEGF to the VEGFR-1 and VEGFR-2 on endothelial cells, thereby reducing tumor angiogenesis and inhibiting tumor growth (15). Atezolizumab is a programmed death-ligand 1 (PD-L1) inhibitor that reverses T-cell-mediated tumor immune evasion by binding to PD-L1 on tumor cells and blocking its interaction with T cells and PD-1 promoting T-cell attack tumor cells and exerting antitumor effects (16). The global, multicenter Phase III clinical trial results of IMbrave150 (17), published in 2020, demonstrated that the Atezo/Bev significantly prolongs the overall survival of patients with intermediate and advanced-stage HCC, with a 12-month survival rate of up to 67.2% and a 42% reduction in the risk of death significantly higher than the clinical efficacy of sorafenib. Thus, the Atezo/Bev regimen has become the first-line systemic treatment for unresectable HCC. However, the sole use of Atezo/Bev typically fails to achieve sustained clinical complete response (CR) or drug-free status, with most cases experiencing progression within 1–1.5 years even with continuous treatment (2). In 2023, Cao et al. (18) reported a clinical study of TACE combined with Atez/Bev versus sole Atez/Bev treatment for advanced HCC patients. Compared to sole Atez/Bev treatment, the combination therapy of TACE with Atez/Bev demonstrated superior overall survival (OS), progression-free survival (PFS), and objective response rate (ORR) for advanced HCC patients, with reliable safety. TACE, as the first-line locoregional treatment for intermediate-stage HCC patients, although demonstrated good short-term efficacy did not lead to a satisfactory long-term prognosis, with a 3-year survival rate of only 26% (19–23). In recent years, the application of novel anti-angiogenic drugs and ICIs in the treatment of HCC has led to higher ORR and longer duration of response (DOR). Combination systemic therapies based on TACE are increasingly being utilized for patients with unresectable HCC who have the potential for conversion. Therefore, combining TACE with the Atezo/Bev regimen has become a new research direction for patients with intermediate HCC in current research.

For patients with intermediate-stage and advanced HCC who have failed first-line treatment, the second-line therapeutic approach becomes particularly crucial. In recent years, numerous second-line therapies have been introduced to treat HCC, among which several combination therapy regimens have yielded promising outcomes. A meta-analysis (24) focusing on second-line treatment for advanced HCC involved 5,488 patients and evaluated 12 treatment regimens. The findings indicated that regorafenib and cabozantinib demonstrated favorable safety and efficacy in individuals resistant to sorafenib, thus serving as viable options for second-line therapy in advanced HCC. Additionally, ICIs have also been examined as novel second-line agents in the treatment of HCC. They included nivolumab (alone or in combination with ipilimumab) and pembrolizumab, two monoclonal antibodies that block the PD-1 pathway and have been approved by the FDA for already treated HCC, following promising results in the CheckMate 040 and KEYNOTE-224 clinical trials, further broadening the treatment landscape (25–27).

Immune-combined TACE therapy remains in the exploratory phase. The IMMUTACE study (28) from Germany in 2020 is one of the earliest research studies to combine TACE with an ICI (nivolumab), involving 49 patients with intermediate-stage HCC, achieving an ORR of 71%. With a median follow-up of 14.6 months, the median PFS reached 6.14 months, and the median overall survival (OS) was 28.32 months meeting its primary endpoints and confirming the safety and efficacy of TACE in combination with ICIs. Various combination therapy regimens primarily involving TACE are continuously being explored, among which the triplet therapy combining TACE with anti-angiogenic drugs and ICIs is considered one of the most promising treatment options. The EMERALD-1 study (29) is the first global multicenter phase III clinical trial to demonstrate positive results of TACE combined with ICIs and anti-angiogenic drugs for locally advanced HCC, and it was reported at the ASCO GI 2024 congress. This study aimed to explore the effectiveness and safety of TACE combined with durvalumab with or without bevacizumab for locally advanced HCC. Analysis of the 616 enrolled patients showed that the median PFS for the TACE combined with durvalumab and bevacizumab group was 15 months, significantly improving PFS compared to the TACE-alone group (8.2 months), reducing the risk of death by 23% compared to sole TACE treatment. Several phase III clinical trials are currently underway. The LEAP-012 study (30) will assess the clinical efficacy of TACE combined with lenvatinib and pembrolizumab for intermediate-stage unresectable HCC patients (NCT04246177). The CheckMate74W trial aims to explore the efficacy and safety of TACE combined with nivolumab with or without ipilimumab for intermediate-stage unresectable HCC (NCT04340193). Both studies are ongoing, and we anticipate achieving encouraging positive results compared to sole TACE treatment.

Relying solely on TACE treatment make it challenging to achieve favorable therapeutic effects. Previous studies have indicated that TACE can lead to increased expression of HIF-1, inducing upregulation of VEGF and platelet-derived growth factor, further promoting angiogenesis and ultimately resulting in tumor recurrence (31, 32). Bevacizumab can enhance the efficacy of TACE by normalizing tumor vessels through the regulation of VEGF, thus improving drug delivery concentration (15). Therefore, combining TACE and bevacizumab can reduce post-TACE angiogenesis in HCC patients, thereby delaying tumor progression and enhancing treatment efficacy. On the other hand, TACE can induce tumor cell necrosis and release tumor-specific antigens, while promoting the recruitment and activation of dendritic cells in the microenvironment, transforming the immunosuppressive microenvironment into an immune-supportive one. Once

combined with immunotherapy, TACE can enable immune checkpoint inhibitors to function better in the activated microenvironment achieving favorable therapeutic effects (33, 34). Therefore, the theoretical synergistic effects of TACE combined with Atezo/Bev may maximize the anticancer effects and effectively enhance the success rate of conversion therapy.

In the IMbrave150 study, the Atezo/Bev regimen appeared to demonstrate more precise therapeutic effects in patients with intermediate-stage (BCLC-B) HCC exhibiting a significantly longer overall survival and progression-free survival compared to advanced-stage HCC (25.8 vs. 17.5 months and 12.6 vs. 6.5 months, respectively). As per RECIST 1.1, the objective response rate for intermediate-stage HCC patients receiving Atezo/Bev systemic treatment is 44%, while it is 27% for advanced-stage HCC patients. This suggests that the Atezo/Bev regimen has a considerable tumor shrinkage effect for intermediate-stage HCC patients potentially offering a more advantageous curative conversion for these patients (35). Kudo et al. (36) conducted a multicenter study of Atezo/Bev regimen treatment for intermediate-stage HCC patients unsuitable for TACE and unresectable, enrolling a total of 110 BCLC-B stage HCC patients. Following systemic treatment with the Atezo/Bev regimen, 38 patients (35%) achieved clinical CR (comprising 7 surgical cases, 13 ablation cases, 15 TACE cases, and 3 cases using Atezo/Bev alone). Among these 38 patients, 25 reached drug-free status (7 surgical cases, 8 ablation cases, and 10 TACE cases), while the remaining 13 patients did not meet the drug-free criteria. During a median observation period of 21.2 months, the 25 patients in the drug-free status did not experience recurrence, whereas among the 13 patients who continued medication, 3 experienced a recurrence. Therefore, achieving a drug-free status can significantly delay tumor progression and prevent tumor recurrence. In this study, it was observed that all seven patients who underwent sequential surgical resection after Atezo/Bev treatment achieved a drug-free status and did not experience tumor recurrence during a median follow-up period of 21.2 months. This, to a certain extent, suggest that curative surgical resection following successful conversion is an extremely effective treatment strategy for preventing tumor recurrence, and achieving a pathological CR could provide these patients with longer disease-free survival and overall survival. However, Kudo's study (36) only evaluated the efficacy of Atezo/Bev therapy in intermediate-stage unresectable HCC patients, and there is currently no internationally reported survival data for curative conversion outcomes of TACE combined with Atezo/Bev in unresectable HCC patients. Theoretically, the amalgamation of both treatments demonstrate a synergistic antineoplastic impact potentially maximizing efficacy and enhancing conversion success rates. In China, Wang et al. (37) conducted a multicenter retrospective study that included 21 patients with intermediate-stage HCC beyond Up-to-Seven Criteria who received TACE combined with Atezo/Bev treatment from March to September 2021. The median follow-up time was 11.7 months, with a best objective response rate (ORR) of 42.9% and a disease control rate (DCR) of 100%. In this study, TACE combined with Atezo/Bev demonstrated promising efficacy and acceptable safety potentially becoming a novel treatment option for intermediate-stage HCC patients. Another multicenter phase II clinical trial called DEMAND (38) is currently ongoing assessing the safety and effectiveness of TACE combined with Atezo/Bev treatment in intermediate-stage unresectable HCC patients. We look forward to the final experimental results of this clinical study.

We present a case of successful R0 resection following therapy involving a combination of TACE and Atezo/Bev regimen in a patient with giant BCLC-B stage (intermediate-stage) unresectable HCC. Due to the multifocality and large volume of the tumor, achieving R0 resection at stage I posed significant challenges. Even with surgical intervention, issues such as insufficient volume of the remaining liver, impaired liver function, and high risk of postoperative recurrence persisted. Remarkably, this patient exhibited significant tumor shrinkage after just two sessions of TACE combined with the Atezo/Bev regimen achieving a clinical PR and ultimately undergoing successful laparoscopic R0 resection. Eleven months postoperatively, no tumor recurrence was observed, and the patient's quality of life remained good. This approach may offer a curative opportunity for a larger cohort of intermediate-stage unresectable HCC patients potentially leading to long-term survival. This reported sample size is limited, which poses certain constraints. Currently, there is a paucity of clinical research on the conversion therapy of unresectable intermediate-stage HCC with this regimen, and its efficacy still necessitate further confirmation through prospective multicenter large-scale randomized controlled trials.

Conclusion

In summary, intermediate-stage HCC represents a potentially curable ailment, with the treatment objective being the attainment of clinical/pathological CR and drug-free status. The combination of TACE with Atezo/Bev regimen may potentially offer improved therapeutic efficacy and conversion resection rates for patients with intermediate-stage unresectable HCC. Upon achieving significant tumor reduction during treatment, a proactive transition to curative surgery can maximize the prognosis of such patients.

Data availability statement

The original contributions presented in the study are included in the article/supplementary material. Further inquiries can be directed to the corresponding author.

Ethics statement

Written informed consent was obtained from the individual(s) for the publication of any potentially identifiable images or data included in this article.

Author contributions

HA: Writing – original draft. TG: Writing – review & editing. YM: Writing – review & editing. GM: Writing – review & editing. WD: Writing – review & editing. WBD: Writing – review & editing. WW: Writing – review & editing. XZ: Writing – review & editing.

Funding

The author(s) declare that no financial support was received for the research, authorship, and/or publication of this article.

Conflict of interest

The authors declare that the research was conducted in the absence of any commercial or financial relationships that could be construed as a potential conflict of interest.

Publisher's note

References

1. Sung H, Ferlay J, Siegel RL, Laversanne M, Soerjomataram I, Jemal A, et al. Global cancer statistics 2020: GLOBOCAN estimates of incidence and mortality worldwide for 36 cancers in 185 countries. *CA Cancer J Clin*. (2021) 71:209–49. doi: 10.3322/caac.21660

2. Sun HC, Zhou J, Wang Z, Liu X, Xie Q, Jia W, et al. Chinese expert consensus on conversion therapy for hepatocellular carcinoma (2021 edition). *Hepatobiliary Surg Nutr*. (2022) 11:227–52. doi: 10.21037/hbsn-21–328

3. Park JW, Chen M, Colombo M, Roberts LR, Schwartz M, Chen PJ, et al. Global patterns of hepatocellular carcinoma management from diagnosis to death: the BRIDGE Study. *Liver Int*. (2015) 35:2155–66. doi: 10.1111/liv.12818

4. Zhou J, Sun H, Wang Z, Cong W, Zeng M, Zhou W, et al. Guidelines for the diagnosis and treatment of primary liver cancer (2022 edition). *Liver Cancer*. (2023) 12:405–44. doi: 10.1159/000530495

5. Tang H, Cao Y, Jian Y, Li X, Li J, Zhang W, et al. Conversion therapy with an immune checkpoint inhibitor and an antiangiogenic drug for advanced hepatocellular carcinoma: A review. *Biosci Trends*. (2022) 16:130–41. doi: 10.5582/bst.2022.01019

6. Zhu XD, Huang C, Shen YH, Ji Y, Ge NL, Qu XD, et al. Downstaging and resection of initially unresectable hepatocellular carcinoma with tyrosine kinase inhibitor and anti-PD-1 antibody combinations. *Liver Cancer*. (2021) 10:320–9. doi: 10.1159/000514313

7. Bruix J, Chan SL, Galle PR, Rimassa L, Sangro B. Systemic treatment of hepatocellular carcinoma: An EASL position paper. *J Hepatol*. (2021) 75:960–74. doi: 10.1016/j.jhep.2021.07.004

8. Llovet JM, Villanueva A, Marrero JA, Schwartz M, Meyer T, Galle PR, et al. Trial design and endpoints in hepatocellular carcinoma: AASLD consensus conference. *Hepatology*. (2021) 73 Suppl 1:158–91. doi: 10.1002/hep.31327

9. Siegel RL, Miller KD, Fuchs HE, Jemal A. Cancer statistics, 2021. *CA Cancer J Clin*. (2021) 71:7–33. doi: 10.3322/caac.21654

10. McGlynn KA, Petrick JL, El-Serag HB. Epidemiology of hepatocellular carcinoma. *Hepatology*. (2021) 73 Suppl 1:4–13. doi: 10.1002/hep.31288

11. Yang X, Xu H, Zuo B, Yang X, Bian J, Long J, et al. Downstaging and resection of hepatocellular carcinoma in patients with extrahepatic metastases after stereotactic therapy. *Hepatobiliary Surg Nutr*. (2021) 10:434–42. doi: 10.21037/hbsn-21–188

12. Qu WF, Ding ZB, Qu XD, Tang Z, Zhu GQ, Fu XT, et al. Conversion therapy for initially unresectable hepatocellular carcinoma using a combination of toripalimab, lenvatinib plus TACE: real-world study. *BJS Open*. (2022) 6. doi: 10.1093/bjsopen/zrac114

13. Gan L, Lang M, Tian X, Ren S, Li G, Liu Y, et al. A retrospective analysis of conversion therapy with lenvatinib, sintilimab, and arterially-directed therapy in patients with initially unresectable hepatocellular carcinoma. *J Hepatocell Carcinoma*. (2023) 10:673–86. doi: 10.2147/JHC.S404675

14. Wu JY, Zhang ZB, Zhou JY, Ke JP, Bai YN, Chen YF, et al. Outcomes of salvage surgery for initially unresectable hepatocellular carcinoma converted by transcatheter arterial chemoembolization combined with lenvatinib plus anti-PD-1 antibodies: A multicenter retrospective study. *Liver Cancer*. (2023) 12:229–37. doi: 10.1159/000528356

15. Garcia J, Hurwitz HI, Sandler AB, Miles D, Coleman RL, Deurloo R, et al. Bevacizumab (Avastin®) in cancer treatment: A review of 15 years of clinical experience and future outlook. *Cancer Treat Rev*. (2020) 86:102017. doi: 10.1016/j.ctrv.2020.102017

16. Dyck L, Mills K. Immune checkpoints and their inhibition in cancer and infectious diseases. *Eur J Immunol*. (2017) 47:765–79. doi: 10.1002/eji.201646875

17. Finn RS, Qin S, Ikeda M, Galle PR, Ducreux M, Kim TY, et al. Atezolizumab plus bevacizumab in unresectable hepatocellular carcinoma. *N Engl J Med*. (2020) 382:1894–905. doi: 10.1056/NEJMoa1915745

18. Cao F, Shi C, Zhang G, Luo J, Zheng J, Hao W. Improved clinical outcomes in advanced hepatocellular carcinoma treated with transarterial chemoembolization plus atezolizumab and bevacizumab: a bicentric retrospective study. *BMC Cancer*. (2023) 23:873. doi: 10.1186/s12885–023-11389-x

19. Lencioni R. Loco-regional treatment of hepatocellular carcinoma. *Hepatology*. (2010) 52:762–73. doi: 10.1002/hep.23725

20. Kudo M, Han KH, Ye SL, Zhou J, Huang YH, Lin SM, et al. A changing paradigm for the treatment of intermediate-stage hepatocellular carcinoma: asia-pacific primary liver cancer expert consensus statements. *Liver Cancer*. (2020) 9:245–60. doi: 10.1159/000507370

21. Kudo M, Kawamura Y, Hasegawa K, Tateishi R, Kariyama K, Shiina S, et al. Management of hepatocellular carcinoma in Japan: JSH consensus statements and recommendations 2021 update. *Liver Cancer*. (2021) 10:181–223. doi: 10.1159/000514174

22. Kuroda C, Sakurai M, Monden M, Marukawa T, Hosoki T, Tokunaga K, et al. Limitation of transcatheter arterial chemoembolization using iodized oil for small hepatocellular carcinoma. *A Study Resected Cases Cancer*. (1991) 67:81–6. doi: 10.1002/1097–0142(19910101)67:1<81::aid-cncr2820670116<3.0.co;2-h

23. Yamashita Y, Matsukawa T, Arakawa A, Hatanaka Y, Urata J, Takahashi M. US-guided liver biopsy: predicting the effect of interventional treatment of hepatocellular carcinoma. *Radiology*. (1995) 196:799–804. doi: 10.1148/radiology.196.3.7644646

24. Solimando AG, Susca N, Argentiero A, Brunetti O, Leone P, De Re V, et al. Second-line treatments for advanced hepatocellular carcinoma: A systematic review and bayesian network meta-analysis. *Clin Exp Med*. (2022) 22:65–74. doi: 10.1007/s10238–021-00727–7

25. Yau T, Kang YK, Kim TY, El-Khoueiry AB, Santoro A, Sangro B, et al. Efficacy and safety of nivolumab plus ipilimumab in patients with advanced hepatocellular carcinoma previously treated with sorafenib: the checkMate 040 randomized clinical trial. *JAMA Oncol*. (2020) 6:e204564. doi: 10.1001/jamaoncol.2020.4564

26. El-Khoueiry AB, Sangro B, Yau T, Crocenzi TS, Kudo M, Hsu C, et al. Nivolumab in patients with advanced hepatocellular carcinoma (CheckMate 040): an open-label, non-comparative, phase 1/2 dose escalation and expansion trial. *Lancet*. (2017) 389:2492–502. doi: 10.1016/S0140–6736(17)31046–2

27. Zhu AX, Finn RS, Edeline J, Cattan S, Ogasawara S, Palmer D, et al. Pembrolizumab in patients with advanced hepatocellular carcinoma previously treated with sorafenib (KEYNOTE-224): a non-randomised, open-label phase 2 trial. *Lancet Oncol*. (2018) 19:940–52. doi: 10.1016/S1470–2045(18)30351–6

28. IMMUTACE. A phase 2 single-arm, open-label study of transarterial chemoembolization in combination with nivolumab performed for intermediate-stage hepatocellular carcinoma. *Gastroenterol Hepatol (N Y)*. (2021) 17:16–7

29. Sun B, Zhang L, Sun T, Ren Y, Cao Y, Zhang W, et al. Safety and efficacy of lenvatinib combined with camrelizumab plus transcatheter arterial chemoembolization for unresectable hepatocellular carcinoma: A two-center retrospective study. *Front Oncol*. (2022) 12:982948. doi: 10.3389/fonc.2022.982948

30. Llovet JM, Vogel A, Madoff DC, Finn RS, Ogasawara S, Ren Z, et al. Randomized phase 3 LEAP-012 study: transarterial chemoembolization with or without lenvatinib plus pembrolizumab for intermediate-stage hepatocellular carcinoma not amenable to curative treatment. *Cardiovasc Intervent Radiol*. (2022) 45:405–12. doi: 10.1007/s00270–021-03031–9

31. Li X, Feng GS, Zheng CS, Zhuo CK, Liu X. Expression of plasma vascular endothelial growth factor in patients with hepatocellular carcinoma and effect of transcatheter arterial chemoembolization therapy on plasma vascular endothelial growth factor level. *World J Gastroenterol*. (2004) 10:2878–82. doi: 10.3748/wjg.v10.i19.2878

32. Wang B, Xu H, Gao ZQ, Ning HF, Sun YQ, Cao GW. Increased expression of vascular endothelial growth factor in hepatocellular carcinoma after transcatheter arterial chemoembolization. *Acta Radiol*. (2008) 49:523–9. doi: 10.1080/02841850801958890

33. Singh P, Toom S, Avula A, Kumar V, Rahma OE. The immune modulation effect of locoregional therapies and its potential synergy with immunotherapy in hepatocellular carcinoma. *J Hepatocell Carcinoma*. (2020) 7:11–7. doi: 10.2147/JHC.S187121

34. Doemel LA, Santana JG, Savic LJ, Gaupp F, Borde T, Petukhova-Greenstein A, et al. Comparison of metabolic and immunologic responses to transarterial chemoembolization with different chemoembolic regimens in a rabbit VX2 liver tumor model. *Eur Radiol*. (2022) 32:2437–47. doi: 10.1007/s00330–021-08337–3

35. Cheng AL, Qin S, Ikeda M, Galle PR, Ducreux M, Kim TY, et al. Updated efficacy and safety data from IMbrave150: Atezolizumab plus bevacizumab vs. sorafenib for unresectable hepatocellular carcinoma. *J Hepatol*. (2022) 76:862–73. doi: 10.1016/j.jhep.2021.11.030

36. Kudo M, Aoki T, Ueshima K, Tsuchiya K, Morita M, Chishina H, et al. Achievement of Complete Response and Drug-Free Status by Atezolizumab plus Bevacizumab Combined with or without Curative Conversion in Patients with Transarterial Chemoembolization-Unsuitable, Intermediate-Stage Hepatocellular Carcinoma: A Multicenter Proof-Of-Concept Study. *Liver Cancer*. (2023) 12:321–38. doi: 10.1159/000529574

37. Wang K, Zhu H, Yu H, Cheng Y, Xiang Y, Cheng Z, et al. Early Experience of TACE Combined with Atezolizumab plus Bevacizumab for Patients with Intermediate-Stage Hepatocellular Carcinoma beyond Up-to-Seven Criteria: A Multicenter, Single-Arm Study. *J Oncol*. (2023) 2023:6353047. doi: 10.1155/2023/6353047

38. Ben Khaled N, Seidensticker M, Ricke J, Mayerle J, Oehrle B, Rössler D, et al. Atezolizumab and bevacizumab with transarterial chemoembolization in hepatocellular carcinoma: the DEMAND trial protocol. *Future Oncol*. (2022) 18:1423–35. doi: 10.2217/fon-2021–1261

frontiers | Frontiers in Medicine

TYPE Original Research
PUBLISHED 13 June 2024
DOI 10.3389/fmed.2024.1391843

OPEN ACCESS

EDITED BY
Marcello Dallio,
University of Campania Luigi Vanvitelli, Italy

REVIEWED BY
Komal Ramani,
Cedars Sinai Medical Center, United States
Vivek Peche,
Washington University in St. Louis, United States

*CORRESPONDENCE
Meijuan Zheng
✉ mjzheng@mail.ustc.edu.cn
Yuanhong Xu
✉ xyhong1964@163.com
Zhongxin Wang
✉ aywzhx78@163.com

†These authors have contributed equally to this work

RECEIVED 26 February 2024
ACCEPTED 30 May 2024
PUBLISHED 13 June 2024

CITATION
Wei X, Tang Y, Zheng M, Xu Y and Wang Z (2024) KEAP1 overexpression is correlated with poor prognosis and immune infiltration in liver hepatocellular carcinoma. *Front. Med.* 11:1391843. doi: 10.3389/fmed.2024.1391843

KEAP1 overexpression is correlated with poor prognosis and immune infiltration in liver hepatocellular carcinoma

Xin Wei, Yigui Tang, Meijuan Zheng*†, Yuanhong Xu*† and Zhongxin Wang*†

Department of Clinical Laboratory, The First Affiliated Hospital of Anhui Medical University, Hefei, China

Purpose: Liver hepatocellular carcinoma (LIHC) is the most common type of liver cancer, but there is a lack of effective indicators for its early diagnosis and prognosis, so we explored the role of KEAP1 in LIHC patients in this study.

Methods: The Cancer Genome Atlas (TCGA) dataset was used to investigate the relationship between KEAP1 expression and clinicopathological features and prognosis of LIHC patients. KEAP1 expression related pathways were enriched by Gene Ontology (GO) and gene set enrichment analysis (GSEA). Besides, KEAP1 expression-related immune infiltration was performed by single-sample GSEA (ssGSEA), and function of immune cells was detected by flow cytometry.

Results: It was found that KEAP1 expression was significantly increased and correlated with overall survival of LIHC patients. A total of 231 differentially expressed genes (DEGs) between LIHC patients with high- and low-KEAP1 expression were found, which associated with various biological pathways. Besides, KEAP1 expression was positively correlated with the infiltration level of T helper cells and Th2 cells but negatively correlated with DCs and cytotoxic cells. Functional analysis revealed that the expression of IL 4 in Th2 cells and CD107a, GrA and GrB in cytotoxic cells was significantly greater in LIHC patients than in HCs. In addition, KEAP1 expression was closely correlated with liver function in LIHC patients.

Conclusion: Highly expressed KEAP1 was closely related to the diagnosis, prognosis, immune cell infiltration, and liver function of LIHC, which might promote the progression of LIHC through regulating cell development, signal transduction, and abnormal immune response. The current study partially revealed the role of KEAP1 in LIHC and provided a potential biomarker for the diagnosis, prognosis and treatment of LIHC.

KEYWORDS

KEAP1, LIHC, biomarker, immune infiltration, liver function

1 Introduction

Liver cancer is the sixth most common malignancy and the fourth leading cause of malignancy-related death worldwide, with 841,080 new cases in 2018. It is estimated that more than 1 million people will develop liver cancer each year by 2025. Liver cancer remains a global challenge, and its incidence is growing worldwide. Liver hepatocellular carcinoma (LIHC) is

the most common type of liver cancer, accounting for approximately 90% of the total cases. Despite the growing need for molecular identification of tumors using tissue biopsies in clinical practice, LIHC diagnosis is often based on noninvasive criteria. Potentially actionable mutations are present in approximately 25% of LIHC; however, this has not yet been translated into clinical practice because molecular information from tissue or liquid biopsies is needed, so noninvasive diagnosis remains a challenge at present (1–3). In addition, effective indicators for the early diagnosis, prognosis and treatment of LIHC are lacking, so it is urgent to explore new molecular targets.

Kelch-like ECH-associated Protein 1 (KEAP1), a Cullin 3-based E3 ubiquitin ligase adaptor subunit, senses a variety of abnormal signals, including oxidation and electrophilic stimulation. The main function of KEAP1 is to regulate the activity of NF-E2-related molecule 2 (Nrf2) and affect the expression of its downstream molecules so as to play different immunomodulatory roles (4). It has been reported that KEAP1 plays an important regulatory role in the occurrence and development of many liver diseases. After competitively binding to KEAP1, P62 can promote an increase of Nrf2 expression, activate the expression of its downstream related molecules (including NQO1, HO1 and FTH1, etc.), inhibit the apoptosis of liver cancer cells induced by iron accumulation, and may participate in promoting the continuous progression of liver cancer (5). Expression of KEAP1 was significantly increased in patients with primary biliary cirrhosis, while the expression of Nrf2 was significantly decreased, resulting in decreased expression of its downstream related molecules (HO-1 and GCLC), which may inhibit oxidative stress in the liver and promote the progression of cirrhosis (6). Our study also revealed that KEAP1 and related target genes were abnormally expressed in hepatocellular carcinoma cells and were closely related to drug resistance in hepatocellular carcinoma (7). However, the association between KEAP1 and LIHC has not yet been characterized.

In this study, we sought to demonstrate the association between KEAP1 and LIHC, and analyzed the prognostic role of KEAP1 in LIHC based on RNA-sequencing (RNA-seq) data from The Cancer Genome Atlas (TCGA). We first analyzed the changes of KEAP1 expression in LIHC, and analyzed the correlation between KEAP1 expression and the severity and prognosis of LIHC. Then, we screened the DEGs associated with KEAP1 expression in LIHC, and performed Gene Ontology (GO) and gene set enrichment analysis (GSEA) on these genes. In addition, we analyzed the relationship between KEAP1 expression and immune infiltration, and further examined the functional changes in related immune cells in LIHC patients. Finally, we analyzed the association between KEAP1 expression and liver function in LIHC patients. This study may provide novel insight into the underlying mechanisms of LIHC tumorigenesis and may have positive implications for enriching the diagnosis, prognosis and treatment of LIHC.

2 Materials and methods

2.1 Data acquisition

Datasets from the TCGA database[1] were included: gene expression data (HTSeq-Counts and HTSeq-FPKM [high-throughput sequencing fragments per kilobase per million]) and the corresponding detailed clinical data from LIHC samples. Level 3 HTSeq-FPKM data were transformed into transcripts per million reads (TPM). 374 LIHC cases and 50 normal cases were included in our study, cases with insufficient or missing data were removed from subsequent data processing. LIHC patients were classified into low- and high-KEAP1 expression groups according to the median KEAP1 expression value.

2.2 Survival analysis

Survival curves were calculated according to the Kaplan–Meier method utilizing the Kaplan–Meier plotter and log-rank test by R (survival) package (V3.6.3)[2]. Cox proportional hazards models estimating the hazard ratio (HR) were established to determine whether KEAP1 was associated with the survival events. HR with 95% confidence intervals and log-rank p-value were calculated via univariate survival analysis (8). The nomogram combining the expression of KEAP1 and clinicopathological risk factors was constructed with the "rms" package and quantitatively assessed by the concordance index (C-index).

2.3 Immune infiltration analysis

The immune infiltration analysis of LIHC for 24 types of immune cells was performed by single-sample gene set enrichment analysis (ssGSEA) method from the GSVA package in R (version 3.6) (9). Markers of the 24 types of immune cells were extracted from the research of Bindea and colleagues (10). Lollipop chart was plotted to examine the correlation of KEAP1 expression with 24 types of immune cell infiltration in LIHC samples with the Spearman correlation analysis. Vioplot was plotted to assess the relationship of KEAP1 and immune cell recruitment with the Wilcoxon rank-sum test.

2.4 Gene set enrichment analysis

GSEA is a computational method that determines whether a defined set of genes exhibits statistically significant and concordant differences between two biological states. GSEA[3] was performed with the R package cluster Profiler (version 3.14.3) to demonstrate the significant functions and pathways between groups expressing high- and low-levels of KEAP1 in LIHC. "c2.cp.v7.2.symbols.gmt [Curated]" from MSigDB Collections[4] was selected as the reference gene set, false discovery rate (FDR) <0.25 and adjusted p-value (p.adj) <0.05 are considered to be significantly enriched (11, 12).

2.5 ROS detection

Dulbecco's Modified Eagle Medium (DMEM, 11966025, Gibco, Grand Island, NY) medium supplemented with 10% FBS (10,099,158,

1 https://portal.gdc.cancer.gov

2 http://www.sthda.com/english/wiki/r-packages

3 https://www.gsea-msigdb.org/gsea/index.jsp

4 https://www.gsea-msigdb.org/gsea/msigdb/

Gibco, Grand Island, NY) was used to adjust the cell concentration at the logarithmic growth stage to 4×10^5/mL. 100 μL of cell suspension was placed in a 96-well round bottom culture plate and cultured at 37°C in a humidified CO_2 incubator. After 12 h, the experimental group was replaced with DMEM medium supplemented with 10% FBS + 10 mmol/L CCl_4 (C032225, Koether, Shanghai, China), and the control group was replaced with DMEM medium supplemented with 10% FBS, and 8 parallel wells were made in each group. After 24 h of continuous culture, the cells and culture medium were collected and put into an ultrasonic grinder to crush the cells, and the cell debris were centrifuged at 10000 rpm/min for 10 min, and the supernuant of each group were detected immediately with ROS ELISA kit (EIA06562h, Xinqidi, Wuhan, China), and the experimental operation was carried out in strict accordance with the reagent instructions. Briefly, 100 μL of specimens or ROS standards with different concentrations were added into the corresponding experimental wells, and incubated at 37°C for 90 min; after washing the plate twice with the washing solution, 100 μL of biotinized ROS antibody working solution was added to each well and incubated at 37°C for 60 min; after washing plate with washing solution for three times, 100 μL of enzyme conjugate working solution was added to each well and incubated at 37°C for 30 min without light; after washing plate with washing liquid for 5 times, add 100 μL of TMB color developing working liquid to each well, and incubate at 37°C for 20 min without light; add 100 μL of the termination solution to each well and mix it well, immediately measure ROS level with an microplate reader (Yantai Addcare Bio-tech Co., Ltd. Shandong, China).

2.6 Patients

Twenty LIHC patients without autoimmune disease were enrolled at the First Affiliated Hospital of Anhui Medical University. All patients were diagnosed and grouped according to the criteria from Bureau of Medical Administration, National Health Commission of the People's Republic of China (13). Twenty age- and sex-matched healthy individuals were recruited as healthy controls (HCs). The study was approved by the ethics committee of the First Affiliated Hospital of Anhui Medical University. Whole blood specimens were obtained from all subjects and peripheral blood mononuclear cells (PBMCs) were isolated by Ficoll density gradient centrifugation on Human Lymphocyte Separation Medium (7,111,012, Dakewe, Shenzhen, China). The clinical and laboratory characteristics of the populations enrolled are summarized in Table 1. Detailed data are presented in Supplementary Table S1.

TABLE 1 Clinical characteristics of the populations enrolled in the study.

Group	HC	LIHC
case	20	20
Sex (male/female)	14/6	16/4
Age (years)	55.00 (41–75)	59.50 (45–73)
TP (g/L)	70.15 (50.50–80.60)	66.85 (48.00–78.20)
ALB (g/L)	43.65 (34.30–50.60)	41.05 (30.30–49.00)
TBIL (μmol/L)	12.13 (7.16–36.80)	20.43 (9.36–216.20)
DBIL (μmol/L)	2.26 (1.10–19.90)	4.53 (1.90–179.20)
IBIL (μmol/L)	9.16 (5.14–14.68)	15.28 (7.09–36.98)
ALT (U/L)	20.50 (5.80–36.80)	38.50 (12.00–435.00)
AST (U/L)	12.40 (4.20–20.60)	54.00 (18.00–443.00)
PLT ($\times 10^9$/L)	165.50 (135.00–350.00)	132.50 (41.00–322.00)
PT (s)	10.00 (9.00–13.00)	10.95 (9.90–15.00)
FIB (g/L)	3.50 (1.80–4.00)	2.60 (1.53–4.10)
AFP (mg/L)	3.40 (1.30–8.00)	12.66 (1.30–100000.00)
HBV-DNA (IU/mL)	ND	750 (ND-5×10^8)
HBsAg+	0	20
HBsAb+	20	0
HBeAg+	0	14
HBeAb+	0	6
HBcAb+	0	20

Data are shown as median and range. TP, total protein; ALB, albumin; TBIL, total bilirubin; DBIL, direct bilirubin; IDBL, indirect bilirubin; ALT, alamine aminotransferase; AST, aspartate aminotransferase; PLT, platelet; PT, prothrombin time; FIB, fibrinogen; AFP, alpha fetal protein; ND, not detected; HC, healthy control; LIHC, liver hepatocellular carcinoma.

2.7 Western blot

Appropriate amount of liver cancer tissues and adjacent tissues were taken, fully ground on ice and cleaved by RIPA (P0013J, Beyotime, Shanghai, China). After centrifugation, supernatant was taken and the protein concentration was detected by BCA protein quantitative kit (P0010, Beyotime, Shanghai, China). 25 μg of protein was taken for sodium dodecyl sulphate-polyacrylamide gel electrophoresis (SDS-PAGE, P0012A, Beyotime, Shanghai, China), and transferred to nitrocellulosa membrane (FFP26, Beyotime, Shanghai, China), which was closed with western blocking solution (P0023B-500 mL, Beyotime, Shanghai, China) at room temperature for 1 h, and then primary antibodies (KEAP1, 1:1000, WL03285; β-actin, 1:1000, WL01372. Wan Class, Shenyang, China) were added and incubated at 4°C overnight. After western wash buffer (P0023C-1 L, Beyotime, Shanghai, China) washing, the secondary antibodies (1,7,000, WLA023, Wan Class, Shenyang, China) were added and incubated at room temperature for 2 h. After western wash buffer washing, ECL luminescent agent (P0018S, Beyotime, Shanghai, China) was added for exposure, and the optical density (OD) value of protein was analyzed by Image J software (National Institutes of Health, Maryland, United States). β-actin was used as standardized control, the ratio of OD value of KEAP1 to β-actin was used as the relative expression of target protein.

2.8 RNA extraction and semiquantitative real-time polymerase chain reaction

Total RNA from PBMCs was isolated using a SteadyPure Tissue and Cell Small RNA Extraction Kit (AG21024, Accurate Biology, Hunan, China) according to the manufacturer's protocol. Gene expression was evaluated using PrimeScript™ RT Master Mix (RR036A, Takara, Japan) and TB Green™ Premix Ex Taq™ II (RR820A, Takara, Japan). The thermocycling conditions consisted of an initial step of 2 min at 50°C and denaturation for 30 s at 95°C, followed by 40 cycles at 95°C for 5 s and 60°C for 35 s, and a melt curve was generated to confirm the specificity of the PCR products. The KEAP1 sequences used were: sence primer (5′→3′), GTGTCC ATTGAGGGTATCCACC, and antisence primer (5′→3′), GCTCAG CGAAGTTGGCGAT. β-actin was used for normalization, and the

sequences were: sence primer (5′→3′), AGCCTCGCCTTTGCCGATCCG, and antisence primer (5′→3′), TCTCTTGCTCTGGGCCTCGTCG. Each sample was analyzed in triplicate, relative gene expression was analyzed with the comparative Ct method ($2^{-\Delta\Delta Ct}$).

2.9 Fluorescence-activated cell sorting analysis

Most antibodies were purchased from BioLegend (San Diego, CA), including allophycocyanin (APC)-conjugated anti-human CD45 mAb (368512), fluorescein isothiocyanate (FITC)-conjugated anti-human CD3 mAb (300306), phycoerythrin-Cy7 (PE/Cy7)-conjugated anti-human CD4 mAb (317414), Brilliant Violet 421™ (BV-421)-conjugated anti-human CD8 mAb (344748), allophycocyanin-Cy7 (APC/Cy7)-conjugated anti-human CD107a mAb (328630), PE-conjugated anti-human perforin mAb (308106), and peridin chlorophyll protein-Cy5.5 (PerCP/Cy5.5)-conjugated anti-human Granzyme B (GrB) mAb (372212). Besides, PE/Cy7-conjugated anti-human Granzyme A (GrA) mAb from Thermo Fisher Scientific (25-9,117-42, Waltham, MA) and PE-conjugated anti-human IL-4 mAb from BD Pharmingen (559,333, San Jose, CA) were used. We detected the functional properties of cytotoxic T cells as follows: APC/Cy7-conjugated anti-human CD107a mAb, PE-conjugated anti-human perforin mAb, PE/Cy7-conjugated anti-human Granzyme A (GrA) mAb and PerCP/Cy5.5-conjugated anti-human Granzyme B (GrB) mAb. The expression of IL-4 was detected to assist in understanding the function of Th2 cells. PBMCs from all subjects were isolated by Ficoll density gradient centrifugation on Lymphoprep (AS1114546, Axis-shield, Norway). For cell surface staining, 2×10^5 PBMCs were taken into a flow tube, washed with 2 mL of 1× cell staining buffer (420,201, BioLegend, San Diego, CA), centrifuged at 1500 rpm/min for 5 min, and the pellet were resuspended in residual buffer. Add appropriate amount of fluorescent antibodies (FITC-conjugated anti-human CD3 mAb, 5 μL; APC-conjugated anti-human CD45 mAb, 4 μL; PE/Cy7-conjugated anti-human CD4 mAb, 4 μL; BV-421-conjugated anti-human CD8 mAb, 3 μL) and incubated at room temperature for 20 min in the dark. Wash with 2 mL of PBS by centrifugation at 1500 rpm/min for 5 min, fully discard the supernatant, add 200 μL of PBS to resuspend pellet and analyzed with BD FACSCanto II (Becton Dickinson, San Jose, CA) and FlowJo Software (TreeStar, Ashland, OR).

2.10 Cell stimulation for intracellular staining

PBMCs (5×10^5) were suspended in 100 μL of Roswell Park Memorial Institute (RPMI)-1640 medium (12,633,012, Gibco, Grand Island, NY) and placed in a 96-well round bottom plate with stimulants (phorbol 12-myristate 13-acetate [PMA, 50 ng/mL] and ionomycin [1 μg/mL]) and GolgiStop (Brefeldin A [5 μg/mL]) (423,303, BioLegend, San Diego, CA) at 37°C in a humidified CO_2 incubator for 4 h. Then, the PBMCs were harvested and washed twice with 2 mL of 1× cell staining buffer by centrifugation at 1500 rpm/min for 5 min, and the pellet were resuspended in residual buffer. Cell surface staining antibodies were added and incubated at room temperature for 20 min in the dark. Wash twice with 1× cell staining buffer and fully discard the supernatant, add 300 μL of Fixation/Permeabilization solution (554,714, BD Pharmingen, San Jose, CA) and incubated at room temperature for 20 min in the dark. Wash twice with 2 mL of 1× Wash Buffer by centrifugation at 1500 rpm/min for 5 min, and the pellet were resuspended in residual buffer. Add appropriate amount of cytokine antibodies (APC/Cy7-conjugated anti-human CD107a mAb, 4 μL; PE-conjugated anti-human perforin mAb, 3 μL; PerCP/Cy5.5-conjugated anti-human GrB mAb, 4 μL; PE/Cy7-conjugated anti-human GrA mAb, 4 μL; PE-conjugated anti-human IL-4 mAb, 3 μL) and incubated at room temperature for 20 min in the dark. After which, protocols for pellet washing and suspension were carried out as described above and analyzed with BD FACSCanto II and FlowJo Software.

2.11 Statistical analysis

Data processing and statistical analysis were performed using R software (version 3.6, R Foundation for Statistical Computing, Vienna, Austria) and GraphPad Prism software (v. 7.0a; GraphPad Software, La Jolla, CA). The Wilcoxon rank-sum test and Wilcoxon signed-rank test were used to analyze the expression of KEAP1 in non-paired and paired samples, respectively. The chi-square test or Fisher's exact test was used to analyze the correlation between the KEAP1 expression level and clinicopathological parameters of LIHC patients. The Kaplan–Meier method and Cox regression model were used to perform survival analyses. A two-sided p-value <0.05 was considered to be significant except where noted. Statistical significance is indicated as follows: $^{***}p < 0.001$, $^{**}p < 0.01$, and $^{*}p < 0.05$.

3 Results

3.1 KEAP1 expression was abnormally elevated in LIHC

KEAP1 expression was significantly higher in LIHC tissues compared with the normal tissues in both non-paired samples (371:160) and paired samples (50:50) based on TCGA databases. Then, we detected KEAP1 expression by western blotting to verify the above results, and found that the expression level of KEAP1 in LIHC tissues was significantly higher than that in adjacent tissues, which was consistent with the above conclusion (Figure 1A). In addition, we analyzed KEAP1 expression in pancarcinoma, and found that KEAP1 expression was elevated in most cancers in both non-paired samples and paired samples except in KICH compared with paired normal tissues (Figures 1B,C). These results suggest that KEAP1 expression may play an important role in the development of liver cancer. Therefore, we further analyzed the correlation between KEAP1 expression and LIHC prognosis. Kaplan–Meier survival analysis revealed that although KEAP1 expression was not a significant predictor of disease-specific survival and progress free interval, KEAP1 expression is associated with overall survival (hazard ratio [HR] = 1.44) in LIHC patients (Figure 1D). Furthermore, we analyzed the relationship between KEAP1 expression and overall survival of LIHC patients during each period. It was found that KEAP1 expression was significantly correlated with the survival time of LIHC patients with different histologic grade (HR = 1.49), pathologic stage (HR = 1.47), and T stage (HR = 1.47) (Figure 1E). LIHC patients with

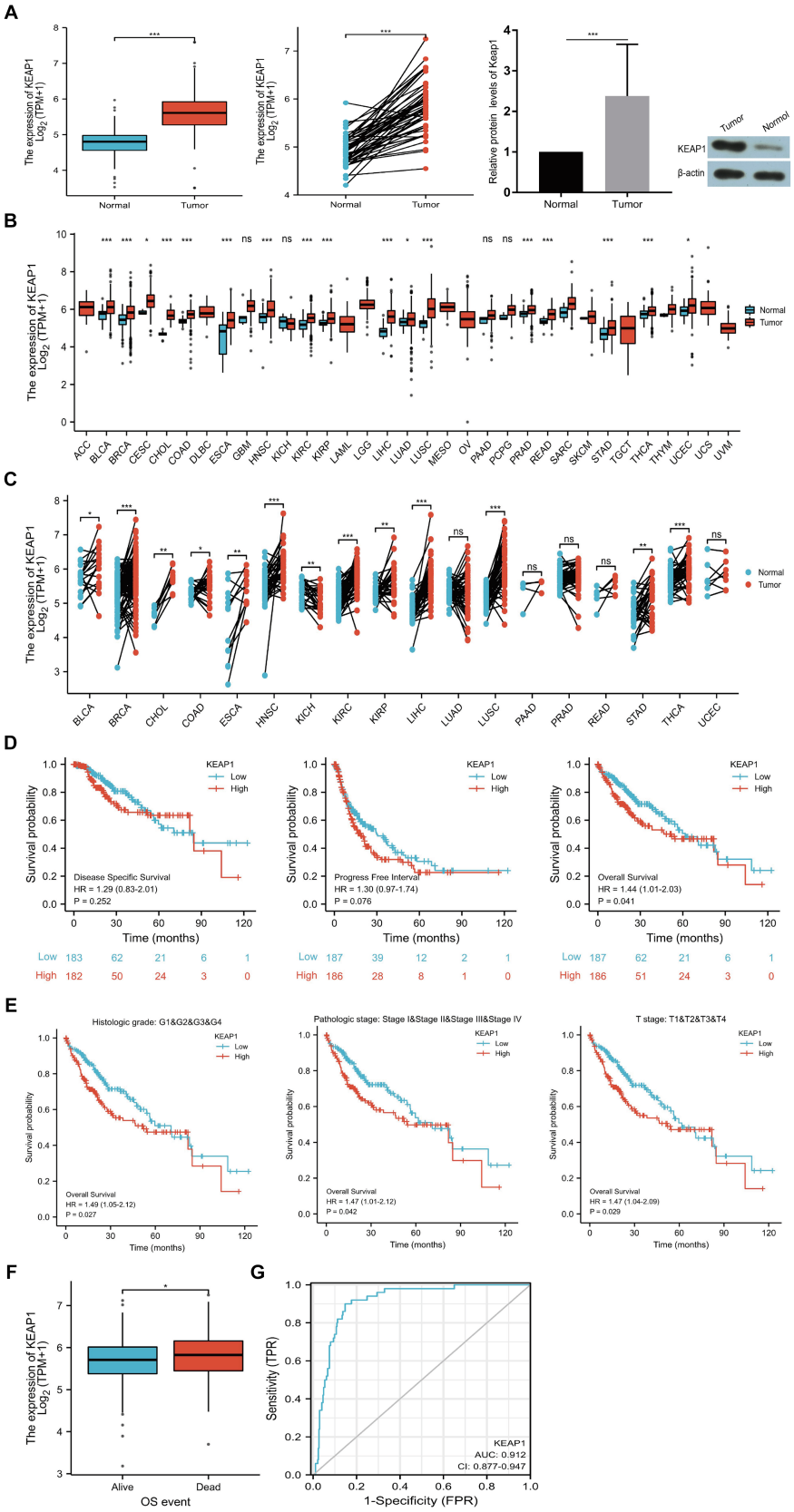

FIGURE 1
KEAP1 overexpression is closely related to LIHC. **(A)** KEAP1 expression in LIHC patients was significantly increased in both paired and non-paired samples. **(B,C)** KEAP1 expression was elevated in most cancers in both paired and non-paired samples. **(D)** KEAP1 expression is associated with overall survival of LIHC patients. **(E)** KEAP1 expression was correlated with the survival time of LIHC patients with different stages. **(F)** LIHC patients with dead outcome had higher KEAP1 expression than those with alive outcome. **(G)** KEAP1 has good diagnostic value for LIHC. Statistical significance is indicated as follows: ***$p < 0.001$, **$p < 0.01$, and *$p < 0.05$. TPM, transcripts per million reads; HR, hazard ratio; LIHC, liver hepatocellular carcinoma.

high KEAP1 expression had lower overall survival than those with low KEAP1 expression. At the same time, LIHC patients with dead outcome had higher KEAP1 expression than those with alive outcome (Figure 1F). Besides, KEAP1 expression showed great diagnostic value (AUC, 0.912) with significant high sensitivity of 0.912 and specificity of 0.853 to identify LIHC tissues from normal tissues (Figure 1G). These results suggest that KEAP1 expression is significantly elevated and is closely related to prognosis in LIHC patients. Detailed data are presented in Supplementary Table S2: S1–S6.

3.2 Associations between KEAP1 expression and clinicopathologic characteristics in LIHC

We extracted and analyzed the demographic and clinical data of LIHC patients with low- (187) and high-KEAP1 expression (187) from the TCGA (Table 2). We further used single gene logistics regression analysis to determine the correlation between KEAP1 expression and clinicopathological characteristics in LIHC patients (Table 3). It was found that KEAP1 expression was positively correlated with pathological stage of LIHC patients (Odds Ratio [OR] = 1.583 for Stage II&Stage III&Stage IV vs. Stage I). To better understand the relevance and mechanisms of KEAP1 expression in LIHC, we investigated the relationship between KEAP1 expression and the clinical characteristics of LIHC patients by univariate Cox regression analysis (Table 4). It was found that high KEAP1 expression correlated with poor survival of LIHC patients. Other clinical characteristics that correlated with poor survival included high T stage, high M stage, high pathologic stage, and with tumor status. To further explore factors associated with survival, multivariate Cox regression analysis was performed, which revealed that tumor status (HR = 1.819) was an independent risk factor for overall survival (Table 4). These results suggest that KEAP1 expression may be correlated with overall survival in LIHC patients and deserves further study.

3.3 KEAP1 related functional annotation and signaling pathways based on GO and GSEA

Results above suggest that KEAP1 expression may play an important role in the prognosis of LIHC patients and is correlated with the overall survival of LIHC patients. Therefore, we conducted relevant studies focusing on KEAP1 expression in LIHC patients, and further extracted and analyzed 56,493 genes from TCGA between patients with high- and low-KEAP1 expression using DESeq2 [1.26.0 version] (14) in R (Supplementary Table S3: S1). There were 231 DEGs between the two groups based on the criteria of logFC >1.5 and p.adj < 0.05, covering 153 upregulated and 78 downregulated genes (Figure 2A) (Supplementary Table S3: S2). Then, DEGs in the HTSeq-Counts were further analyzed by ggplot2 [3.3.3 version] in R. Absolute logFC value of the top 15 DEGs between the two groups were illustrated by heatmaps (Figure 2B). To better understand the functional implications of the 231 DEGs, GO enrichment analysis was performed using the ClusterProfile package (11). The significance cut-off value of GO enrichment analysis was set as p.adj < 0.05, and 30 enriched terms were identified in the GO "biological process"

TABLE 2 Demographic and clinical characteristics of LIHC patients with low- and high-expression of KEAP1 in TCGA.

Characteristic	Low expression of KEAP1	High expression of KEAP1	*p*
n	187	187	
Age, *n* (%)			0.715
<=60	91 (24.4%)	86 (23.1%)	
>60	96 (25.7%)	100 (26.8%)	
Gender, *n* (%)			1.000
Female	61 (16.3%)	60 (16%)	
Male	126 (33.7%)	127 (34%)	
Race, *n* (%)			0.273
Asian	77 (21.3%)	83 (22.9%)	
Black or African American	6 (1.7%)	11 (3%)	
White	99 (27.3%)	86 (23.8%)	
T stage, *n* (%)			0.182
T1	101 (27.2%)	82 (22.1%)	
T2	44 (11.9%)	51 (13.7%)	
T3	37 (10%)	43 (11.6%)	
T4	4 (1.1%)	9 (2.4%)	
N stage, *n* (%)			1.000
N0	124 (48.1%)	130 (50.4%)	
N1	2 (0.8%)	2 (0.8%)	
M stage, *n* (%)			1.000
M0	137 (50.4%)	131 (48.2%)	
M1	2 (0.7%)	2 (0.7%)	
Pathologic stage, *n* (%)			0.149
Stage I	97 (27.7%)	76 (21.7%)	
Stage II	40 (11.4%)	47 (13.4%)	
Stage III	36 (10.3%)	49 (14%)	
Stage IV	3 (0.9%)	2 (0.6%)	
Histologic grade, *n* (%)			0.419
G1	31 (8.4%)	24 (6.5%)	
G2	93 (25.2%)	85 (23%)	
G3	55 (14.9%)	69 (18.7%)	
G4	6 (1.6%)	6 (1.6%)	
AFP (ng/mL), *n* (%)			0.895
<=400	110 (39.3%)	105 (37.5%)	
>400	32 (11.4%)	33 (11.8%)	
Albumin (g/dl), *n* (%)			0.656
<3.5	38 (12.7%)	31 (10.3%)	
>=3.5	118 (39.3%)	113 (37.7%)	
Prothrombin time, *n* (%)			0.455
<=4	103 (34.7%)	105 (35.4%)	
>4	49 (16.5%)	40 (13.5%)	
Child-Pugh grade, *n* (%)			0.495
A	114 (47.3%)	105 (43.6%)	
B	9 (3.7%)	12 (5%)	
C	1 (0.4%)	0 (0%)	

Cases with insufficient or missing data were removed from data processing.

TABLE 3 Logistic regression analysis of association between clinicopathological characteristics and KEAP1 expression in LIHC patients.

Characteristics	Total (*N*)	Odds ratio (OR)	*p* value
T stage (T2&T3&T4 vs. T1)	371	1.493 (0.992–2.251)	0.055
N stage (N1 vs. N0)	258	0.954 (0.113–8.049)	0.963
M stage (M1 vs. M0)	272	1.046 (0.124–8.819)	0.965
Pathologic stage (Stage II & Stage III & Stage IV vs. Stage I)	350	1.583 (1.040–2.419)	0.033
Tumor status (With tumor vs. Tumor free)	355	1.284 (0.843–1.958)	0.245
Age (>60 vs. <=60)	373	1.102 (0.734–1.656)	0.639
Gender (Male vs. Female)	374	1.025 (0.664–1.582)	0.912
Residual tumor (R1&R2 vs. R0)	345	1.321 (0.508–3.540)	0.568
Histologic grade (G2&G3&G4 vs. G1)	369	1.342 (0.756–2.408)	0.318
AFP(ng/mL) (>400 vs. <=400)	280	1.080 (0.620–1.886)	0.785
Child-Pugh grade (B&C vs. A)	241	1.303 (0.540–3.208)	0.556

Cases with insufficient or missing data were removed from data processing.

category, including "stress response to copper ion," "detoxification of copper ion," "stress response to metal ion," and "detoxification of inorganic compound"; 13 enriched terms were identified in the GO "cellular component" category, including "integral component of postsynaptic (synaptic) membrane" and "intrinsic component of synaptic membrane"; and 5 enriched terms were identified in the GO "molecular function" category, including "signaling receptor activator activity," "receptor ligand activity," "hormone activity," and "growth factor activity" (Figure 2C) (Supplementary Table S3: S3). These results suggest that abnormally expressed KEAP1 is associated with the stress response and detoxification of copper ion, synaptic composition, and signaling conduction. Besides, ROS levels in hepatocellular carcinoma cells were detected to assist in determining the oxidative stress role of Keap1 in LIHC. The results showed that under the same stimulation condition, the ROS level of hepatocellular carcinoma cells was significantly reduced after inhibiting Keap1 expression, suggesting that the high expression of Keap1 may promote oxidative stress of hepatocellular carcinoma cells (Figure 2D) (Supplementary Table S3: S4).

To identify key pathways related to KEAP1 expression in LIHC, GSEA was used between the high- and low-KEAP1 expression groups. The results showed that KEAP1 related DEGs mainly enriched in cell development and signal transduction, such as "REACTOME_DNA_REPLICATION" [normalized enrichment score (NES) = 2.525, p.adj = 0.024, FDR = 0.018], "REACTOME_CELL_CYCLE_CHECKPOINTS" [NES = 2.779, p.adj = 0.024, FDR = 0.018], "PID_PLK1_PATHWAY" [NES = 2.704, p.adj = 0.024, FDR = 0.018], "PID_E2F_PATHWAY" [NES = 2.328, p.adj = 0.024, FDR = 0.018] (Figure 2E) (Supplementary Table S3: S5).

3.4 Correlation between KEAP1 expression and immune infiltration in LIHC

Considering that KEAP1 may participate in cell development and signal transduction from the results of GO and GSEA, and the important role of cellular immunity in cancer progression. We further applied ssGSEA to analyze the relationship between KEAP1 expression and immune cell enrichment in LIHC (Figure 3A). We found that KEAP1 expression was positively correlated with the infiltration level of T helper cells ($r = 0.111$, $p = 0.031$) and Th2 cells ($r = 0.156$, $p = 0.002$), while negatively correlated with the infiltration level of DC ($r = -0.131$, $p = 0.011$), and cytotoxic cells ($r = -0.130$, $p = 0.012$) (Figure 3B). Besides, we detected KEAP1 mRNA levels of circulating lymphocytes, and found that KEAP1 mRNA levels of circulating lymphocytes in LIHC patients was significantly higher than that in HCs (Figure 3C). Detailed data are presented in Supplementary Table S4.

3.5 Functional changes of KEAP1 expression related immune infiltration cells in LIHC

The correlation analysis suggest that KEAP1 expression is closely related to immune infiltration in LIHC, so it is particularly necessary to analyze the function of relevant immune cells to assist in judging the immune status of LIHC patients. We selected two broad cell populations (Th2 cells and cytotoxic cells) that are positively and negatively correlated with KEAP1 expression in LIHC patients for functional analysis. Th2 cells mainly mediate immune regulation by secreting IL-4. Therefore, the expression level of IL-4 was analyzed. It was found that the frequency of Th2 cells in LIHC patients was significantly higher than that in HCs, but the absolute number of Th2 cells was not significant different between the two groups (Figures 4A,B). Besides, the expression of IL-4 in Th2 cells of LIHC patients was significantly higher than that of HCs (Figure 4C). Cytotoxic cells secrete perforin and granzyme to mediate the killing function through degranulation. It was found that although the frequency of cytotoxic cells was not significant different between the two groups, the absolute number of cytotoxic cells in LIHC patients was significantly lower than that in HCs (Figures 5A,B). Besides, the expression level of CD107a, GrA and GrB in cytotoxic cells of LIHC patients were significantly higher than that of HCs, but there was no difference in the expression level of perforin between the two groups (Figure 5C). These results suggest that Th2 and cytotoxic cells in LIHC patients may be in an immunoactivated state, and their immune activity is significantly enhanced. Detailed data are presented in Supplementary Table S5.

TABLE 4 Association of clinicopathological characteristics with overall survival using univariate or multivariate cox regression analysis.

Characteristics	Total (*N*)	Univariate analysis		Multivariate analysis	
		Hazard ratio (95% CI)	*p* value	Hazard ratio (95% CI)	*p* value
Age	373				
<=60	177	Reference			
>60	196	1.205 (0.850–1.708)	0.295		
Gender	373				
Female	121	Reference			
Male	252	0.793 (0.557–1.130)	0.200		
T stage	370				
T1	183	Reference			
T2	94	1.431 (0.902–2.268)	0.128	0.000 (0.000-Inf)	0.995
T3	80	2.674 (1.761–4.060)	<0.001	0.952 (0.127–7.130)	0.962
T4	13	5.386 (2.690–10.784)	<0.001	1.793 (0.207–15.561)	0.596
N stage	258				
N0	254	Reference			
N1	4	2.029 (0.497–8.281)	0.324		
M stage	272				
M0	268	Reference			
M1	4	4.077 (1.281–12.973)	0.017	2.186 (0.159–30.109)	0.559
AFP(ng/mL)	279				
<=400	215	Reference			
>400	64	1.075 (0.658–1.759)	0.772		
Pathologic stage	349				
Stage I	173	Reference			
Stage II	86	1.417 (0.868–2.312)	0.164	4329290.072 (0.000-Inf)	0.994
Stage III	85	2.734 (1.792–4.172)	<0.001	2.933 (0.385–22.368)	0.299
Stage IV	5	5.597 (1.726–18.148)	0.004		
Tumor status	354				
Tumor free	202	Reference			
With tumor	152	2.317 (1.590–3.376)	<0.001	1.819 (1.136–2.914)	0.013
Histologic grade	368				
G1	55	Reference			
G2	178	1.162 (0.686–1.969)	0.576		
G3	123	1.185 (0.683–2.057)	0.545		
G4	12	1.681 (0.621–4.549)	0.307		
Residual tumor	344				
R0	326	Reference			
R1&R2	18	1.604 (0.812–3.169)	0.174		
Child-Pugh grade	240				
A	218	Reference			
B&C	22	1.643 (0.811–3.330)	0.168		
KEAP1	373				
Low	187	Reference			
High	186	1.436 (1.015–2.031)	0.041	1.262 (0.805–1.980)	0.310

Cases with insufficient or missing data were removed from data processing.

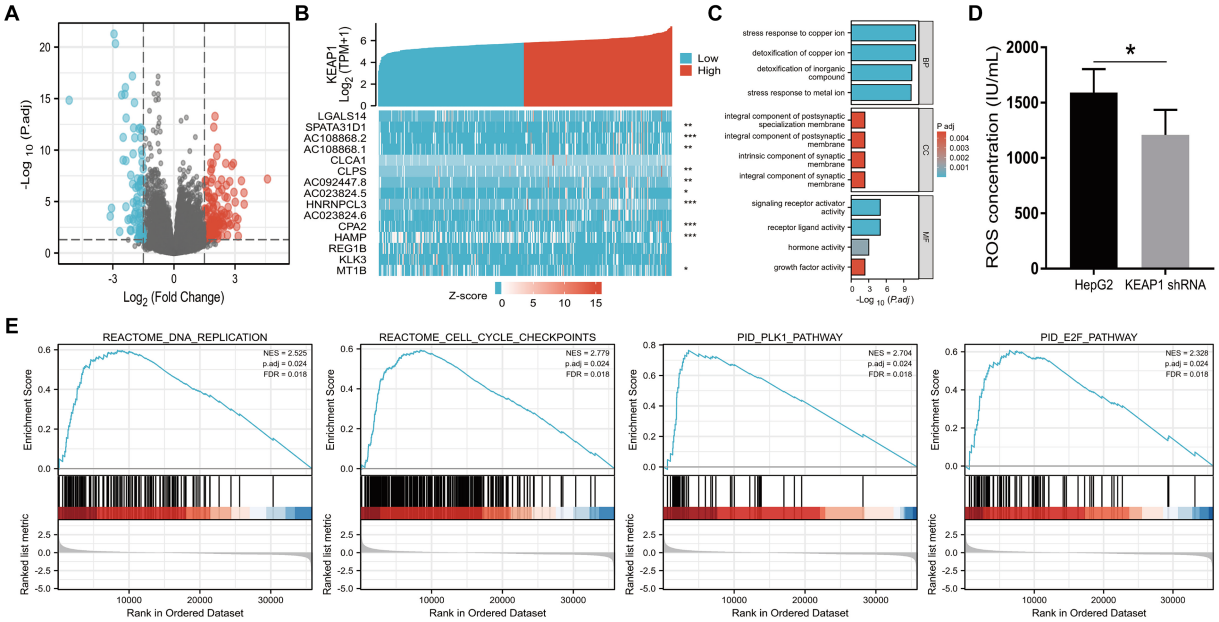

FIGURE 2
KEAP1 related functional annotation and signaling pathways based on GO and GSEA. **(A)** 153 upregulated and 78 downregulated genes between LIHC patients with high- and low-KEAP1 expression based on the criteria of logFC >1.5 and adjusted *p*-value <0.05. **(B)** Absolute logFC value of the top 15 DEGs between LIHC patients with high- and low-KEAP1 expression. **(C)** GO enrichment analysis for DEGs identified between LIHC patients with high- and low-KEAP1 expression groups. **(D)** ROS levels of hepG2 cells was significantly reduced after inhibiting Keap1 expression. KEAP1 shRNA was used to reduce KEAP1 expression in HepG2 cells. **(E)** GSEA for DEGs identified between LIHC patients with high- and low-KEAP1 expression groups. GO, gene ontology; DEGs, differentially expressed genes; ROS, reactive oxygen species.

3.6 KEAP1 expression is closely related to liver function in LIHC

Results above suggest that KEAP1 may play an important role in the development of LIHC. Therefore, we further investigated the relationship between KEAP1 expression and liver function. Correlation analysis revealed that KEAP1 expression was significantly negatively correlated with the level of total protein (TP) and albumin (ALB), and positively correlated with total bilirubin (TBIL), direct bilirubin (DBIL), ALT, AST, and AFP, but not correlated with indirect bilirubin (IBIL), platelet (PLT), prothrombin time (PT) and fibrinogen (FIB) (Figure 6) (Supplementary Tables S1, S4). These results suggest that KEAP1 expression is closely related to liver function in LIHC patients, and elevated KEAP1 expression may promote liver injury.

4 Discussion

Considering the difficulty of treatment and poor prognosis of LIHC, it is extremely necessary to provide timely and effective targets for clinical diagnosis and treatment of LIHC, so as to improve the survival time of patients. KEAP1 has been found to be abnormally elevated in many cancers, such as HNSC, LUSC (15, 16). In this study, we found that KEAP1 was significantly overexpressed in LIHC patients, and found that KEAP1 has a good diagnostic value for LIHC (AUC = 0.912) with high sensitivity (0.912) and specificity (0.853). Therefore, it is necessary to further explore the clinical value of KEAP1 in LIHC. Kaplan–Meier survival analysis and logistics regression analysis revealed that KEAP1 expression was correlated with overall survival of LIHC patients, especially in patients with advanced histologic grade, pathologic stage and T stage. These results suggest that KEAP1 expression is closely related to the diagnosis and prognosis of LIHC. Therefore, we followed up with relevant studies on KEAP1 expression in LIHC. We identified 231 DEGs between LIHC patients with high- and low-KEAP1 expression. GO analysis revealed that these DEGs were mainly involved in stress response and detoxification of inorganic substances, synaptic composition, and signaling conduction. Inorganic is an indispensable part of many key biological pathways, and its abnormal distribution may lead to abnormal cell function and thus biological dysfunction. Rodrigues JFV and colleagues reported that human cells treated with silver nanoparticles upregulated mineral absorption, ferroptosis, protein processing in the endoplasmic reticulum, and mitogen-activated protein kinase signaling pathway expression. At the same time, inorganic compounds and oxidative stress response genes were shared, triggering apoptosis (17). In LIHC patients, KEAP1 expression was closely related to stress response and detoxification of inorganic compounds. Therefore, the mechanism and related pathways of KEAP1 expression regulating the inorganic distribution of LIHC are worth further investigation. The formation of intact synapses is an important part of signal transmission, usually releasing neurotransmitters from the presynaptic membrane to the postsynaptic membrane to transmit excitatory or inhibitory signals (18). Synaptic changes caused by severe stress or trauma can lead to abnormal signal transmission, and the release of a large number of neurotransmitters in the short term may cause irreversible damage to related brain areas, such as the amygdala, and induce mood disorders and mental disorders (19). Differential genes related to KEAP1 expression in LIHC patients are associated with synaptic composition,

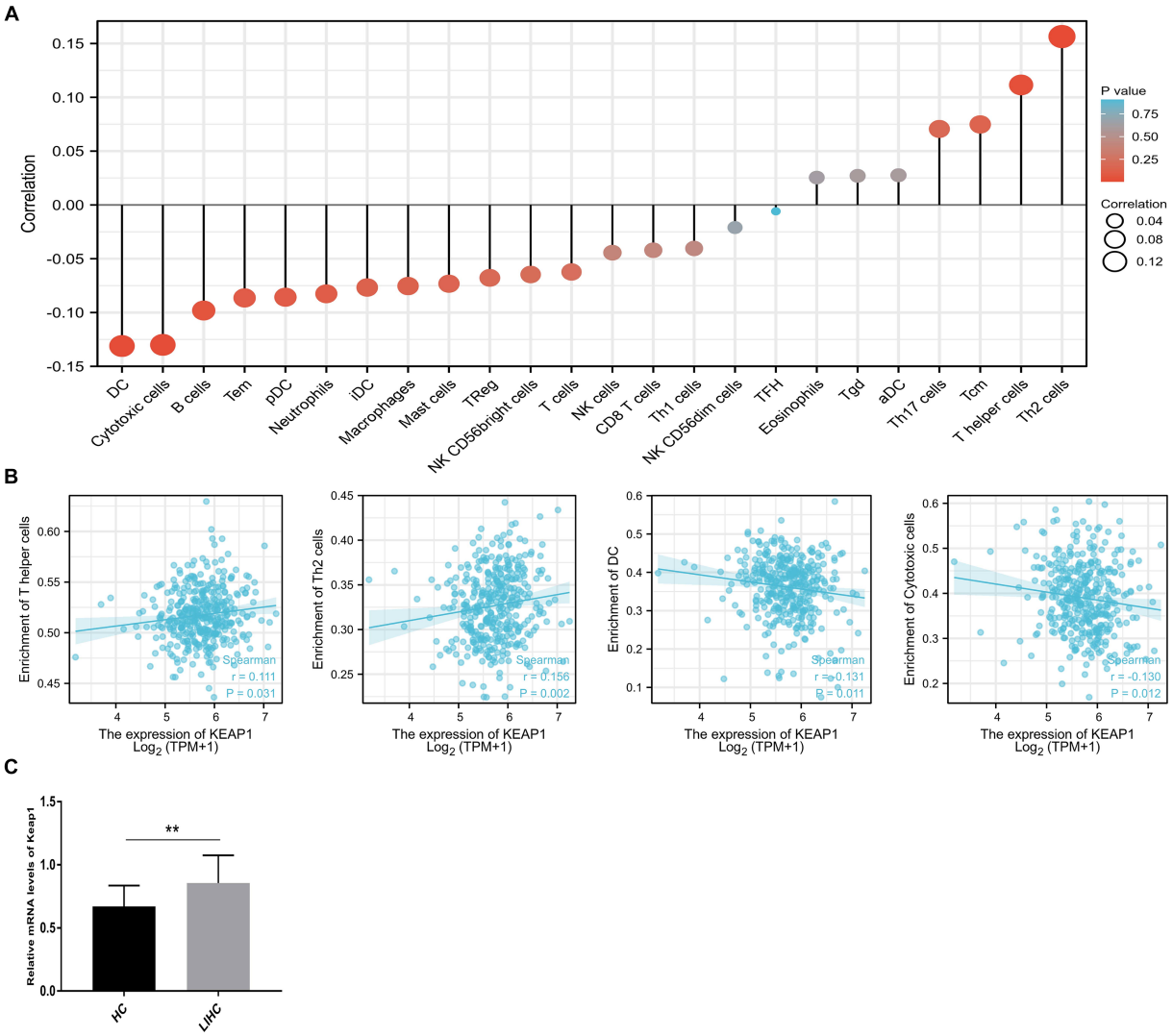

FIGURE 3
Correlation analysis of KEAP1 expression and immune infiltration in LIHC. **(A)** Single-sample GSEA was used to analyze the relationship between KEAP1 expression and immune cell enrichment in LIHC. **(B)** KEAP1 expression was positively correlated with the infiltration level of T helper cells and Th2 cells, while negatively correlated with DC and cytotoxic cells. **(C)** KEAP1 mRNA level of circulating lymphocytes in LIHC patients was significantly higher than that in HCs.

but their role in regulating patients' emotions and related mechanisms remain unclear, which may be worth exploring. In addition, signaling is also an important part for cells to play different biological functions. The expression of different molecules in cells can be regulated by direct contact between cells or sensing changes in the composition of intercellular fluid to play different functions (20). Therefore, whether the signaling related differential gene involved in KEAP1 expression in LIHC patients acts on hepatocytes and related peripheral cells, as well as the effect of its chain reaction on the occurrence and development of LIHC and the related mechanism are questions worth exploring.

In addition, we used GSEA to further analyze key pathways involved in KEAP1 expression related genes in LIHC and found that they are mainly focused on cell development and signal transduction. These results suggest that KEAP1 has a good correlation with LIHC, and the differential genes related to its expression are involved in stress response, synaptic formation, signal transduction, cell development, etc., and are inextricably related to the normal play of cell function. Therefore, it is necessary to further study the relationship between KEAP1 expression and oxidative stress and cell function. We examined the role of KEAP1 in regulating oxidative stress in hepatocellular carcinoma cells, and found that inhibiting KEAP1 expression could significantly reduce ROS levels in hepatocellular carcinoma cells, suggesting that high KEAP1 expression may promote cell dysfunction. Tu et al. systematically introduced the role of KEAP1 in coordination with NRF2 and ARE in mediating and inhibiting inflammation and oxidative stress in various chronic diseases (21), suggesting that KEAP1 may promote inflammation and oxidative stress by inhibiting downstream molecules NRF2 and ARE. Besides, relevant studies have explored the KEAP1-targeting molecule PGAM5 based on the Keap1/Nrf2/ARE pathway, and found that enhancing the expression of PGAM5 can significantly inhibit the expression of KEAP1, thus inhibiting the production of ROS, which is of great value for improving disease progression (22, 23). These studies suggest that the high expression of KEAP1 in LICH tissue may promote the progression of inflammation and oxidative stress in patients, and may improve disease progression in LIHC patients by discovering molecules targeting KEAP1.

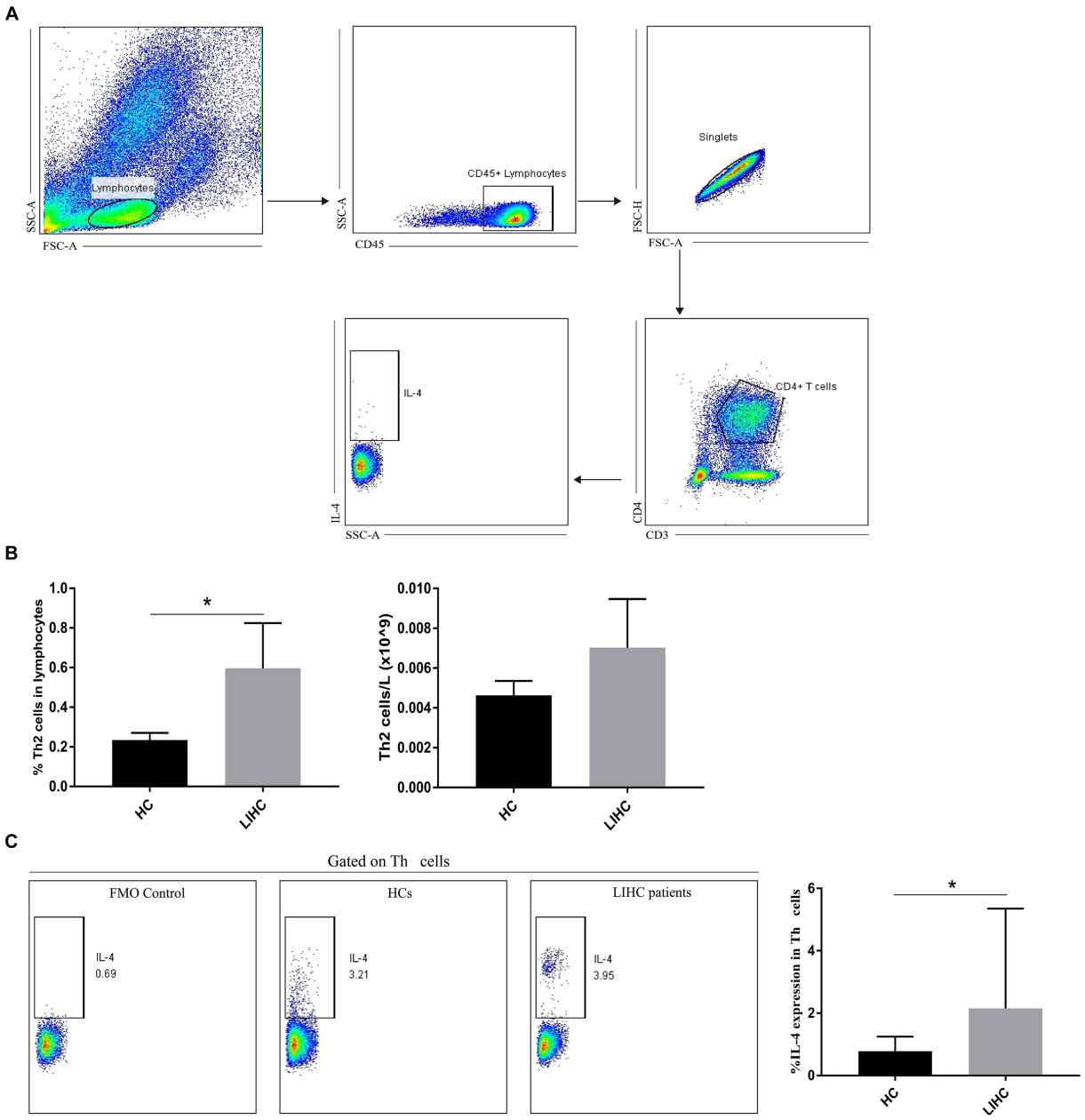

FIGURE 4
Changes of Th2 cells in LIHC patients. **(A)** Gate strategy of IL-4 expression in Th2 cells in flow cytometry. **(B)** The frequency of Th2 cells in LIHC patients was significantly higher than that in HCs, but the absolute number of Th2 cells was not significant different between the two groups. **(C)** The expression of IL-4 in Th2 cells of LIHC patients was significantly higher than that of HCs. FMO (fluorescence minus one) staining was used to distinguish positive from negative thereby helping circle the gate more accurately. HCs, healthy controls.

Immune cells are the main body of immune system to perform immune function. They recognize foreign antigens through specific receptors, directly or indirectly eliminate foreign pathogens, mutated tumor cells and damaged senescent cells, and regulate intercellular immunity by secreting related cytokines to transmit specific information, mediating the normal functions of tissues and the body (16). Therefore, the dysfunction of immune cells may seriously affect the body's health. This study found that KEAP1 expression is closely related to immune cell infiltration, which indirectly proves that keap1 expression may affect the occurrence and development of LIHC. It was found that KEAP1 expression was positively correlated with the infiltration level of T helper cells and Th2 cells, while negatively correlated with the infiltration level of DC and cytotoxic cells, these data can help us to more conveniently and quickly screen out the cell populations that have a greater likelihood of affecting the development of tumors, so as to further perform functional analysis of these cell populations to assist in judging the immune status of LIHC patients. Th cells recognize antigen fragments presented by MHC molecules of antigen-presenting cells mainly through specific receptors on the cell surface, stimulate intracellular cascade reactions, induce secretion of related cytokines, and then regulate the function of target cells and play a role in immune regulation (24). DC can efficiently take up, process

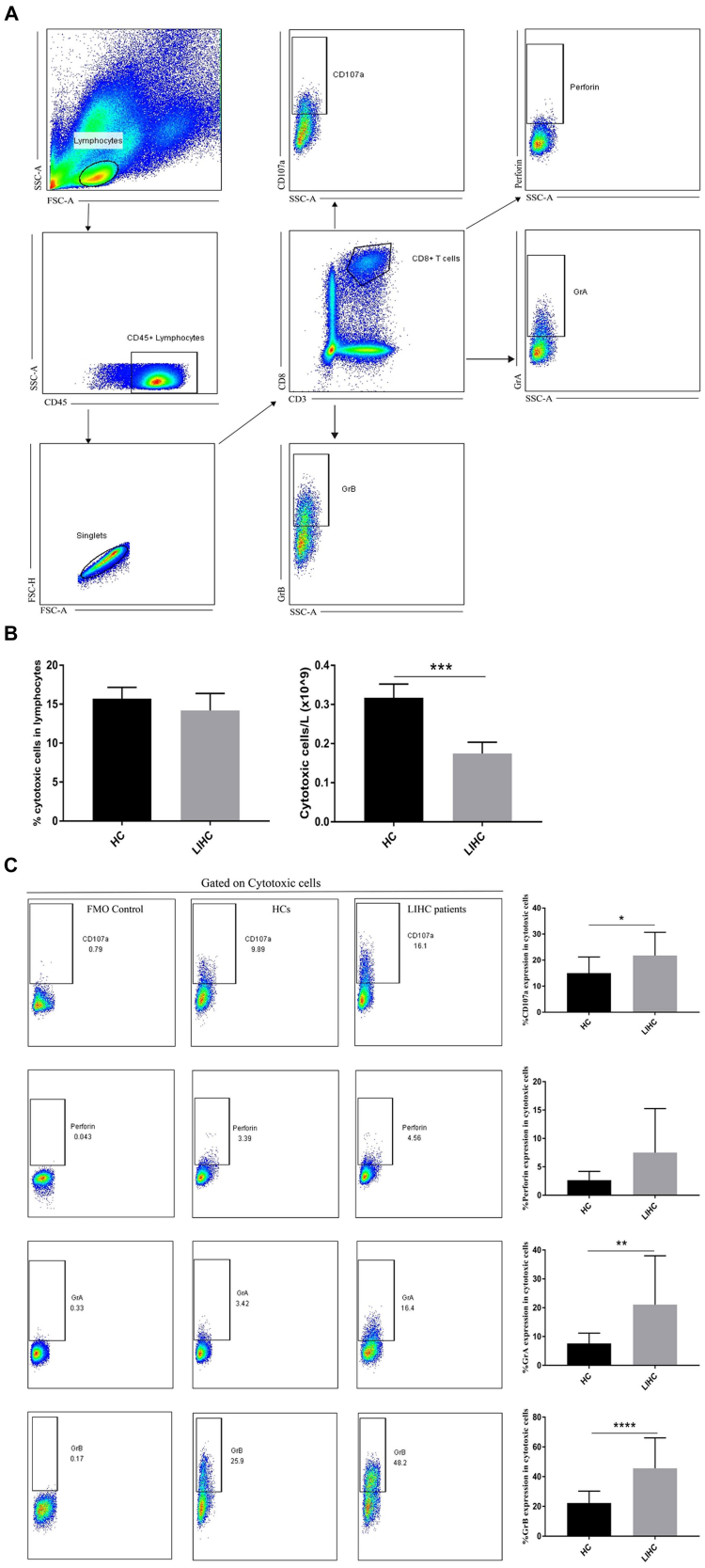

FIGURE 5
Changes of cytotoxic cells in LIHC patients. **(A)** Gate strategy of cytotoxic cell-related cytokine expression in flow cytometry. **(B)** The frequency of cytotoxic cells was not significant different between the two groups, the absolute number of cytotoxic cells in LIHC patients was significantly lower than that in HCs. **(C)** Compared to HCs, the expression of CD107a, GrA and GrB in cytotoxic cells of LIHC patients was significantly increased, while the expression of perforin was not significantly changed. GrA, granzyme A; GrB, granzyme B.

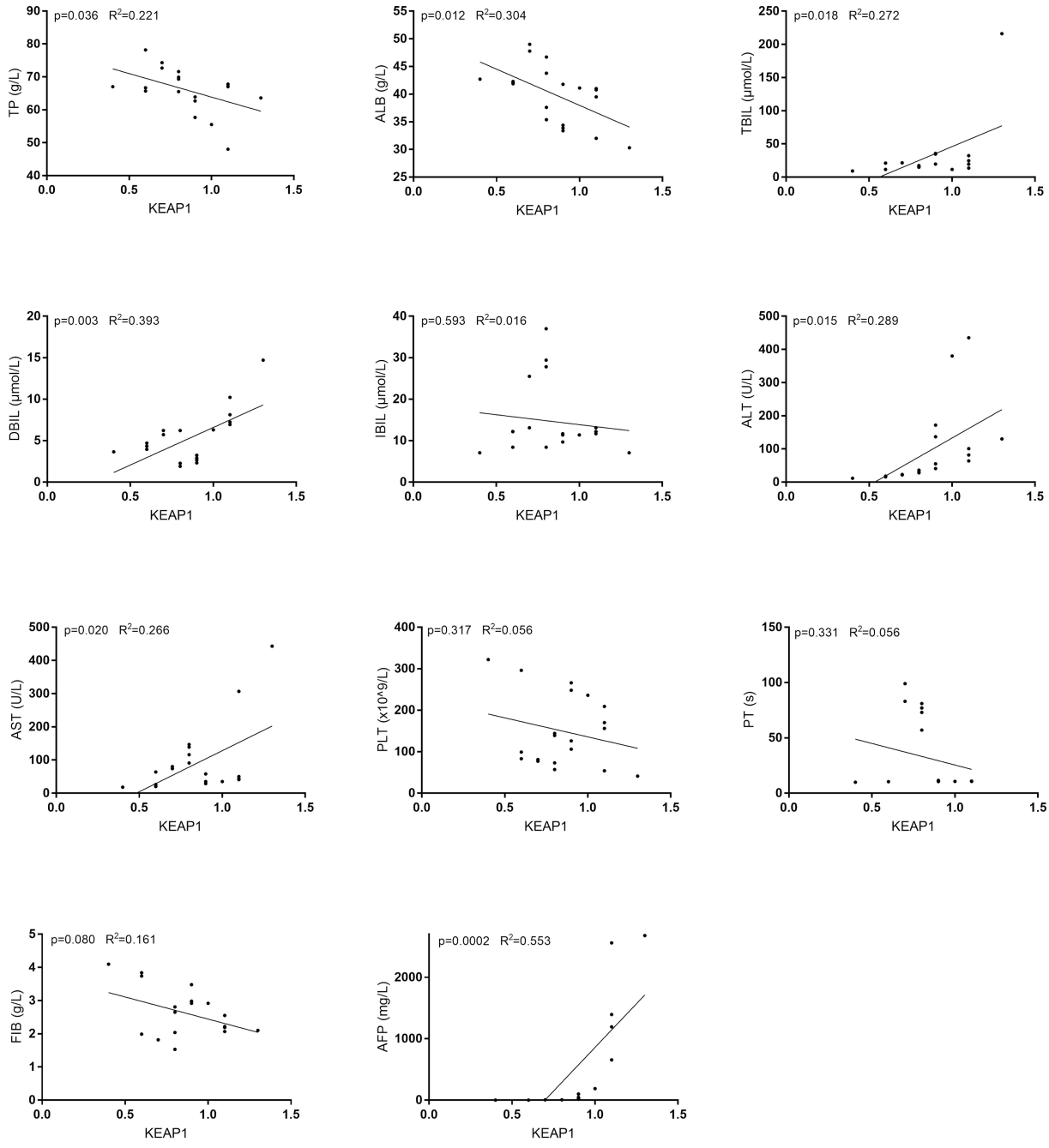

FIGURE 6
KEAP1 expression is closely related to liver function in LIHC. KEAP1 expression was significantly negatively correlated with the level of TP and ALB, and positively correlated with TBIL, DBIL, ALT, AST and AFP, but not correlated with IBIL, PLT, PT, and FIB. TP, total protein; ALB, albumin; TBIL, total bilirubin; DBIL, direct bilirubin; IBIL, indirect bilirubin; PLT, platelet; PT, prothrombin time; FIB, fibrinogen.

and present antigens. Immature DC has strong migration ability, and mature DC can effectively activate the initial T cells, which is the central link to initiate, regulate and maintain the immune response. DC, as the most functional antigen-presenting cells discovered so far, can induce the generation of specific cytotoxic T lymphocytes (25). Cytotoxic T lymphocytes are extremely important members of anti-virus and anti-tumor immunity, they kill target cells by directly contacting or secreting perforin and granzyme, which is an indispensable part of immune defense and immune surveillance (26). In this study, two widespread cell groups (Th2 cells and Cytotoxic cells), which are positively and negatively correlated with KEAP1 expression in LIHC, were selected for functional analysis to assist in judging the immune status of LIHC patients. It was found that the expression level of IL-4 in Th2 cells of LIHC patients was significantly increased, suggesting that its immune regulatory function might be enhanced. In addition, the expression of CD107a in cytotoxic cells of LIHC patients was significantly enhanced, suggesting increased degranulation ability. Perforin and granzyme are the main molecules of cytotoxic cells mediating killing function and are

secreted by degranulation. Therefore, we further examined the expression level of perforin and granzyme in cytotoxic cells of LIHC patients. The results showed that as compared with HCs, although there was no significant change in the expression of perforin in cytotoxic cells of LIHC patients, the expression levels of granzyme A and granzyme B were significantly increased, suggesting that the immune activity of cytotoxic cells in LIHC patients may be enhanced. These results suggest that there may be significant changes in immune cell function in LIHC patients, but the effects of these changes on body immunity and liver immunity, as well as the effects on liver injury and repair still need to be further explored. Besides, we have not further studied the effect of abnormal KEAP1 expression on immune cell function, which is our shortcoming and one of the research directions to be carried out in the future. In addition, our study found that KEAP1 expression was associated with liver function related indicators, and its increase was positively correlated with the increase of aminotransferase and bilirubin, while negatively correlated with the level of TP and ALB, suggesting that the increase of KEAP1 expression may mediate liver injury. Wang et al. found that TNF-α can promote ECV304 cell injury, and this injury may be inhibited by regulating KEAP1-Nrf2 signaling pathway, suggesting that KEAP1 plays a role in cell injury through related pathways (27). However, the mechanism of how KEAP1 mediates liver injury in LIHC patients is still unclear and deserves further study.

In conclusion, this study revealed that highly expressed KEAP1 is closely related to the diagnosis, prognosis, immune infiltration, and liver function of LIHC, which might promote the progression of LIHC through regulating cell development, signal transduction, and abnormal immune responses. The current study partially revealed the role of KEAP1 in LIHC and may have positive implications for enriching the diagnosis, prognosis and treatment of LIHC.

Data availability statement

The datasets presented in this study can be found in online repositories. The names of the repository/repositories and accession number(s) can be found in the article/Supplementary material.

Ethics statement

The studies involving humans were approved by the ethics committee of the First Affiliated Hospital of Anhui Medical University. The studies were conducted in accordance with the local legislation and institutional requirements. The participants provided their written informed consent to participate in this study.

Author contributions

XW: Data curation, Formal analysis, Writing – original draft, Writing – review & editing. YT: Investigation, Software, Writing – original draft. MZ: Conceptualization, Formal analysis, Project administration, Writing – review & editing. YX: Conceptualization, Formal analysis, Project administration, Writing – review & editing. ZW: Conceptualization, Formal analysis, Project administration, Writing – review & editing.

Funding

The author(s) declare that financial support was received for the research, authorship, and/or publication of this article. This work was supported by the Youth Cultivation Program of the First Affiliated Hospital of Anhui Medical University [grant number: 2021kj18].

Acknowledgments

We thank all the volunteers who participated in this study and The Cancer Genome Atlas Program.

Conflict of interest

The authors declare that the research was conducted in the absence of any commercial or financial relationships that could be construed as a potential conflict of interest.

Publisher's note

Supplementary material

The Supplementary material for this article can be found online at: https://www.frontiersin.org/articles/10.3389/fmed.2024.1391843/full#supplementary-material

References

1. Sung H, Ferlay J, Siegel RL, Laversanne M, Soerjomataram I, Jemal A, et al. Global Cancer statistics 2020: GLOBOCAN estimates of incidence and mortality worldwide for 36 cancers in 185 countries. *CA Cancer J Clin*. (2021) 71:209–49. doi: 10.3322/caac.21660

2. Vogel A, Meyer T, Sapisochin G, Salem R, Saborowski A. Hepatocellular carcinoma. *Lancet*. (2022) 400:1345–62. doi: 10.1016/S0140-6736(22)01200-4

3. Llovet JM, Kelley RK, Villanueva A, Singal AG, Pikarsky E, Roayaie S, et al. Hepatocellular carcinoma. *Nat Rev Dis Prim*. (2021) 7:6. doi: 10.1038/s41572-020-00240-3

4. Lu MC, Ji JA, Jiang ZY, You QD. The KEAP1-Nrf2-ARE pathway as a potential preventive and therapeutic target: an update. *Med Res Rev*. (2016) 36:924–63. doi: 10.1002/med.21396

5. Sun X, Ou Z, Chen R, Niu X, Chen D, Kang R, et al. Activation of the p62-KEAP1-NRF2 pathway protects against ferroptosis in hepatocellular carcinoma cells. *Hepatology*. (2016) 63:173–84. doi: 10.1002/hep.28251

6. Wasik U, Milkiewicz M, Kempinska-Podhorodecka A, Milkiewicz P. Protection against oxidative stress mediated by the Nrf2/KEAP1 axis is impaired in primary biliary cholangitis. *Sci Rep*. (2017) 7:44769. doi: 10.1038/srep44769

7. Wu L, Pan C, Wei X, Shi Y, Zheng J, Lin X, et al. lncRNA KRAL reverses 5-fluorouracil resistance in hepatocellular carcinoma cells by acting as a ceRNA against miR-141. *Cell Commun Signal*. (2018) 16:47. doi: 10.1186/s12964-018-0260-z

8. Liu J, Lichtenberg T, Hoadley KA, Poisson LM, Lazar AJ, Cherniack AD, et al. An integrated TCGA Pan-cancer clinical data resource to drive high-quality

survival outcome analytics. *Cell*. (2018) 173:400–416.e11. doi: 10.1016/j.cell.2018.02.052

9. Hänzelmann S, Castelo R, Guinney J. GSVA: gene set variation analysis for microarray and RNA-seq data. *BMC bioinformatics*. (2013) 14:1–15. doi: 10.1186/1471-2105-14-7

10. Bindea G, Mlecnik B, Tosolini M, Kirilovsky A, Waldner M, Obenauf AC, et al. Spatiotemporal dynamics of intratumoral immune cells reveal the immune landscape in human cancer. *Immunity*. (2013) 39:782–95. doi: 10.1016/j.immuni.2013.10.003

11. Yu G, Wang LG, Han Y, He QY. clusterProfiler: an R package for comparing biological themes among gene clusters. *OMICS*. (2012) 16:284–7. doi: 10.1089/omi.2011.0118

12. Subramanian A, Tamayo P, Mootha VK, Mukherjee S, Ebert BL, Gillette MA, et al. Gene set enrichment analysis: a knowledge-based approach for interpreting genome-wide expression profiles. *Proc Natl Acad Sci USA*. (2005) 102:15545–50. doi: 10.1073/pnas.0506580102

13. Bureau of Medical Administration. National Health Commission of the People's Republic of China. Standardization for diagnosis and treatment of hepatocellular carcinoma (2022 edition). *Zhonghua Gan Zang Bing Za Zhi*. (2022) 30:367–88. doi: 10.3760/cma.j.cn501113-20220413-00193

14. Love MI, Huber W, Anders S. Moderated estimation of fold change and dispersion for RNA-seq data with DESeq2. *Genome Biol*. (2014) 15:550. doi: 10.1186/s13059-014-0550-8

15. Mele L, Del Vecchio V, Marampon F, Regad T, Wagner S, Mosca L, et al. β2-AR blockade potentiates MEK1/2 inhibitor effect on HNSCC by regulating the Nrf2-mediated defense mechanism. *Cell Death Dis*. (2020) 11:850. doi: 10.1038/s41419-020-03056-x

16. Liu GY, Zhang W, Chen XC, Wu WJ, Wan SQ. Diagnostic and prognostic significance of KEAP1 mRNA expression for lung Cancer based on microarray and clinical information from Oncomine database. *Curr Med Sci*. (2021) 41:597–609. doi: 10.1007/s11596-021-2378-2

17. Rodrigues JFV, de Souza GAP, Abrahão JS, Amaral RP, de Castro RFG, Malaquias LCC, et al. Integrative transcriptome analysis of human cells treated with silver nanoparticles reveals a distinct cellular response and the importance of inorganic elements detoxification pathways. *Biochim Biophys Acta Gen Subj*. (2022) 1866:130116. doi: 10.1016/j.bbagen.2022.130116

18. Kim JW, Herz J, Kavalali ET, Monteggia LM. A key requirement for synaptic Reelin signaling in ketamine-mediated behavioral and synaptic action. *Proc Natl Acad Sci USA*. (2021) 118:e2103079118. doi: 10.1073/pnas.2103079118

19. Yasmin F, Colangeli R, Morena M, Filipski S, van der Stelt M, Pittman QJ, et al. Stress-induced modulation of endocannabinoid signaling leads to delayed strengthening of synaptic connectivity in the amygdala. *Proc Natl Acad Sci USA*. (2020) 117:650–5. doi: 10.1073/pnas.1910322116

20. Smith NK, Hackett TA, Galli A, Flynn CR. GLP-1: molecular mechanisms and outcomes of a complex signaling system. *Neurochem Int*. (2019) 128:94–105. doi: 10.1016/j.neuint.2019.04.010

21. Tu W, Wang H, Li S, Liu Q, Sha H. The anti-inflammatory and anti-oxidant mechanisms of the Keap1/Nrf2/ARE signaling pathway in chronic diseases. *Aging Dis*. (2019) 10:637–51. doi: 10.14336/AD.2018.0513

22. Holze C, Michaudel C, Mackowiak C, Haas DA, Benda C, Hubel P, et al. Oxeiptosis, a ROS-induced caspase-independent apoptosis-like cell-death pathway. *Nat Immunol*. (2018) 19:130–40. doi: 10.1038/s41590-017-0013-y

23. Li S, Wen P, Zhang D, Li D, Gao Q, Liu H, et al. PGAM5 expression levels in heart failure and protection ROS-induced oxidative stress and ferroptosis by Keap1/Nrf2. *Clin Exp Hypertens*. (2023) 45:2162537. doi: 10.1080/10641963.2022.2162537

24. Basu A, Ramamoorthi G, Albert G, Gallen C, Beyer A, Snyder C, et al. Differentiation and regulation of TH cells: a balancing act for cancer immunotherapy. *Front Immunol*. (2021) 12:669474. doi: 10.3389/fimmu.2021.669474

25. Collin M, Bigley V. Human dendritic cell subsets: an update. *Immunology*. (2018) 154:3–20. doi: 10.1111/imm.12888

26. Raskov H, Orhan A, Christensen JP, Gögenur I. Cytotoxic CD8+ T cells in cancer and cancer immunotherapy. *Br J Cancer*. (2021) 124:359–67. doi: 10.1038/s41416-020-01048-4

27. Wang CM, Li YJ, Li JJ, Zang YL, Cui XH, Song M, et al. Shenlian extract attenuates TNF-α-induced ECV304 injury by regulating Nrf2/Keap1 signaling pathway. *Zhongguo Zhong Yao Za Zhi*. (2021) 46:3402–9. doi: 10.19540/j.cnki.cjcmm.20210224.401

frontiers | Frontiers in Medicine

TYPE Original Research
PUBLISHED 11 July 2024
DOI 10.3389/fmed.2024.1420353

OPEN ACCESS

EDITED BY
Pradeep Kumar Shukla,
University of Tennessee Health Science Center (UTHSC), United States

REVIEWED BY
Komal Ramani,
Cedars Sinai Medical Center, United States
Da Sun,
Wenzhou University, China

*CORRESPONDENCE
Chunxiao Wei
✉ 469077208@qq.com
Zhong Huang
✉ 269481015@qq.com

†These authors have contributed equally to this work and share first authorship

RECEIVED 20 April 2024
ACCEPTED 01 July 2024
PUBLISHED 11 July 2024

CITATION
Li Y, Fang Y, Li D, Wu J, Huang Z, Liao X, Liu X, Wei C and Huang Z (2024) Constructing a prognostic model for hepatocellular carcinoma based on bioinformatics analysis of inflammation-related genes.
Front. Med. 11:1420353.
doi: 10.3389/fmed.2024.1420353

Constructing a prognostic model for hepatocellular carcinoma based on bioinformatics analysis of inflammation-related genes

Yinglian Li[1†], Yuan Fang[1†], DongLi Li[2†], Jiangtao Wu[1], Zichong Huang[1], Xueyin Liao[1], Xuemei Liu[1], Chunxiao Wei[1*] and Zhong Huang[1*]

[1]Department of Oncology, Kaiyuan Langdong Hospital of Guangxi Medical University, Nanning, China, [2]Radiology Department, Guangxi Zhuang Autonomous Region People's Hospital, Nanning, China

Background: This study aims to screen inflammation-related genes closely associated with the prognosis of hepatocellular carcinoma (HCC) to accurately forecast the prognosis of HCC patients.

Methods: Gene expression matrices and clinical information for liver cancer samples were obtained from the Cancer Genome Atlas (TCGA) and the International Cancer Genome Consortium (ICGC). An intersection of differentially expressed genes of HCC and normal and GeneCards yielded inflammation-related genes associated with HCC. Cox regression and the minor absolute shrinkage and selection operator (LASSO) regression analysis to filter genes associated with HCC prognosis. The prognostic value of the model was confirmed by drawing Kaplan–Meier and ROC curves. Select differentially expressed genes between the high-risk and low-risk groups and perform GO and KEGG pathways analyses. CIBERSORT analysis was conducted to assess associations of risk models with immune cells and verified using real-time qPCR.

Results: A total of six hub genes (C3, CTNNB1, CYBC1, DNASE1L3, IRAK1, and SERPINE1) were selected using multivariate Cox regression to construct a prognostic model. The validation evaluation of the prognostic model showed that it has an excellent ability to predict prognosis. A line plot was drawn to indicate the HCC patients' survival, and the calibration curve revealed satisfactory predictability. Among the six hub genes, C3 and DNASE1L3 are relatively low expressed in HCCLM3 and 97H liver cancer cell lines, while CTNNB1, CYBC1, IRAK1, and SERPINE1 are relatively overexpressed in liver cancer cell lines.

Conclusion: One new inflammatory factor-associated prognostic model was constructed in this study. The risk score can be an independent predictor for judging the prognosis of HCC patients' survival.

KEYWORDS

hepatocellular carcinoma, inflammation-related genes, prognostic model, risk score, tumor immune infiltration

1 Introduction

Worldwide, hepatocellular carcinoma (HCC) is the most common malignant tumor. HCC patients are mostly at an advanced stage when diagnosed and have a poor prognosis (1). The most severe result of uncontrolled hepatocyte growth is the occurrence of HCC, whose progression and metastasis are inseparable from the deterioration of the liver regeneration microenvironment (2). The drug therapy for HCC encompasses a variety of treatment modalities. As the first FDA-approved systemic therapy for advanced HCC, Sorafenib remains a cornerstone treatment, primarily due to its ability to extend survival (3, 4). Following Sorafenib, other drugs such as Regorafenib, Cabozantinib, and Lenvatinib have been approved for use (5). These drugs target various tumor growth pathways and angiogenesis pathways (3, 5). Drugs like Nivolumab and Pembrolizumab have shown promise in treating HCC by enhancing the body's immune response against tumor cells (6). Combining Sorafenib with immune checkpoint inhibitors may improve treatment efficacy (7, 8). However, due to the insidious nature of HCC development, high recurrence rate after surgical resection, and high transplantation failure rate, improving the prognosis of HCC patients and identifying new molecular targets for drug development still faces multiple challenges, including those involved in cancer metabolism, immune evasion, and cell survival (9).

Chronic inflammation caused by viral infection significantly increases the possibility of HCC development by activating inflammatory signaling pathways and cytokines (10). The inflammatory pathways are complex and highly interconnected with multiple feedback loops and interactions. This complexity makes it difficult to predict how modulating one pathway might affect others, potentially leading to unintended consequences (11, 12). Thus, inflammation is a significant driver of cancer progression. The expression and role of inflammation-related genes can differ significantly among tumors, complicating the development of universally effective treatments (13, 14). Tumor cells can develop resistance to therapies that target inflammation-related pathways, often through genetic mutations or by activating alternative pathways (15). This adaptation can reduce the long-term efficacy of these treatments (16). Developing computational models that simulate individual responses to therapies targeting inflammation-related genes may help optimize treatment strategies (17, 18). Integrating inflammation-related genes into tumor therapy for conditions like HCC presents significant opportunities. Exploring the correlation between inflammation-related genes and tumor immune status may help further integrate targeted therapy and immunotherapy (19, 20).

Immune inflammation involves the immune system's response to cancer cells, which can either suppress tumor growth or contribute to tumor development and progression (21). Inflammation-related genes are crucial in this context as they can influence the tumor microenvironment, affecting the behavior of HCC. HCC is a highly heterogeneous disease, and the genetic profile can vary significantly among patients, complicating creating a universally applicable model (22). Some studies have identified and evaluated the potential prognostic value of immune-autophagy-related genes in HCC patients (23). The study's assessment was based on the complex interplay between the immune system, autophagy processes, and the tumor microenvironment in liver cancer (24). However, further research is still needed to explore the complex interactions between inflammation-related genes and other pathways in HCC. We identify inflammation-related genes that are significantly altered in HCC. Integrate data from different sources and use statistical and machine learning models to analyze the relationship between the expression of inflammation-related genes and patient survival. Techniques such as the proportional hazards model (25) can be used to estimate risk based on gene expression levels. Due to a more aggressive tumor microenvironment, certain patients with high expression of pro-inflammatory genes may have a poorer prognosis. We also used models to classify patients into risk groups and examine their immune microenvironment. Our model can predict patient survival while helping clinicians plan treatment more efficiently.

2 Materials and methods

2.1 Data acquisition and preparation

This study downloaded the normalized RNA-Seq data set of 371 HCC samples and 50 adjacent normal samples and the corresponding clinical information from the UCSC Xena browser.[1] The clinical information includes follow-up time, survival status, age, gender, TNM stage, and overall stage of HCC patients. Download the LIRI-JP HCC data set of the ICGC database from the Sangerbox platform[2] as an independent validation set for the prognostic model containing RNA-Seq data of 240 HCC tumor samples and corresponding clinical information. The sample data uses standardized count values. Inclusion and exclusion processing criteria: (1) exclude samples without clinical follow-up data; (2) exclude those without TTL data; (3) exclude those without information related to patient survival status; (4) convert ENSEMBL ID to gene symbols, and (5) If multiple gene symbolic expressions exist, the median value is recorded. The clinical data of these samples are shown in Supplementary Table S1. Inflammation-related genes were searched in the GeneCard database using the keyword "inflammation."

2.2 Screening of differentially expressed inflammation-related genes related to HCC

RStudio version 4.1.0 and the "Limma" software package (26) were used to screen differentially expressed genes (DEGs) between HCC and adjacent normal samples. First, genes with an average count of less than one were excluded, and genes were screened based on the criteria that the absolute value of the Log2-transformed fold change (FC) was more significant than or equal to 4, and the significance p value was less than 0.01. The genes that met the conditions were selected as DEGs, among which log2FC greater than 4 is an up-regulated gene, and less than −4 is a down-regulated gene. Use the "ggplot2" R software package (27, 28) to draw a volcano plot to visualize the results. Next, a correlation coefficient greater than six was used as the screening criterion to obtain inflammation-related genes from the GeneCards database (29). Finally, the intersection of DEGs

1 https://xenabrowser.net/datapages/

2 https://dcc.icgc.org/

and inflammation-related genes was used to obtain differentially expressed inflammation-related genes in HCC, and Venny online software[3] (30) was used to draw a Venn diagram for visualization. The "survival" R software package (31) performed Univariate Cox regression analysis (25) on differentially expressed inflammation-related genes in HCC. Genes with p less than 0.05 were differentially expressed inflammation-related genes related to prognosis. This gene is a risk factor for the prognosis of HCC (The hazard Ratio (HR) > 1). This gene is a protective factor for the prognosis of HCC(HR < 1).

2.3 Least absolute shrinkage and selection operator regression and construction of the prognostic model

The 50 paracancerous and HCC samples with missing survival information downloaded from the TCGA database were eliminated, and 365 hepatocellular carcinoma samples were retained as a training set for constructing the prognostic model. To further screen variables, the "glmnet" R software package (32) was used to perform Lasso (Least absolute shrinkage and selection operator is a type of linear regression that includes a penalty equal to the absolute value of the magnitude of coefficients.) regression analysis on the differentially expressed inflammation-related genes related to HCC prognosis screened out in the above Univariate Cox regression analysis to reduce the purpose of the fitting degree of the constructed prognostic model. During the Lasso regression analysis process, 10-fold cross-validation was used to determine the λ value, and the λ with the minor partial likelihood deviation was selected as the optimal λ. Cross-validation in Lasso regression ensures the model is tuned for optimal performance by finding the best regularization parameter (alpha). K-Fold Cross-Validation: Choose the number of folds (typically 5 or 10). Split the dataset into k folds. Each fold will be used once as a validation set, while the remaining $k-1$ folds form the training set. The genes screened by Lasso regression analysis in the previous step were further used to perform Multivariate Cox regression analysis using the "survival" R software package. In the Multivariate Cox regression analysis results, genes with p less than 0.05 were considered independent factors affecting the prognosis of HCC patients. The coefficients for Multivariate Curve Resolution (MCR) analysis (33) were adopted for calculating the RS.

In the TCGA-LIHC cohort, the samples were assigned to a high-risk or low-risk group (cut-off: 50%). The risk score of each HCC patient was calculated according to the prognostic model, and the patients were divided according to the median risk score. Patients whose risk score was higher than the median risk score were divided into high-risk groups. Next, the "survival" software package is used to draw the Kaplan–Meier curve(a statistical tool used in survival analysis to estimate the survival function from lifetime data); the "survival," "survminer," and "timeROC" software packages (22) are used to evaluate the prognosis. The ability of the model to predict the 1-year, 2-year, and 3-year survival rates of HCC patients. Finally, the ROC curves of the 1-year, 2-year, and 3-year survival rates of HCC patients in the prediction training set of age, gender, TNM stage, total stage, and risk score prediction training set were plotted to compare the corresponding AUC values further to illustrate the predictive ability of the prognostic model. Clinicopathological characteristics, including age, gender, TNM stage, total stage, and risk score, were integrated, and the nomogram was constructed using "rms" packages in R.

Akaike information criterion (AIC) (34) is a standard for evaluating the complexity of a statistical model and measuring the goodness of fit of a statistical model to the data. AIC can be expressed as $AIC = 2k - 2\ln(L)$. Where k is the number of parameters and L is the likelihood function. When the complexity of the model increases (k increases), the likelihood function L will also increase, thereby making the AIC smaller. However, when k is too large, the growth rate of the likelihood function slows down, causing the AIC to increase. If the model is too complex, it is easy to cause an Overfitting phenomenon.

2.4 Gene enrichment analysis

To better understand the biological functions of DEGs between high-risk groups and low-risk groups in the training set, four R software packages: "clusterProfiler" (35), "org.Hs.eg.db" (36), "enrich plot," and "GOplot" (37) were used. For GO and KEGG functional enrichment analysis, $p < 0.05$ after correction was set as the screening condition.

2.5 Tumor-infiltrating immune cells

To evaluate the difference in immune infiltration of tumor tissue between high-risk and low-risk groups in the training set and the association between risk score and immune infiltration of tumor tissue. This study used a gene expression matrix to perform ESTIMATE (38) analysis to calculate each sample's stromal score, immune score, ESTIMATE score, and tumor purity. The TIMER algorithm calculated each sample's infiltration of six tumor-infiltrating immune cell subsets (B cells, CD4+ T cells, CD8+ T cells, macrophages, neutrophils, and dendritic cells). Finally, the correlation between the risk score calculated based on the prognostic model and tumor immune infiltration was analyzed.

2.6 Cell line

The normal human liver cell line LO2 and two human hepatocellular carcinoma cell lines (97H and HCCLM3) were purchased from Saiku Biotech Co. The complete medium for culturing cells was prepared using Dulbecco's modified medium (DMEM) with 10% fetal calf serum and 1% double antibody (penicillin/streptomycin).

2.7 Real-time fluorescence quantitative PCR experimental materials

The human regular liver cell line is LO2, and there are two human liver cancer cell lines (97H and HCCLM3). The complete medium for

3 https://bioinfogp.cnb.csic.es/tools/venny/

culturing cells was prepared using Dulbecco's modified medium (DMEM) with 10% fetal calf serum and 1% double antibody (penicillin/streptomycin). Total cellular RNA was extracted using the TRIZOL method. The concentration of extracted RNA was measured by NanoDrop2000 (UV spectroscopy) and was not less than 50ug. Intact total RNA produces clear 28S and 18S rRNA bands when subjected to denaturing gel electrophoresis (2:1). Carry out the entire reverse transcription reaction according to the instructions of TaKaRa Reverse Transcription Kit PrimeScrip™ RT reagent Kit with gDNA Eraser (Perfect Real Time), shown in Supplementary Table S2. Dissolve the FastStart Universal SYBR Green Master (ROX), the upstream primer (Forward primer), and the downstream primer (Reverse primer) on ice for later use. Follow the instructions to prepare the components and configure a 10 μL reaction system. Configure a main tube according to the above features, mix gently with a pipette and centrifuge, and add samples sequentially. Set 4 duplicate wells for each sample. The real-time fluorescence quantitative PCR (qTOWER^3 Series, Analytik Jena, Germany) reaction procedure, shown in Supplementary Table S3, is described in the instructions. The DNA solubilization curve verifies the specificity of the amplification product. From 60 to 98 degrees, the horizontal coordinates of the curve are each temperature point. The vertical coordinate is the change in fluorescence intensity. When the amplification rate of the target genes (C3, CTNNB1, CYBC1, DNASE1L3, IRAK1, SERPINE1) reaches 100%, the cycle threshold is obtained [Linear dynamic range (12–30)] and the relative expression of the target gene mRNA is calculated using the $2^{-\triangle\triangle Ct}$ method. Experimental results were visualized using GraphPad Prism 8 software. The specific primer sequences are shown in Table 1. The suppression test detects the extraction situation. 3 samples using the same method of repeatability (Intra-Assay Variation) to assess the intra-assay variation.

2.8 Statistical method

All statistical analyses were performed using R software (v4.1.0). The stepwise regression method was used to screen Hub genes to construct a prognostic model. The Kaplan–Meier curve compared the prognostic differences between HCC patients in the high-risk and low-risk groups. The *t*-test was used to compare the differences in risk scores between different clinicopathological characteristic groups. $p < 0.05$ (two-sided) was considered statistically significant.

3 Results

3.1 Screening of differentially expressed inflammation-related genes in HCC

Through differential expression analysis, 3,274 DEGs between HCC samples and normal liver samples were obtained, including 2,789 up-regulated genes and 485 down-regulated genes, as shown in the volcano plot in Figure 1A. 303 inflammation-related genes were retrieved from the GeneCards database. Then, we take the intersection between the database and differential genes and call these 49 intersection genes inflammation-related genes (Figure 1B). Then, we used the STRING database (39) to construct a Protein–Protein Interaction (PPI) network of HCC inflammation-related genes. The interaction score was set to 0.7 during PPI analysis, and Cytoscope software visualized the results (Figure 1C).

3.2 GO and KEGG enrichment analysis

We performed GO and KEGG functional enrichment analysis on 49 inflammation-related genes. GO analysis results show that cell functions are significantly enriched in positive regulation of cytokine production, secretory granule lumen, cytokine receptor binding, etc. (Supplementary Figure S1); KEGG pathway analysis shows that it is mainly enriched in NF-κB signaling pathway, cytokine-cytokine receptor interaction, Th17 cell differentiation, etc. (Figure 1D).

3.3 Screening of prognostic model hub genes and construction of a prognostic model

Based on the prognostic information of tumor samples in the training set, univariate Cox regression analysis ($p < 0.05$) was performed on 49 differentially expressed inflammation-related genes in HCC, and 16 genes significantly related to the prognosis of HCC were screened out (C3, CASP3, CTNNB1, CYBC1, and DNASE1L3), (IRAK1, RELA, SERPINE1, SPP1, TGFB1, TNIP1, TTR, UBA1, UBAC2, UBE2L3, and VEGFA), as shown in Figure 1E. Then, Lasso regression analysis was further performed on 16 inflammation-related genes related to the prognosis of HCC patients to obtain 11 genes (C3, CTNNB1, CYBC1, DNASE1L3, IRAK1, SERPINE1, SPP1, UBA1, UBAC2, UBE2L3, and VEGFA), as shown in Figure 1F. Finally, the

TABLE 1 Specific primer sequence.

Gene	Upstream primer	Downstream primer
GAPDH	TGACTTCAACAGCGACACCCA	CACCCTGTTGCTGTAGCCAAA
DNASE1L3	TGGTTGAGGTCTACACGGACGT	GTCAGTCCTCAAGCGGATGTTC
C3	TCACCGTCAACCACAAAGCTGCTACC	TTTCATAGTAGGCTCGGATCTTCCA
CTNNB1	GGCTCTTGTGCGTACTGTCCTTC	CTTGGTGTCGGCTGGTCAGATG
CYBC1	TGTGAGCGTGGAGGAGGAGAAG	CTGGTGATGAGCTTGGCGATGG
IRAK1	GACACGGACACCTTCAGCTTTGG	CAGCCTCCTCAGCCTCCTCTTC
SERPINE1	GGTGCTGGTGAATGCCCTCTAC	TGCTGCCGTCTGATTTGTGGAAG

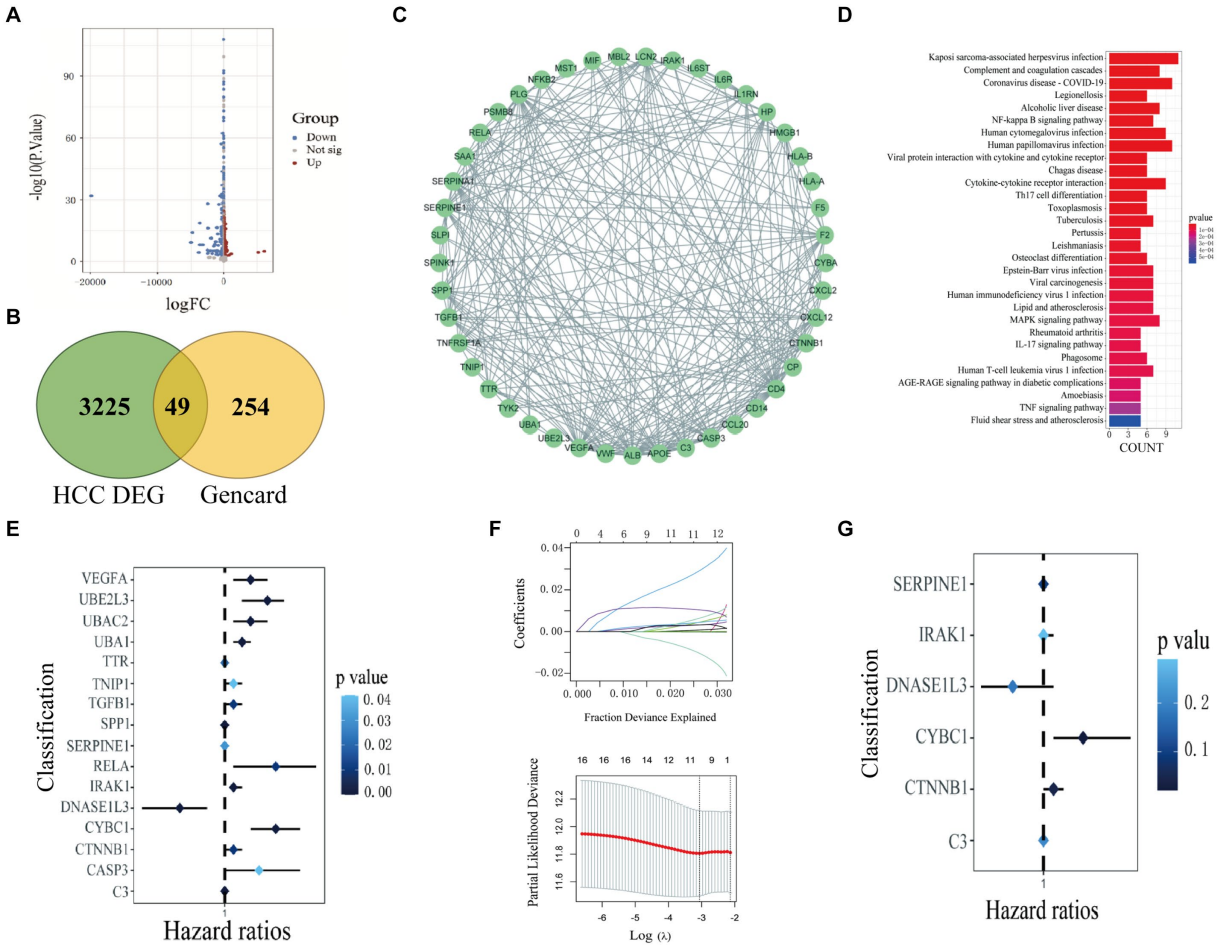

FIGURE 1
Screening of inflammation-related genes in HCC. **(A)** Volcano plot of DEGs in liver cancer; **(B)** Venn diagram of DEGs and inflammation-related genes; **(C)** PPI network of inflammation-related genes in liver cancer. **(D)** KEGG analysis of inflammation-related genes. **(E)** The risk ratio forest plot showed the prognostic value of the genes based on univariate Cox regression analysis. **(F)** Lasso regression analysis and Cross-validation. **(G)** The risk ratio forest plot showed the prognostic value of the genes based on multivariate Cox regression analysis.

above 11 genes were screened using the Step calculation function in multifactor Cox regression analysis based on the AIC information statistic. When AIC was equal to 1316.19, the results were obtained based on 6 Hub genes (C3, CTNNB1, CYBC1, DNASE1L3, the optimal prognostic model constructed by IRAK1, SERPINE1). As shown in Figure 1G, multivariate Cox regression risk showed that CYBC1 (HR = 1.04, 95%CI = 1.01–1.09, $p = 0.02$) among the six Hub genes was an independent prognostic risk factor for HCC patients. A prognostic model is constructed through regression coefficients. In the prognostic model, the risk score calculation formula for each HCC sample is Risk score = (−0.000337128 × C3) + (0.009464722 × CTNNB1) + (0.045920338 × CYBC1) + (−0.035384453 × DNASE1L3) + (0.007516301 × IRAK1) + (0.001958146 × SERPINE1). The risk scores of all HCC patients in the training set were calculated according to the prognostic model formula. Patients with risk scores higher than the median were classified into the high-risk group and others as the low-risk group. Figure 2A shows that the risk scores of HCC patients gradually increase from left to right. It can be seen from Figure 2A that as the risk score increases, the survival time of patients in the high-risk group is shorter (the trend of concentration of scattered points is downward), and the mortality rate is higher (red dots increase). Figure 2A shows the differential expression of six Hub genes between the high-risk and low-risk groups in the form of a heat map. The expression of four genes, SERPINE1, IRAK1, CTNNB1, and CYBC1, was relatively up-regulated in the high-risk group. The expression of C3 and DNASE1L3 Expression was moderately upregulated in the low-risk group.

3.4 Verification of pivot genes

The patients' risk scores in the training set were comprehensively analyzed with the corresponding clinicopathological characteristics (age, gender, TNM stage, and total stage). Single-factor Cox regression analysis showed that the risk score ($p < 0.001$), M stage ($p = 0.01$), N Stage ($p = 0.04$), T stage ($p < 0.001$), and total stage ($p < 0.001$) are significantly related to the prognosis of HCC (Figure 2B). Multivariate Cox regression analysis showed that risk score (HR = 1.52, 95%CI = 1.31–1.75, $p < 0.001$) and M stage (HR = 1.33, 95%CI = 1.02–1.72, $p = 0.03$) are essential factors affecting the prognosis of HCC patients. Independent risk factors (Figure 2C). The ROC curve was used to evaluate the accuracy of the prognostic model, and the AUC

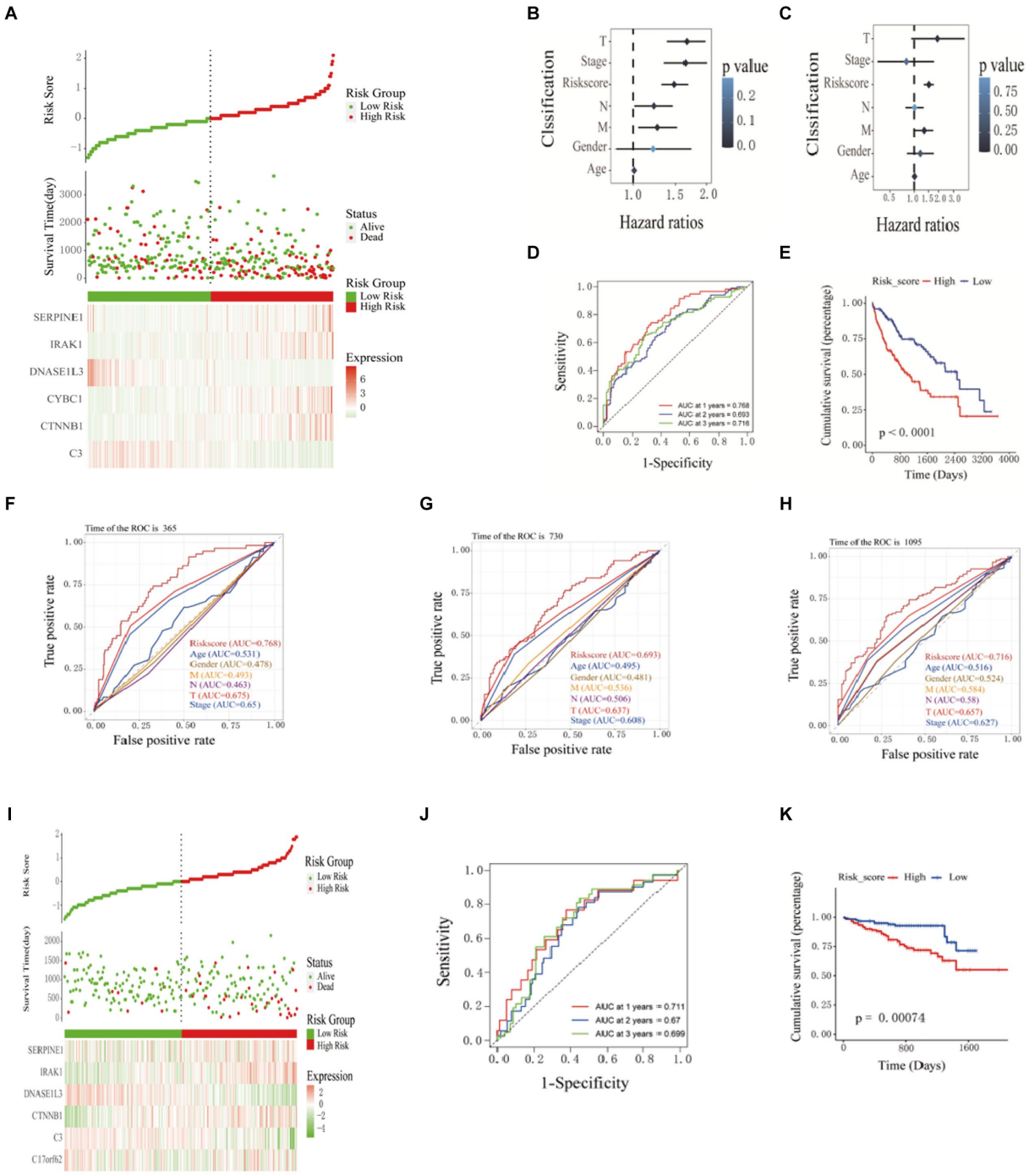

FIGURE 2
Construction and validation of prognostic models. **(A)** Prognostic distribution of HCC, differences in survival status between high-risk and low-risk groups, and heat maps of the expression profiles of the six hub genes. The risk score and clinicopathological features are subjected to univariate **(B)** and multivariate **(C)** Cox regression analysis, as illustrated in the forest plot. **(D)** Kaplan–Meier survival curves and **(E)** time-dependent ROC curves. ROC curve verified the significance of the prognostic model **(F)** 365 days, **(G)** 730 days, and **(H)** 1,065 days. **(I)** Distribution of prognostic index. Survival status of patients in different groups. Heat map of the expression profile of the included inflammation-related genes. **(J-K)** Kaplan-Meier survival curves and time-dependent ROC curves.

values for predicting the 1-, 2-, and 3-year survival rates of HCC patients in the training set were 0.768, 0.693 and 0.716, respectively (Figure 2D). The Kaplan–Meier curve showed that the prognosis of the high-risk group was worse than that of the lower-risk group, and the difference was statistically significant ($p < 0.0001$) (Figure 2E). The ROC curve(is a graphical plot used to evaluate the performance of a binary classifier system. It plots the true positive rate (TPR) against the false positive rate (FPR) at various threshold settings) and was used to verify the predictive performance of the prognostic model. In the ROC curve predicting the 1-year (Figure 2F), 2-year (Figure 2G), and 3-year (Figure 2H) survival rates of HCC patients in the training set, the AUC value of the risk score was always high. Compared with clinicopathological characteristics such as age, gender, TNM stage, and total stage, it indicates that the risk score may be a reliable

predictor of the prognosis of HCC patients. 240 HCC samples from the ICGC database were used as a validation set further to verify the reliability and accuracy of the model. The same formula was used to calculate the risk scores of the 240 HCC samples, and patients higher than the median risk score were divided into high-risk groups; otherwise, they were split into low-risk groups. The risk score distribution, survival time, and mRNA expression level distribution of the six Hub genes of the patients in the validation set are shown in Figure 2I. The AUC values for predicting 1-year, 2-year, and 3-year survival rates were 0.711, 0.67, and 0.699, respectively, (Figure 2J). The Kaplan–Meier curve showed that the prognosis of patients in the high-risk group was worse than that of the lower-risk group, and the difference was statistically significant ($p = 7.4e-4$) (Figure 2K). The research results of the validation and training sets are consistent, indicating that this prognostic model can effectively predict the prognosis of HCC patients.

3.5 Immune infiltration analysis of high and low-risk groups

ESTIMATE analysis found that the stromal cell score difference between the high and low-risk groups in the training set was statistically significant, and the low-risk group had a higher stromal cell score ($p < 0.001$). There was no statistically significant difference in immune cell score, ESTIMATE score, and tumor purity between the high-risk and low-risk groups (Figure 3A). By studying the correlation between the risk score model and the four scores, it was found that the stromal cell score was negatively correlated with the risk score ($R = -0.24$, $p = 3.9e-06$); the ESTIMATE score was negatively correlated with the risk score ($R = -0.13$, $p = 0.013$); tumor purity was positively correlated with risk score ($R = 0.13$, $p = 0.013$) (Figure 3B). Through TIMER analysis, the infiltration abundance of B cells, macrophages, neutrophils, dendritic cells, CD4+ T cells, and CD8+ T cells in HCC was higher in the high-risk group than in the lower-risk group ($p < 0.05$) (Figure 3C). By analyzing the correlation between risk score and immune cell infiltration abundance, it was found that B lymphocytes were positively correlated with risk score ($R = 0.22$, $p = 3.2e-05$); dendritic cells were positively correlated with risk score ($R = 0.26$, $p = 4.4e-07$); macrophages were positively correlated with risk score ($R = 0.26$, $p = 6.7e-07$); neutrophils were positively correlated with risk score ($R = 0.3$, $p = 6e-09$) (Figure 3D).

3.6 Combining clinical data to construct an HCC prognostic nomogram

In this study, the nomogram constructed by combining the clinicopathological characteristics and risk scores of HCC patients in the training set was used to predict the 1-year, 3-year, and 5-year survival probabilities of HCC patients (Figure 4A). C-index equals 0.697 (greater than 0.5). The 3-year actual survival rate was highly consistent with the predicted value, indicating that the constructed nomogram had good accuracy (Figure 4B). In this study, the risk score was closely related to the TNM stage and total Stage, indicating that the prognostic model helps predict the proliferation and metastasis of HCC (Figure 4C). The correlation between the expression of six Hub genes (C3, CYBC1, CTNNB1, DNASE1L3, IRAK1, and SERPINE1) constructed for prognostic modeling and the level of immune cell infiltration was analyzed using the TIMER database. The results showed that the expression of C3 in HCC was closely correlated with the infiltration of B cells, CD4+ T cells, macrophages, neutrophils, and dendritic cells ($p < 0.05$). The expression of CTNNB1 in HCC was closely correlated with the infiltration of B cells, CD4+ T cells, CD8+ T cells, and macrophages ($p < 0.05$). The expression of CYBC1 in HCC was closely correlated with the infiltration of B cells, CD4+ T cells, macrophages, neutrophils, and dendritic cells ($p < 0.05$). DNASE1L3 expression in HCC was closely associated with infiltration of B cells, CD4+ T cells, CD8+ T cells, neutrophils, and dendritic cells ($p < 0.05$). IRAK1 expression in HCC was closely associated with infiltration of B cells, CD8+ T cells, macrophages, and dendritic cells ($p < 0.05$). The expression of SERPINE1 in HCC was closely associated with the infiltration of CD8+ T cells, macrophages, neutrophils, and dendritic cells ($p < 0.05$). These results suggest that the prognostic model Hub genes are closely associated with immune infiltration, and the results are shown in Supplementary Figure S2, with $p < 0.05$ indicated by red boxes. The GEPIA database was further analyzed for six Hub genes, mRNA expression of CYBC1 (HR = 1.7, Logrank $p = 0.0036$), DNASE1L3 (HR = 0.43, Logrank $p = 2e-06$), IRAK1 (HR = 1.7, Logrank $p = 0.0042$), SERPINE1 (HR = 1.5, Logrank $p = 0.027$) mRNA expression correlated with overall survival of hepatocellular carcinoma patients as shown in Supplementary Figure S3. The mRNA expression of C3 ($F = 6.02$, $p = 0.000524$), CYBC1 ($F = 2.66$, $p = 0.0478$), DNASE1L3 ($F = 6.63$, $p = 0.000229$), IRAK1 ($F = 4.67$, $p = 0.00327$), SERPINE1 ($F = 3.73$, $p = 3.73$) and SERPINE1 ($F = 3.73$, $p = 0.0116$) was statistically significant among the groups with different hepatocellular carcinoma clinical staging as shown in Figure 4D.

3.7 Expression in human hepatocellular carcinoma cells and normal cells of the liver

As shown in Figure 5, the expression differences of the six Hub genes C3, CTNNB1, CYBC1, DNASE1L3, IRAK1, and SERPINE1 between human liver cancer cell lines and normal liver cell lines are statistically significant. C3 and DNASE1L3 are significantly different in HCCLM3 and 97H liver cancer cells. The cell lines showed relatively low expression compared with normal liver cells, while CTNNB1, CYBC1, IRAK1, and SERPINE1 showed relatively high expression in HCCLM3 and 97H liver cancer cell lines compared with normal liver cells.

4 Discussion

Studies are developing and validating a systemic immune-inflammatory index based on lymphocyte, neutrophil, and platelet counts and exploring its prognostic value in HCC (40). Other studies have found the prognostic value of prognostic nutritional index (PNI) and systemic immune-inflammatory index in hepatocellular carcinoma (41). Studies have reviewed the utility of inflammatory markers as prognostic tools in patients with resectable HCC (42). It is believed that there is currently a lack of reliable prognostic biomarkers to predict postoperative recurrence of HCC. However, we showed a prognostic model based on six inflammation-related genes, including

10.3389/fmed.2024.1420353

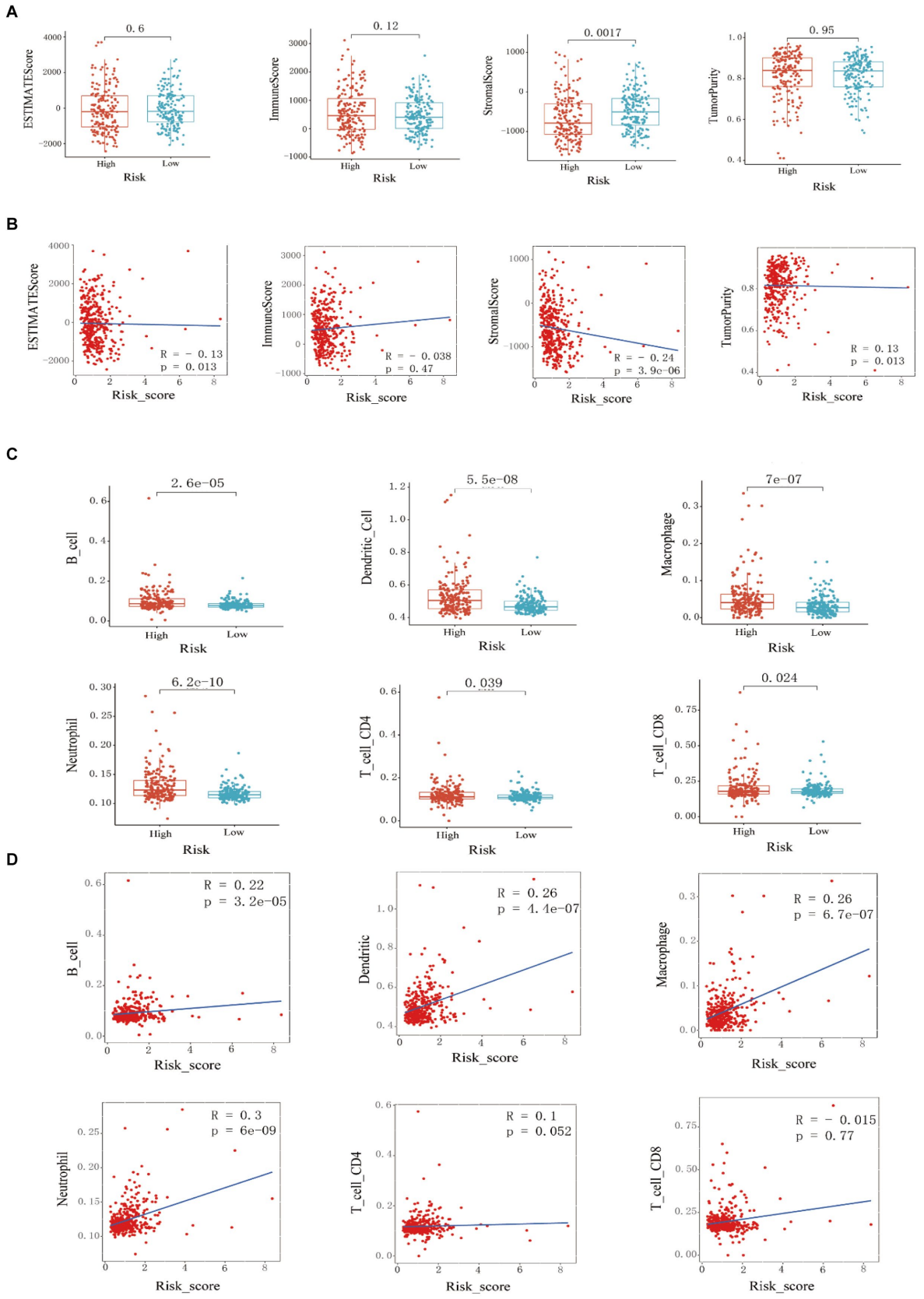

FIGURE 3
Training set immune infiltration analysis. **(A)** Analysis of differences in ESTIMATE scores, immune cell scores, stromal cell scores, and **(B)** tumor purity between high-risk and low-risk groups, and correlation analysis with risk scores. **(C)** Analysis of differences in the infiltration abundance of B cells, macrophages, neutrophils, dendritic cells, CD4+ T cells, and CD8+ T cells between high-risk and low-risk groups, and **(D)** correlation analysis with their respective risk scores.

C3, CTNNB1, CYBC1, DNASE1L3, IRAK1, and SERPINE1, which was established through multi-factor Cox regression analysis. According to the formula, the risk score of each patient is calculated and used as a standard to predict the outcome of HCC patients. The study found that High-risk scores among HCC patients have a worse prognosis than those in the low-risk group. ROC curve analysis of the survival rate of HCC patients found that the risk score has good sensitivity and specificity. The AUC values for predicting 1-year, 2-year, and 3-year survival rates are 0.768, 0.693, and 0.716, respectively, which can be used to predict prognosis for HCC patients. In addition, the predictive ability of the constructed prognostic model was successfully verified using the HCC data set of the ICGC database.

Current studies suggest that changes in the C3 gene and its expression can affect tumor immune response. Excessive activation or inhibition of complement components may lead to tumor progression or immune escape. At the same time, chronic inflammation caused by chronic hepatitis B is usually mediated by complement activation and is a known risk factor for liver cancer. Elevated levels of C3 and other complement components have been observed in HCC patients. Changes in the levels of complement proteins (including C3) in the blood of HCC patients may serve as biomarkers for the diagnosis or prognosis of HCC (43–46). The CTNNB1 gene encodes β-catenin and is involved in the regulation and coordination of cell–cell adhesion and gene transcription. Mutations in the CTNNB1 gene in HCC often lead to the stabilization and accumulation of β-catenin in the nucleus and abnormal activation of the Wnt/β-catenin signaling pathway is associated with the pathogenesis of HCC. HCC tumors with CTNNB1 mutations often show unique histological features and may have a better prognosis than HCC without these mutations. The level and activity of β-catenin represented by CTNNB1 can serve as a biomarker for diagnosing and classifying HCC. The presence of CTNNB1 mutations can also affect the prognosis of HCC patients. Studies have shown that patients with CTNNB1 mutant HCC may respond better to certain treatments, and the role of CTNNB1 in HCC helps develop targeted therapies aimed at inhibiting the Wnt/β-catenin signaling pathway. At the same time, targeting β-catenin signaling with other treatments (such as immune checkpoint inhibitors or traditional chemotherapy) can provide a more effective treatment strategy for HCC patients

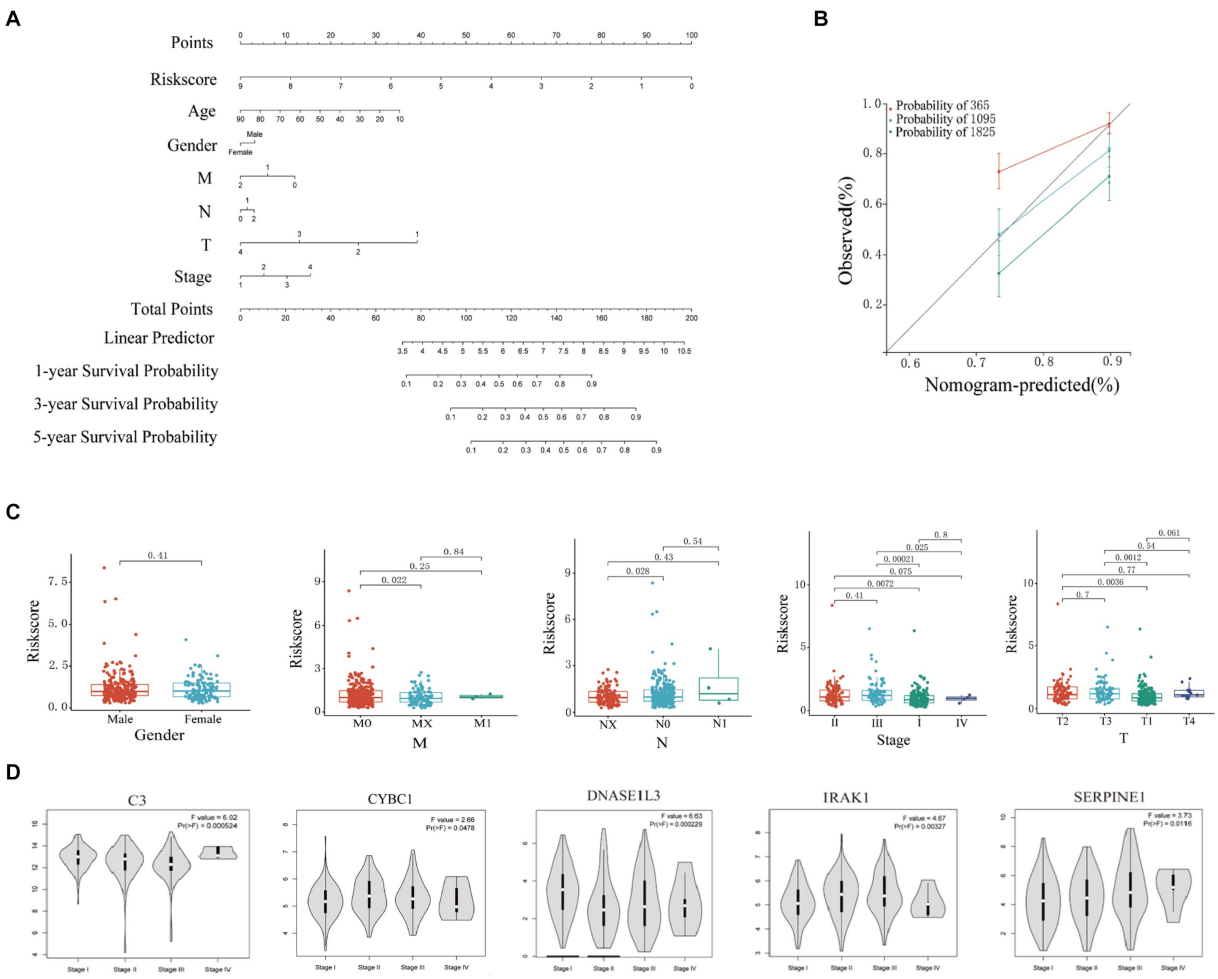

FIGURE 4
Clinical correlation analysis based on training set risk score. **(A)** Nomogram model to predict 1-, 3-, and 5-year survival rates of HCC cases. **(B)** Calibration graphs indicated that predicted 1-, 3-, and 5-year survival rates were close to the actual survival rates. **(C)** Results of correlation analysis between risk score and gender, TNM, and stage. **(D)** Analyze the correlation between the mRNA expression of 6 hub genes based on the GEPIA.

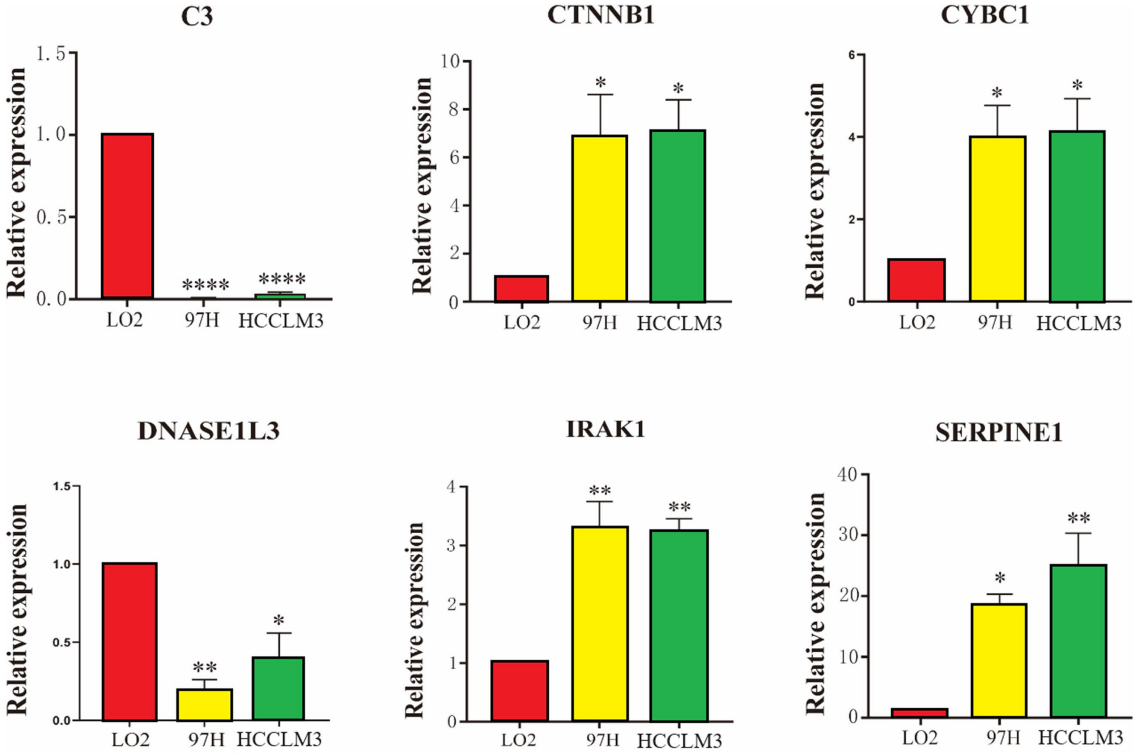

FIGURE 5
Comparison of the mRNA expression levels of six modeled genes in hepatocellular carcinoma and normal liver cells.

(47–53). The CYBC1 gene encodes a protein that acts as a chaperone for cytochrome b-245, which is a component of the NADPH oxidase complex. The CYBC1-cytochrome b-245 complex is essential for producing ROS, and NADPH oxidase and its ROS can affect cancer's development and progression. In chronic inflammation caused by HCC, dysregulated ROS production, which CYBC1 may affect, may lead to a pro-inflammatory environment and promote the development of liver cancer. Alterations in CYBC1 expression or function may affect the immune system's ability to respond to tumor cells (54, 55). The DNASE1L3 gene encodes an enzyme that digests extracellular DNA released during cell death processes such as apoptosis and necrosis. Clearing these DNA fragments maintains homeostasis and prevents excessive inflammation. Chronic inflammation is an important risk factor for liver cancer. The normal function of DNASE1L3 may help maintain genomic stability by preventing the accumulation of DNA fragments, which may otherwise lead to mutations and cancer. Changes in DNASE1L3 expression or activity may serve as a biomarker for HCC (56–62). IRAK1 is a serine/threonine protein kinase that participates in downstream signaling of the IL-1 and TLR pathways. It is essential for activating nuclear factor kappa B (NF-κB) and mitogen-activated protein kinase (MAPK) signaling. Through its role in IL-1 and TLR signaling, IRAK1 can promote the inflammatory microenvironment that promotes the development of liver cancer. Abnormal activation of IRAK1 can lead to sustained activation of the NF-κB and MAPK pathways, promoting cell proliferation, survival, and anti-apoptosis. Elevated IRAK1 expression or activity levels may serve as a biomarker for HCC. At the same time, studies have shown that high IRAK1 expression is associated with poor prognosis in HCC patients (63–66). SERPINE1 (serine protease inhibitor family E member 1) is a gene that encodes a protein that regulates fibrinolysis and plays a role in cell migration, invasion, and angiogenesis. Elevated levels of SERPINE1 are associated with increased tumor growth, invasion, and metastasis in multiple cancers, including HCC. It also plays a role in angiogenesis (forming new blood vessels), essential for tumor growth and metastasis. It interacts with vitronectin and integrins, influencing endothelial cell migration and blood vessel formation. High expression of SERPINE1 is often associated with poor prognosis in HCC patients (67–72). In summary, the six Hub genes in the prognostic model have been confirmed in multiple studies to be involved in the occurrence and development of HCC.

This study also showed a close correlation between HCC and stromal cells (73, 74). ESTIMATE (75) analysis showed that the stromal score in the low-risk group was significantly higher than in the high-risk group, and the difference was statistically significant. Correlation analysis showed that stromal cell and ESTIMATE scores negatively correlated with risk scores. Dense immune cell infiltration is generally associated with a better prognosis because it indicates that the immune system is actively responding to the presence of the tumor. Lower immune cell infiltration or an immune desert state (few immune cells in the tumor microenvironment) is often associated with a poorer prognosis because it indicates that the tumor may have evaded surveillance by the immune system (76). TIMER's (77) algorithm analysis found that the infiltration of B lymphocytes, macrophages, dendritic cells, and neutrophils in HCC tumor cells was positively

correlated with the risk score. Immune cell infiltration plays an important prognostic role in hepatocellular carcinoma (HCC). Studies have shown that immune cells' composition and infiltration level in the tumor microenvironment are closely related to the patient's prognosis (78). Researchers have developed prognostic models based on immune cell infiltration by integrating large-scale and single-cell RNA sequencing data. These models can predict the survival rate and immune checkpoint blockade response of HCC patients (79). The distribution and activity status of different types of immune cells, such as T cells, B cells, and macrophages in the tumor microenvironment, are key prognostic indicators. High levels of anti-tumor immune cells (such as cytotoxic T cells) are generally associated with a better prognosis. In contrast, immunosuppressive cells (such as regulatory T cells) may indicate a poor prognosis (80). Multiple studies have evaluated the effect of immune cell infiltration on HCC prognosis through survival analysis and found that patients with higher immune scores generally have longer survival (52, 78, 81, 82). These patients tend to have higher anti-tumor immune cell infiltration and lower immunosuppressive cell infiltration (83). Studies have shown that combining ICIs with other treatments, such as chemotherapy, radiotherapy, or targeted therapy, can enhance the therapeutic effect. For example, the effect of immunotherapy can be enhanced by inhibiting immunosuppressive cells or promoting the infiltration of anti-tumor immune cells. Suppose there are more regulatory T cells (Tregs) and M2 macrophages in the tumor microenvironment (84, 85). In that case, this may promote tumors to escape immune surveillance, thereby increasing the risk of tumor survival and growth. The high density of cytotoxic T cells (such as CD8+ T cells) and M1 macrophages may enhance the ability to attack tumors and promote the clearance of tumor cells, thereby potentially reducing tumor invasiveness and patient risk (86). Immunotherapy, such as immune checkpoint inhibitors, may be more effective for tumors with high immune cell infiltration (87). Other strategies, such as immune modulators or cell therapies, may be needed for tumors in immune deserts to attract more immune cells to the tumor microenvironment (88, 89).

However, this study also has limitations. First, this study's analysis data come from public data resources such as TCGA, ICGC, and GEPIA (90). They lack their sequencing data. Specific clinical cases need to be collected for experiments to verify the credibility of the constructed prognostic model in predicting the prognosis of HCC patients. In addition, the data sources in public databases also have limitations. The experimental techniques used in different studies, such as different sequencing platforms or chip technologies, may be different. These technical differences will lead to incomparability between data. The data processing and standardization methods may vary, affecting the consistency of the data. Differences in the geographical origin, collection time, and sample processing methods will also introduce variability. Some gene expression data may have missing values, resulting in incomplete data. At the same time, biological differences between different samples in sequencing data, such as individual differences, mixed cell types, etc., may lead to variability in gene expression. Different conditions for sample collection and processing (such as temperature, culture medium, etc.) will affect gene expression. We use different databases and statistical schemes to verify each other to minimize the differences caused by different databases and sequencing batches. Secondly, this study lacks sufficient *in vitro* or *in vivo* experiments to explore the molecular mechanisms by which differentially expressed inflammation-related genes in liver cancer affect the prognosis of HCC patients to confirm the reliability of the GO and KEGG enrichment analysis results of differentially expressed inflammation-related genes in this study. Therefore, Many experiments are needed to prove the mechanical connection between the differential expression of inflammation-related genes and HCC proliferation and metastasis. Finally, the underlying specific mechanisms between differentially expressed inflammation-related genes in HCC and tumor immunity are poorly understood and require further experimental and clinical studies to verify.

5 Conclusion

The mRNA expression of six inflammation-related genes (C3, CTNNB1, CYBC1, DNASE1L3, IRAK1, and SERPINE1) is closely related to the overall survival rate, tumor immune infiltration, and clinical stage of HCC patients. Among them, CYBC1 is an independent risk factor affecting the prognosis of HCC patients. These findings provide a basis for the pathogenesis and clinical treatment of HCC and improve treatment strategies and early screening for HCC patients.

Data availability statement

The original contributions presented in the study are included in the article/Supplementary material, further inquiries can be directed to the corresponding authors.

Ethics statement

Ethical approval was not required for the studies on humans in accordance with the local legislation and institutional requirements because only commercially available established cell lines were used.

Author contributions

YL: Writing – original draft. YF: Writing – original draft. DL: Writing – original draft. JW: Writing – review & editing. ZiH: Writing – review & editing. XueyL: Writing – review & editing. XuemL: Writing – review & editing. CW: Writing – original draft, Writing – review & editing. ZhH: Writing – original draft, Writing – review & editing.

Funding

The author(s) declare financial support was received for the research, authorship, and/or publication of this article. This work was supported by grants from the Guangxi Zhuang Autonomous Region Health Commission Self-funded Research Project (Z20190918 and Z-A20231118).

Conflict of interest

The authors declare that the research was conducted in the absence of any commercial or financial relationships that could be construed as a potential conflict of interest.

Publisher's note

All claims expressed in this article are solely those of the authors and do not necessarily represent those of their affiliated organizations, or those of the publisher, the editors and the reviewers. Any product that may be evaluated in this article, or claim that may be made by its manufacturer, is not guaranteed or endorsed by the publisher.

Supplementary material

The Supplementary material for this article can be found online at: https://www.frontiersin.org/articles/10.3389/fmed.2024.1420353/full#supplementary-material

References

1. Anwanwan D, Singh SK, Singh S, Saikam V, Singh R. Challenges in liver cancer and possible treatment approaches. *Biochim Biophys Acta Rev Cancer*. (1873) 1873:188314. doi: 10.1016/j.bbcan.2019.188314

2. Min LH, Hua YZ. Microenvironment of liver regeneration in liver cancer. *Chin J Integr Med*. (2017) 23:555–60. doi: 10.1007/s11655-017-2806-0

3. Peng SW, Ngo MHT, Kuo YC, Teng MH, Guo CL, Lai HC, et al. Niclosamide revitalizes Sorafenib through insulin-like growth factor 1 receptor (IGF-1R)/Stemness and metabolic changes in hepatocellular carcinoma. *Cancers (Basel)*. (2023) 15:931. doi: 10.3390/cancers15030931

4. Kim DW, Talati C, Kim R. Hepatocellular carcinoma (HCC): beyond sorafenib-chemotherapy. *J Gastrointest Oncol*. (2017) 8:256–65. doi: 10.21037/jgo.2016.09.07

5. Kelley RK, Mollon P, Blanc JF, Daniele B, Yau T, Cheng AL, et al. Comparative efficacy of Cabozantinib and Regorafenib for advanced hepatocellular carcinoma. *Adv Ther*. (2020) 37:2678–95. doi: 10.1007/s12325-020-01378-y

6. Qin S, Chen Z, Fang W, Ren Z, Xu R, Ryoo BY, et al. Pembrolizumab versus placebo as second-line therapy in patients from Asia with advanced hepatocellular carcinoma: a randomized, double-blind, phase III trial. *J Clin Oncol*. (2023) 41:1434–43. doi: 10.1200/JCO.22.00620

7. Schlachterman A, Craft WW, Hilgenfeldt E, Mitra A, Cabrera R. Current and future treatments for hepatocellular carcinoma. *World J Gastroenterol*. (2015) 21:8478–91. doi: 10.3748/wjg.v21.i28.8478

8. Daher S, Massarwa M, Benson AA, Khoury T. Current and future treatment of hepatocellular carcinoma: an updated comprehensive review. *J Clin Transl Hepatol*. (2018) 6:1–10. doi: 10.14218/JCTH.2017.00031

9. Li Y, Zhang R, Xu Z, Wang Z. Advances in Nanoliposomes for the diagnosis and treatment of liver Cancer. *Int J Nanomedicine*. (2022) 17:909–25. doi: 10.2147/IJN.S349426

10. Huang Y, Ge W, Zhou J, Gao B, Qian X, Wang W. The role of tumor associated macrophages in hepatocellular carcinoma. *J Cancer*. (2021) 12:1284–94. doi: 10.7150/JCA.51346

11. Lim CJ, Chew V. Impact of viral etiologies on the development of novel immunotherapy for hepatocellular carcinoma. *Semin Liver Dis*. (2020) 40:131–42. doi: 10.1055/s-0039-3399534

12. Yang YM, Kim SY, Seki E. Inflammation and liver Cancer: molecular mechanisms and therapeutic targets. *Semin Liver Dis*. (2019) 39:026–42. doi: 10.1055/s-0038-1676806

13. Lawal G, Xiao Y, Rahnemai-Azar AA, Tsilimigras DI, Kuang M, Bakopoulos A, et al. The immunology of hepatocellular carcinoma. *Vaccines (Basel)*. (2021) 9:1184. doi: 10.3390/vaccines9101184

14. O'Farrell M, Duke G, Crowley R, Buckley D, Martins EB, Bhattacharya D, et al. FASN inhibition targets multiple drivers of NASH by reducing steatosis, inflammation and fibrosis in preclinical models. *Sci Rep*. (2022) 12:15661. doi: 10.1038/s41598-022-19459-z

15. Desterke C, Chiappini F. Lipid related genes altered in NASH connect inflammation in liver pathogenesis progression to HCC: a canonical pathway. *Int J Mol Sci*. (2019) 20:5594. doi: 10.3390/ijms20225594

16. Ram AK, Pottakat B, Vairappan B. Increased systemic zonula occludens 1 associated with inflammation and independent biomarker in patients with hepatocellular carcinoma. *BMC Cancer*. (2018) 18:572. doi: 10.1186/s12885-018-4484-5

17. Sangro B, Melero I, Wadhawan S, Finn RS, Abou-Alfa GK, Cheng AL, et al. Association of inflammatory biomarkers with clinical outcomes in nivolumab-treated patients with advanced hepatocellular carcinoma. *J Hepatol*. (2020) 73:1460–9. doi: 10.1016/j.jhep.2020.07.026

18. Ruf B, Heinrich B, Greten TF. Immunobiology and immunotherapy of HCC: spotlight on innate and innate-like immune cells. *Cell Mol Immunol*. (2021) 18:112–27. doi: 10.1038/s41423-020-00572-w

19. Liu Z, Lin Y, Zhang J, Zhang Y, Li Y, Liu Z, et al. Molecular targeted and immune checkpoint therapy for advanced hepatocellular carcinoma. *J Exp Clin Cancer Res*. (2019) 38:447. doi: 10.1186/s13046-019-1412-8

20. Miao L, Zhang Z, Ren Z, Li Y. Application of immunotherapy in hepatocellular carcinoma. *Front Oncol*. (2021) 11:699060. doi: 10.3389/fonc.2021.699060

21. Cadinu P, Sivanathan KN, Misra A, Xu RJ, Mangani D, Yang E, et al. Charting the cellular biogeography in colitis reveals fibroblast trajectories and coordinated spatial remodeling. *Cell*. (2024). 187:2010–2028.e30. doi: 10.1016/j.cell.2024.03.013

22. Schulze K, Nault JC, Villanueva A. Genetic profiling of hepatocellular carcinoma using next-generation sequencing. *J Hepatol*. (2016) 65:1031–42. doi: 10.1016/j.jhep.2016.05.035

23. Ma Z, Chen M, Liu XL, Cui H. Identification and verification of a prognostic autophagy-related gene signature in hepatocellular carcinoma. *Sci Rep*. (2024) 14:3032. doi: 10.1038/s41598-024-53565-4

24. Sun Z, Lu Z, Li R, Shao W, Zheng Y, Shi X, et al. Construction of a prognostic model for hepatocellular carcinoma based on immunoautophagy-related genes and tumor microenvironment. *Int J Gen Med*. (2021) 14:5461–73. doi: 10.2147/IJGM.S325884

25. Stel VS, Dekker FW, Tripepi G, Zoccali C, Jager KJ. Survival analysis ii: cox regression. *Nephron Clin Pract*. (2011) 119:c255–60. doi: 10.1159/000328916

26. Ritchie ME, Phipson B, Wu D, Hu Y, Law CW, Shi W, et al. Limma. *Nucleic Acids Res*. (2015) 43:e47. doi: 10.1093/nar/gkv007

27. Wickham H. ggplot2. *Wiley Interdiscip Rev Comput Stat*. (2011) 3:180–5. doi: 10.1002/wics.147

28. Tyner S, Briatte F, Hofmann H. Network visualization with ggplot2. *R J*. (2017) 9:27–59. doi: 10.32614/rj-2017-023

29. Stelzer G, Rosen N, Plaschkes I, Zimmerman S, Twik M, Fishilevich S, et al. The GeneCards suite: From gene data mining to disease genome sequence analyses. *Curr Protoc Bioinformatics* (2016). doi: 10.1002/cpbi.5

30. Oliveros JC. VENNY. An interactive tool for comparing lists with Venn diagrams. Available at: http://bioinfogp.cnb.csic.es/tools/venny/index.html. *BioinfogpCnbCsicEs/Tools/Venny/IndexHtml* (2007).

31. Therneau TM. Survival analysis [R package survival version 3.5–5]. *Comprehensive R archive network (CRAN)* (2021). Available at: https://cran.r-project.org/web/packages/survival/index.html

32. Yang L, Qu Q, Hao Z, Sha K, Li Z, Li S. Powerful identification of large quantitative trait loci using genome-wide R/glmnet-based regression. *J Hered*. (2022) 113:472–8. doi: 10.1093/jhered/esac006

33. Jones HDT, Haaland DM, Sinclair MB, Melgaard DK, Collins AM, Timlin JA. Preprocessing strategies to improve MCR analyses of hyperspectral images. *Chemom Intell Lab Syst*. (2012) 117:149–58. doi: 10.1016/j.chemolab.2012.01.011

34. Burnham KP, Anderson DR. Multimodel inference: understanding AIC and BIC in model selection. *Sociol Methods Res*. (2004) 33:261–304. doi: 10.1177/0049124104268644

35. Wu T, Hu E, Xu S, Chen M, Guo P, Dai Z, et al. clusterProfiler 4.0: a universal enrichment tool for interpreting omics data. *Innovations*. (2021) 2:100141. doi: 10.1016/j.xinn.2021.100141

36. Carlson M, Falcon S, Pages H, Li N. org. Hs. eg. db: Genome wide annotation for Human. *R package version* (2019) 3:3.

37. Walter W, Sánchez-Cabo F, Ricote M. GOplot: an R package for visually combining expression data with functional analysis. *Bioinformatics*. (2015) 31:2912–4. doi: 10.1093/bioinformatics/btv300

38. Hu D, Zhang Z, Zhang Y, Huang K, Li X. Identification of immune related molecular subtypes and prognosis model for predicting prognosis, drug resistance in cervical squamous cell carcinoma. *Front Genet*. (2023) 14:1137995. doi: 10.3389/fgene.2023.1137995

39. Szklarczyk D, Gable AL, Nastou KC, Lyon D, Kirsch R, Pyysalo S, et al. The STRING database in 2021: customizable protein-protein networks, and functional characterization of user-uploaded gene/measurement sets. *Nucleic Acids Res*. (2021) 49:10800. doi: 10.1093/nar/gkab835

40. Chan SL, Wong LL, Chan KCA, Chow C, Tong JHM, Yip TCF, et al. Development of a novel inflammation-based index for hepatocellular carcinoma. *Liver Cancer*. (2020) 9:167–81. doi: 10.1159/000504252

41. Wang D, Hu X, Xiao L, Long G, Yao L, Wang ZM, et al. Prognostic nutritional index and systemic immune-inflammation index predict the prognosis of patients with HCC. *J Gastrointest Surg*. (2021) 25:421–7. doi: 10.1007/s11605-019-04492-7

42. Giannone F, Slovic N, Pessaux P, Schuster C, Baumert TF, Lupberger J. Inflammation-related prognostic markers in resected hepatocellular carcinoma. *Front Oncol*. (2023) 13:1267870. doi: 10.3389/fonc.2023.1267870

43. Suzuki R, Takagi T, Sugimoto M, Sato Y, Irie H, Yomogida Y, et al. Intracellular C3 modulates EMT via the Akt/Smad pathway in pancreatic Cancer cells. *Anticancer Res*. (2022) 42:5743–50. doi: 10.21873/anticanres.16081

44. Yang C, Huang X, Liu Z, Qin W, Wang C. Metabolism-associated molecular classification of hepatocellular carcinoma. *Mol Oncol*. (2020) 14:896–913. doi: 10.1002/1878-0261.12639

45. Li J, Li Y, Li F, Xu L. NK cell marker gene-based model shows good predictive ability in prognosis and response to immunotherapies in hepatocellular carcinoma. *Sci Rep*. (2023) 13:7294. doi: 10.1038/s41598-023-34602-0

46. Liu L, Liu Z, Gao J, Liu X, Weng S, Guo C, et al. CD8+ T cell trajectory subtypes decode tumor heterogeneity and provide treatment recommendations for hepatocellular carcinoma. *Front Immunol*. (2022) 13:964190. doi: 10.3389/fimmu.2022.964190

47. Ogawa K, Kanzaki H, Chiba T, Ao J, Qiang N, Ma Y, et al. Effect of Atezolizumab plus bevacizumab in patients with hepatocellular carcinoma harboring CTNNB1 mutation in early clinical experience. *J Cancer*. (2022) 13:2656–61. doi: 10.7150/jca.71494

48. Murai H, Kodama T, Maesaka K, Tange S, Motooka D, Suzuki Y, et al. Multiomics identifies the link between intratumor steatosis and the exhausted tumor immune microenvironment in hepatocellular carcinoma. *Hepatology*. (2023) 77:77–91. doi: 10.1002/hep.32573

49. Xiao X, Mo H, Tu K. CTNNB1 mutation suppresses infiltration of immune cells in hepatocellular carcinoma through miRNA-mediated regulation of chemokine expression. *Int Immunopharmacol*. (2020) 89:107043. doi: 10.1016/j.intimp.2020.107043

50. Rialdi A, Duffy M, Scopton AP, Fonseca F, Zhao JN, Schwarz M, et al. WNTinib is a multi-kinase inhibitor with specificity against β-catenin mutant hepatocellular carcinoma. *Nat Cancer*. (2023) 4:1157–75. doi: 10.1038/s43018-023-00609-9

51. Senni N, Savall M, Cabrerizo Granados D, Alves-Guerra MC, Sartor C, Lagoutte I, et al. β-Catenin-activated hepatocellular carcinomas are addicted to fatty acids. *Gut*. (2019) 68:322–34. doi: 10.1136/gutjnl-2017-315448

52. Pinyol R, Sia D, Llovet JM. Immune exclusion-WNT/CTNNB1 class predicts resistance to immunotherapies in HCC. *Clin Cancer Res*. (2019) 25:2021–3. doi: 10.1158/1078-0432.CCR-18-3778

53. Charawi S, Just PA, Savall M, Abitbol S, Traore M, Metzger N, et al. LKB1 signaling is activated in CTNNB1-mutated HCC and positively regulates β-catenin-dependent CTNNB1-mutated HCC. *J Pathol*. (2019) 247:435–43. doi: 10.1002/path.5202

54. Mortimer PM, Nichols E, Thomas J, Shanbhag R, Singh N, Coomber EL, et al. A novel mutation in EROS (CYBC1) causes chronic granulomatous disease. *Clin Immunol*. (2023) 255:109761. doi: 10.1016/j.clim.2023.109761

55. Thomas DC, Charbonnier LM, Schejtman A, Aldhekri H, Coomber EL, Dufficy ER, et al. EROS/CYBC1 mutations: decreased NADPH oxidase function and chronic granulomatous disease. *J Allergy Clin Immunol*. (2019) 143:782–785.e1. doi: 10.1016/j.jaci.2018.09.019

56. Chen QY, Li L, Suo DQ. DNase1L3 suppresses hepatocellular carcinoma growth via inhibiting complement autocrine effect. *Neoplasma*. (2021) 68:683–91. doi: 10.4149/neo_2021_201010N1069

57. Sun J, Wang X, Shen Q, Wang M, Chen S, Zhang X, et al. DNASE1L3 inhibits hepatocellular carcinoma by delaying cell cycle progression through CDK2. *Cell Oncol*. (2022) 45:1187–202. doi: 10.1007/s13402-022-00709-1

58. Deng Z, Xiao M, Du D, Luo N, Liu D, Liu T, et al. Dnase1l3 as a prognostic biomarker associated with immune cell infiltration in cancer. *Onco Targets Ther*. (2021) 14:2003–17. doi: 10.2147/OTT.S294332

59. Ouyang B, Xie QQ, Huang W, Wang L, Tang S, Fu J. Diagnostic value of serum DNASE1L3 in hepatitis B virus-related hepatocellular carcinoma. *Clin Lab*. (2021) 67. doi: 10.7754/Clin.Lab.2020.200627

60. Wang S, Ma H, Li X, Mo X, Zhang H, Yang L, et al. DNASE1L3 as an indicator of favorable survival in hepatocellular carcinoma patients following resection. *Aging*. (2020) 12:1171–85. doi: 10.18632/aging.102675

61. Li B, Ge YZ, Yan WW, Gong B, Cao K, Zhao R, et al. DNASE1L3 inhibits proliferation, invasion and metastasis of hepatocellular carcinoma by interacting with β-catenin to promote its ubiquitin degradation pathway. *Cell Prolif*. (2022) 55:e13273. doi: 10.1111/cpr.13273

62. Li N, Zheng X, Chen M, Huang L, Chen L, Huo R, et al. Deficient DNASE1L3 facilitates neutrophil extracellular traps-induced invasion via cyclic GMP-AMP synthase and the non-canonical NF-κB pathway in diabetic hepatocellular carcinoma. *Clin Transl Immunol*. (2022) 11:e1386. doi: 10.1002/cti2.1386

63. Kim SY, Shen Q, Son K, Kim HS, Yang HD, Na MJ, et al. SMARCA4 oncogenic potential via IRAK1 enhancer to activate Gankyrin and AKR1B10 in liver cancer. *Oncogene*. (2021) 40:4652–62. doi: 10.1038/s41388-021-01875-6

64. Cheng BY, Lau EY, Leung HW, Leung CON, Ho NP, Gurung S, et al. Irak1 augments cancer stemness and drug resistance via the ap-1/akr1b10 signaling cascade in hepatocellular carcinoma. *Cancer Res*. (2018) 78:1986. doi: 10.1158/1538-7445.AM2018-1986

65. Chen W, Wei T, Chen Y, Yang L, Wu X. Downregulation of irak1 prevents the malignant behavior of hepatocellular carcinoma cells by blocking activation of the mapks/nlrp3/il-1β pathway. *Onco Targets Ther*. (2020) 13:12787–96. doi: 10.2147/OTT.S260793

66. Ye ZH, Gao L, Wen DY, He Y, Pang YY, Chen G. Diagnostic and prognostic roles of IRAK1 in hepatocellular carcinoma tissues: an analysis of immunohistochemistry and RNA-sequencing data from the cancer genome atlas. *Onco Targets Ther*. (2017) 10:1711–23. doi: 10.2147/OTT.S132120

67. Li LM, Chen C, Ran RX, Huang JT, Sun HL, Zeng C, et al. Loss of TARBP2 drives the progression of hepatocellular carcinoma via miR-145-SERPINE1 Axis. *Front Oncol*. (2021) 11:620912. doi: 10.3389/fonc.2021.620912

68. Divella R, Daniele A, Abbate I, Savino E, Casamassima P, Sciortino G, et al. Circulating levels of PAI-1 and SERPINE1 4G/4G polymorphism are predictive of poor prognosis in HCC patients undergoing TACE. *Transl Oncol*. (2015) 8:273–8. doi: 10.1016/j.tranon.2015.05.002

69. Xiaochun H, Feixiong P, Shengsong O, Xiaojiao W, Yuju X, Yanhua L. Identification and validation of an inflammatory response-related polygenic risk score as a prognostic marker in hepatocellular carcinoma. *Dis Markers*. (2022) 2022:1–14. doi: 10.1155/2022/1739995

70. Zhang Q, Feng Z, Gao M, Guo L. Determining novel candidate anti-hepatocellular carcinoma drugs using interaction networks and molecular docking between drug targets and natural compounds of SiNiSan. *PeerJ*. (2021) 9:e10745. doi: 10.7717/peerj.10745

71. Song L, Su X, Lu Y, Hua D, Gao Z. An inflammation-associated prognosis model for hepatocellular carcinoma based on adenylate Uridylate- (AU-) rich element genes. *Mediat Inflamm*. (2023) 2023:1–17. doi: 10.1155/2023/2613492

72. Divella R, Mazzocca A, Gadaleta C, Simone G, Paradiso A, Quaranta M, et al. Influence of plasminogen activator inhibitor-1 (SERPINE1) 4G/5G polymorphism on circulating SERPINE-1 antigen expression in HCC associated with viral infection. *Cancer Genomics Proteomics*. (2012) 9:193–8. doi: 10.1016/j.jep.2006.05.032

73. Papadakos SP, Machairas N, Stergiou IE, Arvanitakis K, Germanidis G, Frampton AE, et al. Unveiling the yin-Yang balance of M1 and M2 macrophages in hepatocellular carcinoma: role of exosomes in tumor microenvironment and immune modulation. *Cells*. (2023) 12:2036. doi: 10.3390/cells12162036

74. Xu R, Wu Q, Gong Y, Wu Y, Chi Q, Sun D. A novel prognostic target-gene signature and nomogram based on an integrated bioinformatics analysis in hepatocellular carcinoma. *Biocell*. (2022) 46:1261–88. doi: 10.32604/biocell.2022.018427

75. Chiarotti F, Venerosi A. Epidemiology of autism spectrum disorders: a review of worldwide prevalence estimates since 2014. *Brain Sci*. (2020) 10:274. doi: 10.3390/brainsci10050274

76. Hickey JW, Haist M, Horowitz N, Caraccio C, Tan Y, Rech AJ, et al. T cell-mediated curation and restructuring of tumor tissue coordinates an effective immune response. *Cell Rep*. (2023) 42:113494. doi: 10.1016/j.celrep.2023.113494

77. Mulyadi AM, Sihombing AVR, Hendrawan H, Marpaung E, Malisan J, Arianto D, et al. Subaryata, Siregar NAM, et al. effect of traffic lights countdown Timer and motorcycle lanes as an approach to the red box for motorcycles in Bali Island. *Infrastructures (Basel)*. (2022) 7:127. doi: 10.3390/infrastructures7100127

78. Dai K, Liu C, Guan G, Cai J, Wu L. Identification of immune infiltration-related genes as prognostic indicators for hepatocellular carcinoma. *BMC Cancer*. (2022) 22:496. doi: 10.1186/s12885-022-09587-0

79. Wei Y, Lan C, Yang C, Liao X, Zhou X, Huang X, et al. Robust analysis of a novel PANoptosis-related prognostic gene signature model for hepatocellular carcinoma immune infiltration and therapeutic response. *Sci Rep*. (2023) 13:14519. doi: 10.1038/s41598-023-41670-9

80. Wu D, Li Y. Application of adoptive cell therapy in hepatocellular carcinoma. *Immunology*. (2023) 170:453–69. doi: 10.1111/imm.13677

81. He Z, Zhang J, Huang W. Diagnostic role and immune correlates of programmed cell death-related genes in hepatocellular carcinoma. *Sci Rep*. (2023) 13:20509. doi: 10.1038/s41598-023-47560-4

82. Hartwell HJ, Petrosky KY, Fox JG, Horseman ND, Rogers AB. Prolactin prevents hepatocellular carcinoma by restricting innate immune activation of c-Myc in mice. *Proc Natl Acad Sci USA*. (2014) 111:11455–60. doi: 10.1073/pnas.1404267111

83. Zhao M, Xu P, Shi W, Wang J, Wang T, Li P. Icariin exerts anti-tumor activity by inducing autophagy via AMPK/mTOR/ULK1 pathway in triple-negative breast cancer. *Cancer Cell Int*. (2024) 24:74. doi: 10.1186/s12935-024-03266-9

84. Davidsson S, Fiorentino M, Giunchi F, Eriksson M, Erlandsson A, Sundqvist P, et al. Infiltration of M2 macrophages and regulatory T cells plays a role in recurrence of renal cell carcinoma. *Eur Urol Open Sci*. (2020) 20:62–71. doi: 10.1016/j.euros.2020.06.003

85. You JA, Gong Y, Wu Y, Jin L, Chi Q, Sun D. WGCNA, LASSO and SVM algorithm revealed RAC1 correlated M0 macrophage and the risk score to predict the survival of hepatocellular carcinoma patients. *Front Genet*. (2022) 12:730920. doi: 10.3389/fgene.2021.730920

86. Witonsky S, Buechner-Maxwell V, Santonastasto A, Pleasant R, Werre S, Wagner B, et al. Can levamisole upregulate the equine cell-mediated macrophage (M1) dendritic cell (DC1) T-helper 1 (CD4 Th1) T-cytotoxic (CD8) immune response in vitro? *J Vet Intern Med*. (2019) 33:889–96. doi: 10.1111/jvim.15404

87. Hu X, Zhu H, Chen B, He X, Shen Y, Zhang X, et al. Tubulin alpha 1b is associated with the immune cell infiltration and the response of HCC patients to immunotherapy. *Diagnostics*. (2022) 12:858. doi: 10.3390/diagnostics12040858

88. Wang K, Wu J, Yang Z, Zheng B, Shen S, Ru WR, et al. Hyperactivation of β-catenin signal in hepatocellular carcinoma recruits myeloid-derived suppressor cells through PF4-CXCR3 axis. *Cancer Lett*. (2024) 586:216690. doi: 10.1016/j.canlet.2024.216690

89. Li J, Wang W, Zhou Y, Liu L, Zhang G, Guan K, et al. m6A regulator-associated modification patterns and immune infiltration of the tumor microenvironment in Hepatocarcinoma. *Front Cell Dev Biol*. (2021) 9:687756. doi: 10.3389/fcell.2021.687756

90. Zhou W, Zhang Y, Zhang S, Yang Z. Absent in melanoma 1-like (AIM1L) serves as a novel candidate for overall survival in hepatocellular carcinoma. *Bioengineered*. (2021) 12:2750–62. doi: 10.1080/21655979.2021.1939636

frontiers | Frontiers in Medicine

TYPE Original Research
PUBLISHED 17 July 2024
DOI 10.3389/fmed.2024.1419058

OPEN ACCESS

EDITED BY
Liliana Chemello,
University of Padua, Italy

REVIEWED BY
Surjeet Dalal,
Amity University Gurgaon, India
Jiasheng Cao,
Zhejiang University, China

*CORRESPONDENCE
Liang Peng
✉ wsfirefly@126.com

RECEIVED 17 April 2024
ACCEPTED 24 June 2024
PUBLISHED 17 July 2024

CITATION
Zhang M, Kuang B, Zhang J, Peng J, Xia H, Feng X and Peng L (2024) Enhancing prognostic prediction in hepatocellular carcinoma post-TACE: a machine learning approach integrating radiomics and clinical features.
Front. Med. 11:1419058.
doi: 10.3389/fmed.2024.1419058

Enhancing prognostic prediction in hepatocellular carcinoma post-TACE: a machine learning approach integrating radiomics and clinical features

Mingqi Zhang[1,2], Bingling Kuang[3], Jingxuan Zhang[3], Jingyi Peng[2], Haoming Xia[4], Xiaobin Feng[4,5] and Liang Peng[1]*

[1]Department of Gastroenterology, First Affiliated Hospital of Guangzhou Medical University, Guangzhou Medical University, Guangzhou, Guangdong, China, [2]The Second Clinical School of Guangzhou Medical University, Guangzhou Medical University, Guangzhou, Guangdong, China, [3]Nanshan College, Guangzhou Medical University, Guangzhou, Guangdong, China, [4]School of Clinical Medicine, Tsinghua University, Beijing, China, [5]Hepato-Pancreato-Biliary Center, Beijing Tsinghua Changgung Hospital, School of Clinical Medicine, Tsinghua University, Beijing, China

Objective: This study aimed to investigate the use of radiomics features and clinical information by four machine learning algorithms for predicting the prognosis of patients with hepatocellular carcinoma (HCC) who have been treated with transarterial chemoembolization (TACE).

Methods: A total of 105 patients with HCC treated with TACE from 2002 to 2012 were enrolled retrospectively and randomly divided into two cohorts for training ($n = 74$) and validation ($n = 31$) according to a ratio of 7:3. The Spearman rank, random forest, and univariate Cox regression were used to select the optimal radiomics features. Univariate Cox regression was used to select clinical features. Four machine learning algorithms were used to develop the models: random survival forest, eXtreme gradient boosting (XGBoost), gradient boosting, and the Cox proportional hazard regression model. The area under the curve (AUC) and C-index were devoted to assessing the performance of the models in predicting HCC prognosis.

Results: A total of 1,834 radiomics features were extracted from the computed tomography images of each patient. The clinical risk factors for HCC prognosis were age at diagnosis, TNM stage, and metastasis, which were analyzed using univariate Cox regression. In various models, the efficacy of the combined models generally surpassed that of the radiomics and clinical models. Among four machine learning algorithms, XGBoost exhibited the best performance in combined models, achieving an AUC of 0.979 in the training set and 0.750 in the testing set, demonstrating its strong prognostic prediction capability.

Conclusion: The superior performance of the XGBoost-based combined model underscores its potential as a powerful tool for enhancing the precision of prognostic assessments for patients with HCC.

KEYWORDS

machine learning, hepatocellular carcinoma, prognosis, radiomics, clinical features

1 Introduction

Primary liver cancer is the sixth most common cancer globally and the third leading cause of cancer-related deaths worldwide. Hepatocellular carcinoma (HCC) constitutes approximately 75–85% of all primary liver cancer cases (1). There are many treatment options for HCC, including local ablation therapy, liver transplantation, liver resection, transarterial chemoembolization (TACE), radiation therapy, and systemic treatment. Presently, surgical resection stands as the principal treatment approach for HCC. However, due to HCC often presenting without distinct early symptoms, many patients are already at the intermediate stage [Barcelona Clinic Liver Cancer (BCLC) B stage] according to the BCLC staging system at the time of diagnosis, missing the optimal timing for treatment (2). This limits the choice of treatment options and affects the patient's prognosis.

The TACE is a minimally invasive technique that uses imaging guidance to diminish the blood supply to a tumor. Through a catheter inserted into an artery, contrast materials are administered to block the tumor's blood vessels, thereby halting the growth of new blood vessels and causing cell death in the tumor. According to European and American HCC management guidelines, TACE is a commonly used interventional treatment method for patients with intermediate to advanced HCC, effectively delaying disease progression and providing a chance of survival for some patients (3–7).

Owing to considerable variability within the patients, the effectiveness and safety of TACE treatment for individuals with intermediate to advanced HCC can differ (8). Therefore, before treatment begins, an objective method must be available to accurately predict the prognosis of patients with HCC treated with TACE. For patients with HCC who are not expected to benefit from TACE, alternative treatment methods should be considered, such as using sorafenib or lenvatinib, while preserving liver function as much as possible to extend overall survival (OS) (9–11).

In recent years, with the advancement of imaging technology and the development of big data analysis techniques, radiomics has emerged as a new research field. Radiomics transforms medical images into high-dimensional, quantitative, and minable data through deep feature extraction and data analysis, quantifying tumor phenotypic characteristics and heterogeneity, and is considered a potential biomarker for personalized cancer treatment (12). Moreover, machine learning methods excel at handling the intricate interactions among complex variables, which is difficult for traditional models (13). Nowadays, some studies have reported substantial progress in the diagnosis, treatment response, and prognosis prediction of HCC by combining radiomics features, clinical information, and computer technology, especially in TACE treatment for patients with HCC (14–16). However, predicting prognosis for patients with HCC with the use of radiomics or clinical information by different machine learning algorithms has not been fully explored, and their performance may vary in different scenarios.

Therefore, this study aimed to develop and validate different prediction models using four machine learning algorithms. It includes radiomics, clinical, and combined models incorporating clinical information and radiomics features. The purpose of these models is to predict the OS of patients with HCC after TACE treatment, providing new insights and effective strategies for selecting treatment options.

2 Materials and methods

2.1 Patients

To obtain the requisite data, we used the public data repository, The Cancer Imaging Archive (TCIA, https://www.cancerimagingarchive.net/) database. We collected the data of 105 patients with HCC who were treated with TACE from 2002 to 2012. The inclusion criteria specified that TACE must be the sole first-line or initial bridging therapy, accompanied by the availability of multiphasic contrast material enhanced computed tomography (CT) images at baseline, free from any image artifacts such as surgical clips. More information can be found in previous studies (17–19).

Patients were randomly divided into two categories at a ratio of 7:3: a training cohort ($n = 74$) and a testing cohort ($n = 31$). The training cohort was used to build the predictive models, while the testing cohort was used to validate the performance of the predictive model.

2.2 Image acquisition and segmentation

The dataset used was taken from TCIA and consisted of CT images from 105 patients. More information can be found in the TCIA database and previous studies (17–19). For the dataset from TCIA, expert radiologists meticulously annotated CT images from 105 patients using specialized software, focusing on the precise delineation of tumors and anatomical structures. Adhering to a standardized protocol, they outlined regions of interest on each slice, with their work undergoing rigorous review in consensus meetings to ensure accuracy and consistency.

2.3 Radiomics features

2.3.1 Radiomics features extraction

Feature extraction was based on Python 3.7 and implemented using the PyRadiomics software[1] (20). The algorithms for obtaining radiomics features were referenced from the Image Biomarker Standardization Initiative (21). The extracted radiomics features can be divided into three groups: (1) first-order statistical features; (2) shape features, including two-dimensional and three-dimensional characteristics; and (3) texture features, including gray level co-occurrence matrix, gray level run length matrix, gray level size zone matrix, gray level dependence matrix, and neighborhood gray-tone difference matrix.

2.3.2 Radiomics features selection

Initially, within the training dataset, the Spearman rank correlation coefficient was used to determine the inter-feature correlations, retaining one feature from any pair with a correlation coefficient exceeding 0.9 to eliminate highly redundant features. To maximally preserve the descriptive power of features, a greedy recursive elimination strategy was applied for feature filtering, wherein

1 http://PyRadiomics.readthedocs.io/en/latest

the most redundant feature in the current set was removed at each iteration.

Subsequently, further selection was performed using random forests, an ensemble learning method based on decision trees that assesses the contribution of each feature to the model's predictive performance. By evaluating the role of feature splits in the trees, random forests determined the extent to which feature splits improve model accuracy. Feature importance helped identify the most influential features for predicting the target variable (survival time).

Finally, univariate Cox proportional regression analysis was used to evaluate the impact of each variable on survival time. In this analysis, each variable was examined in relation to survival time separately, to ascertain its effect on survival risk. This method identified variables for subsequent model construction by calculating the hazard ratio and corresponding statistical significance (p-value) for each feature, incorporating variables from univariate regression analyses with a p-value of <0.05.

2.4 Clinical features selection

In the initial data preparation phase, features with more than 20% missing values were excluded to maintain the integrity and reliability of the dataset. This step was crucial to ensuring the robustness and comprehensiveness of the clinical information used for modeling. Following this, to simplify the model and enhance its interpretability, continuous variables were converted into binary variables (dichotomization). This process involved setting a threshold for each feature, above which values were coded as 1 and below as 0, thus categorizing patients into two distinct groups based on each feature's presence or absence.

For feature selection, univariate Cox proportional hazards regression analysis was used on the training set. This statistical method was used to assess the impact of each feature on the OS of patients with HCC, identifying variables that significantly affected the outcome. Features with a p-value less than 0.1 in this analysis were considered statistically significant and were selected for further modeling.

2.5 Construction and validation of models for survival prediction

The application of machine learning algorithms was carefully tailored, with specific parameters set to optimize their performance for radiomics and clinical data. The Cox proportional hazard regression model (Coxph) was parameterized to evaluate the risk factors with adjustments to its baseline hazard function and regression coefficients to suit the survival data. For the random survival forest (RSF) algorithm, many decision trees were constructed to improve prediction accuracy, with parameters such as the number of trees, maximum depth, and minimum samples per leaf tuned to prevent overfitting while capturing the complex interactions within the data. Gradient Boosting was utilized to minimize errors sequentially using decision trees, where the learning rate and the number of trees were critical parameters to balance bias and variance effectively. Finally, eXtreme gradient boosting (XGBoost) was used, as it is known for its efficiency and scalability. Parameters such as the learning rate, maximum depth of trees, and the number of estimators were optimized to enhance the model's ability to accurately predict the outcomes of patients with HCC. To validate these models, a 5-fold cross-validation method was used, assessing their prediction accuracy through the average area under the curve (AUC) on the testing cohort, thus ensuring a robust evaluation of each algorithm's predictive power.

2.6 Statistical analysis

Statistical analysis was conducted using R software version 4.2.3.[2] The normality of continuous data was tested using the Shapiro–Wilk test, with normally distributed data presented as mean ± standard deviation ($\bar{x} \pm s$), and differences between two groups were analyzed using independent sample t-tests. Non-normally distributed data were presented as M (Q1, Q3), with differences between groups analyzed using the Mann–Whitney U-test. Categorical data were compared using the chi-square test, with a p-value of <0.05 considered statistically significant. OS was regarded as the primary outcome. Receiver operating characteristic (ROC) curves were generated using the "pROC" package. The model that achieved the highest AUC was chosen as the best prediction model. ROC curves and C-index were used to assess the predictive capability of different models for the prognosis of patients with HCC treated with TACE.

3 Results

3.1 Clinical baseline characteristics of patients

Table 1 displays the clinical characteristics of patients in the training cohort ($n = 74$) and the testing cohort ($n = 31$). A total of 12, 24, 66, and 3 patients were in BCLC stages A, B, C, and D, respectively. In the training cohort, most patients (71.62%) were diagnosed at age over 60 years, and 66.22% were men. Additionally, most patients were not diagnosed with vascular invasion (82.43%) or diabetes (66.22%). Moreover, 74.32% of the patients had cirrhosis, and 94.59% had metastasis. No significant differences were observed in clinical characteristics between the training and testing cohorts ($p > 0.05$).

3.2 Radiomics features screening results

A total of 1,834 radiomics features were initially extracted. Using the Spearman rank correlation coefficient to assess the inter-feature correlations, 233 features were retained. Subsequent selection through random forests resulted in the preservation of 13 features owing to the importance scores. Finally, univariate Cox regression analysis included three variables ($p < 0.05$), comprising two first-order features and one texture feature. Among these, the feature square_glcm_ClusterShade made the most significant contribution. Detailed information about the process is depicted in Figures 1, 2. All selected features were utilized in constructing the radiomics and combined models.

2 http://www.r-project.org

TABLE 1 Baseline of 105 enrolled patients from TCIA.

Characteristics	Training cohort (*N* = 74)	Testing cohort (*N* = 31)	*P*
OS, No. (%)			0.98
Alive	9 (12.16%)	3 (9.68%)	
Dead	65 (87.84%)	28 (90.32%)	
OS.time (weeks), mean (*SD*)	128.03 (106.22)	123.13 (97.57)	0.93
Hepatitis, No. (%)			1.00
No	38 (51.35%)	16 (51.61%)	
Yes	36 (48.65%)	15 (48.39%)	
Age at diagnosis (years), No. (%)			1.00
<=60	21 (28.38%)	9 (29.03%)	
>60	53 (71.62%)	22 (70.97%)	
Sex, No. (%)			0.80
Male	49 (66.22%)	19 (61.29%)	
Female	25 (33.78%)	12 (38.71%)	
Smoking, No. (%)			0.21
No	29 (39.19%)	17 (54.84%)	
Yes	45 (60.81%)	14 (45.16%)	
Alcohol, No. (%)			0.38
No	32 (43.24%)	17 (54.84%)	
Yes	42 (56.76%)	14 (45.16%)	
Diabetes, No. (%)			1.00
No	49 (66.22%)	21 (67.74%)	
Yes	25 (33.78%)	10 (32.26%)	
Cirrhosis, No. (%)			1.00
No	19 (25.68%)	8 (25.81%)	
Yes	55 (74.32%)	23 (74.19%)	
Child-Pugh, No. (%)			0.29
A	63 (85.14%)	23 (74.19%)	
B or C	11 (14.86%)	8 (25.81%)	
Tumor nodularity, No. (%)			0.95
Uninodular	36 (48.65%)	16 (51.61%)	
Multinodular	38 (51.35%)	15 (48.39%)	
Vascular invasion, No. (%)			0.16
No	61 (82.43%)	21 (67.74%)	
Yes	13 (17.57%)	10 (32.26%)	
Metastasis, No. (%)			0.71
No	70 (94.59%)	28 (90.32%)	
Yes	4 (5.41%)	3 (9.68%)	
AFP(ng/mL) , No. (%)			0.76
<400	54 (72.97%)	21 (67.74%)	
>=400	20 (27.03%)	10 (32.26%)	
Okuda, No. (%)			0.26
Stage I	53 (71.62%)	18 (58.06%)	
Stage II or III	21 (28.38%)	13 (41.94%)	
TNM, No. (%)			1.00
Stage I or II	40 (54.05%)	17 (54.84%)	
Stage III or IV	34 (45.95%)	14 (45.16%)	
BCLC, No. (%)			0.16
Stage A or B	29 (39.19%)	7 (22.58%)	
Stage C or D	45 (60.81%)	24 (77.42%)	

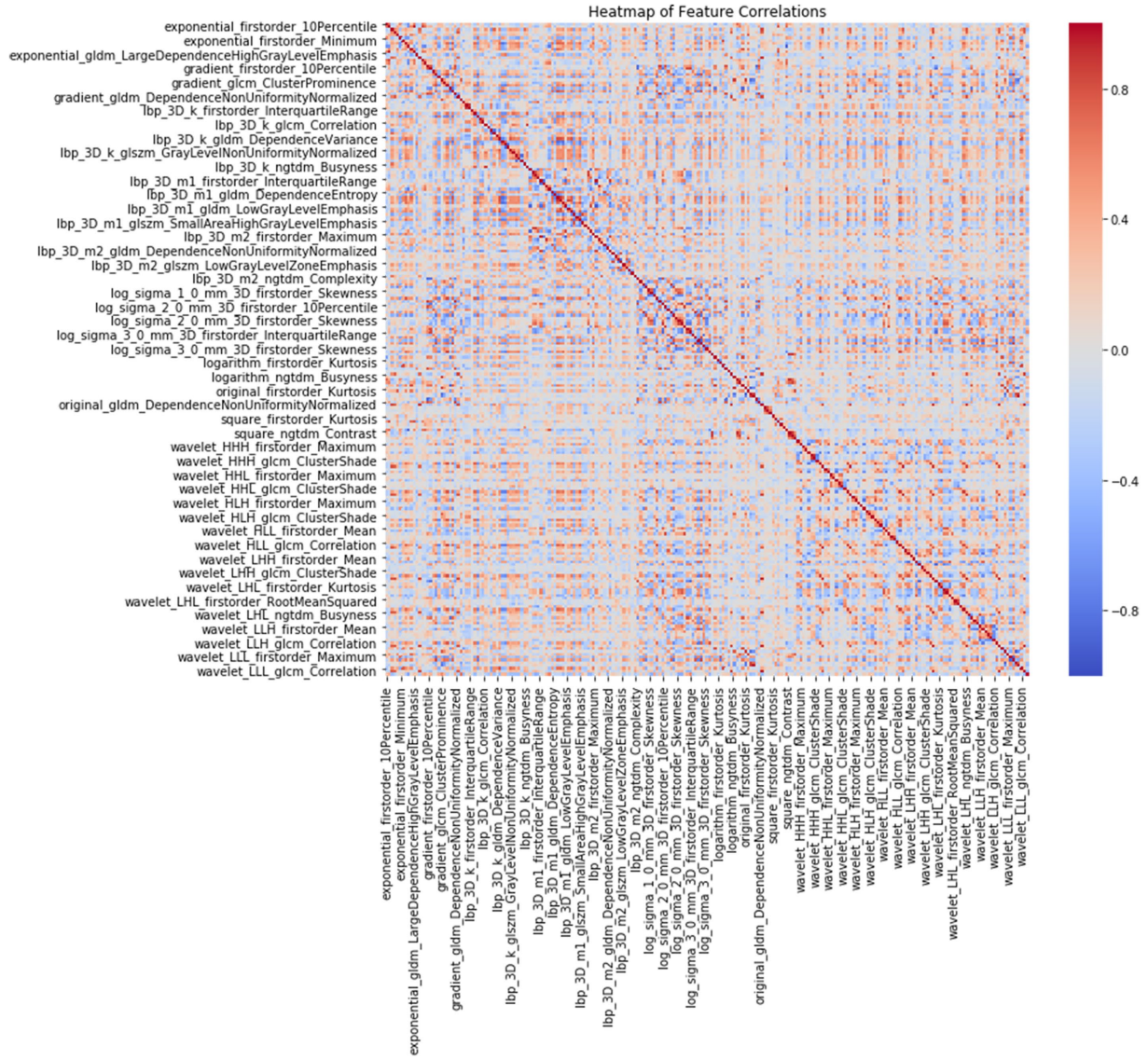

FIGURE 1
Heatmap of 233 radiomics features correlations according to Spearman rank correlation coefficient.

3.3 Clinical characteristics included analysis

The clinical characteristics of patients in the training cohort are presented in Table 2. Based on the univariate Cox proportional hazards regression analysis within the training cohort ($p \leq 0.1$), only age at diagnosis, TNM staging, and metastasis were associated with OS in patients with HCC. Age at diagnosis helped in understanding the survival prognosis, with older age potentially indicating a poorer outcome. The TNM stage, an indicator of cancer progression, provided crucial information on tumor size, lymph node involvement, and the extent of metastasis. The presence of metastasis, indicating the spread of cancer to other parts of the body, was another critical factor influencing survival rates. These findings underscored the importance of these variables in predicting the survival outcomes of patients with HCC. They were used to refine the predictive model for better accuracy and clinical relevance.

3.4 Model performance

Model performance is shown in Tables 3, 4. ROC curves for each model in the training and testing cohorts are shown in Figure 3. Among all machine learning models, the evaluation of combined models generally outperformed the radiomics or clinical models in predicting HCC prognosis in the training and testing cohorts. Specifically, the XGBoost model in the combined models showed the best performance, achieving an AUC of 0.979 in the training cohort and an AUC of 0.750 in the testing cohort, demonstrating strong prognostic prediction capability. The AUC of the combined model was significantly higher than

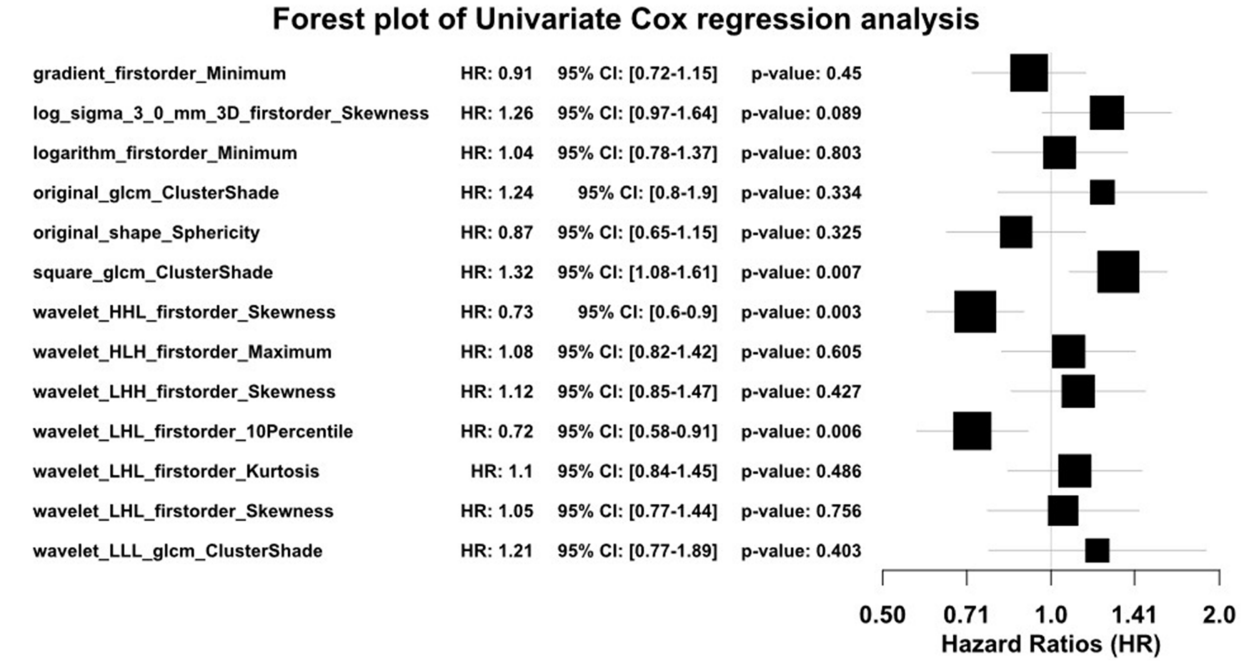

FIGURE 2
Forest plot of radiomics features selection with univariate Cox regression analysis.

TABLE 2 Clinical variables for predicting survival in the univariate Cox analysis.

Variable	Hazard ratio	HR_CI_Lower	HR_CI_Upper	*P*
Progressed	1.43	0.87	2.36	0.16
Hepatitis	0.72	0.44	1.19	0.20
Age at diagnosis	1.79	0.99	3.23	0.05
Sex	1.46	0.87	2.45	0.16
Smoking	1.08	0.64	1.82	0.76
Alcohol	0.85	0.52	1.41	0.54
Family history of cancer	1.05	0.63	1.74	0.86
Family history of liver cancer	0.82	0.30	2.28	0.71
Diabetes	1.16	0.69	1.94	0.57
Personal history of cancer	1.07	0.54	2.11	0.84
Cirrhosis	0.69	0.40	1.20	0.19
Performance status	1.23	0.75	2.02	0.40
Child-Pugh	1.42	0.72	2.80	0.31
Tumor nodularity	1.24	0.76	2.04	0.39
Vascular invasion	1.49	0.81	2.75	0.20
Metastasis	6.53	2.22	19.25	0.00
Lymph nodes	1.23	0.61	2.49	0.57
Portal Vein Thrombosis	1.76	0.86	3.57	0.12
Tumor involvement	0.91	0.48	1.71	0.77
AFP	1.15	0.65	2.04	0.64
CLIP	1.49	0.72	3.05	0.28
Okuda	1.02	0.60	1.75	0.93
TNM	1.53	0.93	2.52	0.09
BCLC	1.21	0.73	2.00	0.47

TABLE 3 Performance of different machine learning algorithms in the training cohort.

	AUC	C-Index	Accuracy	Sensitivity	Precision	F1
Clinical models						
Coxph	0.726	0.604	0.838	0.892	0.892	0.892
Gradient boosting	0.718	0.570	0.838	0.892	0.892	0.892
RSF	0.728	0.579	0.838	0.892	0.892	0.892
XGBoost	0.706	0.556	0.838	0.892	0.892	0.892
Radiomics models						
Coxph	0.781	0.663	0.730	0.708	0.708	0.708
Gradient boosting	0.800	0.652	0.743	0.723	0.723	0.723
RSF	0.822	0.674	0.757	0.738	0.738	0.738
XGBoost	0.990	0.979	0.881	0.892	0.892	0.092
Combined models						
Coxph	0.834	0.692	0.824	0.831	0.831	0.831
Gradient boosting	0.805	0.656	0.743	0.723	0.723	0.723
RSF	0.862	0.696	0.757	0.738	0.738	0.738
XGBoost	0.979	0.985	0.922	0.938	0.938	0.938

TABLE 4 Performance of different machine learning algorithms in the testing cohort.

	AUC	C-Index	Accuracy	Sensitivity	Precision	F1
Clinical models						
Coxph	0.524	0.575	0.742	0.821	0.821	0.821
Gradient boosting	0.613	0.579	0.742	0.821	0.821	0.821
RSF	0.571	0.590	0.742	0.821	0.821	0.821
XGBoost	0.649	0.585	0.742	0.821	0.821	0.821
Radiomics models						
Coxph	0.690	0.615	0.516	0.500	0.500	0.500
Gradient boosting	0.607	0.558	0.613	0.643	0.643	0.643
RSF	0.583	0.554	0.645	0.679	0.679	0.679
XGBoost	0.702	0.534	0.623	0.650	0.650	0.650
Combined models						
Coxph	0.655	0.615	0.806	0.857	0.857	0.857
Gradient boosting	0.631	0.560	0.613	0.607	0.607	0.607
RSF	0.607	0.578	0.645	0.679	0.679	0.679
XGBoost	0.750	0.512	0.758	0.879	0.879	0.879

that of the XGBoost clinical model (AUC = 0.706) and the XGBoost radiomics model (AUC = 0.990). In contrast, the clinical model exhibited a lower AUC, with particularly weaker performance observed in the Coxph and RSF algorithms. In the training cohort, the Coxph and RSF algorithms demonstrated an AUC of 0.726 and 0.728, respectively, while in the testing cohort, the AUC decreased to 0.524 and 0.571, respectively. The clinical models displayed consistent accuracy across all algorithms, with an accuracy of 0.838 in the training and 0.742 in the testing cohorts. Conversely, the radiomics models and the combined models exhibited significant fluctuations in accuracy across different algorithms.

4 Discussion

Primary liver cancer is the sixth most common cancer globally. Most patients are diagnosed at an intermediate stage according to the BCLC staging system (stage B), for which TACE is considered the preferred treatment option. This plays an important role in managing patients with HCC (1, 7). However, the treatment response to TACE among patients with HCC often exhibits considerable individual variability, and liver function usually declines in patients with intermediate-stage HCC compared with healthy individuals. Moreover, TACE is highly likely to impose an additional burden on the liver; therefore, accurate preoperative

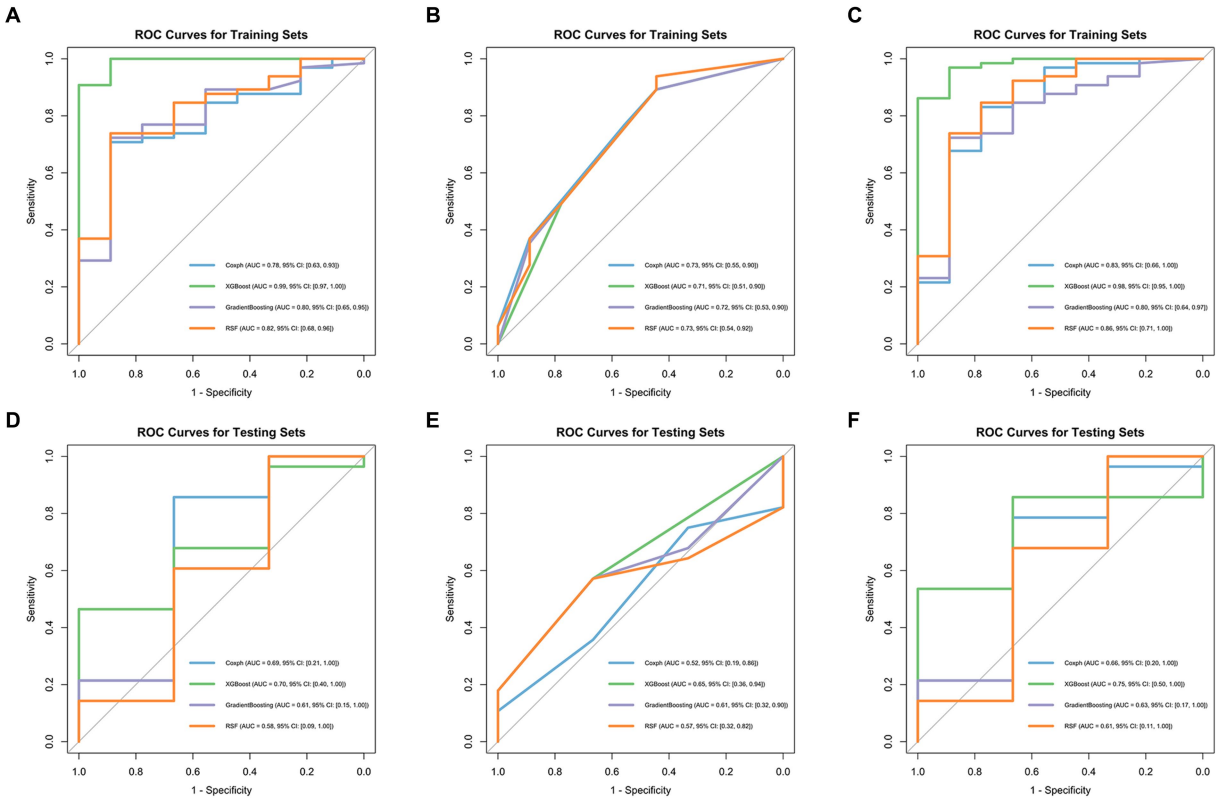

FIGURE 3
ROC curves of four machine learning algorithms in the training cohort: radiomics models **(A)**, clinical models **(B)**, and combined models **(C)**, in the testing cohort: radiomics models **(D)**, clinical models **(E)**, and combined models **(F)**.

prediction is crucial for treating and managing patients with HCC (22). In this study, we constructed four machine learning models based on patients' CT images and clinical information. The combined models outperformed single-feature models in predicting the prognosis of patients with HCC treated with TACE, with the XGBoost combined model demonstrating the best performance.

Recently, the rapid advancement of radiomics has enhanced the accuracy of clinical diagnosis and prognosis assessment. Radiomics extracts tissue and lesion characteristics, converting potential pathological and physiological information in images into mineable high-dimensional quantitative image features for analysis, training, and validation, providing a powerful tool for modern medicine to address clinical problems (23, 24). This applies to HCC as well, where radiomics is extensively used. Liu et al. (25) investigated the OS of patients with HCC after hepatectomy. Feng et al. (26) built a radiomics model to predict the macrotrabecular-massive subtype in patients with HCC. Xia et al. (27) extracted radiomics features from images to predict microvascular invasion status in patients with HCC. Tong et al. (28) and Khodabakhshi et al. (29) have also confirmed that radiomics features can predict the prognosis of many cancers. This suggests the potential of radiomics in predicting the prognosis of patients with HCC after TACE. Therefore, in our study, we opted to incorporate radiomics features into constructing machine learning models. We selected three radiomics features, including two first-order features and one texture feature: square_glcm_ClusterShade, wavelet_HHL_firstorder_Skewness, and wavelet_LHL_firstorder_10Percentile.

However, interpreting the relationship between radiomics features and complex tumor biological processes remains challenging, prompting the inclusion of clinical information in our analysis. Regarding clinical information, our study identified age at diagnosis, metastasis, and TNM stage as significant variables affecting the prognosis of patients with HCC, with metastasis occurrence being the most critical variable based on importance scores. Combined models using clinical information and radiomics features outperformed radiomics or clinical models, echoing findings from previous studies. Ning et al. (30) conducted a study that combined radiomics signatures and clinical information to predict early recurrence in HCC. The combined model demonstrated the highest predictive power in the training and validation datasets, with AUCs of 0.846 and 0.737, respectively. Fang et al. (31) and Geng et al. (32) also drew a similar conclusion consistent with our results, where the combined model was a better predictor than the clinical or radiomics models.

Machine learning is widely applied in the medical field because of its high predictive accuracy (33). To date, various machine learning algorithms have been utilized to predict survival, prognosis, and treatment efficacy in patients with intermediate or advanced HCC treated with TACE. However, previous studies usually limit themselves to a single machine

learning algorithm for analysis and modeling (34, 35). Considering the different features and scopes of application of various machine learning algorithms, this study used four advanced algorithms: XGBoost, RSF, gradient boosting, and Coxph to build models predicting the OS of patients with HCC under TACE treatment. Our results suggested that XGBoost performed the best among all machine learning algorithms, especially in the combined model constructed after merging radiomics and clinical features, with an AUC of 0.979 in the training and 0.750 in the testing sets, significantly outperforming other algorithms, thereby proving its strong predictive efficiency. According to other studies, XGBoost has been proven to have a better predictive performance than other machine learning algorithms, consistent with our results (36–38). XGBoost is a scalable and highly accurate machine learning library that breaks through the computational limits of gradient boosting tree algorithms. The XGBoost algorithm iteratively optimizes the structure of trees to minimize the loss function, introduces L1 regularization to reduce the number of leaf nodes of decision trees, and introduces L2 regularization to reduce the weight of leaf nodes of decision trees, among other iterative optimizations, enhancing the model's generalization ability. XGBoost is distinct from other machine learning algorithms because it captures complex and non-linear relationships between features and outcomes. It efficiently processes complex, high-dimensional data, handles missing values effectively, and prevents overfitting. This makes XGBoost particularly well-suited for high-dimensional data scenarios such as radiomics. Our study demonstrated the great potential of the XGBoost in accurately predicting the prognosis of patients with HCC treated with TACE, especially when based on radiomics features and clinical characteristics. Apart from machine learning, we have also identified other advanced algorithms, such as deep learning, which have achieved notable successes in various fields (39, 40). However, because of the limited sample size in this study, machine learning might be a more suitable choice. In the future, we will obtain more samples for further in-depth research.

The limitations of this study included: (1) The ideal TACE candidates are patients in BCLC stage B; however, most patients ($n = 70$) were in BCLC stages C and D. (2) Data were selected in a single center, and external validation from other research centers is needed to improve the universality of the predictive model. (3) The sample size was small. (4) The relatively small number of patients included could have led to model overfitting, and increasing the number of cases would enhance the model's generalizability. (5) This study was retrospective, lacking a prospective study, and subject to selection bias. (6) An easy-to-use application designed for machine learning algorithms is lacking.

5 Conclusion

The purpose of this study was to investigate how four machine learning algorithms utilize radiomics features and clinical information to predict the prognosis of patients with HCC treated with TACE. By applying feature selection methods and testing various machine learning algorithms, it was found that the combined model notably outperformed those based solely on radiomics or clinical features. Among the four algorithms, XGBoost emerged as the most effective, demonstrating the model's enhanced predictive power in forecasting patient outcomes. This underscores the potential of integrating radiomics and clinical data through advanced machine learning techniques such as XGBoost to improve prognostic predictions in patients with HCC.

Data availability statement

Publicly available datasets were analyzed in this study. This data can be found here: https://www.cancerimagingarchive.net/collection/hcc-tace-seg/#citations.

Author contributions

MZ: Conceptualization, Data curation, Methodology, Software, Writing – original draft. BK: Investigation, Methodology, Writing – original draft. JZ: Data curation, Methodology, Writing – original draft. JP: Software, Writing – original draft. XH: Methodology, Software, Writing – original draft. LP: Conceptualization, Funding acquisition, Writing – review & editing. XF: Writing – original draft, Funding acquisition, Software.

Funding

The author(s) declare that financial support was received for the research, authorship, and/or publication of this article. This research project was supported by Basic Research Project of Dengfeng Hospital (grant agreement 2023A03J0339) and Natural Science Foundation of Beijing (Grant No. Z190024).

Conflict of interest

The authors declare that the research was conducted in the absence of any commercial or financial relationships that could be construed as a potential conflict of interest.

Publisher's note

References

1. Sung H, Ferlay J, Siegel RL, Laversanne M, Soerjomataram I, Jemal A, et al. Global Cancer statistics 2020: Globocan estimates of incidence and mortality worldwide for 36 cancers in 185 countries. *CA Cancer J Clin*. (2021) 71:209–49. doi: 10.3322/caac.21660

2. Chakraborty E, Sarkar D. Emerging therapies for hepatocellular carcinoma (Hcc). *Cancers*. (2022) 14:2798. doi: 10.3390/cancers14112798

3. Marrero JA, Kulik LM, Sirlin CB, Zhu AX, Finn RS, Abecassis MM, et al. Diagnosis, staging, and Management of Hepatocellular Carcinoma: 2018 practice guidance by the American Association for the Study of Liver Diseases. *Hepatology*. (2018) 68:723–50. doi: 10.1002/hep.29913

4. Heimbach JK, Kulik LM, Finn RS, Sirlin CB, Abecassis MM, Roberts LR, et al. Aasld guidelines for the treatment of hepatocellular carcinoma. *Hepatology*. (2018) 67:358–80. doi: 10.1002/hep.29086

5. Galle PR, Forner A, Llovet JM, Mazzaferro V, Piscaglia F, Raoul J-L, et al. Easl clinical practice guidelines: management of hepatocellular carcinoma. *J Hepatol*. (2018) 69:182–236. doi: 10.1016/j.jhep.2018.03.019

6. Vogel A, Martinelli E, Vogel A, Cervantes A, Chau I, Daniele B, et al. Updated treatment recommendations for hepatocellular carcinoma (Hcc) from the Esmo clinical practice guidelines. *Ann Oncol*. (2021) 32:801–5. doi: 10.1016/j.annonc.2021.02.014

7. Reig M, Forner A, Rimola J, Ferrer-Fàbrega J, Burrel M, Garcia-Criado Á, et al. Bclc strategy for prognosis prediction and treatment recommendation: the 2022 update. *J Hepatol*. (2022) 76:681–93. doi: 10.1016/j.jhep.2021.11.018

8. Zq W, Yw Z. Transcatheter arterial chemoembolization followed by surgical resection for hepatocellular carcinoma: a focus on its controversies and screening of patients Most likely to benefit. *Chin Med J*. (2021) 134:2275–86. doi: 10.1097/CM9.0000000000001767

9. Kudo M. A new treatment option for intermediate-stage hepatocellular carcinoma with high tumor burden: initial Lenvatinib therapy with subsequent selective Tace. *Liver Cancer*. (2019) 8:299–311. doi: 10.1159/000502905

10. Arizumi T, Ueshima K, Minami T, Kono M, Chishina H, Takita M, et al. Effectiveness of Sorafenib in patients with Transcatheter arterial chemoembolization (Tace) refractory and intermediate-stage hepatocellular carcinoma. *Liver Cancer*. (2015) 4:253–62. doi: 10.1159/000367743

11. Kudo M, Han K-H, Ye S-L, Zhou J, Huang Y-H, Lin S-M, et al. A changing paradigm for the treatment of intermediate-stage hepatocellular carcinoma: Asia-Pacific primary liver Cancer expert consensus statements. *Liver Cancer*. (2020) 9:245–60. doi: 10.1159/000507370

12. Lambin P, Leijenaar RTH, Deist TM, Peerlings J, de Jong EEC, van Timmeren J, et al. Radiomics: the bridge between medical imaging and personalized medicine. *Nat Rev Clin Oncol*. (2017) 14:749–62. doi: 10.1038/nrclinonc.2017.141

13. Avanzo M, Wei L, Stancanello J, Vallières M, Rao A, Morin O, et al. Machine and deep learning methods for Radiomics. *Med Phys*. (2020) 47:e185–202. doi: 10.1002/mp.13678

14. Sun Z, Shi Z, Xin Y, Zhao S, Jiang H, Li J, et al. Contrast-enhanced Ct imaging features combined with clinical factors to predict the efficacy and prognosis for Transarterial chemoembolization of hepatocellular carcinoma. *Acad Radiol*. (2023) 30:S81–91. doi: 10.1016/j.acra.2022.12.031

15. Niu XK, He XF. Development of a computed tomography-based Radiomics nomogram for prediction of Transarterial chemoembolization refractoriness in hepatocellular carcinoma. *World J Gastroenterol*. (2021) 27:189–207. doi: 10.3748/wjg.v27.i2.189

16. Kong C, Zhao Z, Chen W, Lv X, Shu G, Ye M, et al. Prediction of tumor response via a pretreatment Mri Radiomics-based nomogram in Hcc treated with Tace. *Eur Radiol*. (2021) 31:7500–11. doi: 10.1007/s00330-021-07910-0

17. Clark K, Vendt B, Smith K, Freymann J, Kirby J, Koppel P, et al. The Cancer imaging archive (Tcia): maintaining and operating a public information repository. *J Digit Imaging*. (2013) 26:1045–57. doi: 10.1007/s10278-013-9622-7

18. Morshid A, Elsayes KM, Khalaf AM, Elmohr MM, Yu J, Kaseb AO, et al. A machine learning model to predict hepatocellular carcinoma response to Transcatheter arterial chemoembolization. *Radiol Artif Intell*. (2019) 1:e180021. doi: 10.1148/ryai.2019180021

19. Moawad AW, Morshid A, Khalaf AM, Elmohr MM, Hazle JD, Fuentes D, et al. Multimodality annotated hepatocellular carcinoma data set including pre-and post-Tace with imaging segmentation. *Sci Data*. (2023) 10:33. doi: 10.1038/s41597-023-01928-3

20. van Griethuysen JJM, Fedorov A, Parmar C, et al. Computational Radiomics System to Decode the Radiographic Phenotype. *Cancer Res*. (2017) 77:e104–e107. doi: 10.1158/0008-5472.CAN-17-0339

21. Zwanenburg A, Vallières M, Abdalah MA, et al. The Image Biomarker Standardization Initiative: Standardized Quantitative Radiomics for High-Throughput Image-based Phenotyping. *Radiology*. (2020) 295:328–338. doi: 10.1148/radiol.2020191145

22. Raoul J-L, Forner A, Bolondi L, Cheung TT, Kloeckner R, de Baere T. Updated use of Tace for hepatocellular carcinoma treatment: how and when to use it based on clinical evidence. *Cancer Treat Rev*. (2019) 72:28–36. doi: 10.1016/j.ctrv.2018.11.002

23. Lambin P, Rios-Velazquez E, Leijenaar R, Carvalho S, van Stiphout RGPM, Granton P, et al. Radiomics: extracting more information from medical images using advanced feature analysis. *Eur J Cancer*. (2012) 48:441–6. doi: 10.1016/j.ejca.2011.11.036

24. Bera K, Braman N, Gupta A, Velcheti V, Madabhushi A. Predicting Cancer outcomes with Radiomics and artificial intelligence in radiology. *Nat Rev Clin Oncol*. (2022) 19:132–46. doi: 10.1038/s41571-021-00560-7

25. Liu Y, Wei X, Zhang X, Pang C, Xia M, Du Y. Ct Radiomics combined with clinical variables for predicting the overall survival of hepatocellular carcinoma patients after hepatectomy. *Transl Oncol*. (2022) 26:101536. doi: 10.1016/j.tranon.2022.101536

26. Feng Z, Li H, Liu Q, Duan J, Zhou W, Yu X, et al. Ct Radiomics to predict macrotrabecular-massive subtype and immune status in hepatocellular carcinoma. *Radiology*. (2023) 307:e221291. doi: 10.1148/radiol.221291

27. Xia T-Y, Zhou Z-H, Meng X-P, Zha J-H, Yu Q, Wang W-L, et al. Predicting microvascular invasion in hepatocellular carcinoma using Ct-based Radiomics model. *Radiology*. (2023) 307:e222729. doi: 10.1148/radiol.222729

28. Tong H, Sun J, Fang J, Zhang M, Liu H, Xia R, et al. A machine learning model based on pet/Ct Radiomics and clinical characteristics predicts tumor immune profiles in non-small cell lung Cancer: a retrospective multicohort study. *Front Immunol*. (2022) 13:859323. doi: 10.3389/fimmu.2022.859323

29. Khodabakhshi Z, Amini M, Mostafaei S, Haddadi Avval A, Nazari M, Oveisi M, et al. Overall survival prediction in renal cell carcinoma patients using computed tomography Radiomic and clinical information. *J Digit Imaging*. (2021) 34:1086–98. doi: 10.1007/s10278-021-00500-y

30. Ning P, Gao F, Hai J, Wu M, Chen J, Zhu S, et al. Application of Ct Radiomics in prediction of early recurrence in hepatocellular carcinoma. *Abdom Radiol*. (2020) 45:64–72. doi: 10.1007/s00261-019-02198-7

31. Fang C, An X, Li K, Zhang J, Shang H, Jiao T, et al. A nomogram based on Ct Radiomics and clinical risk factors for prediction of prognosis of hypertensive intracerebral hemorrhage. *Comput Intell Neurosci*. (2022) 2022:9751988. doi: 10.1155/2022/9751988

32. Geng X, Zhang Y, Li Y, Cai Y, Liu J, Geng T, et al. Radiomics-clinical nomogram for preoperative lymph node metastasis prediction in esophageal carcinoma. *J Radiol*. (2024) 97:652–9. doi: 10.1093/bjr/tqae009

33. Deo RC. Machine learning in medicine. *Circulation*. (2015) 132:1920–30. doi: 10.1161/CIRCULATIONAHA.115.001593

34. Zhang X, He Z, Zhang Y, Kong J. Prediction of initial objective response to drug-eluting beads Transcatheter arterial chemoembolization for hepatocellular carcinoma using Ct Radiomics-based machine learning model. *Front Pharmacol*. (2024) 15:1315732. doi: 10.3389/fphar.2024.1315732

35. Zhou W, Lv Y, Hu X, Luo Y, Li J, Zhu H, et al. Study on the changes of Ct texture parameters before and after Hcc treatment in the efficacy evaluation and survival predication of patients with Hcc. *Front Oncol*. (2022) 12:957737. doi: 10.3389/fonc.2022.957737

36. Zhang Y-B, Yang G, Bu Y, Lei P, Zhang W, Zhang D-Y. Development of a machine learning-based model for predicting risk of early postoperative recurrence of hepatocellular carcinoma. *World J Gastroenterol*. (2023) 29:5804–17. doi: 10.3748/wjg.v29.i43.5804

37. Huang Y, Chen H, Zeng Y, Liu Z, Ma H, Liu J. Development and validation of a machine learning prognostic model for hepatocellular carcinoma recurrence after surgical resection. *Front Oncol*. (2021) 10:593741. doi: 10.3389/fonc.2020.593741

38. Peng H-Y, Duan S-J, Pan L, Wang M-Y, Chen J-L, Wang Y-C, et al. Development and validation of machine learning models for non-alcoholic fatty liver disease. *Hepatob Pancreat Dis*. (2023) 22:615–21. doi: 10.1016/j.hbpd.2023.03.009

39. Lilhore UK, Dalal S, Simaiya S. A cognitive security framework for detecting intrusions in Iot and 5g utilizing deep learning. *Comput Secur*. (2024) 136:103560. doi: 10.1016/j.cose.2023.103560

40. Lilhore UK, Manoharan P, Simaiya S, Alroobaea R, Alsafyani M, Baqasah AM, et al. Hidm: hybrid intrusion detection model for industry 4.0 networks using an optimized Cnn-Lstm with transfer learning. *Sensors*. (2023) 23:7856. doi: 10.3390/s23187856

frontiers | Frontiers in Pharmacology

TYPE Systematic Review
PUBLISHED 29 July 2024
DOI 10.3389/fphar.2024.1443551

OPEN ACCESS

EDITED BY
Pradeep Kumar Shukla,
University of Tennessee Health Science Center (UTHSC), United States

REVIEWED BY
Ka Zhang,
Sun Yat-sen University, China
Naresh Poondla,
Icahn School of Medicine at Mount Sinai, United States

*CORRESPONDENCE
Aidong Wang,
wangaidong@enzemed.com

RECEIVED 04 June 2024
ACCEPTED 08 July 2024
PUBLISHED 29 July 2024

CITATION
Hu L, Yang C, Qiao Y and Wang A (2024), A systematic review and meta-analysis comparing the impact of tenofovir and entecavir on the prognosis of hepatitis B virus-related hepatocellular carcinoma patients undergoing liver resection.
Front. Pharmacol. 15:1443551.
doi: 10.3389/fphar.2024.1443551

A systematic review and meta-analysis comparing the impact of tenofovir and entecavir on the prognosis of hepatitis B virus-related hepatocellular carcinoma patients undergoing liver resection

Lingbo Hu[1,2], Chao Yang[3], Yingli Qiao[1,2] and Aidong Wang[1,2]*

[1]Department of Hepatopancreatobiliary Surgery, Taizhou Hospital of Zhejiang Province Affiliated to Wenzhou Medical University, Taizhou, Zhejiang, China, [2]Department of Hepatopancreatobiliary Surgery, Enze Hospital, Taizhou Enze Medical Center (Group), Taizhou, Zhejiang, China, [3]Department of Blood Purification, Taizhou Hospital of Zhejiang Province Affiliated to Wenzhou Medical University, Taizhou, Zhejiang, China

Background: Tenofovir (TDF) and entecavir (ETV) are highly effective and well-tolerated nucleos(t)ide analogs commonly prescribed for hepatitis B virus (HBV) treatment. Yet, it is unclear whether survival outcomes differ for HBV-related hepatocellular carcinoma (HCC) patients treated with ETV and TDF. Thus, this meta-analysis aimed to compare the prognostic effectiveness of ETV and TDF in HBV-related HCC patients.

Methods: We comprehensively searched four databases, PubMed, Web of Science, Embase, and the Cochrane Library, to identify pertinent studies utilizing keywords "entecavir," "tenofovir," "hepatocellular carcinoma," and "liver resection." Our primary outcomes of interest encompassed overall survival (OS), recurrence-free survival (RFS), early recurrence, and late recurrence. The statistical effect size for these measures was expressed in terms of hazard ratios (HRs).

Results: Our search yielded 10 studies encompassing 11 datasets involving 7,400 patients. Our meta-analysis revealed that patients treated with TDF achieved better OS (HR = 0.53; 95% confidence interval [CI] = 0.40–0.70, $p < 0.0001$), RFS (HR = 0.68; 95% CI = 0.57–0.80; $p < 0.0001$), early recurrence (HR = 0.80; 95% CI = 0.67–0.94; $p < 0.0077$), and late recurrence (HR = 0.64; 95% CI = 0.43–0.97; $p = 0.0368$). We detected publication bias potentially affecting OS but not RFS.

Conclusion: Our findings demonstrated that TDF outperformed ETV regarding RFS for HBV-related HCC patients. However, to bolster the evidence and establish more conclusive conclusions, further validation via extensive and high-quality randomized controlled trials is essential.

Systematic Review Registration: https://www.crd.york.ac.uk/prospero/#recordDetails, identifier CRD 42024542579.

KEYWORDS

hepatocellular carcinoma, entecavir, tenofovir, liver resection, meta-analysis, prognosis

Introduction

Liver cancer is the sixth most common cancer globally and third leading cause of mortality (Sung et al., 2021), with hepatocellular carcinoma (HCC) constituting roughly 90% of the cases (Llovet et al., 2021). The considerable recurrence rate following liver resection contributes to an unfavorable prognosis in HCC patients (Llovet et al., 2021). Persistent hepatitis B virus (HBV) replication significantly elevates the risk of HCC recurrence. Nucleos(t)ide analog therapy, reducing the virus load, has the potential to substantially prolong overall survival (OS) and minimize tumor recurrence in HCC patients (Huang et al., 2015; Wang et al., 2020).

Tenofovir (TDF) and entecavir (ETV) are highly effective and well-tolerated nucleos(t)ide analogs used for HBV treatment. However, observations suggest that TDF may confer a significantly lower risk of HCC than ETV in patients with chronic hepatitis B (Choi et al., 2023). This finding prompts questions regarding whether the roles of TDF and ETV in the prognosis of HBV-associated HCC after liver resection differ. While some studies suggest a more favorable efficacy of TDF than ETV in the prognosis of HBV-related HCC patients (Choi et al., 2021; Qi et al., 2021), others have indicated similar efficacy of both drugs on the prognosis (Kao et al., 2023; Liang et al., 2024). Thus, we executed a meta-analysis to compare their prognostic efficacy following liver resection in HBV-related HCC patients.

Materials and methods

This review has been registered in the PROSPERO database (registration No. CRD 42024542579).

Search strategy

On 19 March 2024, we systematically searched the Web of Science, PubMed, Embase, and Cochrane Library utilizing a combination of MeSH terms and keywords, focusing on HCC, liver resection, entecavir, and tenofovir. Supplementary Table S1 lists the comprehensive details of the search strategy.

Inclusion criteria

We used the PICOS criteria for inclusion, where P indicates that patients with HBV-related HCC received liver resection; I indicates that TDF was adopted after liver resection; C indicates that ETV was adopted after liver resection; O indicates that outcomes included overall survival (OS), recurrence-free survival (RFS), early recurrence, or late recurrence; and S indicates that retrospective studies and randomized controlled trials (RCTs) were legal.

Exclusion criteria

Non-comparative studies, case reports, abstracts, comments, and reviews were excluded. In the cases of overlapping patient cohorts, only the foremost study, determined by factors such as superior quality, larger sample size, or the most recent publication, was included.

Definition

OS and RFS were characterized as the duration from surgery to death and tumor recurrence, respectively. Early recurrence and late recurrence were specified as a recurrence within 2 years and 2 or more years post-liver resection, respectively.

Quality assessment and data extraction

Two researchers independently performed quality assessment and data extraction using the Newcastle–Ottawa scale (NOS) for non-RCTs with scores of up to 9 points (Wells et al., 2014), and the Cochrane risk assessment tool was used for RCTs (Sterne et al., 2019). Study details, such as tumor characteristics, patient information, the first author, and the publication year, were extracted using pre-designed, standardized forms. Outcomes, including OS, RFS, early recurrence, and late recurrence, were extracted from original reports or via data conversion using ReviewManager software (version 5.3). Any disagreements between researchers were resolved by a third party.

Statistical analysis

Hazard ratio (HR) and 95% confidence interval (CI) values were determined using the inverse variance method. Heterogeneity was evaluated through the Q statistic and I^2, with I^2 of 25% and 50% denoting low and moderate heterogeneity, respectively. Heterogeneity sources were explored using either meta-regression with the random-effects model for studies with $I^2 > 50\%$ or subgroup analysis. A leave-one-out sensitivity analysis was applied to assess the robustness of the conclusion. Funnel plots were used to examine publication bias, and its influence on the results was further analyzed using the trim-and-fill method. All analyses were conducted using the R program (version 4.4.0). Statistically significant difference was deemed at $p < 0.05$.

Results

Study search and inclusion

A thorough search produced 147 articles, which were reduced to 102 after eliminating duplicates. After reviewing titles and abstracts, 22 records were retained. Twelve studies were excluded due to duplicated data, incorrect comparisons, and inappropriate article types (Figure 1). Consequently, this meta-analysis incorporated 10 studies (Zhang et al., 2018; Choi et al., 2021; Qi et al., 2021; Shen et al., 2022; Tsai et al., 2022; Wang et al., 2022; Kao et al., 2023; Li et al., 2023; Linye et al., 2023; Liang et al., 2024).

Study characteristics

Ten studies, comprising 11 datasets and involving 7,400 patients, compared TDF and ETF efficacy in HBV-related HCC prognosis. Among them, nine were from China, and one was from Korea. Two were retrospective studies, one was an RCT, and the rest were retrospective studies using propensity analysis

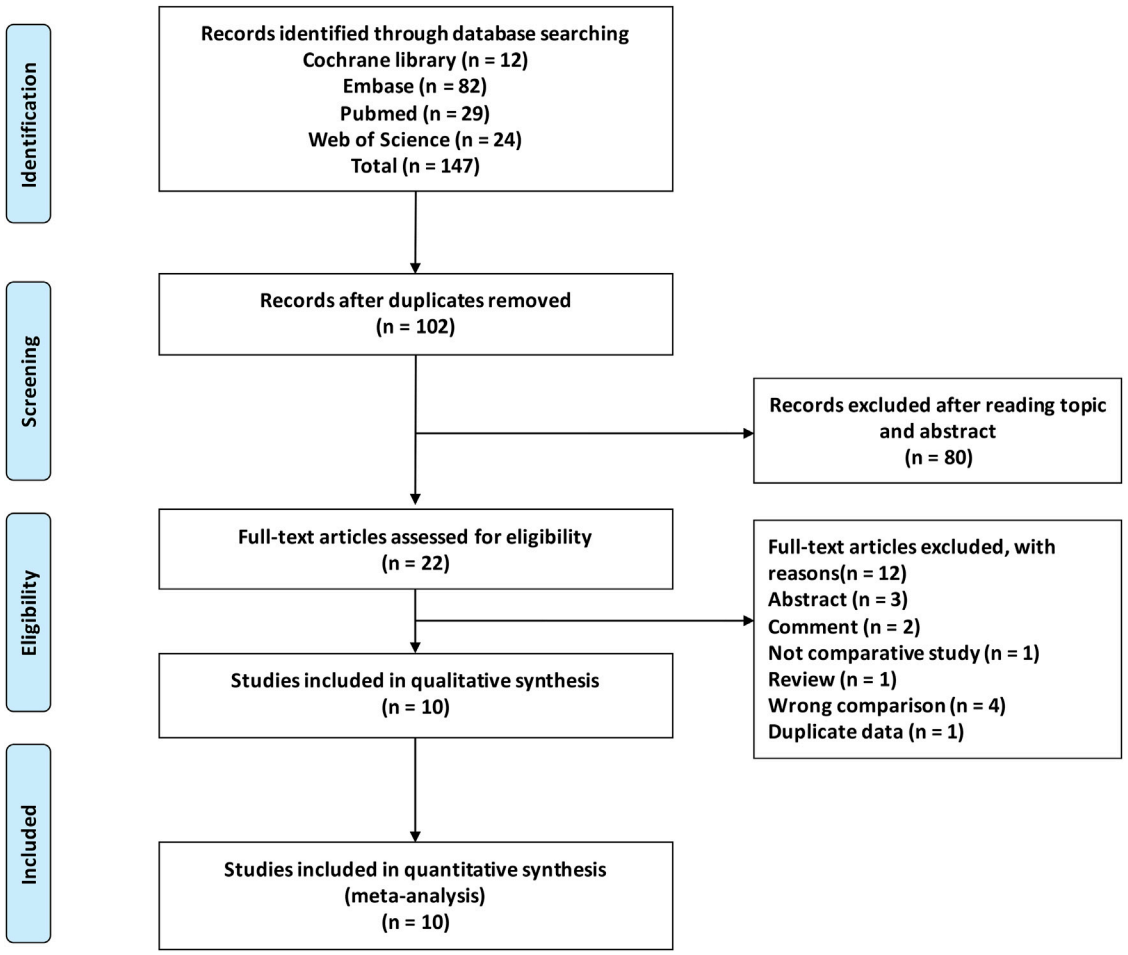

FIGURE 1
Flowchart depicting the selection process of studies.

(including propensity-score matching, propensity-score overlap weighting, and inverse probability of treatment weighting). Three studies exclusively included patients at the Barcelona Clinical Liver Cancer Staging (BCLC) 0 or A stage. Table 1 lists the detailed patient and tumor characteristics.

Quality assessment

Supplementary Tables S2, S3 list the quality assessment details of the included studies. Of the nine non-RCT studies, two scored 7 points, two scored 8 points, and five scored 9 points. Thus, the two studies with 7 points were deemed as moderate-quality, and the remaining seven were classified as high-quality. For the RCT, the blind method implementation was not elucidated in the article, with all other domains showing low risk.

Outcomes

HR values for OS were reported in eight studies comprising nine datasets and analyzed based on the random-effects model. The aggregated data indicated that patients treated with TDF achieved superior OS (HR, 0.53; 95% CI, 0.40–0.70; $p < 0.0001$) (Figure 2). Ten studies with 11 datasets documented the HR values for RFS, which was analyzed with the random-effects model. The combined data suggested that patients treated with TDF achieved better RFS (HR, 0.68; 95% CI, 0.57–0.80; $p < 0.0001$) (Figure 2).

The 1-, 3-, and 5-year OS rates were reported in five, five, and four studies, respectively, and analyzed using the random-effects model due to the observed heterogeneity. The pooled results revealed a higher 5-year OS rate with TDF (5-year RR, 1.19; 95% CI, 1.04–1.35; $p = 0.0113$) but similar 1- and 3-year OS rates (Figure 3). Similarly, 1-, 3-, and 5-year RFS rates were documented in five, five, and four studies, respectively, and analyzed using the random-effects model, with the exception of the 3-year RFS rate, which presented low heterogeneity. The synthesized data revealed higher 3- and 5-year RFS rates with TDF (3-year RR, 1.14; 95% CI, 1.08–1.20; $p < 0.0001$; 5-year RR, 1.31; 95% CI, 1.13–1.53; $p = 0.0005$), with similar 1-year RFS rates (Figure 3).

The studies with four datasets that reported HR values for early recurrence were analyzed using the fixed-effects model. The pooled data indicated that patients treated with TDF achieved better early

TABLE 1 Features of the incorporated studies.

Study	NOS score	Design	Country	Group	Sample size	Age year	Gender male/female	HBV DNA copy/mL	HBeAg positive n (%)
Liang 2024	7	R	China	ETV	59	56 ± 12	53/6	12 (<1,000) 47 (≥1,000)	14 (23.7)
PO cohort				TDF	31	56 ± 14	28/3	12 (<1,000) 19 (≥1,000)	16 (51.6)
Liang 2024	7	R	China	ETV	51	59 ± 11	40/11	33 (<1,000) 18 (≥1,000)	17 (33.3)
PPO cohort				TDF	55	57 ± 12	45/10	34 (<1,000) 21 (≥1,000)	14 (25.5)
He 2023	NA	RCT	China	ETV	74	49.78 ± 11.95	66/8	57 (<2,000) 17 (≥2,000)	22 (29.7)
				TDF	74	50.97 ± 12.17	63/11	55 (<2,000) 19 (≥2,000)	16 (21.6)
Li 2023	9	PSM 1:1	China	ETV	989	58.3 ± 9.8	884/145	3.3 ± 1.8 (log copies/mL)	270 (27.3)
				TDF	989	58.4 ± 10.5	851/138	3.3 ± 1.8 (log copies/mL)	261 (26.4)
Kao 2023	9	PS overlap weighting	China	ETV	1,365	58.22 ± 11.14	1,143/222	NA	NA
				TDF	432	56.13 ± 10.79	367/65	NA	NA
Wang 2022	8	PSM 2:1	China	ETV	403	49.0 (18–80)[a]	344/59	116 (undetectable) 77 (<2,000) 210 (≥2,000)	117 (29.0)
				TDF	265	49.0 (18–79)[a]	231/34	73 (undetectable) 58 (<2,000) 134 (≥2,000)	77 (29.1)
Tsai 2022	8	PSM 2:1	China	ETV	146	56.4 ± 10.9	127/19	65 (undetectable) 15 (<2,000) 65 (≥2,000)	27 (18.5)
				TDF	73	56.5 ± 10.6	64/9	29 (undetectable) 11 (<2,000) 32 (≥2,000)	16 (21.7)
Shen 2022	9	IPTW	China	ETV	533	412 (≤60) 121 (>60)	450/83	162 (≤1,000) 371 (>1,000)	115 (21.6)
				TDF	62	52 (≤60) 10 (>60)	52/10	24 (≤1,000) 38 (>1,000)	15 (24.2)
Qi 2021	9	PSM 2:1	China	ETV	288	49.3 ± 10.6	248/40	131 (≤1,000) 157 (>1,000)	56 (23.0)
				TDF	144	49.9 ± 10.7	122/22	68 (≤1,000) 76 (>1,000)	29 (24.1)
Choi 2021	9	PSM 1:1	Korea	ETV	567	54.6 ± 8.6	430/137	238 (undetectable) 151 (<2,000) 178 (≥2,000)	137 (24.2)
				TDF	567	54.7 ± 9.3	433/134	236 (undetectable) 150 (<2,000) 181 (≥2,000)	149 (26.3)
Zhang 2018	7	R	China	ETV	126	55 (26–73)[a]	107/19	4.1 (3.0–5.1)[a] (log copies/mL)	88 (69.84)
				TDF	107	52 (25–69)[a]	82/25	3.7 (3.0–4.7)[a] (log copies/mL)	76 (71.03)

(Continued on following page)

10.3389/fphar.2024.1443551

TABLE 1 (Continued) Features of the incorporated studies.

Cirrhosis n (%)	AFP ng/mL	BCLC stage	MVI positive n (%)	Tumor size cm	Tumor number single/ multiple	Tumor differentiation	Satellite nodule n (%)
45 (76.3)	29 (<20) 30 (≥20)	29 (0/A) 30 (B)	30 (50.8)	6.2 ± 2.6	34/25	12 (P) 47 (M + H)	NA
20 (64.5)	17 (<20) 14 (≥20)	20 (0/A) 11 (B)	17 (54.8)	6.7 ± 2.6	22/9	10 (P) 21 (M + H)	NA
32 (62.7)	24 (<20) 27 (≥20)	29 (0/A) 22 (B)	17 (33.3)	6.4 ± 3.8	36/15	9 (P) 42 (M + H)	NA
37 (67.3)	26 (<20) 29 (≥20)	37 (0/A) 18 (B)	20 (36.4)	5.6 ± 3.2	37/18	15 (P) 40 (M + H)	NA
54 (73.0)	30 (<20) 44 (≥20)	21 (0) 53 (A)	17 (23.0)	3.05 ± 0.89	16/58	32 (P + M) 42 (H)	4 (5.4)
55 (74.3)	28 (<20) 46 (≥20)	32 (0) 42 (A)	19 (25.7)	2.91 ± 0.82	53/21	35 (P + M) 39 (H)	3 (4.1)
360 (36.4)	543.2 ± 6,339.4	98 (0) 747 (A) 144 (B)	477 (48.2)	4.2 (0.3–25.0)[a]	811/178	NA	NA
362 (36.6)	461 ± 3,065.8	120 (0) 743 (A) 126 (B)	471 (47.6)	4.1 (0.5–23.1)[a]	823/166	NA	NA
1,015 (74.36)	1,017 (<20) 230 (≥20)	155 (0) 806 (A) 404 (B)	NA	4.26 ± 3.24	NA	434 (P) 740 (M) 106 (H)	NA
334 (77.31)	313 (<20) 86 (≥20)	59 (0) 262 (A) 111 (B)	NA	3.78 ± 2.4	NA	114 (P) 259 (M) 34 (H)	NA
233 (57.8)	184 (<20) 219 (≥20)	29 (0) 330 (A) 44 (B)	94 (23.3)	5.5 (0.8–19.0)§	349/54	144 (P) 198 (M) 61 (H)	NA
164 (61.9)	128 (<20) 137 (≥20)	22 (0) 214 (A) 29 (B)	54 (20.4)	5.5 (0.9–19.5)§	229/36	96 (P) 130 (M) 39 (H)	NA
84 (57.5)	70 (<20) 76 (≥20)	34 (0) 112 (A)	50 (34.2)	2.6 ± 1.0	127/19	10 (P) 107 (M) 29 (H)	7 (4.8)
44 (60.3)	34 (<20) 39 (≥20)	19 (0) 54 (A)	25 (34.2)	2.7 ± 1.0	64/9	6 (P) 50 (M) 17 (H)	4 (5.5)
446 (83.7)	263(≤400) 270 (>400)	NA	205 (38.5)	8.5 (6.3–12.0)[b]	450/83	262 (P) 269 (M) 2 (H)	85 (15.9)
56 (90.3)	29 (≤400) 33 (>400)	NA	23 (37.1)	8.5 (6.5–11.0)[b]	50/12	33 (P) 29 (M) 0 (H)	6 (9.7)

(Continued on following page)

10.3389/fphar.2024.1443551

TABLE 1 (Continued) Features of the incorporated studies.

Cirrhosis n (%)	AFP ng/mL	BCLC stage	MVI positive n (%)	Tumor size cm	Tumor number single/ multiple	Tumor differentiation	Satellite nodule n (%)
243 (84.3)	179(≤400) 109 (>400)	18 (0) 212 (A) 19 (B) 39 (C)	87 (30.2)	5.5 ± 3.3	253/35	155 (P) 132 (M) 1 (H)	22 (7.6)
120 (83.3)	86 (≤400) 58 (>400)	10 (0) 107 (A) 8 (B) 19 (C)	44 (30.5)	5.6 ± 3.8	128/14	76 (P) 66 (M) 2 (H)	11 (7.6)
340 (60.0)	297 (<20) 270 (≥20)	151 (0) 416 (A)	157 (27.7)	2.7 (2.0–4.0)[b]	545/22	193 (P) 353 (M) 21 (H)	22 (3.9)
333 (58.7)	296 (<20) 271 (≥20)	142 (0) 425 (A)	148 (26.1)	2.8 (2.0–4.1)[b]	540/27	194 (P) 360 (M) 13 (H)	22 (3.9)
37 (29.36)	109 (10.3–1,210)[a]	NA	NA	4.4 (2.6–8.5)[a]	NA	NA	NA
59 (55.14)	97.5 (7.8–1,210)[a]	NA	NA	3.8 (2.8–9.7)[a]	NA	NA	NA

Note: PO cohort, in this cohort, patients received entecavir or tenofovir post-operation; PPO cohort, in this cohort, patients received entecavir or tenofovir pre-operation and post-operation; NOS, Newcastle–Ottawa scale; R, retrospective study; RCT, randomized controlled trial; PSM, propensity score matching; PS overlap weighting, propensity-score overlap weighting; IPTW, inverse probability of treatment weighting; ETV, entecavir; TDF, tenofovir; HBV, hepatitis B virus; NA, not available; HBeAg, hepatitis B e antigen; AFP, alpha-fetoprotein; BCLC, Barcelona clinical liver cancer; MVI, microvascular invasion; P, poorly differentiated; M, moderately differentiated; H, highly differentiated.

[a]data are presented as the median and range.

[b]data are presented as the median and inter-quartile range.

10.3389/fphar.2024.1443551

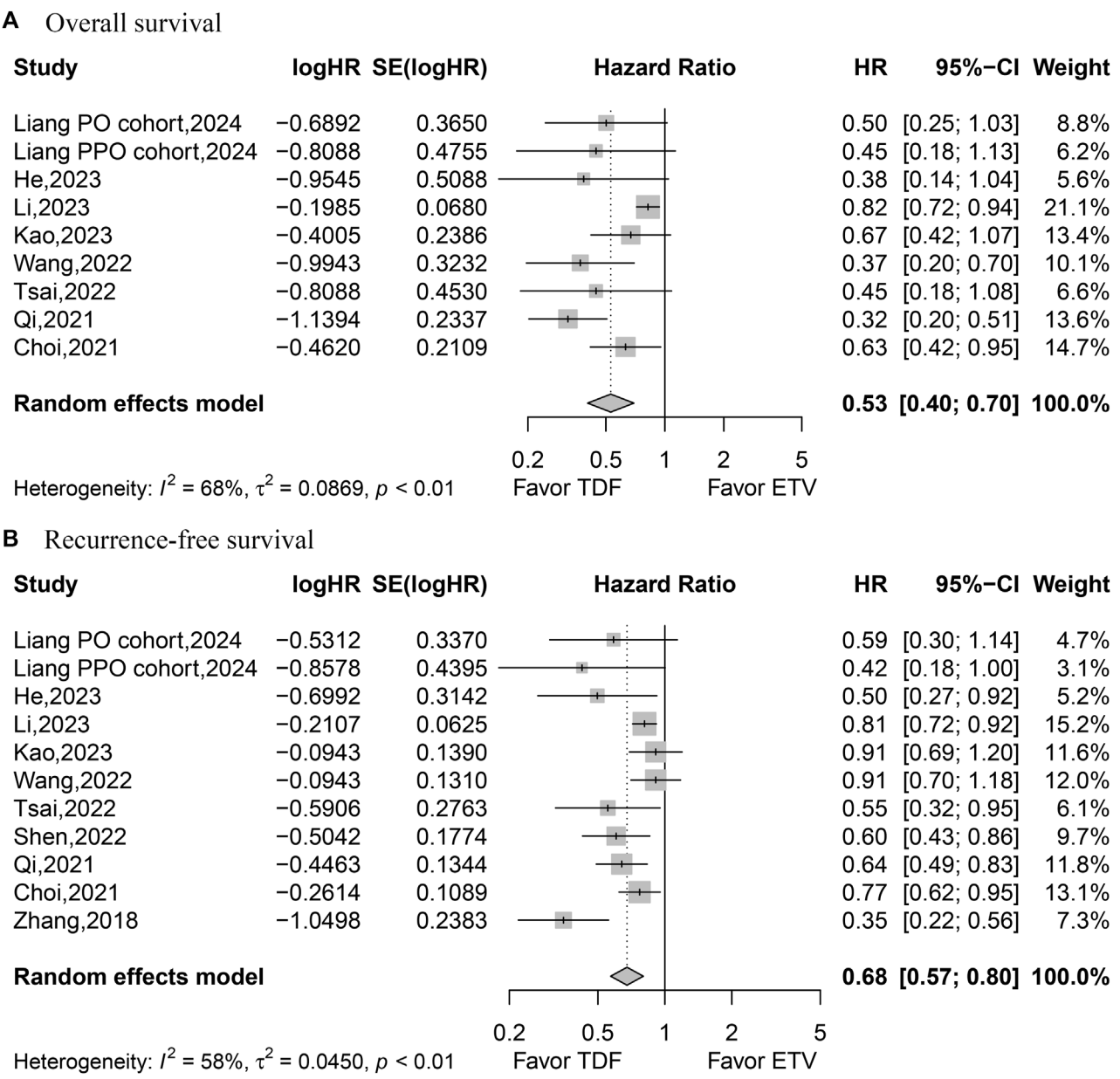

FIGURE 2
Forest plot for overall survival **(A)** and recurrence-free survival **(B)**.

recurrence outcomes (HR, 0.80; 95% CI, 0.67–0.94; p < 0.0077) (Figure 4). Furthermore, four studies with four datasets reporting HR values for late recurrence were analyzed with the random-effects model. The combined data suggested that patients treated with TDF achieved better late recurrence (HR, 0.64; 95% CI, 0.43–0.97; p = 0.0368) (Figure 4).

Meta-regression, subgroup analyses, and sensitivity analyses

Meta-regression was performed only for RFS due to the smaller number of OS datasets (<10). The results revealed the sample size and retrospective study design as the heterogeneity sources (Supplementary Figure S1). Subgroup analyses were conducted for retrospective studies, propensity analysis studies combined with RCT, studies that only included BCLC early-stage HCC, studies conducted in China, and available patient characteristics. Figure 5 shows that patients receiving TDF achieved better OS and RFS in subgroup analyses. In the sensitivity analysis of OS, the overall heterogeneity decreased after the removal of the study conducted by Li, indicating that this study is one of the sources of heterogeneity but does not affect the results of the meta-analysis. This study was a propensity score matching (PSM) study with high quality and the largest sample size (Supplementary Figure S2). The sensitivity analysis for RFS indicated that the result was stable (Supplementary Figure S2B). Additionally, the sensitivity analyses indicated that the early recurrence and late recurrence results were

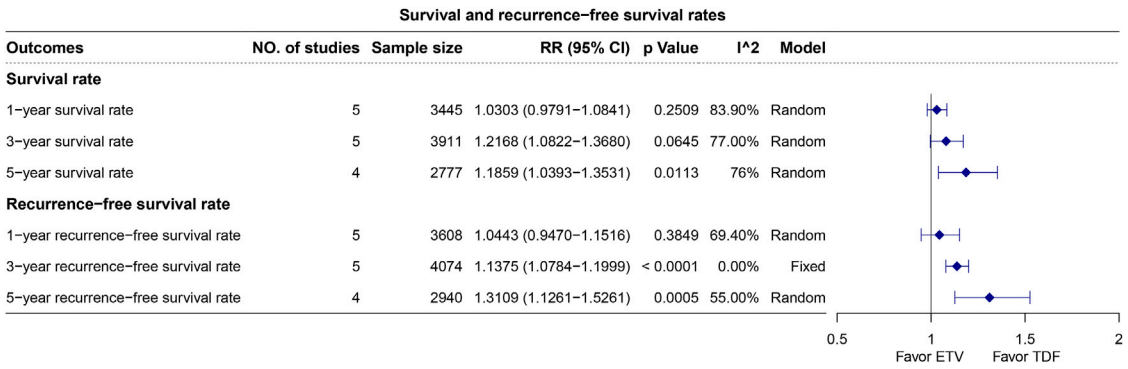

FIGURE 3
Plot for the overall survival and recurrence-free survival rates.

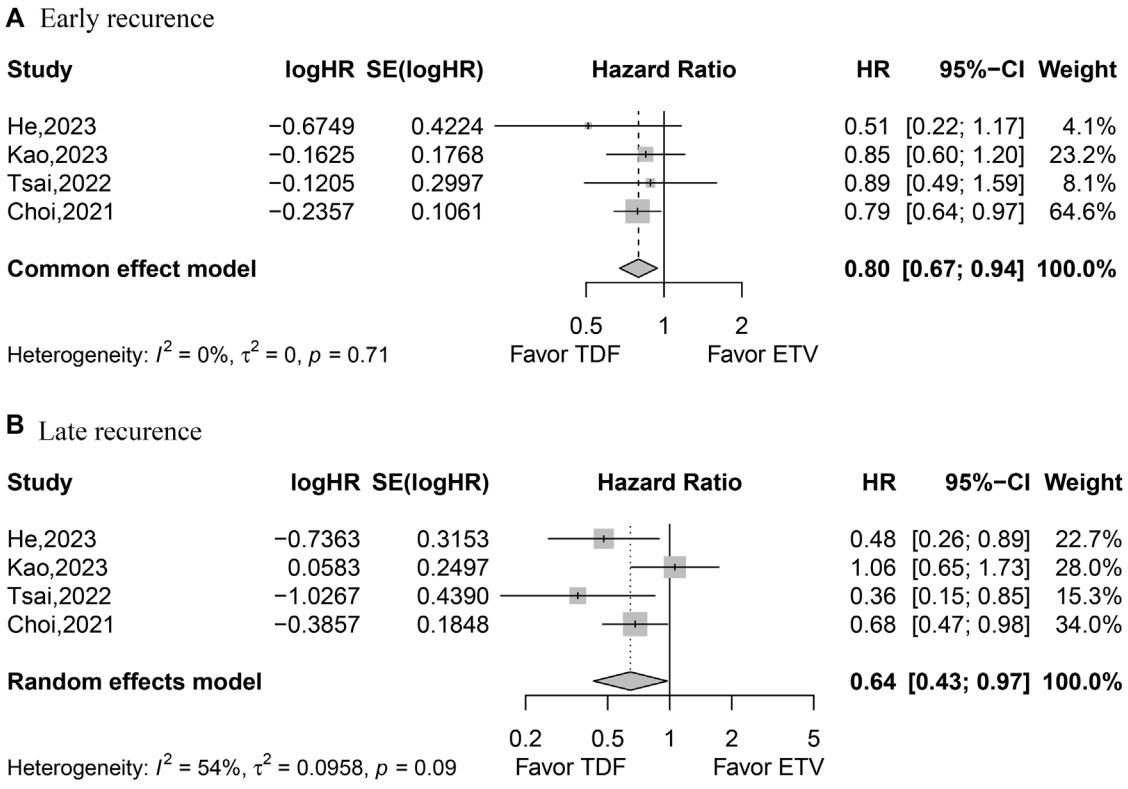

FIGURE 4
Forest plot for early recurrence **(A)** and late recurrence **(B)**.

less stable (Supplementary Figures S2C, D). The studies by Kao et al. and Choi et al. would affect the results of early recurrence and late recurrence.

Publication bias

Funnel plots with the Egger test revealed publication bias in OS and RFS but not in early recurrence and late recurrence (Supplementary Figure S3). Contour-enhanced funnel plots for OS and RFS indicated filled studies in the white area ($p < 0.05$), suggesting that publication bias affected the meta-analysis results (Supplementary Figures S4A, B). After filling potential unpublished studies, the meta-analysis showed superior RFS for patients receiving TDF compared to ETV, while OS remained similar between TDF and ETV recipients (Supplementary Figure S5).

Discussion

In our meta-analysis, HBV-related HCC patients on TDF exhibited better OS, RFS, early recurrence, and late recurrence.

10.3389/fphar.2024.1443551

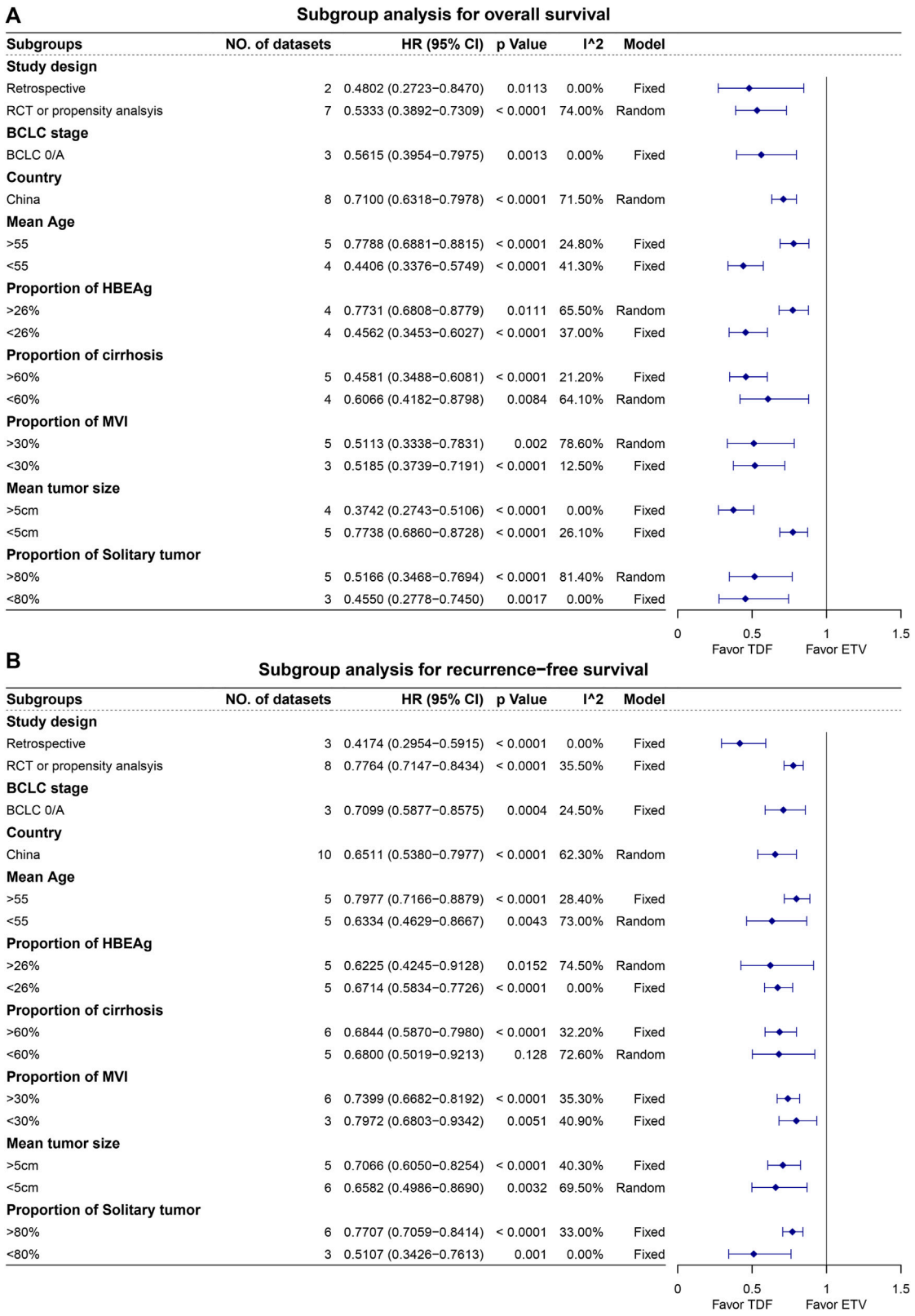

FIGURE 5
Subgroup analysis for overall survival **(A)** and recurrence-free survival **(B)**.

Previous meta-analyses that mainly compared TDF and ETV for HBV-related HCC prognosis (Giri et al., 2023; Liu et al., 2023; Kong et al., 2024) included patients receiving various treatments, such as liver transplantation, radiofrequency ablation, and liver resection, inevitably introducing bias. We focused solely on HCC patients undergoing liver resection to minimize bias from different treatments. Additionally, we comprehensively analyzed the result reliability. The meta-regression analysis revealed the heterogeneity sources, urging for larger, higher-quality studies. The subgroup analyses by study design and tumor stage supported our findings. Moreover, publication bias was identified. Addressing publication bias by filling the potentially unpublished studies revealed the consistently better efficacy of TDF on RFS over ETV, questioning its superiority on OS. This increases our confidence in the hypothesis that TDF can lead to better outcomes for HCC patients than ETV. Additionally, we advocate for publishing articles with negative or conflicting conclusions. Based on the meta-analysis, we believe that TDF is superior to ETV in improving RFS. The current research suggested that the improvement in RFS with TDF is due to its superior HBV-DNA suppression and anti-inflammatory effects compared to ETV (12). Therefore, TDF is more suitable as an antiviral medication for postoperative patients with higher viral loads.

Our study is subject to some constrains. First, the majority of the incorporated studies were non-RCTs. Although they demonstrated high quality, the inherent bias cannot be fully addressed by propensity analysis. Second, all studies were performed in Asia, potentially restricting the generalizability of our findings to other populations. Third, heterogeneity was present. Although we conducted a meta-regression analysis to explore its source, the subgroup analysis supported the reliability of our results. Fourth, publication bias was identified. However, using the trim-and-fill method, we observed the consistent efficacy of TDF over ETV in terms of RFS. Lastly, some studies had relatively small sample sizes, potentially impacting the robustness of our findings.

Conclusion

Our meta-analysis demonstrated the superiority of TDF over ETV in RFS for HBV-related HCC patients. These findings carry significant implications for postoperative antiviral therapy selection. However, further extensive, high-quality RCTs are necessary to bolster evidence and draw more conclusive recommendations.

Data availability statement

The original contributions presented in the study are included in the article/Supplementary Material; further inquiries can be directed to the corresponding author.

Author contributions

LH: conceptualization, data curation, formal analysis, methodology, software, visualization, writing–original draft, and writing–review and editing. CY: data curation and writing–review and editing. YQ: funding acquisition, validation, and writing–review and editing. AW: funding acquisition, validation, and writing–review and editing.

Funding

The author(s) declare that financial support was received for the research, authorship, and/or publication of this article. This research was sponsored by the Zhejiang Provincial Basic Public Welfare Research Project (No. LTGY23H030008), the Taizhou Science and Technology Planning Project (Nos 20ywb25 and 22ywa34), the Medical and Health Technology Plan of Zhejiang Province (Nos 2021RC140 and 2024KY1825), and the Taizhou High-level Talents Special Support Program (the third level).

Acknowledgments

The authors thank TopEdit (www.topeditsci.com) for the English language editing of this manuscript.

Conflict of interest

The authors declare that the research was conducted in the absence of any commercial or financial relationships that could be construed as a potential conflict of interest.

Publisher's note

Supplementary material

The Supplementary Material for this article can be found online at: https://www.frontiersin.org/articles/10.3389/fphar.2024.1443551/full#supplementary-material

References

Choi, J., Jo, C., and Lim, Y. S. (2021). Tenofovir versus entecavir on recurrence of hepatitis B virus–related hepatocellular carcinoma after surgical resection. *Hepatology* 73 (2), 661–673. doi:10.1002/hep.31289

Choi, W. M., Yip, T. C., Wong, G. L., Kim, W. R., Yee, L. J., Brooks-Rooney, C., et al. (2023). Hepatocellular carcinoma risk in patients with chronic hepatitis B receiving tenofovir-vs. entecavir-based regimens: individual patient data meta-analysis. *J. Hepatol.* 78 (3), 534–542. doi:10.1016/j.jhep.2022.12.007

Giri, S., Agrawal, D., Afzalpurkar, S., Gopan, A., Angadi, S., and Sundaram, S. (2023). Tenofovir versus entecavir for tertiary prevention of hepatocellular carcinoma in chronic hepatitis B infection after curative therapy: a

systematic review and meta-analysis. *J. Viral Hepat.* 30 (2), 108–115. doi:10.1111/jvh.13766

G. A. Wells, G. Wells, B. Shea, B. Shea, D. O'Connell, J. Peterson, et al. (2014). *The newcastle-ottawa Scale (NOS) for assessing the quality of nonrandomised studies in meta-analyses*. (Ottawa: The Ottawa Hospital).

Huang, G., Lau, W. Y., Wang, Z. G., Pan, Z. Y., Yuan, S. X., Shen, F., et al. (2015). Antiviral therapy improves postoperative survival in patients with hepatocellular carcinoma: a randomized controlled trial. *Ann. Surg.* 261 (1), 56–66. doi:10.1097/SLA.0000000000000858

Kao, W. Y., Tan, E. C. H., Lee, H. L., Huang, Y. H., Huo, T. I., Chang, C. C., et al. (2023). Entecavir versus tenofovir on prognosis of hepatitis B virus-related hepatocellular carcinoma after curative hepatectomy. *Alimentary Pharmacol. Ther.* 57 (11), 1299–1312. doi:10.1111/apt.17438

Kong, Q., Yi, M., Teng, F., and Chen, Z. (2024). Enhanced prognosis of HCC patients undergoing radical treatments with tenofovir versus entecavir: a meta-analysis based on propensity score matching studies. *Asian J. Surg.* 47 (1), 55–62. doi:10.1016/j.asjsur.2023.09.057

Li, P. P., Wang, Y. Y., Yu, J., Yu, J. D., Tao, Q. F., Zhang, J. W., et al. (2023). Tenofovir vs entecavir among patients with HBV-related HCC after resection. *Jama Netw. Open* 6 (10), e2340353. doi:10.1001/jamanetworkopen.2023.40353

Liang, Y., Zhong, D., Zhang, Z., Su, Y., Yan, S., Lai, C., et al. (2024). Impact of preoperative antiviral therapy on the prognosis of hepatitis B virus-related hepatocellular carcinoma. *BMC Cancer* 24 (1), 291. doi:10.1186/s12885-024-12031-0

Linye, H., Zijing, X., Xiaoyun, Z., Zhihui, L., Tianfu, W., and Chuan, L. (2023). Tenofovir versus entecavir on the prognosis of hepatitis B-related hepatocellular carcinoma after surgical resection: a randomised controlled trial. *Int. J. Surg. Lond. Engl.* 109 (10), 3032–3041. doi:10.1097/JS9.0000000000000554

Liu, H., Han, C. L., Tian, B. W., Ding, Z. N., Yang, Y. F., Ma, Y. L., et al. (2023). Tenofovir versus entecavir on the prognosis of hepatitis B virus-related hepatocellular carcinoma: a systematic review and meta-analysis. *Expert Rev. Gastroenterol. Hepatol.* 17 (6), 623–633. doi:10.1080/17474124.2023.2212161

Llovet, J. M., Kelley, R. K., Villanueva, A., Singal, A. G., Pikarsky, E., Roayaie, S., et al. (2021). Hepatocellular carcinoma. *Nat. Rev. Dis. Prim.* 7 (1), 6. doi:10.1038/s41572-020-00240-3

Qi, W., Shen, J., Dai, J., Wu, Y., Zhang, Y., Leng, S., et al. (2021). Comparison of nucleoside and nucleotide analogs in the recurrence of hepatitis B virus-related hepatocellular carcinoma after surgical resection: a multicenter study. *Cancer Med.* 10 (23), 8421–8431. doi:10.1002/cam4.4348

Shen, J., Qi, W., Dai, J., Leng, S., Jiang, K., Zhang, Y., et al. (2022). Tenofovir vs. entecavir on recurrence of hepatitis B virus-related hepatocellular carcinoma beyond Milan criteria after hepatectomy. *Chin. Med. J.* 135 (3), 301–308. doi:10.1097/CM9.0000000000001864

Sterne, J. A. C., Savović, J., Page, M. J., Elbers, R. G., Blencowe, N. S., Boutron, I., et al. (2019). RoB 2: a revised tool for assessing risk of bias in randomised trials. *Bmj* 366, l4898. doi:10.1136/bmj.l4898

Sung, H., Ferlay, J., Siegel, R. L., Laversanne, M., Soerjomataram, I., Jemal, A., et al. (2021). Global cancer statistics 2020: GLOBOCAN estimates of incidence and mortality worldwide for 36 cancers in 185 countries. *CA Cancer J. Clin.* 71 (3), 209–249. doi:10.3322/caac.21660

Tsai, M. C., Wang, C. C., Lee, W. C., Lin, C. C., Chang, K. C., Chen, C. H., et al. (2022). Tenofovir is superior to entecavir on tertiary prevention for BCLC stage 0/A hepatocellular carcinoma after curative resection. *Liver Cancer* 11 (1), 22–37. doi:10.1159/000518940

Wang, X. H., Hu, Z. L., Fu, Y. Z., Hou, J. Y., Li, W. X., Zhang, Y. J., et al. (2022). Tenofovir vs. entecavir on prognosis of hepatitis B virus-related hepatocellular carcinoma after curative resection. *J. Gastroenterology* 57 (3), 185–198. doi:10.1007/s00535-022-01855-x

Wang, Z. Y., Tao, Q. F., Wang, Z. H., Lin, K. Y., Huang, G., Yang, Y., et al. (2020). Antiviral therapy improves post-operative survival outcomes in patients with HBV-related hepatocellular carcinoma of less than 3 cm - a retrospective cohort study. *Am. J. Surg.* 219 (4), 717–725. doi:10.1016/j.amjsurg.2019.05.016

Zhang, M., Wang, D., Liu, H., and Li, H. (2018). Tenofovir decrease hepatocellular carcinoma recurrence in chronic hepatitis B patients after liver resection. *Infect. Agents Cancer* 13 (1), 19. doi:10.1186/s13027-018-0191-8

frontiers | Frontiers in Oncology

TYPE Original Research
PUBLISHED 13 August 2024
DOI 10.3389/fonc.2024.1422119

OPEN ACCESS

EDITED BY
Liliana Chemello,
University of Padua, Italy

REVIEWED BY
Basen Li,
Huazhong University of Science and Technology, China
Antonio Giovanni Solimando,
University of Bari Aldo Moro, Italy
Shaofeng Duan,
Shanghai United Imaging Healthcare Co., Ltd., China

*CORRESPONDENCE
Xueqin Zhang
13962981245@163.com
Tao Zhang
ntsyzhangtao@sina.com

RECEIVED 23 April 2024
ACCEPTED 29 July 2024
PUBLISHED 13 August 2024

CITATION
Zhang J, Liu M, Qu Q, Lu M, Liu Z, Yan Z, Xu L, Gu C, Zhang X and Zhang T (2024) Radiomics analysis of gadoxetic acid-enhanced MRI for evaluating vessels encapsulating tumour clusters in hepatocellular carcinoma.
Front. Oncol. 14:1422119.
doi: 10.3389/fonc.2024.1422119

Radiomics analysis of gadoxetic acid-enhanced MRI for evaluating vessels encapsulating tumour clusters in hepatocellular carcinoma

Jiyun Zhang[1], Maotong Liu[1], Qi Qu[1], Mengtian Lu[1], Zixin Liu[1], Zuyi Yan[1], Lei Xu[1], Chunyan Gu[2], Xueqin Zhang[1*] and Tao Zhang[1*]

[1]Department of Radiology, Affiliated Nantong Hospital 3 of Nantong University, Nantong Third People's Hospital, Nantong, Jiangsu, China, [2]Department of Pathology, Affiliated Nantong Hospital 3 of Nantong University, Nantong Third People's Hospital, Nantong, Jiangsu, China

Purpose: The aim of this study was to develop an integrated model that combines clinical-radiologic and radiomics features based on gadoxetic acid-enhanced MRI for preoperative evaluating of vessels encapsulating tumour clusters (VETC) patterns in hepatocellular carcinoma (HCC).

Methods: This retrospective study encompassed 234 patients who underwent surgical resection. Among them, 101 patients exhibited VETC-positive HCC, while 133 patients displayed VETC-negative HCC. Volumes of interest were manually delineated for entire tumour regions in the arterial phase (AP), portal phase (PP), and hepatobiliary phase (HBP) images. Independent predictors for VETC were identified through least absolute shrinkage and selection operator (LASSO) regression and multivariable logistic regression analysis, utilising radiomics-AP, PP, HBP, along with 24 imaging features and 19 clinical characteristics. Subsequently, the clinico-radiologic model, radiomics model, and integrated model were established, with a nomogram visualising the integrated model. The performance for VETC prediction was evaluated using a receiver operating characteristic curve.

Results: The integrated model, composed of 3 selected traditional imaging features (necrosis or severe ischemia [OR=2.457], peripheral washout [OR=1.678], LLR_AP (Lesion to liver ratio_AP) [OR=0.433] and radiomics-AP [OR=2.870], radiomics-HBP [OR=2.023], radiomics-PP [OR=1.546]), showcased good accuracy in predicting VETC patterns in both the training (AUC=0.873, 95% confidence interval [CI]: 0.821-0.925)) and validation (AUC=0.869, 95% CI:0.789-0.950) cohorts.

Conclusion: This study established an integrated model that combines traditional imaging features and radiomic features from gadoxetic acid-enhanced MRI, demonstrating good performance in predicting VETC patterns.

KEYWORDS

hepatocellular carcinoma, vessels encapsulating tumour clusters, radiomics, gadoxetic acid, magnetic resonance imaging

1 Introduction

Hepatocellular carcinoma (HCC) stands as one of the most prevalent primary hepatic malignancies, with an annual global incidence of approximately 500,000 cases, a figure that continues to ascend each year (1, 2). Surgical resection and liver transplantation offer potential curative options for HCC patients, however such patients have high recurrence rates (3), and the precise underlying mechanisms governing metastasis and recurrence remain incompletely elucidated.

Epithelial-mesenchymal transition (EMT), a classical metastatic mechanism, is intricately linked to cancer recurrence and metastasis, and has been correlated with shortened survival among HCC patients (4). EMT-mediated metastasis has been identified as a driver of microvascular invasion (MVI), a crucial prognostic factor for HCC post-surgical intervention (5). Nevertheless, within clinical realms, a notable proportion of patients, devoid of MVI and other high-risk conventional clinical parameters, experience relapses subsequent to therapeutic resection. This underscores the inadequacy in comprehensively depicting the heterogeneity and underpinning mechanisms of HCC metastasis and recurrence.

Fang et al. (6) present an alternative mode of HCC metastasis, termed as the EMT-independent "vessels encapsulating tumour clusters" (VETC), characterised by a sinusoidal network of functional blood vessels that entirely envelop sections of the primary tumour. The VETC phenotype, deemed a dependable pathological parameter, exerts an impact on survival and exhibits significant associations with overall survival (OS) and early recurrence (6–9). The comprehension of HCC's VETC status could indeed have far-reaching implications for future treatments (10), to be able to apply precision medicine to HCC treatment.

Fang et al. (11)have indicated that the VETC pattern might serve as a dependable marker for selecting HCC patients who could potentially benefit from sorafenib treatment. VETC-positive tumours might respond to lenvatinib treatment because of gene expression analyses of VETC-positive tumours (10, 12, 13). Because VETC formation is dependent on Ang2, Ang2 inhibitors may be promising in the treatment of VETC-positive HCC. VETC-positive tumours are associated with CTNNB1 mutations and the Wnt/b-catenin signalling pathway activation (7, 12–14). Lin et al. (15) demonstrated significant benefits of adjuvant TACE in terms of time to recurrence and OS in VETC-positive HCC patients. Therefore, VETC status may provide guidance for the prevention and treatment of HCC recurrence. However, the postoperative diagnosis of VETC necessitates surgical specimens. Consequently, it holds immense importance to develop the ability to preoperatively evaluate the VETC pattern, necessitating further research.

To the best of our knowledge, only a handful of studies have endeavoured to delineate the imaging characteristics of the VETC pattern in HCC (9, 16–18). Prior investigations (9, 16–18) have showcased that preoperative CT or MRI features could be harnessed to characterise the VETC pattern. However, despite its potential utility, the analysis of image features is inherently subjective and suffers from limitations in terms of repeatability. Radiomics, a burgeoning field of imaging analysis, can extract a multitude of high-dimensional quantitative features from multimodal medical images, subsequently unravelling the connections between these features and the tumour's diagnosis, pathology, and prognosis (19). Recently, a limited number of studies have employed radiomics to forecast the VETC pattern based on MRI (20–23). Yu et al. (20) formulated a gadoxetic acid-enhanced MRI radiomics model to preoperatively predict VETC, 1,316 quantitative features from intratumoural and peritumoural regions of HCCs were extracted and used four different machine learning algorithms to generate impressive AUROCs (>0.90). Chu et al. (22), on the other hand, employed a deep learning framework based on 3D CNN for multitask learning to predict VETC using preoperative gadoxetic acid-enhanced MRI, albeit with a focus on HBP phases that did not encompass multiphase contrast-enhanced MRI. Recently, Xue Dong et al (23) employed dynamic contrast-enhanced MRI with extracellular contrast agents to construct models, demonstrating that a deep learning radiomic model based on the peritumoural portal phase yielded optimal performance. However, there is no widely accepted criteria for preoperative imaging diagnosis of VETC, and more studies are needed to find more robust evidence.

In this investigation, we conducted an analysis of MR images following the Liver Imaging Reporting and Data System (LI-RADS) v2018 (24) guidelines based on gadoxetic acid–enhanced MRI. Subsequently, these findings were amalgamated with radiomics data to formulate predictions regarding the VETC pattern and overall patient prognosis in cases of HCC.

Hence, the principal aim of this research was to formulate an integrated model that fuses clinical-radiologic data and radiomics-derived features on gadoxetic acid-enhanced MRI scans. This model serves the purpose of preoperatively evaluating the VETC pattern in hepatocellular carcinoma (HCC).

2 Materials and methods

2.1 Patients

This retrospective study was conducted at a sole medical institution. Ethical clearance was obtained from the local institutional ethics review board, written informed consent was waived. Our investigation focused on patients who underwent surgical confirmation of HCC between January 2013 and December 2020 within our institution. Detailed criteria for inclusion and exclusion are provided in Figure 1A. Enrolled patients were randomly partitioned into a training set and a validation set in a 7:3 ratio, as illustrated in Figure 1A.

2.2 Clinical characteristics

Clinical variables and preoperative laboratory data were meticulously extracted from the patients' medical records, as outlined in Table 1. All clinical and laboratory data were procured within a one-week window prior to or subsequent to the gadoxetic acid-enhanced MRI examination.

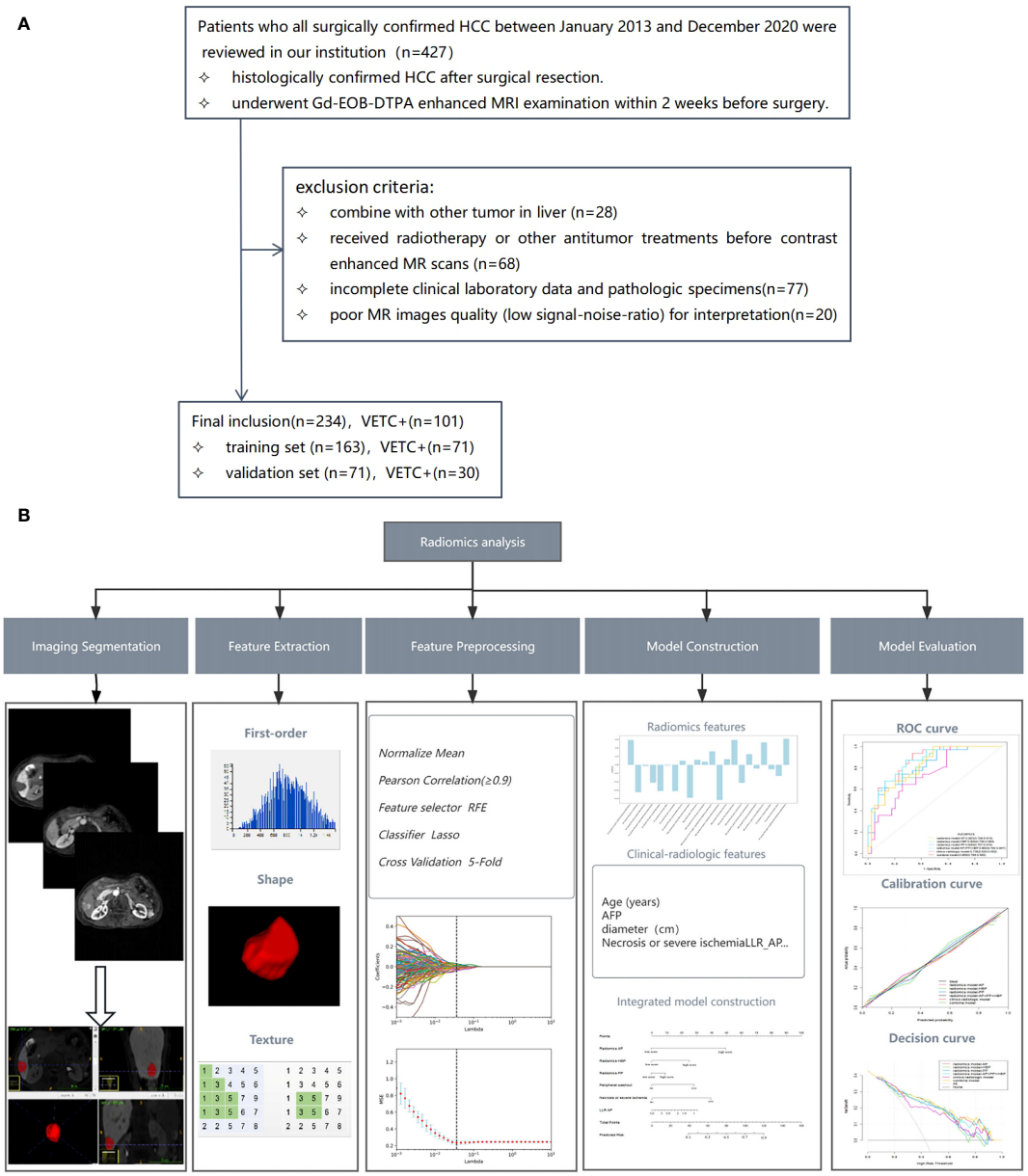

FIGURE 1
Flowchart illustrating the patient selection process **(A)** and the workflow for radiomics analysis **(B)**. *RFE*, recursive feature elimination; *LASSO*, least absolute shrinkage and selection operator; *AFP*, alpha-fetoprotein; *LLR*, lesion to liver ratio; *AP*, arterial phase; *ROC*, receiver operating characteristic.

2.3 Histopathology

All surgical specimens underwent thorough evaluation by an accomplished pathologist (G.C.Y.) with over two decades of experience in the analysis of hepatic pathology. The VETC pattern is characterised by the presence of sinusoid-like vessels that form intricate network patterns, encapsulating individual clusters of tumour cells, either in their entirety or partially within the tumour. This pattern was discerned through CD34 immunostaining during imaging (25). In this study, tumour sections displaying a discernible VETC pattern, accounting for a minimum of 5% of the tumour's area, were classified as VETC+. Additionally, the other histopathological attributes were documented in Table 1.

2.4 Follow up

Post-surgery, patients were subjected to regular follow-up appointments spaced between intervals of 3 to 6 months. These sessions involved assessments based on alpha-fetoprotein (AFP) levels, ultrasonography, and either CT or MRI. Recurrence was

TABLE 1 Baseline clinical characteristics and pathological parameters and radiologic factors of the training and validation set.

Characteristics	Training set			Validation set		
	VETC-(92)	VETC+(71)	P -value *	VETC-(41)	VETC+(30)	P-value *
Age (years) *b*	60 (52, 67)	57 (51, 64)	0.072	62.00 (53.00, 65.00)	54.00 (51.00, 59.00)	0.033
Sex (male)	64 (69.57)	46 (64.79)	0.519	29 (70.73)	27 (90)	0.05
AFP *b*	8.18 (3.64, 59.94)	19.00 (3.18, 300.00)	0.201	8.82 (4.53, 101.10)	17.65 (3.56, 97.24)	0.839
PIVKA-II *b*	44.36 (21.47, 179.42)	162.67 (61.45, 384.36)	<0.001	61.07 (25.34, 184.32)	88.28 (40.37, 502.90)	0.068
ALB *a*	40.20 ± 5.02	40.24 ± 4.32	0.955	41.84 ± 5.84	40.84 ± 4.83	0.445
TBIL *b*	17.00 (12.45, 21.08)	15.30 (11.30, 20.20)	0.241	16.30 (12.70, 19.60)	18.30 (13.10, 22.40)	0.264
ALT *b*	30.50 (22.00, 56.50)	35.00 (20.00, 48.00)	0.749	29.00 (22.00, 43.00)	36.00 (22.00, 67.00)	0.511
AST *b*	37.00 (26.00, 56.00)	37.00 (25.00, 51.00)	0.679	37.00 (28.00, 48.00)	36.50 (25.00, 57.00)	0.903
ALP *b*	84.00 (65.00, 108.00)	94.00 (60.00, 112.00)	0.861	93.00 (72.50, 123.00)	80.50 (66.00, 110.00)	0.116
GGT *b*	40.50 (27.00, 72.00)	45.00 (31.00, 70.00)	0.422	56.00 (30.00, 96.00)	37.00 (25.00, 96.00)	0.744
PLT *b*	112.50 (74.50, 158.50)	119.00 (86.00, 173.00)	0.549	117.00 (78.00, 151.00)	100.00 (71.00, 145.00)	0.284
PT *b*	11.85 (10.95, 13.30)	12.00 (11.40, 12.60)	0.489	11.90 (11.10, 12.90)	11.95 (11.10, 12.80)	0.784
APRI *b*	0.39 (0.19, 0.69)	0.30 (0.21, 0.51)	0.429	0.34 (0.20, 0.66)	0.38 (0.25, 0.58)	0.629
Cause of liver disease (HBV,others)	85, 7	65,6	0.844	35,6	26,4	1
Child-Pugh (A,B)	81,11	61,10	0.688	36,5	22,8	0.119
Pathological						
Diameter (cm)b	2.45 (1.40, 3.90)	3.00 (2.00, 4.50)	0.017	2.70 (1.60, 4.00)	2.70 (2.00, 5.80)	0.5642
Number of tumour (single,multi)	79,13	58,13	0.47	36,5	19,11	0.015
MVI (%)	82 (89.13)	41 (57.74)	<0.001	33 (80.49)	15 (50)	0.007
Edmondson grade (I-II,III-IV)	31,61	5,66	<0.001	8,33	2,28	0.174
MTM (%)	0	10 (14.08)	<0.001	0	2 (6.67)	0.175
Capsule infiltration	4 (4.35)	9 (12.68)	0.052	3 (7.32)	5 (16.67)	0.269
Inflammatory infiltrates	75 (81.52)	44 (61.97)	0.005	31 (75.61)	19 (63.33)	0.263
Gross vascular invasion	3 (3.26)	3 (4.23)	1	12.44)	2 (6.67)	0.57
Satellite nodule	1 (1.09)	2 (2.82)	0.581	2 (4.88)	4 (13.33)	0.233
CK7+ (%)	51 (55.43)	32 (45.07)	0.189	27 (65.85)	16 (53.33)	0.286
CK19+ (%)	24 (26.09)	16 (22.54)	0.601	13 (31.71)	7 (23.33)	0.438
Radiology Factors						
LI-RADS major features						
Nonrim arterial phase hyperenhancement (%)	60 (65.22)	36 (50.70)	0.062	23 (56.10)	14 (46.67)	0.432
Nonperipheral washout (%)	61 (66.30)	36 (50.70)	0.044	23 (56.10)	14 (46.67)	0.432
Enhancing capsule (%)	58 (63.04)	55 (77.46)	0.048	35 (85.37)	27 (90)	0.724
LI-RADS ancillary features (favouring HCC in particular)						
Nonenhancing capsule (%)	3 (3.26)	5 (7.04)	0.297	0 (0.00)	2 (6.57)	0.175
Mosaic architecture (%)	10 (10.87)	6 (8.45)	0.607	5 (12.20)	2 (6.57)	0.691

(Continued)

TABLE 1 Continued

Characteristics	Training set			Validation set		
	VETC-(92)	VETC+(71)	P -value *	VETC-(41)	VETC+(30)	P-value *
LI-RADS ancillary features (favouring HCC in particular)						
Nodule-in-nodule architecture (%)	7 (7.61)	1 (1.41)	0.139	3 (7.32)	0 (0.00)	0.258
Fat in mass (%)	14 (15.22)	16 (22.54)	0.232	8 (19.51)	6 (20)	0.959
Blood products in mass (%)	12 (13.04)	12 (16.90)	0.491	8 (19.51)	6 (20)	0.959
LI-RADS ancillary features (favouring malignancy, not HCC in particular)						
Transitional phase hypointensity (%)	91 (98.91)	70 (98.59)	1	40 (97.56)	30 (100)	1
Restricted diffusion (%)	91 (98.91)	71 (100)	1	41 (100)	30 (100)	1
Mild-moderate T2 hyperintensity (%)	91 (98.91)	71 (100)	1	41 (100)	30 (100)	1
Corona enhancement (%)	23 (25)	25 (35.21)	0.156	16 (39.02)	9 (30)	0.432
Fat sparing in solid mass (%)	77 (83.70)	52 (73.24)	0.103	33 (80.49)	24 (80)	0.959
Hepatobiliary phase hypointensity (%)	92 (100)	71 (100)	1	40 (97.56)	30 (100)	1
Iron sparing in solid mass (%)	88 (95.65)	70 (98.59)	0.388	41 (100)	29 (96.67)	0.423
LI-RADS M features						
Rim arterial phase hyperenhancement (%)	28 (30.43)	35 (49.30)	0.014	17 (41.46)	14 (46.67)	0.662
Portal phase peripheral washout (%)	10 (10.87)	30 (42.25)	0	10 (24.39)	9 (30)	0.598
Delayed central enhancement (%)	6 (6.52)	2 (2.82)	0.468	0 (0.00)	0 (0.00)	0.598
Targetoid TP or HBP appearance (%)	20 (21.74)	14 (19.72)	0.753	12 (29.27)	6 (20)	0.375
Targetoid restriction (%)	21 (22.83)	21 (29.58)	0.329	13 (31.71)	9 (30)	0.878
Necrosis or severe ischemia (%)	15 (16.30)	31 (43.66)	<0.001	7 (17.07)	13 (43.33)	0.015
Infiltrative appearance (%)	14 (15.22)	13 (18.31)	0.599	6 (14.63)	4 (13.33)	1
Non LI-RADS high-risk features						
Non-Smooth tumour margin (%)	20 (21.74)	22 (30.99)	0.181	12 (69.27)	7 (23.33)	0.577
Peritumoural hypointensity on HBP (%)	24 (26.09)	27 (38.03)	0.103	19 (46.34)	13 (43.33)	0.801
Quantitative indicators						
LLR_AP *b*	1.37 (1.21, 1.58)	1.17 (1.09, 1.36)	0.014	1.50 (1.23, 1.73)	1.12 (1.03, 1.24)	<0.001
LLR_PP *b*	0.55 (0.46, 0.62)	0.53 (0.46, 0.63)	0.398	0.56 (0.48, 0.62)	0.48 (0.46, 0.59)	0.107
LLR_HBP *b*	0.89 (0.67, 1.09)	0.78 (0.65, 1.09)	0.044	0.98 (0.79, 1.26)	0.75 (0.69, 0.97)	<0.001

Categorical variables are presented as N (%) according to different levels.
[a]Data are presented as mean ± standard deviation.
[b]Data are presented as median (interquartile range).
VETC, vessels encapsulating tumour clusters; AFP, alpha-fetoprotein; PIVKA-II, protein induced by vitamin K absence-II; ALT, alanine aminotransferase; AST, aspartate aminotransferase; ALB, serum albumin; TB, serum total bilirubin; GGT, gamma-glutamyl transferase; ALP, alkaline phosphatase; PLT, platelet count; PT, prothrombin time; APRI=AST/PLT; HBV, hepatitis B virus; MVI, microvascular invasion; MTM, macrotrabecular-massive; LI-RADS, Liver Imaging Reporting and Data System; LLR, lesion to liver ratio; AP, arterial phase; PP, portal phase; HBP, hepatobiliary phase; TP, transitional phase.
* T test results for continuous variables with normal distribution, Wilcoxon test results for continuous variables with abnormal distribution, and chisquare test or Fisher exact test results for categorical variables.

determined by the appearance of new intrahepatic lesions and/or instances of extrahepatic metastases. The culmination of the follow-up period was in April 2022. The duration between the surgical intervention date and the earliest manifestation of tumour recurrence defined the recurrence-free survival (RFS) period.

2.5 Magnetic resonance imaging examination

Detailed information regarding the MRI equipment and parameters can be found in Supplementary Text 1 and Supplementary Table 1.

2.6 Analysis of radiologic features

Two radiologists, referred to as Reader 1 (M.T.L.) and Reader 2 (L.X.) endowed with professional experience of 6 years and 10 years respectively, independently scrutinised all imaging data and gauged the corresponding parameters, blinded to clinical, laboratory, and pathologic information. Following the individual assessments, the two readers convened two weeks later for a collective review. Any disparities that emerged were harmonised through intervention by a senior radiologist (X.Q.Z.), who possessed 18-year experience in abdominal MRI diagnostics. While individual scores were utilised for the computation of inter-observer concordance, consensus scores were employed for the ultimate analysis.

The imaging attributes encompassed both major and ancillary features, consistent with the LI-RADS v2018 (24). Moreover, a range of other high-risk imaging features of interest (as outlined in Table 1) were included. A detailed exposition of the imaging feature definitions can be found in Supplementary Table 2. When patients have multiple lesions, the largest substantial lesion was selected for analyses.

Quantitative assessment was employed to evaluate the signal intensity (SI) of lesion-to-liver ratio (LLR), expressed as LLR = SI_{tumor}/SI_{liver}. Additional particulars are elaborated upon in Supplementary Text 2.

2.7 Tumour segmentation and radiomics feature extraction

The radiomic analysis process is illustrated in Figure 1B. Gd-EOB-DTPA-enhanced MR AP, PP and HBP images were exported as digital imaging data and communications in medicine (DICOM) for mat. All images were transferred into the ITK-SNAP software (www.itksnap.org) for tumour segmentation. A team of two radiologists, known as Reader 3 (Q.Q.) and Reader 4 (J.Y.Z.), each with professional experience spanning 4 years and 6 years respectively, undertook the task of manually delineating three-dimensional volumes of interest (VOI) for the entire tumour. The ROI was manually delineated on each axial slice of the AP, PP, and HBP images, covering the entire tumour, and finally a volume of interest (VOI) representing the tumour area was presented. To ensure robustness, 30 patients were randomly selected and independently reviewed by both Reader 3 and Reader 4, from which interobserver intra-class correlation coefficients (ICC) were computed,ICC≥0.8 indicated high consistency, 0.5–0.79 middle, and<0.5 low. Moreover, within this subset, Reader 4 repeated the process of tumour segmentation and intraobserver ICCs were calculated. The subsequent segmentation of the remaining images was exclusively performed by Reader 4.

Utilising an open-source software package (https://github.com/salan668/FAE), all radiomics features were extracted and preprocessed. For each MRI sequence (including arterial phase (AP), portal phase (PP), and hepatobiliary phase (HBP) imaging), a total of 1050 quantitative radiomics features were extracted from the VOI of the tumour. These encompassed first-order statistics, shape, and texture features. Texture features comprised gray level co-occurrence matrix (GLCM), gray level run length matrix (GLRLM), gray level size zone matrix (GLSZM), gray level dependence matrix (GLDM), and neighboring gray tone difference matrix (NGTDM). Features exhibiting ICC values greater than 0.80 were selected for subsequent analysis. A Pearson correlation coefficients (PCCs) test was subsequently executed, and features boasting coefficients exceeding 0.90 were excluded to mitigate redundancy. Then we used the least absolute shrinkage and selection operator (LASSO) to reduce the redundancy and dimensionality of the features of each single sequence and to determine the hyper-parameter (e.g. the number of features) of model, we applied cross validation with 5-fold on the training data set. Under the optimal lambda value, features exhibiting non-zero characteristic coefficients were identified and subsequently utilised. These features denoted the correlation between the radiomic feature and VETC pattern, contributing to the final establishment of the radiomics model.

2.8 Model construction and validation

For radiomics model, we analysed each single sequence to built model separately and combine model, namely radiomics model_AP, radiomics model_PP, radiomics model_HBP, and radiomics model_AP+PP+HBP. The threshold of radiomics model was determined using receiver operating characteristic (ROC) analysis by maximising the Youden index.

Clinical characteristics and radiologic features with a P value <0.05 in univariate logistic regression analysis were entered into multivariate logistic regression analysis using the stepwise method. Akaike's information criterion (AIC) was used for model reduction, and the model with the minimum AIC value was used to generate the clinico-radiologic model.

Subsequently, the radiomics features and clinico-radiologic features were amalgamated to establish the integrated model, visualised through a nomogram. The nomogram was built based on each β regression coefficient in the multivariable regression model. Model performance was assessed via the receiver operating characteristic (ROC) curve. The optimal threshold was identified through ROC analysis, aiming to maximise the Youden index. The area under the curve (AUC), accuracy, sensitivity, specificity, positive predictive value (PPV), and negative predictive value (NPV) were computed for evaluation. Calibration curves were employed to assess the performance of the nomogram. Furthermore, the clinical utility of the nomograms was evaluated by quantifying the net benefits through decision curve analysis (DCA).

2.9 Statistical analysis

Continuous variables were expressed as means with corresponding standard deviations or medians with interquartile ranges, while categorical data were represented as numbers and percentages. The Student's t-test or Mann-Whitney U-test was utilised for comparing continuous variables, while Fisher's exact

test or χ^2 test was employed for categorical variables. The Cohen's kappa statistic was employed to assess interobserver agreement for traditional radiologic features. The interpretation of kappa values followed the criteria: $\kappa > 0.80$ denoting excellent agreement, $0.50 \leq \kappa \leq 0.80$ representing good agreement, and $\kappa < 0.50$ indicating poor agreement.

The Kaplan-Meier method was utilised to compute RFS and generate survival curves, with the log-rank test used for assessing statistical significance. All statistical analyses were conducted utilising R software (version 3.6.0) and SPSS 20.0. A significance level of <0.05 was adopted for all analyses.

3 Results

3.1 Basic clinico-radiologic characteristics

A total of 234 cases were encompassed within this study, of which 101 (43.16%) were pathologically ascribed to possess the VETC pattern. Comprehensive clinical characteristics pertaining to both the training and testing cohorts are outlined in Table 1. The majority of clinical characteristics and radiological factors exhibited no statistically significant disparities between the training and validation sets, as delineated in Supplementary Table 3.

Several clinical attributes displayed notable discrepancies between the VETC-positive and VETC-negative groups (Supplementary Table 3). The ICC stood at ≥0.8 for 62.96% of radiological features, and within the range of 0.5–0.79 for 37.04% of features (Supplementary Table 4).

3.2 Development of VETC-predicting models

3.2.1 Clinico-radiologic model

The multivariable logistic regression unveiled peripheral washout (OR = 6.493; 95% CI: 2.485-16.967), necrosis or severe ischemia (OR = 4.756; 95% CI: 1.964-11.516), targetoid TP or HBP appearance (OR = 1.307; 95% CI: 0.101-1.935), and LLR_AP (OR = 0.082; 95% CI: 0.012-0.459) as independent risk factors for the VETC pattern in Supplementary Table 5.

3.2.2 Radiomics model

Initially, 966 AP radiomics features, 924 PP radiomics features, and 987 HBP radiomics features were included, each displaying ICC exceeding 0.8. Ultimately, 8 AP radiomics features, 3 PP radiomics features, and 11 HBP radiomics features were identified, as illustrated in Supplementary Figure 1. The resultant radiomics model (R-score) is expounded upon in Supplementary Table 6.

3.2.3 Integrated model

In the multivariate regression analysis, radiomics-AP (OR = 2.87; 95% CI: 1.293-3.704), radiomics-HBP (OR = 2.023; 95% CI: 1.012-3.398), radiomics-PP (OR = 1.546; 95% CI: 0.089-1.882), necrosis or severe ischemia (OR = 2.457; 95% CI: 1.133-7.367), peripheral washout (OR = 1.678; 95% CI: 1.046-2.423), and LLR_AP (OR = 0.433; 95% CI: 0.221-0.435) emerged as independent prognostic factors for histologic VETC (Table 2, Figure 2A). Notably, the Wilcoxon test exhibited a significant distinction between the Nomo scores of VETC+ and VETC- classifications, as determined by the integrated model ($p < 0.01$) (Figure 2B).

3.3 Performance of the three models in the training and validation set

Table 3 succinctly presents the predictive performance metrics of the clinico-radiologic model, radiomics model, integrated model, and individual risk factors. The AUC of the clinical-radiologic model was lower than that of the radiomics model and integrated model (Z = 2.501 and 3.063, $p = 0.012$ and 0.002) in the training cohort and (Z = 2.497 and 3.200, $p = 0.013$ and 0.001)

TABLE 2 Univariate and multivariate analysis of preoperative radiomics and clinico-radiologic factors in prediction VETC.

Factors	Univariate analysis		Multivariate analysis	
	p value	OR (95% CI)	*p* value	OR (95% CI)
Radiomics-AP	<0.001	4.074 (1.661-2.59)	<0.001	2.870 (1.293-3.704)
Radiomics-PP	<0.001	0.672 (0.053-0.962)	0.047	1.546 (0.089-1.882)
Radiomics-HBP	<0.001	1.900 (0.266-2.703)	0.025	2.023 (1.012-3.398)
Diameter cm	0.027	1.203 (1.021-1.416)		
Peripheral washout	<0.001	4.738 (2.146-10.459)	0.034	1.678 (1.046-2.423)
Targetoid TP or HBP appearance	0.037	2.365 (1.053-5.311)		
Necrosis or severe ischemia	<0.001	4.833 (2.238-10.441)	<0.001	2.457 (1.133-7.367)
LLR_AP	<0.001	0.026 (0.004-0.148)	0.021	0.433 (0.221-0.435)

VETC, Vessels encapsulating tumour clusters; LLR, Lesion to liver ratio; AP, arterial phase; PP, portal phase; HBP, hepatobiliary phase; TP, transitional phase; CI, Confidence interval; OR, Odds ratio.

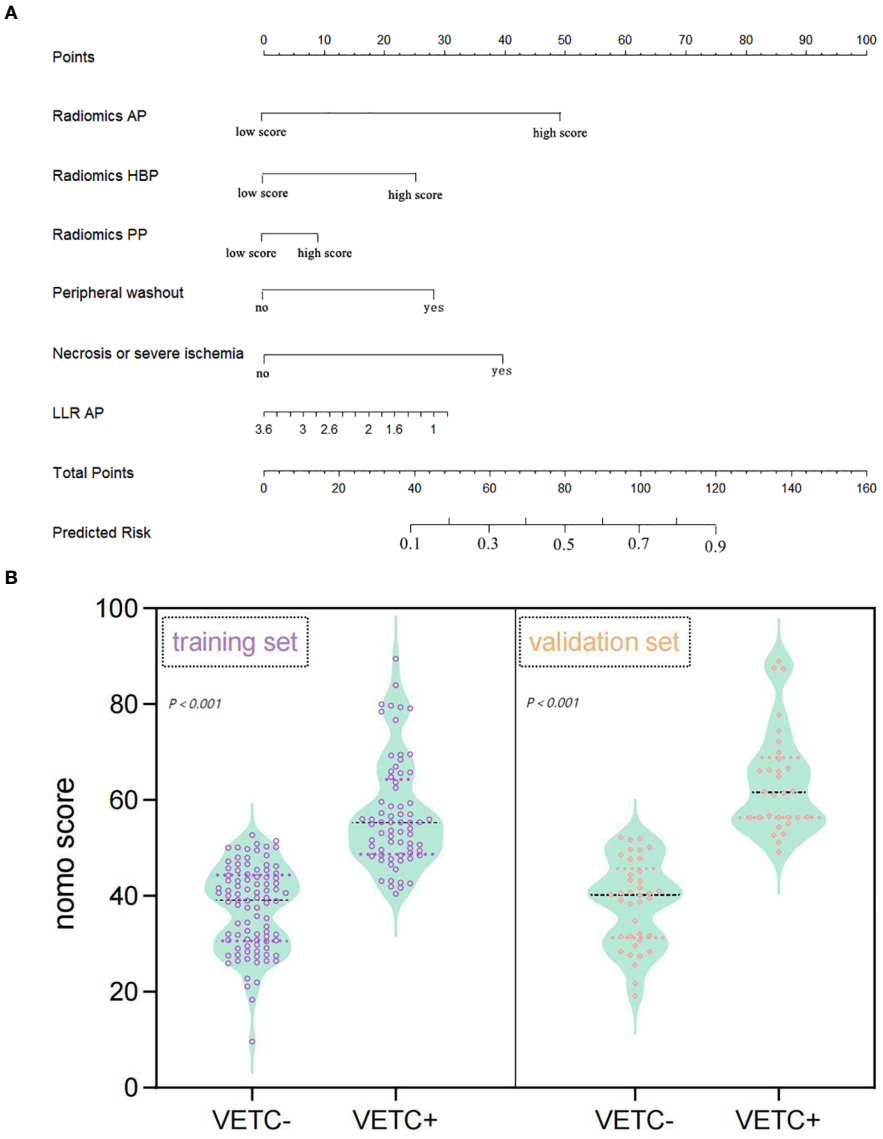

FIGURE 2
Nomogram representing the integrated model for evaluating the VETC pattern, alongside a violin plot depicting nomo-score distribution in VETC+ and VETC- groups. **(A)** The nomogram displays proportional regression coefficients of individual predictors. **(B)** Wilcoxon test demonstrates significant distinction in Nomo scores between VETC+ and VETC- groups based on the integrated model, observed in both the training and validation sets (p<0.01). *VETC*, vessels encapsulating tumour clusters; *LLR*, lesion to liver ratio; *AP*, arterial phase; *PP*, portal phase; *HBP*, hepatobiliary phase.

in the validation cohort, while the AUC of the radiomics model was inferior to the integrated model (Z = 0.422, p = 0.673) in the training cohort and (Z = 0.164, p = 0.870) in the validation cohort (Figures 3A, B).

The calibration curves of the clinical-radiologic model, radiomics model, and integrated model for predicting VETC exhibited robust agreement across both the training and validation sets (Figures 3C, D). Decisive DCA curves were employed to predict VETC utilising the clinical-radiologic model, radiomics model, and integrated model, each showcased in Figures 3E, F. Two examples of the integrated model of the nomogram was shown in Supplementary Figure 2.

3.4 Predictors of survival

As of April 2022, 233 patients (99.57%) had concluded their recurrence-free survival (RFS) follow-up. The RFS rates at 1, 2, 3, 4, and 5 years stood at 93.8%, 86.4%, 78.9%, 75.1%, and 69.6%, respectively.

In the entirety of the cohort (n = 233), VETC+ HCC demonstrated a notably inferior RFS when juxtaposed with VETC- HCC (all p < 0.05). The median RFS was 21 months (95% CI: 15.69–26.31) for those manifesting VETC and 54 months (95% CI: 43.09–80.91) for those without VETC (log-rank test, p < 0.001) (Figure 4A). Analogously, consistent findings

TABLE 3 Performance of the three models and risk factors in the training and validation sets.

Models	Cutoff*	Training set				Validation set			
		AUC (95% CI)	Sensitivity	Specificity	Accuracy	AUC (95% CI)	Sensitivity	Specificity	Accuracy
Peripheral.washout	–	0.734 (0.568-0.700)	38.57% (28.03-50.30)	88.30% (80.09-93.50)	67.07% (59.55-73.81)	0.707 (0.498-0.716)	41.94% (26.39-59.26)	79.49% (64.21-89.47)	62.86% (51.13-73.25)
Necrosis or severe ischemia	–	0.743 (0.576-0.711)	41.43% (30.62-53.13)	87.23% (78.85-92.69)	67.68% (60.18-74.38)	0.714 (0.501-0.727)	48.39% (31.97-65.16)	74.36% (58.76-85.59)	62.86% (51.13-73.25)
LLR_AP	1.123	0.671 (0.587-0.755)	95.71% (87.65-99.02)	51.06% (41.12-60.93)	70.12% (62.71-76.62)	0.675 (0.546-0.804)	100.00% (86.91-100.00)	48.72% (33.86-63.80)	71.43% (59.89-80.73)
Clinico-radiologic model	0.464	0.816 (0.752-0.880)	68.57% (56.93-78.28)	80.85% (71.66-87.62)	75.61% (68.47-81.57)	0.736 (0.620-0.852)	64.52% (46.88-78.95)	74.36% (58.76-85.59)	70.00% (58.41-79.51)
Radiomics model_AP	0.432	0.857 (0.800-0.913)	80.00% (69.06-87.82)	77.66% (68.18-84.97)	78.66% (71.74-84.27)	0.823 (0.728-0.918)	93.55% (78.25-99.24)	66.67% (50.91-79.44)	78.57% (67.50-86.67)
Radiomics model_PP	0.508	0.822 (0.756-0.887)	75.71% (64.42-84.33)	82.98% (74.02-89.35)	79.88% (73.05-85.34)	0.809 (0.709-0.909)	96.77% (82.42-100.82)	51.28% (36.20-66.14)	71.43% (59.89-80.73)
Radiomics model_HBP	0.471	0.831 (0.768-0.894)	71.43% (59.89-80.73)	84.04% (75.21-90.20)	78.66% (71.74-84.27)	0.809 (0.707-0.910)	74.19% (56.54-86.51)	74.36% (58.76-85.59)	74.29% (62.90-83.15)
Radiomics model_AP +PP+HBP	0.295	0.863 (0.809-0.918)	84.29% (73.84-91.17)	74.47% (64.76-82.25)	78.66% (71.74-84.27)	0.865 (0.783-0.947)	87.10% (70.54-95.48)	71.79% (56.10-83.58)	78.57% (67.50-86.67)
Integrated model	0.475	0.873 (0.821-0.925)	78.57% (67.50-86.67)	81.91% (72.84-88.49)	80.49% (73.71-85.87)	0.869 (0.789-0.950)	100.00% (86.91-100.00)	51.28% (36.20-66.14)	72.86% (61.39-81.95)

*Receiver operating characteristic analysis by maximising the Youden index.
AUC, area under the curve; PPV, positive predictive value; NPV, negative predictive value; LLR, lesion to liver ratio; AP, arterial phase; PP, portal phase; HBP, hepatobiliary phase; CI, confidence interval.

emerged from the integrated model analysis: Patients predicted to possess the VETC pattern by the integrated model exhibited a median RFS of 21 months (95% CI: 13.32–25.51), whereas those predicted to lack VETC by the integrated model had a median RFS of 62 months (42.3–93.7) (log-rank test, $p < 0.001$) (Figure 4B).

4 Discussion

In this study, we systematically developed and validated clinico-radiologic, radiomics, and integrated models for preoperatively evaluating VETC in HCC. These models ingeniously incorporated pivotal clinical, radiological risk factors, and radiomics features extracted from gadoxetic acid-enhanced MRI. Our findings underscored the superior predictive capacity of the integrated model in comparison to the individual clinico-radiologic and radiomics models. Among the risk factors analysed, namely radiomics-AP, radiomics-HBP, peripheral washout, and necrosis or severe ischemia emerged as significant predictors.

In the validation set, the AUC (95% CI) of the integrated model was 0.869(0.789-0.950), the sensitivity was 100.00%(86.91-100.00), and the specificity was 71.28%(36.20-76.14). Recently, Dong et al (23) compares deep neural network and machine learning (ML) classifiers for evaluating VETC status, and finally a deep learning model performed well in the preoperative assessment of VETC status, the AUC was 0.844 (95% CI, 0.735–0.921), the sensitivity was 77.3%, and the specificity was 82.2%. However, in our study the AUC values, sensitivity, were slightly higher than theirs. Fan et al (16) used qualitative and quantitative imaging features of Gd-EOB-DTPA-enhanced MRI to investigate HCC with VETC, the AUC value of the nomogram was 0.885 (95% CI, 0.824–0.946). Their team (21) combined of the two texture features for identifying VETC-positive HCC achieved an AUC value of 0.844 (95% CI, 0.777, 0.910) with a sensitivity of 80.8% (95% CI, 70.1%, 91.5%) and specificity of 74.1% (95% CI, 64.5%, 83.6%). Yu et al (20) developed a Gd-EOB-DTPA-enhanced MRI radiomics model for preoperative prediction of VETC, the peritumoural radiomics model achieved an AUC of 0.909, however this study was only based on HBP and the qualitative feature analysis was not included in this study. Chen et al (17) developed the nomogram integrating gadoxetate disodium-enhanced MRI features for estimating VETC in HCC, showed good discrimination with a C-index of 0.870 (development cohort) and 0.862 (validation cohort), also in our study the AUC values were slightly higher than theirs. The study differed from previous works

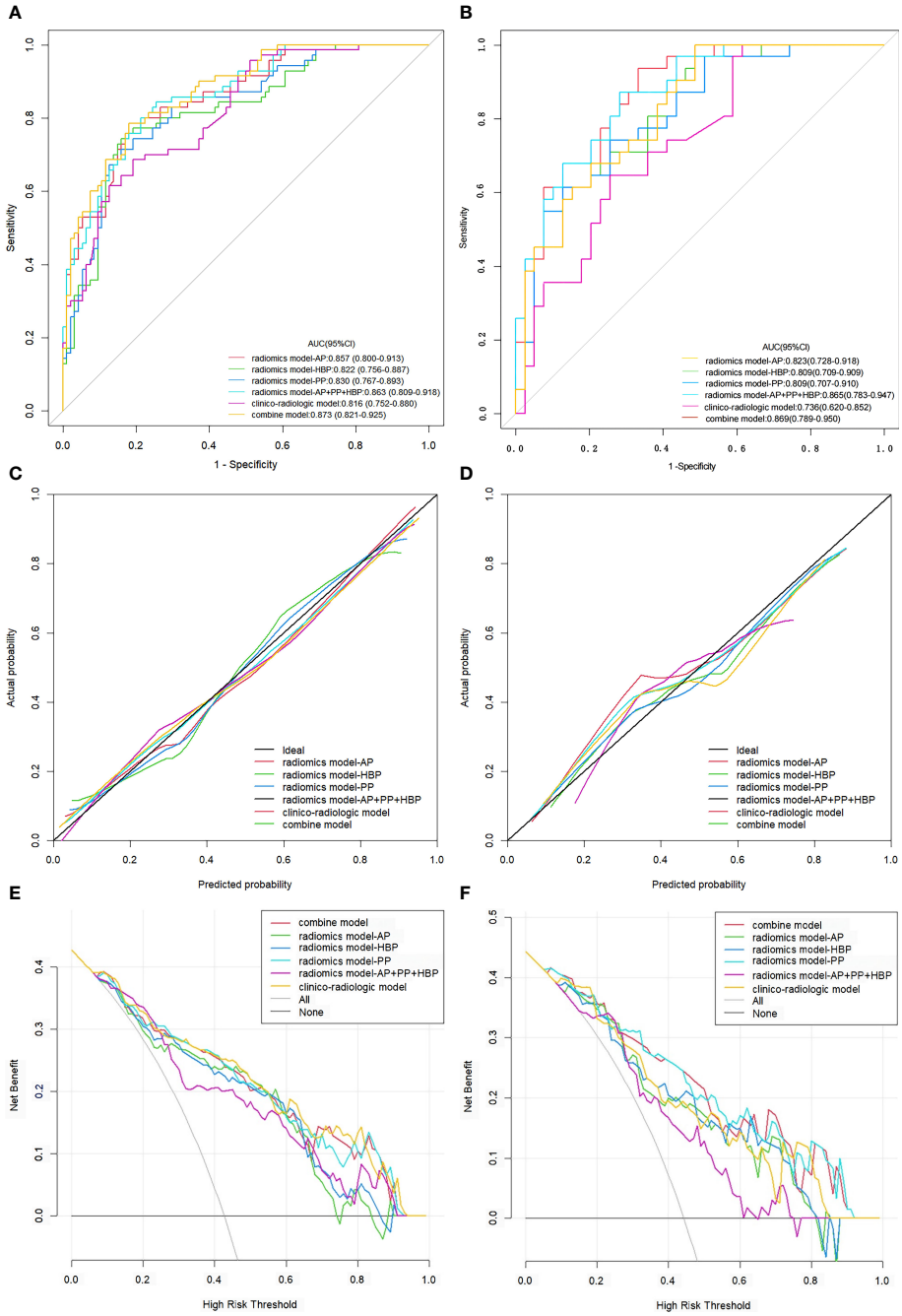

FIGURE 3
ROC curves, calibration curves, and DCA for various models evaluating the VETC pattern. **(A, B)** ROC curves for VETC pattern assessment in the training set **(A)** and validation set **(B)**. **(C, D)** Calibration curves for VETC assessment in the training **(C)** and validation set **(D)**.The diagonal 45-degree line indicates perfect prediction. **(E, F)** DCA for VETC assessment in the training **(E)** and validation set **(F)**. The vertical axis represents the value of net benefit, and the horizontal axis represents the threshold level. The coloured line is the expected net benefit of per patient based on each models. *ROC*, receiver operating characteristics; *DCA*, decision curve analysis; *VETC*, vessels encapsulating tumour clusters; *AUC*, area under the curve; *AP*, arterial phase; *PP*, portal phase; *HBP*, hepatobiliary phase.

in that it analysed the imaging features of gadoxetic acid-enhanced MRI, based on the LI-RADS version 2018 criteria. As a standardised reporting system, LI-RADS v2018 is widely used in routine practice, and identifying imaging characteristics of relevant LI-RAD may help select appropriate treatment options and optimise the management of HCC patients. Therefore, this study tried to analyse the comprehensive image characteristics of the lesions as much as possible, and analysed the radiomics features from multiphase contrast-enhanced MRI.

Our findings highlighted a close relationship between the VETC pattern in HCC and specific attributes such as portal phase peripheral washout, necrosis or severe ischemia, as well as the presence of targetoid appearances during TP or HBP, along with the LLR_AP. The work of Feng et al. (9) demonstrated an independent

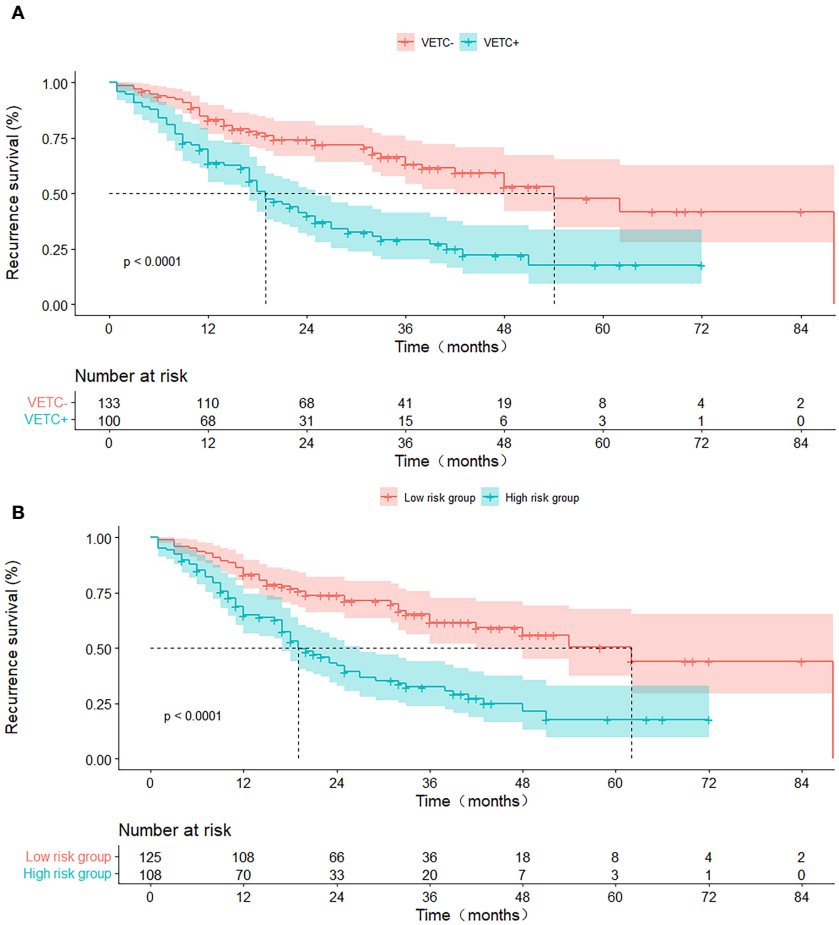

FIGURE 4
RFS curves stratified by histologic VETC pattern **(A)** and integrated model-predicted VETC pattern **(B)**, presented through Kaplan-Meier analysis. *VETC*, vessels encapsulating tumour clusters; *RFS*, recurrence-free survival.

connection between intratumour necrosis and the manifestation of the VETC pattern. As tumoural cells proliferate and expand, the resulting increased distance from the existing vascular supply induces hypoxia. Rapidly growing HCCs experience both new angiogenesis and hypoxia, leading to conspicuous necrosis (26). Notably, portal phase peripheral washout and targetoid appearances during the TP or HBP are likely to be associated with peripheral arterialisation and heightened cellular density, alongside central ischemia and necrosis. Therefore, while the presence of a targetoid appearance might suggest a non-HCC malignancy and trigger LI-RADS M categorisation, this does not preclude the possibility of HCC, particularly in cases of poorly differentiated HCC (27). The results of this study showed that the LLR arterial stage of VETC-positive HCC was lower than that of VETC-negative HCC, contrary to the study of Fan et al. (16). This discrepancy could potentially be attributed to the fact that VETC-positive HCC in our study exhibited a higher proportion of necrosis or severe ischemia.

Radiomics bears significant potential in enhancing clinical decision-making, especially in the realm of oncology (28). The VETC pattern encompasses heterogeneous angiogenesis within HCC behaviour, and in this study radiomic features were extracted from intratumoural regions, capturing biological properties linked to intratumoural heterogeneities. We conducted a rigorous canonical screening of radiomic features for the purpose of developing machine learning models, and subsequently employed validation sets to verify the stability of the integrated models. The AUC value (0.809-0.865) in the validation set of radiomics models were similar to the AUC value (0.822-0.873) in the training set, indicating that the model can be generalised from the training set to the validation set, and the performance is stable. For the model to gain broad acceptance and recognition, we will proceed to verify its robustness and generalisation capabilities in other cohorts in the future. Specifically, the radiomics model based on arterial phase (AP) data outperformed the radiomics models based on portal phase (PP) and hepatobiliary phase (HBP) data in the training and validation sets respectively. Our investigation encompassed 17 texture features, 4 first-order features, and a solitary original feature. These texture features, encompassing measures such as energy, homogeneity, correlation, entropy, dissimilarity, and second-order metrics (21), collectively captured intratumoural heterogeneity, aligning with previous research (20). Notably, the majority of features were derived from wavelet analysis, signifying that the features extracted from preprocessed images exhibited greater stability compared to those from the original images (20). Particularly, GLSZM features emerged at the forefront. Noteworthy examples include

HBP_VOItumor_waveletHLL_glszm_SizeZoneNonUniformity and HBP_VOItumor_original_glszm_GrayLevelNonUniformity, which might relate to intratumoural texture heterogeneity attributed to factors like tumour cellularity, micronecrosis, and inflammation (23). In our study, wavelet analysis and GLSZM features demonstrated significant stability and predictive capability. Wavelet analysis captures different frequency components of the image through multi-scale decomposition, while GLSZM features reflect the spatial distribution of gray levels in the image. These features not only enhance model performance but also improve image resolution and feature extraction accuracy. The application of these features allows the model to better distinguish between different lesion types and demonstrates stronger capability in predicting patient prognosis. This finding partly elucidates the impressive performance of the VETC model. Intriguingly, 11 features were sourced from HBP data, highlighting the significance of gadoxetic acid-enhanced MRI in diagnosing VETC patterns.

Remarkably, the integrated model offered valuable information regarding the risk of VETC, which could potentially contribute to elucidating the correlation between tumour aggressiveness and prognosis. Moreover, the integrated model estimated VETC pattern had a similar result to the VETC status identified by CD34 immunostaining in predicting recurrence. The integrated model stratified patients into high-risk or low-risk VETC-positive HCCgroups. It may help clinicians define treatment plans, such as whether to consider the type of surgical resection, anatomic resection or non-anatomic resection, and whether to include adjuvant therapy (i.e., TACE). And sorafenib prolonged survival in patients with VETC-positive HCCs but not VETC-negative ones. Finally, given the observed responses of VETC-positive tumours to multikinase inhibitors (11), they may be considered before and after curative resection or liver transplant(ation) as (neo)adjuvant therapy to treat micrometastases and reduce recurrence. Thus, non-invasive identification of VETC-positive HCC can guide individualised management decisions, potentially selecting the treatment regimen that is likely to provide the greatest benefit to the individual patient.

Nonetheless, several limitations merit consideration in this study. Firstly, this was a single-center study, lack of external validation from other medical centres. Secondly, being retrospective, the study could potentially be influenced by selection bias. Thirdly, due to the short follow-up period for certain patients, the study excluded comprehensive overall survival analysis, potentially limiting its ability to comprehensively capture long-term outcomes and recurrence patterns. Lastly, our focus was exclusively on the VETC pattern; thus, exploring the interplay between the VETC pattern and other risk-related pathological factors, such as microvascular invasion (MVI), necessitates further investigation. Future studies will necessitate prospective studies and additional multi-center cohorts to further substantiate the integrated model. Furthermore, overall survival analysis will be include in these studies, thereby affording a deeper and more encompassing understanding of the prognostic significance of our integrated model. Future studies will explore whether the integration of MRI with other advanced imaging technologies (such as CT and PET) will further improve the accuracy and robustness of the predictive model. To enhance the interpretability of the model and mitigate the potential for overfitting, we aim to employ advanced image processing algorithms, while refining and optimising the radiomics feature extraction and selection procedure. Hepatitis C virus (HCV) is one of the leading causes of chronic liver disease, cirrhosis, and hepatocellular carcinoma, resulting in major global public health concerns (29). However, in this study the majority of patients were HBV-positive. The question of whether the integrated model is also applicable to HCV cohorts or patients with other liver diseases necessitates further investigation, so in the future an external sets with HCV will be included to prove the generalisation of the model. Indeed, the EMT pathway has been shown in mixed tumours with both VETC-positive and VETC-negative components, suggesting traditional HCC treatments are still required in addition to anti-VETC agents (30). Ultimately, we need to prospectively investigate interventions specific for VETC-positive (and VETC-negative) HCCs, including clinical treatment regimen or combination therapy regimen.

5 Conclusion

This study has developed an integrated model that combines traditional imaging features and radiomic features extracted from gadoxetic acid-enhanced MRI. The integrated model demonstrates good predictive performance for the VETC pattern in HCC.

Data availability statement

The raw data supporting the conclusions of this article will be made available by the authors, without undue reservation.

Author contributions

JZ: Supervision, Data curation, Investigation, Methodology, Software, Writing – original draft, Conceptualization, Visualization. MaL: Conceptualization, Data curation, Formal analysis, Investigation, Methodology, Software, Writing – original draft. QQ: Data curation, Investigation, Writing – review & editing, Validation. MeL: Data curation, Investigation, Validation, Writing – review & editing. ZL: Data curation, Investigation, Validation, Writing – review & editing. ZY: Data curation, Investigation, Validation, Writing – review & editing. LX: Data curation, Investigation, Validation, Writing – review & editing. CG: Data curation, Writing – review & editing, Conceptualization. XZ: Conceptualization, Writing – review & editing, Formal analysis, Investigation, Project administration, Supervision, Visualization. TZ: Project administration, Supervision, Writing – review & editing, Funding acquisition, Resources.

Funding

The author(s) declare financial support was received for the research, authorship, and/or publication of this article. This study has received funding by 2023 medical research project of Jiangsu Provincial Health Committee (Z2023091) and Infection Imaging Research Project of Jiangsu Research Hospital Society (GY202203) and Nantong Science and Technology Plan Project (MS22022056).

Conflict of interest

The authors declare that the research was conducted in the absence of any commercial or financial relationships that could be construed as a potential conflict of interest.

Publisher's note

Supplementary material

The Supplementary Material for this article can be found online at: https://www.frontiersin.org/articles/10.3389/fonc.2024.1422119/full#supplementary-material

References

1. Sung H, Ferlay J, Siegel RL, Laversanne M, Soerjomataram I, Jemal A, et al. Global cancer statistics 2020: GLOBOCAN estimates of incidence and mortality worldwide for 36 cancers in 185 countries. *CA Cancer J Clin*. (2021) 71:209–49. doi: 10.3322/caac.21660

2. Baecker A, Liu X, La Vecchia C, Zhang ZF. Worldwide incidence of hepatocellular carcinoma cases attributable to major risk factors. *Eur J Cancer Prev*. (2018) 27:205–12. doi: 10.1097/CEJ.0000000000000428

3. Marrero JA, Kulik LM, Sirlin CB, Zhu AX, Finn RS, Abecassis MM, et al. Diagnosis, staging, and management of hepatocellular carcinoma: 2018 practice guidance by the American association for the study of liver diseases. *Hepatology*. (2018) 68:723–50. doi: 10.1002/hep.29913

4. Yamada S, Okumura N, Wei L, Fuchs BC, Fujii T, Sugimoto H, et al. Epithelial to mesenchymal transition is associated with shorter disease-free survival in hepatocellular carcinoma. *Ann Surg Oncol*. (2014) 21:3882–90. doi: 10.1245/s10434-014-3779-2

5. Shah SA, Cleary SP, Wei AC, Yang I, Taylor BR, Hemming AW, et al. Recurrence after liver resection for hepatocellular carcinoma: risk factors, treatment, and outcomes. *Surgery*. (2007) 141:330–9. doi: 10.1016/j.surg.2006.06.028

6. Fang JH, Zhou HC, Zhang C, Shang LR, Zhang L, Xu J, et al. A novel vascular pattern promotes metastasis of hepatocellular carcinoma in an epithelial-mesenchymal transition-independent manner. *Hepatology*. (2015) 62:452–65. doi: 10.1002/hep.27760

7. Renne SL, Woo HY, Allegra S, Rudini N, Yano H, Donadon M, et al. Vessels encapsulating tumor clusters (VETC) is a powerful predictor of aggressive hepatocellular carcinoma. *Hepatology*. (2020) 71:183–95. doi: 10.1002/hep.30814

8. Lin WP, Xing KL, Fu JC, Ling YH, Li SH, Yu WS, et al. Development and validation of a model including distinct vascular patterns to estimate survival in hepatocellular carcinoma. *JAMA Netw Open*. (2021) 4:e2125055. doi: 10.1001/jamanetworkopen.2021.25055

9. Feng Z, Li H, Zhao H, Jiang Y, Liu Q, Chen Q, et al. Preoperative CT for characterization of aggressive macrotrabecular-massive subtype and vessels that encapsulate tumor clusters pattern in hepatocellular carcinoma. *Radiology*. (2021) 300:219–29. doi: 10.1148/radiol.2021203614

10. Liu K, Dennis C, Prince DS, Marsh-Wakefield F, Santhakumar C, Gamble JR, et al. Vessels that encapsulate tumour clusters vascular pattern in hepatocellular carcinoma. *JHEP Rep*. (2023) 5:100792. doi: 10.1016/j.jhepr.2023.100792

11. Fang JH, Xu L, Shang LR, Pan CZ, Ding J, Tang YQ, et al. Vessels that encapsulate tumor clusters (VETC) pattern is a predictor of sorafenib benefit in patients with hepatocellular carcinoma. *Hepatology*. (2019) 70:824–39. doi: 10.1002/hep.30366

12. Zhang P, Ono A, Fujii Y, Hayes CN, Tamura Y, Miura R, et al. The presence of vessels encapsulating tumor clusters is associated with an immunosuppressive tumor microenvironment in hepatocellular carcinoma. *Int J Cancer*. (2022) 151:2278–90. doi: 10.1002/ijc.34247

13. Matsuda K, Kurebayashi Y, Masugi Y, Yamazaki K, Ueno A, Tsujikawa H, et al. Immunovascular microenvironment in relation to prognostic heterogeneity of WNT/β-catenin-activated hepatocellular carcinoma. *Hepatol Res*. (2023) 53:344–56. doi: 10.1111/hepr.13869

14. Kurebayashi Y, Matsuda K, Ueno A, Tsujikawa H, Yamazaki K, Masugi Y, et al. Immunovascular classification of HCC reflects reciprocal interaction between immune and angiogenic tumor microenvironments. *Hepatology*. (2022) 75:1139–53. doi: 10.1002/hep.32201

15. Lin C, He Y, Liu M, Wu A, Zhang J, Li S, et al. Vessels that encapsulate tumor clusters (VETC) predict cTACE response in hepatocellular carcinoma. *J Hepatocell Carcinoma*. (2023) 10:383–97. doi: 10.2147/JHC.S395903

16. Fan Y, Yu Y, Hu M, Wang X, Du M, Guo L, et al. Imaging features based on Gd-EOB-DTPA-enhanced MRI for predicting vessels encapsulating tumor clusters (VETC) in patients with hepatocellular carcinoma. *Br J Radiol*. (2021) 94:20200950. doi: 10.1259/bjr.20200950

17. Chen FM, Du M, Qi X, Bian L, Wu D, Zhang SL, et al. Nomogram estimating vessels encapsulating tumor clusters in hepatocellular carcinoma from preoperative gadoxetate disodium-enhanced MRI. *J Magn Reson Imaging*. (2023) 57:1893–905. doi: 10.1002/jmri.28488

18. Yang J, Dong X, Wang G, Chen J, Zhang B, Pan W, et al. Preoperative MRI features for characterization of vessels encapsulating tumor clusters and microvascular invasion in hepatocellular carcinoma. *Abdom Radiol (NY)*. (2023) 48:554–66. doi: 10.1007/s00261-022-03740-w

19. Parekh VS, Jacobs MA. Deep learning and radiomics in precision medicine. *Expert Rev Precis Med Drug Dev*. (2019) 4:59–72. doi: 10.1080/23808993.2019.1585805

20. Yu Y, Fan Y, Wang X, Zhu M, Hu M, Shi C, et al. Gd-EOB-DTPA-enhanced MRI radiomics to predict vessels encapsulating tumor clusters (VETC) and patient prognosis in hepatocellular carcinoma. *Eur Radiol*. (2022) 32:959–70. doi: 10.1007/s00330-021-08250-9

21. Fan Y, Yu Y, Wang X, Hu M, Du M, Guo L, et al. Texture analysis based on gd-EOB-DTPA-enhanced MRI for identifying vessels encapsulating tumor clusters (VETC)-positive hepatocellular carcinoma. *J Hepatocell Carcinoma*. (2021) 8:349–59. doi: 10.2147/JHC.S293755

22. Chu T, Zhao C, Zhang J, Duan K, Li M, Zhang T, et al. Application of a convolutional neural network for multitask learning to simultaneously predict microvascular invasion and vessels that encapsulate tumor clusters in hepatocellular carcinoma. *Ann Surg Oncol*. (2022) 29:6774–83. doi: 10.1245/s10434-022-12000-6

23. Dong X, Yang J, Zhang B, Li Y, Wang G, Chen J, et al. Deep learning radiomics model of dynamic contrast-enhanced MRI for evaluating vessels encapsulating tumor clusters and prognosis in hepatocellular carcinoma. *J Magn Reson Imaging*. (2024) 59:108–19. doi: 10.1002/jmri.28745

24. CT/MRI Liver Imaging Reporting and Data System version 2018 . American College of Radiology Web site. Available online at: https://www.acr.org/Clinical-Resources/Reporting-andData-Systems/LI-RADS/CTMRI-LI-RADS-v2018 (Accessed 1 December 2018).

25. Akiba J, Nakayama M, Sadashima E, Kusano H, Kondo R, Mihara Y, et al. Prognostic impact of vessels encapsulating tumor clusters and macrotrabecular patterns in hepatocellular carcinoma. *Pathol Res Pract*. (2022) 238:154084. doi: 10.1016/j.prp.2022.154084

26. Tohme S, Yazdani HO, Liu Y, Loughran P, van der Windt DJ, Hai H, et al. Hypoxia mediates mitochondrial biogenesis in hepatocellular carcinoma to promote tumor growth through HMGB1 and TLR9 interaction. *Hepatology*. (2017) 66:182–97. doi: 10.1002/hep.29184

27. Rhee H, An C, Kim HY, Yoo JE, Park YN, Kim MJ. Hepatocellular carcinoma with irregular rim-like arterial phase hyperenhancement: more aggressive pathologic features. *Liver Cancer*. (2019) 8:24–40. doi: 10.1159/000488540

28. Gillies RJ, Kinahan PE, Hricak H. Radiomics: images are more than pictures, they are data. *Radiology*. (2016) 278:563–77. doi: 10.1148/radiol.2015151169

29. Guntipalli P, Pakala R, Kumari Gara S, Ahmed F, Bhatnagar A, Endaya Coronel MK. Worldwide prevalence, genotype distribution and management of hepatitis C. *Acta Gastroenterol Belg*. (2021) 84:637–56. doi: 10.51821/ageb

30. He C, Zhou Z, Jiang H, Yin Z, Meng S, Zhang J, et al. Epithelial-mesenchymal transition is superior to vessels-encapsulate tumor cluster in promoting metastasis of hepatocellular carcinoma: a morphological evidence. *J Cancer*. (2017) 8:39–47. doi: 10.7150/jca.16736

frontiers | Frontiers in Medicine

TYPE Original Research
PUBLISHED 27 September 2024
DOI 10.3389/fmed.2024.1452188

OPEN ACCESS

EDITED BY
Marcello Dallio,
University of Campania Luigi Vanvitelli, Italy

REVIEWED BY
Mohammadsadegh Nikdad,
Universitätsmedizin Greifswald, Germany
Tamer A. Addissouky,
University of Menoufia, Egypt

*CORRESPONDENCE
Youming Ding
✉ dingym@whu.edu.cn
Kailiang Zhao
✉ zhaokl1983@whu.edu.cn

†These authors have contributed equally to this work and share first authorship

RECEIVED 20 June 2024
ACCEPTED 18 September 2024
PUBLISHED 27 September 2024

CITATION
Shen J, Zhou Y, Pei J, Yang D, Zhao K and Ding Y (2024) Development of prognostic models for advanced multiple hepatocellular carcinoma based on Cox regression, deep learning and machine learning algorithms. *Front. Med.* 11:1452188. doi: 10.3389/fmed.2024.1452188

Development of prognostic models for advanced multiple hepatocellular carcinoma based on Cox regression, deep learning and machine learning algorithms

Jie Shen[1†], Yu Zhou[1†], Junpeng Pei[2], Dashuai Yang[1], Kailiang Zhao[1*] and Youming Ding[1*]

[1]Department of Hepatobiliary Surgery, Renmin Hospital of Wuhan University, Wuhan, China, [2]Department of Hepatobiliary Surgery, 521 Hospital of Norinco Group, Xi'an, China

Background: Most patients with multiple hepatocellular carcinoma (MHCC) are at advanced stage once diagnosed, so that clinical treatment and decision-making are quite tricky. The AJCC-TNM system cannot accurately determine prognosis, our study aimed to identify prognostic factors for MHCC and to develop a prognostic model to quantify the risk and survival probability of patients.

Methods: Eligible patients with HCC were obtained from the Surveillance, Epidemiology, and End Results (SEER) database, and then prognostic models were built using Cox regression, machine learning (ML), and deep learning (DL) algorithms. The model's performance was evaluated using C-index, receiver operating characteristic curve, Brier score and decision curve analysis, respectively, and the best model was interpreted using SHapley additive explanations (SHAP) interpretability technique.

Results: A total of eight variables were included in the follow-up study, our analysis identified that the gradient boosted machine (GBM) model was the best prognostic model for advanced MHCC. In particular, the GBM model in the training cohort had a C-index of 0.73, a Brier score of 0.124, with area under the curve (AUC) values above 0.78 at the first, third, and fifth year. Importantly, the model also performed well in test cohort. The Kaplan–Meier (K-M) survival analysis demonstrated that the newly developed risk stratification system could well differentiate the prognosis of patients.

Conclusion: Of the ML models, GBM model could predict the prognosis of advanced MHCC patients most accurately.

KEYWORDS

advanced multiple hepatocellular carcinoma, prognosis, machine learning, deep learning, gradient boosted machine

1 Introduction

Hepatocellular carcinoma (HCC), the sixth most common cancer in the world, has an insidious onset, rapid progression and poor prognosis, making it more difficult to treat (1). Accurately assessing the prognosis of HCC patients may provide clinicians reference values to develop more effective treatment plans. AJCC-TNM and Barcelona Clinic Liver Cancer

(BCLC) staging are the most commonly used staging systems for HCC, but they are unable to take into account the effects of treatment, age, and other important factors, thus, they seem to have poor accuracy (2). Recently, a large number of scholars have used nomograms to study cancer (3, 4), which were built based on multifactorial Cox regression analyses with fixed weights assigned, and the accuracy is sometimes unsatisfactory (5). Machine Learning (ML) enables computers to learn from large-scale, disparate healthcare data and then make decisions or predictions without being explicitly programmed. ML models offer considerable advantages over traditional statistical models for tasks such as diagnosis, classification and survival prediction (6, 7). DL is a branch of ML that uses a ML technique called artificial neural networks to extract patterns and make predictions from large datasets, and is particularly well suited to solving complex computational problems (8).

MHCC is classified into two types, one is intrahepatic metastasis, which is the result of intrahepatic metastasis of solitary tumor nodule, and the other is multicentric origin, which is the primary HCC (9). There are few studies on the prognosis of MHCC, making treatment more difficult (10). Previous studies have revealed that tumor size, Alpha-Fetal Protein (AFP) level, surgical treatment, microvascular invasion and hepatic functional status were important risk factors affecting patients' recurrence or Overall Survival (OS) (11–13). As for surgery, although many studies have consistently shown that surgery is beneficial in MHCC (11, 14, 15), there are no studies that indicate whether patients with advanced MHCC can benefit from it.

The aim of this study is to construct prognostic models based on Cox regression, ML and DL algorithms using a large dataset from the SEER database, to predict the prognosis of patients with advanced MHCC, thus helping clinicians to optimize their decisions.

2 Methods

2.1 Selection of patients and study variables

Data on patients, who were diagnosed with HCC between 2000 and 2020, were obtained with SEER*Stat software (version 8.4.2). The SEER database is publicly accessible and does not require approval by the ethics institutional review board. External validation data were obtained from Renmin Hospital of Wuhan University. Variables included in the study were age, sex, race, tumor size, tumor primary site and regional lymph surgery information, months from diagnosis to treatment, AJCC-TNM stage, histological grade, radiotherapy, chemotherapy, AFP, sequence of systemic therapy and surgery, number and sequence of malignant tumors, a total of 15 variables. Patient inclusion criteria: (1) Patients diagnosed with HCC between 2000 and 2020 (histologic type International Classification of Disease for Oncology third edition = 8,170–8,175) (ICD-O3); (2) CS extension records as multiple nodules; (3) TNM stage was stage III or IV. The exclusion criteria are as follows: (1) Data missing or not clearly recorded, grouping disputed data; (2) Survival time is not recorded or less than 1 month; (3) A patient has two or more medical records, the last one shall prevail. The detailed selection process was shown in Figure 1.

2.2 Variable selection and construction of prognostic models

We randomly divided 1707 advanced MHCC patients into a training cohort and test cohort in a 7:3 ratio. Univariate and multivariate Cox were successively used to screen variables with prognostic significance, that is, Variables with hazard ratio (HR) more or less than 1 and statistically significant were retained. Use R software (version 4.2.1), open-source Python library scikit-survival (version 0.21.0) and PyTorch (Python version 3.11.4) to build prediction models (16).

2.3 Evaluation and selection of the best prediction model

Calculating C-index and Brier score to assess the accuracy of model prediction, receiver operating characteristic (ROC) curves and decision curve analysis (DCA) curves for the 1st, 3rd, and 5th year were then continued to be plotted to compare the accuracy of the models and potential clinical benefit (17). We determined the best cut off value for risk grouping by X-tile software, then K-M curves were used to compare the differences in OS of advanced MHCC patients in different risk stratification groups.

2.4 Interpretation of GBM model

The explanation of the model was divided into two parts: SHAP plot and the prediction website based on JAVA. SHAP is a model interpretation package developed in Python, for each prediction sample, the SHAP value is assigned to each feature. The larger the absolute value of SHAP, the greater the influence of the feature, and the sign of the value indicates whether the feature has a positive or negative effect on the result (18, 19). In order to better present the results and make it easier for the reader to use the model, an interactive website was established. By entering the required clinical information, 1-, 3-, and 5-year survival probability and risk score can be automatically calculated.

2.5 Statistical analysis

All statistical analyses were performed by R software (version 4.2.1.) and Python (version 3.11.4.) The "survival" package and "survminer" package were used for univariate and multivariate Cox regression analysis, forest mapping. Hazard ratio (HR) > 1 indicates that the factor is a risk factor, while HR < 1 indicates it is a protective factor. The "rms" package was used to draw the nomogram. Survival distributions were compared using the log-rank test. All tests were two-sided and p values less than 0.05 were considered statistically significant.

3 Results

3.1 Baseline characteristics in the training and test cohorts

A total of 1707 advanced MHCC patients were enrolled in our study, including 1,195 (70%) in the training cohort and 512

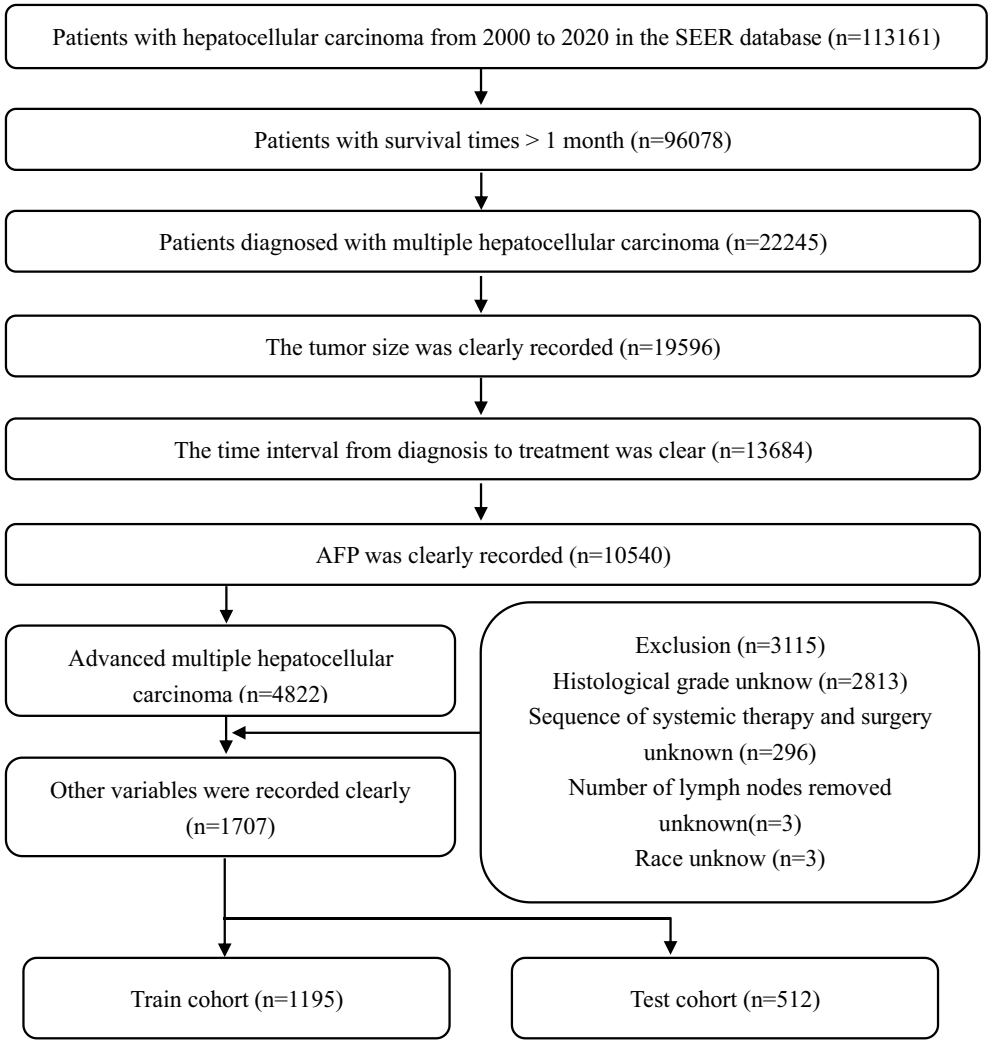

FIGURE 1
Flow chart of patients' selection in the training and test cohorts from the SEER database.

(30%) in the internal test cohort, the information for the external cohort can be obtained from Supplement Sheet 1. Most of these patients only had HCC, and their histological grading was in grades I to III, with a predominance of grade II. The vast majority of patients were at stage IIIA in the AJCC-TNM staging, i.e., there were multiple lesions in liver and any one of the lesions was more than 5 cm in size without lymph node or major vascular invasion. Because of this, the vast majority of tumor size was greater than 5 cm, but dimensions greater than 10 cm were rare. AFP is often considered as a marker for HCC, although the sensitivity and specificity are not satisfactory. In this study, AFP was abnormal in more than 70% of patients with advanced MHCC. In terms of treatment, not many patients were treated immediately after being diagnosed, they were more likely to choose to receive treatment after one to 2 months, and, of course, more than 10% of patients still went for treatment in the fourth month or later. There is a gap in research regarding surgery in advanced MHCC. Nearly 70% of the patients in this study did not undergo surgical treatment, still more than 20% underwent partial hepatectomy, in addition, almost all patients did not undergo lymph node dissection. Table 1 detailed the baseline information of the patients with advanced MHCC in this study.

3.2 Screening for statistically significant prognostic factors

A total of 15 variables were included in the study, after univariate Cox analysis, as shown in Supplementary Table S1, four variables: age, race, number of malignant tumors and radiotherapy were excluded. A multivariate analysis was conducted immediately afterward, the results showed that TNM stage, histological grade, months from diagnosis to treatment, primary site surgery, tumor size, regional lymph surgery, AFP and sequence of malignant tumors were independent prognostic factors for patients with advanced MHCC, therefore, a total of 8 prognostic factors with statistical significance (Figure 2A).

As shown in the figure, it is clear that patients with AJCC-TNM staging at stage IV had a higher risk of death than those at stage IIIA, and stage IIIB may be a false positive because the proportion of

TABLE 1 Demographic and clinical characteristics of patients with advanced MHCC.

Variable	Overall		Train cohort		Test cohort	
	Sample size	Percentage	Sample size	Percentage	Sample size	Percentage
Total	1707		1,195		512	
Histological grade[a]						
I	488	28.59%	331	27.70%	157	30.66%
II	791	46.34%	557	46.61%	234	45.71%
III	400	23.43%	287	24.02%	113	22.07%
IV	28	1.64%	20	1.67%	8	1.56%
TNM stage						
IIIA	1,236	72.41%	860	71.97%	376	73.43%
IIIB	8	0.47%	6	0.50%	2	0.39%
IIIC	117	6.85%	80	6.69%	37	7.23%
IV	346	20.27%	249	20.84%	97	18.95%
Diagnosis to treat[b]						
Zero	272	15.93%	197	16.49%	75	14.65%
One	576	33.74%	397	33.22%	179	34.95%
Two	408	23.90%	294	24.60%	114	22.27%
Three	228	13.36%	159	13.31%	69	13.48%
4 or more	223	13.07%	148	12.38%	75	14.65%
Primary site surgery						
No surgery	1,162	68.07%	811	67.87%	351	68.55%
Local tumor destruction	103	6.03%	80	6.69%	23	4.50%
Partial hepatectomy	394	23.09%	270	22.59%	124	24.22%
Liver transplantation	48	2.81%	34	2.85%	14	2.73%
Tumor size						
< 5 cm	133	7.79%	95	7.95%	38	7.42%
5 ~ 10 cm	1,066	62.45%	744	62.26%	322	62.89%
> 10 cm	508	29.76%	356	29.79%	152	29.69%
Lymph surgery						
No	1,591	93.20%	1,108	92.72%	483	94.33%
Biopsy	9	0.53%	8	0.67%	1	0.20%
Yes	107	6.27%	79	6.61%	28	5.47%
AFP						
Negative	437	25.60%	292	24.44%	145	28.32%
Borderline	7	0.41%	5	0.42%	2	0.39%
Positive	1,263	73.99%	898	75.14%	365	71.29%
Sequence number[c]						
One primary only	1,388	81.31%	971	81.26%	417	81.45%
1st of 2 or more	58	3.40%	42	3.51%	16	3.13%
Not 1st of 2 or more	261	15.29%	182	15.23%	79	15.42%

[a]"Grade" refers to histological grade. In pathological reports, highly differentiated ICC corresponds to "Grade I," moderately differentiated ICC corresponds to "Grade II," poorly differentiated ICC corresponds to "Grade III," and undifferentiated ICC corresponds to "Grade IV".

[b]"Diagnosis to Treat" refers to time interval from diagnosis to treatment.

[c]"Sequence number" refers to the order in which the cancers in a patient's lifetime compared to ICC. "One primary only" means that the patient has only ICC in his or her lifetime. "1st of 2 or more" "1st of 2 or more" means that the ICC is the patient's first malignant tumor, but later developed other tumors. "not 1st primary" means that the patient had other tumors prior to ICC.

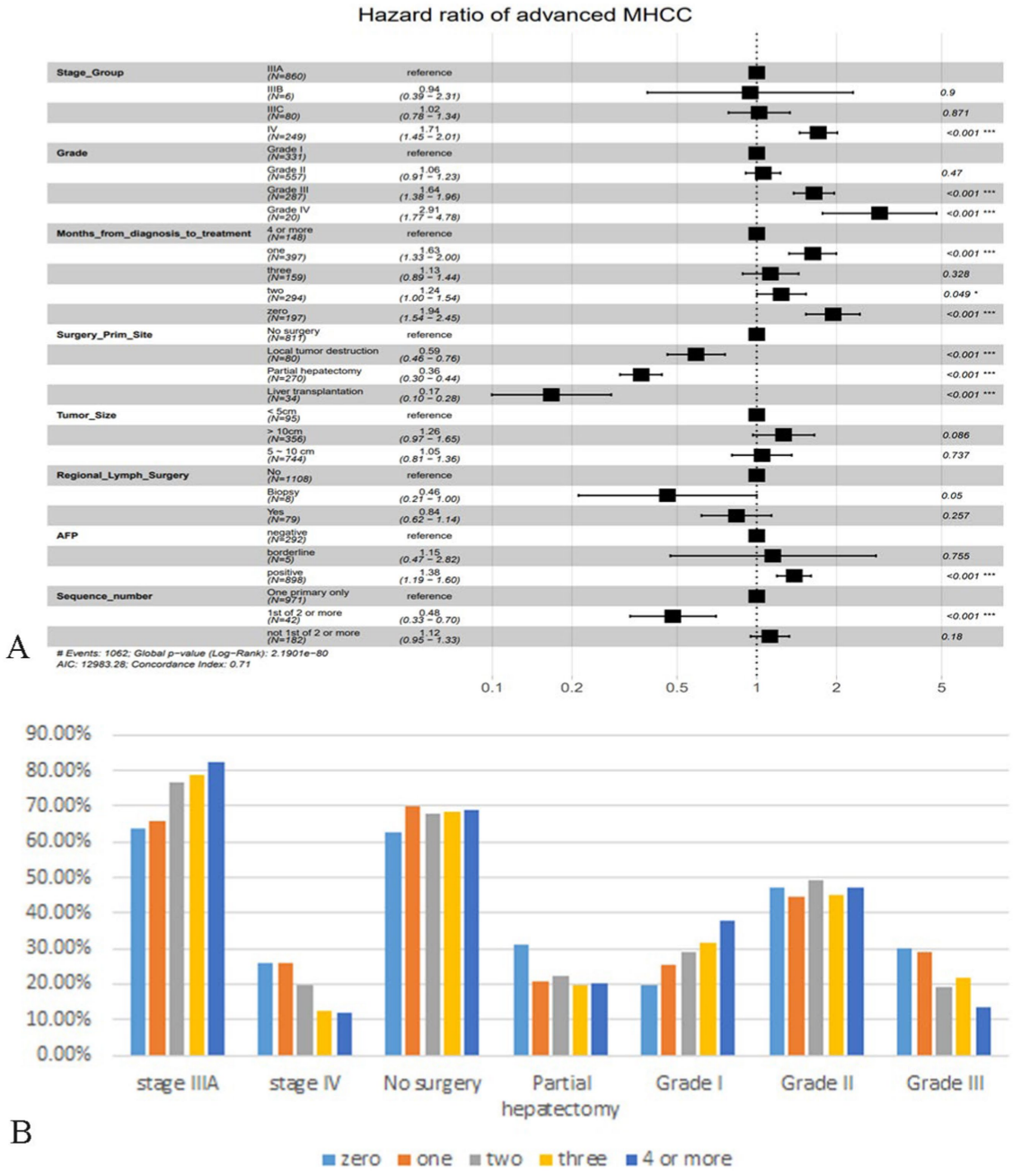

FIGURE 2
Demonstration of multivariate Cox regression analysis and analysis of patients in different months from diagnosis to treatment. **(A)** Forest plot based on multivariate Cox regression analysis. **(B)** Bar plot of important features of advanced MHCC patients in different months from diagnosis to treatment. The vertical coordinate is the percentage of the feature subgroup in the group.

patients was too small. The results regarding histologic grade were consistent with popular knowledge that the lower the degree of differentiation, the correspondingly lower the OS of the patient. Surprisingly, "time interval from diagnosis to treatment" was not the factor that patients who were treated immediately had a better prognosis, patients who were treated immediately after diagnosis or who received treatment a month later had a significantly higher risk of death than those who were delayed for 4 months or more. We tried to analyze whether it was influenced by other factors, selecting some of the important ones. Figure 2B showed that "zero" or "one" group had a significantly lower proportion of patients in stage IIIA than the "4 or more" group, and a significantly higher proportion in stage IV (Figure 2B). The same trend was observed in the factor histological grade, so they may have influenced the significance of the factor "months from diagnosis to treatment" on prognosis. As for surgery for tumor lesions, liver transplantation (LT) remained the best treatment modality, greatly reducing the risk of death, and failure to undergo surgery appeared to be the highest risk. In this study, we did not find significant variability between subgroups of tumor size and subgroups of regional lymph surgery. The risk of death was significantly higher

in the AFP-positive group than in the negative group, and surprisingly, the risk of death in MHCC patients who recurred other primary tumors was instead lower than that of MHCC only, which we discussed in the Discussion section.

3.3 Evaluation and comparison of prognostic models

Based on the training cohort, we first constructed a nomogram model using R software (Figure 3A), which is a visualization of multivariate Cox regression analysis with the same performance as Cox proportional hazards (CPH) model (20). Nomogram is convenient to use, but it is not hard to notice from Supplementary Table S2 that although its Brier score is not high, its C-index is 0.71, which is unsatisfactory. So based on ML and DL algorithms, we constructed CPH, survival tree, random survival forest (RSF), GBM and DeepSurv model, a total of five models, and optimized the parameters of models with five-fold cross-validation (Supplementary Table S3; Supplement Sheet 1). We first calculated their C-index, Brier score to evaluate the models as shown in Supplementary Table S2. Obviously, the GBM model performed the best with a high C-index of 0.73 and a low Brier score of 0.111. We then plotted the ROC curves for the 1st, 3rd, and 5th year of the five models (Figures 3B–D), and we can note that the GBM model always had the highest area under the curve (AUC) values, followed by the DeepSurv model. Interestingly, the AUC values gradually increased with time, suggesting that the GBM model is more accurate in predicting long-term prognosis. DCA curves showed (Figures 3E–G) that using our models to guide treatment can bring benefits to patients, with the GBM and DeepSurv models leading to more benefits for patients with advanced MHCC. In summary, it is not difficult to conclude that the GBM model outperformed the other models, so we selected the GBM model for subsequent evaluation and research.

3.4 Validation of GBM performance and development of a risk stratification system

We performed internal and external tests. Internal and external test cohorts consisted of 512 and 41 patients, respectively. The mean AUC values of GBM model over the period from the 1st to the 72nd month was 0.772 and increased over time (Figure 4A). In external cohort, the average AUC value was 0.771, which is surprisingly high in the first year (Figure 4B) its C-index was 0.702 and Brier score was 0.129 in internal test cohort, with C-index of 0.691 and Brier score of 0.136 in external test cohort (Supplementary Table S4). Calibration curves revealed that the model's predictions were highly consistent with the actual situation (Figures 4C–E). Therefore, the GBM model still performed well in the test cohort. Figure 4F showed the poor ability of TNM stage to differentiate patients' prognosis (Figure 4F), to assess the model's ability to differentiate patients' OS, we developed a risk stratification system based on the total risk score of each patient in the training cohort and determined the optimal cut off value using X-tile software (Figure 4G). Patient risk scores were determined from the GBM model's predictions and they ranged from between −1.7 and 2.1, with lower than −0.1 being low risk, higher than 1.0 being high risk, and in between being intermediate risk. Following this, we plotted the K-M survival curves for the three risk subgroups (Figure 4H), which showed significant differences in prognosis among the different subgroups, with the high-risk group having the worst prognosis and the low-risk group having a better prognosis. The prognosis of external test cohort was similarly well differentiated (Figure 4I).

3.5 Interpretation of GBM model and feature importance

Features with higher mean Shapley values are more important for prognosis, and in the SHAP plot (Figure 5A), the features were listed in descending order of importance. Among them, whether the tumor primary site was operated on was the most important. In addition, a positive SHAP value increases the probability of death, i.e., the higher the value, the higher the risk of death, and vice versa. The results suggested that histological grade of grade III and TNM stage of stage IV increased the probability of death. As for "tumor primary site surgery," no surgery generally increased the probability of death, but it is not difficult to find that in a considerable number of cases, no surgery would increase the probability of survival. Three patients from the training cohort were selected for the prognostic demonstration (Figures 5B–D). The first patient underwent partial hepatectomy, which increased the probability of death, while the next two patients had the opposite effect, with an increase in the probability of death due to no surgical intervention. Therefore, many patients with advanced MHCC may have lost the opportunity for surgery at the time of diagnosis, and it is necessary to strictly grasp the indications for surgery in order to make the patients benefit from surgery. To facilitate the use of our prognostic model by clinicians, we built a website,[1] which allows users to directly input their own data for prediction of OS and risk score. Controlling for the same other features and then inputting a different treatment to determine if the prediction improves or decreases, by which they can also preliminarily assess whether a treatment is beneficial.

4 Discussion

The morbidity and mortality rates of HCC are increasing annually, and the treatment of MHCC is more complicated than that of solitary HCC, and once it reaches an advanced stage, the prognosis of the patient is quite dismal (21). Importantly, clinicians need to balance commonly used treatments at this stage, and there is a lack of effective predictive models to the extent that some patients are not treated rationally enough (22). Our research is an attempt to build predictive models for advanced MHCC patients using well-established Cox regression, ML and DL algorithms.

Our results indicated that the GBM model had the best prediction accuracy with a C-index of 0.730 and a Brier score of 0.111, and the AUCs for the 1st year, 3rd year, and 5th year were higher than 0.78 with an increasing trend. In addition, the GBM model still performed well in the test cohort, which demonstrated that our model is quite

1 http://39.101.130.191:8888/mhcc

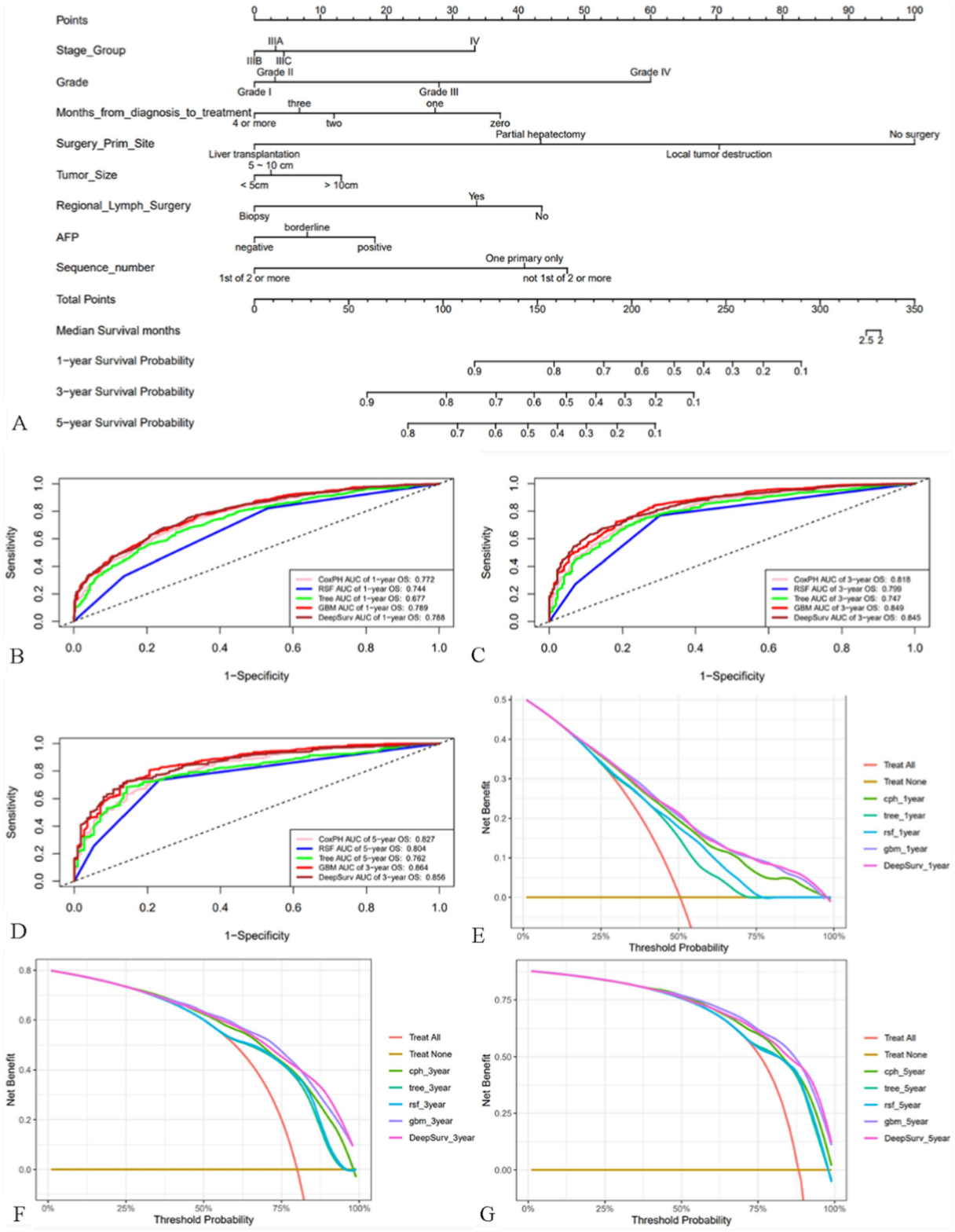

FIGURE 3
Nomogram of patients with advanced MHCC and evaluation of the performance of the five models. **(A)** Nomogram of patients with advanced MHCC. **(B–D)** ROC curves for prognostic models predicting 1-, 3-, and 5-year OS in the training cohort. (**E–G**) DCA curves of prognostic models for 1-year, 3-year, and 5-year OS prediction in the training cohort.

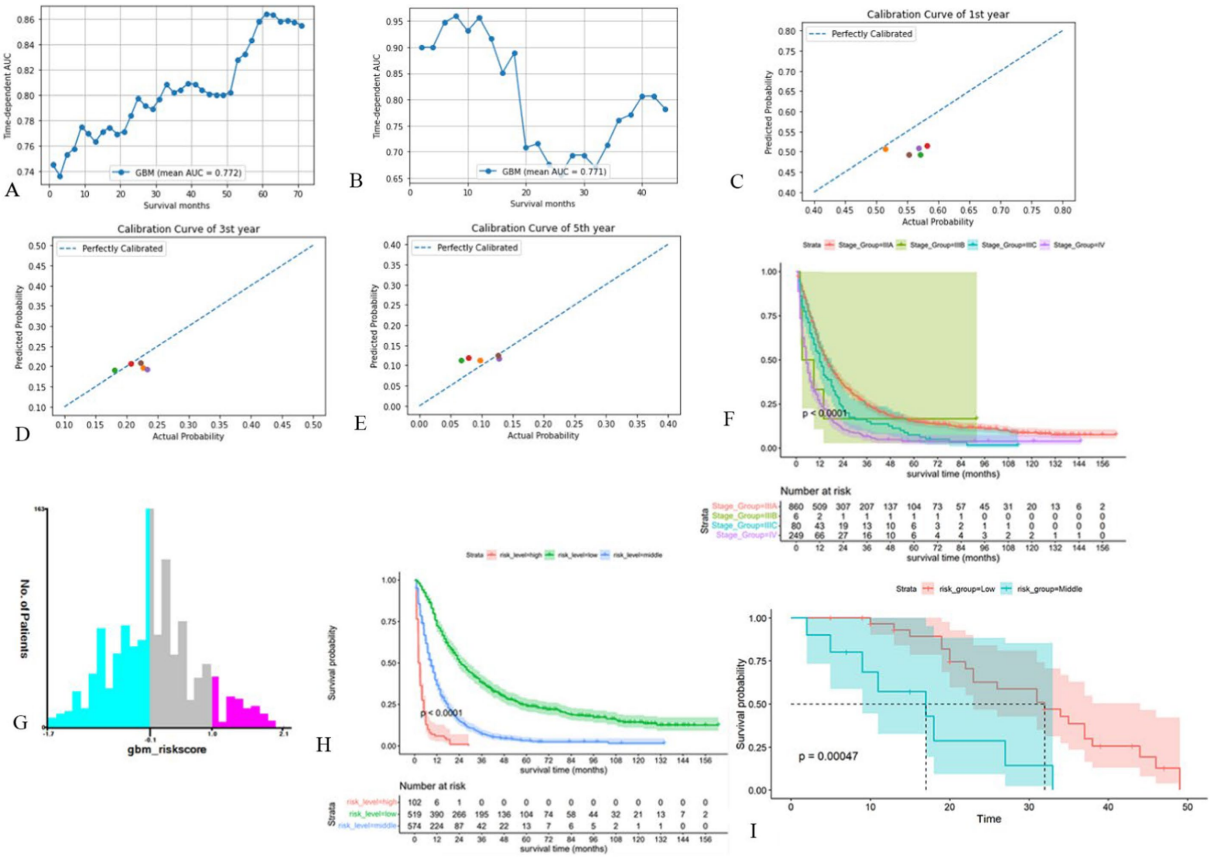

FIGURE 4
Validation of the GBM model and development of new risk stratification system. (**A, B**) Time-dependent AUC for the GBM model in internal test cohort (**A**) and external test cohort (**B**). (**C-E**) Calibration curves of first (**C**), third (**D**) and fifth (**E**) year in the internal test cohort. (**F**) Survival curves based on AJCC-TNM stage. (**G**) Cut off values for optimal grouping determined using X-tile. (**H**) K-M survival curves based on new risk stratification system. (**I**) K-M survival curves of external test cohort based on new risk stratification system (Only one of these patients was high risk and was merged into the intermediate risk group).

reliable in terms of prediction accuracy. The DCA curves indicated that the use of our GBM model maximized the survival benefit for patients with advanced MHCC. DeepSurv model uses a DL neural network to integrate Cox proportional hazards, which performed slightly weaker with the GBM model in this study.

According to Cox regression analysis, our model included 8 variables, which were shown in Table 1. The higher the histological grade, the worse the differentiation, the later the TNM stage, and the worse the OS of HCC patients, which has been recognized by the public. AFP is currently the most commonly used tumor marker for HCC, and according to the Asian HCC guidelines, the serum biomarker AFP is recommended as one of the monitoring and diagnostic tools for HCC (23, 24), however, many non-cancer sources involving liver and other organs may also lead to elevated AFP and thus have lower sensitivity and specificity (25). Limited literatures addressed the clinical significance of regional lymph node dissection during surgery in patients with HCC, a study by Yang et al. based on the SEER database reported that regional lymph node dissection was not an independent prognostic factor for OS (26). Another report showed a significantly higher incidence of postoperative ascites and a significantly lower overall tumor recurrence rate for liver surgery combined with regional lymph node dissection versus no lymph node dissection, although there was no difference in OS rates (27). The clinical significance of regional lymph node dissection in advanced MHCC remains to be studied. As for surgery for primary tumor sites, multivariate Cox results demonstrated that liver surgery improved OS for patients with advanced MHCC in general, and liver transplantation in particular. However, the subsequent SHAP figure indicated that a considerable number of patients with advanced MHCC were not suitable for surgical treatment, and no surgery was a kind of protection. Although a number of studies on MHCC have shown that hepatectomy (28, 29), LT, and even combined ablation therapy were effective treatment strategies for MHCC (30), Bartolini et al. (11) reported that surgery should be subject to strict indications in order to benefit specific patients, especially for patients with advanced MHCC. Our model may help clinicians make decisions, but further test is needed. For solitary HCC, tumor size often affects treatment and prognosis (31), but in our study, for advanced MHCC, there did not appear to be a significant difference in risk of death between different tumor sizes.

Interestingly, sequence of malignant tumors and interval from diagnosis to treatment showed results that seemed to differ from popular perception. Patients with HCC alone had worse OS than those who developed other primary tumors after HCC, and we found that other researchers have reported similar results (32, 33). They noted that patients with only one cancer may die prematurely due to poor health or a higher degree of malignancy of the tumor, with no

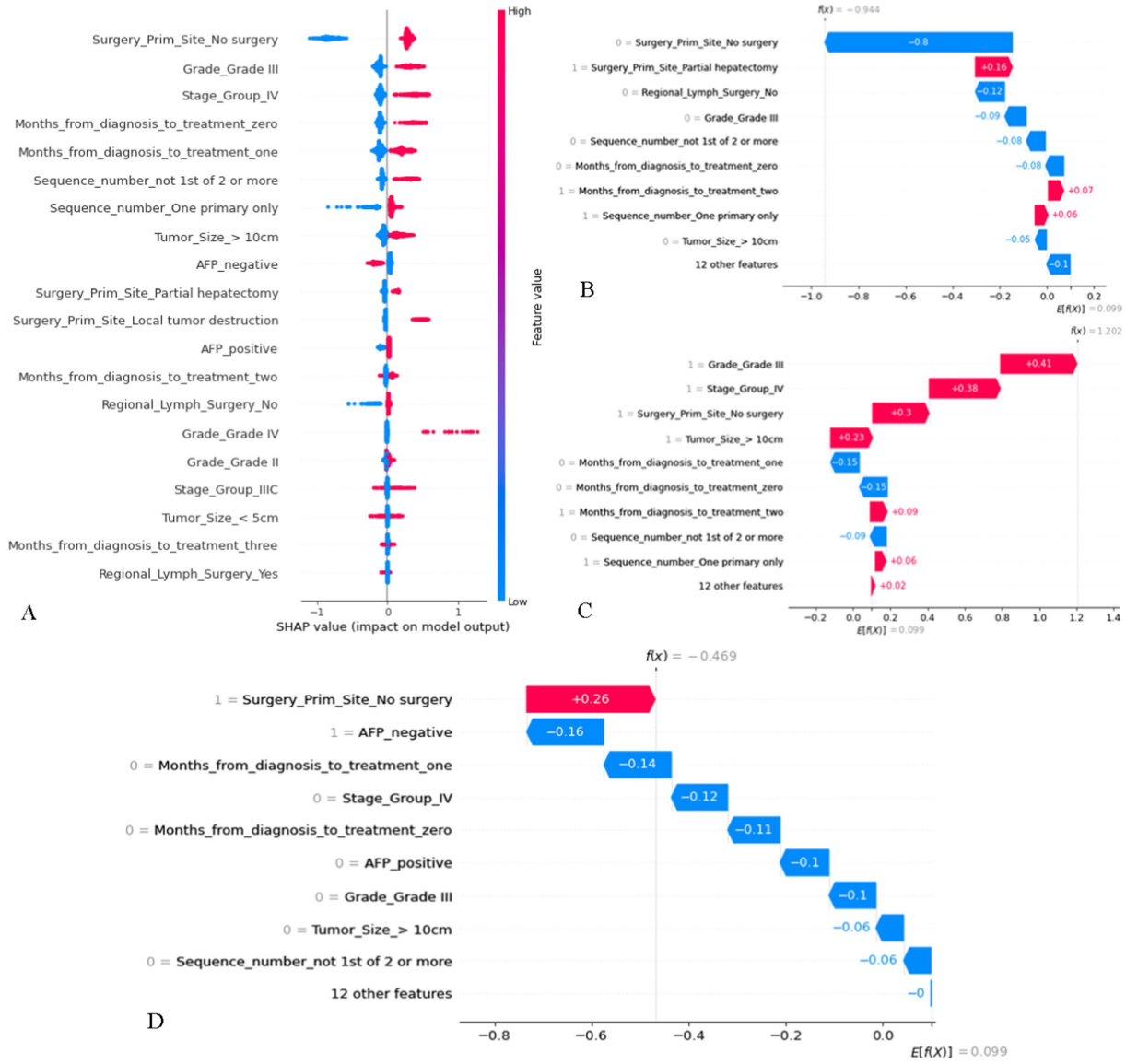

FIGURE 5
The SHAP plot of the GBM model. (**A**) SHAP beeswarm summary plot on the impact of input variables on the GBM model's prediction. (**B**) The local SHAP plot of patient #1. Patient #1: 74-year-old male, survival time was 96 months, alive. AJCC TNM stage was IIIA, Histological grade was II, tumor size = 6.0 cm, AFP was positive. She was treated 2 months after diagnosis, underwent partial hepatectomy and regional lymph surgery, only had HCC in his life. (**C**) The local SHAP plot of patient #2. Patient #2: 42-year-old male, survival time was 2 months, died. AJCC TNM stage was IV, Histological grade was III, tumor size = 13.0 cm, AFP was negative. She was treated 2 months after diagnosis, no tumor site and regional lymph surgery, only had HCC in his life. (**D**) The local SHAP plot of patient #3. Patient #3: 82-year-old male, survival time was 7 months, died. AJCC TNM stage was IIIA, Histological grade was II, tumor size = 5.9 cm, AFP was negative. She was treated 1 month after diagnosis, no tumor site and regional lymph surgery. Only had HCC in his life. The red ribbons in the local SHAP plot represent risk factors that lead to a poor prognosis, whereas the blue ribbons are the relatively protective factors.

chance of getting other tumors, and that re-emergence of other tumors occurs only in patients who have been survival for a long time. Secondly, patients with HCC only may have defective immune surveillance, leading to "immune escape," while reoccurrence of other tumors may activate cancer-related immune mechanisms. Finally, patients who re-emerge with other tumors will inevitably receive additional anti-tumor treatments, and these subsequent treatments may act as concurrent anti-HCC therapies. There is no uniformity in the literature regarding the impact of the time interval between diagnosis and treatment on prognosis. One study reported that time delay from diagnosis to treatment did not significantly affect OS in HCC patients (34), but Tsai et al. reported that the longer the time interval between diagnosis and treatment of early liver cancer, the lower the OS was (35). Therefore, randomized controlled trials may be needed to clarify the clinical significance of this factor.

Our research is advanced. We first applied multiple algorithms to construct prognostic models for patients with advanced MHCC, which were evaluated by multiple methods, and ultimately the more superior GBM model was selected among five models. To our knowledge, this is the first model for advanced MHCC. Visualization

and application promotion of ML models are difficult problems, we used SHAP technique for model interpretation and built a prediction website to solve this problem well. Despite a substantial amount of published research indicating that AI-based systems demonstrate significant advantages in improving the accuracy and efficiency of HCC screening, diagnosis, and tumor characterization, there is still a need for rigorous multicenter prospective validation studies and the validation of standardized multimodal datasets (36, 37). Secondly, the SEER database only covers cancer data in the U.S. Our study would be more convincing if more data were obtained. Due to the limitations of the SEER database, some variables that may be important, such as BCLC stage, genetic factors and targeted therapies, are not available. Having access to these variables may improve the performance of the model.

5 Conclusion

A total of eight variables were independent prognostic factors, which were included in the model to predict the prognosis of patients with advanced MHCC, and the GBM model could provide a more accurate prediction of patients' OS.

Data availability statement

Publicly available datasets were analyzed in this study. This data can be found at: the Surveillance, Epidemiology, and End Results (SEER) database (https://seer.cancer.gov/mortality/).

Ethics statement

The studies involving humans were approved by the Clinical Research Ethics Committee, Renmin Hospital of Wuhan University. The studies were conducted in accordance with the local legislation and institutional requirements. Written informed consent for participation was not required from the participants or the participants' legal guardians/next of kin in accordance with the national legislation and institutional requirements.

Author contributions

JS: Writing – review & editing, Writing – original draft, Visualization, Validation, Software, Methodology, Investigation, Data curation, Conceptualization. YZ: Writing – original draft, Resources, Methodology, Formal analysis. JP: Writing – review & editing, Resources, Data curation. DY: Writing – review & editing, Validation, Methodology. KZ: Writing – review & editing, Project administration, Funding acquisition. YD: Writing – review & editing, Project administration, Funding acquisition.

Funding

The author(s) declare that financial support was received for the research, authorship, and/or publication of this article. This research was funded by the national key research and development program of China (2022YFC2407304), Natural Science Foundation of Hubei Province (2022CFB122) and National Natural Science Foundation of China (82370654).

Acknowledgments

Thanks to Yang Hao for his contributions in building online websites using JAVA.

Conflict of interest

The authors declare that the research was conducted in the absence of any commercial or financial relationships that could be construed as a potential conflict of interest.

Publisher's note

Supplementary material

The Supplementary material for this article can be found online at: https://www.frontiersin.org/articles/10.3389/fmed.2024.1452188/full#supplementary-material

References

1. Qi W, Dai J, Qiu Z, Wu Y, Wen T, Xie F, et al. Nomogram to predict liver surgery-specific complications for hepatocellular carcinoma: a multicenter study. *Eur J Surg Oncol.* (2023) 49:107119. doi: 10.1016/j.ejso.2023.107119

2. Torimura T, Iwamoto H. Treatment and the prognosis of hepatocellular carcinoma in Asia. *Liver Int.* (2022) 42:2042–54. doi: 10.1111/liv.15130

3. Wang Y, Li J, Xia Y, Gong R, Wang K, Yan Z, et al. Prognostic nomogram for intrahepatic cholangiocarcinoma after partial hepatectomy. *J Clin Oncol Off J Am Soc Clin Oncol.* (2013) 31:1188–95. doi: 10.1200/jco.2012.41.5984

4. Hyder O, Marques H, Pulitano C, Marsh JW, Alexandrescu S, Bauer TW, et al. A nomogram to predict long-term survival after resection for intrahepatic cholangiocarcinoma: an eastern and Western experience. *JAMA Surg.* (2014) 149:432–8. doi: 10.1001/jamasurg.2013.5168

5. Ji GW, Jiao CY, Xu ZG, Li XC, Wang K, Wang XH. Development and validation of a gradient boosting machine to predict prognosis after liver resection for intrahepatic cholangiocarcinoma. *BMC Cancer.* (2022) 22:258. doi: 10.1186/s12885-022-09352-3

6. Ngiam KY, Khor IW. Big data and machine learning algorithms for health-care delivery. *Lancet Oncol.* (2019) 20:e262–73. doi: 10.1016/s1470-2045(19)30149-4

7. Addissouky TA, Sayed IETE, Ali MMA, Wang Y, Baz AE, Khalil AA, et al. Latest advances in hepatocellular carcinoma management and prevention through advanced technologies. *Egypt Liver J.* (2024) 14:2. doi: 10.1186/s43066-023-00306-3

8. Tran KA, Kondrashova O, Bradley A, Williams ED, Pearson JV, Waddell N. Deep learning in cancer diagnosis, prognosis and treatment selection. *Genome Med*. (2021) 13:152. doi: 10.1186/s13073-021-00968-x

9. Yamamoto S, Midorikawa Y, Nagae G, Tatsuno K, Ueda H, Moriyama M, et al. Spatial and temporal expansion of intrahepatic metastasis by molecularly-defined clonality in multiple liver cancers. *Cancer Sci*. (2020) 111:601–9. doi: 10.1111/cas.14282

10. Li C, Liu JY, Peng W, Wen TF, Yan LN, Yang JY, et al. Liver resection versus transplantation for multiple hepatocellular carcinoma: a propensity score analysis. *Oncotarget*. (2017) 8:81492–500. doi: 10.18632/oncotarget.20623

11. Bartolini I, Nelli T, Russolillo N, Cucchetti A, Pesi B, Moraldi L, et al. Multiple hepatocellular carcinoma: long-term outcomes following resection beyond actual guidelines. An Italian multicentric retrospective study. *Am J Surg*. (2021) 222:599–605. doi: 10.1016/j.amjsurg.2021.01.023

12. Shindoh J, Kobayashi Y, Kawamura Y, Akuta N, Kobayashi M, Suzuki Y, et al. Microvascular invasion and a size cutoff value of 2 cm predict long-term oncological outcome in multiple hepatocellular carcinoma: reappraisal of the American joint committee on Cancer staging system and validation using the surveillance, epidemiology, and end-results database. *Liver Cancer*. (2020) 9:156–66. doi: 10.1159/000504193

13. Ryu T, Takami Y, Wada Y, Sasaki S, Imamura H, Ureshino H, et al. Combined hepatectomy and microwave ablation for multifocal hepatocellular carcinoma: long-term outcomes and prognostic factors. *Asian J Surg*. (2021) 44:186–91. doi: 10.1016/j.asjsur.2020.05.008

14. Nojiri K, Tanaka K, Takeda K, Ueda M, Matsuyama R, Taniguchi K, et al. The efficacy of liver resection for multinodular hepatocellular carcinoma. *Anticancer Res*. (2014) 34:2421–6.

15. Li ZL, Yu JJ, Guo JW, Sui CJ, Dai BH, Zhang WG, et al. Liver resection is justified for multinodular hepatocellular carcinoma in selected patients with cirrhosis: a multicenter analysis of 1,066 patients. *Eur J Surg Oncol*. (2019) 45:800–7. doi: 10.1016/j.ejso.2018.12.016

16. Pölsterl SJJMLR. Scikit-survival: a library for time-to-event analysis built on top of scikit-learn. *JMLR*. (2020) 21:1–6.

17. Dankers F, Traverso A, Wee L, van Kuijk SMJ. Prediction modeling methodology In: P Kubben, M Dumontier and A Dekker, editors. Fundamentals of clinical data science. Springer: Cham (2019). 101–20.

18. Lundberg SM, Lee S-I. A unified approach to interpreting model predictions. Proceedings of the 31st International Conference on Neural Information Processing Systems; California, USA: Curran Associates Inc; (2017). 4768–4777.

19. Lin J, Yin M, Liu L, Gao J, Yu C, Liu X, et al. The development of a prediction model based on random survival Forest for the postoperative prognosis of pancreatic Cancer: a SEER-based study. *Cancers*. (2022) 14:667. doi: 10.3390/cancers14194667

20. Yang L, Zhou Y, Wang G, Liu D, Chen B, Pu D, et al. Clinical features and prognostic factors of combined small cell lung cancer: development and validation of a nomogram based on the SEER database. *Transl Lung Cancer Res*. (2021) 10:4250–65. doi: 10.21037/tlcr-21-804

21. Cassese G, Han HS, Lee E, Lee B, Lee HW, Cho JY, et al. Laparoscopic versus open liver resection for multiple hepatocellular carcinoma within and beyond the Milan criteria: an eastern-Western propensity score-matched analysis. *J Hepatobiliary Pancreat Sci*. (2024) 31:2–11. doi: 10.1002/jhbp.1384

22. Colagrande S, Inghilesi AL, Aburas S, Taliani GG, Nardi C, Marra F. Challenges of advanced hepatocellular carcinoma. *World J Gastroenterol*. (2016) 22:7645–59. doi: 10.3748/wjg.v22.i34.7645

23. Omata M, Cheng AL, Kokudo N, Kudo M, Lee JM, Jia J, et al. Asia-Pacific clinical practice guidelines on the management of hepatocellular carcinoma: a 2017 update. *Hepatol Int*. (2017) 11:317–70. doi: 10.1007/s12072-017-9799-9

24. Xie DY, Ren ZG, Zhou J, Fan J, Gao Q. Critical appraisal of Chinese 2017 guideline on the management of hepatocellular carcinoma. *Hepatob Surg Nutr*. (2017) 6:387–96. doi: 10.21037/hbsn.2017.11.01

25. Wang W, Wei C. Advances in the early diagnosis of hepatocellular carcinoma. *Genes Dis*. (2020) 7:308–19. doi: 10.1016/j.gendis.2020.01.014

26. Yang A, Xiao W, Ju W, Liao Y, Chen M, Zhu X, et al. Prevalence and clinical significance of regional lymphadenectomy in patients with hepatocellular carcinoma. *ANZ J Surg*. (2019) 89:393–8. doi: 10.1111/ans.15096

27. Ravaioli M, Ercolani G, Grazi GL, Cescon M, Dazzi A, Zanfi C, et al. Safety and prognostic role of regional lymphadenectomy for primary and metastatic liver tumors. *Updat Surg*. (2010) 62:27–34. doi: 10.1007/s13304-010-0008-9

28. Shen WF, Wu L, Dong H, Sui CJ, Dai BH, Shen RX, et al. Hepatic resection for multiple hepatocellular carcinoma less than 5 cm: a prospective comparative study. *Hepato Gastroenterol*. (2014) 61:173–80.

29. Donadon M, Fontana A, Procopio F, Del Fabbro D, Cimino M, Viganò L, et al. Dissecting the multinodular hepatocellular carcinoma subset: is there a survival benefit after hepatectomy? *Updat Surg*. (2019) 71:57–66. doi: 10.1007/s13304-019-00626-3

30. Tada T, Kumada T, Toyoda H, Nakamura S, Endo Y, Kaneoka Y, et al. A validation study of combined resection and ablation therapy for multiple hepatocellular carcinoma. *Clin Radiol*. (2022) 77:114–20. doi: 10.1016/j.crad.2021.10.012

31. Usta S, Kayaalp C. Tumor diameter for hepatocellular carcinoma: why should size matter? *J Gastrointest Cancer*. (2020) 51:1114–7. doi: 10.1007/s12029-020-00483-z

32. Heo J, Noh OK, Oh YT, Chun M, Kim L. Second primary cancer after liver transplantation in hepatocellular carcinoma: a nationwide population-based study. *Hepatol Int*. (2017) 11:523–8. doi: 10.1007/s12072-017-9824-z

33. Wang S, Hu S, Huang S, Su L, Guo Q, Wu B, et al. Better survival and prognosis in SCLC survivors after combined second primary malignancies: a SEER database-based study. *Medicine*. (2023) 102:e32772. doi: 10.1097/md.0000000000032772

34. Rao A, Rich NE, Marrero JA, Yopp AC, Singal AG. Diagnostic and therapeutic delays in patients with hepatocellular carcinoma. *J Natl Comp Cancer Netw*. (2021) 19:1063–71. doi: 10.6004/jnccn.2020.7689

35. Tsai WC, Kung PT, Wang YH, Kuo WY, Li YH. Influence of the time interval from diagnosis to treatment on survival for early-stage liver cancer. *PLoS One*. (2018) 13:e0199532. doi: 10.1371/journal.pone.0199532

36. Addissouky T, Sayed I, Ali M, Alubiady M. Realizing the promise of artificial intelligence in hepatocellular carcinoma through opportunities and recommendations for responsible translation. *J Online Inform*. (2024) 9:70–9. doi: 10.15575/join.v9i1.1297

37. Chatzipanagiotou OP, Loukas C, Vailas M, Machairas N, Kykalos S, Charalampopoulos G, et al. Artificial intelligence in hepatocellular carcinoma diagnosis: a comprehensive review of current literature. *J Gastroenterol Hepatol*. (2024). doi: 10.1111/jgh.16663

frontiers | Frontiers in Medicine

TYPE Original Research
PUBLISHED 16 October 2024
DOI 10.3389/fmed.2024.1460505

OPEN ACCESS

EDITED BY
Liliana Chemello,
University of Padua, Italy

REVIEWED BY
Pablo Rodríguez Carnero,
La Princesa University Hospital, Spain
Emina Talakic,
Medical University of Graz, Austria

*CORRESPONDENCE
Peng Peng
✉ doublep@126.com

†These authors have contributed equally to this work and share first authorship

RECEIVED 06 July 2024
ACCEPTED 30 September 2024
PUBLISHED 16 October 2024

CITATION
Peng F, Luo C, Ning X, Xiao F, Guan K, Tang C, Huang F, Liang J and Peng P (2024) Computed tomography image quality in patients with primary hepatocellular carcinoma: intraindividual comparison of contrast agent concentrations.
Front. Med. 11:1460505.
doi: 10.3389/fmed.2024.1460505

Computed tomography image quality in patients with primary hepatocellular carcinoma: intraindividual comparison of contrast agent concentrations

Fei Peng†, Chaotian Luo†, Xiaojing Ning†, Fangyan Xiao, Kaiming Guan, Cheng Tang, Fuling Huang, Junli Liang and Peng Peng*

Department of Radiology, The First Affiliated Hospital of Guangxi Medical University, Nanning, China

Objective: This study aimed to assess the impact of the different concentrations of iodine contrast agents used on the quality of computed tomography (CT) images obtained intraindividually in hepatocellular carcinoma patients.

Methods: In this retrospective study, data from a cohort of 29 patients diagnosed with primary hepatocellular carcinoma who had undergone two preoperative CT-enhanced examinations within a 3-month timeframe were analyzed. Each patient was randomly assigned to receive either a low-concentration contrast agent (300 mg I/mL iohexol) or a high-concentration contrast agent (350 mg I/mL iohexol) for the first scan and the alternative contrast agent for the second scan. CT images of different liver regions of each patient were compared between low-and high-concentration scans using their before-and-after control design. Subjective image quality scores for portal vein images were also assessed.

Results: The findings of this study indicate that patients in the high-concentration group presented significantly elevated CT values across various anatomical regions, including the liver parenchyma, abdominal aorta, and hepatic portal vein, compared to those in the low-concentration group ($p < 0.05$). Moreover, the high-concentration group demonstrated superior subjective image ratings ($p < 0.05$). Nevertheless, there was no statistically significant difference in the CT values observed in liver cancer parenchyma scans at different phases between the two groups ($p > 0.05$).

Conclusion: In summary, using a high-concentration iodine contrast agent is efficient in enhancing the visual clarity of the liver parenchyma, the aorta, and the portal vein in individuals diagnosed with primary hepatocellular carcinoma.

KEYWORDS

contrast agent, iodine concentration, hepatocellular carcinoma, comparative study, computed tomography

1 Introduction

Hepatocellular carcinoma (HCC) is the sixth most prevalent neoplastic disorder worldwide and the third leading cause of cancer-related death (1). Early diagnosis of HCC is crucial for improving patient outcomes. With advances in medical imaging technology, dynamic contrast-enhanced computed tomography (CT) is regarded as one of the best non-invasive diagnostic imaging techniques for HCC (2). The quality of CT images is pivotal for tumor detection, staging, and the formulation of treatment plans, and the use of contrast agents is a key element in enhancing image quality.

Several studies, both domestic and international, have demonstrated that the concentration of contrast agent used significantly affects the enhancement of the hepatic vasculature and parenchyma. High-concentration contrast agents offer superior vascular enhancement, thereby improving the contrast between tumors and normal liver tissues. However, these agents typically have relatively high viscosities, which may restrict their iodine delivery rates (IDRs) (3–5). Conversely, low-concentration contrast agents, while generally less viscous, may not provide adequate enhancement to meet clinical demands for image quality (6).

Although previous studies have explored the impact of varying contrast agent concentrations on liver imaging, few have focused specifically on the HCC patient population (7–11). Particularly in clinical practice, selecting the most appropriate contrast agent concentration based on different stages of HCC remains an unresolved issue. Traditional independent sample designs may be susceptible to inter-individual variability. To address this, our study employs an intraindividual control design. This design allows for direct comparison of low-and high-concentration contrast agents within the same patient, effectively controlling for individual differences and enhancing the reliability of the results. Moreover, our research introduces a subjective image quality score, offering a novel perspective to the existing literature, which has not been thoroughly explored in previous studies.

This study aimed to evaluate the CT image quality in HCC patients using different iodine concentrations of contrast media, employing a within-subject before-and-after control design. This approach can more sensitively detect the impact of contrast agent concentration changes on image quality, thereby providing a more optimized protocol for the use of contrast agents in clinical practice.

2 Methods

2.1 Patient population

This study was conducted in accordance with the principles set forth in the Declaration of Helsinki and was approved by the Medical Ethics Committee of the First Affiliated Hospital of Guangxi Medical University (Approval No: 2024-E159-01); the requirement for informed consent from the participating patients was waived. A retrospective analysis of patients who met specific criteria and were treated at the First Affiliated Hospital of Guangxi Medical University from May 2017 to July 2022 was conducted. The inclusion criteria were as follows: (1) diagnosed with HCC through clinical or pathological confirmation; (2) underwent upper abdominal CT contrast-enhanced examinations with the same scanning parameters and contrast agent injection protocols; (3) underwent imaging follow-up examinations within 3 months using both a low-concentration iodine contrast agent (iohexol) and a high-concentration iodine contrast agent (ioversol); and (4) did not undergo chemotherapy, surgery, interventional therapy, or radiofrequency ablation during the follow-up period. The exclusion criteria were as follows: (1) patients with tumor size change of more than 15% or new metastases during the follow-up period; (2) patients with portal vein thrombosis or vascular anomalies causing abnormal liver perfusion; (3) poor image quality that could affect diagnosis; and (4) incomplete clinical data. This study used a before-and-after controlled study design for each patient; for the first scan, patients were randomly assigned to either the low-concentration group, in which 300 mg I/mL iohexol was used, or the high-concentration group, in which 350 mg I/mL ioversol was used, and for the second scan, they were assigned to the group they had not been in for the first scan. Because each patient was scanned using both low-and high-concentration contrast agents, two sets of data were obtained. The characteristics of the patients are shown in Table 1.

TABLE 1 Demographic and clinical findings related to the study patients ($n = 29$).

Characteristics	Value
Mean age, years	53.52 ± 10.86 (33–77)
Sex	
Male	26
Female	3
Weight, kg	60.25 ± 9.21 (48–80)
Body mass index, kg/m^{-2}	22.05 ± 22.05 (17.81–30.11)
Child–Pugh class	
Class A	17
Class B	10
Class C	2
Time interval between serial CT examinations, days	55.19 ± 22.42 (14–90)

Values are presented as the mean ± SD (range).

2.2 Image acquisition and contrast medium injection parameters

Prior to the examination, all patients underwent a pre-examination procedure that involved the insertion of a 20-G indwelling needle into the forearm vein. This needle was used before and after the procedure. The patients also received training on how to cooperate by holding their breath. The study utilized a Siemens Somatom Definition Flash dual-source CT scanner (Siemens Healthcare, Forchheim, Germany) for the CT scanning protocol. Prior to the examination, all patients provided informed consent by signing a CT enhancement consent form. The patients were placed in the supine position with their hands elevated toward the sides of the head and neck. The scanning region extended from the upper part of the diaphragm to the lower edge of the liver. The tube voltage was set at 120 kV, and the tube current was automatically determined via the automatic tube current mode on the basis of the patient's body size.

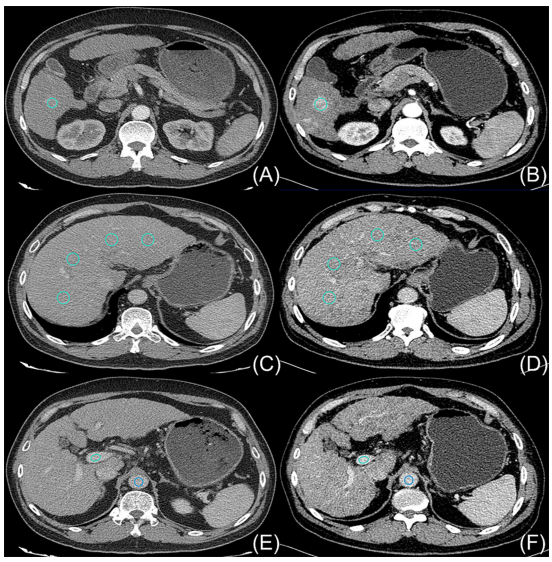

FIGURE 1
On 24 August 2018, a 54-year-old man with hepatocellular carcinoma underwent initial upper abdominal enhanced CT imaging in which a contrast agent concentration of 300 mg I/mL was used (A,C,E); this patient was subsequently examined on 6 November 2018 using an increased contrast agent concentration of 350 mg I/mL (B,D,F). The light blue circles indicate the ROIs outlining the hepatocellular carcinoma parenchyma (A,B), the liver parenchyma (C,D), and the portal vein (E,F). The dark blue circles in (E,F) indicate the ROIs outlining the aorta.

After enhancement, both plain scanning and three-phase scanning were conducted in spiral mode, with a collimator width of 1.2 mm × 32, a pitch of 0.8, a rotation speed of 0.5 s/rotation, an acquisition matrix of 256 × 256, a layer thickness of 5 mm, and a layer spacing of 5 mm.

After the routine scan, a high-pressure injector was employed to administer contrast agents intravenously via the right antecubital vein of the forearm. For the initial scan, the contrast agent used was either iohexol (300 mgI/mL) provided by Beijing Beilu Pharmaceuticals Co., Ltd., or iohexol (350 mgI/mL) supplied by Jiangsu Hengrui Medicine Co., Ltd. The second scan utilized the contrasting agent not used in the first, with each administration totaling 85 mL at a flow rate of 3.0 mL/s. Subsequently, 30 mL of a saline solution was injected at the same rate. The contrast agent injection protocol employed contrast agent tracking and automatic triggering scan technology, with a specific focus on the abdominal aorta as the region of interest. Monitoring of contrast agent arrival occurred simultaneously with injection of the contrast agent, and arterial phase imaging was automatically initiated 10 s after the CT value in the region of interest reached 100 Hounsfield units. Following a 25–30 s interval after the arterial phase, portal vein phase CT scanning commenced. Delayed phase imaging was conducted 70–90 s after the initiation of the portal vein phase. Thin-slice reconstruction was performed using a soft tissue window setting with a window width of 240 Hounsfield units, a window level of 50 Hounsfield units, a slice thickness of 2 mm, and a 2 mm interslice gap. To maintain consistency in scanning conditions, all procedures were performed by the same team of radiologic technologists, adhering strictly to the same scanning protocol.

2.3 Quantitative analysis

To ensure consistency in the selection of ROIs and to maximize the reduction of variability, this study adopted standardized protocols. Two radiologists, each with over 5 years of professional experience, independently delineated ROIs using the picture archiving and communication system (PACS) and assessed the quality of portal venous phase images, blinded to the study hypotheses. ROI selection deliberately avoided areas with artifacts or major vessels, with particular attention to placing ROIs in regions of homogeneous tissue enhancement. Before the commencement of the study, the radiologists participated in calibration exercises to ensure consistent ROI selection. A third radiologist reviewed a portion of the ROIs and performed an inter-rater reliability analysis on the data from the first two radiologists. Any discrepancies were resolved through consensus.

The radiologists manually measured the CT values (in Hounsfield units, HU) for the arterial, venous, and delayed phases of the liver cancer parenchyma imaging on cross-sections with a reconstructed layer thickness of 2 mm. To obtain the mean CT values of the HCC, liver parenchyma, abdominal aorta, and portal vein during different phases, circular or ovoid regions of interest (ROIs) measuring $100 \pm 10\,mm^2$ were placed at the level of the portal vein. The average CT values obtained by both radiologists were then calculated to generate the final results. The ROIs are outlined schematically in Figure 1.

The details of the measurement procedure are as follows:

(1) To ensure anatomical uniformity, anatomical references such as the branches of the hepatic artery, the portal vein, or the hepatic vein, as well as the shapes of lesions caused by the hepatocellular carcinoma, along with the presence of additional structures such as the spleen, pancreas, ribs, and vertebrae, were considered for each patient. This approach was adopted to maintain consistency in the positioning and dimensions of both the initial and subsequent ROIs.
(2) Four ROIs were delineated on the hepatic parenchyma; they were located in the right anterior-posterior and left medial-lateral regions of the right and left liver lobes. Particular care was taken to select areas that exhibited consistent and homogeneous enhancement and that maintained normal parenchymal characteristics. Any regions that displayed alterations in focal density, the presence of large blood vessels, or noticeable artifacts were deliberately excluded from consideration, and the resulting average values were calculated.
(3) During the process of delimiting the hepatocellular carcinoma tissue, meticulous attention was given to excluding the incorporation of liquefied necrotic regions and guaranteeing the consistency of outlines in terms of both area and location.
(4) In relation to the abdominal aorta, singular ROIs that encapsulated 90% or more of the cross-sectional area of each aorta were established. Particular emphasis was placed on circumventing the presence of calcifications and soft plaques within the aortic wall.
(5) The portal vein was chosen as the reference point for measurement. To ensure consistency, all the measurements were repeated three times at three consecutive levels, and the mean of the three measurements was calculated.

2.4 Visual analysis

This study employed a 5-point scale to evaluate image quality, where 1 denotes poor quality and 5 signifies excellent quality. These scores were subsequently converted into categories for statistical analysis. The rating criteria are as follows:

(1) 1 Point: Poor vessel enhancement, blurred borders, or severe artifacts hindering diagnosis.
(2) 2 Points: Blurred vessel borders, still allowing the identification of the portal vein trunk and the assessment of obvious filling defects in portal vein branches of grades 1 and 2 but not in those of lower grades.
(3) 3 Points: Clear visualization of the main portal vein trunk, enabling the evaluation of filling defects in grade 4 or higher branches.
(4) 4 Points: Evident enhancement of blood vessels at all portal vein levels, albeit with slightly rough vessel borders.
(5) 5 Points: Highly pronounced vessel enhancement with clear borders (9).

Two radiologists independently assessed the image quality and calculated the average score. A third radiologist reviewed a portion of the images and conducted a consistency analysis of the ratings provided by the initial two physicians.

2.5 Statistical analysis

Assessment of normality of the CT values for hepatocellular carcinoma parenchyma, liver parenchyma, aorta, and portal vein after enhancement in three stages was conducted using the Shapiro–Wilk test. A paired-samples *t*-test was applied to compare the CT values between the high and low iodine contrast concentration groups across different scan stages (hepatocellular carcinoma parenchyma, hepatic parenchyma, abdominal aorta, and portal vein).

Two physicians conducted a kappa consistency test to assess the subjective image quality. The hierarchical information obtained from the subjective image quality scores was then compared within matched groups via a paired-sample Wilcoxon signed rank-sum test. All statistical analyses were performed using IBM SPSS Statistics 24, with a significance level set at $p < 0.05$.

3 Results

The present study included 29 patients who were longitudinally divided into two groups on the basis of the iodine concentration of the contrast agent administered: a low-concentration group and a high-concentration group. The patient's demographic and clinical characteristics are listed in Table 1.

The disparities in the CT values measured during the arterial phase, the portal venous phase, and the delayed phase in the high-and low-concentration groups of hepatocellular carcinoma patients were not statistically significant ($p > 0.05$) (Figure 2). The differences between the two groups in the CT values measured during the arterial phase of hepatic parenchymal enhancement were not statistically significant ($p > 0.05$) (Figure 3). However, significant differences between the two groups in the CT values during the portal venous phase and the delayed phase of hepatic parenchymal enhancement were observed ($p < 0.05$), and statistically significant differences in the CT values measured during the arterial phase, the portal venous phase, and the delayed phase of the aorta and portal vein were evident in both groups ($p < 0.05$) (Figure 4).

There was a substantial level of concordance between the two physicians in the subjective evaluation of image quality in the two

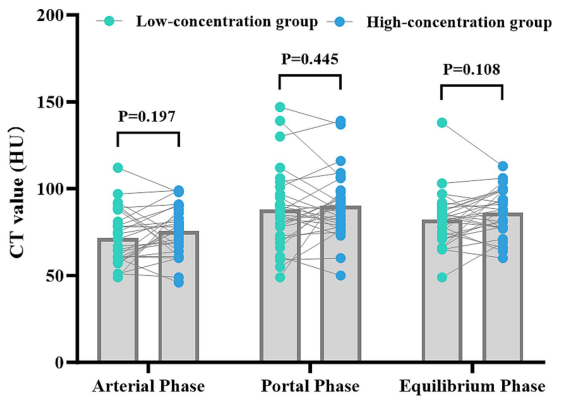

FIGURE 2
Comparison of the differences in CT values for parenchymal enhancement of hepatocellular carcinoma lesions between the two groups of hepatocellular carcinoma patients. The horizontal coordinates represent the scanning stage (arterial, portal venous, or delayed), and the vertical coordinates represent the mean CT values (HUs). There were no statistically significant differences in the CT values for parenchymal enhancement of hepatocellular carcinoma lesions between the two groups at any of the three scanning stages ($p > 0.05$).

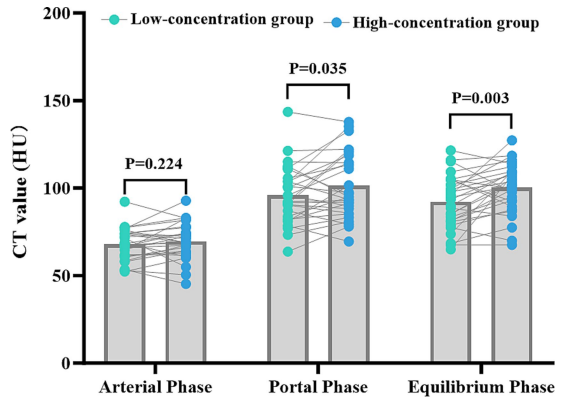

FIGURE 3
Comparison of the differences in liver parenchymal enhancement CT values between the two groups of patients. The horizontal coordinates represent the scanning stages (arterial, portal venous, and delayed), and the vertical coordinates represent the mean CT values (HUs). There was no statistically significant difference ($p>0.05$) between the two groups of patients in the liver parenchymal enhancement CT values in the arterial phase. However, there were statistically significant differences ($p<0.05$) between the two groups of patients in the liver parenchymal enhancement CT values in the portal venous and delayed phases, with patients in the high-concentration group having higher CT values.

groups as indicated by a high level of agreement (Kappa = 0.625, $p < 0.001$). The images obtained from patients in the low-concentration group were assigned image quality scores of 2.44 ± 0.12, whereas those obtained from patients in the high-concentration group achieved scores of 3.30 ± 0.67. In particular, the high-concentration group presented significantly higher scores than did the low-concentration group ($Z = 3.819$, $p < 0.001$), emphasizing the statistically significant difference (Figure 5).

4 Discussion

In this study, the effects of the concentration of iodine contrast agent used on the quality of CT images obtained from liver cancer patients were evaluated using an intraindividual comparison design. The results indicate that using a high concentration of contrast agent significantly improves the CT image values for the liver parenchyma, the abdominal aorta, and the portal vein as well as the image quality scores. This provides an important reference for the selection of the appropriate contrast concentration to be used in clinics. The results of this study thus support the use of high-concentration contrast agents in CT-enhanced scanning of patients with hepatocellular carcinoma. High-concentration contrast agents can provide better vascular enhancement and improve the contrast between the tumor and the surrounding tissues, thus improving image quality and contributing to the early detection and diagnosis of tumors. The use of high-concentration contrast can also enhance the visualization of the vascular structure of the abdominal aorta and portal vein, and this can help in vascular reconstruction and assessment, providing more accurate information for clinical treatment planning.

Several previous studies have supported that using high concentrations of contrast can improve the quality of CT images in patients with hepatocellular carcinoma (9–14). Jo et al. (11) used different concentrations of iodine contrast in two scans of patients with chronic liver disease and showed that the use of a high-concentration iodine contrast agent (Iomephenol 400) significantly improved CT values of the aorta, portal vein, and hepatic parenchyma in both the portal and delayed phases, thereby improving the image quality of each phase. This observation aligns with the findings of our study. Nevertheless, the study was constrained by an extended interval of approximately 271 days between the initial and follow-up CT scans. Despite the exclusion of patients with a weight change exceeding 5% during that period, conditions such as hepatomegaly and diffuse liver disease may have altered hepatic parenchymal perfusion, consequently impacting the contrast-enhanced features in the liver. In contrast, our study exclusively enrolled patients whose initial and follow-up CT scans were collected within a three-month interval. Furthermore, the introduction of a subjective image quality score further validates and demonstrates the robustness of our study results. In a circulation phantom study, Mihl et al. (15) observed that intravascular attenuation remained relatively stable when different contrast agents with varying iodine concentrations were administered at constant IDRs. It is possible to achieve target attenuation levels with contrast agent concentrations as low as 240 mg I/mL while keeping the IDR constant. However, this necessitates a higher injection rate, which may increase patient discomfort and the risk of extravasation. Conversely, it has been suggested that lower iodine contrast concentrations may be more evenly distributed within vessels because of their lower viscosity, potentially leading to a more consistent contrast distribution. This, in turn, could improve the visualization of smaller vessel segments (16). The advantage of a high IDR is partially offset by the slower and less uniform mixing of the contrast agent with the blood in the vessel, because of its higher viscosity and injection pressure. Additionally, individual patient factors such as heart rate, cardiac output, and body mass index add further complexity to the relationship between contrast concentration and vascular enhancement (17, 18). Nevertheless, the findings of our present study indicate that high-concentration contrast agents yield superior enhancement values compared to their low-concentration counterparts. The intrasubject

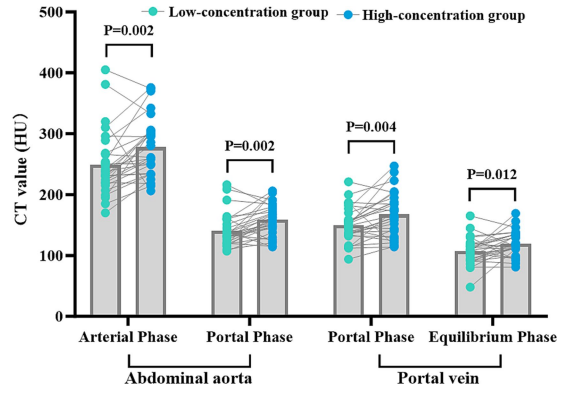

FIGURE 4
Comparison of CT values for abdominal aortic and portal vein enhancement in the two groups. The horizontal coordinates represent the scanning phases (arterial, portal, and delayed), and the vertical coordinates represent the mean CT values (HU). The CT values for abdominal aortic and portal vein enhancement in the arterial, portal venous, and delayed phases were significantly different in the two groups ($p < 0.05$), with higher CT values in the HU group.

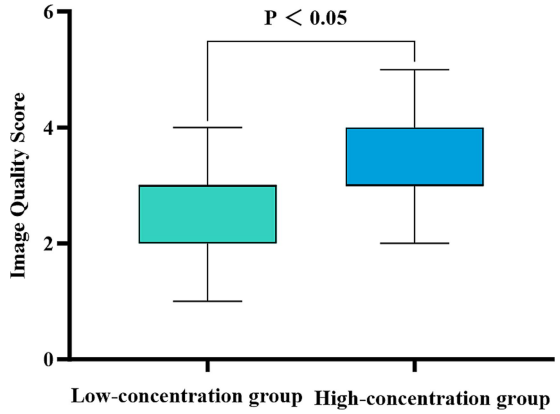

FIGURE 5
Comparison of the subjective image quality scores for the two groups of patients. The horizontal coordinate represents the scanning phase (arterial, portal venous, and delayed), and the vertical coordinate represents the average image quality score. The patients in the high-concentration group had significantly higher image quality scores than those in the low-concentration group ($p < 0.001$).

controlled design adopted in our study offers greater statistical efficiency and clinical relevance over traditional independent sample designs, thus lending stronger support to our conclusions.

In specific clinical contexts, the use of a low concentration (300 mg I/L) of contrast material is advantageous for procedures such as CT screening and the diagnosis of hepatocellular carcinoma. Conversely, preoperative CT angiography requires a relatively high concentration of iodine contrast agent (350–370 mg I/L) to meet the standards of image quality. Although, generally, enhanced CT arterial phase images allow for arterial vasculature reconstruction, their quality is inferior to that achieved through CTA. It is worth noting that individuals diagnosed with hepatocellular carcinoma typically undergo a minimum of two CT-enhanced examinations throughout their diagnosis and treatment. This not only increases the financial burden but also raises concerns related to radiation exposure and potential physical harm to the patient.

The utilization of high-concentration contrast agents holds promise for simultaneously acquiring dual imaging modalities, streamlining examination procedures, and alleviating patient burden. The bolus volume of the high-concentration iodinated contrast agent was smaller than that of the low-concentration iodinated contrast agent (19). Administration of a high-concentration contrast agent at a fixed injection rate leads to rapid iodine delivery per unit time, resulting in earlier and greater peak arterial enhancement, albeit for a shorter period. However, hepatic enhancement remains unaffected (20). Under the premise of maintaining iodine flow rates, low-concentration iodinated contrast can also achieve comparable vascular imaging effects (21). However, this necessitates higher injection rates, and this may induce contrast extravasation, particularly in liver cancer patients, given their typically advanced age and the need for prolonged vascular access with associated drug stimulation, rendering administration of contrast at a high flow rate contrast administration impractical. Using a high-concentration iodinated contrast agent is an alternative approach that employs high injection rates to increase iodine delivery rates (16). Hence, increasing the contrast agent concentration is an optimal choice for liver cancer diagnosis and preoperative vascular reconstruction in a single examination setting.

In most recent assessments of the effectiveness of high-versus low-concentration imaging, the researchers have employed statistical methods to mitigate the effects of variations in fundamental patient characteristics. However, numerous patient-related factors, including body mass index, cardiac output, age, sex, venous access, and the presence of cirrhosis, portal hypertension, and other pathologies impacting organ enhancement, influence contrast imaging efficacy. The crossover design used in the current study was intended to mitigate the effects of several confounding variables, such as body weight, cardiac output, and the type and severity of cirrhosis, by utilizing each patient as their own control. However, our study has certain limitations. Although the time interval between the two consecutive CT examinations was restricted to 3 months and the order in which each contrast agent was used was randomized to reduce potential bias, we acknowledged that changes in tumor characteristics during this period could introduce variability. Factors such as tumor growth, the emergence of new lesions, or alterations in tumor vascularity might potentially influence the contrast enhancement patterns observed on CT scans. Moreover, this study focused solely on comparing 300 mg I/mL iohexol and 350 mg I/mL ioversol. Future research could consider including a wider variety of iodine contrast agents for comparative analysis. Additionally, as a single-center study with a relatively small sample size, the generalizability of the results may be limited. Therefore, future studies should increase the sample size, conduct large-scale, multicenter prospective studies, and perform stratified analyses based on disease stage, the presence or absence of cirrhosis, and other significant patient characteristics. This approach would further explore the differences in contrast agent concentration response among various patient populations, thereby providing more robust scientific evidence for clinical practice.

5 Conclusion

Our research demonstrated that the use of a high-concentration iodine contrast agent in routine CT enhancement scans of the upper abdomen effectively enhances the clarity of images of the liver parenchyma, the abdominal aorta, and the portal vein in patients with hepatocellular carcinoma. This enhanced imaging technique facilitates the reconstruction of hepatocellular carcinoma-associated blood vessels in patients in advanced stages of the disease, potentially limiting the need for supplementary CT examinations.

Data availability statement

The data analyzed in this study is subject to the following licenses/restrictions: the dataset used in support of the findings of this study are available from the corresponding author at email address upon request. Requests to access these datasets should be directed to PP, doublep@126.com.

Ethics statement

The studies involving humans were approved by The Ethics Committee of the First Affiliated Hospital of Guangxi Medical University. The studies were conducted in accordance with the local legislation and institutional requirements. The participants provided their written informed consent to participate in this study. Written informed consent was obtained from the individual(s) for the publication of any potentially identifiable images or data included in this article.

Author contributions

FP: Conceptualization, Formal analysis, Methodology, Validation, Visualization, Writing – original draft, Writing – review & editing, Data curation, Funding acquisition, Investigation, Project administration, Resources, Software, Supervision. CL: Data curation, Investigation, Project administration, Supervision, Writing – original draft, Writing – review & editing, Conceptualization, Formal analysis, Funding acquisition, Methodology, Resources, Software, Validation, Visualization. XN: Conceptualization, Data curation, Formal analysis, Investigation, Software, Supervision, Validation, Visualization, Project administration, Writing – review & editing, Funding acquisition, Methodology, Resources, Writing – original draft. FX: Funding acquisition, Validation, Writing – review & editing, Formal analysis,

Methodology. KG: Formal analysis, Investigation, Validation, Writing – review & editing, Data curation, Project administration, Software, Supervision. CT: Project administration, Writing – review & editing, Conceptualization, Funding acquisition, Software, Validation, Visualization. FH: Formal analysis, Investigation, Methodology, Validation, Writing – review & editing. JL: Formal analysis, Project administration, Supervision, Writing – review & editing. PP: Conceptualization, Data curation, Formal analysis, Funding acquisition, Investigation, Methodology, Project administration, Resources, Software, Supervision, Validation, Visualization, Writing – original draft, Writing – review & editing.

Funding

The author(s) declare that financial support was received for the research, authorship, and/or publication of this article. This study was supported by research grants from the National Natural Science Foundation of China (No. 81760305 and No. 81641066), the Open Project of NHC Key Laboratory of Thalassemia Medicine (No. GJWJWDP202306), the Natural Science Foundation of Guangxi Zhuang Autonomous Region (No. 2023GXNSFAA026009), the Key Laboratory of Children's Disease Research in Guangxi's Colleges and Universities, the Education Department of Guangxi Zhuang Autonomous Region (No. GXCDR2023001), the Guangxi Medical and Health Appropriate Technology Development and Promotion Application Project (No. S2022072), and the Advanced Innovation Teams and Xinghu Scholars Program of Guangxi Medical University (No. 202110598039).

Acknowledgments

We are grateful to all the people who have helped us with our article.

Conflict of interest

The authors declare that the research was conducted in the absence of any commercial or financial relationships that could be construed as a potential conflict of interest.

Publisher's note

References

1. Rumgay H, Arnold M, Ferlay J, Lesi O, Cabasag CJ, Vignat J, et al. Global burden of primary liver cancer in 2020 and predictions to 2040. *J Hepatol*. (2022) 77:1598–606. doi: 10.1016/j.jhep.2022.08.021

2. Haj-Mirzaian A, Kadivar A, Kamel IR, Zaheer A. Updates on imaging of liver tumors. *Curr Oncol Rep*. (2020) 22:46. doi: 10.1007/s11912-020-00907-w

3. McDermott M, Kemper C, Barone W, Jost G, Endrikat J. Impact of CT injector technology and contrast media viscosity on vascular enhancement: evaluation in a circulation phantom. *Br J Radiol*. (2020) 93:20190868. doi: 10.1259/bjr.20190868

4. Faggioni L, Gabelloni M. Iodine concentration and optimization in computed tomography angiography: current issues. *Investig Radiol*. (2016) 51:816–22. doi: 10.1097/RLI.0000000000000283

5. Rengo M, Caruso D, De Cecco CN, Lucchesi P, Bellini D, Maceroni MM, et al. High concentration (400 mgI/mL) versus low concentration (320 mgI/mL) iodinated contrast media in multi detector computed tomography of the liver: a randomized, single Centre, non-inferiority study. *Eur J Radiol*. (2012) 81:3096–101. doi: 10.1016/j.ejrad.2012.05.017

6. Shen Y, Hu X, Zou X, Zhu D, Li Z, Hu D. Did low tube voltage CT combined with low contrast media burden protocols accomplish the goal of "double low" for patients? An overview of applications in vessels and abdominal parenchymal organs over the past 5 years. *Int J Clin Pract*. (2016) 70:B5–B15. doi: 10.1111/ijcp.12861

7. Jiang J, Zhang M, Ji Y, Li C, Fang X, Zhang S, et al. An individualized contrast-enhanced liver computed tomography imaging protocol based on body mass index in 126 patients seen for liver cirrhosis. *Med Sci Monit*. (2021) 27:e932109. doi: 10.12659/MSM.932109

8. Dong X-Y, Fang T-S, Yuan J-X, Liang Z-H, Li J-H. Discussion on the effect of different concentrations of contrast media on CT imaging of hepatic veins based on BSA and fixed iodine rate. *Comput Tomogr Theory Appl*. (2021) 30:466–76. doi: 10.15953/j.1004-4140.2021.30.04.07

9. Wang W, Zhao Z, Qin Z, Cai Y, Ju S-H. Comparison of different contrast agent concentrations in CT portal venography. *Chin J Radiol*. (2020) 54:413–6. doi: 10.3760/cma.j.cn112149-20190830-00732

10. Du Y, Wang Y-N, Wang Q, Qi X-H, Shi G-F, Jia L-T, et al. A comparison of the use of contrast media with different iodine concentrations for enhanced computed tomography. *Front Physiol*. (2023) 14:1141135. doi: 10.3389/fphys.2023.1141135

11. Jo BG, Song YG, Shim SG, Kim YW. Comparison of enhancement and image quality: different iodine concentrations for liver on 128-slice multidetector computed tomography in the same chronic liver disease patients. *Korean J Intern Med*. (2016) 31:461–9. doi: 10.3904/kjim.2014.210

12. Awai K, Takada K, Onishi H, Hori S. Aortic and hepatic enhancement and tumor-to-liver contrast: analysis of the effect of different concentrations of contrast material at multi-detector row helical CT. *Radiology*. (2002) 224:757–63. doi: 10.1148/radiol.2243011188

13. Sofue K, Tsurusaki M, Kawasaki R, Fujii M, Sugimura K. Evaluation of hypervascular hepatocellular carcinoma in cirrhotic liver: comparison of different concentrations of contrast material with multi-detector row helical CT—a prospective randomized study. *Eur J Radiol*. (2011) 80:e237–42. doi: 10.1016/j.ejrad.2010.10.006

14. Guerrisi A, Marin D, Nelson RC, De Filippis G, Di Martino M, Barnhart H, et al. Effect of varying contrast material iodine concentration and injection technique on the conspicuity of hepatocellular carcinoma during 64-section MDCT of patients with cirrhosis. *Br J Radiol*. (2011) 84:698–708. doi: 10.1259/bjr/21539234

15. Mihl C, Wildberger JE, Jurencak T, Yanniello MJ, Nijssen EC, Kalafut JF, et al. Intravascular enhancement with identical iodine delivery rate using different iodine contrast media in a circulation phantom. *Investig Radiol*. (2013) 48:813–8. doi: 10.1097/RLI.0b013e31829979e8

16. Bae KT. Intravenous contrast medium administration and scan timing at CT: considerations and approaches. *Radiology*. (2010) 256:32–61. doi: 10.1148/radiol.10090908

17. Fleischmann U, Pietsch H, Korporaal JG, Flohr TG, Uder M, Jost G, et al. Impact of contrast media concentration on low-kilovolt computed tomography angiography: a systematic preclinical approach. *Investig Radiol*. (2018) 53:264–70. doi: 10.1097/RLI.0000000000000437

18. Behrendt FF, Plumhans C, Keil S, Mühlenbruch G, Das M, Seidensticker P, et al. Contrast enhancement in chest multidetector computed tomography: intraindividual comparison of 300 mg/mL versus 400 mg/mL iodinated contrast medium. *Acad Radiol*. (2009) 16:144–9. doi: 10.1016/j.acra.2008.05.008

19. Aschoff AJ, Catalano C, Kirchin MA, Krix M, Albrecht T. Low radiation dose in computed tomography: the role of iodine. *Br J Radiol*. (2017) 90:20170079. doi: 10.1259/bjr.20170079

20. Zhu Z, Zhao X-M. The application of high concentration iodine-based contrast media (400 mg/mL) in abdominal CT imaging. *Chin J Radiol*. (2020) 54:385–8. doi: 10.3760/cma.j.cn112149-20191028-00866

21. Van Cauteren T, Van Gompel G, Nieboer KH, Willekens I, Evans P, Macholl S, et al. Improved enhancement in CT angiography with reduced contrast media iodine concentrations at constant iodine dose. *Sci Rep*. (2018) 8:17493. doi: 10.1038/s41598-018-35918-y

frontiers | Frontiers in Oncology

TYPE Original Research
PUBLISHED 08 November 2024
DOI 10.3389/fonc.2024.1446386

OPEN ACCESS

EDITED BY
Liliana Chemello,
University of Padua, Italy

REVIEWED BY
Vivek Peche,
Washington University in St. Louis, United States
Basen Li,
Huazhong University of Science and Technology, China

*CORRESPONDENCE
Ailian Liu
liuailian@dmu.edu.cn

†These authors have contributed equally to this work

RECEIVED 09 June 2024
ACCEPTED 21 October 2024
PUBLISHED 08 November 2024

CITATION
Zhao Y, Wang S, Wang Y, Li J, Liu J, Liu Y, Ji H, Su W, Zhang Q, Song Q, Yao Y and Liu A (2024) Deep learning radiomics based on contrast enhanced MRI for preoperatively predicting early recurrence in hepatocellular carcinoma after curative resection. *Front. Oncol.* 14:1446386. doi: 10.3389/fonc.2024.1446386

Deep learning radiomics based on contrast enhanced MRI for preoperatively predicting early recurrence in hepatocellular carcinoma after curative resection

Ying Zhao[1†], Sen Wang[2,3†], Yue Wang[1], Jun Li[1], Jinghong Liu[1], Yuhui Liu[4], Haitong Ji[4], Wenhan Su[4], Qinhe Zhang[1], Qingwei Song[1], Yu Yao[2,3] and Ailian Liu[1,5*]

[1]Department of Radiology, The First Affiliated Hospital, Dalian Medical University, Dalian, China, [2]Chengdu Institute of Computer Application, Chinese Academy of Sciences, Chengdu, China, [3]School of Computer Science and Technology, University of Chinese Academy of Sciences, Beijing, China, [4]College of Medical Imaging, Dalian Medical University, Dalian, China, [5]Dalian Engineering Research Center for Artificial Intelligence in Medical Imaging, Dalian, China

Purpose: To explore the role of deep learning (DL) and radiomics-based integrated approach based on contrast enhanced magnetic resonance imaging (CEMRI) for predicting early recurrence (ER) in hepatocellular carcinoma (HCC) patients after curative resection.

Methods: Total 165 HCC patients (ER, *n* = 96 vs. non-early recurrence (NER), *n* = 69) were retrospectively collected and divided into a training cohort (*n* = 132) and a validation cohort (*n* = 33). From pretreatment CEMR images, a total of 3111 radiomics features were extracted, and radiomics models were constructed using five machine learning classifiers (logistic regression, support vector machine, k-nearest neighbor, extreme gradient Boosting, and multilayer perceptron). DL models were established via three variations of ResNet architecture. The clinical-radiological (CR), radiomics combined with clinical-radiological (RCR), and deep learning combined with RCR (DLRCR) models were constructed. Model discrimination, calibration, and clinical utilities were evaluated by receiver operating characteristic curve, calibration curve, and decision curve analysis, respectively. The best-performing model was compared with the widely used staging systems and preoperative prognostic indexes.

Results: The RCR model (area under the curve (AUC): 0.841 and 0.811) and the optimal radiomics model (AUC: 0.839 and 0.804) achieved better performance than the CR model (AUC: 0.662 and 0.752) in the training and validation cohorts, respectively. The optimal DL model (AUC: 0.870 and 0.826) outperformed the radiomics model in the both cohorts. The DL, radiomics, and CR predictors (aspartate aminotransferase (AST) and tumor diameter) were combined to construct the DLRCR model. The DLRCR model presented the best performance over any model, yielding an AUC, an accuracy, a sensitivity, a

specificity of 0.917, 0.886, 0.889, and 0.882 in the training cohort and of 0.844, 0.818, 0.800, and 0.846 in the validation cohort, respectively. The DLRCR model achieved better clinical utility compared to the clinical staging systems and prognostic indexes.

Conclusion: Both radiomics and DL models derived from CEMRI can predict HCC recurrence, and DL and radiomics-based integrated approach can provide a more effective tool for the precise prediction of ER for HCC patients undergoing resection.

KEYWORDS

hepatocellular carcinoma, early recurrence, magnetic resonance imaging, deep learning, radiomics

Introduction

Hepatocellular carcinoma (HCC) is the most common primary hepatic malignancy and the third leading cause of cancer-related deaths worldwide (1). Although surgical resection has been considered as the first-line curative treatment for early-stage HCC patients with well-preserved liver function, the high recurrence rates after resection still remain a major hurdle, and 70% of the patients occur recurrence within 5 years (2). Patients with early recurrence (ER) within 2 years after operation are at high risk for poor prognosis (3), whose are potential candidates for clinical trials of adjuvant systemic therapies (4). Thus, the identification of patients with high recurrent risk at early stage is critical for prognostication surveillance and thus facilitating the implementation of individualized treatment.

Several identified predictors for HCC recurrence include various pathological markers related to tumor aggressiveness, such as tumor size, microvascular invasion, surgical margin, and Edmondson-Steiner grade, as reported in published studies (3, 5, 6). However, preoperative prediction of HCC recurrence risk remains difficult, and thus a noninvasive tool with adequate information about tumor characterization that enables to accurately estimate prognosis is needed. Magnetic resonance imaging (MRI) is the ideal technique for non-invasive diagnosis and surveillance of HCC due to its high soft tissue contrast and multiparametric imaging. Previous studies have reported that conventional radiological features including non-smooth tumor margin, incomplete/without tumor capsule, peritumoral enhancement, and hypointensity on hepatobiliary phase can predict clinical outcomes (7–9); however, these features interpreted by radiologists indicate high subjectivity, difficulty in quantification, and lack of metrics about tumor heterogeneity.

In recent years, radiomics has emerged as a promising tool to facilitate precision diagnosis and prognosis of HCC with increases in the scale of medical imaging data and development of artificial intelligence (AI) techniques. Radiomics can convert medical images into high-throughput and quantitative handcrafted features using computer algorithms to capture intratumoral pathophysiology and heterogeneity. Key radiomics features are selected and harnessed to construct robust and reproducible imaging markers for clinicians, from diagnosis assistance to therapeutic guidance (10, 11). Recent studies have utilized MRI-based radiomics containing intratumoral and/or peritumoral regions to predict HCC recurrence with promising predictive results (12, 13).

Furthermore, deep learning (DL), as the state-of-the-art machine learning (ML) technique in the field of AI, has been successfully applied in many pattern recognition tasks, which can bring revolutionary changes in health care (14). DL is a type of representation learning method allowing computational models that are composed of multiple processing layers to automatically learn representations of data by transforming the input information into multiple levels of abstractions (14, 15). It has been proven to be very good at discovering intricate structures in high-dimensional data and is therefore applicable to reveal complex relationships between multimodal images and challenging clinical questions with very little engineering by hand (15, 16). Previous studies of deep learning applied to pathological indicator classification and prognosis prediction in HCC have reported superior performance compared to those by conventional imaging modality or even better than radiomics (17, 18). Notely, a ML framework integrating handcrafted radiomics features with DL features has an emerging trend for achieving satisfying predictive performance in some specific clinical tasks (18, 19). Nevertheless, only a few studies (18, 20) have applied DL and radiomics-based integrated approach for HCC recurrence prediction, in which the traditional ML method was used for dimensionality reduction and fusion model construction.

The aim of the present study was to develop and validate radiomics and DL models based on preoperative multi-phase contrast enhanced magnetic resonance imaging (CEMRI) for predicting ER of HCC patients after curative resection. Furthermore, we evaluated the predictive capacity of the

combined model incorporating DL, radiomics, and clinical-radiological features. We assumed that the proposed DL and radiomics-based integrated approach can improve recurrence prediction accuracy, thus creating a better risk stratification and enhancing the overall prognosis of HCC patients after surgical resection.

Materials and methods

Patients

This retrospective study was approved and the requirement for the informed consent was waived by the Institutional Review Board of our hospital (approval number: PJ-KS-KY-2022-180), and was carried out in accordance with the Declaration of Helsinki. Between August 2007 and May 2021, we retrospectively recruited 290 consecutive patients with pathologically confirmed HCC who performed preoperative abdominal MRI examination at our institution. The inclusion criteria were as follows: (1) patients received curative (R0) resection without any prior antitumoral treatments; (2) patients with pathological confirmation of HCC; (3) patients performed CEMRI examination within two weeks before resection. The exclusion criteria were as follows: (1) unavailable or incomplete clinical or imaging data (n = 5); (2) small HCC lesions less than 10 mm in diameter (n = 3); (3) poor image quality or severe motion artifacts (n = 4); (4) loss to follow-up within 2 years after resection (n = 113). The flow chart of this study population is shown in Figure 1. Ultimately, a total of 165 HCC patients were recruited in the study. The patients were randomly divided at a ratio of 8:2 into the training and validation cohorts.

Baseline clinical characteristics, including age, gender, history of hepatitis B or C, alpha-fetoprotein (AFP), alanine aminotransferase (ALT), aspartate aminotransferase (AST), γ-glutamyltranspeptadase (GGT), total bilirubin (TBIL), albumin (ALB), and Child-Pugh class, were retrospectively collected.

MRI acquisition

MRI was performed using a 1.5 T or 3.0 T MR scanner (Signa, HDXT, GE Healthcare, USA) with an eight-channel phased array body coil. MRI protocols included in- and opposed-phase fast-spoiled gradient-recalled echo T1-weighted imaging (T1WI), fat-suppressed fast spin-echo T2-weighted imaging (T2WI), and contrast enhanced imaging with fat-suppressed T1-weighted fast-spoiled gradient-recalled echo sequence. The contrast enhanced images consisted of arterial phase (AP), portal venous phase (PVP), and delayed phase (DP) images, which were obtained at 40 s, 70 s, and 90 s, respectively. Gd-diethylenetriamine pentaacetic acid (Gd-

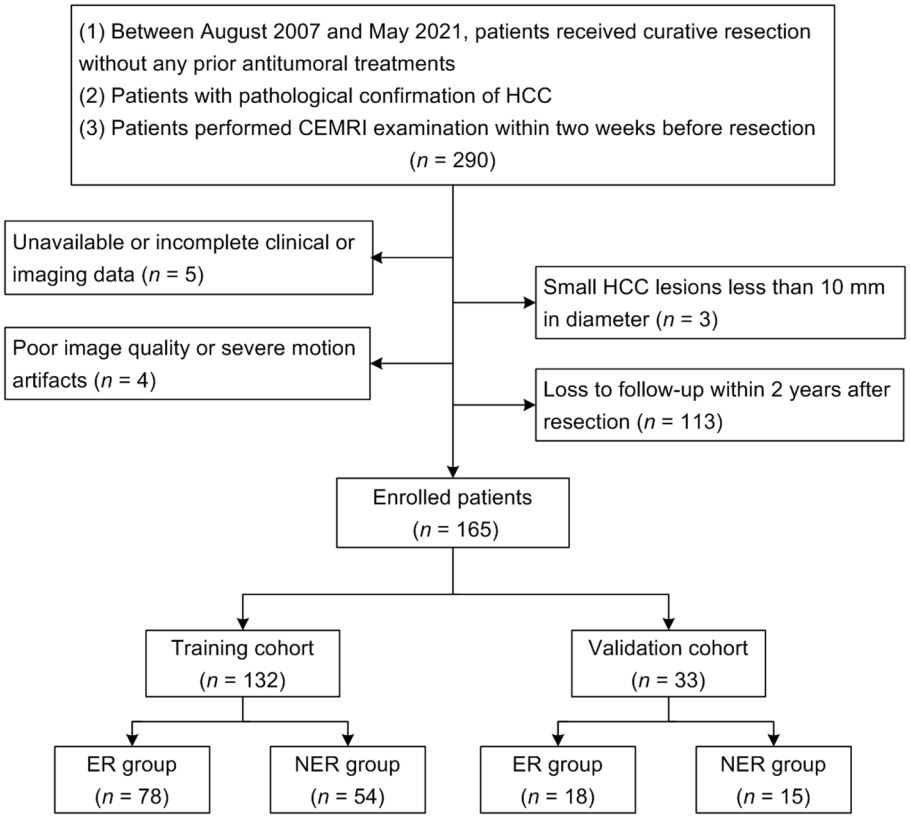

FIGURE 1
The flow chart of this study population.

DTPA) (Bayer Schering Pharma AG, Germany) was injected at a patient weight-dependent dose of 0.1 mmol/kg and an injection rate of 2.5 mL/s through a median cubital vein. Of the 165 HCC patients described above, 74 patients were examined with a 1.5 T MR system, and the other 91 patients with a 3.0 T MR system. Detailed parameters of imaging acquisition protocols are listed in Supplementary Material S1.

Evaluation of MRI features

All MR images were retrospectively assessed by two radiologists with 10 (radiologist 1, Y.Z.) and 5 (radiologist 2, Y.W.) years of experience in abdominal MRI interpretation, who were blinded to clinical, pathological, and follow-up information. If there was any disagreement between radiologists during the imaging analysis, the images were evaluated by another senior radiologist of 20 (radiologist 3, J.H.L.) years of experience in abdominal MRI.

MRI features included the following: (1) tumor diameter (the maximum axial diameter including the capsule measured on PVP images) (21); (2) tumor number (unifocal or multifocal); (3) tumor margin (smooth or non-smooth); (4) intratumor necrosis (hypointensity on T1WI, hyperintensity on T2WI, and no enhancement of part of the tumor on all enhanced phases); (5) intratumor hemorrhage (heterogeneous hyperintensity on T1WI and hypointensity on T2WI); (6) tumor encapsulation (a peripheral rim of uniform and smooth hyperenhancement on PVP or DP images) (22); (7) arterial peritumoral enhancement (a zone of irregular and patchy hyperenhancement surrounding the tumor on AP images, becoming isointensity compared with normal liver parenchyma on DP images) (23); (8) radiological cirrhosis (surface irregularity and nodularity, shrunken of liver, widening of fissures, accompanied by ascites or signs of portal hypertension).

Follow up

All patients were regularly followed up once every 3 months for 2 years after curative resection. Serum AFP level, liver function tests, and imaging examinations (included contrast enhanced computed tomography (CECT) or CEMRI) were conducted to monitor recurrence of HCC. The censored follow-up date was May 2023. Early recurrence was defined as new intrahepatic lesions and/or extrahepatic metastasis within 2 years after resection confirmed by typical imaging features or histopathology.

Image segmentation and preprocessing

Preoperative MR images of AP, PVP, and DP were exported as digital imaging data and communications in medicine (DICOM) format. The images in DICOM format were converted to NIFTI format. All images were resampled to the same voxel size of $1 \times 1 \times 1$ mm via linear interpolation algorithm to standardize the voxel spacing. Intensity normalization of images was performed to correct the scanner effect. Three dimensional segmentation of the whole tumor was performed on each phase using open source software ITK-SNAP (version 3.6.0, http://www.itksnap.org/). The volume of interests (VOIs) of all patients were manually delineated slice-by-slice along the visible borders of the tumor by radiologist 1 (Y.Z.). In terms of multifocal HCCs, the largest nodule was selected as the delineated lesion. Thirty tumors were randomly selected and then repeatedly segmented by two abdominal radiologists (radiologists 1 and 2, Y.Z. and Y.W.) independently to evaluate the intra- and inter-observer reproducibility of the radiomics features.

Radiomics feature extraction

A total of 1037 radiomics features were extracted from each enhanced phase using Pyradiomics package implemented in Python (version 3.7.11, https://www.python.org/). Radiomics features were comprised of the following five categories: (1) histogram features (n = 18); (2) shape features (n = 14); (3) texture features (n = 75, including gray level co-occurrence matrix (GLCM), gray level run length matrix (GLRLM), neighborhood gray tone difference matrix (NGTDM), gray level dependence matrix (GLDM), and gray level size zone matrix (GLSZM)); (4) wavelet features (n = 186); (5) Laplacian of Gaussian features (n = 744). The extracted radiomics features were in accordance with feature definitions described by the image biomarker standardization initiative (IBSI) reporting guidelines (24). Detailed descriptions of these radiomics features are provided in Supplementary Material S2. Next, values of radiomics features were standardized using the z-score normalization based on the mean and standard deviation values from the training cohort to eliminate the differences in the value scales of the radiomics features (19).

Feature selection and radiomics model construction

Figure 2 shows the workflow of radiomics and DL analysis. We devised a three-step strategy for dimensionality reduction and robust feature selection. First, the intraclass correlation coefficients (ICCs) were used to assess the intra- and inter-observer reproducibility of radiomics features, and features with ICC > 0.90 (excellent stability) were selected. Second, the independent sample t test or Mann-Whitney U test was conducted to select the features that were statistically different between ER and non-early recurrence (NER) groups. The P value threshold for the significant features was set at 0.05. Finally, the least absolute shrinkage and selection operator (LASSO) algorithm, with penalty parameter tuning conducted by 5-fold cross-validation, was then utilized to identify the most top-ranked features for predicting HCC recurrence. Five commonly used ML classifiers, including logistic regression (LR), support vector machine (SVM), k-nearest neighbor (KNN), extreme gradient Boosting (XG-Boost), and multilayer perceptron (MLP), were used to build radiomics models.

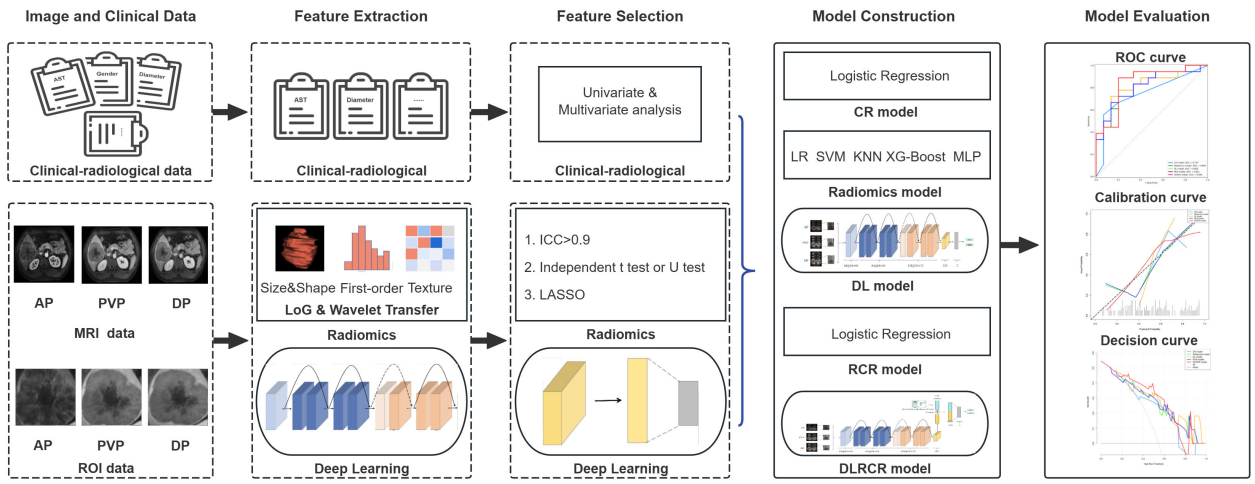

FIGURE 2
The workflow of radiomics and deep learning (DL) analysis in the current study. The volume of interests (VOIs) from contrast enhanced MR images in three phases [arterial phase (AP), portal venous phase (PVP), and delayed phase (DP)] were extracted for feature development in both radiomics and DL models. The clinical and radiological data were collected for clinical-radiological (CR) model construction. Following feature selection, chosen radiomics features were merged with CR risk factors to build an integrated radiomics combined with clinical-radiological (RCR) model. Furthermore, DL features were combined with both CR and radiomics features to develop a comprehensive deep learning combined with RCR (DLRCR) model. The discrimination, calibration, and clinical utilities were evaluated by receiver operating characteristic curve, calibration curve, and decision curve analysis, respectively.

Deep learning model construction

For DL analysis, the PVP and DP images were registered to AP images respectively using QuickRigid registration of the Antspy (https://github.com/ANTsX/ANTsPy). Three consecutive slices with the maximum cross-sectional tumor area were selected, and the tumor regions were cropped and resized into 256 × 256 pixels. Considering that a large amount of training data could improve the performance of the model, we adopted data augmentation strategies to increase the number of ROIs, including rotation, scaling, flipping, and shifting. Since ResNet architecture has showed promising performance in multiple computer vision tasks (25), we chose two variations of ResNet architecture with different numbers of layers, including ResNet-18 and ResNet-34, as our basic architecture for model training. Because the parameters of the two variations are excessive and an overfitting error easily occurs in the small-scale liver tumor image datasets, we optimized the original ResNet-18 architecture by reducing the network's depth to ResNet-10.

The detailed network architecture of the CNN is shown in Figure 3. The first part of the CNN included a 64 7×7 convolution layer, a normalization module, and a max pooling layer. After going through all these layers, we obtained a feature map of the input ROI. The following structures of the CNN contained four 64 3×3 convolution bottleneck modules and four 128 3×3 convolution bottleneck modules, in which all the bottleneck modules were employed from the ResNet. The raw feature map of the ROI was sequentially processed by these bottleneck modules, enabling the acquisition of ROI features at distinct scales. Shallow features learn more detailed structure information, while deep features can express high-level semantic features. After the last convolution operation, feature maps extracted by the backbone network were converted into feature vectors through global average pooling. These feature vectors were then concatenated and fed into the fully connected layer for HCC recurrence prediction. Additionally, to better explore the important features or patterns the DL model identified, we employed Score-CAM method for visual interpretation (26). Unlike gradient-based methods, Score-CAM removes the reliance on gradients by determining the weight of each activation map based on its forward-passing score for the target class. The final results were obtained through a linear combination of these weights and the corresponding activation maps.

The training and testing processes were conducted on the platform of GeForce GTX3060 graphics processing unit (NVIDIA, Santa Clara, Calif). The proposed framework was implemented by the Python programming language (https://www.python.org/) on the open source deep learning framework MONAI in conjunction with PyTorch (version 1.9.0 https://pytorch.org). The cross-entropy loss function of the DL model was minimized by the gradient descent algorithm. The number of training iteration was 200, and the batch size was 64. To reduce the risk of overfitting, the technique of early stopping was adopted. The learning rate was initialized by 1e-4 with the decay value of 1e–4 and momentum of 0.9.

Clinical-radiological and combined models construction

To identify clinical and radiological predictors associated with HCC recurrence, the univariate logistic regression was employed

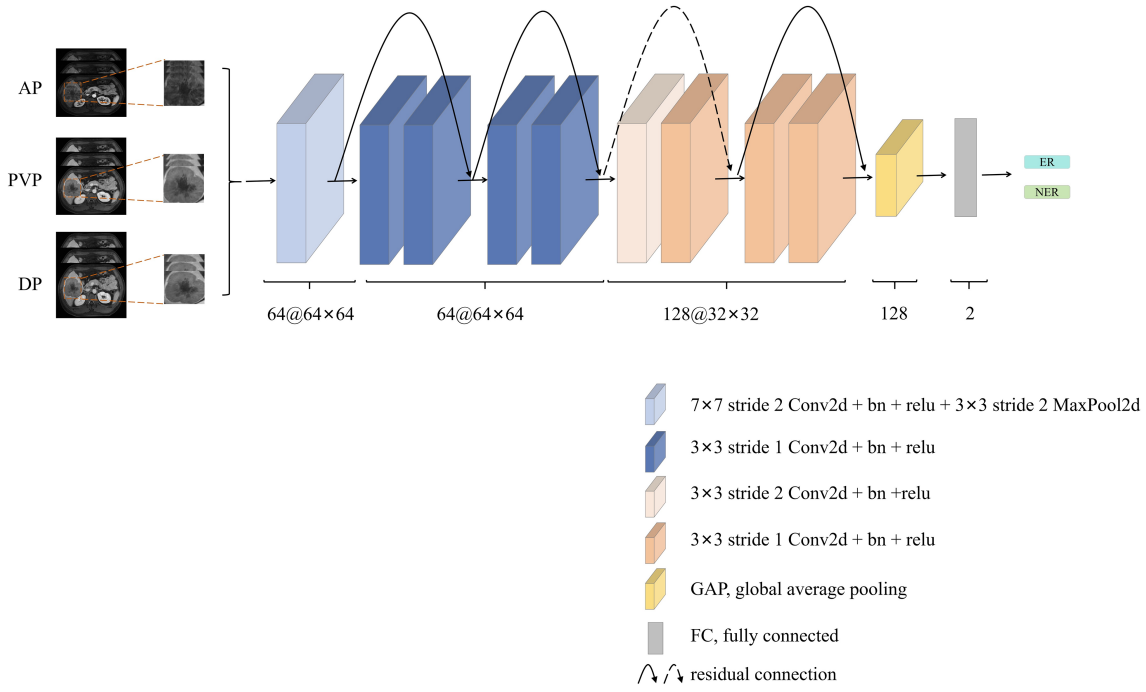

FIGURE 3
The network architecture of the deep learning (DL) model. The architecture involved concatenating three phase contrast enhanced MR images [arterial phase (AP), portal venous phase (PVP), and delayed phase (DP)], which were then fed into the ResNet-10. Subsequent to convolutional layers feature extraction, early recurrence (ER) prediction was performed through the fully connected layer. This architecture utilized the combination of multi-phase information and ResNet-10's convolutional capabilities to achieve accurate ER prediction.

and factors with P value of < 0.05 were further included in the multivariate logistic regression analysis. A clinical-radiological (CR) model was established based on the chosen CR independent risk factors by using logistic regression.

The radiomics combined with clinical-radiological (RCR) model, which incorporated the selected radiomics features derived from the highest performance radiomics model with CR risk factors for predicting tumor recurrence, was established using the proposed best-performing ML classifier.

These radiomics features belong to the low-level features of the manual design, while ResNet extracts the high-level semantic features. The combination of high-level DL features with CR and radiomics features can better describe the characteristics of the tumor and improve the capability of HCC recurrence prediction. We identified the DL model with the best performance for recurrence prediction based on the AUC and confirmed the preferably ResNet architecture variation. The high-level DL features and CR and radiomics features were combined with the fully connected layer to conduct joint training via the best-performing ResNet architecture variation, and were further applied to construct deep learning combined with RCR (DLRCR) model. Detailed diagram depicting the proposed fusion network architecture is listed in Supplementary Material S3. The DLRCR model performance was compared with the widely used Barcelona Clinic Liver Cancer (BCLC) staging system (27) and Chinese National Liver Cancer (CNLC) staging system (28), preoperative Early Recurrence After Surgery for Liver Tumor (ERASL) model (29), and some inflammation-based prognostic indexes (neutrophil-to-lymphocyte ratio (NLR), platelet-to-lymphocyte ratio (PLR), and lymphocyte-to-monocyte ratio (LMR)) (30).

Statistical analysis

R software (version 3.4.1, https://www.r-project.org/) and Python software (version 3.7.11, https://www.python.org/) were used for statistical analyses. Continuous variables among clinical-radiological characteristics were compared using the independent sample t test or Mann-Whitney U test, and categorical variables were analyzed using the chi-squared test or Fisher's exact test. The inter-observer consistency of radiological features was assessed using Kappa test (kappa value determination: $\kappa > 0.80$, excellent; $0.60 < \kappa \leq 0.80$, substantial; $0.40 < \kappa \leq 0.60$, moderate; $\kappa \leq 0.40$, poor). To evaluate the performance of different models, predictive accuracy, sensitivity, and specificity were measured using receiver operating characteristic (ROC) curve and the area under the curve (AUC) was calculated. Comparisons between the AUCs of different predictive models were performed using the Delong's test. We also performed stratified analysis on the subgroups of MRI scanner of the optimal radiomics model. We used ROC curve and AUC to evaluate model performance on the subpopulations. Model fit was assessed via calibration curves. The clinical utility of the models was evaluated using decision curve analysis (DCA). All statistical tests were two-sided, and $P < 0.05$ was considered statistically significant.

Results

Baseline characteristics

The final study cohort consisted of 165 patients (male: 138; median age, 59 years; range, 31-83 years) and was divided into the training cohort (n = 132) and the validation cohort (n = 33). Among the 165 patients, 96 (58.18%) patients were diagnosed with ER within 2 years, and 69 (41.82%) patients did not have ER. There was not significantly different in the ER rate between the training and validation cohorts (59.09% vs. 54.55%, P = 0.782). The median time to recurrence for all patients with ER was 7 months (range, 1-24 months). No significant differences of clinical-radiological characteristics were found between the training and validation cohorts (P = 0.081-1.000). Clinical-radiological data are summarized in Table 1.

Radiomics and DL models development and evaluation

A total of 3111 radiomics features for three phase CEMR images were extracted. After intra- and inter-observer reproducibility analysis, 2739 features had ICC ≥ 0.9 and were performed for further analysis. 961 features with significant differences that aided in predicting recurrence were then identified. LASSO algorithm ultimately allowed the selection of 34 features, which were input into five ML classifiers for radiomics models building. The selected radiomics features and the corresponding coefficients are presented in Supplementary Material S4.

The performance comparisons among five classifiers are shown in Table 2, and ROC curves are presented in Supplementary Material S5. The radiomics models showed moderate to good discrimination in the both cohorts (AUC: training cohort, 0.839 - 1.000; validation cohort, 0.626 - 0.804). It demonstrated that the LR classifier performed the best with the AUCs of 0.839 (95% confidence interval (CI), 0.772 - 0.906) and 0.804 (95%CI, 0.650 - 0.957) in the training and validation cohorts, respectively. There was no significant difference in the AUCs of LR classifier between the training and validation cohorts (P = 0.436), which indicated that the model showed non overfitting and high robust; while significant differences in the AUCs of SVM, KNN, XG-Boost, and MLP classifiers between the training and validation cohorts were found (P < 0.05). The accuracy, sensitivity, and specificity of the best-performing radiomics model (LR classifier) were 0.780, 0.885, and 0.630 in the training cohort, and 0.727, 0.833, and 0.600 in the validation cohort, respectively. The stratified analysis showed that the optimal radiomics model (LR classifier) was not influenced by MRI scanners with different magnetic field strength in the training cohort (1.5 T: AUC, 0.882 (95%CI, 0.796 - 0.968); 3.0 T: AUC, 0.834 (95%CI, 0.743 - 0.925), P = 0.457) and the validation cohort (1.5 T: AUC, 0.880 (95%CI, 0.696 - 1.000); 3.0 T: AUC, 0.762 (95%CI, 0.538 - 0.986), P = 0.430).

Predictive performances and ROC curves of DL models are shown in Supplementary Material S6. The AUCs of ResNet-18 and ResNet-34 models were 0.700 (95%CI, 0.608 - 0.792) and 0.611 (95%CI, 0.511 - 0.712) in the training cohort, and 0.704 (95%CI, 0.517 - 0.890) and 0.619 (95%CI, 0.414 - 0.823) in the validation cohort, respectively. Compared with ResNet-18 and ResNet-34 models, the ResNet-10 model achieved the best performance with an AUC, an accuracy, a sensitivity, and a specificity of 0.870 (95% CI, 0.806 - 0.934), 0.803, 0.861, 0.733 in the training cohort, respectively, and an AUC, an accuracy, a sensitivity, and a specificity of 0.826 (95%CI, 0.682 - 0.970), 0.788, 0.824, and 0.750 in the validation cohort, respectively. The DL (ResNet-10) model obtained better performance than radiomics (LR) model (AUC: training, 0.870 vs. 0.839; validation, 0.826 vs. 0.804). In addition, we computed activation maps and visualized the AP, PVP, and DP images, where the darker the color in the activation map, the more significant the region's importance. The highlighted regions in the map were primarily concentrated on the tumor margins. The visualization results of the DL model are showed in Figure 4.

Clinical-radiological and combined models construction and evaluation

Inter-observer agreements on the MR imaging features were excellent (kappa-value range: 0.834 to 1.000). Univariate and multivariate analyses of clinical-radiological characteristics for predicting tumor recurrence in the training cohort are shown in Table 3. The univariate analysis demonstrated that AFP, AST, and tumor diameter were significant CR factors for discriminating the ER and NER groups in the training cohort (all P < 0.05). The multivariate analysis showed that AST (OR = 2.490; 95% CI: 1.140 - 5.440; P = 0.020) and tumor diameter (OR = 2.510; 95% CI: 1.080 - 5.820; P = 0.030) were independent risk factors for predicting ER in HCC patients. The CR model was built based on the two risk factors, which achieved an AUC of 0.662 (95%CI, 0.574 - 0.749) in the training cohort and 0.752 (95%CI, 0.593 - 0.911) in the validation cohort, respectively (Table 4; Figures 5A, B).

The RCR model was constructed integrating the remained radiomics features, AST, and tumor diameter using logistic regression classifier. Furthermore, the DL features, the chosen radiomics features, AST, and tumor diameter were input into the fully connected layer via ResNet-10 architecture to build the DLRCR model. The AUCs of RCR model were 0.841 (95%CI, 0.774 - 0.908) and 0.811 (95%CI, 0.661 - 0.962), which performed better than CR model (Delong's test: training, P < 0.001; validation, P = 0.440). The DLRCR model outperformed the CR, radiomics, DL, and RCR models, yielding an AUC, an accuracy, a sensitivity, a specificity of 0.917 (95%CI, 0.963 - 0.972), 0.886, 0.889, and 0.882 in the training cohort and of 0.844 (95%CI, 0.702 - 0.987), 0.818, 0.800, and 0.846 in the validation cohort, respectively (Table 4; Figures 5A, B). The Delong's test showed a significant difference of the AUCs between the DLRCR model and the CR model in the training cohort (P < 0.001), while there was no significant difference in the validation cohort (P = 0.232). Delong's test of different predictive models in the both cohorts is shown in Supplementary Material S7. Calibration curves for the probability of ER demonstrated good model agreements between prediction and observation in the both cohorts (Figures 6A, B). DCA curves

10.3389/fonc.2024.1446386

TABLE 1 Patient clinical-radiological characteristics.

Characteristics	Training cohort (*n* = 132)			Validation cohort (*n* = 33)			*P* value
	ER group (*n* = 78)	NER group (*n* = 54)	*P* value	ER group (*n* = 18)	NER group (*n* = 15)	*P* value	
Gender (*n*, [%])			0.355			1.000	0.958
Male	68 (87.2)	43 (79.6)		15 (83.3)	12 (80.0)		
Female	10 (12.8)	11 (20.4)		3 (16.7)	3 (20.0)		
Age (years, mean ± SD)	58.35 ± 10.59	58.38 ± 10.60	0.604	57.81 ± 10.84	56.81 ± 10.26	0.758	0.642
History of hepatitis B or C (*n*, [%])			0.733			1.000	0.199
Positive	61 (78.2)	40 (74.1)		11 (61.1)	10 (66.7)		
Negative	17 (21.8)	14 (25.9)		7 (38.9)	5 (33.3)		
AFP (IU/ml) (*n*, [%])			0.046			0.607	0.397
≤ 400	57 (73.1)	48 (88.9)		15 (83.3)	14 (93.3)		
> 400	21 (26.9)	6 (11.1)		3 (16.7)	1 (6.67)		
ALT (U/L) (*n*, [%])			0.234			1.000	1.000
≤ 50	52 (66.7)	42 (77.8)		13 (72.2)	11 (73.3)		
> 50	26 (33.3)	12 (22.2)		5 (27.8)	4 (26.7)		
AST (U/L) (*n*, [%])			0.016			1.000	0.128
≤ 40	42 (53.8)	41 (75.9)		14 (77.8)	12 (80.0)		
> 40	36 (46.2)	13 (24.1)		4 (22.2)	3 (20.0)		
GGT (U/L) (*n*, [%])			0.084			0.923	0.785
≤ 60	36 (46.2)	34 (63.0)		11 (61.1)	8 (53.3)		
> 60	42 (53.8)	20 (37.0)		7 (38.9)	7 (46.7)		
TBIL (umol/L) (*n*, [%])			0.424			0.108	0.081
≤ 19	53 (67.9)	41 (75.9)		14 (77.8)	15 (100)		
> 19	25 (32.1)	13 (24.1)		4 (22.2)	0 (0.00)		
ALB (g/L) (*n*, [%])			0.624			0.266	1.000
< 40	29 (37.2)	17 (31.5)		4 (22.2)	7 (46.7)		
≥ 40	49 (62.8)	37 (68.5)		14 (77.8)	8 (53.3)		
Child-Pugh class (*n*, [%])			1.000			—	0.127
A	71 (91.0)	49 (90.7)		18 (100)	15 (100)		
B	7 (9.0)	5 (9.3)		0 (0.00)	0 (0.00)		
Tumor diameter (*n*, [%])			0.024			0.009	0.899
≤ 5 cm	48 (61.5)	44 (81.5)		8 (44.4)	14 (93.3)		
> 5 cm	30 (38.5)	10 (18.5)		10 (55.6)	1 (6.7)		
Tumor number (*n*, [%])			0.442			0.346	0.776
Unifocal	66 (84.6)	49 (90.7)		14 (77.8)	14 (93.3)		
Multifocal	12 (15.4)	5 (9.3)		4 (22.2)	1 (6.7)		
Tumor margin (*n*, [%])			0.567			0.266	0.550
Smooth	44 (56.4)	34 (63.0)		10 (55.6)	12 (80.0)		
Non-smooth	34 (43.6)	20 (37.0)		8 (44.4)	3 (20.0)		

(Continued)

TABLE 1 Continued

Characteristics	Training cohort (*n* = 132)			Validation cohort (*n* = 33)			*P* value
	ER group (*n* = 78)	NER group (*n* = 54)	*P* value	ER group (*n* = 18)	NER group (*n* = 15)	*P* value	
Intratumoral necrosis (*n*, [%])			0.523			1.000	0.399
Present	30 (38.5)	17 (31.5)		8 (44.4)	7 (46.7)		
Absent	48 (61.5)	37 (68.5)		10 (55.6)	8 (53.3)		
Intratumoral hemorrhage (*n*, [%])			0.258			0.064	0.573
Present	24 (30.8)	11 (20.4)		9 (50.0)	2 (13.3)		
Absent	54 (69.2)	43 (79.6)		9 (50.0)	13 (86.7)		
Tumor encapsulation (*n*, [%])			0.284			0.674	0.891
Present	56 (71.8)	44 (81.5)		15 (83.3)	11 (73.3)		
Absent	22 (28.2)	10 (18.5)		3 (16.7)	4 (26.7)		
Arterial peritumoral enhancement (*n*, [%])			0.424			0.447	0.525
Present	25 (32.1)	13 (24.1)		5 (27.8)	7 (46.7)		
Absent	53 (67.9)	41 (75.9)		13 (72.2)	8 (53.3)		
Radiological cirrhosis (*n*, [%])			0.731			1.000	0.133
Present	54 (69.2)	35 (64.8)		9 (50.0)	8 (53.3)		
Absent	24 (30.8)	19 (35.2)		9 (50.0)	7 (46.7)		

Data are shown as number of patients, with the percentage in parentheses. ER, early recurrence; NER, non-early recurrence; SD: standard deviation; AFP, alpha-fetoprotein; ALT, alanine aminotransferase; AST, aspartate aminotransferase; GGT,γ-glutamyltranspeptadase; TBIL, total bilirubin; ALB; albumin.

showed that the DLRCR model achieved more net benefit compared with other models for most of the threshold probabilities (Figures 7A, B).

In the training cohort, the DLRCR model demonstrated superior performance than BCLC system (0.565; 95%CI, 0.507 - 0.623), CNLC system (0.610; 95%CI, 0.529 - 0.692), preoperative ERASL model (0.550; 95%CI, 0.485 - 0.616), NLR (0.561; 95%CI, 0.476 - 0.646), PLR (0.544; 95%CI, 0.462- 0.626), and LMR (0.507; 95%CI, 0.422 - 0.592) ($P < 0.05$). In the validation cohort, the AUC of the DLRCR model was significantly higher than that of BCLC system (0.615; 95%CI, 0.513 - 0.717), preoperative ERASL model (0.572; 95%CI, 0.433 - 0.711), NLR (0.483; 95%CI, 0.307 - 0.660), PLR (0.467; 95%CI, 0.296 - 0.637), and LMR (0.489; 95%CI, 0.313 - 0.665) ($P < 0.05$), except for CNLC system (0.774; 95%CI, 0.635 -

TABLE 2 Discrimination performance of different classifiers in the training and validation cohorts.

Model		AUC (95% CI)	Accuracy	Sensitivity	Specificity	*P* value
LR model	TC	0.839 (0.772 - 0.906)	0.780	0.885	0.630	0.436
	VC	0.804 (0.650 - 0.957)	0.727	0.833	0.600	
SVM model	TC	0.971 (0.935 - 1.000)	0.932	0.987	0.852	0.003
	VC	0.641 (0.439 - 0.842)	0.636	0.889	0.333	
KNN model	TC	0.874 (0.816 - 0.931)	0.803	0.821	0.778	0.031
	VC	0.637 (0.439 - 0.835)	0.515	0.500	0.533	
XG-Boost model	TC	0.934 (0.888 - 0.980)	0.871	0.846	0.907	0.028
	VC	0.722 (0.547 - 0.897)	0.667	0.556	0.800	
MLP model	TC	1.000 (1.000 - 1.000)	1.000	1.000	1.000	<0.001
	VC	0.626 (0.429 - 0.823)	0.606	0.667	0.533	

LR, logistic regression; SVM, support vector machine; KNN, k-nearest neighbor; XG-Boost, extreme gradient Boosting; MLP, multilayer perceptron; TC, training cohort; VC, validation cohort; AUC, area under the curve; CI, confidence interval.

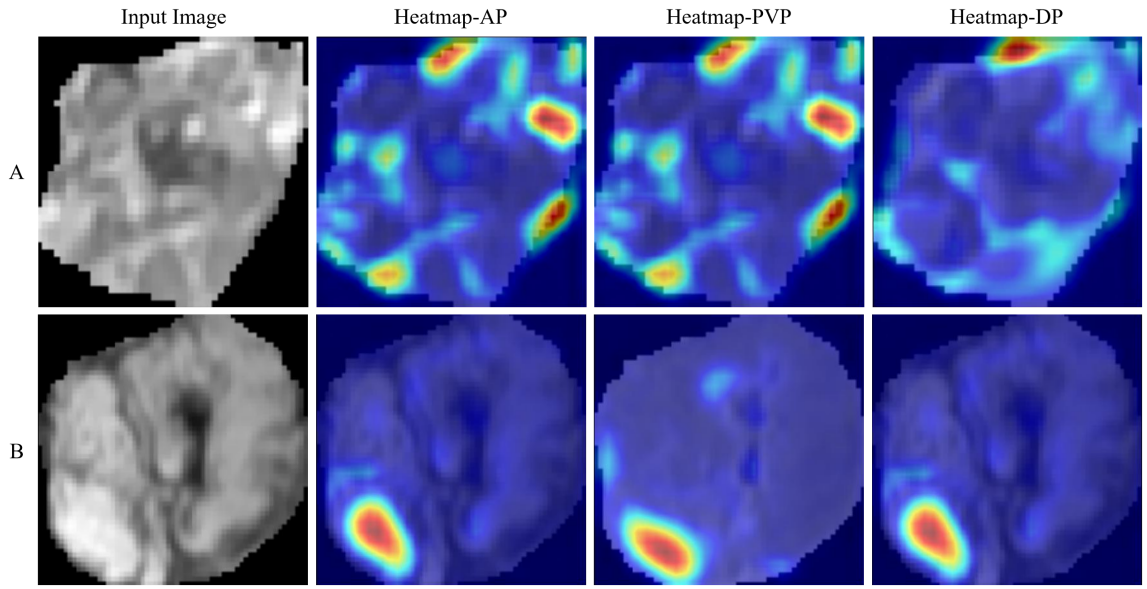

FIGURE 4
Visualization results for the early recurrence case **(A)** and non-early recurrence case **(B)**. Input images represent the cropped tumor regions fed into the model. Heatmaps are standard jet colormaps overlaid on the original input images, where red indicates areas of the highest relevance to the classification, followed by yellow, while green and blue regions indicate weaker predictive relevance. AP, PVP, and DP denote arterial phase, portal venous phase, and delayed phase, respectively.

TABLE 3 Univariate and multivariate analyses of clinical-radiological characteristics for predicting early recurrence in the training cohort.

Variables	Univariate analysis		Multivariate analysis	
	Odd ratio (95% CI)	*P* value	Odd ratio (95% CI)	*P* value
Gender	1.74 (0.68 - 4.44)	0.25	—	—
Age	1.01 (0.98 - 1.04)	0.65	—	—
History of hepatitis B or C	1.26 (0.56 - 2.83)	0.58	—	—
AFP	2.95 (1.10 - 7.89)	0.03	—	—
ALT	1.75 (0.79 - 3.88)	0.17	—	—
AST	2.70 (1.26 - 5.82)	0.01	2.49 (1.14 - 5.44)	0.02
GGT	1.98 (0.98 - 4.03)	0.06	—	—
T-BIL	1.49 (0.68 - 3.26)	0.32	—	—
ALB	0.78 (0.37 - 1.62)	0.50	—	—
Child-Pugh class	0.97 (0.29 - 3.22)	0.96	—	—
Tumor diameter	2.75 (1.21 - 6.27)	0.02	2.51 (1.08 - 5.82)	0.03
Tumor number	1.78 (0.59 - 5.39)	0.31	—	—
Tumour margin	1.31 (0.65 - 2.67)	0.45	—	—
Intratumoral necrosis	0.74 (0.35 - 1.53)	0.41	—	—
Intratumoral hemorrhage	0.58 (0.25 - 1.30)	0.19	—	—
Tumor encapsulation	1.73 (0.74 - 4.03)	0.20	—	—
Arterial peritumoral enhancement	0.67 (0.31 - 1.47)	0.32	—	—
Radiological cirrhosis	0.82 (0.39 - 1.71)	0.60	—	—

Variables with $P < 0.05$ in the univariate analysis were included in the multivariate logistic regression analysis. AFP, alpha-fetoprotein; ALT, alanine aminotransferase; AST, aspartate aminotransferase; GGT,γ-glutamyltranspeptadase; TBIL, total bilirubin; ALB; albumin.

TABLE 4 Discrimination performance of different models in the training and validation cohorts.

Model		AUC (95% CI)	Accuracy	Sensitivity	Specificity	*P* value
CR model	TC	0.662 (0.574 - 0.749)	0.652	0.654	0.648	0.334
	VC	0.752 (0.593 - 0.911)	0.727	0.667	0.800	
Radiomics model	TC	0.839 (0.772 - 0.906)	0.780	0.885	0.630	0.681
	VC	0.804 (0.650 - 0.957)	0.727	0.833	0.600	
DL model	TC	0.870 (0.806 - 0.934)	0.803	0.861	0.733	0.584
	VC	0.826 (0.682 - 0.970)	0.788	0.824	0.750	
RCR model	TC	0.841 (0.774 - 0.908)	0.773	0.872	0.630	0.722
	VC	0.811 (0.661 - 0.962)	0.727	0.833	0.600	
DLRCR model	TC	0.917 (0.963 - 0.972)	0.886	0.889	0.882	0.355
	VC	0.844 (0.702 - 0.987)	0.818	0.800	0.846	

CR, clinical-radiological; DL, deep learning; RCR, radiomics combined with clinical-radiological; DLRCR, deep learning combined with RCR; TC, training cohort; VC, validation cohort; AUC, area under the curve; CI, confidence interval.

0.914) (P = 0.492). Predictive performances and ROC curves of clinical prediction methods are provided in Supplementary Material S8.

Discussion

In this study, we developed and validated radiomics and DL models based on multi-phase CEMR images using different ML classifiers and CNN architectures for preoperatively predicting early recurrence of HCC patients after curative resection. Furthermore, we proposed a novel DL and radiomics-based integrated approach for HCC recurrence prediction that combined DL, radiomics, and clinical-radiological data. Our study found that the optimal DL model improved the performance over the radiomics model. The DLRCR model exhibited superior predictive efficiency over any model in predicting HCC recurrence and better clinical utility compared to clinical prediction methods (BCLC system, CNLC system, preoperative ERASL model, and some inflammation-based prognostic indexes). This DL and radiomics-based integrated strategy can provide a promising tool for accurate prediction of recurrence, which may potentially guide individualized treatment and survival monitoring of HCC patients.

Early-stage HCC still has a high recurrence rate after resection. In our study, 58.18% of HCC patients occurred postoperative ER. Accurate preoperative prediction of ER is critical for risk stratification and appropriate therapeutic strategies adjustment, contributing to improve patients overall survival (OS). Currently, a number of studies have developed clinical model based on the independent risk factors to predict ER, which obtained the AUCs from 0.606 to 0.715 (13, 16, 21, 22). However, the estimated clinical metrics are limited and the predictive performance is still required

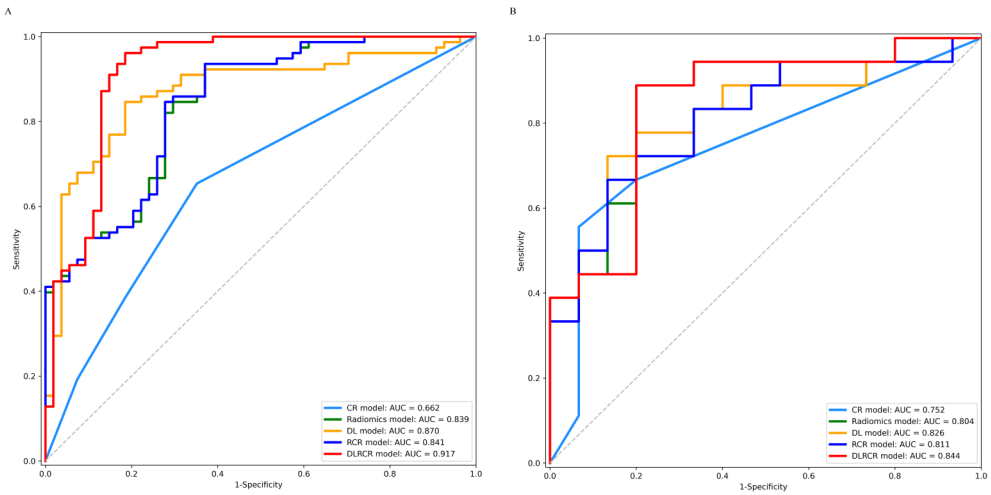

FIGURE 5
ROC curves for the clinical-radiological (CR) model, radiomics model, deep learning (DL) model, radiomics combined with clinical-radiological (RCR) model, and deep learning combined with RCR (DLRCR) model in the training cohort **(A)** and the validation cohort **(B)**.

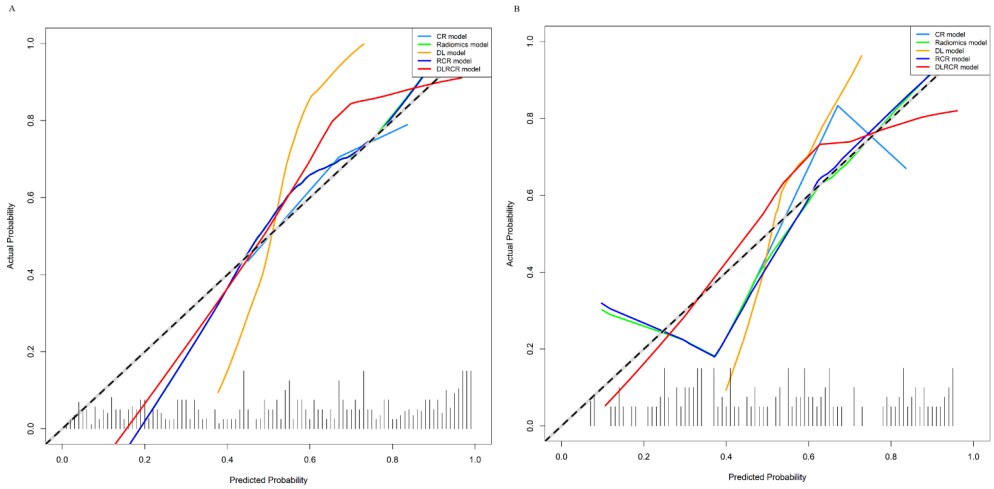

FIGURE 6
Calibration curves of various models in the training cohort **(A)** and the validation cohort **(B)**. The curves assess the models' goodness-of-fit. The x-axis represents the predicted probability, and the y-axis represents the actual probability. The dashed line represents the ideal prediction by a perfect model. The solid line represents the predictive performance of the model. If the solid line is closer to the dashed line, it means a better goodness-of-fit.

to be improved. With the development of ML technology, a large amount of quantitative radiomics data have been used to construct more predictive models than those developed by clinical characteristics. In the present study, the multivariate analysis demonstrated that AST and tumor diameter were significant risk factors for ER prediction in patients with HCC, consistent with the results of other studies (3, 7, 12, 13). A recent study proved that the AST level > 40 U/L was independent predictor for poor recurrence-free survival (RFS) and OS (7). A multicenter study of 628 HCC patients demonstrated that the larger tumor diameter was closely associated with ER after liver resection for solitary HCC (3). We developed CEMRI-based radiomics models using five commonly used ML classifiers (LR, SVM, KNN, XG-Boost, and MLP) and evaluated its role in predicting ER. Our study showed that the LR classifier obtained better performance and robustness than the other four classifiers, which were consistent with previous studies (31–33). Logistic regression has advantages that it does not require a value with a normal distribution and can resist noisy interference and prevent overfitting using regularization (31). The radiomics model with LR classifier had a higher ability to predict ER than the clinical-radiological model (ΔAUC: training, 0.177; validation, 0.052). Furthermore, the combined model integrating clinical-radiological characteristics with radiomics features based on CEMRI was constructed and achieved improved performance compared with the clinical-radiological model (ΔAUC: training, 0.179; validation, 0.059). Nonetheless, the radiomics method relies

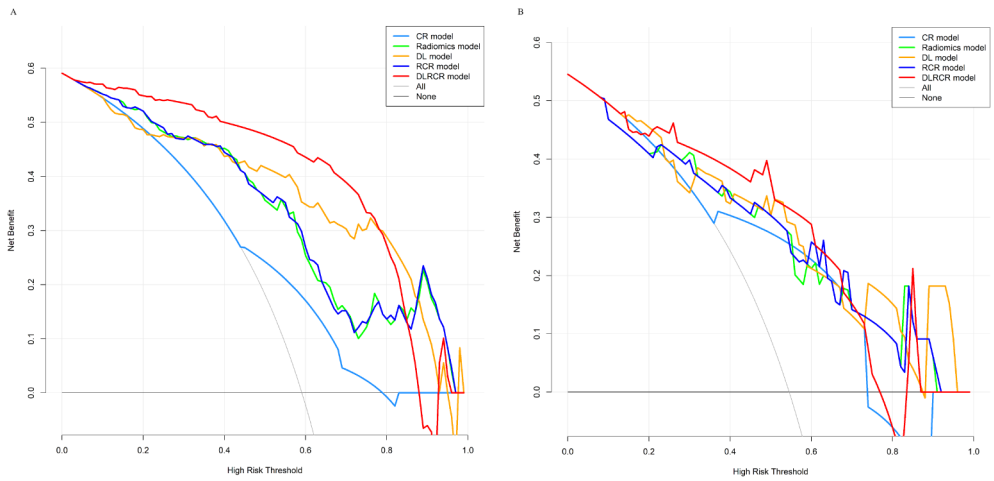

FIGURE 7
Decision curve analysis for different models in the training cohort **(A)** and the validation cohort **(B)**. The x-axis represents the threshold probability for high risk, and the y-axis denotes the net benefit. The DLRCR model obtained more net benefit compared with other models, treat-all strategy (gray line), and treat-none strategy (horizontal black line) across the majority range of threshold probabilities.

on predefined feature engineering that the extraction and selection of "hand-engineered" features are still complicated, subjective, time-consuming, and lack of stable reproducibility, thus limiting their clinical applicability (34, 35).

The emerging DL approach has advantages in automatically learning and hierarchically organizing task-adaptive high-level image features with less manpower and time (36). It can achieve higher accuracy, reproducibility, and predictive performance compared to conventional radiomics method (37). Two recent studies utilizing DL algorithms based on preoperative CECT images showed moderate performances for HCC recurrence prediction with the AUCs of 0.723 and 0.730 in the validation cohort, respectively (38, 39). In contrast, the development of DL model using MR images maybe more promising due to the higher soft tissue contrast of MR imaging compared to CT. Kucukkaya et al. (40) conducted a MRI-based DL research on 120 HCC patients undergoing surgical resection, thermal ablation, or orthotopic liver transplantation for postoperative recurrence prediction within six different time frames (range 1 - 6 years), showing two-year recurrence and average AUCs of 0.750 and 0.760 in the test cohort, respectively. However, that study had limited sample size, lower predictive performance, and lacked of model comparisons of different CNN architectures. Gao et al. (18) reported that DL method based on multi-sequence MR images for predicting early recurrence of HCC, achieving the AUC and accuracy of 0.813 and 0.755 in the validation cohort, which were slightly lower than our DL model (AUC: 0.826; accuracy: 0.788). Compared to the above two studies (18, 40), our DL model are trained in an end-to-end fashion, which simplifies the process by eliminating intermediate steps and reducing potential sources of error thus improving predictive capacity. A recent study reported by Wang et al. (41) constructed a DL model based on Gd-EOB-DTPA-enhanced MRI using VGG-19 network for prediction of HCC early recurrence post-hepatectomy. Compared to the VGG-19 prediction model (41), our DL (ResNet-10) model has the following advantages: firstly, our model lies in its incorporation of residual connections, which allows it to achieve excellent performance with fewer parameters and effectively addresses the vanishing gradient problem during the training of deeper networks; secondly, we implemented a weighted approach for each class in the cross-entropy loss to address class imbalance in the network; finally, our model achieved better performance metrics in the validation cohort (AUC: 0.826 vs. 0.759; accuracy: 0.788 vs. 0.775).

In the current study, we established three DL models using different neural network layers of ResNet architecture (ResNet-10, ResNet-18, and ResNet-34), and the shallower ResNet-10 model obtained better ER predictive performance compared to the other two DL models (ΔAUC: training, 0.170 - 0.259; validation, 0.122 - 0.207). Overfitting is a problem in DL field that becomes more serious with the more superimposed neural network layers there are (42). Specifically, as the number of layers in a model increases, it can learn progressively more complex features and patterns. However, if the data is insufficient or lacks diversity, the model may finally learn irrelevant information (noise) that is specific to the training set, leading to a decline in performance in the validation or test set. In our study, we primarily focused on model simplification technique to tackle overfitting, which allowed us to achieve superior predictive performance by using a smaller number of neural network layers. And this improvement can be attributed to two key aspects: firstly, having fewer neural network layers results in a lower model complexity, which can help reduce the risk of overfitting, especially when training data is limited; secondly, shallow neural networks can effectively capture global patterns and key features within the data, particularly for tasks with relatively simple structures or lower dimensions, where deeper models often do not provide significant performance improvements. Some studies have reached similar results that shallow neural networks can achieve comparable or even superior performance to deeper networks for specific tasks (43, 44). Additionally, the visualization analysis of the DL model demonstrated that the highlighted regions in the heatmap were primarily concentrated on the tumor margins, indicating that the features in these areas are crucial in supporting the model's decisions. This may be interpreted that the non-smooth tumor margin and incomplete/without tumor capsule are closely related to prognosis of HCC patients (7, 8).

Recently, the DL and radiomics-based integrated strategy incorporating interpretable radiomics features with high-level temporal and spatial DL features has been demonstrated as a state-of-the-art quantitative tool and can be used to predict tumor behavior and prognosis due to its higher predictive accuracy (18–20, 45). However, studies of using DL and radiomics-based model for predicting early recurrence in HCC patients after curative resection are scarce, and to the best of our knowledge, only two studies have been conducted recently (18, 20). In a recent study (20), the clinical & deep learning-based radiomics model and deep learning-based radiomics model based on AP and PVP images of preoperative CECT showed better distinguished performance than the radiological model for prediction of 3-year recurrence rate of HCC after resection (AUC: 0.831 vs. 0.796 vs. 0.732). Gao et al (18) have further constructed a DL and radiomics-based combined model based on multi-sequence MR images, which demonstrated superior discriminative ability than the DL or radiomics model alone for ER prediction (AUC: 0.840 vs. 0.813 vs. 0.780). However, that study ignored routine clinical and radiological information that were useful and interpretable for predicting recurrence. Our study found that the DLRCR model achieved improvements in the AUC, accuracy, sensitivity, and specificity for predicting ER compared to the DL model or the RCR model alone, indicating that the combination of high-level DL features along with radiomics and clinical-radiological data maximized the predictive performance of ER. Compared with the only MRI-related study reported by Gao et al. (18), our study may have the following advantages: firstly, our study contained routine clinical information and conventional radiological features, which could provide more information about tumor characteristics; secondly, our DLRCR model possessed higher accuracy (0.818 vs. 0.777), sensitivity (0.800 vs. 0.769), and specificity (0.846 vs. 0.779) than the combined model in the validation cohort in that study, although the AUC (0.844 vs. 0.840) was comparable; finally, as opposed to the traditional approach of employing machine learning for dimensionality reduction and model building, our primary objective is to construct a neural network through the integration of DL,

radiomics, and clinical-radiological data, which may automatically learn complementary information from multimodal data and thereby enhancing model performance.

Our study has several limitations. Firstly, the potential selection bias may exist due to the retrospective nature of the study. Secondly, this was a single-center study with relatively small samples. Our study have employed various strategies such as data augmentation, regularization, early stopping, and model simplification techniques to avoid overfitting and improve predictive performance. A large-scale and multi-center dataset is required to validate reliability and robustness of prediction models and to provide a better generalization of our results in the future. Thirdly, the VOIs were outlined manually by radiologists, thus is time- and labor-consuming, and limiting the model usefulness of our study. Further research is considered to design a DL framework integrating HCC automatic segmentation and recurrence prediction. Fourthly, the DL method is regarded as "black box" and lacks interpretability that is a challenge to explain the correlation between relevant features and results. To interpret important features or patterns identified by the DL model, we performed visual interpretation using Score-CAM method. In the future, we will try to continuously optimize our DL network to improve its predictive performance and interpretability. Finally, the value of our method for improving long-term survival in patients with HCC remains unclear, we will further explore the capacity of MRI DL and radiomics-based integrated approach for predicting OS of HCC patients after surgical resection.

In conclusion, CEMRI-based radiomics and DL models performed well in predicting HCC early recurrence after curative resection. Importantly, a novel DL and radiomics-based combined model incorporating clinical-radiological, radiomics, and high level DL features was proposed as a more effective method for the prediction of early recurrence for HCC patients. The integrated approach has potential to refine the prognosis and guide individualized treatment strategies for patients with HCC.

Data availability statement

The raw data supporting the conclusions of this article will be made available by the authors, without undue reservation.

Ethics statement

The studies involving humans were approved by the Institutional Review Board of the First Affiliated Hospital of Dalian Medical University. The studies were conducted in accordance with the local legislation and institutional requirements. The ethics committee/institutional review board waived the requirement of written informed consent for participation from the participants or the participants' legal guardians/next of kin because this was a retrospective study.

Author contributions

YZ: Conceptualization, Data curation, Formal analysis, Funding acquisition, Investigation, Methodology, Software, Validation, Visualization, Writing – original draft. SW: Conceptualization, Formal analysis, Methodology, Software, Validation, Visualization, Writing – original draft. YW: Formal analysis, Software, Validation, Writing – original draft. JL: Formal analysis, Software, Validation, Writing – original draft. JHL: Formal analysis, Validation, Writing – original draft, Data curation, Visualization. YL: Formal analysis, Validation, Writing – original draft, Software. HJ: Formal analysis, Software, Writing – original draft. WS: Formal analysis, Software, Writing – original draft. QZ: Formal analysis, Software, Writing – original draft, Validation. QS: Data curation, Supervision, Writing – review & editing. YY: Supervision, Writing – review & editing, Methodology, Project administration. AL: Project administration, Supervision, Writing – review & editing, Conceptualization, Data curation, Resources.

Funding

The author(s) declare that financial support was received for the research, authorship, and/or publication of this article. This work was supported by the Dalian Young Stars of Science and Technology Project Support Program (No. 2022RQ074) and Dalian Medical Science Research Program (No. 2212011).

Conflict of interest

The authors declare that the research was conducted in the absence of any commercial or financial relationships that could be construed as a potential conflict of interest.

Publisher's note

Supplementary material

The Supplementary Material for this article can be found online at: https://www.frontiersin.org/articles/10.3389/fonc.2024.1446386/full#supplementary-material

References

1. Sung H, Ferlay J, Siegel RL, Laversanne M, Soerjomataram I, Jemal A, et al. Global cancer statistics 2020: GLOBOCAN estimates of incidence and mortality worldwide for 36 cancers in 185 countries. *CA Cancer J Clin*. (2021) 71:209–49. doi: 10.3322/caac.21660

2. Marrero JA, Kulik LM, Sirlin CB, Zhu AX, Finn RS, Abecassis MM, et al. Diagnosis, staging, and management of hepatocellular carcinoma: 2018 practice guidance by the American association for the study of liver diseases. *Hepatology*. (2018) 68:723–50. doi: 10.1002/hep.29913

3. Jung SM, Kim JM, Choi GS, Kwon CHD, Yi NJ, Lee KW, et al. Characteristics of early recurrence after curative liver resection for solitary hepatocellular carcinoma. *J Gastrointest Surg*. (2019) 23:304–11. doi: 10.1007/s11605-018-3927-2

4. Bruix J, Takayama T, Mazzaferro V, Chau GY, Yang J, Kudo M, et al. Adjuvant sorafenib for hepatocellular carcinoma after resection or ablation (STORM): a phase 3, randomised, double-blind, placebo-controlled trial. *Lancet Oncol*. (2015) 16:1344–54. doi: 10.1016/S1470-2045(15)00198-9

5. Lim KC, Chow PK, Allen JC, Chia GS, Lim M, Cheow PC, et al. Microvascular invasion is a better predictor of tumor recurrence and overall survival following surgical resection for hepatocellular carcinoma compared to the Milan criteria. *Ann Surg*. (2011) 254:108–13. doi: 10.1097/SLA.0b013e31821ad884

6. Nitta H, Allard MA, Sebagh M, Golse N, Ciacio O, Pittau G, et al. Ideal surgical margin to prevent early recurrence after hepatic resection for hepatocellular carcinoma. *World J Surg*. (2021) 45:1159–67. doi: 10.1007/s00268-020-05881-9

7. Wu F, Ni X, Sun H, Zhou C, Huang P, Xiao Y, et al. An MRI-based prognostic stratification system for medical decision-making of multinodular hepatocellular carcinoma patients beyond the Milan criteria. *J Magn Reson Imaging*. (2023) 58:1918–29. doi: 10.1002/jmri.28724

8. Mo ZY, Chen PY, Lin J, Liao JY. Pre-operative MRI features predict early post-operative recurrence of hepatocellular carcinoma with different degrees of pathological differentiation. *Radiol Med*. (2023) 128:261–73. doi: 10.1007/s11547-023-01601-0

9. Qu Q, Lu M, Xu L, Zhang J, Liu M, Jiang J, et al. A model incorporating histopathology and preoperative gadoxetic acid-enhanced MRI to predict early recurrence of hepatocellular carcinoma without microvascular invasion after curative hepatectomy. *Br J Radiol*. (2023) 96:20220739. doi: 10.1259/bjr.20220739

10. Lévi-Strauss T, Tortorici B, Lopez O, Viau P, Ouizeman DJ, Schall B, et al. Radiomics, a promising new discipline: example of hepatocellular carcinoma. *Diagnostics (Basel)*. (2023) 13:1303. doi: 10.3390/diagnostics13071303

11. Wei J, Jiang H, Zhou Y, Tian J, Furtado FS, Catalano OA. Radiomics: A radiological evidence-based artificial intelligence technique to facilitate personalized precision medicine in hepatocellular carcinoma. *Dig Liver Dis*. (2023) 55:833–47. doi: 10.1016/j.dld.2022.12.015

12. Zhao Y, Wu J, Zhang Q, Hua Z, Qi W, Wang N, et al. Radiomics analysis based on multiparametric MRI for predicting early recurrence in hepatocellular carcinoma after partial hepatectomy. *J Magn Reson Imaging*. (2021) 53:1066–79. doi: 10.1002/jmri.27424

13. Chong H, Gong Y, Pan X, Liu A, Chen L, Yang C, et al. Peritumoral dilation radiomics of gadoxetate disodium-enhanced MRI excellently predicts early recurrence of hepatocellular carcinoma without macrovascular invasion after hepatectomy. *J Hepatocell Carcinoma*. (2021) 8:545–63. doi: 10.2147/JHC.S309570

14. Chan HP, Samala RK, Hadjiiski LM, Zhou C. Deep learning in medical image analysis. *Adv Exp Med Biol*. (2020) 1213:3–21. doi: 10.1007/978-3-030-33128-3_1

15. LeCun Y, Bengio Y, Hinton G. Deep learning. *Nature*. (2015) 521:436–44. doi: 10.1038/nature14539

16. Wang F, Chen Q, Chen Y, Zhu Y, Zhang Y, Cao D, et al. A novel multimodal deep learning model for preoperative prediction of microvascular invasion and outcome in hepatocellular carcinoma. *Eur J Surg Oncol*. (2023) 49:156–64. doi: 10.1016/j.ejso.2022.08.036

17. Jiang YQ, Cao SE, Cao S, Chen JN, Wang GY, Shi WQ, et al. Preoperative identification of microvascular invasion in hepatocellular carcinoma by XGBoost and deep learning. *J Cancer Res Clin Oncol*. (2021) 147:821–33. doi: 10.1007/s00432-020-03366-9

18. Gao W, Wang W, Song D, Yang C, Zhu K, Zeng M, et al. A predictive model integrating deep and radiomics features based on gadobenate dimeglumine-enhanced MRI for postoperative early recurrence of hepatocellular carcinoma. *Radiol Med*. (2022) 127:259–71. doi: 10.1007/s11547-021-01445-6

19. Dong X, Yang J, Zhang B, Li Y, Wang G, Chen J, et al. Deep learning radiomics model of dynamic contrast-enhanced MRI for evaluating vessels encapsulating tumor clusters and prognosis in hepatocellular carcinoma. *J Magn Reson Imaging*. (2023) 59:108–19. doi: 10.1002/jmri.28745

20. Lv C, He N, Yang JJ, Xiao JJ, Zhang Y, Du J, et al. Prediction of 3-year recurrence rate of hepatocellular carcinoma after resection based on contrast-enhanced CT: a single-centre study. *Br J Radiol*. (2023) 96:20220702. doi: 10.1259/bjr.20220702

21. Ji GW, Zhu FP, Xu Q, Wang K, Wu MY, Tang WW, et al. Radiomic features at contrast-enhanced CT predict recurrence in early stage hepatocellular carcinoma: A multi-institutional study. *Radiology*. (2020) 294:568–79. doi: 10.1148/radiol.2020191470

22. Yan M, Zhang X, Zhang B, Geng Z, Xie C, Yang W, et al. Deep learning nomogram based on Gd-EOB-DTPA MRI for predicting early recurrence in hepatocellular carcinoma after hepatectomy. *Eur Radiol*. (2023) 33:4949–61. doi: 10.1007/s00330-023-09419-0

23. Chen Y, Chen J, Zhang Y, Lin Z, Wang M, Huang L, et al. Preoperative prediction of cytokeratin 19 expression for hepatocellular carcinoma with deep learning radiomics based on gadoxetic acid-enhanced magnetic resonance imaging. *J Hepatocell Carcinoma*. (2021) 8:795–808. doi: 10.2147/JHC.S313879

24. Zwanenburg A, Vallières M, Abdalah MA, Aerts HJWL, Andrearczyk V, Apte A, et al. The image biomarker standardization initiative: standardized quantitative radiomics for high-throughput image-based phenotyping. *Radiology*. (2020) 295:328–38. doi: 10.1148/radiol.2020191145

25. Yang J, Dong X, Wang F, Jin S, Zhang B, Zhang H, et al. A deep learning model based on MRI for prediction of vessels encapsulating tumour clusters and prognosis in hepatocellular carcinoma. *Abdom Radiol (NY)*. (2024) 49:1074–83. doi: 10.1007/s00261-023-04141-3

26. Früh M, Fischer M, Schilling A, Gatidis S, Hepp T. Weakly supervised segmentation of tumor lesions in PET-CT hybrid imaging. *J Med Imaging (Bellingham)*. (2021) 8:054003. doi: 10.1117/1.JMI.8.5.054003

27. Reig M, Forner A, Rimola J, Ferrer-Fàbrega J, Burrel M, Garcia-Criado Á, et al. BCLC strategy for prognosis prediction and treatment recommendation: The 2022 update. *J Hepatol*. (2022) 76:681–93. doi: 10.1016/j.jhep.2021.11.018

28. Zhou J, Sun H, Wang Z, Cong W, Zeng M, Zhou W, et al. Guidelines for the diagnosis and treatment of primary liver cancer (2022 edition). *Liver Cancer*. (2023) 12:405–44. doi: 10.1159/000530495

29. Chan AWH, Zhong J, Berhane S, Toyoda H, Cucchetti A, Shi K, et al. Development of pre and post-operative models to predict early recurrence of hepatocellular carcinoma after surgical resection. *J Hepatol*. (2018) 69:1284–93. doi: 10.1016/j.jhep.2018.08.027

30. She S, Shi J, Zhu J, Yang F, Yu J, Dai K. Impact of inflammation and the immune system on hepatocellular carcinoma recurrence after hepatectomy. *Cancer Med*. (2024) 13:e7018. doi: 10.1002/cam4.7018

31. Cui H, Sun Y, Zhao D, Zhang X, Kong H, Hu N, et al. Radiogenomic analysis of prediction HER2 status in breast cancer by linking ultrasound radiomic feature module with biological functions. *J Transl Med*. (2023) 21:44. doi: 10.1186/s12967-022-03840-7

32. Wu J, Liu A, Cui J, Chen A, Song Q, Xie L. Radiomics-based classification of hepatocellular carcinoma and hepatic haemangioma on precontrast magnetic resonance images. *BMC Med Imaging*. (2019) 19:23. doi: 10.1186/s12880-019-0321-9

33. Chong H, Gong Y, Zhang Y, Dai Y, Sheng R, Zeng M. Radiomics on gadoxetate disodium-enhanced MRI: non-invasively identifying glypican 3-positive hepatocellular carcinoma and postoperative recurrence. *Acad Radiol*. (2023) 30:49–63. doi: 10.1016/j.acra.2022.04.006

34. Liu Z, Wang S, Dong D, Wei J, Fang C, Zhou X, et al. The applications of radiomics in precision diagnosis and treatment of oncology: opportunities and challenges. *Theranostics*. (2019) 9:1303–22. doi: 10.7150/thno.30309

35. Liu Y, Wang B, Mo X, Tang K, He J, Hao J. A deep learning workflow for mass-forming intrahepatic cholangiocarcinoma and hepatocellular carcinoma classification based on MRI. *Curr Oncol*. (2022) 30:529–44. doi: 10.3390/curroncol30010042

36. Parmar C, Barry JD, Hosny A, Quackenbush J, Aerts HJWL. Data analysis strategies in medical imaging. *Clin Cancer Res*. (2018) 24:3492–9. doi: 10.1158/1078-0432.CCR-18-0385

37. Huang JL, Sun Y, Wu ZH, Zhu HJ, Xia GJ, Zhu XS, et al. Differential diagnosis of hepatocellular carcinoma and intrahepatic cholangiocarcinoma based on spatial and channel attention mechanisms. *J Cancer Res Clin Oncol*. (2023) 149:10161–8. doi: 10.1007/s00432-023-04935-4

38. Wang W, Chen Q, Iwamoto Y, Han X, Zhang Q, Hu H, et al. Deep learning-based radiomics models for early recurrence prediction of hepatocellular carcinoma with multi-phase CT images and clinical data. *Annu Int Conf IEEE Eng Med Biol Soc*. (2019) 2019:4881–4. doi: 10.1109/EMBC.2019.8856356

39. Kinoshita M, Ueda D, Matsumoto T, Shinkawa H, Yamamoto A, Shiba M, et al. Deep learning model based on contrast-enhanced computed tomography imaging to predict postoperative early recurrence after the curative resection of a solitary hepatocellular carcinoma. *Cancers (Basel)*. (2023) 15:2140. doi: 10.3390/cancers15072140

40. Kucukkaya AS, Zeevi T, Chai NX, Raju R, Haider SP, Elbanan M, et al. Predicting tumor recurrence on baseline MR imaging in patients with early-stage hepatocellular carcinoma using deep machine learning. *Sci Rep*. (2023) 13:7579. doi: 10.1038/s41598-023-34439-7

41. Wang T, Chen H, Chen Z, Li M, Lu Y. Prediction model of early recurrence of multimodal hepatocellular carcinoma with tensor fusion. *Phys Med Biol*. (2024) 69. doi: 10.1088/1361-6560/ad4f45

42. Lai YC, Wu KC, Chang CJ, Chen YJ, Wang KP, Jeng LB, et al. Predicting overall survival with deep learning from 18F-FDG PET-CT images in patients with hepatocellular carcinoma before liver transplantation. *Diagnostics (Basel)*. (2023) 13:981. doi: 10.3390/diagnostics13050981

43. Yuan Q, Wei Z, Guan X, Jiang M, Wang S, Zhang S, et al. Toxicity prediction method based on multi-channel convolutional neural network. *Molecules*. (2019) 24:3383. doi: 10.3390/molecules24183383

44. Zhu M, Ren B, Richards R, Suriawinata M, Tomita N, Hassanpour S. Development and evaluation of a deep neural network for histologic classification of renal cell carcinoma on biopsy and surgical resection slides. *Sci Rep*. (2021) 11:7080. doi: 10.1038/s41598-021-86540-4

45. Li M, Fan Y, You H, Li C, Luo M, Zhou J, et al. Dual-energy CT deep learning radiomics to predict macrotrabecular-massive hepatocellular carcinoma. *Radiology*. (2023) 308:e230255. doi: 10.1148/radiol.230255

frontiers | Frontiers in Medicine

TYPE Original Research
PUBLISHED 13 November 2024
DOI 10.3389/fmed.2024.1464610

OPEN ACCESS

EDITED BY
Pradeep Kumar Shukla,
University of Tennessee Health Science Center (UTHSC), United States

REVIEWED BY
Fei Peng Conrad,
University of Texas Southwestern Medical Center, United States
Qingfei Zhang,
University of Chinese Academy of Sciences, China

*CORRESPONDENCE
Yin Cao
✉ caoyin19901@163.com
Guang Zhang
✉ zhangguang5566@163.com

†These authors have contributed equally to this work

RECEIVED 14 July 2024
ACCEPTED 28 October 2024
PUBLISHED 13 November 2024

CITATION
Hu L, Shi W, Liu K, Ma D, Xin Q, Wang Z, Cao Y and Zhang G (2024) EGFR bypass activation mediates acquired resistance to regorafenib in hepatocellular carcinoma.
Front. Med. 11:1464610.
doi: 10.3389/fmed.2024.1464610

EGFR bypass activation mediates acquired resistance to regorafenib in hepatocellular carcinoma

Lili Hu[1,2†], Weiwei Shi[1,3†], Kua Liu[4], Ding Ma[5], Qilei Xin[6], Zhongxia Wang[1], Yin Cao[1,4*] and Guang Zhang[1,4*]

[1]Division of Hepatobiliary and Transplantation Surgery, Department of General Surgery, Nanjing Drum Tower Hospital, The Affiliated Hospital of Medical School, Nanjing University, Nanjing, China, [2]Department of Oncological Surgery, The First People's Hospital of Lianyungang, The First Affiliated Hospital of Kangda College of Nanjing Medical University, Lianyungang, China, [3]Department of Obstetrics and Gynecology, School of Medicine, Zhongda Hospital, Southeast University, Nanjing, China, [4]Jiangsu Key Laboratory of Molecular Medicine, Medical School, National Institute of Healthcare Data Science at Nanjing University, Nanjing University, Nanjing, China, [5]Department of Gastroenterology, Third Xiangya Hospital, Central South University, Changsha, China, [6]Jinan Microecological Biomedicine Shandong Laboratory, Jinan, China

Background: Regorafenib, a tyrosine kinase inhibitor (TKI), is used in the treatment of unresectable hepatocellular carcinoma (HCC). However, the occurrence of acquired resistance limits its antitumor efficacy. While multiple studies have highlighted the crucial role of bypass activation in acquired TKI resistance, few have focused on bypass activation in regorafenib resistance in HCC.

Methods: High-throughput proteomics was used to identify differential proteins associated with bypass activation between acquired regorafenib-resistant cells and parental cells. The ability of epidermal growth factor receptor (EGFR) bypass inhibition to reverse resistance was evaluated both *in vitro* and *in vivo* using direct microscopic observation, the CCK-8 assay, colony formation assay, Annexin V-FITC/propidium iodide double staining, cell cycle analysis, western blotting, and a xenograft model.

Results: The expression of EGFR, a member of the receptor tyrosine kinase (RTK) family, was significantly increased in acquired regorafenib-resistant HCC cells compared with parental cells. Pharmacological inhibition of EGFR with gefitinib restored the sensitivity of regorafenib-resistant HCC cells to regorafenib. In a xenograft mouse model, gefitinib sensitized resistant tumors to regorafenib. Additionally, levels of RAS, RAF, and P-ERK1/2, components of the downstream EGFR signaling pathway, were positively associated with EGFR expression.

Conclusion: EGFR overexpression promotes acquired resistance to regorafenib through RAS/RAF/ERK bypass activation in HCC. Inhibition of EGFR restores sensitivity to regorafenib, and the combination of gefitinib and regorafenib demonstrates significant antitumor efficacy both *in vivo* and *in vitro*. These findings suggest that this combination could be a potential strategy for patients with advanced HCC.

KEYWORDS

regorafenib, acquired resistance, EGFR, bypass activation, combination therapy, HCC

1 Introduction

Based on the global cancer statistics of 2020, primary liver cancer was the sixth most commonly diagnosed cancer and the third leading cause of cancer-related death worldwide (1). Hepatocellular carcinoma (HCC) accounts for nearly 90% of all primary liver cancers (2). However, the majority of patients with HCC are diagnosed at an advanced stage, by which time they have lost the opportunity for potential curative treatments such as surgical resection or liver transplantation (3). Therefore, these patients primarily rely on systemic therapies, particularly targeted therapies (4).

Regorafenib, approved by the Food and Drug Administration (FDA) in 2017, is a second-line treatment for patients with advanced HCC (5). This drug is an oral tyrosine kinase inhibitor (TKI) that targets multiple receptor tyrosine kinases (RTKs), such as angiogenic RTKs (VEGFR-1, -2, and -3 and TIE-2), oncogenic RTKs (c-KIT and RET), stromal RTKs (PDGFR-β and FGFR1), and intracellular signaling kinases (c-RAF/RAF-1, BRAF, and BRAFV600E) (6). A clinical study demonstrated that regorafenib was the first drug to show survival benefits in patients with unresectable HCC following sorafenib failure (7). Unfortunately, most patients with HCC eventually develop acquired resistance to regorafenib after a period of treatment (8), resulting in treatment failure and tumor progression (9). Therefore, it is essential to investigate the underlying mechanisms of this resistance and explore potential strategies to overcome it.

To date, few studies have investigated acquired resistance to regorafenib in HCC. Studies on other TKIs have shown that activation of bypass signaling is a nearly universal mechanism of acquired resistance across multiple cancer types (10). Bypass activation occurs when nontargeted RTKs are overexpressed or alternative downstream compounds are abnormally activated, reducing TKI inhibition efficacy (11). For example, the downstream signaling pathways of epidermal growth factor receptor (EGFR), such as Akt or ERK, were aberrantly activated, promoting tumor cell proliferation and leading to EGFR-TKI afatinib resistance in head and neck squamous cell carcinoma (12). Increased activation of PDGFR-β and IGF-IR is frequently observed in patients with melanoma undergoing TKI treatment (13). In breast carcinoma, JNK bypass activation modulates acquired resistance to the HER2-TKI lapatinib (14). Given the prevalence of bypass activation, combining TKIs with inhibitors targeting bypass signaling has become a popular regimen for managing acquired TKI resistance (15). The key to combination therapy lies in the accurate identification of aberrantly activated bypass signaling. However, whether bypass activation is involved in acquired regorafenib resistance in HCC and which specific bypass signaling pathway is activated remains unclear.

In this study, we established regorafenib-resistant HCC cells using a stepwise dose-escalation method and identified aberrantly activated pathways through proteomic analysis. Moreover, combination therapy was used to assess whether inhibition of bypass signaling could reverse regorafenib resistance both *in vitro* and *in vivo*. This study aimed to provide an experimental foundation for the clinical therapy of regorafenib resistance in HCC.

2 Materials and methods

2.1 Cell culture

The human HCC cell lines, SMMC-7721 and MHCC97H, were purchased from the Cell Bank of the Chinese Academy of Sciences (Shanghai, China). The cells were cultured in Dulbecco's modified Eagle's medium (DMEM) supplemented with 10% fetal bovine serum, 100 units/mL penicillin, and 100 mg/mL streptomycin sulfate. They were maintained in a humidified incubator at 37°C with an atmosphere of 5% CO_2.

2.2 Establishment of regorafenib-resistant HCC cells

Acquired regorafenib-resistant HCC cells (97H-R and 7721-R) were established by treating MHCC97H and SMMC-7721 cells, respectively, with gradually increasing concentrations of regorafenib for over 6 months, as described in our previous studies (16).

2.3 CCK-8 assay

Cells (10,000 cells/well) were seeded into 96-well plates and cultured for 24 h. CCK-8 solution (10 μL/well; Selleck, Wuhan, China) was added, and the plates were incubated for 1–2 h. Then, the absorbance at 450 nm was measured using a microplate reader (Bio-Rad, CA, United States), and cell viability was determined.

2.4 Cell cycle assay

Cells (1×10^6 cells/well) were harvested after various treatments and fixed in 70% ethanol at −20°C for 2 h. After two washes with PBS and centrifugation, the cells were stained with propidium iodide (PI; 10 μg/mL) and RNase A (100 μg/mL) at room temperature for 30 min, followed by their detection using a BD FACSCalibur flow cytometer (Becton Dickinson, San Jose, CA, United States). The distribution of cells in different phases of the cell cycle was analyzed using FlowJo software (Tree Star, San Carlos, CA, United States).

2.5 Annexin V-FITC/PI double staining assay

Cells (1×10^6 cells/well) were collected and resuspended in 500 μL of binding buffer. Then, 5 μL of Annexin V-FITC staining solution and 5 μL of PI staining solution were added to the suspension, followed by incubation for 30 min at room temperature. Fluorescence intensity was measured using a BD FACSCalibur cytometer (Becton Dickinson), and the percentage of apoptotic cells was determined using FlowJo software (Tree Star).

2.6 Colony formation assay

Cells (1,000 cells/well) were plated in six-well plates and monitored for 7–14 days to assess colony growth. Afterward, the cells were fixed with 4% paraformaldehyde for 20 min, washed, and incubated with 0.4% crystal violet solution for 30 min. The cells were then washed with PBS, dried, and counted. Colonies containing more than 30 cells were included in the count.

2.7 Protein isolation and western blotting

Cells were lysed on ice for 5 min using 150 μL of lysis buffer (Beyotime, Shanghai, China) containing 1% protease inhibitors (Thermo Fisher Scientific, Waltham, MA, United States). The lysates were then harvested and centrifuged at 12,000 × g for 5 min at 4°C. Protein concentrations were determined using a BCA kit (Thermo Fisher Scientific). Equal amounts of protein (20 μg/lane) were separated by sodium dodecyl sulfate-polyacrylamide gel electrophoresis (SDS-PAGE), transferred onto polyvinylidene difluoride (PVDF) membranes, and blocked with 5% nonfat dry milk for 1 h at room temperature. Immunoblotting was performed by incubating the membranes with primary antibodies overnight at 4°C, followed by incubation with secondary antibodies the next day. Protein signals were detected using an enhanced chemiluminescence reagent (EMD Millipore, Billerica, MA, United States).

2.8 Bioinformatic analysis

Differentially expressed proteins (DEPs) were identified using the following reference thresholds: a fold change of 1.2 and a p-value of <0.05. Gene Ontology (GO) analysis was performed via the GO Database[1] using Blast2GO (version 3.3.5). The GO functions of DEPs, including biological process (BP), molecular function (MF), and cellular component (CC), were analyzed.

2.9 HCC orthotopic xenograft assay

The study protocol was approved by the Institutional Ethics Committee of the Affiliated Drum Tower Hospital, Nanjing Medical University. We sourced six-week-old male BALB/c nude mice from the Model Animal Research Center at Nanjing University and maintained them in accordance with the institution's guidelines. Two nude mice were subcutaneously injected with 1×10^7 regorafenib-resistant MHCC-97H cells in 100 μL of PBS. Once the tumors reached a volume of 100 mm^3, they were excised, dissected into 1 mm^3 segments, and implanted subcutaneously on the dorsal side near the right armpit of the mice. The mice were then randomly assigned to four groups and received oral treatments of either vehicle control, regorafenib, gefitinib, or a combination of regorafenib and gefitinib. The dosages were 20 mg/kg for regorafenib and 50 mg/kg for gefitinib, administered orally once daily for an initial period of 21 days. Body weight and tumor volume were monitored every 2 days. After 4 weeks of treatment, the mice were euthanized, and the tumors were collected for further analysis.

2.10 Hematoxylin and eosin (H&E) staining

Tissues fixed with 4% paraformaldehyde were embedded in paraffin and sectioned into 5 μm thick slices. The tissue sections were deparaffinized in xylene, rehydrated through a graded series of ethanol, and washed in PBS. They were then stained with hematoxylin, agitated for 30 s, and rinsed in water. Subsequently, they were stained with eosin, agitated for 10–30 s, and rinsed in water. After staining, the sections were dehydrated, mounted, and covered with a cover slip. Microscopic examination was performed using a microscope (BX50; Olympus, Tokyo, Japan).

2.11 Statistical analysis

PSS 19.0 statistical software (IBM Corp., Chicago, IL, United States) was used for data analysis. Data are presented as means ± SD from triplicate experiments. Comparisons between two groups were performed using the Student's t-test. Significance among multiple groups was determined by one-way analysis of variance followed by the Student–Newman–Keuls *post hoc* test. A p-value of <0.05 was considered to indicate a statistically significant difference.

3 Results

3.1 EGFR is overexpressed in regorafenib-resistant HCC cell lines

Regorafenib-resistant HCC cell lines were established using MHCC97H and SMMC-7721 cell lines through a stepwise dose-escalation method and were designated as 97H-R and 7721-R, respectively. The successful establishment of regorafenib-resistant HCC cells was confirmed using the CCK-8 assay. The IC_{50} values for regorafenib (Table 1) were markedly higher in the resistant cells (97H-R: 16.85 μM; 7721-R: 12.27 μM) compared with the parental cells (97H: 6.266 μM; 7721: 5.431 μM). Based on high-throughput proteomics analysis, we identified DEPs between MHCC97H and 97H-R cells. These DEPs were used to generate a heatmap (Figure 1A), which demonstrated a significant difference in protein expression between the resistant and parental cells. The detailed list of DEPs is provided in Supplementary Table S1. GO enrichment analysis showed that the DEPs were primarily enriched in cell division under the CC

TABLE 1 IC_{50} values of regorafenib in parental HCC cells and regorafenib-resistant HCC cells.

Cell line	IC_{50} (μM)
97H	5.378
97H-R	16.85
7721	5.431
7721R	12.27

1 http://www.geneontology.org

10.3389/fmed.2024.1464610

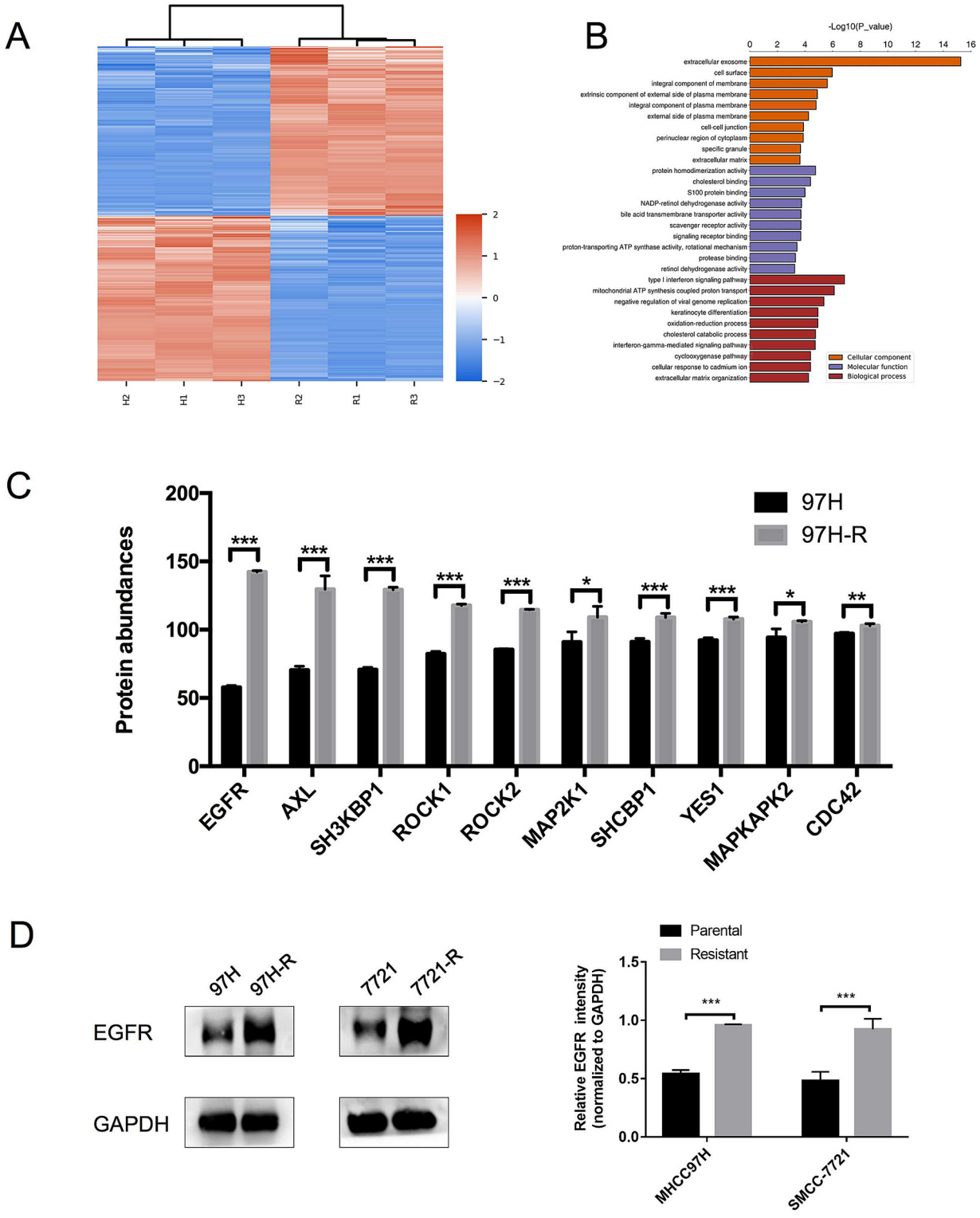

FIGURE 1
Expression levels of EGFR in regorafenib-resistant HCC cells and parental cells. (A) Volcano plot of DEPs between parental cells and regorafenib-resistant HCC cells. (B) GO enrichment analysis for DEPs. (C) The top 10 proteins associated with RTK pathways overexpressed in 97H-R cells compared with MHCC97H cells. (D) Protein expression levels of EGFR in parental and regorafenib-resistant HCC cells, as measured by western blotting. Results are representative of three independent experiments. Error bars represent the mean ± SD from a representative experiment. *$p < 0.05$ and ***$p < 0.001$.

subcategory (Figure 1B). EGFR, a key member of the tyrosine kinase receptor family, was the most overexpressed protein associated with RTK pathways. The protein level of EGFR in 97H-R cells was 2.46-fold higher than that in MHCC97H cells (Figure 1C). Western blotting analysis further confirmed that the protein expression of EGFR was significantly upregulated in regorafenib-resistant cells compared with parental cells ($p < 0.001$; Figure 1D). These results indicate that EGFR might mediate regorafenib resistance in HCC.

3.2 Pharmacological inhibition of EGFR using gefitinib restores the regorafenib sensitivity in regorafenib-resistant HCC cells

To assess the role of EGFR in regorafenib resistance in HCC, we used gefitinib, a selective inhibitor of EGFR. We first evaluated the effect of gefitinib on the viability of 97H-R and 7721-R cells using the CCK-8 assay. Treatment with gefitinib alone at concentrations up to 20 μM for 48 h had minimal inhibitory effect on the viability of 97H-R cells, while the inhibitory concentration for 7721-R cells was 10 μM (Figure 2A). However, when combined with regorafenib, the viability of 97H-R cells decreased after treatment with 20 μM gefitinib for 48 h (10 μM gefitinib for 7721-R cells; Figure 2B). The IC_{50} values for regorafenib in 97H-R and 7721-R cells also decreased following gefitinib supplementation (Table 2). These results indicate that EGFR inhibition reverses regorafenib resistance in HCC cells.

3.3 Combination of gefitinib and regorafenib exhibits strong antitumor potency *in vitro*

We further evaluated the antitumor efficacy of the combination treatment with gefitinib and regorafenib *in vitro*. The results showed that both the number and cell state of 97H-R and 7721-R cells were decreased when exposed to the combination of regorafenib and gefitinib, as observed through direct microscopy. In contrast, treatment with either regorafenib or gefitinib alone had minimal impact on the cell number or cell state of these two cell lines (Figure 3A). The proportion of apoptotic cells was significantly higher in the combination treatment group compared with the other groups (97H-R: $p < 0.001$; 7721-R: $p < 0.001$; Figure 3B). Moreover, the combination treatment increased the number of cells arrested in the G1 phase (Figure 3C) and reduced colony formation (Figure 3D) by 97H-R and 7721-R cells. To further confirm the differential effects of gefitinib and regorafenib on cell apoptosis, we measured the protein levels of two apoptotic cascade-related proteins, B-cell leukemia/lymphoma 2 (Bcl2) and cleaved poly ADP-ribose polymerase (PARP). The effects on cell proliferation were verified by examining the expression levels of cyclin D1 and cyclin-dependent kinases 2 and 4 (CDK2 and CDK4). The alterations in the

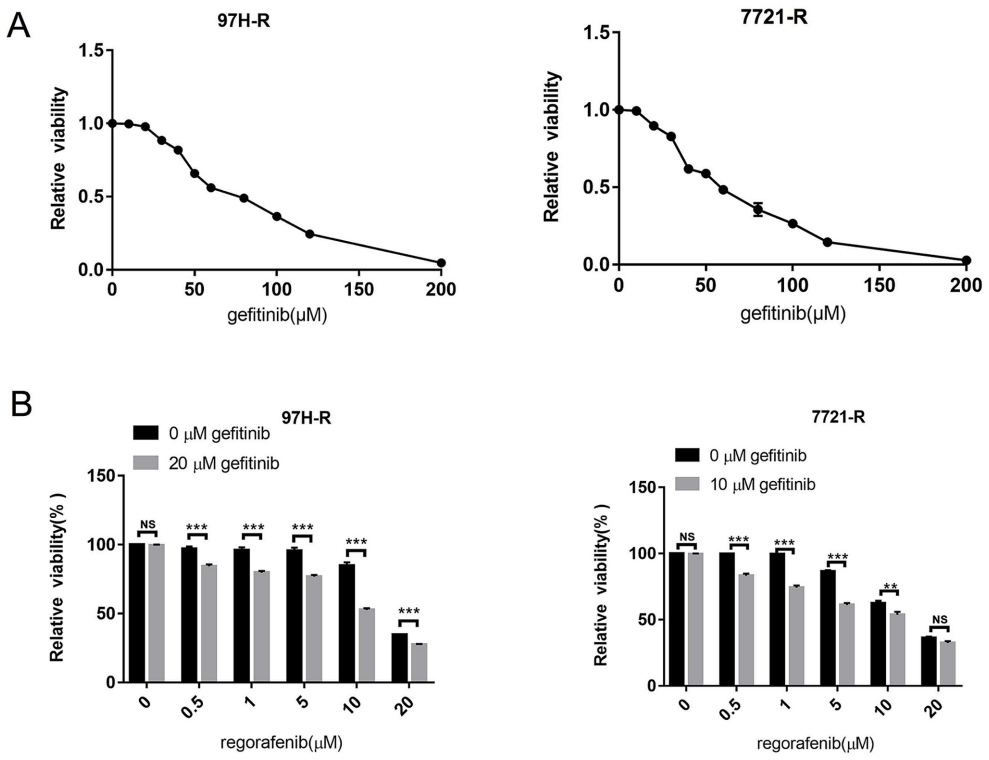

FIGURE 2
Effect of EGFR inhibition on the reversal of regorafenib resistance. (A) 97H-R cells were treated with 20 μM gefitinib, and 7721-R cells were treated with 10 μM gefitinib for 48 h. The impact of gefitinib on the viability of regorafenib-resistant HCC cells was evaluated using the CCK-8 assay. (B) The viability of regorafenib-resistant HCC cells treated with regorafenib, with or without gefitinib, was measured. The results are representative of three independent experiments. Error bars represent the mean ± SD from a representative experiment. $^{**}p < 0.01$ and $^{***}p < 0.001$.

TABLE 2 IC_{50} values of regorafenib in regorafenib-resistant HCC cells exposed to gefitinib and control group cells.

Cell line	Group	IC_{50} (μM)
97H-R	0 μM gefitinib	15.12
	20 μM gefitinib	6.156
7721-R	0 μM gefitinib	12.31
	10 μM gefitinib	7.142

protein levels of Bcl2, cleaved PARP, cyclin D1, CDK2, and CDK4 further confirmed that the combination of gefitinib and regorafenib indeed promoted cell apoptosis and inhibited the proliferation of regorafenib-resistant HCC cells (Figure 3E). These results suggest that inhibition of EGFR may reduce regorafenib resistance in HCC cells.

3.4 Gefitinib supplementation reverses regorafenib-resistant HCC tumor growth in a mouse model

This study further investigated whether inhibition of EGFR by gefitinib could reverse regorafenib resistance in a nude mouse xenograft model established with 97H-R cells. No significant difference in body weight was observed between the drug-treated mice and the vehicle-treated controls, and no mice died during the treatment, indicating minimal systemic toxicity from the drugs (Figure 4A). Furthermore, H&E staining of lung, kidney, liver and heart tissues indicated barely any difference between the groups (Supplementary Figure S1). As shown in Figures 4B,C, treatment with either regorafenib or gefitinib alone produced a mild tumor inhibitory effect compared with the vehicle control, while the combination of the two drugs significantly inhibited tumor growth. The volume and weight of the tumors at the end confirmed that supplementation with gefitinib sensitized regorafenib-resistant HCC tumors to regorafenib treatment (Figure 4D). These results indicate that combination therapy with gefitinib and regorafenib exerts a strong tumor-inhibitory effect *in vivo*.

3.5 EFGR regulates acquired regorafenib resistance in HCC via RAS/RAF/ERK signaling activation

Although we confirmed that EGFR overexpression promotes acquired regorafenib resistance in HCC, the underlying molecular mechanisms remained unclear. Previous studies have identified the RAS/RAF/ERK signaling as an important downstream pathway of EGFR (17, 18). Therefore, we first measured the protein levels of RAS, c-RAF, and ERK1/2, as well as the phosphorylation of ERK1/2, in regorafenib-resistant cells (97H-R and 7721-R) and their corresponding parental cells (MHCC97H and SMMC-7721). No significant differences in ERK1/2 protein levels were observed between MHCC97H and 97H-R cells; however, the protein levels of RAS, c-RAF, and P-ERK1/2 were markedly higher in 97H-R cells compared with those in MHCC97H cells (Figure 5A). Similar results were obtained for SMMC-7721 and 7721-R cells. Additionally, we assessed the protein levels of RAS, c-RAF, ERK1/2, and P-ERK1/2 following EGFR inhibition by gefitinib in 97H-R and 7721-R cells. EGFR inhibition significantly reduced the elevated expression of RAS, c-RAF, and P-ERK1/2. Furthermore, these protein levels were significantly decreased after combined treatment with regorafenib and gefitinib (Figure 5B). These findings indicate that EGFR overexpression promotes regorafenib resistance by activating the RAS/RAF/ERK signaling pathway.

4 Discussion

Acquired resistance is a highly complex challenge in cancer treatment that limits the effectiveness of TKI therapies (19). Multiple mechanisms mediate the acquired resistance to regorafenib in HCC, such as immunosuppression (20), gut microbiome (21), and oxidative stress (22). However, the key factor driving this resistance remains unknown. This study is the first to demonstrate that EGFR plays a crucial role in mediating acquired resistance to regorafenib through activation of the RAS/RAF/ERK pathway in HCC. In addition, gefitinib, a selective inhibitor of EGFR, showed high potential to enhance the sensitivity of regorafenib-resistant HCC cells to regorafenib.

EGFR belongs to the subfamily of RTKs. Ligand binding induces EGFR dimerization, leading to the phosphorylation of intracellular tyrosine residues, which activates downstream pathways that regulate critical BPs, such as cell proliferation, migration, metastasis, and survival (23). Abnormal expression or activation of EGFR and its downstream pathways is common in various cancers, such as gastric cancer (24), colorectal cancer (25), and breast cancer (26). In HCC, high EGFR expression has been associated with poor prognosis (27). Moreover, Jin et al. (28) reported that EGFR activation limits the response of patients with HCC to lenvatinib (another TKI used for HCC therapy) and that EGFR inhibition sensitizes HCC to lenvatinib. However, it remains unclear whether EGFR mediates acquired regorafenib resistance in HCC. Our study is the first to show that EGFR is overexpressed in regorafenib-resistant HCC cells. To further investigate the role of EGFR in the acquired resistance of HCC to regorafenib, we performed various *in vitro* and *in vivo* experiments to determine whether EGFR inhibition by gefitinib could restore regorafenib sensitivity in HCC. We found that the combination of regorafenib with gefitinib significantly inhibited the growth and proliferation of regorafenib-resistant HCC cells and induced cell apoptosis. Upon EGFR inhibition by gefitinib, the IC_{50} of regorafenib for the two types of acquired-resistant cells decreased significantly. Additionally, our experimental results demonstrated that the combination therapy of regorafenib and gefitinib markedly inhibited tumor growth in a xenograft model of regorafenib-resistant HCC cells, compared with treatment with regorafenib or gefitinib alone. Taken together, these findings confirm that EGFR overexpression facilitates regorafenib resistance in HCC. Furthermore, our results suggest that the EGFR inhibitor gefitinib has the potential to reverse regorafenib resistance, offering significant clinical value for the treatment of regorafenib-resistant patients with HCC. Although regorafenib and gefitinib target different tyrosine kinases, there is an overlap in the intracellular signaling pathways they inhibit, such as the RAS/RAF/ERK and PI3K/Akt pathways (29, 30). On the one side, this may contribute to the synergistic antitumor effect of the

10.3389/fmed.2024.1464610

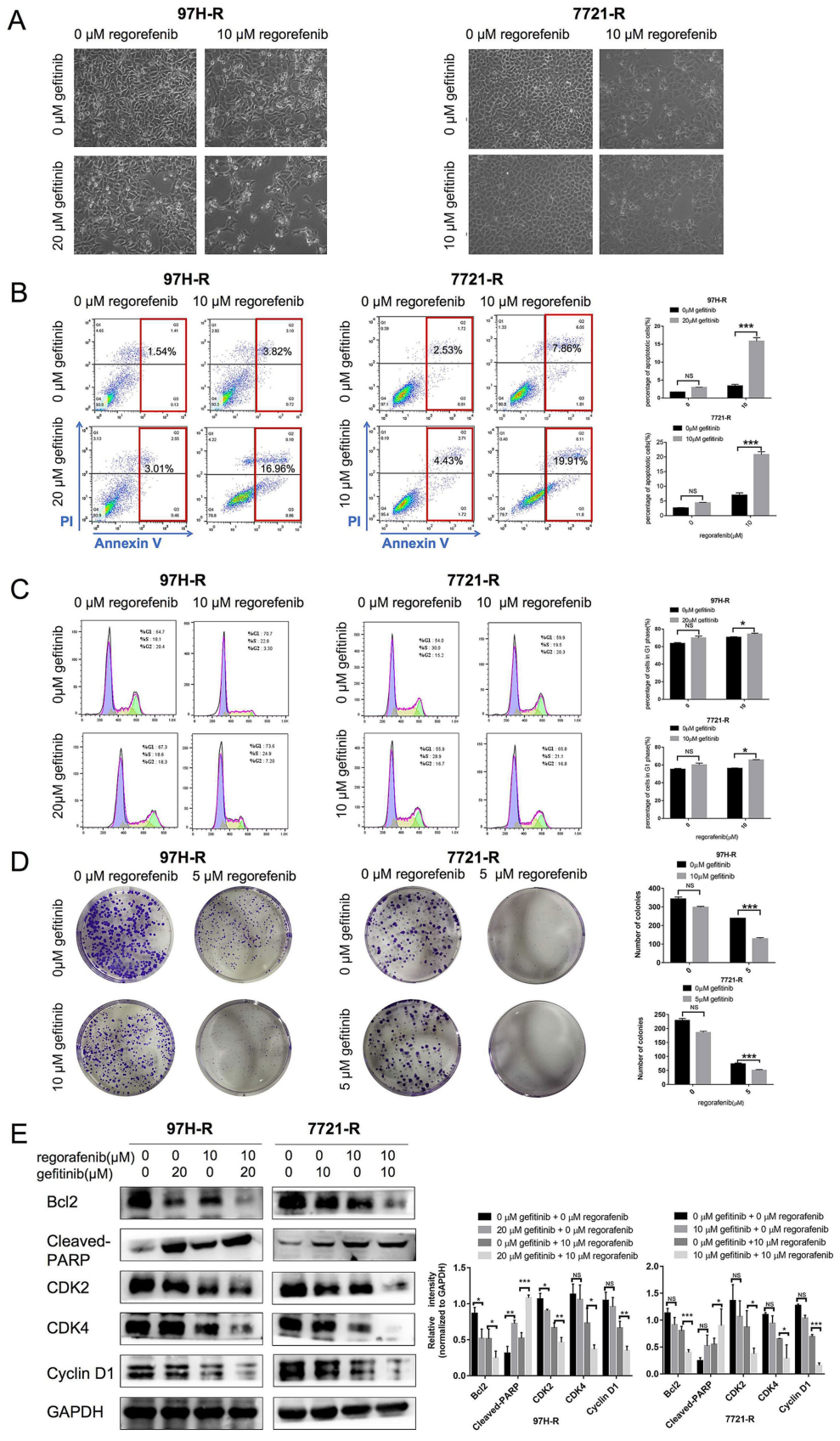

FIGURE 3
Effect of regorafenib and gefitinib combination treatment on the proliferation and apoptosis of regorafenib-resistant HCC cells. (A) Regorafenib-resistant HCC cells were treated with gefitinib and regorafenib for 48 h. Representative images of cell morphology were captured. Subsequently, (B) the

(Continued)

FIGURE 3 (Continued)
apoptosis rate was measured using the Annexin V-FITC/PI double-staining assay. (C) Cell cycle distribution was analyzed by flow cytometry, and (D) cell proliferation was evaluated using the colony formation assay. (E) The expression levels of Bcl-2, cleaved PARP, cyclin D1, CDK2, and CDK4 were examined by western blotting. The concentrations of regorafenib and gefitinib in all assays for 97H-R cells were 10 and 20 μM for 48 h, respectively, except for the colony formation assay (5 and 10 μM, 10 days). For all assays in 7721-R cells, the concentrations were 10 and 10 μM for 48 h, respectively, except for the colony formation assay (5 and 5 μM, 10 days). The results represent three independent experiments. Error bars indicate the mean ± SD from a representative experiment. *$p < 0.05$, **$p < 0.01$, and ***$p < 0.001$.

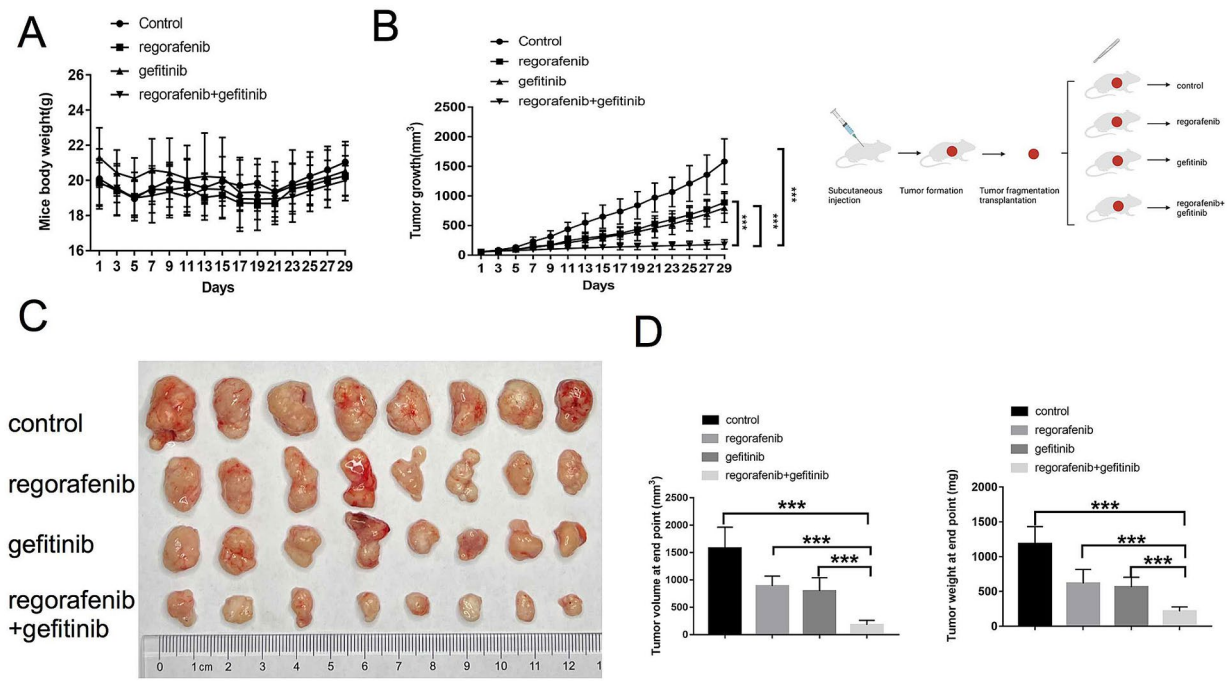

FIGURE 4
Effects of regorafenib resistance reversal by gefitinib in a xenograft nude mouse model of HCC. (A) Body weight of nude mice during drug treatment. (B) Tumor growth of subcutaneous xenograft tumors in nude mice during drug treatment. (C) Images of tumors harvested from nude mice treated with vehicle, regorafenib, gefitinib, or a combination of regorafenib and gefitinib. (D) Average volume and weight of subcutaneous xenograft tumors harvested from nude mice at the study's endpoint. Error bars represent the mean ± SD. **$p < 0.01$ and *$p < 0.001$.

regorafenib and gefitinib combination in HCC (31). On the other hand, the abnormal activation of these same target cellular pathways has the potential to induce cross-resistance to both drugs (32). In our study, the regorafenib-resistant HCC cells did not develop resistance to gefitinib. One possible explanation is that gefitinib's inhibitory effect on the RAS/RAF/ERK is stronger than that of regorafenib.

Bypass activation is a critical cause of acquired TKI resistance, which reactivates key downstream signals to promote cancer cell proliferation and/or survival despite the inhibition of the original targets (33). EGFR, a member of the RTK family, is not a target of regorafenib but is overexpressed in regorafenib-resistant HCC cells. We hypothesized that EGFR bypass activation regulates acquired regorafenib resistance in HCC, though the key downstream signal of EGFR remains unknown. This study demonstrates that the RAS/RAF/ERK pathway plays a role in the acquired resistance to regorafenib in HCC. Western blot analysis showed higher levels of RAS, c-RAF, and P-ERK1/2 in regorafenib-resistant cells compared with parental cells. Since inhibition of the RAS/RAF/ERK pathway is a primary antitumor mechanism of regorafenib, EGFR overexpression-mediated activation of the RAS/RAF/ERK pathway counteracts regorafenib's inhibitory effects, resulting in acquired resistance in HCC. Similar bypass activation phenomena have been observed in acquired erlotinib resistance in non-small cell lung cancer (NSCLC), where AXL, an RTK subfamily member, increased and activated Akt/MAPK downstream signaling, leading to a loss of erlotinib's effectiveness in blocking the Akt/MAPK pathway (34). Bypass IGF1R/RAS/RAF/ERK activation has also been reported to drive sorafenib resistance in HCC (35). Although we identified EGFR/RAS/RAF/ERK bypass activation as a contributor to acquired regorafenib resistance in HCC, the reasons for EGFR overexpression remain unclear. Further experiments are needed to explore the underlying mechanisms.

5 Conclusion

Collectively, our findings suggest that EGFR overexpression mediates acquired resistance to regorafenib in HCC through downstream RAS/

10.3389/fmed.2024.1464610

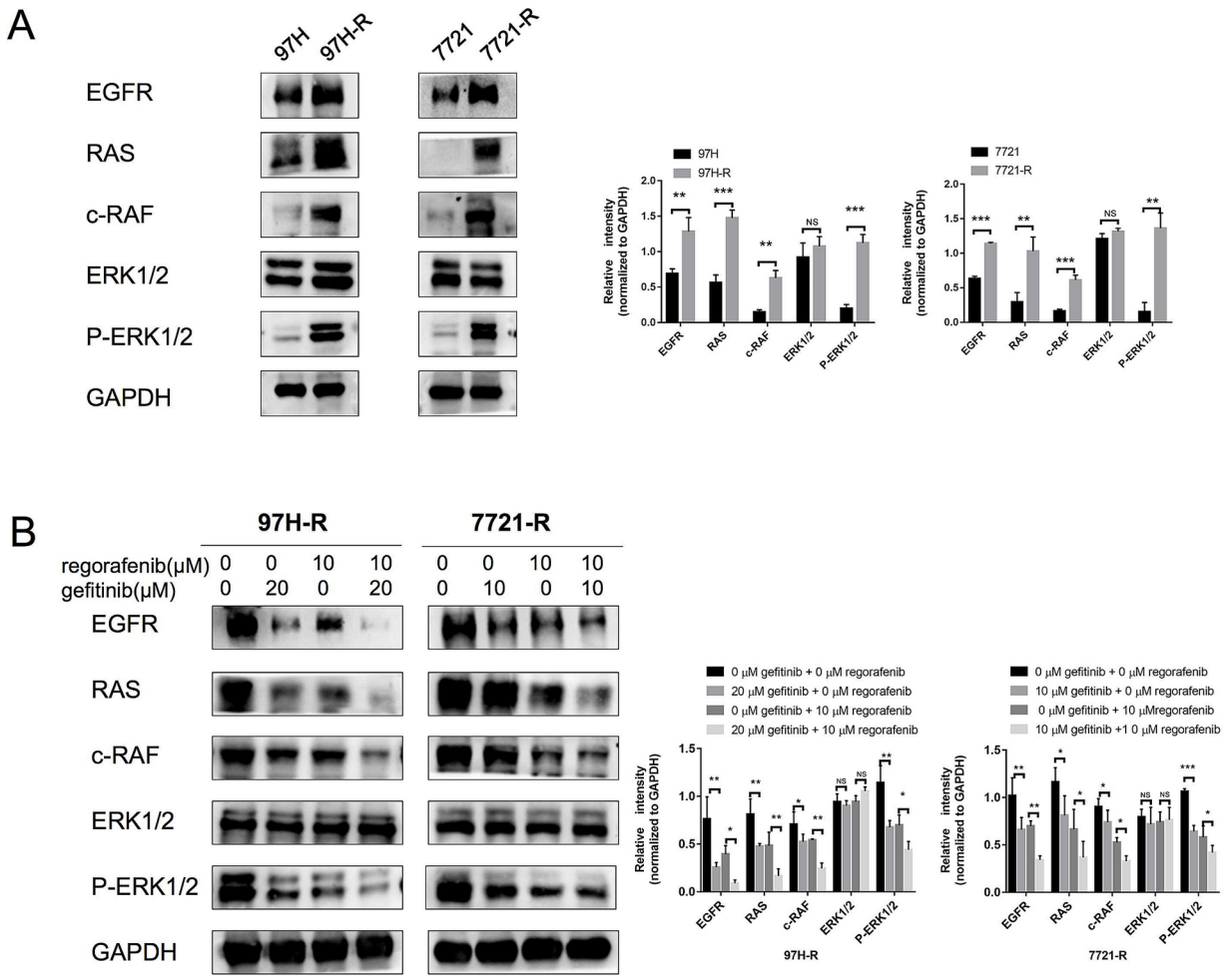

FIGURE 5
Protein levels of RAS, c-RAF, and ERK1/2 and the phosphorylation level of ERK1/2 in HCC cells. (A) The expression levels of RAS, c-RAF, ERK1/2, and P-ERK1/2 in both parental and regorafenib-resistant HCC cells were examined by western blotting. (B) 97H-R cells were treated with 10 μM regorafenib and 20 μM gefitinib for 48 h, while 7721-R cells were treated with 10 μM regorafenib and 10 μM gefitinib for 48 h. The expression levels of RAS, c-RAF, ERK1/2, and P-ERK1/2 were then examined. Error bars represent the mean ± SD from a representative experiment. *$p < 0.05$, **$p < 0.01$, and ***$p < 0.001$.

RAF/ERK bypass activation. Most notably, the combination of regorafenib with gefitinib inhibits proliferation and promotes apoptosis in regorafenib-resistant HCC cells, indicating that EGFR inhibition by gefitinib has the potential to overcome acquired resistance to regorafenib treatment. Our study provides new insights into therapeutic strategies for patients with advanced HCC exhibiting regorafenib resistance.

Data availability statement

The raw data supporting the conclusions of this article will be made available by the authors, without undue reservation.

Ethics statement

The animal study was approved by the Ethics Committee of the Drum Tower Clinical College of Nanjing Medical University (2016-057-01). Animal experiments were also approved by the Animal Ethics Committee of Nanjing Medical University (Nanjing, China) (Approval Code: 2111041, Approval Date: 17 November 2021). Animal experiments is conducted in accordance with ARRIVE Guidelines and the US Public Health Service Policy on the Humane Care and Use of laboratory animals. The study was conducted in accordance with the local legislation and institutional requirements.

Author contributions

LH: Investigation, Writing – original draft. WS: Investigation, Writing – original draft. KL: Formal analysis, Writing – original draft. DM: Investigation, Writing – original draft. QX: Investigation, Writing – original draft. ZW: Funding acquisition, Validation, Writing – review & editing. YC: Writing – review & editing. GZ: Data curation, Project administration, Writing – review & editing.

Funding

The author(s) declare that financial support was received for the research, authorship, and/or publication of this article. The research was supported by the Shandong Provincial Laboratory Project (SYS202202); the National Natural Science Foundation of China (82272819 and 81972888); the Research Project of Jinan Microecological Biomedicine Shandong Laboratory (JNL202219B, JNL202204A, and JNL2023017D); the Primary Research & Development Plan of Jiangsu Province (BE2022840); and the Open Project of Chinese Materia Medica First-Class Discipline of Nanjing University of Chinese Medicine (2020YLXK007).

Conflict of interest

The authors declare that the research was conducted in the absence of any commercial or financial relationships that could be construed as a potential conflict of interest.

Publisher's note

Supplementary material

The Supplementary material for this article can be found online at: https://www.frontiersin.org/articles/10.3389/fmed.2024.1464610/full#supplementary-material

SUPPLEMENTARY DATA SHEET 1
DEPs between MHCC97H and 97H-R cells.

SUPPLEMENTARY FIGURE 1
HE staining of lung, kidney, liver and heart.

References

1. Sung H, Ferlay J, Siegel RL, Laversanne M, Soerjomataram I, Jemal A, et al. Global cancer statistics 2020: GLOBOCAN estimates of incidence and mortality worldwide for 36 cancers in 185 countries. *CA Cancer J Clin*. (2021) 71:209–49. doi: 10.3322/caac.21660

2. Sia D, Villanueva A, Friedman SL, Llovet JM. Liver cancer cell of origin, molecular class, and effects on patient prognosis. *Gastroenterology*. (2017) 152:745–61. doi: 10.1053/j.gastro.2016.11.048

3. Raoul JL, Forner A, Bolondi L, Cheung TT, Kloeckner R, de Baere T. Updated use of TACE for hepatocellular carcinoma treatment: how and when to use it based on clinical evidence. *Cancer Treat Rev*. (2019) 72:28–36. doi: 10.1016/j.ctrv.2018.11.002

4. Chakraborty E, Sarkar D. Emerging therapies for hepatocellular carcinoma (HCC). *Cancers*. (2022) 14:2798. doi: 10.3390/cancers14112798

5. Fan Y, Xue H, Zheng H. Systemic therapy for hepatocellular carcinoma: current updates and outlook. *J Hepatocell Carcinoma*. (2022) 9:233–63. doi: 10.2147/jhc.S358082

6. Teufel M, Seidel H, Köchert K, Meinhardt G, Finn RS, Llovet JM, et al. Biomarkers associated with response to regorafenib in patients with hepatocellular carcinoma. *Gastroenterology*. (2019) 156:1731–41. doi: 10.1053/j.gastro.2019.01.261

7. Bruix J, Qin S, Merle P, Granito A, Huang YH, Bodoky G, et al. Regorafenib for patients with hepatocellular carcinoma who progressed on sorafenib treatment (RESORCE): a randomised, double-blind, placebo-controlled, phase 3 trial. *Lancet*. (2017) 389:56–66. doi: 10.1016/s0140-6736(16)32453-9

8. Jiang L, Li L, Liu Y, Lu L, Zhan M, Yuan S, et al. Drug resistance mechanism of kinase inhibitors in the treatment of hepatocellular carcinoma. *Front Pharmacol*. (2023) 14:1097277. doi: 10.3389/fphar.2023.1097277

9. Xing R, Gao J, Cui Q, Wang Q. Strategies to improve the antitumor effect of immunotherapy for hepatocellular carcinoma. *Front Immunol*. (2021) 12:783236. doi: 10.3389/fimmu.2021.783236

10. Noguchi K. Novel mechanisms of resistance to investigational molecularly targeted drugs. *Yakugaku Zasshi*. (2017) 137:151–60. doi: 10.1248/yakushi.16-00229-6

11. Alexander PB, Wang XF. Resistance to receptor tyrosine kinase inhibition in cancer: molecular mechanisms and therapeutic strategies. *Front Med*. (2015) 9:134–8. doi: 10.1007/s11684-015-0396-9

12. Wang D, Chen Y, Huang J, Zhang Y, Sun C, Shen Y. Glucocorticoid reduces the efficacy of afatinib on the head and neck squamous cell carcinoma. *Biocell*. (2023) 47:329–38. doi: 10.32604/biocell.2023.023489

13. Wang XD, Kim C, Zhang Y, Rindhe S, Cobb MH, Yu Y. Cholesterol regulates the tumor adaptive resistance to MAPK pathway inhibition. *J Proteome Res*. (2021) 20:5379–91. doi: 10.1021/acs.jproteome.1c00550

14. Manole S, Richards EJ, Meyer AS. JNK pathway activation modulates acquired resistance to EGFR/HER2-targeted therapies. *Cancer Res*. (2016) 76:5219–28. doi: 10.1158/0008-5472.Can-16-0123

15. Drilon A, Sharma MR, Johnson ML, Yap TA, Gadgeel S, Nepert D, et al. SHP2 inhibition sensitizes diverse oncogene-addicted solid tumors to re-treatment with targeted therapy. *Cancer Discov*. (2023) 13:1789–801. doi: 10.1158/2159-8290.Cd-23-0361

16. Shi W, Zhang S, Ma D, Yan D, Zhang G, Cao Y, et al. Targeting SphK2 reverses acquired resistance of regorafenib in hepatocellular carcinoma. *Front Oncologia*. (2020) 10:694. doi: 10.3389/fonc.2020.00694

17. Hong CS, Sun EG, Choi JN, Kim DH, Kim JH, Ryu KH, et al. Fibroblast growth factor receptor 4 increases epidermal growth factor receptor (EGFR) signaling by inducing amphiregulin expression and attenuates response to EGFR inhibitors in colon cancer. *Cancer Sci*. (2020) 111:3268–78. doi: 10.1111/cas.14526

18. He M, Wang X, Chen W, Zhang J, Xiong Y, Cao L, et al. PTPIP51 inhibits non-small-cell lung cancer by promoting PTEN-mediated EGFR degradation. *Life Sci*. (2022) 297:120293. doi: 10.1016/j.lfs.2021.120293

19. Holohan C, Van Schaeybroeck S, Longley DB, Johnston PG. Cancer drug resistance: an evolving paradigm. *Nat Rev Cancer*. (2013) 13:714–26. doi: 10.1038/nrc3599

20. Li Q, Zhao Z, Pei F, Kang C, Duan F. IKBIP is a predictive biomarker related to immunosuppressive microenvironment in digestive system malignancies. *Discov Med*. (2023) 35:57–72. doi: 10.24976/Discov.Med.202335174.7

21. Guo C, Kong L, Xiao L, Liu K, Cui H, Xin Q, et al. The impact of the gut microbiome on tumor immunotherapy: from mechanism to application strategies. *Cell Biosci*. (2023) 13:188. doi: 10.1186/s13578-023-01135-y

22. Zhuang Y, Liu K, He Q, Gu X, Jiang C, Wu J. Hypoxia signaling in cancer: implications for therapeutic interventions. *MedComm*. (2020) 2023:e203. doi: 10.1002/mco2.203

23. Levantini E, Maroni G, Del Re M, Tenen DG. EGFR signaling pathway as therapeutic target in human cancers. *Semin Cancer Biol*. (2022) 85:253–75. doi: 10.1016/j.semcancer.2022.04.002

24. Cui F, Zhang X. Correlation between the overexpression of epidermal growth factor receptor and pathological features of gastric cancer: a meta-analysis. *Transl Cancer Res*. (2021) 10:406–16. doi: 10.21037/tcr-20-2035

25. Deng YM, Zhao C, Wu L, Qu Z, Wang XY. Cannabinoid receptor-1 suppresses M2 macrophage polarization in colorectal cancer by downregulating EGFR. *Cell Death Discov*. (2022) 8:273. doi: 10.1038/s41420-022-01064-8

26. Vieira P, Jesus V, Cândido MA, Pacheco-Soares C, Castilho M, Raniero L. Specific nanomarkers fluorescence: *in vitro* analysis for EGFR overexpressed cells in triple-negative breast cancer and malignant glioblastoma. *Photodiagn Photodyn Ther*. (2022) 39:102997. doi: 10.1016/j.pdpdt.2022.102997

27. Nikolova D, Trajkovska M, Trpcevska EN, Eftimov A, Jovanovik R, Janevska V. Epidermal growth factor receptor immunohistochemical expression in hepatocellular carcinoma without epidermal growth factor receptor exons 18–21 mutations. *Rom J Intern Med*. (2022) 60:153–9. doi: 10.2478/rjim-2022-0006

28. Jin H, Shi Y, Lv Y, Yuan S, Ramirez CFA, Lieftink C, et al. EGFR activation limits the response of liver cancer to lenvatinib. *Nature*. (2021) 595:730:734. doi: 10.1038/s41586-021-03741-7

29. Subramonian D, Phanhthilath N, Rinehardt H, Flynn S, Huo Y, Zhang J, et al. Regorafenib is effective against neuroblastoma *in vitro* and *in vivo* and inhibits the RAS/MAPK, PI3K/Akt/mTOR and Fos/Jun pathways. *Br J Cancer*. (2020) 123:568–79. doi: 10.1038/s41416-020-0905-8

30. Yi YW, Hong W, Kang HJ, Kim HJ, Zhao W, Wang A, et al. Inhibition of the PI3K/AKT pathway potentiates cytotoxicity of EGFR kinase inhibitors in triple-negative breast cancer cells. *J Cell Mol Med*. (2013) 17:648–56. doi: 10.1111/jcmm.12046

31. Pasini F, Fraccon AP, Modena Y, Bencivenga M, Giacopuzzi S, La Russa F, et al. Targeted therapies for advanced and metastatic adenocarcinoma of the gastroesophageal junction: is there something new? *Gastric Cancer*. (2017) 20:31–42. doi: 10.1007/s10120-016-0626-0

32. Afshar S, Sedighi Pashaki A, Najafi R, Nikzad S, Amini R, Shabab N, et al. Cross-resistance of acquired radioresistant colorectal cancer cell line to gefitinib and regorafenib. *Iran J Med Sci*. (2020) 45:50–8. doi: 10.30476/ijms.2019.44972

33. Aldonza MBD, Reyes RDD, Kim YS, Ku J, Barsallo AM, Hong JY, et al. Chemotherapy confers a conserved secondary tolerance to EGFR inhibition via AXL-mediated signaling bypass. *Sci Rep*. (2021) 11:8016. doi: 10.1038/s41598-021-87599-9

34. Wang F, Liu X, Bartholdy BA, Cheng H, Halmos B. Blockade of AXL activation overcomes acquired resistance to EGFR tyrosine kinase inhibition in non-small cell lung cancer. *Transl Cancer Res*. (2019) 8:2425–38. doi: 10.21037/tcr.2019.09.61

35. Xu Y, Huang J, Ma L, Shan J, Shen J, Yang Z, et al. MicroRNA-122 confers sorafenib resistance to hepatocellular carcinoma cells by targeting IGF-1R to regulate RAS/RAF/ERK signaling pathways. *Cancer Lett*. (2016) 371:171–81. doi: 10.1016/j.canlet.2015.11.034

frontiers | Frontiers in Pharmacology

TYPE Original Research
PUBLISHED 06 January 2025
DOI 10.3389/fphar.2024.1449603

OPEN ACCESS

EDITED BY
Marcello Dallio,
University of Campania Luigi Vanvitelli, Italy

REVIEWED BY
Song Yang,
Capital Medical University, China
Dong Ji,
Peking University, China
Yuanxin Shi,
Affiliated Hospital of Zunyi Medical University, China

*CORRESPONDENCE
Zhiyun Yang,
yangzhiyun66@163.com

†These authors have contributed equally to this work

RECEIVED 15 June 2024
ACCEPTED 13 December 2024
PUBLISHED 06 January 2025

CITATION
Yan H, Zhou D, Liu X, Wang P, Jiang T and Yang Z (2025) Survival analysis of patients with hepatocellular carcinoma based on the ratio of platelet count to spleen diameter.
Front. Pharmacol. 15:1449603.
doi: 10.3389/fphar.2024.1449603

Survival analysis of patients with hepatocellular carcinoma based on the ratio of platelet count to spleen diameter

Huiwen Yan[1†], Dongdong Zhou[1,2†], Xiaoli Liu[1†], Peng Wang[1], Tingting Jiang[1] and Zhiyun Yang[1*]

[1]Center for Integrative Medicine, Beijing Ditan Hospital, Capital Medical University, Beijing, China, [2]Rehabilitation Medicine, People's Hospital of Daxing'anling Region, Daxing'anling, Heilongjiang, China

Background: In China, 80% of Hepatocellular Carcinoma (HCC) is associated with cirrhosis. Portal hypertension, the most common outcome of cirrhosis progression, has a high incidence. Platelet count/spleen diameter ratio (PSL) with a cut-off value of 909 can predict the presence of esophagogastric varices and thus portal hypertension, which is also an independent risk factor for early recurrence and late recurrence of hepatocellular carcinoma after resection. Therefore, the effect of PSL on the overall survival (OS) of patients with HCC is necessary. The aim of this study was to apply a new method to establish and validate a model for predicting the prognosis of patients based on PSL with HCC.

Methods: A total of 1,104 patients with clinical diagnosed with HCC following non-surgical therapy randomly divided the patients into a primary cohort and a validation cohort in a ratio of 7:3, in which 772 HCC patients were in the primary cohort and a total of 332 HCC patients were in the validation cohort. Through Lasso-Cox analysis, the independent predictors of OS of training cohort were included in nomogram1, and the independent predictors of Cox regression analysis were included in nomogram2. Nomogram1 and nomogram2 used consistency index (C-index), AUC and time-dependent ROC curves in the training cohort, respectively, and the calibration curves were plotted. All suggest that nomogram1 is better than nomogram2. We get similar results in the validation cohort.

Results: The C-index of nomogram1was 0.792 (95%CI: 0.772–0.812), which was superior to nomogram2 (0.788) and traditional modes (0.631–0.712). The AUC of nomogram1 was 0.866 (95%CI: 0.840–0.889). In the validation cohort, the nomogram1 still gave good discrimination (C-index: 0.769, 95%CI: 0.740–0.798; AUC: 0.867, 95%CI: 0.826–0.902). Calibration plots for 3-year OS probabilities showed the good agreement between nomogram1 predictions and actual observations. In addition, we found that the decision curve analysis of nomogram1 and nomogram2 was also meaningful.

Conclusion: Novel nomogram containing PSL, based on LASSO Cox regression, had higher predictive efficacy for 3-year overall survival in patients with HCC.

KEYWORDS

hepatocellular carcinoma, the ratio of platelet count to spleen diameter, LASSO Cox regression, nomogram, prognosis

Background

According to the latest global cancer statistics for 2021, Hepatocellular Carcinoma (HCC) is the fourth leading cause of cancer death worldwide (Sung et al., 2021). There are about 906,000 new cases of HCC and 803,000 deaths each year. Among them, the death rate of HCC patients in China accounts for half of the global total (Torre et al., 2015). Therefore, HCC is a major public health problem in China. Platelet count is an independent risk factor for the development of HCC, which may be involved in the development (Akuta et al., 2012; Wang et al., 2013), progression and metastasis of HCC (Franco et al., 2015; Menter et al., 2014). However, the relationship between PLT and HCC prognosis remains controversial. Some studies have found that patients with low PLT have poor prognosis after HCC. (Wu et al., 2012; Roayaie et al., 2013). At the same time, studies have found that HCC patients with high PLT have a high risk of tumor metastasis and vascular invasion and are associated with poor prognosis (Morimoto et al., 2014; Lee et al., 2015). However, the etiology may affect platelets, such as long-term drinking can inhibit bone marrow tissue hyperplasia and hepatitis B virus can affect platelets, so this single index is not stable. In recent years, it has been proposed that the ratio of platelet count (PC) to spleen diameter (SD) (PSL) is better than a single index. Taking 909 as the cutoff value, the presence of esophagogastric varices can be accurately predicted, with a negative predictive value (NPV) of 100%, and the degree of varices can also be evaluated (Colli et al., 2017). Blood routine examination and abdominal B-ultrasound examination are both extremely routine clinical examinations, and the data are easy to obtain, reproducible, and do not increase additional costs, which has obvious cost-benefit advantages (Mangone et al., 2012). Meanwhile, Marasco et al. (2019) showed that PSL < 909 was an independent risk factor for early recurrence and late recurrence after HCC resection, which was related to the prognosis of HCC. However, the study was limited to patients undergoing surgery. Therefore, it is necessary to investigate the effect of PSL on overall survival (OS) of HCC patients.

Predicting the prognosis of HCC patients and grading their risk, and early intervention of patients are effective strategies to improve the survival of HCC patients. The current prognostic models for HCC patients mainly include Okuda, TNM, BCLC, Child and CLIP. The predictors of these prognostic models mainly focused on tumor burden, liver function, life status, etc. At the same time, these classical models were built earlier and contain relatively single predictors, so their predictive effect on some specific groups is unknown (Dongdong et al., 2020). Therefore, it is necessary to use new methods to screen out more comprehensive prognostic predictors and construct simple visual prognostic prediction models.

The least absolute shrinkage and selection operator (LASSO) Cox regression is a method for variable selection and contraction in Cox proportional hazards model proposed by Tibshirani (1997) in 1997. LASSO Cox regression analysis was used to construct the penalty function and obtain a more refined model. Our team applied Lasso Cox regression to screen model factors for patients with A-fetoprotein-negative liver cancer, and the prediction effect of the constructed model was significantly higher than other prognostic prediction models (Zhou et al., 2021). However, the use of LASSO Cox regression model of liver cancer patients to screen factors, and then build models, its predictive effect due to other prognostic models, to be further verified.

The aim of this study was to analyze the relationship between platelet count to spleen diameter ratio and prognosis of patients with liver cancer, and to construct a model including platelet count to spleen diameter ratio to predict long-term survival of patients with liver cancer using LASSO Cox regression. In addition, the constructed model was compared with the traditional staging system to determine whether it could provide more accurate prognostic prediction. According to the constructed LASSO Cox regression model, different prognostic risk groups were identified, and early intervention was carried out to reduce the mortality of patients.

Methods

Patient selection

A retrospective study was conducted on 2,580 patients with HCC treated at Beijing Ditan Hospital of Capital Medical University from January 2012 to December 2017. The Ethics Committee of Beijing Ditan Hospital approved the study and waived the requirement for informed consent. Patients with HCC were initially included based on the results of ultrasound, computed tomography (CT), and magnetic resonance imaging (MRI). The exclusion criteria were: (1) human immunodeficiency virus (HIV) infection; (2) metastatic liver cancer; (3) incomplete data; and (4) having undergone radical surgical treatments.

Patients who underwent radical surgical treatments were excluded to focus on the prognostic assessment of those receiving non-surgical therapies. This focus allows for the development of a prognostic model tailored to patients who are not candidates for surgery, which is particularly important since a substantial proportion of HCC patients present at an advanced stage or have comorbidities precluding surgical intervention.

The definition of comprehensive treatment with traditional Chinese medicine (TCM) was the documented use of TCM in medical records after the diagnosis of HCC. Finally, 1,104 HCC patients with complete clinical data were randomly divided into a training cohort and a validation cohort in a ratio of 7:3. The follow-up period for this study was 3 years or until the patient's death, with the final deadline for follow-up set as December 2020.

Demographics and clinical data

The data provided by patients for the first visit include: general background, such as gender, age, smoking history, drinking history, family history of HBV, family history of HCC, traditional Chinese medicine (TCM), etiology; Laboratory indicators like white blood cell count (WBC), neutrophil to lymphocyte ratio (NLR), red blood cell count (WBC), hemoglobin (HGB), platelet (PLT), platelet count/spleen diameter ratio (PSL), alanine aminotransferase (ALT), aspartate aminotransferase (AST), total bilirubin (TBIL), albumin (ALB), lactate dehydrogenase (LDH), gamma-glutamyl transpeptidase (GGT), alkaline phosphatase (ALP), acetylcholinesterase (CHE), total cholesterol (TC), triglyceride

TABLE 1 Characteristics of the clinical profile of the modeling group and validation group of patients with HCC.

Characters	Training cohort (n = 772)	Validation cohort group (n = 332)	*p*-value
General Features			
Gender (Female/Male)	152/620 (19.7/80.3)	66/266 (19.9/80.1)	0.942
Age (<50/≥50)	173/599 (22.4/77.6)	68/264 (20.5/79.5)	0.477
Smoke (No/Yes)	465/307 (60.2/39.8)	201/131 (60.5/39.5)	0.923
Drink (No/Yes)	481/291 (62.3/37.7)	222/110 (66.9/33.1)	0.148
Hypertension (No/Yes)	560/212 (72.5/27.5)	245/87 (73.8/26.2)	0.667
DM (No/Yes)	579/193 (75.0/25.0)	269/63 (81.0/19.0)	0.030
Hyperlipidemia (No/Yes)	726/64 (94.0/6.0)	312/20 (94.0/6.0)	0.966
CHD (No/Yes)	750/22 (97.2/2.8)	324/8 (97.6/2.4)	0.680
Cirrhosis (No/Yes)	70/702 (9.1/90.9)	35/297 (10.5/89.5)	0.444
HS (No/Yes)	510/262 (66.1/33.9)	205/127 (61.7/38.3)	0.169
Family history of HBV (No/Yes)	539/233 (69.8/30.2)	238/94 (71.7/28.3)	0.533
Family history of HCC (No/Yes)	745/27 (96.5/3.5)	324/8 (97.6/2.4)	0.344
TCM (No/Yes)	375/397 (48.6/51.4)	151/181 (45.5/54.5)	0.345
Etiology			
HBV	740 (95.9)	323 (97.3)	0.510
HCV	10 (1.3)	3 (0.9)	
Others	22 (2.8)	6 (1.8)	
Complications			
Ascites (No/Yes)	435/337 (56.3/43.7)	186/146 (56.0/44.0)	0.921
HE (No/Yes)	754/18 (97.7/2.3)	325/7 (97.9/2.1)	0.819
Laboratory indicators			
WBC (≤10/>10*10^9/L)	751/21 (97.3/2.7)	323/9 (97.3/2.7)	0.993
NLR (≤2/>2)	291/481 (37.7/62.3)	136/196 (41.0/59.0)	0.306
RBC (<4/≥4*10^12/L)	387/385 (50.1/49.9)	172/160 (51.8/48.2)	0.609
HGB (<110/≥110 g/L)	194/578 (25.1/74.9)	75/257 (22.6/77.4)	0.367
PLT (<100/≥100*10^9/L)	472/300 (61.1/38.9)	209/123 (63.0/37.0)	0.570
PSL (<909/≥909)	524/248 (67.9/32.1)	230/102 (69.3/30.7)	0.646
ALT (≤50/>50 U/L)	576/196 (74.6/25.4)	255/77 (76.8/23.2)	0.438
AST (≤40/>40 U/L)	405/367 (52.5/47.5)	186/146 (56.0/44.0)	0.276
TBIL (≤18.8/>18.8 μmol/L)	389/383 (50.4/49.6)	160/172 (48.2/51.8)	0.503
ALB (<40/≥40 g/L)	534/238 (69.2/30.8)	234/98 (70.5/29.5)	0.664
LDH (≤250/>250 U/L)	673/99 (87.2/12.8)	295/37 (88.9/11.1)	0.436
GGT (≤60/>60 U/L)	426/346 (55.2/44.8)	188/144 (56.6/43.4)	0.658
ALP (≤125/>125 U/L)	560/212 (72.5/27.5)	248/84 (74.7/25.3)	0.458
CHE (≤4,000/>4000 U/L)	345/427 (44.7/55.3)	144/188 (43.4/56.6)	0.687
TC (≤18.8/>18.8 mmol/L)	753/19 (97.5/2.5)	327/5 (98.5/1.5)	0.318
TG (≤1.71/>1.71 mmol/L)	728/44 (94.3/5.7)	310/22 (93.4/6.6)	0.551

(Continued on following page)

TABLE 1 (*Continued*) Characteristics of the clinical profile of the modeling group and validation group of patients with HCC.

Characters	Training cohort (n = 772)	Validation cohort group (n = 332)	*p*-value
CR (≤111/>111μmoI/L)	737/35 (95.5/4.5)	313/19 (94.3/5.7)	0.401
PTA (<70/≥70%)	275/497 (35.6/64.4)	115/217 (34.6/65.4)	0.754
AFP (≤400/>400 ng/mL)	521/251 (67.5/32.5)	230/102 (69.3/30.7)	0.559
CRP (<5/≥5 mg/L)	209/563 (27.1/72.9)	98/234 (29.5/70.5)	0.406
Child			
A	403 (52.2)	171 (51.5)	0.238
B	258 (33.4)	124 (37.3)	
C	111 (14.4)	37 (11.2)	
HBV-related features			
HBV-DNA (≤500/>500 IU/mL)	330/442 (42.7/57.3)	156/176 (47.0/53.0)	0.193
HbsAg (≤250/>250 IU/mL)	228/544 (29.5/70.5)	111/221 (33.4/66.6)	0.198
HBeAg (No/Yes)	453/319 (58.7/41.3)	197/135 (59.3/40.7)	0.838
Tumor-related features			
Tumor multiplicity (Single/Multiple)	434/338 (56.2/43.8)	172/160 (51.8/48.2)	0.177
Tumor size (<5 cm, ≥5 cm)	569/203 (73.7/26.3)	234/98 (70.5/29.5)	0.270
PVTT (No/Yes)	451/321 (58.4/41.6)	202/130 (60.8/39.2)	0.452
BCLC			
0	42 (5.4)	16 (4.8)	0.245
A	240 (31.1)	101 (30.4)	
B	252 (32.6)	130 (39.2)	
C	127 (16.5)	48 (14.5)	
D	111 (14.4)	37 (11.1)	
TNM			
I	229 (29.7)	98 (29.5)	0.661
II	138 (17.9)	64 (19.3)	
III	394 (51.0)	168 (50.6)	
IV	11 (1.4)	2 (0.6)	

(TG), creatinine (CR), prothrombin time activity (PTA), C reactive protein (CRP); Tumor-related features like alpha fetoprotein (AFP), portal vein tumor thrombus (PVTT).

Statistical analysis

In this study, we used SPSS 24.0 (IBM, Chicago, IL, USA), R software (version 3.6.3; http://www.Rproject.org) and MedCalc 19.2.0 for statistical analysis. We implemented a stratified random sampling approach to divide patients into training and validation cohorts in a 7:3 ratio, ensuring similar distributions of key clinical variables across both cohorts. The stratification was performed based on the outcome variable to maintain balance in prognostic factors. The randomization process was conducted using the "caret" package. The "glmnet" package in R 3.6.3 is used for Lasso-Cox regression and "nomogramEx" package is used to build nomogram. On the basis of establishing nomogram, "foreign", "survival", "nricens", "stdca" and "rms" packages are used to analyze C index and calibration curve, to score NRI and IDI, and to draw decision curve. Analyze and draw time-dependent ROC curves with the "time ROC" package. The total score of each patient was calculated according to nomogram, and the patients with high, medium and low prognostic risk were divided into three groups according to the quartile. MedCalc 19.2.0 was used to draw Kaplan-Meier curves in low risk group, medium risk group and high risk group. The two-tailed P-value < 0.05 was statistically significant.

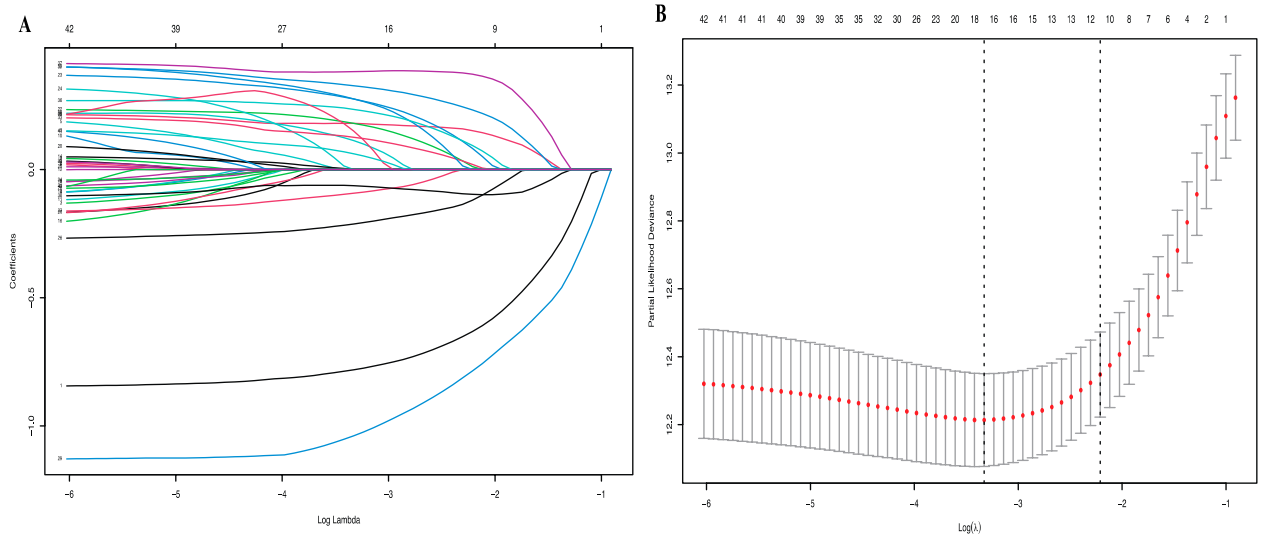

FIGURE 1
(A) LASSO coefficient profiles of the 42 risk factors; **(B)** 11 risk factors selected using LASSO Cox regression analysis. The two dotted vertical lines were drawn at the optimal scores by minimum criteria and 1-s.e. criteria.

Results

Basic characteristics

A total of 1104 HCC patients who met the inclusion and exclusion criteria were included in this study. The patients were randomly divided into the modeling cohort and the validation cohort at a ratio of 7:3, with 772 HCC patients in the modeling cohort and 332 HCC patients in the validation cohort. To enhance the objectivity and simplicity of the model, continuous variables were converted to categorical variables using clinically normal laboratory test values as cutoffs.

The majority of the study population was male (80.3% vs. 80.1%; $P = 0.942$), patients older than 50 years (77.6% vs. 79.5%; $P = 0.477$). More than half of the patients using TCM (51.4% vs. 54.5%; $P = 0.444$). In addition, the majority of patients had cirrhosis (90.9% vs. 89.5%; $p = 0.444$), with HBV infection as the main cause (95.9% vs. 97.3%; $p = 0.510$), with HBsAg positivity (70.5% vs. 66.6%; $p = 0.198$). More than half of the patients had platelet/spleen diameters <909 (67.9% vs. 79.3%; $p = 0.646$); Almost half of the patients in TNM III (51.0% vs. 50.6%; $P = 0.661$); Most patients were still in stage 0-B BCLC (69.1% vs. 74.4%; $P = 0.245$), child-Pugh A-B patients accounted for the majority (85.6% vs. 88.8%; $P = 0.238$), (73.7% vs. 70.5%; $P = 0.270$) had tumor diameter <5 cm (Table 1).

Biomarker selection

All available clinical indicators listed in Table 1, including general patient characteristics, etiology, comorbidities, laboratory indicators, hepatitis B-related characteristics and tumor-related characteristics, were analyzed using the LASSO Cox regression model to identify potential prognostic factors. All available clinical indicators were subjected to LASSO Cox regression, with a significant correlation between TCM, ascites, PVTT, tumor number, tumor size, RBC, HGB, PSL, CR, TBIL, LDH, GGT, ALP, CHE, TC, AFP and OS at minimum values (Figure1A); Further disciplinary regression was performed to take 1-s.e. criteria TCM, ascites, PVTT, tumor number, tumor size, RBC, PSL, TBIL, GGT, ALP and CHE as independent risk factors for HCC (Figure 1B).

Cox univariate analysis of all clinical indicators revealed significant associations between OS and factors such as TCM usage, cirrhosis, HS, ascites, HE, PVTT, HBV-DNA, tumor number, tumor size, NLR, RBC, HGB, PSL, CR, AST, TBIL, ALB, LDH, GGT, ALP, CHE, PTA, AFP and CRP. Subsequent Cox multivariate analysis identified TCM usage, PVTT, tumor number, tumor size, PSL, CR, LDH, GGT and ALP were independent risk factors for prognosis in HCC (Table 2). And the COX analysis results of PFS were shown in Supplementary Table S1.

Establish and evaluate nomogram

Based on the statistical results, we established two prognostic nomograms—Nomogram 1 and Nomogram 2—to predict the overall survival of HCC patients (Figure 2). Nomogram 1 incorporated the following independent prognostic factors: TCM usage, PVTT, tumor number, tumor size, PSL, Cr, LDH, GGT, and ALP. Each variable was assigned a score based on its relative contribution to the prognosis, allowing for individualized risk prediction by summing the total score. Nomogram 2 included the same variables as Nomogram 1, except that the PSL ratio was replaced by its individual components—platelet count and spleen diameter—as separate variables. This nomogram also assigned scores to each variable to calculate a total prognostic score.

To compare and evaluate the performance of the two nomograms, we calculated the concordance index (C-index) and the area under the receiver operating characteristic curve (AUC). In

TABLE 2 Univariate and multivariate cox hazards analysis of the training cohort with OS.

	Univariate analysis		Multivariate analysis	
Characteristic	HR (95% CI)	*p*	HR (95% CI)	*p*
TCM				
No/Yes	0.319 (0.265–0.385)	<0.001	0.423 (0.346–0.518)	<0.001
Cirrhosis				
No/Yes	2.655 (1.761–4.004)	<0.001		
HS				
No/Yes	2.369 (1.978–2.838)	<0.001		
PHT				
No/Yes	2.206 (1.833–2.655)	<0.001		
Ascites				
No/Yes	2.772 (2.311–3.325)	<0.001		
HE				
No/Yes	2.013 (1.223–3.315)	0.006		
PVTT				
No/Yes	2.621 (2.189–3.139)	<0.001	1.482 (1.215–1.808)	<0.001
HBV-DNA (IU/mL)				
≤500, >500	1.295 (1.080–1.552)	0.005		
Tumor multiplicity				
Single/ Multiple	1.771 (1.481–2.117)	<0.001	1.308 (1.084–1.579)	0.005
Tumor size (cm)				
<5, ≥5	1.912 (1.576–2.320)	<0.001	1.442 (1.153–1.803)	0.001
NLR				
≤2, >2	1.641 (1.355–1.988)	<0.001		
RBC (10^12/L)				
<4, ≥4	0.393 (0.326–0.473)	0.001		
HGB (g/L)				
<110, ≥110	0.416 (0.344–0.503)	<0.001		
PLT (*10^9/L)				
<100,≥100	0.353 (0.287–0.435)	<0.001		
PSL				
<909,≥909	0.206 (0.160–0.265)	<0.001	0.317 (0.220–0.458)	<0.001
CR (μmol/L)				
<111, ≥111	2.542 (1.764–3.663)	<0.001	2.200 (1.254–3.858)	0.006
AST (U/L)				
<40, ≥40	2.083 (1.739–2.494)	<0.001		
TBIL (μmol/L)				
<18.8, ≥18.8	2.473 (2.056–2.975)	<0.001		
ALB (g/L)				
<40, ≥40	0.423 (0.340–0.527)	<0.001		
LDH(U/L)				
<250, ≥250	2.057 (1.621–2.611)	<0.001	1.555 (1.204–2.008)	0.001
GGT (U/L)				
<60, ≥60	1.931 (1.615–2.308)	<0.001	1.336 (1.078–1.656)	0.008
ALP(U/L)				
≤125, >125	3.017 (2.503–3.636)	<0.001	1.481 (1.177–1.862)	0.001
CHE(U/L)				
≤4,000, >4,000	0.347 (0.289–0.417)	<0.001		
PTA (%)				
<70, ≥70	0.413 (0.345–0.495)	<0.001		
AFP (ng/mL)				
≤400, >400	1.372 (1.138–1.654)	0.001		
CRP (mg/L)				
<5, ≥5	1.253 (1.022–1.536)	0.030		

(Continued in next column)

TABLE 2 (*Continued*) Univariate and multivariate cox hazards analysis of the training cohort with OS.

the modeling cohort, Nomogram 1 had a C-index of 0.792 and an AUC of 0.866, while Nomogram 2 had a C-index of 0.788 and an AUC of 0.854 (Table 3). Time-dependent ROC curves showed that over time, the predictive efficiencies of both models were not significantly different and both significantly outperformed traditional models such as Child-Pugh, BCLC, ALBI, and TNM staging systems (Figure 3).

The calibration curve for the 3-year OS probability indicated that the predictions made by Nomogram 1 had the best agreement

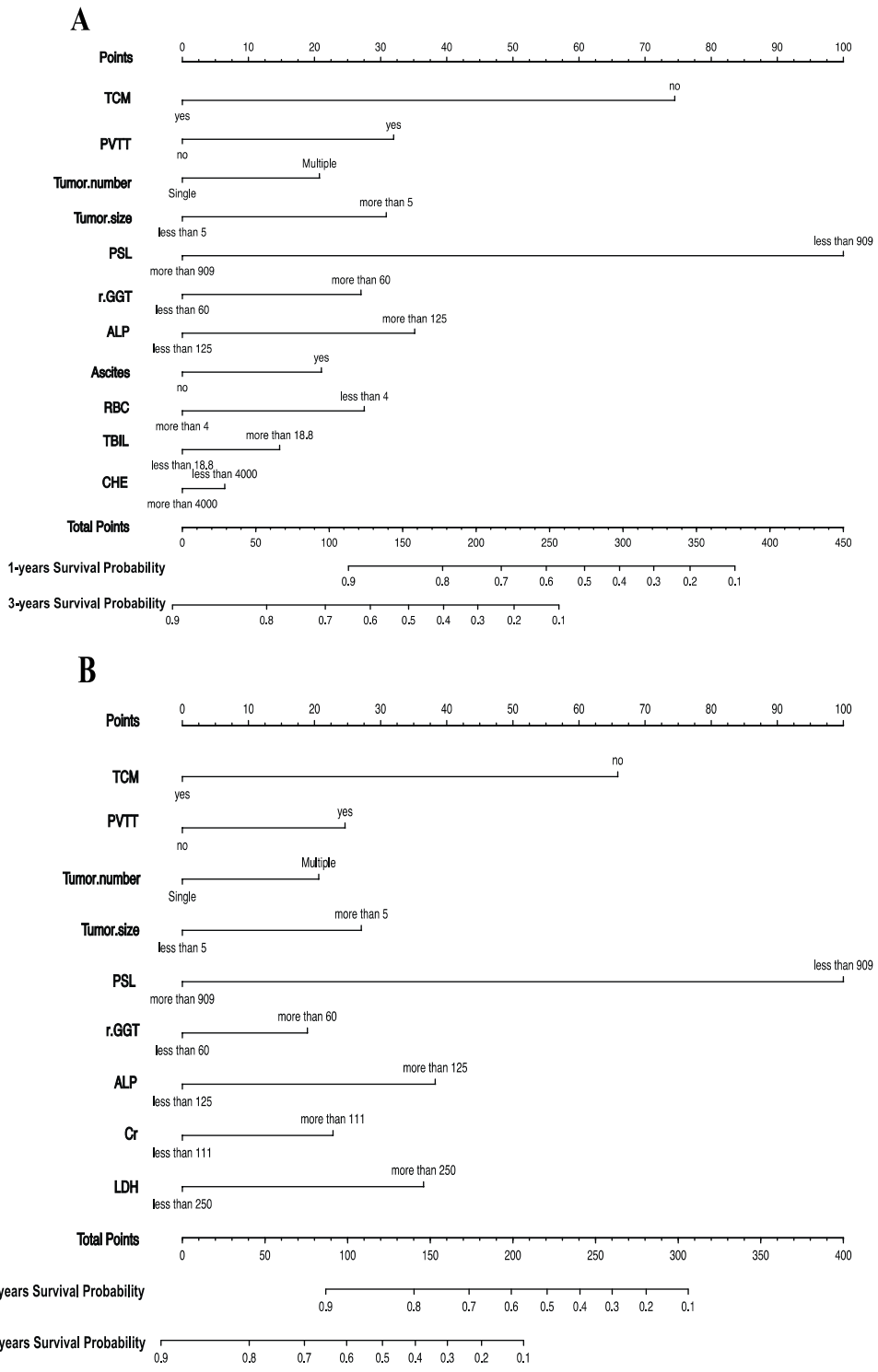

FIGURE 2
(A) Nomogram1 including TCM, PVTT, Tumor number, Tumor size, PSL, GGT, ALP, Ascites, RBC, TBIL and CHE, for one- and 3-years overall survival (OS) in patients with HCC; **(B)** Nomogram2 including TCM, PVTT, Tumor number, Tumor size, PSL, GGT, ALP, Cr and LDH, for one- and 3-years overall survival (OS) in patients with HCC. The nomogram1 and nomogram2 are valued to obtain the probability of one- and 3-years survival by adding up the points identified on the points scale for each variable.

with the actual observations (Figure 4). Decision curve analysis demonstrated that both nomograms provided meaningful clinical net benefits, with Nomogram 1 showing a slightly higher net benefit than Nomogram 2 in the modeling cohort; both yielded a net benefit exceeding 50% (Figure 5). Similar trends were observed in the validation cohort. Therefore, we concluded that Nomogram 1, which incorporates the PSL ratio, is more effective in predicting the prognosis of HCC patients.

TABLE 3 C-index and AUC of prognostic staging systems for Training and Validation cohort.

Models	Training cohort				Validation cohort			
	C-index	95% CI	AUC	95% CI	C-index	95% CI	AUC	95% CI
Nomogram1	0.792	0.772–0.812	0.866	0.840–0.889	0.769	0.740–0.798	0.867	0.826–0.902
Nomogram2	0.788	0.768–0.808	0.854	0.827–0.878	0.761	0.732–0.790	0.856	0.813–0.892
Child	0.648	0.628–0.668	0.702	0.668–0.734	0.634	0.603–0.665	0.679	0.626–0.729
BCLC	0.676	0.654–0.698	0.736	0.704–0.767	0.665	0.634–0.696	0.714	0.662–0.762
ALBI	0.631	0.609–0.653	0.686	0.652–0.718	0.623	0.590–0.656	0.676	0.622–0.732
TNM	0.648	0.626–0.670	0.697	0.663–0.729	0.625	0.592–0.658	0.682	0.629–0.732
CLIP	0.712	0.690–0.734	0.751	0.719–0.781	0.693	0.660–0.726	0.733	0.682–0.780
Okuda	0.664	0.642–0.686	0.717	0.684–0.749	0.655	0.626–0.684	0.710	0.658–0.758

Risk stratification based on nomograms

Methods and criteria for risk stratification

To assess the prognostic utility of the nomograms, we divided patients into different risk groups based on their total nomogram scores. Each patient's total score was calculated using the points specified in the nomogram. Then, based on the quartiles of the total scores, patients were classified into low-risk, middle-risk, and high-risk groups. Specifically, the lowest 25% of total scores constituted the low-risk group, the highest 25% constituted the high-risk group, and the remaining 50% formed the middle-risk group.

Survival analyses derived from nomogram 1

Based on Nomogram 1 developed in this study, we stratified patients into low-risk, medium-risk, and high-risk groups, demonstrating good discrimination in both the modeling and validation cohorts. In the modeling cohort (n = 772), the low-, medium-, and high-risk groups comprised 194, 385, and 193 patients, respectively. The median overall survival (OS) was not reached in the low-risk group, while it was 25.57 ± 0.99 months in the medium-risk group and 5.37 ± 0.75 months in the high-risk group ($P < 0.001$). Using the low-risk group as a reference, the hazard ratios (HRs) for OS were 4.46 (95% CI: 3.68–5.41; $P < 0.001$) for the medium-risk group and 14.02 (95% CI: 10.38–18.95; $P < 0.001$) for the high-risk group (Figure 6A). In the validation cohort (n = 332), with 75 low-risk, 173 medium-risk, and 84 high-risk patients, the median OS was not reached in the low-risk group, whereas it was 25.57 ± 0.96 months in the medium-risk group and 5.70 ± 1.11 months in the high-risk group ($P < 0.001$). The HRs for OS were 5.11 (95% CI: 3.82–6.83; $P < 0.001$) for the medium-risk group and 15.08 (95% CI: 9.67–23.51; $P < 0.001$) for the high-risk group compared to the low-risk group (Figure 6B).

Regarding progression-free survival (PFS), in the modeling cohort, the HRs were 4.41 (95% CI: 3.51–5.54; $P < 0.001$) for the medium-risk group and 12.82 (95% CI: 9.37–17.56; $P < 0.001$) for the high-risk group compared to the low-risk group (Figure 6C). In the validation cohort, the HRs for PFS were 6.26 (95% CI: 4.31–9.09; $P < 0.001$) for the medium-risk group and 19.81 (95% CI: 11.99–32.74; $P < 0.001$) for the high-risk group (Figure 6D).

Application of the nomogram model

We incorporated all the variables from Nomogram 1 into a decision tree in the modeling cohort to visualize the hierarchical importance of prognostic factors (Figure 7). The decision tree revealed that the PSL ratio was the most significant contributor to the model, appearing at the first level. Patients with PSL >909 who were also receiving TCM had significantly higher survival rates compared to those with PSL <909 and not using TCM. This hierarchical stratification underscores the critical role of PSL and TCM usage in influencing patient outcomes.

Discussion

Patients with hepatitis B virus-associated hepatocellular carcinoma are often associated with liver dysfunction, portal hypertension and splenomegaly, resulting in abnormal platelet counts and abnormal coagulation (Yang et al., 2011). Thrombocytopenia, also known as low platelet count, is common in chronic liver disease due to a lack of sufficient thrombopoietin in normal liver tissue and/or increased platelet destruction due to splenomegaly (Hayashi et al., 2014; Peck-Radosavljevic, 2017). There is much talk about the relationship between PLT counts and HCC prognosis. Roayaie et al. (2013) concluded that a PLT count <150 was associated with a poor prognosis after resection of hepatocellular carcinoma. Morimoto et al. (2014) and Lee et al. (2015) reported that high PLT counts promoted extrahepatic metastasis of HCC and were associated with poor prognosis, respectively. Meanwhile, Kondo et al. found that postoperative survival in HCC patients was not associated with low PLT counts (Kondo et al., 2012). However, their studies did not take into account the fact that platelets may be affected by different factors, such as chronic alcohol consumption, which can inhibit bone marrow tissue proliferation, or hepatitis B virus, which can affect platelet production, suggesting that this single indicator is not stable. Whether the combination of spleen diameter, as a clinically imaging-accessible indicator, would yield a better predictive outcome was the focus of our study.

Various columnar maps have been developed to predict the prognosis of certain cancers and have been shown to be more accurate than traditional staging systems. However, it is mostly

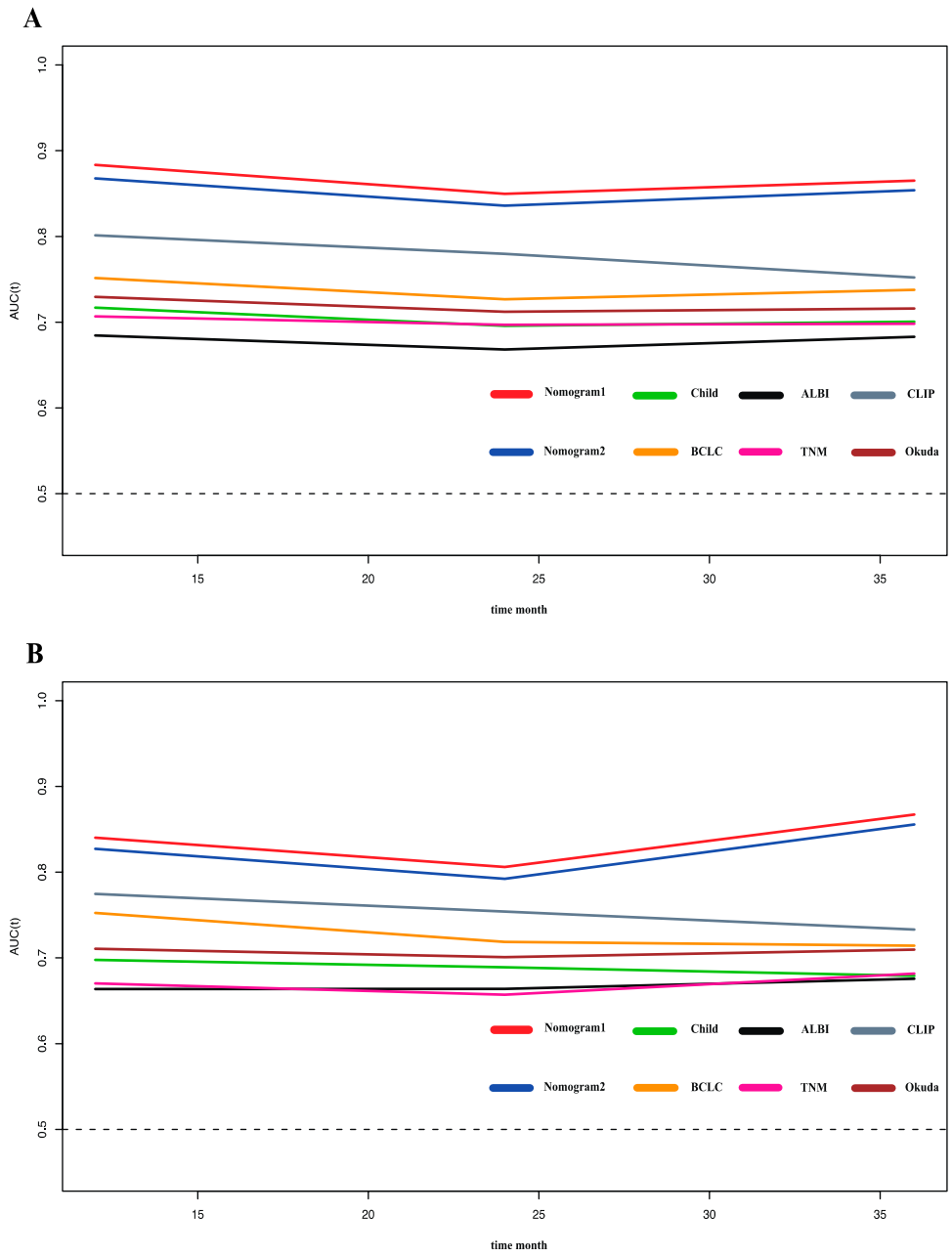

FIGURE 3
Time-ROC curve of the eight models in the primary and validation cohort. Red line: Nomogram1; Blue line: Nomogram2; Green line: Child-pugh; Yellow line: BCLC stage; Black line: ALBI; Pink line: TNM; Gray line: CLIP; deep red line: Okuda. **(A)** Time-ROC curve of the eight models in the primary. **(B)** Time-ROC curve of the eight models in the validation cohort.

limited to forward stepwise Cox regression risk factor screening, which is not conducive to small sample size and multi-indicator model screening (Iasonos et al., 2008). LASSO Cox regression was chosen for this study due to its capacity to handle high-dimensional data and select significant variables in the presence of multicollinearity. By applying a penalty function, this method minimizes overfitting and improves the predictive performance of the model. Compared to traditional stepwise regression, LASSO Cox regression provides a more robust approach for constructing prognostic models in complex clinical datasets (Tibshirani, 1997). A previous study by our team found that model variables for prognosis prediction of AFP-negative HCC patients screened by applying LASSO Cox regression had better precision and resolution than those screened by forward stepwise Cox regression (Zhou et al., 2021).

The study retrospectively included 1104 HCC patients, with the modelling and validation cohorts randomised in a 7:3 ratio. The nomogram1 and nomogram2 were constructed by LASSO Cox regression and Forward Stepwise Cox regression with the selection of independent risk factors. We found that the C index, AUC, time-dependent ROC, specificity, PPV, and calibration curve of nomogram1 were superior to those of nonogram2 in the

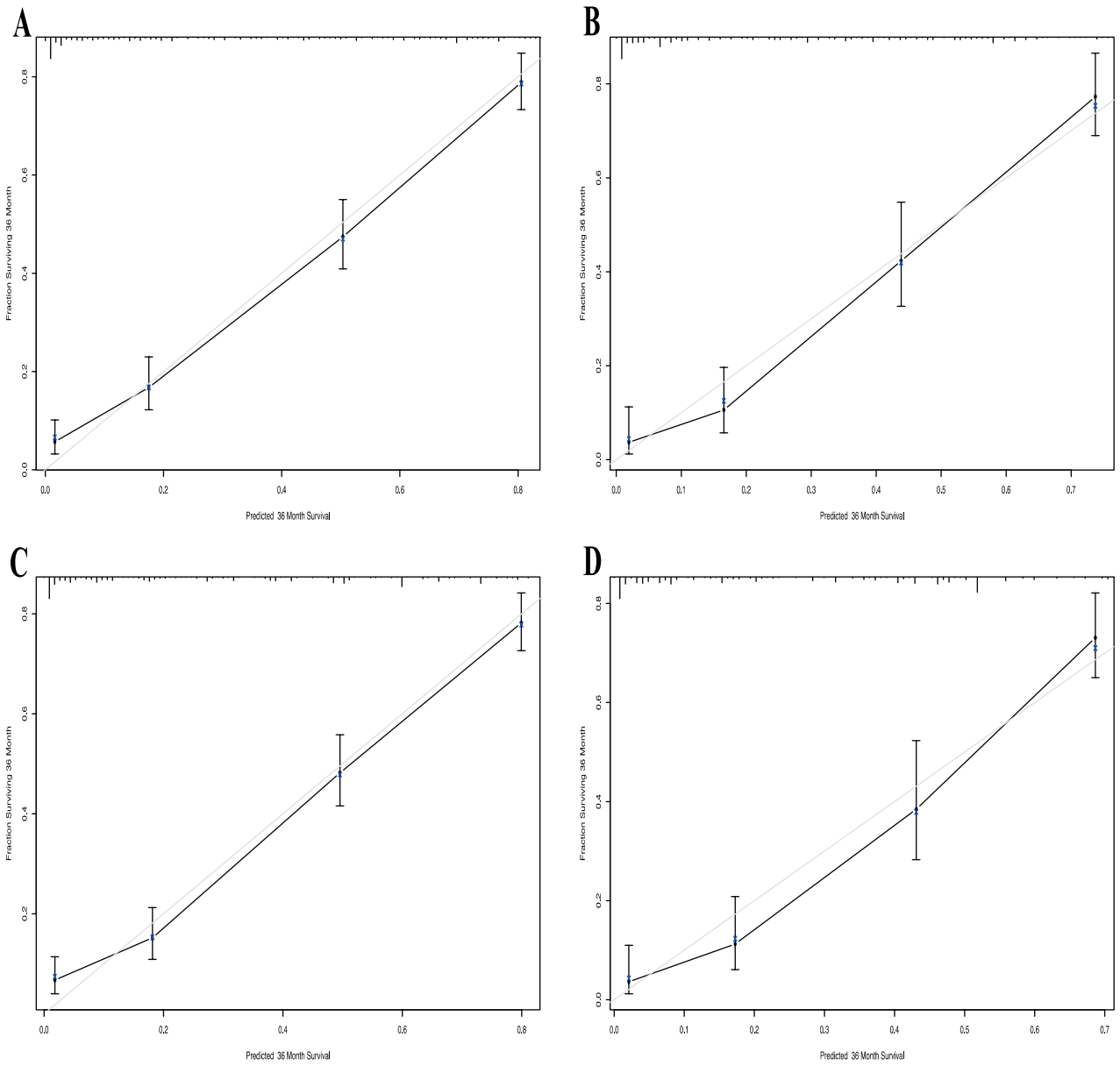

FIGURE 4
Calibration curve of the nomogram1 and nomogram2 in the primary and validation cohort, with the x-axes are actual survival estimated by the nomogram, the y-axes are observed survival calculated by the Kaplan-Meier method. **(A)** Three-year survival OS in the primary cohort in nomogram1. **(B)** Three-year OS in the validation cohort in nomogram1. **(C)** Three-year survival OS in the primary cohort in nomogram2. **(D)** Three-year OS in the validation cohort in nomogram2.

modelling cohort. They were similar in terms of sensitivity, NPV, and decision curves. Both were significantly higher than traditional models (Child, BCLC, ALBI, TNM, CLIP, Okuda, etc.). We get similar results in the validation cohort. Meanwhile, multiple studies have shown that tumor number, PVTT and tumor size are the main risk factors for predicting OS (Sun et al., 2019; Liu S. et al., 2019; Park et al., 2016; Pang et al., 2015a; Yu et al., 2019; Liu et al., 2020), which is consistent with our findings. The present study found TCM to be an independent risk factor for HCC prognosis, which is the same as our team's previous findings (Liu X. et al., 2019). Notably, we found that GGT and ALP are key biomarkers closely associated with the progression of HCC disease. Research has shown that preoperative elevation of ALT and GGT is associated with HCC mortality (Xu et al., 2014). The impact of GGT on tumorigenesis may be mediated through intracellular oxidative stress pathways. Numerous pieces of evidence suggest that GGT catalyzed degradation of glutathione can synergistically generate free radicals, leading to lipid peroxidation, which is closely associated with the occurrence of various malignant tumors, including HCC. This may partially explain the association between GGT and HCC (Pompella et al., 2007). An increase in ALP indicates the possibility of biliary obstruction, liver tissue damage, or bone metastasis, further indicating the severity and progression of the disease. Research has shown that ALP, as a marker for the differentiation of embryonic stem cells and other stem cells in bone

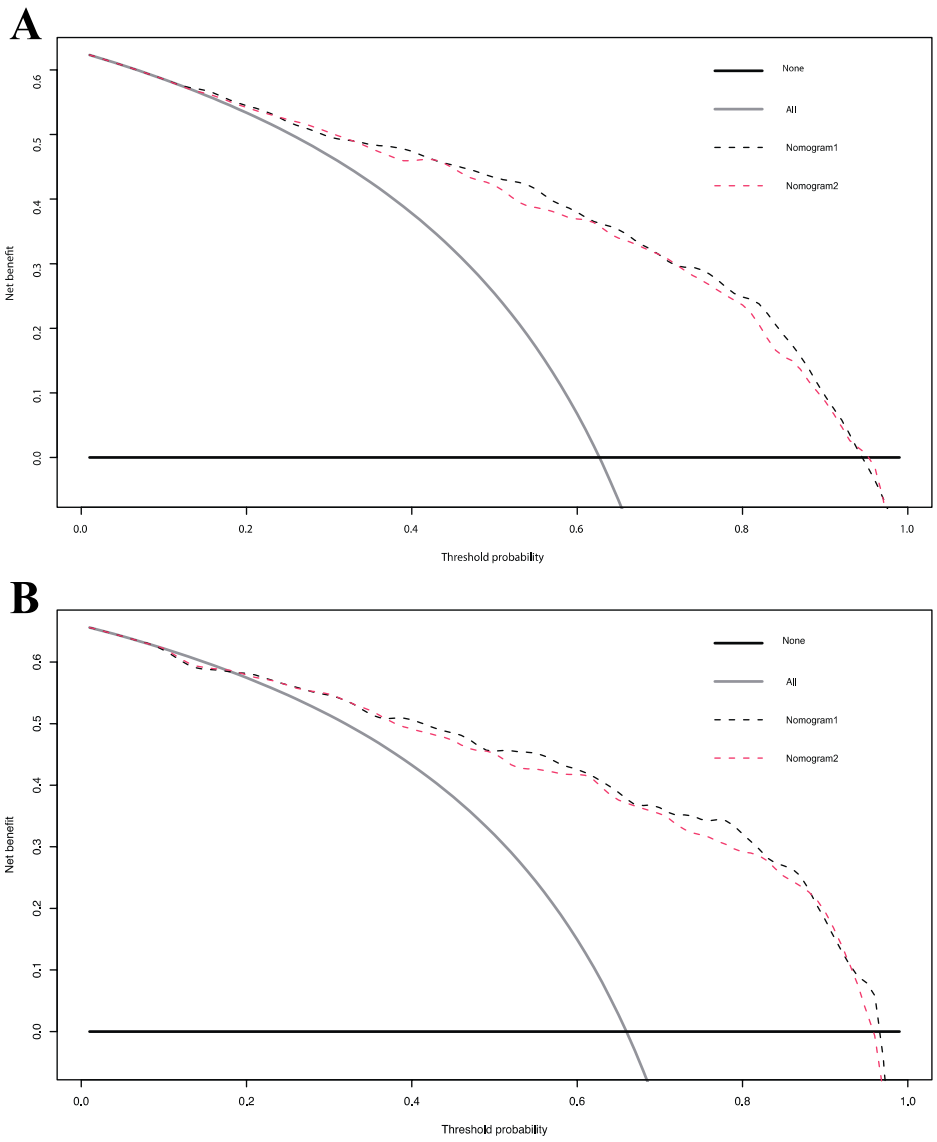

FIGURE 5
Decision curve analysis for overall survival in the primary and validation cohort. Black line: All patients dead. Gray line: None patients dead. Black dashed line: Model of nomogram1. Gray dashed line: Model of nomogram2. **(A)** Decision curve analysis for overall survival in the primary. **(B)** Decision curve analysis for overall survival in the validation cohort.

and adipose tissue, plays a key role in tumor proliferation and progression, and is commonly associated with bile stasis and hepatitis (Yamamoto et al., 2003). Interestingly, the GGT/ALT ratio is a potential effective factor in predicting vascular invasion and prognosis in HBV related HCC patients (Zhao et al., 2021).

However, there are few reports on PSL as a major risk factor for predicting OS in patients. Studies have shown that PLT levels change from initial inflammation through subsequent cirrhosis to the eventual formation of cancer, and that reduced PLT levels increase in-hospital and short-term mortality in patients with liver cancer, in addition to having an impact on long-term survival (Pang et al., 2015b; Maithel et al., 2011). However, the molecular mechanism is not known. In parallel, studies have found that low platelet levels in patients undergoing liver resection and radiofrequency ablation increase the risk of complications and tumour recurrence in patients (Amano et al., 2011; Kaibori et al., 2013). Kubo et al. prospectively included 202 patients with HCV-associated hepatocellular carcinoma undergoing tumour resection and found that only PLT levels were an independent risk factor for prognosis in patients with hepatocellular carcinoma, with levels significantly correlating with the severity of liver fibrosis ($p < 0.05$) (Kubo et al., 2004). It has been shown that a decrease in PLT levels is significantly associated with an increase in AFP levels (Akuta et al., 2012; Kobeisy et al., 2012). PLT levels are usually lower in early tumour stages due to low tumour load, hypersplenism and other factors such as reduced production of thrombopoietin and increased capture of platelets by the spleen (Kondo et al., 2013), where platelets are less affected by tumour factors. In advanced stages of the tumour, the tumour itself secretes more thrombopoietin (Cheng et al., 2019), which increases the platelet count and interacts with cirrhosis and

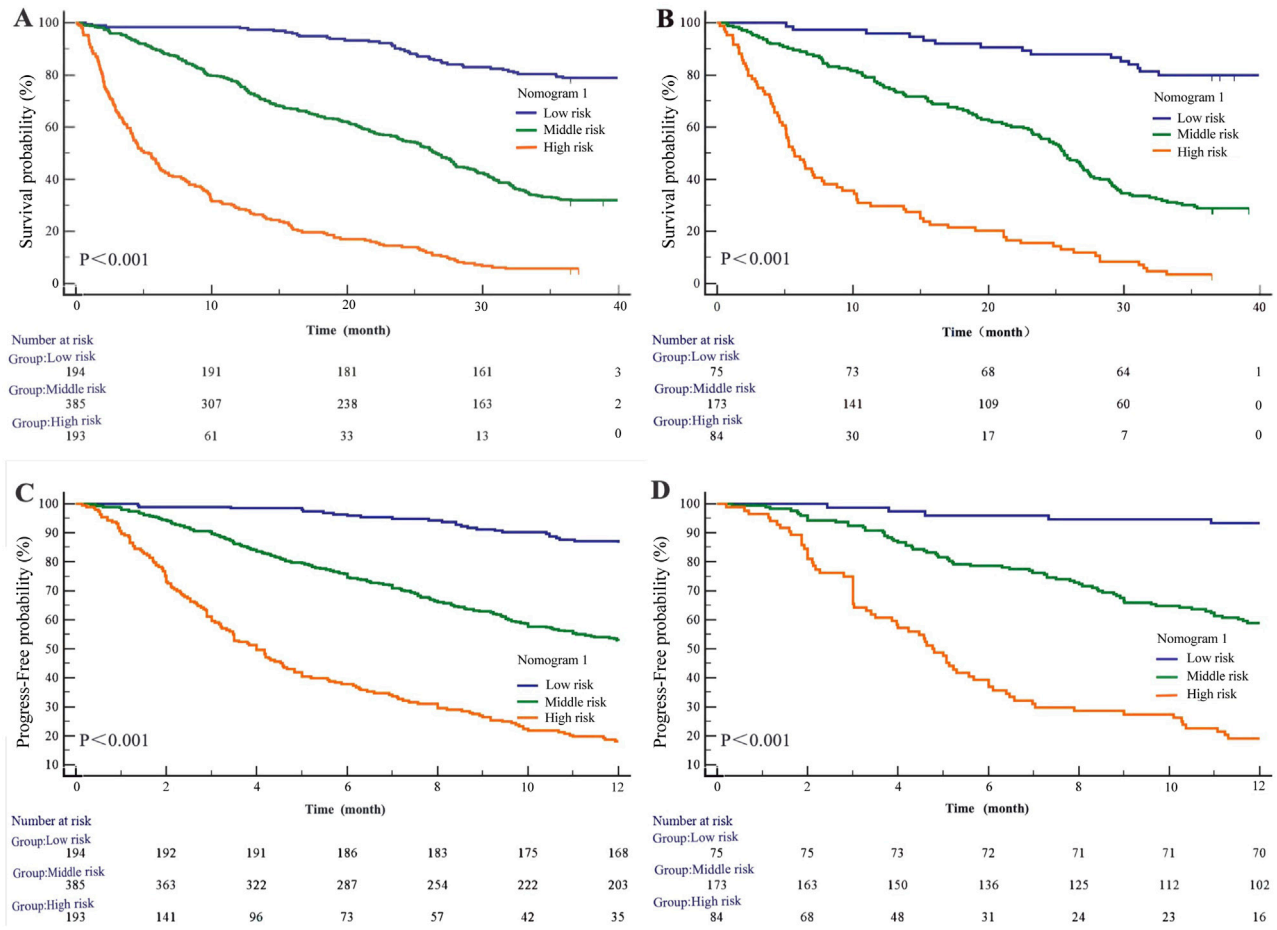

FIGURE 6
Kaplan-Meier survival curves of nomogram1. **(A)** OS in the primary cohort; **(B)** OS in the validation cohort; **(C)** PFS in the primary cohort; **(D)** PFS in the validation cohort.

thrombocytopenia. Platelet counts do not fully reflect the extent of cirrhosis. Thus, a single platelet index cannot predict the cirrhosis status of patients and the prognosis of patients with hepatocellular carcinoma. At the same time, higher platelet levels release more proteins, nucleotides and bioactive lipids that promote extravasation of primary liver cancer cells during the interaction of PLT with cancer cells in the bloodstream, sustaining cancer progression (Franco et al., 2015). In assessing the relationship between HCC and PLT, CarRBI et al. observed that PLT stimulated the growth and invasion of HCC cell lines *in vitro* (Carr et al., 2014). Our study also showed that in advanced tumour stages, patients with PVTT but normal or elevated PLT counts had larger tumours than those with thrombocytopenia. This finding also confirms that PLT significantly enhances the high adhesion of hepatocellular carcinoma cell lines. In addition, Tsuguru et al. found that antiplatelet therapy improved overall survival in patients with hepatocellular carcinoma (Hayashi et al., 2020). The spleen also plays a critical role in HCC pathophysiology. Splenomegaly, often associated with portal hypertension in cirrhotic patients, significantly affects platelet kinetics. The enlarged spleen may sequester platelets, leading to thrombocytopenia, which not only reflects liver dysfunction but also alters the systemic inflammatory and immune responses critical to tumor progression. Study shown that preoperative spleen volume is an independent predictor of late recurrence in HCC patients (Yang et al., 2024). By incorporating spleen diameter into PSL, this ratio provides a composite measure that captures both platelet activity and the severity of portal hypertension, making it a potentially robust prognostic indicator for HCC. In this study, PLT was not found to be an independent risk factor for the prognosis of hepatocellular carcinoma. However, in combination with spleen length diameter, the constructed PSL was one of the independent risk factors affecting the prognosis of patients with HCC. This provides new ideas for future research. Furthermore, the application of PSL in different therapeutic contexts warrants exploration. For instance, PSL could be investigated as a biomarker to stratify patients for targeted therapies or immunotherapies. Elevated PSL may indicate patients with lower tumor burden and better immune function, potentially identifying those who are more likely to benefit from immune checkpoint inhibitors. Conversely, patients with reduced PSL may require tailored therapeutic strategies to address underlying portal hypertension and associated complications. These potential applications expand the clinical significance of PSL and warrant further research to validate its utility in guiding personalized treatment strategies.

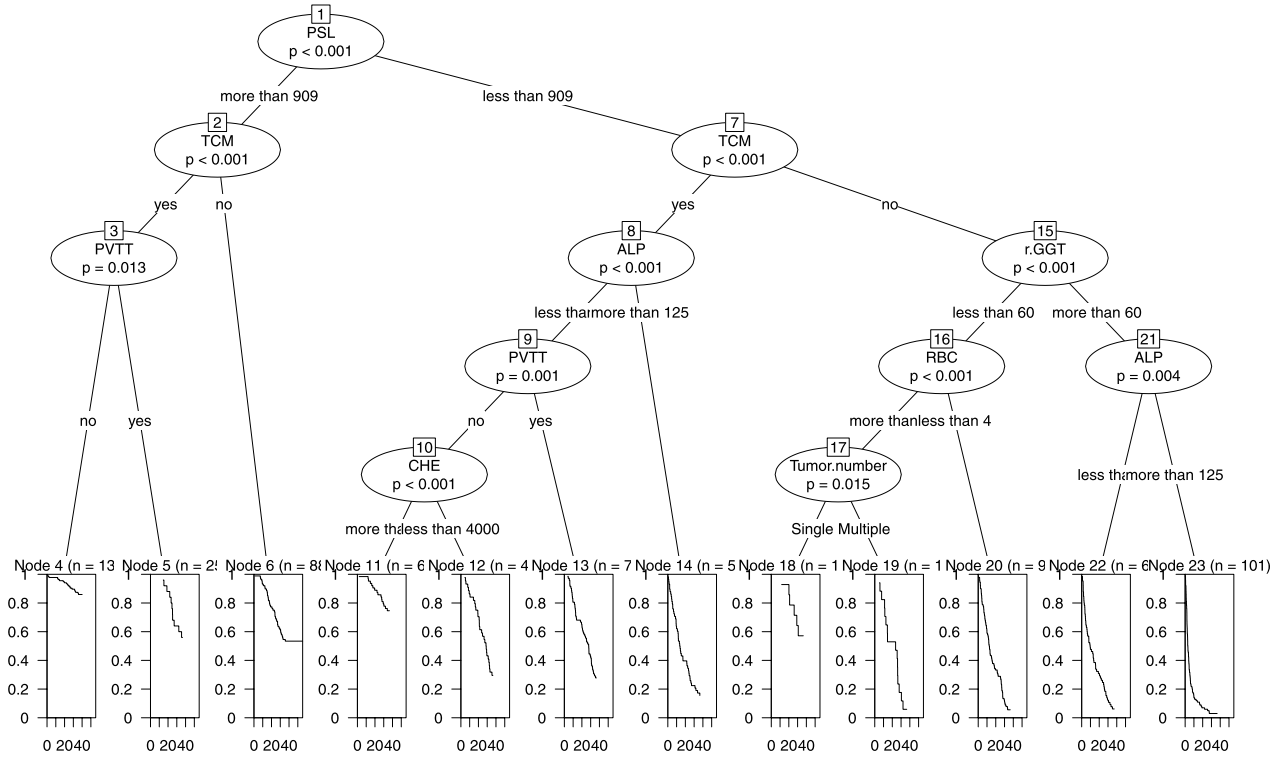

FIGURE 7
Decision Tree of nomogram1 in the primary cohort including PSL, TCM, PVTT, ALP, GGT, RBC, CHE and tumor number.

Despite the strengths of this study, several limitations should be acknowledged. Firstly, as a single-center study, the generalizability of our findings may be limited due to potential data bias. To address this, we recommend future studies to incorporate multicenter cohorts for external validation. Such studies would be critical to confirm the utility of PSL in diverse populations and healthcare settings, ensuring that our prognostic model is broadly applicable in clinical practice. Secondly, we did not explore the mechanisms underlying tumor factor-induced thrombocytopenia in depth, and further research is needed to elucidate these pathophysiological processes. Additionally, one limitation is the absence of detailed data on first-line treatments such as tyrosine kinase inhibitors (TKIs), immune checkpoint blockers (ICBs), chemotherapy, transarterial chemoembolization (TACE), and radiofrequency ablation. Due to the constraints of retrospective data collection, we could not include these variables in our analysis. Future prospective studies should incorporate comprehensive treatment data to validate and refine our prognostic model further, allowing for an assessment of how these therapies interact with the identified prognostic factors.

Conclusion

In conclusion, this study applied factors from the LASSO Cox regression screening model to develop and validate a visual nomogram for predicting 3-year overall survival in HCC patients based on PSL. In this study, it was shown that PSL <909 is one of the independent risk factors for 3-year overall survival and progression-free survival in HCC patients.

Data availability statement

The raw data supporting the conclusions of this article will be made available by the authors, without undue reservation.

Ethics statement

The studies involving humans were approved by the ethical committee at Capital Medical University's Beijing Ditan Hospital. The studies were conducted in accordance with the local legislation and institutional requirements. The ethics committee/institutional review board waived the requirement of written informed consent for participation from the participants or the participants' legal guardians/next of kin because this study obtained information from previous case samples, and the study risk was extremely small. Therefore, unnecessary identity details were omitted from the paper and informed consent was waived through ethical approval.

Author contributions

HY: Methodology, Validation, Writing–original draft, Writing–review and editing. DZ: Data curation, Formal Analysis, Visualization, Writing–original draft. XL: Software, Writing–review

and editing. PW: Investigation, Methodology, Writing–review and editing. TJ: Project administration, Writing–review and editing. ZY: Funding acquisition, Resources, Writing–review and editing.

Funding

The author(s) declare that financial support was received for the research, authorship, and/or publication of this article. This work was supported by the National Natural Science Foundation of China (No. 82104781), Young Talent Training Project of Beijing Hospital Authority (QML20231801), the National Natural Science Foundation of China (No. 82274479), High-level Public Health Technical Personnel Construction Project (Subject leaders-02-16), Dengfeng Talent Support Program of Beijing Municipal Administration of Hospitals (No. DFL20191803), Beijing Hospitals Authority Clinical Medicine Development of Special Funding Support (No. ZYLX202127), the Special Fund of Capital Health Research and Development (No. 2020-2-2173).

Acknowledgments

The authors would like to thank the Beijing Ditan Hospital of Capital Medical University database for the support.

Conflict of interest

The authors declare that the research was conducted in the absence of any commercial or financial relationships that could be construed as a potential conflict of interest.

The reviewer SY declared a shared affiliation with the authors to the handling editor at the time of review.

Publisher's note

Supplementary material

The Supplementary Material for this article can be found online at: https://www.frontiersin.org/articles/10.3389/fphar.2024.1449603/full#supplementary-material

References

Akuta, N., Suzuki, F., Seko, Y., Kawamura, Y., Sezaki, H., Suzuki, Y., et al. (2012). Complicated relationships of amino acid substitution in hepatitis C virus core region and IL28B genotype influencing hepatocarcinogenesis. *Hepatology* 56 (6), 2134–2141. doi:10.1002/hep.25949

Amano, H., Tashiro, H., Oshita, A., Kobayashi, T., Tanimoto, Y., Kuroda, S., et al. (2011). Significance of platelet count in the outcomes of hepatectomized patients with hepatocellular carcinoma exceeding the Milan criteria. *J. Gastrointest. Surg.* 15 (7), 1173–1181. doi:10.1007/s11605-011-1538-2

Carr, B. I., Cavallini, A., D'Alessandro, R., Refolo, M. G., Lippolis, C., Mazzocca, A., et al. (2014). Platelet extracts induce growth, migration and invasion in human hepatocellular carcinoma *in vitro*. *BMC Cancer* 14, 43. doi:10.1186/1471-2407-14-43

Cheng, Y. Q., Wang, K., Zhang, X. P., Wei, X. B., Jiang, Y. B., Hu, Y. R., et al. (2019). Thrombocytopenia: a prognostic factor for hepatocellular carcinoma patients with portal vein tumor thrombus after hepatectomy. *J. Gastroenterol. Hepatol.* 34 (7), 1214–1221. doi:10.1111/jgh.14537

Colli, A., Gana, J. C., Yap, J., Adams-Webber, T., Rashkovan, N., Ling, S. C., et al. (2017). Platelet count, spleen length, and platelet count-to-spleen length ratio for the diagnosis of oesophageal varices in people with chronic liver disease or portal vein thrombosis. *Cochrane Database Syst. Rev.* 4 (4), CD008759. doi:10.1002/14651858.CD008759.pub2

Dongdong, Z., Xiaoli, L., Tingting, J., Hao, Y., Yuyong, J., and Zhiyun, Y. (2020). Analysis and comparison of common prognostic prediction models for liver cancer. *Chin. J. Clin. Oncol.* 47 (24), 1281–1286. doi:10.3969/j.issn.1000-8179.2020.24.149

Franco, A. T., Corken, A., and Ware, J. (2015). Platelets at the interface of thrombosis, inflammation, and cancer. *Blood* 126 (5), 582–588. doi:10.1182/blood-2014-08-531582

Hayashi, H., Beppu, T., Shirabe, K., Maehara, Y., and Baba, H. (2014). Management of thrombocytopenia due to liver cirrhosis: a review. *World J. Gastroenterol.* 20 (10), 2595–2605. doi:10.3748/wjg.v20.i10.2595

Hayashi, T., Shibata, M., Oe, S., Miyagawa, K., Honma, Y., and Harada, M. (2020). Antiplatelet therapy improves the prognosis of patients with hepatocellular carcinoma. *Cancers (Basel)* 12 (11), 3215. doi:10.3390/cancers12113215

Iasonos, A., Schrag, D., Raj, G. V., and Panageas, K. S. (2008). How to build and interpret a nomogram for cancer prognosis. *J. Clin. Oncol.* 26 (8), 1364–1370. doi:10.1200/JCO.2007.12.9791

Kaibori, M., Kubo, S., Nagano, H., Hayashi, M., Haji, S., Nakai, T., et al. (2013). Clinicopathological features of recurrence in patients after 10-year disease-free survival following curative hepatic resection of hepatocellular carcinoma. *World J. Surg.* 37 (4), 820–828. doi:10.1007/s00268-013-1902-3

Kobeisy, M. A., Morsy, K. H., Galal, M., Sayed, S. K., Ashmawy, M. M., and Mohammad, F. M. (2012). Clinical significance of elevated alpha-foetoprotein (AFP) in patients with chronic hepatitis C without hepatocellular carcinoma in upper Egypt. *Arab. J. Gastroenterol.* 13 (2), 49–53. doi:10.1016/j.ajg.2012.06.004

Kondo, K., Chijiiwa, Y., Otani, K., Kai, M., Ohuchida, J., and Chijiiwa, K. (2012). Characteristics and surgical outcome of HCC patients with low platelet count. *Hepatogastroenterology* 59 (119), 2269–2272. doi:10.5754/hge10649

Kondo, R., Yano, H., Nakashima, O., Tanikawa, K., Nomura, Y., and Kage, M. (2013). Accumulation of platelets in the liver may be an important contributory factor to thrombocytopenia and liver fibrosis in chronic hepatitis C. *J. Gastroenterol.* 48 (4), 526–534. doi:10.1007/s00535-012-0656-2

Kubo, S., Tanaka, H., Shuto, T., Takemura, S., Yamamoto, T., Uenishi, T., et al. (2004). Correlation between low platelet count and multicentricity of hepatocellular carcinoma in patients with chronic hepatitis C. *Hepatol. Res.* 30 (4), 221–225. doi:10.1016/j.hepres.2004.10.005

Lee, C. H., Lin, Y. J., Lin, C. C., Yen, C. L., Shen, C. H., Chang, C. J., et al. (2015). Pretreatment platelet count early predicts extrahepatic metastasis of human hepatoma. *Liver Int.* 35 (10), 2327–2336. doi:10.1111/liv.12817

Liu, S., Li, H., Guo, L., Zhang, B., Zhou, B., Zhang, W., et al. (2019a). Tumor size affects efficacy of adjuvant transarterial chemoembolization in patients with hepatocellular carcinoma and microvascular invasion. *Oncologist* 24 (4), 513–520. doi:10.1634/theoncologist.2018-0305

Liu, X., Hou, Y., Wang, X., Yu, L., Wang, X., Jiang, L., et al. (2020). Machine learning-based development and validation of a scoring system for progression-free survival in liver cancer. *Hepatol. Int.* 14 (4), 567–576. doi:10.1007/s12072-020-10046-w

Liu, X., Li, M., Wang, X., Dang, Z., Yu, L., Wang, X., et al. (2019b). Effects of adjuvant traditional Chinese medicine therapy on long-term survival in patients with hepatocellular carcinoma. *Phytomedicine* 62, 152930. doi:10.1016/j.phymed.2019.152930

Maithel, S. K., Kneuertz, P. J., Kooby, D. A., Scoggins, C. R., Weber, S. M., Martin, R. C., et al. (2011). Importance of low preoperative platelet count in selecting patients for resection of hepatocellular carcinoma: a multi-institutional analysis. *J. Am. Coll. Surg.* 212 (4), 638–648. doi:10.1016/j.jamcollsurg.2011.01.004

Mangone, M., Moretti, A., Alivernini, F., Papi, C., Orefice, R., Dezi, A., et al. (2012). Platelet count/spleen diameter ratio for non-invasive diagnosis of oesophageal varices: is it useful in compensated cirrhosis? *Dig. Liver Dis.* 44 (6), 504–507. doi:10.1016/j.dld.2011.12.016

Marasco, G., Colecchia, A., Colli, A., Ravaioli, F., Casazza, G., Bacchi Reggiani, M. L., et al. (2019). Role of liver and spleen stiffness in predicting the recurrence of hepatocellular carcinoma after resection. *J. Hepatol.* 70 (3), 440–448. doi:10.1016/j.jhep.2018.10.022

Menter, D. G., Tucker, S. C., Kopetz, S., Sood, A. K., Crissman, J. D., and Honn, K. V. (2014). Platelets and cancer: a casual or causal relationship: revisited. *Cancer Metastasis Rev.* 33 (1), 231–269. doi:10.1007/s10555-014-9498-0

Morimoto, Y., Nouso, K., Wada, N., Takeuchi, Y., Kinugasa, H., Miyahara, K., et al. (2014). Involvement of platelets in extrahepatic metastasis of hepatocellular carcinoma. *Hepatol. Res.* 44 (14), E353–E359. doi:10.1111/hepr.12315

Pang, Q., Qu, K., Bi, J. B., Liu, S. S., Zhang, J. Y., Song, S. D., et al. (2015b). Thrombocytopenia for prediction of hepatocellular carcinoma recurrence: systematic review and meta-analysis. *World J. Gastroenterol.* 21 (25), 7895–7906. doi:10.3748/wjg.v21.i25.7895

Pang, Q., Qu, K., Zhang, J. Y., Song, S. D., Liu, S. S., Tai, M. H., et al. (2015a). The prognostic value of platelet count in patients with hepatocellular carcinoma: a systematic review and meta-analysis. *Med. Baltim.* 94 (37), e1431. doi:10.1097/MD.0000000000001431

Park, Y., Kim, S. U., Kim, B. K., Park, J. Y., Kim, D. Y., Ahn, S. H., et al. (2016). Addition of tumor multiplicity improves the prognostic performance of the hepatoma arterial-embolization prognostic score. *Liver Int.* 36 (1), 100–107. doi:10.1111/liv.12878

Peck-Radosavljevic, M. (2017). Thrombocytopenia in chronic liver disease. *Liver Int.* 37 (6), 778–793. doi:10.1111/liv.13317

Pompella, A., Corti, A., Paolicchi, A., Giommarelli, C., and Zunino, F. (2007). Gamma-glutamyltransferase, redox regulation and cancer drug resistance. *Curr. Opin. Pharmacol.* 7 (4), 360–366. doi:10.1016/j.coph.2007.04.004

Roayaie, S., Obeidat, K., Sposito, C., Mariani, L., Bhoori, S., Pellegrinelli, A., et al. (2013). Resection of hepatocellular cancer ≤2cm: results from two Western centers. *Hepatology* 57 (4), 1426–1435. doi:10.1002/hep.25832

Sun, J., Yang, L., Shi, J., Liu, C., Zhang, X., Chai, Z., et al. (2019). Postoperative adjuvant IMRT for patients with HCC and portal vein tumor thrombus: an open-label randomized controlled trial. *Radiother. Oncol.* 140, 20–25. doi:10.1016/j.radonc.2019.05.006

Sung, H., Ferlay, J., Siegel, R. L., Laversanne, M., Soerjomataram, I., Jemal, A., et al. (2021). Global cancer statistics 2020: GLOBOCAN estimates of incidence and mortality worldwide for 36 cancers in 185 countries. *CA Cancer J. Clin.* 71 (3), 209–249. doi:10.3322/caac.21660

Tibshirani, R. (1997). The Lasso method for variable selection in the Cox model. *Stat. Med.* 16 (4), 385–395. doi:10.1002/(sici)1097-0258(19970228)16:4<385::aid-sim380>3.0.co;2-3

Torre, L. A., Bray, F., Siegel, R. L., Ferlay, J., Lortet-Tieulent, J., and Jemal, A. (2015). Global cancer statistics, 2012. *CA Cancer J. Clin.* 65 (2), 87–108. doi:10.3322/caac.21262

Wang, J. H., Chang, K. C., Kee, K. M., Chen, P. F., Yen, Y. H., Tseng, P. L., et al. (2013). Hepatocellular carcinoma surveillance at 4- vs. 12-month intervals for patients with chronic viral hepatitis: a randomized study in community. *Am. J. Gastroenterol.* 108 (3), 416–424. doi:10.1038/ajg.2012.445

Wu, W. C., Chiou, Y. Y., Hung, H. H., Kao, W. Y., Chou, Y. H., Su, C. W., et al. (2012). Prognostic significance of computed tomography scan-derived splenic volume in hepatocellular carcinoma treated with radiofrequency ablation. *J. Clin. Gastroenterol.* 46 (9), 789–795. doi:10.1097/MCG.0b013e31825ceeb5

Xu, X. S., Wan, Y., Song, S. D., Chen, W., Miao, R. C., Zhou, Y. Y., et al. (2014). Model based on γ-glutamyltransferase and alkaline phosphatase for hepatocellular carcinoma prognosis. *World J. Gastroenterol.* 20 (31), 10944–10952. doi:10.3748/wjg.v20.i31.10944

Yamamoto, K., Awogi, T., Okuyama, K., and Takahashi, N. (2003). Nuclear localization of alkaline phosphatase in cultured human cancer cells. *Med. Electron Microsc.* 36 (1), 47–51. doi:10.1007/s007950300006

Yang, C., Tan, J., Chen, Y., Wang, Y., Qu, Y., Chen, J., et al. (2024). Prediction of late recurrence after curative-intent resection using MRI-measured spleen volume in patients with hepatocellular carcinoma and cirrhosis. *Insights Imaging* 15 (1), 31. doi:10.1186/s13244-024-01609-8

Yang, J. D., Kim, W. R., Coelho, R., Mettler, T. A., Benson, J. T., Sanderson, S. O., et al. (2011). Cirrhosis is present in most patients with hepatitis B and hepatocellular carcinoma. *Clin. Gastroenterol. Hepatol.* 9 (1), 64–70. doi:10.1016/j.cgh.2010.08.019

Yu, L., Liu, X., Wang, X., Dang, Z., Jiang, Y., Wang, X., et al. (2019). Impact of gender as a prognostic factor in HBV-related Hepatocellular Carcinoma: the survival strength of female patients in BCLC stage 0-B. *J. Cancer* 10 (18), 4237–4244. doi:10.7150/jca.33430

Zhao, Z., Zhu, Y., Ni, X., Lin, J., Li, H., Zheng, L., et al. (2021). Serum GGT/ALT ratio predicts vascular invasion in HBV-related HCC. *Cancer Cell Int.* 21 (1), 517. doi:10.1186/s12935-021-02214-1

Zhou, D., Liu, X., Wang, X., Yan, F., Wang, P., Yan, H., et al. (2021). A prognostic nomogram based on LASSO Cox regression in patients with alpha-fetoprotein-negative hepatocellular carcinoma following non-surgical therapy. *BMC Cancer* 21 (1), 246. doi:10.1186/s12885-021-07916-3

frontiers | Frontiers in Pharmacology

TYPE Original Research
PUBLISHED 07 January 2025
DOI 10.3389/fphar.2024.1499269

OPEN ACCESS

EDITED BY
Marcello Dallio,
University of Campania Luigi Vanvitelli, Italy

REVIEWED BY
Qun Tang,
Nanchang University, China
Jin Zhang,
University of Mississippi Medical Center, United States

*CORRESPONDENCE
Shiping Wen,
wensp@sysucc.org.cn
Yanzhang Hao,
hyz022@126.com

†These authors have contributed equally to this work

RECEIVED 20 September 2024
ACCEPTED 18 December 2024
PUBLISHED 07 January 2025

CITATION
Zhao Z, Jiang X, Wen S and Hao Y (2025) Efficiency and safety of HAIC combined with lenvatinib and tislelizumab for advanced hepatocellular carcinoma with high tumor burden: a multicenter propensity score matching analysis.
Front. Pharmacol. 15:1499269.
doi: 10.3389/fphar.2024.1499269

Efficiency and safety of HAIC combined with lenvatinib and tislelizumab for advanced hepatocellular carcinoma with high tumor burden: a multicenter propensity score matching analysis

Zhonghua Zhao[1†], Xiongying Jiang[2†], Shiping Wen[3*] and Yanzhang Hao[1*]

[1]Department of Oncology, Binzhou Medical University Hospital, Binzhou, Shandong, China, [2]Department of Interventional Radiology, Sun Yat-sen Memorial Hospital, Sun Yat-sen University, Guangzhou, China, [3]Department of Minimally Invasive Interventional Therapy, State Key Laboratory of Oncology in South China, Guangdong Provincial Clinical Research Center for Cancer, Sun Yat-Sen University Cancer Center, Guangzhou, China

Purpose: The present work focused on assessing whether hepatic arterial infusion chemotherapy (HAIC) combined with lenvatinib and tislelizumab was safe and effective on advanced hepatocellular carcinoma (HCC) showing high tumor burden.

Methods: In the present multicenter retrospective study, treatment-naive advanced HCC patients (BCLC stage C) showing high tumor burden (maximum diameter of intrahepatic lesion beyond 7 cm) treated with lenvatinib and tislelizumab with or without HAIC were reviewed for eligibility from June 2020 to June 2023. Baseline differences between groups were mitigated by propensity score matching (PSM). Our primary endpoint was overall survival (OS); and secondary endpoints included adverse events (AEs), progression-free survival (PFS), disease control rate (DCR) and objective response rate (ORR) according to RECIST 1.1 criteria, respectively.

Results: After eligibility reviewed, total 162 patients treated with lenvatinib and tislelizumab were enrolled: 63 patients with HAIC (HTP group), and the remaining 99 patients without HAIC (TP group). After PSM 1:1, 47 cases were evenly divided into each group. Of them, HTP group showed significant prolonged median OS compared with TP group (16.6 versus 21.0 months; hazard ratio [HR]: 0.26, 95% confidence interval [CI]: 0.35–0.98; $p = 0.039$), and median PFS of HTP group was also prolonged (8.9 versus 11.6 months; HR: 0.55, 95% CI: 0.34–0.87; $p = 0.010$). Higher DCR and ORR could be observed in HTP relative to TP groups (ORR: 53.2% versus 17.0%, $p < 0.001$; DCR: 87.2% versus 61.7%, $p = 0.004$). The severe AEs (grade 3/4) and all grades were comparable between the groups, while all of these AEs could be controlled, and AEs of grade 5 were not reported.

Conclusion: HAIC combined with lenvatinib and tislelizumab is the candidate treatment for advanced HCC patients because of its improved prognosis and acceptable safety.

KEYWORDS

hepatocellular carcinoma, hepatic arterial infusion chemotherapy, tyrosine kinase inhibitors, programmed cell death protein-1 inhibitors, propensity score matching

1 Introduction

Hepatocellular carcinoma (HCC) ranks the 6th place among cancers with regard to its morbidity and the 3rd place among factors inducing cancer-associated mortality worldwide in 2022, and the harm is even greater in China (Bray et al., 2024). The main reason is that the diagnosis in over 70% cases is made at the advanced stage in China, when radical treatment is unfeasible, resulting in extremely poor prognosis (Younossi et al., 2023). In the past decades, lots of novel therapy methods have been developed for cancer treatment, including nanotechnology, targeted therapy, immunotherapy and so on (Zhu et al., 2024; Liu et al., 2023; Dai et al., 2024). As recommended by the Barcelona Clinic Liver Cancer (BCLC) classification system, systemic treatment with immunotherapy and targeted therapy can be applied in advanced HCC, and the life expectancy has obviously improved (Reig et al., 2022).

Sorafenib has been recommended to be a first-line treatment for advanced HCC from 2008, which is effective in the SHARP and Oriental clinical trial (Llovet et al., 2008; Cheng et al., 2009). Until 2017, lenvatinib shows comparable overall survival (OS) and significantly improved progression-free survival (PFS), objective response, time to progression (TTP), as well as postponed life quality decline to sorafenib among untreated, non-resectable HCC cases (Kudo et al., 2018). Based on the result, lenvatinib has become a novel preferred option for advanced HCC. Besides, multiple programmed cell death protein 1 (PD-1) inhibitors gain approval for HCC, including first-line or second-line therapy options. Among them, tislelizumab is promising in treating HCC, and exhibited durable antitumor effect and favorable OS among advanced HCC cases from the front-line cohort in RATIONALE 301 study, comparing to sorafenib (Qin et al., 2023).

Next, with the positive result of the IMbrave150 study, targeted therapy combined with immunotherapy is becoming a preferred option for advanced hepatocellular carcinoma (Finn et al., 2020a). Except for bevacizumab, tyrosine kinase inhibitors (TKIs) combined with immunotherapy have also undergone extensive clinical trials and practice. Lenvatinib combined with pembrolizumab as the first-line therapy displays good antitumor effect in the KEYNOTE-524 phase 1b study, the median OS was 22.0 months, and the median PFS was 8.6 months, accompanied by controllable safety (Finn et al., 2020b). Unfortunately, though LEAP-002 phase III study demonstrated that lenvatinib combined with pembrolizumab could significantly improve prognosis, it could not reach specific significance in terms of prolonged OS and PFS compared with lenvatinib plus placebo, indicating that the therapeutic effect of combination therapy needs to be further enhanced (Llovet et al., 2023).

FOLFOX-based hepatic artery infusion chemotherapy (HAIC) can effectively treat advanced HCC, which can substantially increase OS in comparison with sorafenib (Lyu et al., 2022). HAIC can transfer sustained high drug concentration to the tumors, and induce the great local anticancer efficacy, resulting in effectively shrinking intrahepatic lesions, especially for those with high tumor burden (Chen et al., 2023). In addition, it has reported that chemotherapy can exert synergistic anti-tumor effects with immunotherapy and targeted therapy in various types of cancer (Ye et al., 2023; Tubridy et al., 2024), and many studies have also demonstrated that HAIC combined with PD-1 inhibitors and TKIs can improve survival outcomes for advanced HCC (Zhang et al., 2023; Lin et al., 2023). However, it remains unclear whether the triple combination therapy is safe and effective on advanced HCC with high tumor burden.

Therefore, the present work focused on investigating whether HAIC combined with lenvatinib and tislelizumab versus lenvatinib plus tislelizumab was effective and safe in the treatment of advanced HCC with high tumor burden.

2 Methods

2.1 Participants

Advanced (BCLC stage C) HCC cases receiving lenvatinib and tislelizumab treatment from June 2020 to June 2023 were enrolled into the present retrospective study and divided into HTP group (triple combination of HAIC, lenvatinib and tislelizumab) and TP group (lenvatinib and tislelizumab) according to treatment option.

Patients below were included: (1) those with the age of 18–75 years; (2) those with radiological or pathological diagnosis of HCC in line with guidelines of the American Association for the Study of Liver Diseases (AASLD); (3) BCLC C stage, either with extrahepatic metastasis or portal vein thrombus (PVTT); (4) maximum diameter of intrahepatic lesion beyond 7cm; (5) no previous anti-HCC therapy; (6) Child-Pugh class A or B, ALBI class 1 or 2, and Eastern Cooperative Oncology Group Performance Status score (ECOG PS) 0 or 1; (7) without additional malignant diseases within 5 years; (8) received at least six cycles of tislelizumab, 3 months of lenvatinib, and two cycles of HAIC in the HTP group; (9) at least 12 months from enrollment to cut-off time; and (10) sufficient follow-up and medical data. Patients below were excluded: (1) pathologically diagnosed as fibrolamellar HCC, sarcomatous HCC, or combined hepatocellular cholangiocarcinoma (HCC-CC); (2) active upper gastrointestinal bleeding or coagulation dysfunction; (3) therapy regimen discontinued or changed with no appropriate reason; and (4) without informed consent. Imaging examinations like enhanced computed tomography (CT) and magnetic resonance imaging (MRI), and laboratory test results were obtained in 1 week prior to initiating treatment.

This work was approved by ethics committee of our institutions. This study did not require informed consent because of its retrospective design.

2.2 Treatment procedures

HAIC was performed by experienced interventional physicians at each center. The detailed procedure of HAIC with oxaliplatin, fluorouracil, and leucovorin (FOLFOX) combination therapy was described previously (Lyu et al., 2022; Lyu et al., 2018a; Lyu et al., 2018b). To be specific, the tumor-feeding branch of hepatic artery was inserted with a catheter tip selectively according to the tumor size, location, and arterial supply. The following regimen was administered: oxaliplatin (CENEXI-Laboratoires THISSEN S.A.) (130 mg/m^2, 0–2 h on day 1), leucovorin (Qilu Pharmaceutical Co., Ltd.) (200 mg/m^2, 2–4 h on day 1), fluorouracil (Qilu Pharmaceutical Co., Ltd.) (400 mg/m^2 bolus within 15 min, and 2,400 mg/m^2 > 46 h on days 1 and 2). Repetitive HAIC was determined to perform at intervals of 3 weeks with no more than 8 cycles according to operators' evaluation.

Patients in both groups received oral administration of lenvatinib (Eisai Co., Ltd.) at 8 mg (≤60 kg) or 12 mg (>60 kg) in line with body weight, and 200 mg tislelizumab (BeiGene., Ltd.) intravenously every 3 weeks. Lenvatinib administration was conducted on day 1 during HAIC, whereas tislelizumab was given through intravenous injection on day 2 just after HAIC was completed in HTP group, while they were admitted at the same day in the TP group. If patients were intolerable due to the toxicities, lenvatinib or tislelizumab was reduced or discontinued until the disappearance of adverse events (AEs). A multidisciplinary team (MDT) was responsible for determining the change of transfer to salvage liver resection. Hepatectomy was carried out under the hands of experienced surgeons.

2.3 Efficacy and safety assessment

The primary endpoint was overall survival (OS), and the secondary endpoints included adverse events (AEs), progression-free survival (PFS), disease control rate (DCR) and objective response rate (ORR) according to RECIST 1.1 criteria, respectively. Contrast-enhanced CT or MRI was completed in 2 cycles and evaluated by 2 radiologists with rich experienced in liver disease. If there was any discrepancy in the results, it was evaluated by another senior radiologist and resolved by consensus. Treatment efficacy was evaluated based on the response evaluation criteria in solid tumor (RECIST) version 1.1. ORR referred to complete response (CR) or partial response (PR) rate in patients. DCR referred to CR, PR or stable disease (SD) rate in patients. OS referred to the duration between admission and death of all causes. PFS referred to the duration between admission and death of all causes or disease progression. We recorded AEs throughout the treatment and rated them in line with CTCAE version 5.0 (Freites-Martinez et al., 2021).

2.4 Propensity score matching (PSM) analysis

This study used PSM analysis for reducing selection bias while balancing the baseline features between groups. Besides, variables that could affect the response to treatment and outcomes, such as age, gender, etiology, Child-Pugh class, Eastern Cooperative Oncology Group of Performance Status (ECOG-PS), AFP, number of intrahepatic lesions, tumor size, albumin-bilirubin (ALBI) grade, extrahepatic metastasis, and portal vein tumor thrombus (PVTT), were identified by stepwise logistic regression with forward selection methods performed by R software (version 4.0.3; R Foundation Inc., Vienna, Austria). To minimize bias, improve simplicity and interpretability, and reduce variance, we adopted the 1:1 nearest-neighbor matching algorithm at the 0.2 caliper.

2.5 Statistical analysis

Statistical analysis was performed with SPSS27.0 (SPSS, Chicago, IL, United States) and R software (version 4.0.3; R Foundation Inc., Vienna, Austria). The continuous-variable normality test was performed using the Shapiro-Wilk normality test. Continuous data were represented by median (interquartile range, IQR) or mean ± standard deviation, and analyzed by Mann-Whitney U test or student t test according to normality. Categorical data were represented by number and percentages and compared by fisher exact test or χ^2 test. OS and PFS of time-to-event variables were estimated by Kaplan-Meier analysis, whereas log-rank test was conducted to analyze between-group differences. Risk factors related to survival were identified by univariable and multivariable Cox regression. Factors satisfying $p < 0.1$ from univariate regression were incorporated into multivariate regression. $p < 0.05$ (two-tailed) stood for statistical significance.

3 Results

3.1 Participants

Figure 1 displays the patient selection process. Altogether 162 advanced HCC patients with high tumor burden were enrolled, including 63 receiving the triple combination of HAIC plus lenvatinib and tislelizumab (HTP group), and the remaining 99 undergoing lenvatinib and tislelizumab without HAIC (TP group). Patients were followed up for a median period of 29.7 (95% Confidence interval [CI]: 18.4–38.9) and 24.9 (95% CI: 12.8–30.5) months till 30 June 2024, respectively. Age, ALBI class and extrahepatic metastasis were significantly different in both groups. PSM 1:1 ratio assigned 47 cases to every group for reducing the bias. Supplementary Table S1 shows the institutional distribution. Basic patient features were comparable in both groups following PSM ($p > 0.2$) (Table 1).

Prior to PSM, HTP group received median 4 cycles of HAIC (range: 2–8), 16 cycles of tislelizumab (range: 8–28), and 7.9 months of lenvatinib (range: 3.0–18.7), and patients in the TP group received median 12 cycles of tislelizumab (range: 6–23) and 5.1 months of lenvatinib (range: 3.0–15.2).

3.2 Tumor response

The treatment response was assessed before and following PSM according to RECIST 1.1 criteria (Table 2). Before PSM, HTP group

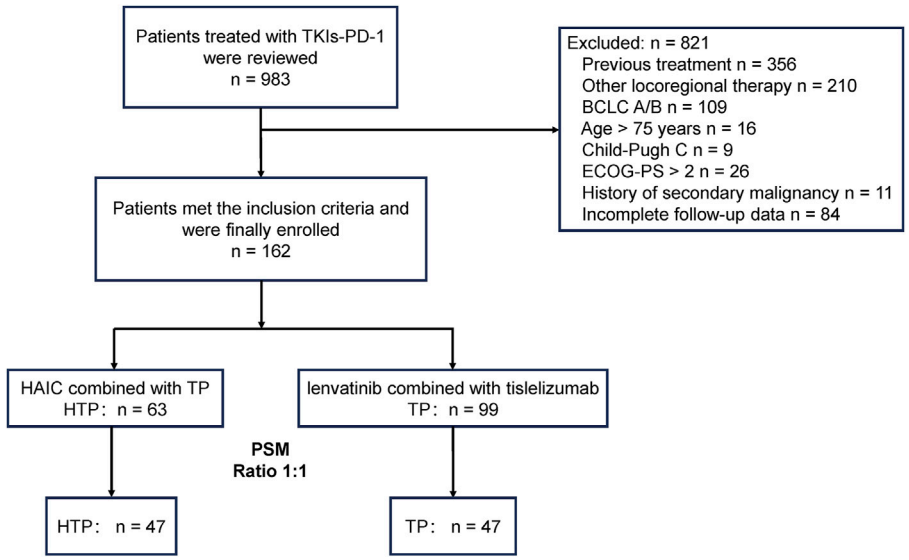

FIGURE 1
Patient selection flowchart. A patient might meet several exclusion criteria, but they were excluded only once from the uppermost criteria. PSM, propensity score matching; HTP, HAIC combined with lenvatinib and tislelizumab; TP, lenvatinib combined with tislelizumab; HAIC, hepatic arterial infusion chemotherapy; BCLC, Barcelona Clinic Liver Cancer; ECOG, Eastern Cooperative Oncology Group; PS, performance score.

showed increased ORR (58.7% versus 24.2%, $p < 0.001$) and DCR (88.9% versus 64.6%, $p < 0.001$), compared to TP group. After matching, HTP group also achieved higher rates of ORR (53.2% versus 17.0%, $p < 0.001$) and DCR (87.2% versus 61.7%, $p = 0.004$). Besides, the conversion rate to hepatectomy of HTP group was significant higher (before PSM: 1.0% versus 15.9%, $p < 0.001$; following PSM: 2.1% versus 17.0%, $p = 0.015$), as well.

3.3 Survival endpoints

Before PSM, there were 69 deaths (69.7%) from TP group and 41 (65.1%) from HTP group at the end follow-up time. HTP group had significantly prolonged OS (24.8 months, 95% CI: 20.7–29.3) compared with TP group (13.4 months, 95% CI: 12.5–17.7; HR: 0.36, 95% CI: 0.24–0.55, $p < 0.001$). Besides, HTP group also showed the markedly prolonged median PFS compared to TP group (13.3 months, 95% CI: 10.8–14.9 versus 7.1 months, 95% CI: 6.4–9.0; HR: 0.41, 95% CI: 0.28–0.59, $p < 0.001$). Of these 47 PSM pairs, HTP group also demonstrated evidently prolonged median OS than TP group (21.0 months, 95% CI: 20.1–29.3 versus 16.6 months, 95% CI: 13.1–25.8; HR: 0.58, 95% CI: 0.35–0.98, $p = 0.039$). Further, HTP group had prolonged median PFS compared with TP group (11.6 months, 95% CI: 10.4–14.9 versus 8.9 months, 95% CI: 6.6–13.3; HR: 0.55, 95% CI: 0.34–0.87, $p = 0.010$), as well (Figure 2).

3.4 Univariate and multivariate regression

This study carried out univariate and multivariate regression for identifying predictive factors for OS and PFS (Table 3). As revealed by multivariate Cox regression, triple combination treatment independently predicted the risk of OS and PFS. Besides, PVTT independently predicted the risk of OS. Etiology, extrahepatic metastasis and Child-Pugh class independently predicted the risk of PFS.

3.5 Subgroup analysis

This work drew forest plots for illustrating comparison among subgroups (Figure 3). As for the OS (Figure 3A) and PFS (Figure 3B), HTP group exhibited more beneficial effects in nearly every subgroup in comparison with TP group, indicating the effectiveness of HAIC, lenvatinib and tislelizumab combination therapy on advanced HCC patients with high tumor burden in each subgroup.

3.6 Progression reason analysis

Altogether 4 ways for tumor progression were detected, including extrahepatic metastasis, intrahepatic metastasis, local lesion progression, and death. For HTP and TP groups, there were respective 55 and 86 patients who have progressed at the cut-off follow-up time, and the proportion of four ways were 32.6%, 36.0%, 22.1% and 9.3% versus 21.8%, 27.3%, 21.8% and 29.1%. HTP group had lower proportion of intrahepatic metastasis and lesion progression compared with TP group (Supplementary Figure S1).

3.7 Subsequent treatments

At the end of follow-up, 78 and 39 patients in the HTP and TP group, respectively, experienced tumor progression (except for those

10.3389/fphar.2024.1499269

TABLE 1 Basic patient features before and following PSM.

Characteristic	Before PSM			Following PSM		
	TP n = 63	HTP n = 99	*p*	TP n = 47	HTP n = 47	*p*
Age (mean ± SD, year)	50 ± 12	45 ± 12	0.016	48 ± 11	47 ± 12	0.634
Age (year)			0.065			0.680
<50	45 (45.5%)	38 (60.3%)		23 (48.9%)	25 (53.2%)	
≥50	54 (54.5%)	25 (39.7%)		24 (51.1%)	22 (46.8%)	
Sex			0.174			0.748
Male	89 (89.9%)	52 (82.5%)		42 (89.4%)	41 (87.2%)	
Female	10 (10.1%)	11 (17.5%)		5 (10.6%)	6 (12.8%)	
ECOG-PS			0.070			>0.999
0	88 (88.9%)	61 (96.8%)		45 (95.7%)	45 (95.7%)	
1	11 (11.1%)	2 (3.2%)		2 (4.3%)	2 (4.3%)	
Etiology			0.799			>0.999
HBV	90 (90.9%)	58 (92.1%)		44 (93.6%)	44 (93.6%)	
Others	9 (9.1%)	5 (7.9%)		3 (6.4%)	3 (6.4%)	
Child-Pugh			0.115			>0.999
A	87 (87.9%)	60 (95.2%)		43 (91.5%)	44 (93.6%)	
B	12 (12.1%)	3 (4.8%)		4 (8.5%)	3 (6.4%)	
ALBI			0.044			0.680
1	39 (39.4%)	35 (55.6%)		24 (51.1%)	22 (46.8%)	
2	60 (60.6%)	28 (44.4%)		23 (48.9%)	25 (53.2%)	
AFP (μg/L)			0.652			0.836
<400	42 (42.4%)	29 (46.0%)		23 (48.9%)	22 (46.8%)	
≥400	57 (57.6%)	34 (54.0%)		24 (51.1%)	25 (53.2%)	
Intrahepatic lesion			0.054			0.472
Single	21 (21.2%)	22 (34.9%)		10 (21.3%)	13 (27.7%)	
Multiple	78 (78.8%)	41 (65.1%)		37 (78.7%)	34 (72.3%)	
Size (mean ± SD, cm)	12.2 ± 3.3	12.6 ± 3.4	0.367	12.4 ± 3.6	12.4 ± 3.3	0.931
Size (cm)			0.444			0.815
<10	29 (29.3%)	15 (23.8%)		13 (27.7%)	12 (25.5%)	
≥10	70 (70.7%)	48 (76.2%)		34 (72.3%)	35 (74.5%)	
PVTT			0.333			0.789
Presence	83 (83.8%)	49 (77.8%)		39 (83.0%)	38 (80.9%)	
Absence	16 (16.2%)	14 (22.2%)		8 (17.0%)	9 (19.1%)	
Extrahepatic metastasis			0.041			0.391
Presence	54 (54.5%)	24 (38.1%)		15 (31.9%)	19 (40.4%)	
Absence	45 (45.5%)	39 (61.9%)		32 (68.1%)	28 (59.6%)	

Continuous and categorical data are indicated by mean ± SD and n (%) separately.

P values were obtained by the two-sided Welch *t*-test and Pearson's χ^2 test.

PSM, propensity score matching; HTP, HAIC plus lenvatinib and tislelizumab; TP, lenvatinib plus tislelizumab; HAIC, hepatic arterial infusion chemotherapy; ECOG, eastern cooperative oncology group; PS, performance score; ALBI, albumin-bilirubin; AFP, alpha-fetoprotein; PVTT, portal vein tumor thrombus.

TABLE 2 Therapeutic effect assessed through RECIST 1.1 criteria before and following PSM.

Response	Before PSM			Following PSM		
	TP (n = 99)	HTP (n = 63)	*p*	TP (n = 47)	HTP (n = 47)	*p*
Complete response	0 (0)	0 (0)		0 (0)	0 (0)	
Partial response	24 (24.2%)	37 (58.7%)		8 (17.0%)	25 (53.2%)	
Stable disease	40 (40.4%)	19 (30.2%)		21 (44.7%)	16 (34.0%)	
Progression disease	35 (35.4%)	7 (11.1%)		18 (38.3%)	6 (12.8%)	
Objective response rate	24 (24.2%)	37 (58.7%)	<0.001	8 (17.0%)	25 (53.2%)	<0.001
Disease control rate	64 (64.6%)	56 (88.9%)	<0.001	29 (61.7%)	41 (87.2%)	0.004
Conversion to hepatectomy	1 (1.0%)	10 (15.9%)	<0.001	1 (2.1%)	8 (17.0%)	0.015

Summary of optimal response.
Data are indicated by n (%).
p values were obtained by the two-sided χ^2 test.
PSM, propensity score matching; RECIST, response evaluation criteria in solid tumors; HTP, HAIC plus lenvatinib and tislelizumab; TP, lenvatinib plus tislelizumab; HAIC, hepatic arterial infusion chemotherapy.

due to death). Additionally, 55 (70.5%) and 32 (82.1%) patients in the two groups, separately, underwent subsequent treatment. In TP and HTP groups, HAIC combined with lenvatinib plus tislelizumab (34.5%), and TACE combined with lenvatinib and tislelizumab (31.3%) were the most frequently adopted subsequent treatments. TACE and HAIC remained the preferred options for locoregional treatment, while atezolizumab plus bevacizumab and regorafenib were the preferred options for systemic treatment after progression (Supplementary Table S2).

3.8 Safety

As exhibited in Table 4, overall incidence rates of AEs in HTP and the TP group were 82.5% and 80.1%, respectively. In HTP group, AEs including decreased appetite (77.8%), neurologic toxicity (60.3%), and leukopenia (57.1%) occurred at the highest frequency, whereas severe AEs (grade 3/4) with the highest occurrence frequency included abdominal pain (7.9%), diarrhea (7.9%), and proteinuria (7.9%). In TP group, AEs like hypertension (52.5%), decreased appetite (41.4%), and elevated AST (33.3%) occurred at the highest frequency, and severe AEs with the highest frequency included proteinuria (10.1%), diarrhea (7.1%) and hypertension (7.1%). Though the overall incidence of any grade and severe AEs was higher in HTP group, there were no significant difference between the two groups. Obviously, HAIC-related (e.g., hypertension and hand-foot skin reaction) AEs was significantly higher in HTP group, but these AEs could be managed, and no treatment-related death happened.

4 Discussion

The present multicenter clinical study is the first to examine whether HAIC plus lenvatinib and tislelizumab was as effective and safe as lenvatinib plus tislelizumab for advanced HCC with high tumor burden, and the triple combination therapy significantly improved survival and tumor response compared with the dual combination therapy. Besides, PSM was conducted for eliminating group heterogeneities, a relatively large sample size was included among diverse centers, and long-time follow-ups were performed. At last, no matter in PSM cohort or the whole cohort, HTP group showed significantly prolonged OS and PFS comparing to TP group. Noteworthily, triple combination therapy induced the increased AEs rate, while efficient measures were adopted for mitigating AEs.

According to current guidelines, locoregional therapy, mainly referring to TACE, has been recommended to be the first-line therapy for immediate-stage HCC, while systemic treatment remains the preferred option in advanced stage HCC (Singal et al., 2023; Vogel and Martinelli, 2021). Although the dual immunotherapies atezolizumab-bevacizumab and durvalumab-tremelimumab have been shown to result in better OS and PFS than sorafenib, lenvatinib remained the first-line choice for PVTT patients in China, giving the rather high cost of the dual immunotherapies and the prevalent risk of gastric bleeding due to cirrhosis. However, in the phase 3 randomized controlled study of LEAP 002, lenvatinib plus pembrolizumab failed to meet the pre-specified statistical significance on OS, even though the combination therapy achieved the longest median OS time ever reported in first-line HCC studies. Hence, it is worth noting that locoregional treatment and systemic treatment should complement each other rather than be mutually exclusive, especially for those with high-risk factors, including high tumor burden or extrahepatic metastasis. Locoregional therapy can reduce the tumor burden in a relatively short time, while systemic therapy can effectively control the intrahepatic and extrahepatic lesions in a relatively longer period, resulting in an enhanced synergistic anti-tumor effect (Cappuyns et al., 2024; Brown et al., 2023). As reported, an increasing number of clinical trials have demonstrated that locoregional therapy, including TACE or HAIC, combined with TKIs and/or PD-1 inhibitors possessed favorable outcomes in advanced HCC patients, comparing to monotherapy or dual combination therapy (Kulik and El-Serag, 2019). As reported in a phase II clinical study (TRIPLET), HAIC combined with camrelizumab and apatinib for HCC in BCLC C stage demonstrated encouraging results and manageable safety. Over 50% of the

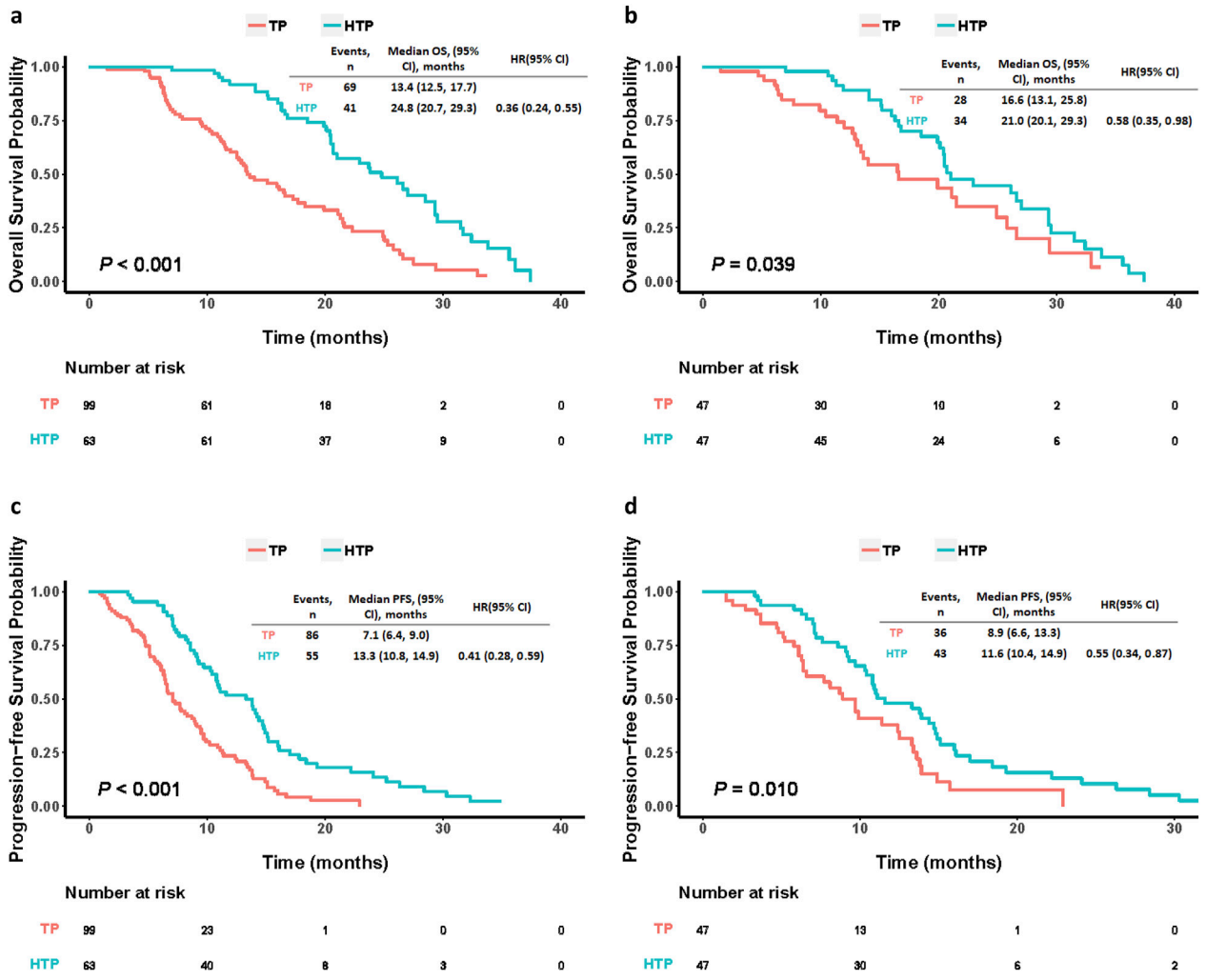

FIGURE 2
Kaplan-Meier curves comparing OS and PFS among patients who underwent HAIC plus lenvatinib and tislelizumab (HTP) or lenvatinib plus tislelizumab (TP) before **(A, B)** and after **(C, D)** PSM. *p* values were calculated using Log-rank test. PSM, propensity score matching; HTP, HAIC combined with lenvatinib and tislelizumab; TP, lenvatinib combined with tislelizumab; HAIC, hepatic arterial infusion chemotherapy; OS, overall survival; PFS, progression-free survival; HR, hazard ratio; CI, confidence interval.

enrolled patients had high risk factors, including Vp3/4 or extrahepatic metastasis. The median PFS was 10.38c months, and the ORR and DCR were 77.1% and 97.1%, respectively (Chen et al., 2023), consistent with our study.

Some rationales were proposed for combining HAIC rather than TACE as the locoregional treatment in the study. First, previous studies have demonstrated that comparing with TACE, FOLFOX-HAIC results in favorable tumor response and superior outcomes for advanced HCC due to the direct delivery high-dose chemotherapeutic drugs into tumor via hepatic artery (Li et al., 2021). As a result, Chinese guidelines have recommended HAIC rather TACE as one of first-line options for advanced HCC, particularly for patients with high tumor burden (Xie et al., 2023). Second, TACE can induce hypoxia in the tumor microenvironment, which may activate hypoxia-inducible factors (HIFs) and promote tumor survival, angiogenesis, and subsequent recurrence (Gai et al., 2020). Third, many embolization particles are required for embolizing large-sized HCC, probably leading to an increased risk of hepatic functional reserve deterioration, nontarget embolization, and postembolization syndrome (Roehlen et al., 2023). Finally, total embolization is not easy for large-sized HCC due to extrahepatic collateral arteries (Li et al., 2022).

We also carried out subgroup analyses on OS and PFS according to different factors. HTP group showed the clinical benefits for almost all the subgroups. Nonetheless, broad 95% CI ranges were observed in females, patients of Child-Pugh class B, and those without HBV infection, probably associated with the small sample size in each subgroup.

When analyzing various endpoints to PFS, HTP group had obviously lower proportion of intrahepatic metastasis and local lesion progression comparing to TP group. These findings suggested that HAIC, as a locoregional approach, could play an important role in controlling intrahepatic and local recurrence, and the triple combination therapy could exert the synergistic anticancer efficacy. Expectedly, intrahepatic and local recurrence mainly restricted the survival benefits of systemic therapy. Therefore, the

TABLE 3 Univariate and multivariate regression of predictive factors for survival post-treatment.

Variables	OS				PFS			
	Univariate regression		Multivariate regression		Univariate regression		Multivariate regression	
	HR (95% CI)	*P*	HR (95% CI)	*P*	HR (95% CI)	*P*	HR (95% CI)	*P*
Treatment (HTP)	0.36 (0.24–0.55)	<0.001	0.40 (0.26–0.61)	<0.001	0.41 (0.28–0.59)	<0.001	0.45 (0.31–0.65)	<0.001
Age (≥50 years)	0.95 (0.65–1.40)	0.811			0.89 (0.64–1.24)	0.494		
Sex (Male)	1.34 (0.73–2.44)	0.343			1.66 (1.01–2.74)	0.048	1.82 (0.85–3.16)	0.133
ECOG-PS (1)	2.17 (1.13–4.19)	0.021	1.62 (0.78–3.36)	0.199	1.38 (0.76–2.50)	0.289		
Etiology (Others)	1.50 (0.84–2.68)	0.174			1.70 (0.97–2.97)	0.064	2.32 (1.28–4.22)	0.006
Child-Pugh (B)	1.67 (0.89–3.13)	0.112			1.91 (1.07–3.41)	0.028	1.93 (1.07–3.49)	0.028
ALBI (2)	1.15 (0.79–1.68)	0.477			1.16 (0.83–1.62)	0.385		
Number (Multiple)	1.31 (0.85–2.02)	0.221			1.51 (1.03–2.22)	0.035	1.27 (0.86–1.90)	0.233
Size (≥10 cm)	1.18 (0.77–1.80)	0.451			0.72 (0.50–1.04)	0.083	0.75 (0.52–1.09)	0.132
AFP (≥400ug/L)	1.39 (0.94–2.06)	0.097	1.28 (0.84–1.96)	0.255	1.09 (0.78–1.52)	0.628		
PVTT (Presence)	2.14 (1.22–3.77)	0.008	1.89 (1.06–3.36)	0.030	1.00 (0.65–1.54)	0.985		
Metastasis (Presence)	0.98 (0.67–1.43)	0.903			1.52 (1.09–2.14)	0.015	1.44 (1.00–2.07)	0.047

Univariable and multivariable Cox regression conducted for identifying survival-related factors. Factors satisfying $p < 0.1$ upon univariate regression were incorporated for multivariate regression. $p < 0.05$ (two-sided) stands for statistical significance.

HTP, HAIC plus lenvatinib and tislelizumab; TP, lenvatinib plus tislelizumab; HAIC, hepatic arterial infusion chemotherapy; ECOG, eastern cooperative oncology group; PS, performance score; ALBI, albumin-bilirubin; AFP, alpha-fetoprotein; PVTT, portal vein tumor thrombus; OS, overall survival; PFS, progression-free survival.

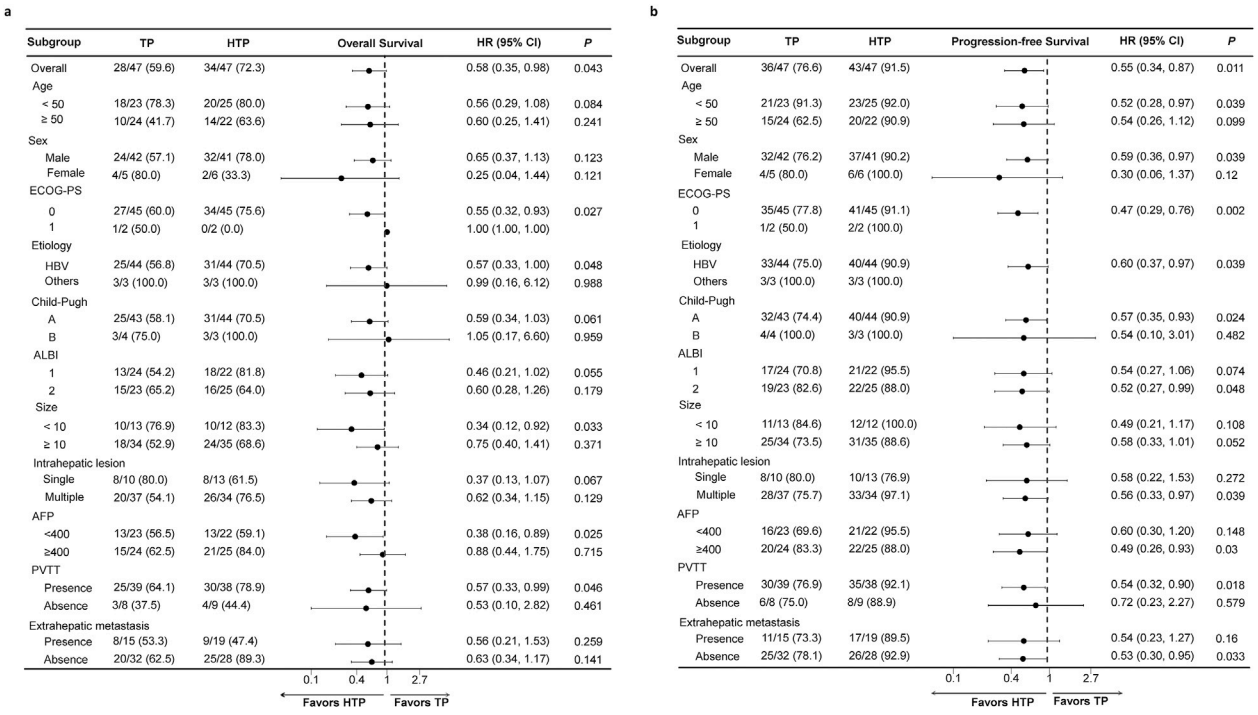

FIGURE 3
Forest plots based on OS **(A)** and PFS **(B)** of each subgroup. *p* values were calculated using Log-rank test. PSM, propensity score matching; HTP, HAIC combined with lenvatinib and tislelizumab; TP, lenvatinib combined with tislelizumab; HAIC, hepatic arterial infusion chemotherapy; OS, overall survival; PFS, progression-free survival; HR, hazard ratio; CI, confidence interval; ECOG, Eastern Cooperative Oncology Group; PS, performance score; ALBI, albumin-bilirubin; AFP, alpha-fetoprotein; PVTT, portal vein tumor thrombus.

TABLE 4 Treatment-associated adverse events.

Adverse events	Any grade			Grade 3/4		
	HTP (n = 63)	TP (n = 99)	*P*	HTP (n = 63)	TP (n = 99)	*P*
Overall incidence	52 (82.5%)	80 (80.1%)	0.782	22 (34.9%)	37 (37.4%)	0.752
Abdominal pain	35 (55.6%)	18 (28.6%)	0.000	5 (7.9%)	1 (1.0%)	0.033
Nausea	29 (46.0%)	21 (21.2%)	0.001	3 (4.8%)	2 (2.0%)	0.378
Diarrhea	31 (49.2%)	24 (24.2%)	0.001	5 (7.9%)	7 (7.1%)	0.837
Fever	26 (41.3%)	4 (4.0%)	0.000	1 (1.6%)	2 (2.0%)	1.000
Decreased appetite	49 (77.8%)	41 (41.4%)	0.000	2 (3.2%)	3 (3.0%)	1.000
Rush	13 (20.6%)	29 (29.3%)	0.220	2 (3.2%)	4 (4.0%)	1.000
Fatigue	25 (39.7%)	19 (19.2%)	0.004	2 (3.2%)	3 (3.0%)	1.000
Hypoproteinemia	16 (25.4%)	21 (21.2%)	0.536	2 (3.2%)	2 (2.0%)	0.643
Elevated bilirubin	19 (30.2%)	25 (25.3%)	0.494	3 (4.8%)	4 (4.0%)	1.000
Elevated ALT	31 (49.2%)	25 (25.3%)	0.002	2 (3.2%)	1 (1.0%)	0.561
Elevated AST	29 (46.0%)	33 (33.3%)	0.105	1 (1.6%)	1 (1.0%)	1.000
Hypothyroidism	4 (6.3%)	6 (6.1%)	1.000	1 (1.6%)	1 (1.0%)	1.000
Neurologic toxicity	38 (60.3%)	6 (6.1%)	0.000	4 (6.3%)	0 (0)	0.022
Leukopenia	36 (57.1%)	17 (17.2%)	0.000	3 (4.8%)	1 (1.0%)	0.300
Thrombocytopenia	25 (39.7%)	29 (29.3%)	0.171	4 (6.3%)	6 (6.1%)	1.000
Hypertension	20 (31.7%)	52 (52.5%)	0.009	3 (4.8%)	7 (7.1%)	0.742
Hand-foot skin reaction	18 (28.6%)	29 (29.3%)	0.921	3 (4.8%)	7 (7.1%)	0.742
Dysphonia	5 (7.9%)	14 (14.1%)	0.231	0 (0.0%)	1 (1.0%)	1.000
Proteinuria	11 (17.5%)	28 (28.3%)	0.116	5 (7.9%)	10 (10.1%)	0.643
Bleeding (gingiva)	4 (6.3%)	8 (8.1%)	0.767	1 (1.6%)	3 (3.0%)	1.000
Joint pain	11 (17.4%)	25 (25.3%)	0.245	3 (4.8%)	6 (6.1%)	1.000
Immunity-related AEs	9 (14.3%)	17 (17.2%)	0.626	2 (3.2%)	5 (5.1%)	0.707

Data are represented by n (%).
p values were determined by two-sided χ^2 test.
HTP, HAIC combined with lenvatinib and tislelizumab; TP, lenvatinib combined with tislelizumab; HAIC, hepatic arterial infusion chemotherapy; ALT, alanine transaminase; AST, aspartate aminotransferase.

combination with HAIC probably further improved prognosis (Yuan et al., 2023).

The ration of subsequent therapy was higher in HTP group (82.1% versus 70.5%), suggesting that treatment following progression might be conducted at a higher frequency among patients receiving HAIC plus lenvatinib and tislelizumab. This may be explained from two aspects. First, triple combination therapy provided superior efficacy, improving the compliance of patients. Second, triple combination therapy significantly prolonged survival, providing more opportunities for subsequent treatments.

In addition to favorable outcomes, HAIC combined with lenvatinib and tislelizumab increased AEs rate to some extent. The higher HAIC-related AEs incidence took place, consistent with those in previous trials of HAIC. However, those AEs could be controllable using corresponding supporting medications, without aggravating the condition or treatment discontinuation. HTP group had increased AEs incidence relative to locoregional therapy or systemic therapy in the previous studies (Kudo et al., 2018; Qin et al., 2023; Llovet et al., 2023; Lyu et al., 2018a), the reasons of which may be that the enrolled patients in the study were with worse baseline levels, and the systemic therapy aggravated the toxicity of HAIC. Abdominal pain resulting from arteria vasospasm in oxaliplatin infusion was also a common HAIC-specific AE. So far, abdominal pain cannot be effectively avoided, with the exception of the prescription of pain/spasm relieving agents or slowing down oxaliplatin infusion (Wu et al., 2021; Proietti et al., 2007). Collectively, HAIC combined with lenvatinib and tislelizumab showed acceptable safety and tolerability.

Certain limitations should be noted in the present work. First, due to the retrospective nature, selection bias could not be avoided. Though PSM was conducted for minimizing between-group heterogeneities, there were still endogenous differences due to unmeasured confounders, population differences, temporal bias, exclusion of non-matched cases, and information bias. Consequently, more prospective randomized controlled studies should be conducted for validating our

results. Second, since the study primarily included HBV-positive individuals, it is important to note that HCC in patients with HBV infection can differ biologically and clinically from HCC in individuals with other etiologies, such as hepatitis C virus (HCV) or non-alcoholic fatty liver disease (NAFLD). The treatment responses, prognosis, and underlying mechanisms of HCC may vary across these different patient populations. It should acknowledge that the findings may not be fully applicable to non-HBV patients, especially in regions where HCV or NAFLD-related HCC is more common. Third, the patient cohort being sourced mainly from Chinese medical centers is another important limitation. The genetic, environmental, and healthcare-related factors in China may differ from those in other countries or regions, such as Europe or North America. These differences could impact treatment response and outcomes. It is important to state that the study's results may not be directly applicable to populations in other parts of the world, particularly where the prevalence of HBV and other risk factors for HCC may differ significantly. The study should call for further validation in more diverse cohorts from different geographic regions to confirm the external validity of the findings. Finally, we just enrolled cases undergoing tislelizumab treatment, and further exploration is warranted for determining if the same results are attained using other PD-1 inhibitors.

5 Conclusion

In conclusion, comparing to lenvatinib plus tislelizumab, HAIC plus lenvatinib and tislelizumab achieves markedly improved OS, PFS, and ORR for advanced HCC with high tumor burden, and this combination treatment is safe. Before prospective results are revealed, our results support applying the triple combination treatment for advanced HCC with high tumor burden.

Data availability statement

The original contributions presented in the study are included in the article/Supplementary Material, further inquiries can be directed to the corresponding authors.

Ethics statement

The studies involving humans were approved by the Binzhou Medical University Hospital, Sun Yat-sen Memorial Hospital, and Sun Yat-Sen University Cancer Center. The studies were conducted in accordance with the local legislation and institutional requirements. The participants provided their written informed consent to participate in this study.

Author contributions

ZZ: Data curation, Formal Analysis, Writing–original draft, Writing–review and editing. XJ: Data curation, Formal Analysis, Writing–original draft, Writing–review and editing. SW: Conceptualization, Data curation, Formal Analysis, Writing–original draft, Writing–review and editing. YH: Conceptualization, Writing–original draft, Writing–review and editing.

Funding

The author(s) declare that no financial support was received for the research, authorship, and/or publication of this article.

Conflict of interest

The authors declare that the research was conducted in the absence of any commercial or financial relationships that could be construed as a potential conflict of interest.

Publisher's note

Supplementary material

The Supplementary Material for this article can be found online at: https://www.frontiersin.org/articles/10.3389/fphar.2024.1499269/full#supplementary-material

References

Bray, F., Laversanne, M., Sung, H., Ferlay, J., Siegel, R. L., Soerjomataram, I., et al. (2024). Global cancer statistics 2022: GLOBOCAN estimates of incidence and mortality worldwide for 36 cancers in 185 countries. *CA Cancer J. Clin.* 74 (3), 229–263. doi:10.3322/caac.21834

Brown, Z. J., Tsilimigras, D. I., Ruff, S. M., Mohseni, A., Kamel, I. R., Cloyd, J. M., et al. (2023). Management of hepatocellular carcinoma: a review. *Jama Surg.* 158 (4), 410–420. doi:10.1001/jamasurg.2022.7989

Cappuyns, S., Corbett, V., Yarchoan, M., Finn, R. S., and Llovet, J. M. (2024). Critical appraisal of guideline recommendations on systemic therapies for advanced hepatocellular carcinoma: a review. *Jama Oncol.* 10 (3), 395–404. doi:10.1001/jamaoncol.2023.2677

Chen, Q. F., Lyu, N., Wang, X., Jiang, X. Y., Hu, Y., Chen, S., et al. (2023). Cost-effectiveness and prognostic model of hepatic arterial infusion chemotherapy for hepatocellular carcinoma with high tumor burden and/or Vp4 tumor thrombus compared with sorafenib: a post-hoc analysis of the FOHAIC-1 trial. *Int. J. Surg.* 109 (12), 3929–3939. doi:10.1097/JS9.0000000000000683

Cheng, A. L., Kang, Y. K., Chen, Z., Tsao, C. J., Qin, S., Kim, J. S., et al. (2009). Efficacy and safety of sorafenib in patients in the Asia-Pacific region with advanced hepatocellular carcinoma: a phase III randomised, double-blind, placebo-controlled trial. *Lancet Oncol.* 10 (1), 25–34. doi:10.1016/S1470-2045(08)70285-7

Dai, J., Ashrafizadeh, M., Aref, A. R., Sethi, G., and Ertas, Y. N. (2024). Peptide-functionalized, -assembled and -loaded nanoparticles in cancer therapy. *Drug Discov. Today* 29 (7), 103981. doi:10.1016/j.drudis.2024.103981

Finn, R. S., Ikeda, M., Zhu, A. X., Sung, M. W., Baron, A. D., Kudo, M., et al. (2020b). Phase ib study of lenvatinib plus pembrolizumab in patients with unresectable hepatocellular carcinoma. *J. Clin. Oncol.* 38 (26), 2960–2970. doi:10.1200/JCO.20.00808

Finn, R. S., Qin, S., Ikeda, M., Galle, P. R., Ducreux, M., Kim, T. Y., et al. (2020a). Atezolizumab plus bevacizumab in unresectable hepatocellular carcinoma. *N. Engl. J. Med.* 382 (20), 1894–1905. doi:10.1056/NEJMoa1915745

Freites-Martinez, A., Santana, N., Arias-Santiago, S., and Viera, A. (2021). Using the common terminology criteria for adverse events (CTCAE - version 5.0) to evaluate the severity of adverse events of anticancer therapies. *Actas Dermosifiliogr. Engl. Ed.* 112 (1), 90–92. doi:10.1016/j.ad.2019.05.009

Gai, X., Zhou, P., Xu, M., Liu, Z., Zheng, X., and Liu, Q. (2020). Hyperactivation of IL-6/STAT3 pathway leaded to the poor prognosis of post-TACE HCCs by HIF-1α/SNAI1 axis-induced epithelial to mesenchymal transition. *J. Cancer* 11 (3), 570–582. doi:10.7150/jca.35631

Kudo, M., Finn, R. S., Qin, S., Han, K. H., Ikeda, K., Piscaglia, F., et al. (2018). Lenvatinib versus sorafenib in first-line treatment of patients with unresectable hepatocellular carcinoma: a randomised phase 3 non-inferiority trial. *Lancet* 391 (10126), 1163–1173. doi:10.1016/S0140-6736(18)30207-1

Kulik, L., and El-Serag, H. B. (2019). Epidemiology and management of hepatocellular carcinoma. *Gastroenterology* 156 (2), 477–491. doi:10.1053/j.gastro.2018.08.065

Li, Q. J., He, M. K., Chen, H. W., Fang, W. Q., Zhou, Y. M., Xu, L., et al. (2022). Hepatic arterial infusion of oxaliplatin, fluorouracil, and leucovorin versus transarterial chemoembolization for large hepatocellular carcinoma: a randomized phase III trial. *J. Clin. Oncol.* 40 (2), 150–160. doi:10.1200/JCO.21.00608

Li, S., Lyu, N., Han, X., Li, J., Lai, J., He, M., et al. (2021). Hepatic artery infusion chemotherapy using fluorouracil, leucovorin, and oxaliplatin versus transarterial chemoembolization as initial treatment for locally advanced hepatocellular carcinoma: a propensity score-matching analysis. *J. Vasc. Interv. Radiol.* 32 (9), 1267–1276.e1. doi:10.1016/j.jvir.2021.06.008

Lin, Z., Chen, D., Hu, X., Huang, D., Chen, Y., Zhang, J., et al. (2023). Clinical efficacy of HAIC (FOLFOX) combined with lenvatinib plus PD-1 inhibitors vs. TACE combined with lenvatinib plus PD-1 inhibitors in the treatment of advanced hepatocellular carcinoma with portal vein tumor thrombus and arterioportal fistulas. *Am. J. Cancer Res.* 13 (11), 5455–5465.

Liu, Y., Wang, Y., Yang, Y., Weng, L., Wu, Q., Zhang, J., et al. (2023). Emerging phagocytosis checkpoints in cancer immunotherapy. *Signal Transduct. Target Ther.* 8 (1), 104. doi:10.1038/s41392-023-01365-z

Llovet, J. M., Kudo, M., Merle, P., Meyer, T., Qin, S., Ikeda, M., et al. (2023). Lenvatinib plus pembrolizumab versus lenvatinib plus placebo for advanced hepatocellular carcinoma (LEAP-002): a randomised, double-blind, phase 3 trial. *Lancet Oncol.* 24 (12), 1399–1410. doi:10.1016/S1470-2045(23)00469-2

Llovet, J. M., Ricci, S., Mazzaferro, V., Hilgard, P., Gane, E., Blanc, J. F., et al. (2008). Sorafenib in advanced hepatocellular carcinoma. *N. Engl. J. Med.* 359 (4), 378–390. doi:10.1056/NEJMoa0708857

Lyu, N., Kong, Y., Mu, L., Lin, Y., Li, J., Liu, Y., et al. (2018a). Hepatic arterial infusion of oxaliplatin plus fluorouracil/leucovorin vs. sorafenib for advanced hepatocellular carcinoma. *J. Hepatol.* 69 (1), 60–69. doi:10.1016/j.jhep.2018.02.008

Lyu, N., Lin, Y., Kong, Y., Zhang, Z., Liu, L., Zheng, L., et al. (2018b). FOXAI: a phase II trial evaluating the efficacy and safety of hepatic arterial infusion of oxaliplatin plus fluorouracil/leucovorin for advanced hepatocellular carcinoma. *Gut* 67 (2), 395–396. doi:10.1136/gutjnl-2017-314138

Lyu, N., Wang, X., Li, J. B., Lai, J. F., Chen, Q. F., Li, S. L., et al. (2022). Arterial chemotherapy of oxaliplatin plus fluorouracil versus sorafenib in advanced hepatocellular carcinoma: a biomolecular exploratory, randomized, phase III trial (FOHAIC-1). *J. Clin. Oncol.* 40 (5), 468–480. doi:10.1200/JCO.21.01963

Proietti, S., De Baere, T., Bessoud, B., Doenz, F., Qanadli, S. D., Schnyder, P., et al. (2007). Interventional management of gastroduodenal lesions complicating intra-arterial hepatic chemotherapy. *Eur. Radiol.* 17 (8), 2160–2165. doi:10.1007/s00330-006-0552-3

Qin, S., Kudo, M., Meyer, T., Bai, Y., Guo, Y., Meng, Z., et al. (2023). Tislelizumab vs sorafenib as first-line treatment for unresectable hepatocellular carcinoma: a phase 3 randomized clinical trial. *Jama Oncol.* 9 (12), 1651–1659. doi:10.1001/jamaoncol.2023.4003

Reig, M., Forner, A., Rimola, J., Ferrer-Fàbrega, J., Burrel, M., Garcia-Criado, Á., et al. (2022). BCLC strategy for prognosis prediction and treatment recommendation: the 2022 update. *J. Hepatol.* 76 (3), 681–693. doi:10.1016/j.jhep.2021.11.018

Roehlen, N., Stoehr, F., Müller, L., Luxenburger, H., Gairing, S. J., Reincke, M., et al. (2023). Prediction of postembolization syndrome after transarterial chemoembolization of hepatocellular carcinoma and its impact on prognosis. *Hepatol. Commun.* 7 (10), e0252. doi:10.1097/HC9.0000000000000252

Singal, A. G., Llovet, J. M., Yarchoan, M., Mehta, N., Heimbach, J. K., Dawson, L. A., et al. (2023). AASLD Practice Guidance on prevention, diagnosis, and treatment of hepatocellular carcinoma. *Hepatology* 78 (6), 1922–1965. doi:10.1097/HEP.0000000000000466

Tubridy, E. A., Taunk, N. K., and Ko, E. M. (2024). Treatment of node-positive endometrial cancer: chemotherapy, radiation, immunotherapy, and targeted therapy. *Curr. Treat. Options Oncol.* 25 (3), 330–345. doi:10.1007/s11864-023-01169-x

Vogel, A., and Martinelli, E., (2021). Updated treatment recommendations for hepatocellular carcinoma (HCC) from the ESMO Clinical Practice Guidelines. *Ann. Oncol.* 32 (6), 801–805. doi:10.1016/j.annonc.2021.02.014

Wu, Z., Guo, W., Chen, S., and Zhuang, W. (2021). Determinants of pain in advanced HCC patients recieving hepatic artery infusion chemotherapy. *Invest. New Drugs* 39 (2), 394–399. doi:10.1007/s10637-020-01009-x

Xie, D., Shi, J., Zhou, J., Fan, J., and Gao, Q. (2023). Clinical practice guidelines and real-life practice in hepatocellular carcinoma: a Chinese perspective. *Clin. Mol. Hepatol.* 29 (2), 206–216. doi:10.3350/cmh.2022.0402

Ye, F., Dewanjee, S., Li, Y., Jha, N. K., Chen, Z. S., Kumar, A., et al. (2023). Advancements in clinical aspects of targeted therapy and immunotherapy in breast cancer. *Mol. Cancer* 22 (1), 105. doi:10.1186/s12943-023-01805-y

Younossi, Z. M., Wong, G., Anstee, Q. M., and Henry, L. (2023). The global burden of liver disease. *Clin. Gastroenterol. Hepatol.* 21 (8), 1978–1991. doi:10.1016/j.cgh.2023.04.015

Yuan, Y., He, W., Yang, Z., Qiu, J., Huang, Z., Shi, Y., et al. (2023). TACE-HAIC combined with targeted therapy and immunotherapy versus TACE alone for hepatocellular carcinoma with portal vein tumour thrombus: a propensity score matching study. *Int. J. Surg.* 109 (5), 1222–1230. doi:10.1097/JS9.0000000000000256

Zhang, T. Q., Geng, Z. J., Zuo, M. X., Li, J. B., Huang, J. H., Huang, Z. L., et al. (2023). Camrelizumab (a PD-1 inhibitor) plus apatinib (an VEGFR-2 inhibitor) and hepatic artery infusion chemotherapy for hepatocellular carcinoma in Barcelona Clinic Liver Cancer stage C (TRIPLET): a phase II study. *Signal Transduct. Target Ther.* 8 (1), 413. doi:10.1038/s41392-023-01663-6

Zhu, H., Sun, H., Dai, J., Hao, J., and Zhou, B. (2024). Chitosan-based hydrogels in cancer therapy: drug and gene delivery, stimuli-responsive carriers, phototherapy and immunotherapy. *Int. J. Biol. Macromol.* 282 (Pt 2), 137047. doi:10.1016/j.ijbiomac.2024.137047

frontiers | Frontiers in Medicine

TYPE Systematic Review
PUBLISHED 29 January 2025
DOI 10.3389/fmed.2024.1511511

OPEN ACCESS

EDITED BY
Pradeep Kumar Shukla,
University of Tennessee Health Science Center (UTHSC), United States

REVIEWED BY
Ali Reza Safarpour,
Gastroenterohepatology Research Center, Iran
Jianhai Guo,
Peking University, China

*CORRESPONDENCE
Gang Cheng
✉ chenggang63@hotmail.com
Xin Zhao
✉ sxdteyyzx@163.com

†These authors share first authorship

RECEIVED 15 October 2024
ACCEPTED 20 December 2024
PUBLISHED 29 January 2025
CORRECTED 29 August 2025

CITATION
Tuersun A, Mohetaer M, Hou G and Cheng G (2025) Meta-analysis of the efficiency and safety of neoadjuvant therapy with immune checkpoint inhibitors in resectable hepatocellular carcinoma. *Front. Med.* 11:1511511. doi: 10.3389/fmed.2024.1511511

Meta-analysis of the efficiency and safety of neoadjuvant therapy with immune checkpoint inhibitors in resectable hepatocellular carcinoma

Adili Tuersun[1], Munire Mohetaer[2], Guanxin Hou[3] and Gang Cheng[4]*

[1]School of Life Sciences and Biopharmaceutics, Shenyang Pharmaceutical University, Shenyang, Liaoning, China, [2]School of Business Administration, Shenyang Pharmaceutical University, Shenyang, China, [3]Department of Pharmacy, General Hospital of Northern Theater Command, Shenyang, China, [4]Department of Pharmacy, Shenyang Pharmaceutical University, Shenyang, China

Purpose: Immunotherapy as a neoadjuvant treatment approach has achieved certain therapeutic effects in various types of cancer. However, in the specific cancer type of hepatocellular carcinoma (HCC), standardized protocols for neoadjuvant immunotherapy remain to be defined. This systematic review and meta-analysis focus on evaluating the efficacy and safety of neoadjuvant immunotherapy in the treatment of HCC, aiming to provide a robust basis for clinical decision-making.

Methods: This study systematically searched databases such as PubMed, EMBASE, the Cochrane Library, and conference proceedings to identify clinical trials focusing on patients with HCC undergoing neoadjuvant immunotherapy. The Review Manager 5.4 software was applied to estimate the odds ratio (OR) of effect sizes and their corresponding 95% confidence intervals (CI).

Results: Immune checkpoint inhibitors (ICIs) demonstrate significant efficacy in improving pathological outcomes and safety profiles in patients with resectable hepatocellular carcinoma (HCC). Specifically, ICIs significantly increase the pathological complete response (pCR) rate (OR = 0.23, 95% CI [0.14, 0.37], $p < 0.00001$) and major pathological response (MPR) rate (OR = 0.47, 95% CI [0.32, 0.70], $p = 0.0002$). They also markedly enhance the objective response rate (ORR) (OR = 0.42, 95% CI [0.28, 0.63], $p < 0.0001$). Furthermore, ICIs potentially improve the surgical resection rate (OR = 3.91, 95% CI [2.05, 7.45], $p < 0.0001$) and reduce the incidence of grade 3–4 treatment-related adverse events (TRAEs) (OR = 0.27, 95% CI [0.17, 0.44], $p < 0.00001$), indicating both therapeutic benefits and acceptable toxicity profiles.

Conclusion: Neoadjuvant immunotherapy shows promise in the treatment of resectable HCC. Nonetheless, to further validate its efficacy, more large-scale, well-designed clinical trials are necessary to provide conclusive evidence.

Systematic review registration: This comprehensive review adheres to the PRISMA (Preferred Reporting Items for Systematic Reviews and Meta-Analyses) standards and has been carried out as per a preregistered protocol (PROSPERO registration number: CRD42024560660).

KEYWORDS

neoadjuvant immunotherapy, hepatocellular carcinoma, meta-analysis, safety, efficiency

Highlights

- Neoadjuvant immunotherapy shows a 47% Major Pathological Response in resectable HCC.
- Complete Pathological Response achieved in 24% of patients post-neoadjuvant therapy.
- Objective Response Rate reaches 42% with neoadjuvant immunotherapy in HCC.
- Grade 3-4 Treatment-Related Adverse Event Rate is 27% in neoadjuvant immunotherapy.
- Systematic review emphasizes the need for large-scale trials to validate immunotherapy efficacy in HCC.

1 Introduction

Primary liver cancer (PLC) ranks sixth among malignant tumors and is the third leading cause of cancer-related deaths worldwide. Approximately 906,000 new cases emerge annually, with 830,000 fatalities (1). Currently, a variety of treatment modalities for hepatocellular carcinoma (HCC) are available, including surgical resection, liver transplantation, transarterial chemoembolization (TACE), ablation therapy, and pharmacological treatments. These therapeutic approaches collectively form an integrated treatment system aimed at providing personalized treatment plans. Despite surgical resection being an effective means for long-term survival, the majority of patients are diagnosed at an advanced stage, missing the optimal timing for surgery. Even with surgical intervention, the long-term survival rate for nearly 70% of patients remains poor, with a high risk of recurrence within 5 years. Therefore, improving the resection rate, reducing recurrence, establishing effective treatment plans and predictive indicators, and selecting patient subgroups likely to benefit have become key to treating HCC (2).

Immune checkpoint inhibitors (ICIs) are a class of targeted therapeutic drugs that act on specific receptors on the surface of cytotoxic T lymphocytes. These receptors include Cytotoxic T-Lymphocyte Associated Protein 4 (CTLA-4) and Programmed Cell Death Protein 1 (PD-1). ICIs enhance T-cell activity by blocking the interaction of these receptors with CD80/CD86 and PD-L1, thereby promoting an attack on tumor cells. Tumor cells often create an immunosuppressive microenvironment by upregulating the expression of immune checkpoint molecules to evade immune clearance (3). ICIs can block the interaction of these molecules with ligands on T cells, activating them to infiltrate tumor tissue and trigger cytotoxic T-cell responses, restoring antitumor immune reactions. In the early stages of HCC, the tumor microenvironment already exhibits immunosuppressive characteristics, such as an increase in regulatory T cells, a decline in the ratio of effector T cells to regulatory T cells, and a reduction in NK cells and dendritic cells. Studies have shown that an increase in CD4+ T cells is associated with prolonged recurrence-free time, memory CD8+ T cells are linked to a reduced risk of recurrence, and an increase in effector CD8+ T cells is correlated with an increased risk of recurrence. Additionally, an increase in PD-L1 expression levels is associated with shorter recurrence-free time (4, 5).

With enhanced screening for high-risk groups, an increasing number of early-stage HCC patients are being identified and given the opportunity for surgical resection. A phase II clinical trial by Kaseb et al. showed that preoperative treatment with nivolumab, either alone or in combination with ipilimumab, had good safety, with 25% of patients achieving pathological complete response (pCR) (6). A phase Ib clinical trial by Pinateo et al. confirmed the safety and tolerability of the combination therapy (7). Marron et al.'s study demonstrated that cemiplimab as neoadjuvant therapy can significantly promote tumor necrosis, supporting the application of neoadjuvant immunotherapy in HCC treatment (8).

Global liver cancer treatment guidelines have included immune checkpoint inhibitors, especially drugs targeting the PD-1/PD-L1 pathway, providing a new direction for neoadjuvant therapy in HCC. Neoadjuvant therapy shows potential to transform tumors into a "resectable cure" state, but there are still few clinical studies, and its efficacy and safety require further validation. A standardized protocol for neoadjuvant immunotherapy has not yet been established, and challenges remain in the standardization of treatment and patient selection. Therefore, in-depth research and clinical trials are crucial for determining the optimal application strategy and timing of neoadjuvant immunotherapy in the treatment of HCC.

2 Materials and methods

This comprehensive review adheres to the PRISMA (Preferred Reporting Items for Systematic Reviews and Meta-Analyses) standards (9) and has been carried out as per a preregistered protocol (PROSPERO registration number: CRD42024560660).

2.1 Search strategy

This study conducted a comprehensive search of the PubMed, EMBASE, and Cochrane Library electronic databases to gather relevant literature. To ensure the completeness of the materials, we also manually checked the reference lists of related literature and reviewed conference abstracts and reports, covering a time range from 2010 to May 2024. When conducting the literature search, we first identified key terms using Medical Subject Headings (MeSH) terminology and constructed a comprehensive search strategy using Boolean logical operators. The search keywords we used included "Hepatocellular Carcinoma (HCC)," "Neoadjuvant Therapy," "Immune Checkpoint Inhibitors (ICIs)," as well as their synonyms and related derived terms. The specific search strategy, using PubMed as an example, is as follows:

#1	"Randomized controlled trials as topic" [MeSH Terms] OR "random allocation" [MeSH Terms] OR "placebos" [MeSH Terms].
#2	"Carcinoma, Hepatocellular" [MeSH Terms] OR "Liver Cell Carcinoma, Adult" [MeSH Terms] OR "Liver Cancer, Adult" [MeSH Terms] OR "Adult Liver Cancer" [MeSH Terms] OR "Cancer, Adult Liver" [MeSH Terms] OR "Cancers, Adult Liver" [MeSH Terms] OR "Liver Cancers, Adult" [MeSH Terms] OR "Liver Cell Carcinoma" [MeSH Terms] OR "Carcinoma, Liver Cell" [MeSH Terms] OR "Carcinomas, Liver Cell" [MeSH Terms] OR "Cell Carcinoma, Liver" [MeSH Terms] OR "Cell Carcinomas, Liver" [MeSH Terms] OR "Hepatocellular Carcinoma" [MeSH Terms] OR "Hepatoma" [MeSH Terms].

#3	"Immune Checkpoint Inhibitors" [Title/Abstract] OR "Checkpoint Inhibitors, Immune" [Title/Abstract] OR "Immune Checkpoint Blockers" [Title/Abstract] OR "Checkpoint Blockers, Immune" [Title/Abstract] OR "PD L1 Inhibitors" [Title/Abstract] OR "Blockade, PD-1-PD-L1" [Title/Abstract] OR "PD 1 PD L1 Blockade" [Title/Abstract] OR "CTLA-4 Inhibitors" [Title/Abstract] OR "Cytotoxic T-Lymphocyte-Associated Protein 4 Inhibitors" [Title/Abstract] OR "Inhibitor, PD-1" [Title/Abstract].
#4	#1 AND #2 AND #3.

2.2 Study selection process

This study strictly adhered to the framework of Patients, Interventions, Comparisons, Outcomes, and Study design (PICOS) to establish the inclusion and exclusion criteria. The specific inclusion criteria are as follows:

(1) Patients (P): The study subjects were patients diagnosed with resectable hepatocellular carcinoma (HCC), encompassing a diverse population without restrictions on gender or age. (2) Interventions (I): The study employed immune checkpoint inhibitors as neoadjuvant therapeutic agents.
(2) Comparisons (C): This study did not specify a comparison group but focused on the effects of the single intervention.
(3) Outcomes (O): The study must report at least one of the following primary outcome measures: Major Pathologic Response (MPR), Pathological Complete Response (pCR), the incidence of Grade 3–4 Treatment-Related Adverse Events (TRAEs) including liver function abnormalities, skin reactions, neurotoxicity, cardiotoxicity, infections, etc. (10), Objective Response Rate (ORR), and resection rate.
(4) Study design (S): The study design must be an original research article, including single-arm or non-randomized controlled trials, to ensure the reliability and validity of the results.

The exclusion criteria are as follows:

(1) The study subjects were patients with unresectable primary or metastatic HCC.
(2) Participants had received immunotherapy or other systemic treatments prior to the study.
(3) The literature was a duplicate publication of a research report.
(4) The literature type was non-original research, such as reviews, meta-analyses, case reports, or case series.

2.3 Data extraction

This study involved two authors independently screening literature and extracting data to ensure the objectivity of the results. In cases of disagreement, a third author was involved to resolve the dispute. Subsequently, we conducted a comprehensive search of the selected articles and conducted an in-depth analysis of their full texts.

We meticulously recorded key information for each included study, including but not limited to: the first author and publication year; clinical trial registration number (NCT number); the intervention measures and treatment strategies used in the study; the type of article, including study design and methodology; the specific immune checkpoint inhibitor drugs used; the sample size of the study; and the primary outcome measures, including pCR, MPR, Grade 3–4 TRAEs, ORR, and resection rate.

Through this method, we ensured the completeness and traceability of the study data, providing a solid foundation for subsequent data analysis and interpretation of results.

2.4 Quality assessment of studies

To evaluate the quality of non-randomized studies, this research utilized the Methodological Index for Non-Randomized Studies (MINORS) as the assessment tool. This evaluation instrument includes a series of specific criteria such as the clarity of the study's objectives, consistency in patient inclusion, anticipated data collection, appropriateness of endpoints reflecting the study's objectives, objectivity in endpoint assessment, completeness of follow-up, dropout rate below 5%, and consideration of sample size estimation. Each criterion is scored on a scale from 0 to 2: 0 indicates not reported, 1 indicates reported but inadequate, and 2 indicates reported and fully detailed. This scoring mechanism ensures a meticulous assessment of the study quality, aiding in the identification of potential biases and limitations within the research. The specific scoring details and results are presented in Table 1.

2.5 Data analysis

In this study, we utilized Review Manager 5.4 software for calculations and graphical representations. For single-arm studies lacking a control group, we employed an appropriate transformation method to handle binary outcome data, facilitating subsequent statistical analysis. The specific transformation process adheres to the following formula: $P = \ln(\text{odds}) = \ln[X/(n\text{-}X)]$, where n represents the total sample size, X is the number of observed events, and P denotes the event occurrence rate. Furthermore, the standard error of the occurrence rate, SE(p), can be calculated using the formula: $SE(p) = SE[\ln(\text{odds})] = [1/X + 1/n - X]^{\wedge 1/2}$ (11).

Based on the aforementioned transformation, we further estimated the Odds Ratio (OR) and its 95% Confidence Interval (CI) using the following formula: $P_f = OR/1 + OR$. Concurrently, the actual event occurrence rate P_f and its 95% CI were calculated using the formulas: $LL = LLOR/1 + LLOR$ and $UL = ULOR/1 + ULOR$ (11).

3 Results

3.1 Study selection process and results

A total of 161 relevant studies were initially identified. After removing duplicates, 130 studies were obtained. Following the review of titles and abstracts, 14 studies were ultimately included (6, 8, 12–23), as depicted in Figure 1.

TABLE 1 Methodological Index for Non-Randomized Studies (MINORS) assessment tool.

Author/year	A	B	C	D	E	F	G	H	I	G	K	L	Score
Shi, Y. H/2021 (12)	2	2	2	2	1	2	2	0	–	–	–	–	13
Su, Y/2021 (13)	2	2	2	2	2	2	2	0	–	–	–	–	14
Ho, W. J/2021 (14)	2	2	2	2	2	2	2	0	–	–	–	–	14
Marron/2022 (8)	2	2	2	2	1	2	2	0	–	–	–	–	13
Xia, Y/2022 (15)	2	2	2	2	2	2	2	0	–	–	–	–	14
Kaseb/2022 (6)	2	2	2	2	2	2	2	0	2	2	2	2	22
Chen, S/2022 (16)	2	2	2	2	1	2	2	0	–	–	–	–	13
Bai, X/2022 (17)	2	2	2	2	2	2	2	0	–	–	–	–	14
Song, T. Q/2023 (18)	2	2	2	2	1	2	2	0	–	–	–	–	13
D'Alessio/2023 (19)	2	2	2	2	2	2	2	0	–	–	–	–	14
Sun, H. C/2023 (20)	2	2	2	2	2	2	2	0	–	–	–	–	14
Wang, K (21)	2	2	2	2	2	2	2	0	2	2	2	2	22
Qin, S (22)	2	2	2	2	2	2	2	0	2	2	2	2	22
Kaseb, A (23)	2	2	2	2	2	2	2	0	2	2	2	2	22

A: The study's aim is clearly stated. B: The coherence of patient inclusion is maintained. C: Data collection is conducted as expected. D: The endpoints appropriately reflect the study's objectives. E: The evaluation of endpoints is objective. F: Sufficient follow-up time is ensured. G: The dropout rate is below 5%. H: Sample size estimation is performed. I: Additional criteria for evaluating studies with control groups. J: The selection of the control group is appropriate. K: The control group is contemporaneous. L: The baseline comparability between groups is ensured. M: Statistical analysis is conducted appropriately.

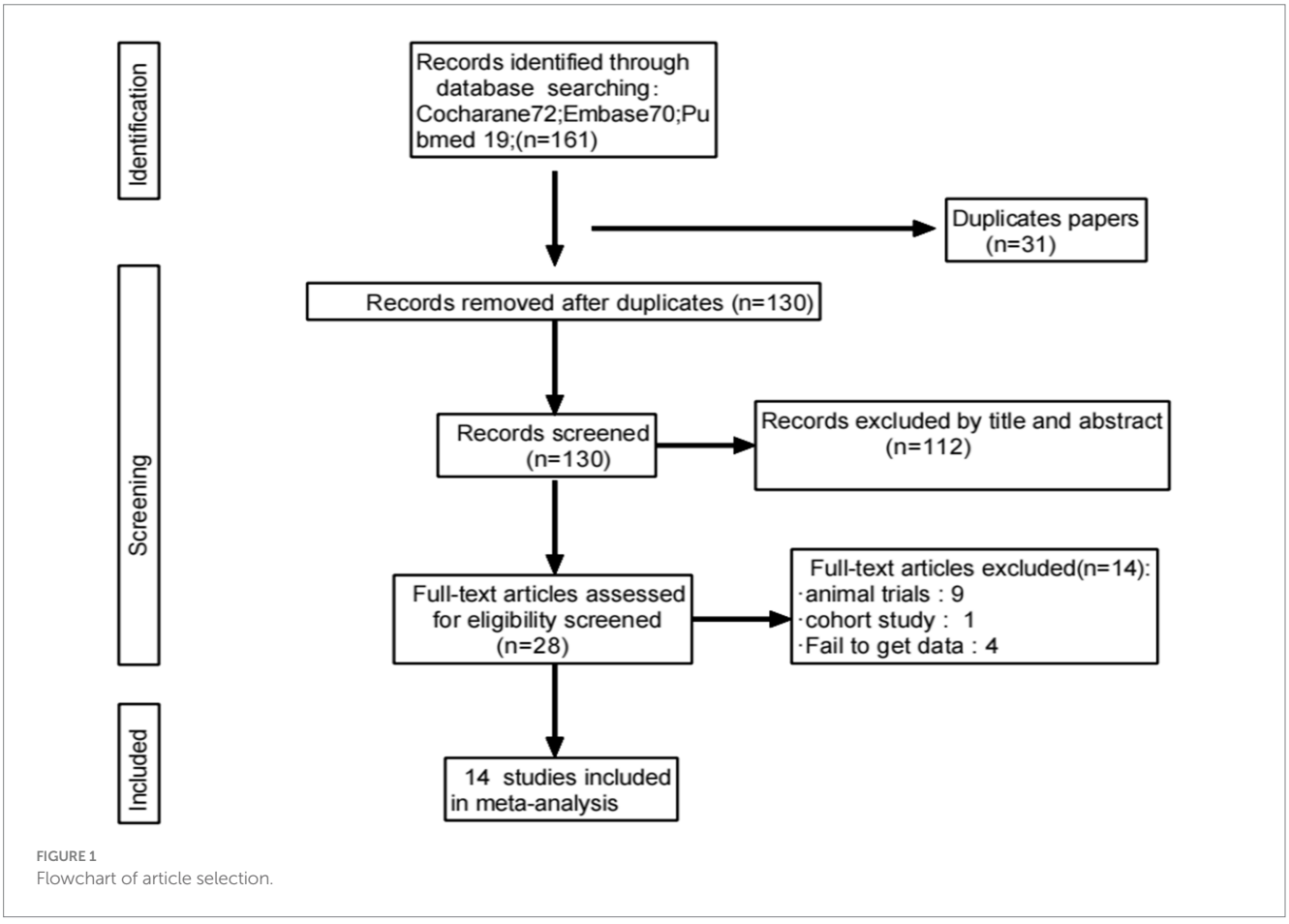

FIGURE 1
Flowchart of article selection.

3.2 Basic characteristics of included literature

A total of 14 articles were included in this study, covering a variety of neoadjuvant therapy drugs, including Tremelimumab, Nivolumab, Cemiplimab, and Camrelizumab. The incidence of pCR ranged from 5.9 to 38%, the incidence of MPR ranged from 17.6 to 56%, and the incidence of Grade 3–4 TRAEs ranged from 10 to 41.4%. The specific study characteristics and outcome data are detailed in Table 2.

3.3 Efficacy outcomes of immune checkpoint inhibitors

In this meta-analysis, a total of 10 studies reported the incidence of pCR. The results of the heterogeneity test indicated that there was no significant heterogeneity among the included studies ($p = 0.35$, $I^2 = 10\%$). Further analysis revealed that ICIs have a statistically significant benefit in increasing the pCR rate, with an OR of 0.23, 95% CI (0.14, 0.37), and a p-value less than 0.00001, indicating a highly statistically significant effect (see Figure 2) for specifics.

In this meta-analysis, a total of 8 studies reported the MPR rate. The results of the heterogeneity test indicated that there was no significant heterogeneity among these studies ($p = 0.41$, $I^2 = 2\%$). A pooled analysis of these studies revealed that ICIs have a statistically significant benefit in increasing the MPR rate, with an OR of 0.47, 95% CI (0.32, 0.70), and a p-value of 0.0002, indicating a statistically significant effect of ICIs in promoting MPR (see Figure 3) for specifics.

In this meta-analysis, a total of 6 studies reported the overall response rate (ORR). The results of the heterogeneity test showed significant heterogeneity ($p = 0.06$, $I^2 = 52\%$), suggesting that caution should be exercised when interpreting the results. Despite the heterogeneity, the pooled analysis indicated that ICIs have a significant statistical benefit in increasing the ORR, with an OR of 0.42, 95% CI (0.28, 0.63), and a p-value less than 0.0001. This result suggests that ICIs have a potential therapeutic effect in promoting ORR (see Figure 4) for specifics.

3.4 Safety outcomes of immune checkpoint inhibitors

In this meta-analysis, a total of 10 studies reported the surgical resection rate. The results of the heterogeneity test showed significant heterogeneity ($p < 0.00001$, $I^2 = 82\%$). Despite the significant heterogeneity, the pooled analysis results indicate that ICIs have a potential benefit in increasing the surgical resection rate, with an OR of 3.91, 95% CI (2.05, 7.45), and a p-value less than 0.0001 (see Figure 5) for specifics.

Additionally, the use of ICIs is closely associated with the incidence of treatment-related adverse events (TRAEs). A total of 10 studies reported the incidence of grade 3–4 TRAEs. The results of the heterogeneity test showed significant heterogeneity ($p = 0.0003$, $I^2 = 71\%$). The pooled analysis results suggest that ICIs have a potential benefit in reducing the incidence of grade 3–4 TRAEs, with an OR of 0.27, 95% CI (0.17, 0.44), and a p-value less than 0.00001 (see Figure 6) for specifics.

3.5 Subgroup analysis

Subgroup analyses were conducted to assess the impact of various treatment regimens on clinical outcomes, including pCR, MPR, ORR, TRAEs, and surgical resection rates. This evaluation

TABLE 2 Characteristics of neoadjuvant immunotherapy studies in patients with hepatocellular carcinoma.

Author	Register number	Nation	Patient number	Neoadjuvant therapy	pCR (%)	MPR (%)	Grade 3–4 TRAEs (%)	ORR (%)	Resection rate (%)
Shi, Y. H (12)	NCT03867370	China	18	Tremelimumab/Tremelimumab + Lenvatinib	6.3	–	16.7	–	51.7
Su, Y (13)	NCT03510871	China	29	Nivolumab + Ipilimumab	–	33.3	41.4	–	80
Ho, W. J (14)	NCT03299946	USA	15	Nivolumab + Cabozantinib	8.3	33.3	13.3	–	95.2
Marron, T. U (8)	NCT03916627	USA	21	Cemiplimab	15	20	10	15	94.4
Xia, Y (15)	NCT04297202	China	20	Camrelizumab + Apatinib	5.9	17.6	16.7	16.7	74.1
Kaseb, A. O (6)	NCT03222076	USA	30	Nivolumab / Nivolumab + Ipilimumab	25	30	33	–	–
Chen, S (16)	NCT04615143	China	11	Tislelizumab	9.1	–	–	18.2	–
Bai, X (17)	NCT04930315	China	32	Camrelizumab + Apatinib	9.1	27.3	–	–	70.8
Song, T. Q (18)	NCT04834986	China	24	Tislelizumab + Lenvatinib	17.6	35.3	–	54.2	84
D'Alessio, A (19)	NCT03682276	UK	25	Nivolumab + Ipilimumab	38	56	–	29	56.7
Sun, H. C (20)	NCT04843943	China	30	Sintilimab + Bevacizumab	–	–	23.3	26.7	–
Wang, K (21)	ChiCTR2000037655	China	198	Sintilimab	–	–	12.4	–	–
Qin, S (22)	NCT04102098	China	668	Atezolizumab + Bevacizumab	–	–	27	–	87.5
Kaseb, A (23)	–	USA	14	Nivolumab + Ipilimumab	28.6	–	35.7	–	85.7

"–": Not report.

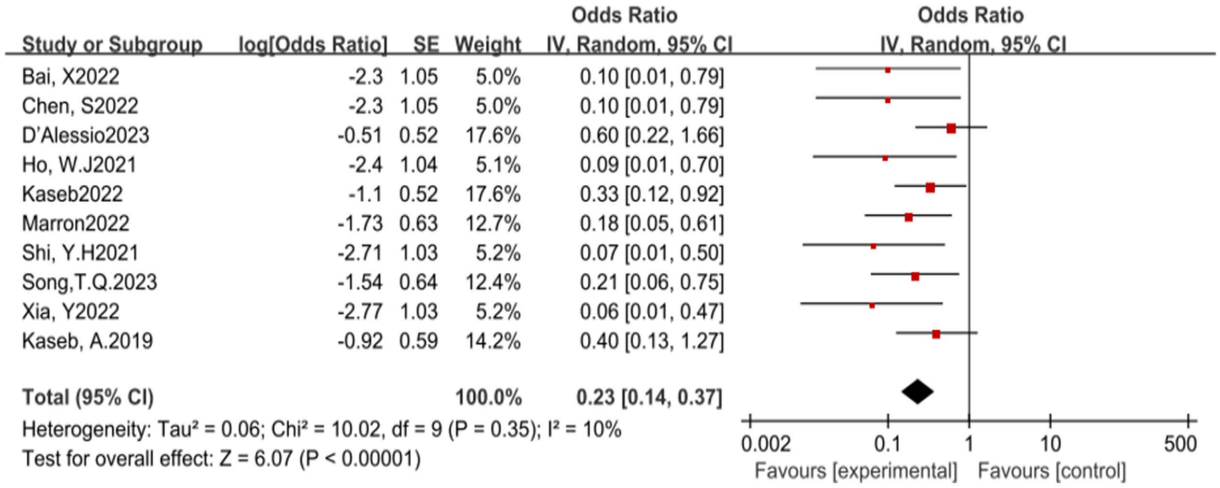

FIGURE 2
Forest plot of pCR outcomes with immune checkpoint inhibitors.

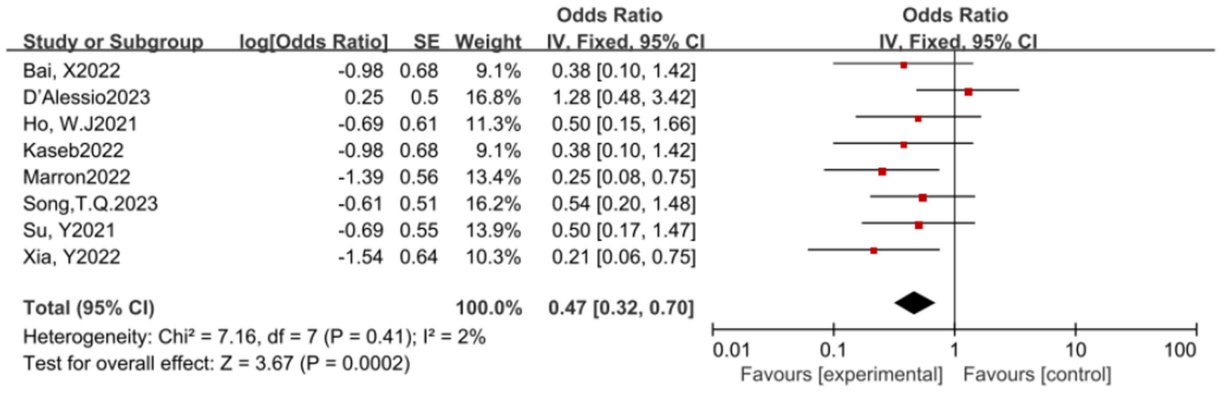

FIGURE 3
Forest plot of MPR outcomes with immune checkpoint inhibitors.

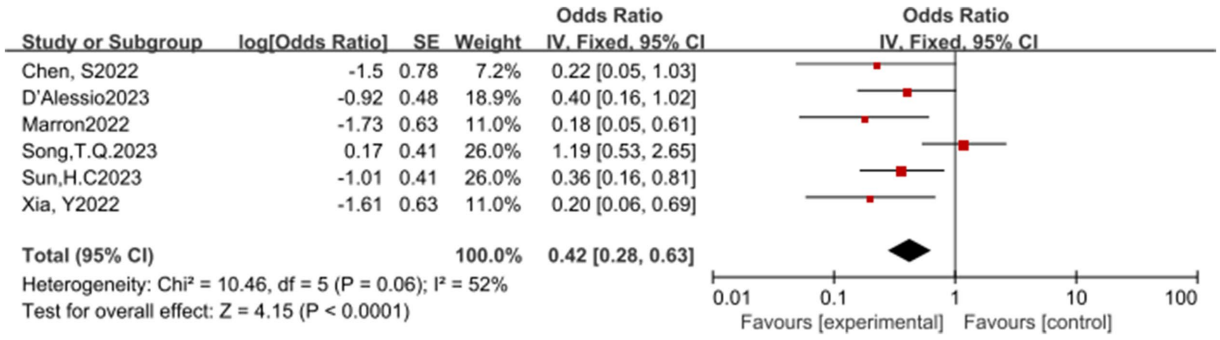

FIGURE 4
Forest plot of ORR outcomes with immune checkpoint inhibitors.

aimed to determine the differential effects of treatments on efficacy and safety profiles and their overall influence on patient outcomes.

The subgroup analysis revealed no significant efficacy differences between the three immune checkpoint inhibitors (ICIs) when used as monotherapies (Figures 7A–C). In terms of safety, nivolumab

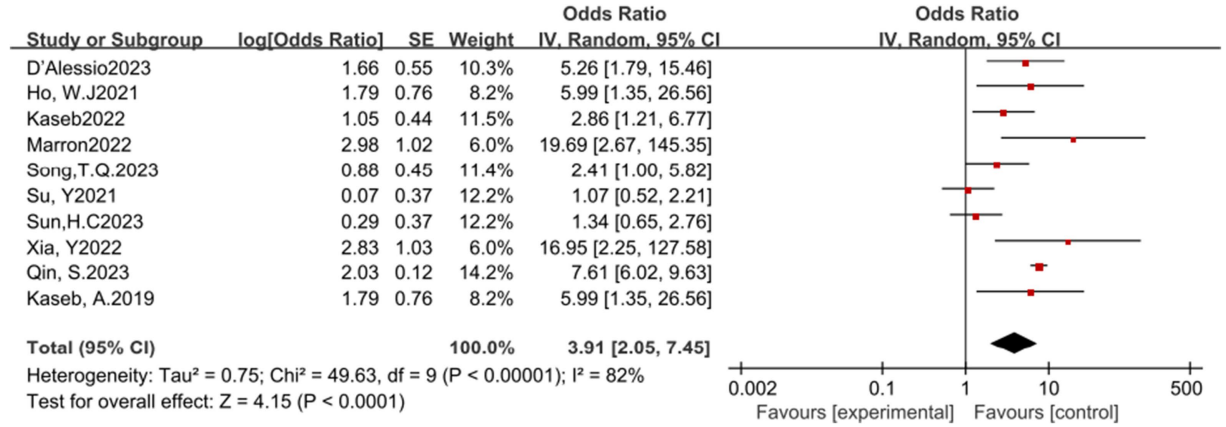

FIGURE 5
Forest plot of surgical resection rate outcomes with immune checkpoint inhibitors.

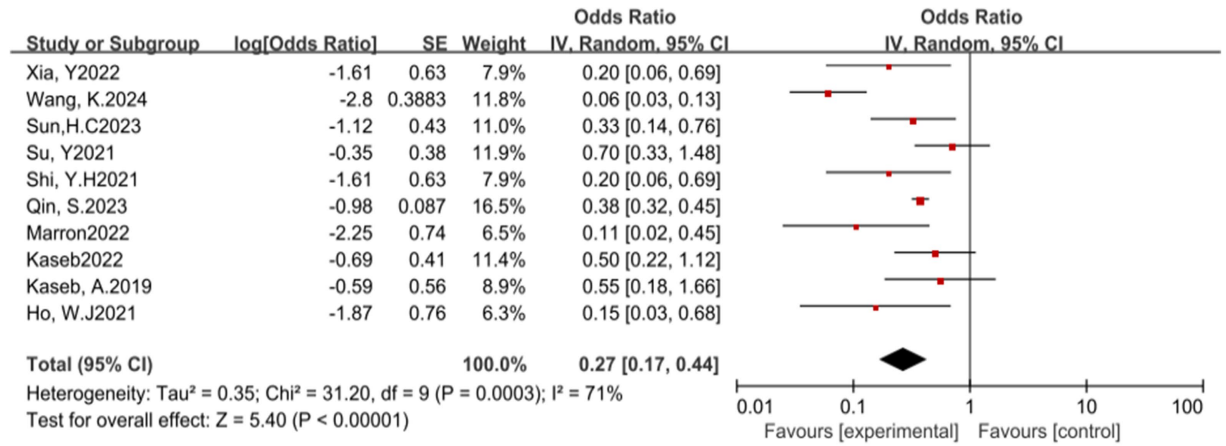

FIGURE 6
Forest plot of grade 3–4 treatment-related adverse events (TRAEs) outcomes with immune checkpoint inhibitors.

monotherapy (Figure 7D) exhibited a higher OR for adverse events compared to Cemiplimab, indicating a statistically significant difference. Conversely, Cemiplimab monotherapy showed a higher OR for the rate of excision (Figure 7E) than nivolumab, the difference was statistically significant.

In the analysis of various immunotherapeutic combinations, dual immune checkpoint inhibitor (ICI) therapy demonstrated a superior combined odds ratio (OR) for pathological complete response (pCR) compared to monotherapy (Figure 8), and monotherapy showed a higher combined OR than the combination of immunotherapy with targeted therapy, both exhibiting statistical significance. No significant differences were observed across groups for major pathological response (MPR) (Figure 9) and objective response rate (ORR) (Figure 10). Conversely, the combined OR for adverse events with dual ICI therapy was elevated compared to monotherapy, and monotherapy had a lower combined OR than the targeted therapy-immunotherapy combination, indicating significant inter-group variations (Figure 11). Surgical excision rates (Figure 12) remained consistent across all groups.

4 Discussion

The present study underscores the substantial therapeutic benefits of neoadjuvant immunotherapy in patients with resectable HCC, with a meta-analysis yielding an ORR of 0.37 (95% CI: 0.20–0.69). Notably, the highest ORR reported was 54.2% (18), underscoring the potential of neoadjuvant immunotherapy to enhance surgical outcomes. Corresponding pCR and MPR rates were 0.23 (95% CI: 0.14–0.37) and 0.47 (95% CI: 0.32–0.70), respectively, suggesting a promising role for this treatment modality in HCC management (24).

Despite the potential of neoadjuvant immunotherapy in improving surgical resection opportunities for liver cancer patients, current data on postoperative survival rates are limited. Most relevant studies are ongoing, leading to a scarcity of existing statistical data for assessing the long-term efficacy of neoadjuvant immune checkpoint inhibitor therapy in HCC. In this meta-analysis, only four studies provided specific statistical results. The study by Kaseb et al. (6) revealed that median progression-free survival (PFS) with nivolumab monotherapy was 9.4 months, with a 95% CI of 1.47 to not estimable

(NE), whereas the PFS median significantly extended to 19.53 months with nivolumab combined with ipilimumab, with a 95% CI of 2.33 to NE. Additionally, other studies (15, 20) reported data on event-free survival (EFS) and recurrence-free survival (RFS). The median EFS was 13.8 months, with a 95% CI of 10.3 to 17.3, and the one-year RFS rate was 53.85%, with a 95% CI of 24.77 to 75.99%. However, due to the limitation of follow-up time, no studies have reported data on overall survival (OS) yet. These preliminary results suggest that neoadjuvant immunotherapy may have a positive impact on improving the prognosis of patients with HCC, but longer follow-up and more data are needed to fully assess its long-term effects on patient survival rates.

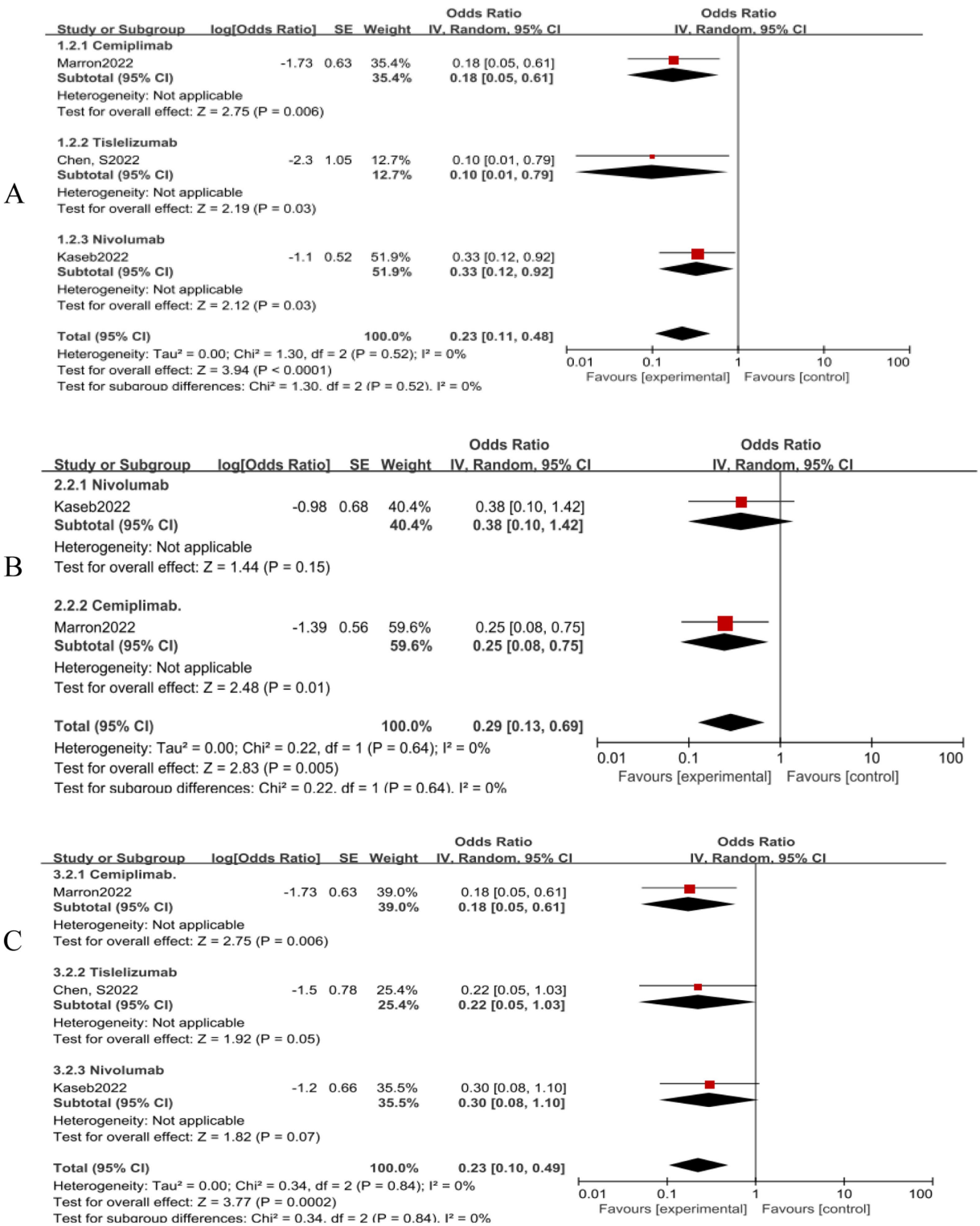

FIGURE 7 (Continued)

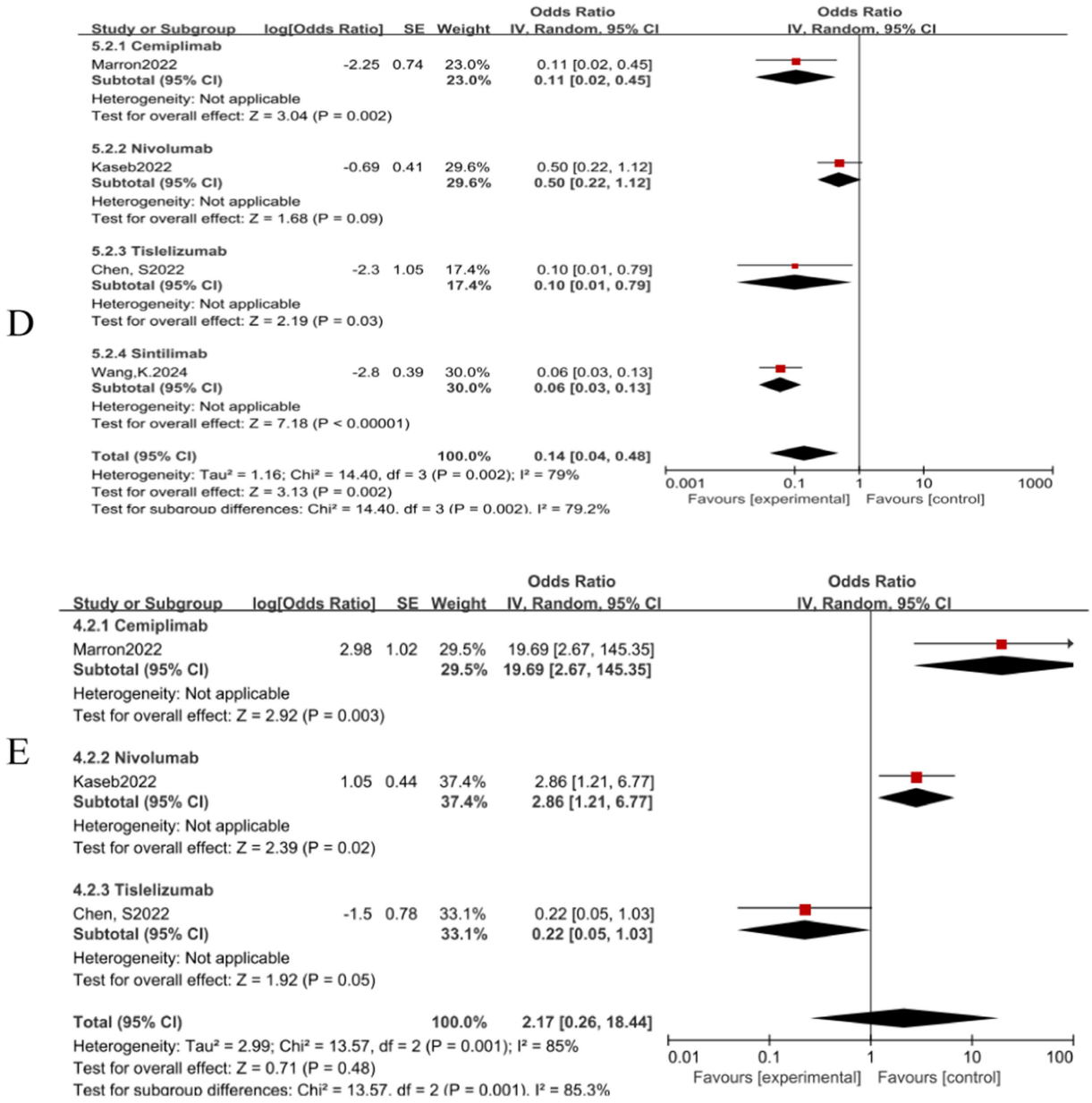

FIGURE 7
Subgroup analyses of immune checkpoint inhibitor drug types for **(A)** pCR, **(B)** MPR, **(C)** ORR, **(D)** Grade3–4 TRAEs and **(E)** Resection Rate. pCR, pathological complete response; MPR, major pathological response; ORR, Overall Response Rate; TRAEs, treatment-related adverse events.

In studies of other tumor types, a significant correlation between pathological response and patient survival has been established (25). This study further explores this correlation in patients with HCC through similar statistical analysis. Ho et al. (14) found a correlation between achieving MPR and long-term disease-free survival (DFS). Currently, all patients have surpassed 230 days in DFS, suggesting the potential impact of pathological response on long-term patient prognosis. Kaseb et al. (6) also reported a positive effect of MPR on recurrence-free survival (RFS) and observed a significant difference ($p = 0.049$). Additionally, Xia et al. (15) noted higher RFS rates in patients achieving pCR or MPR, although this difference did not reach statistical significance, possibly due to the small sample size in the study. These results indicate that pathological response may be a potential predictor of prognosis in patients with HCC. However, to validate these preliminary findings, further research and a larger sample size are required to establish the exact relationship between pathological response and patient survival.

The safety assessment of neoadjuvant immunotherapy revealed an odds ratio (OR) of grade 3–4 treatment-related adverse events (TRAEs) of 0.27, with a 95% confidence interval (CI) ranging from 0.17 to 0.44. These immune therapy-related adverse reactions are mostly manageable, aligning with the

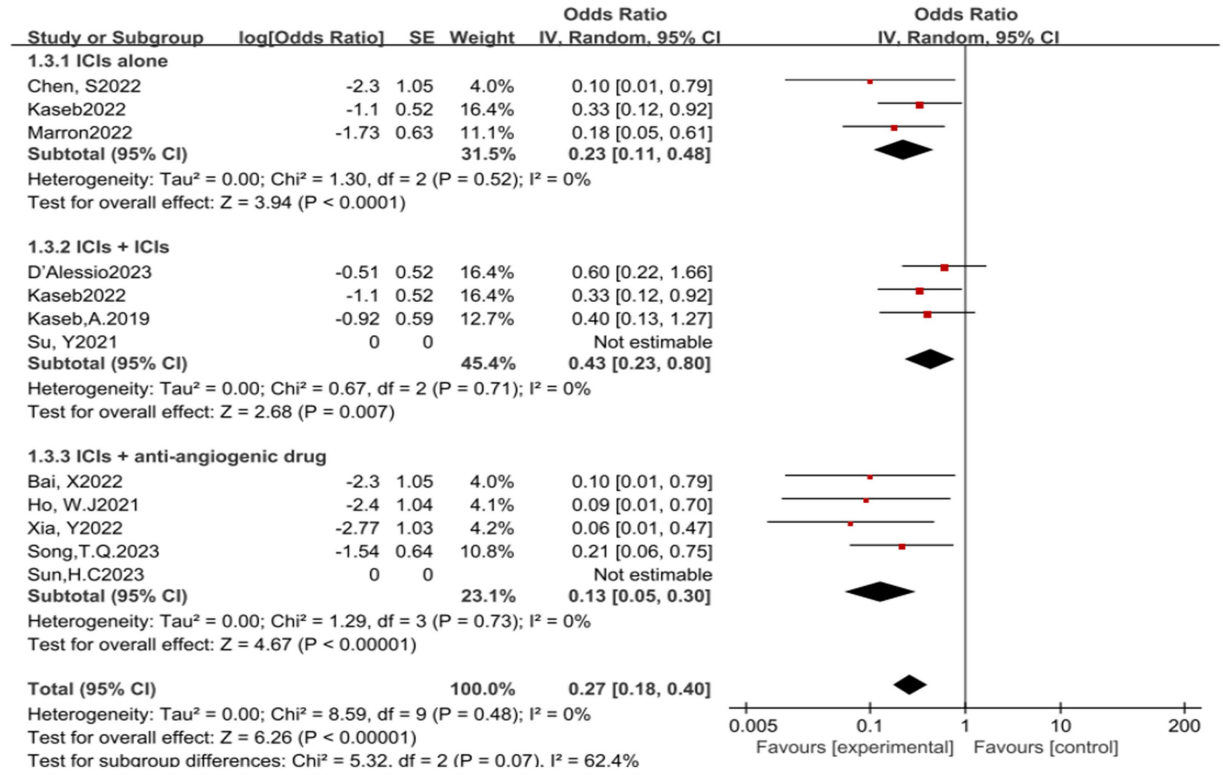

FIGURE 8
Subgroup analyses based on neoadjuvant immune checkpoint inhibitor combinations for pCR. pCR, pathological complete response.

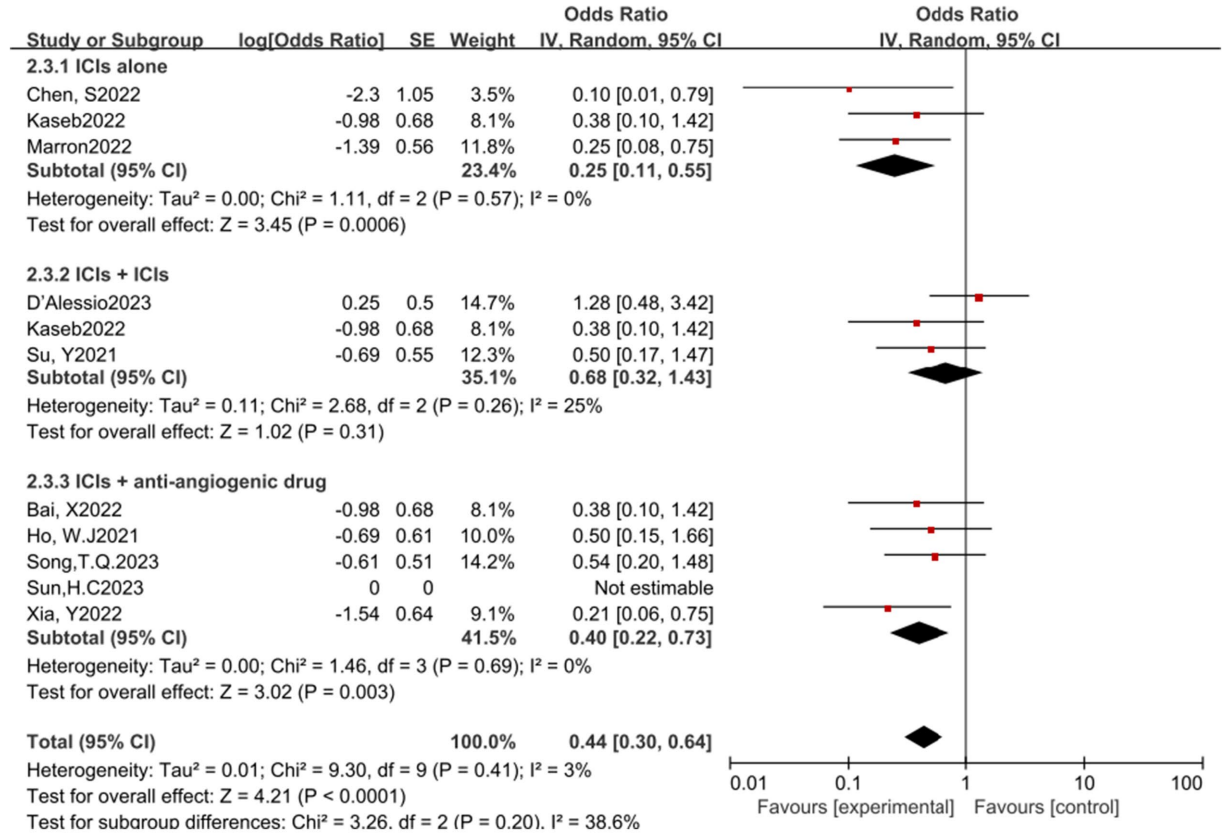

FIGURE 9
Subgroup analyses based on neoadjuvant immune checkpoint inhibitor combinations for MPR. MPR, major pathological response.

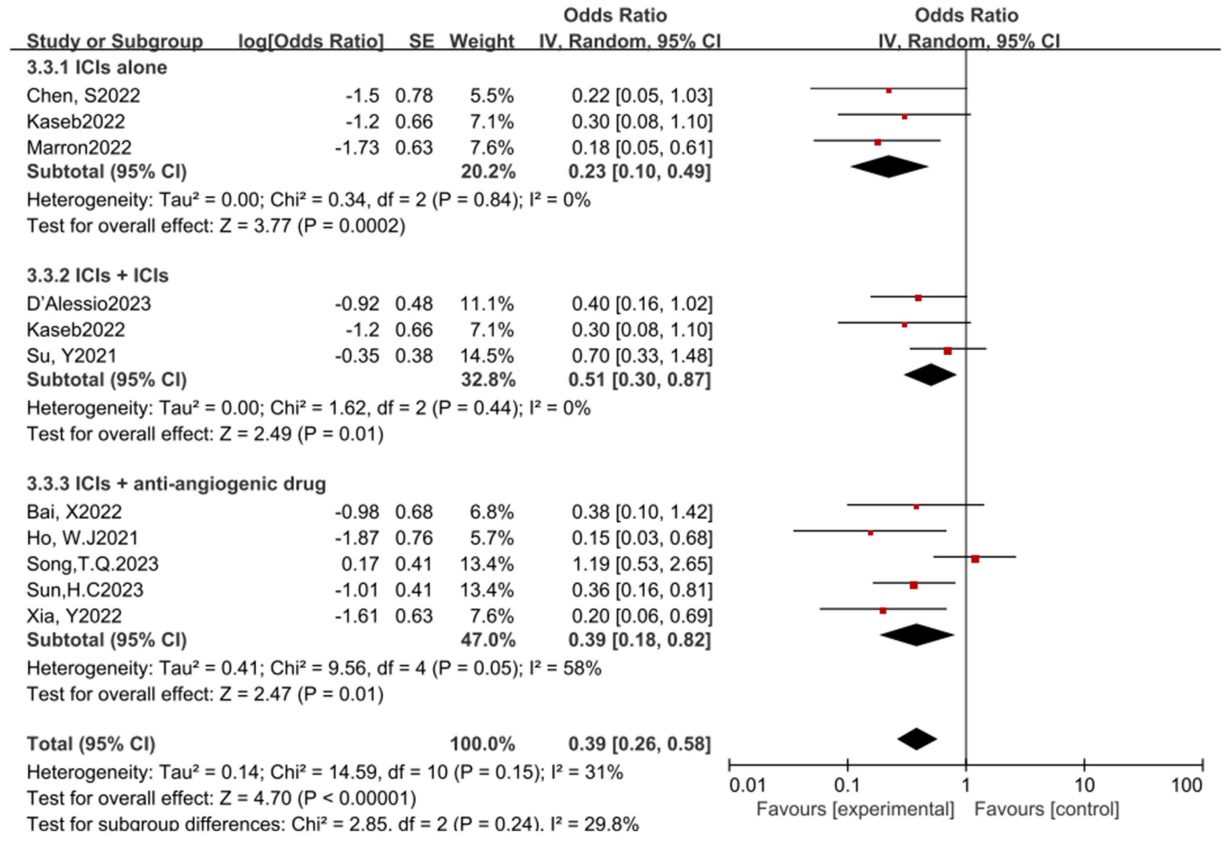

FIGURE 10
Subgroup analyses based on neoadjuvant immune checkpoint inhibitor combinations for ORR. ORR, Overall Response Rate.

findings from a recent study that evaluated the safety profile of immunotherapies in gastrointestinal tumors, which reported similar manageable adverse event profiles (26). In particular, a study on the combination therapy of nivolumab and ipilimumab (6) indicated a higher proportion of grade 3–4 TRAEs compared to monotherapy. However, the observed 20% difference (95% CI of 14.7 to 38.7%, $p = 0.69$) was not statistically significant, suggesting that different combination therapy regimens may elicit varied therapeutic responses and safety profiles. Therefore, optimizing drug use to maximize patient benefit should be a priority in future treatment strategies. Additionally, the overall surgical resection rate following neoadjuvant immunotherapy exhibited an OR of 3.91, with a 95% CI of 2.05 to 7.45. While the majority of patients proceeded with surgery as scheduled, a subset may lose surgical eligibility due to disease progression or face increased toxicity risks. Comprehensive preparation and management by medical teams for potential perioperative risks are crucial to maximize patient benefit and ensure treatment safety (20).

Subgroup analyses did not detect significant efficacy disparities among the three single-agent immune checkpoint inhibitors (ICIs). In contrast, dual ICI therapy showed superior efficacy compared to single-agent therapy, which in turn was more effective than the combination with targeted therapy. Interestingly, the rate of Grade 3–4 treatment-related adverse events (TRAEs) was notably lower with the combination of targeted therapy and immunotherapy, highlighting a reverse pattern in safety profiles. Despite the widespread clinical use of both targeted and immune therapies in HCC, monotherapy approaches may result in resistance and limited benefits, underscoring the potential advantages of combination treatments. The IMbrave150 trial (27) illustrated marked enhancements in both the one-year survival rate, which increased to 67.2%, and the median progression-free survival (mPFS), extended to 6.8 months, among untreated patients with advanced HCC who were treated with the combination of atezolizumab and bevacizumab. This regimen has been endorsed by the FDA and CSCO as a first-line therapy for advanced HCC. Additional regimens, including lenvatinib combined with pembrolizumab, sintilimab in conjunction with bevacizumab, and camrelizumab paired with apatinib, have demonstrated encouraging outcomes (28–31). At the mechanistic level, research indicates that immune-modulating agents help to reestablish a supportive immune microenvironment, whereas anti-VEGF therapies such as bevacizumab alleviate immunosuppression and promote vascular normalization, enhancing drug delivery. This strategy enables the use of lower doses of immune checkpoint inhibitors (ICIs), which in turn reduces the likelihood of adverse reactions (32, 33). In our subgroup analysis, the combination of targeted therapy and immunotherapy did not exhibit significant

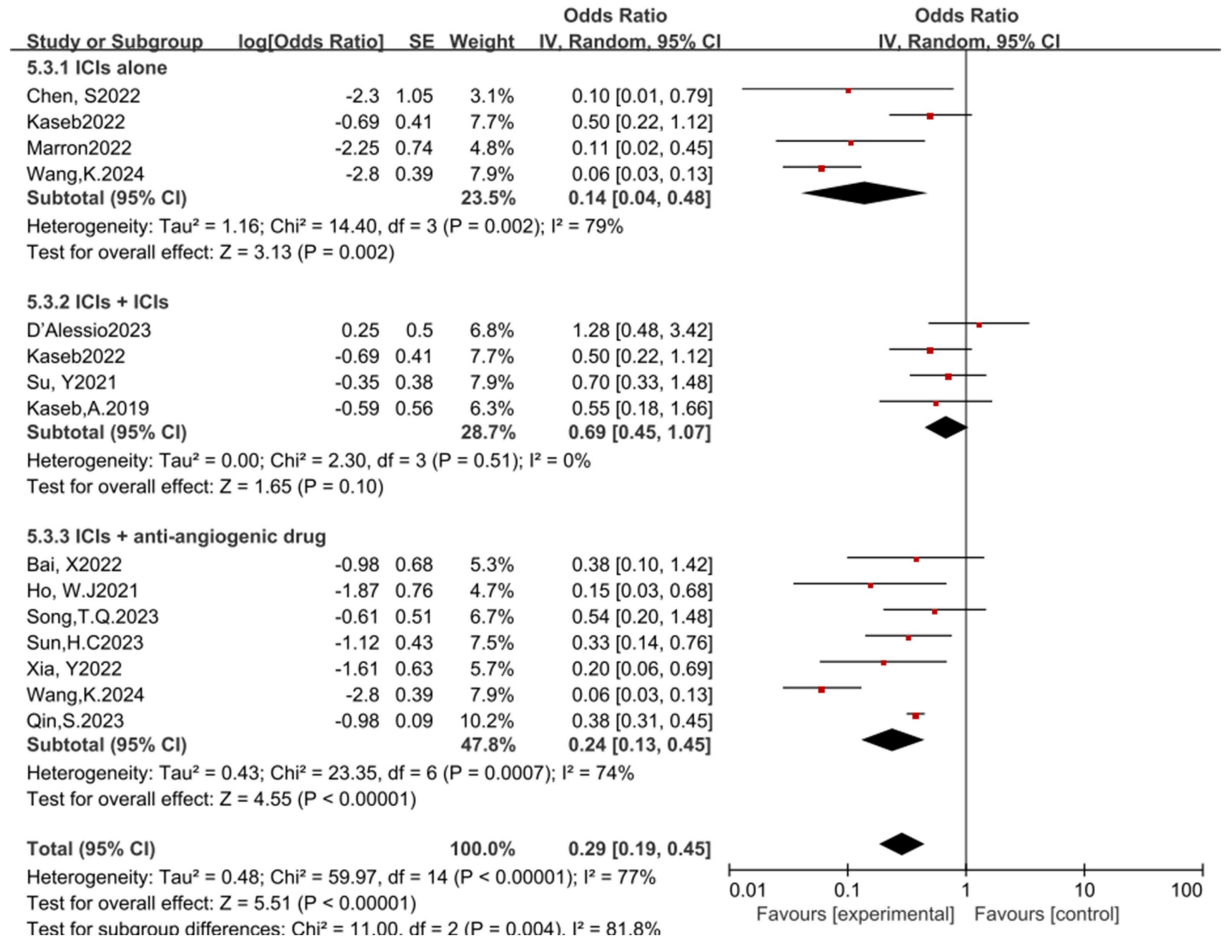

FIGURE 11
Subgroup analyses based on neoadjuvant immune checkpoint inhibitor combinations for Grade 3–4 TRAEs. TRAEs, treatment-related adverse events.

superiority. However, considering the limited follow-up duration, the potential for long-term survival benefits after surgery warrants further investigation, which could inform the selection of optimal treatment strategies in future clinical practice.

The application of immunotherapy in HCC treatment is burgeoning, with studies demonstrating significant long-term survival advantages for patients who respond to therapy (34). However, the challenge remains to identify patients who are more likely to benefit from treatment, a necessity underscored by the variable responses observed in clinical practice. In pivotal trials for primary liver cancer, such as CheckMate040 (35) and CheckMate459 (36), a PD-L1 expression threshold of 1% or higher was associated with improved median OS and ORR (35). Contrarily, the KEYNOTE224 (36) study found no significant correlation between tumor cell PD-L1 expression levels and treatment response rates (36). Beyond PD-L1, other potential biomarkers, including gut microbiota, circulating tumor DNA (ctDNA), and tumor-infiltrating lymphocytes, have been investigated for their predictive value in HCC treatment (37). However, these biomarkers require validation in large prospective studies to clarify their specificity and sensitivity. In this analysis, studies by Xia (15) and Ho (14) identified tumor-infiltrating B cells and dendritic cells (DCs) as potential biomarkers for antitumor immunotherapy. They noted that higher post-treatment DC levels correlated with a reduced risk of patient recurrence. D'Alessio (19) highlighted immune cell infiltration, peripheral cfDNA, and gut microbiota composition as predictive factors for the efficacy of the Nivolumab plus Ipilimumab regimen. Similar findings have been corroborated across various tumor types, including melanoma, colorectal cancer, and lung cancer (38). The ongoing development of precise and effective biomarker combinations or multidimensional predictive models aims to identify patient populations most likely to benefit from immunotherapy, thereby optimizing survival outcomes (8).

This study acknowledges its limitations, including inconsistencies across included studies, incomplete data sources, and a dearth of biomarker information, which restrict the analysis of long-term benefits of neoadjuvant therapy. Future research must address these limitations to more accurately assess the potential long-term impact of neoadjuvant therapy on patient prognosis.

5 Conclusion

Overall, neoadjuvant immunotherapy has shown effectiveness and safety in patients with resectable hepatocellular carcinoma.

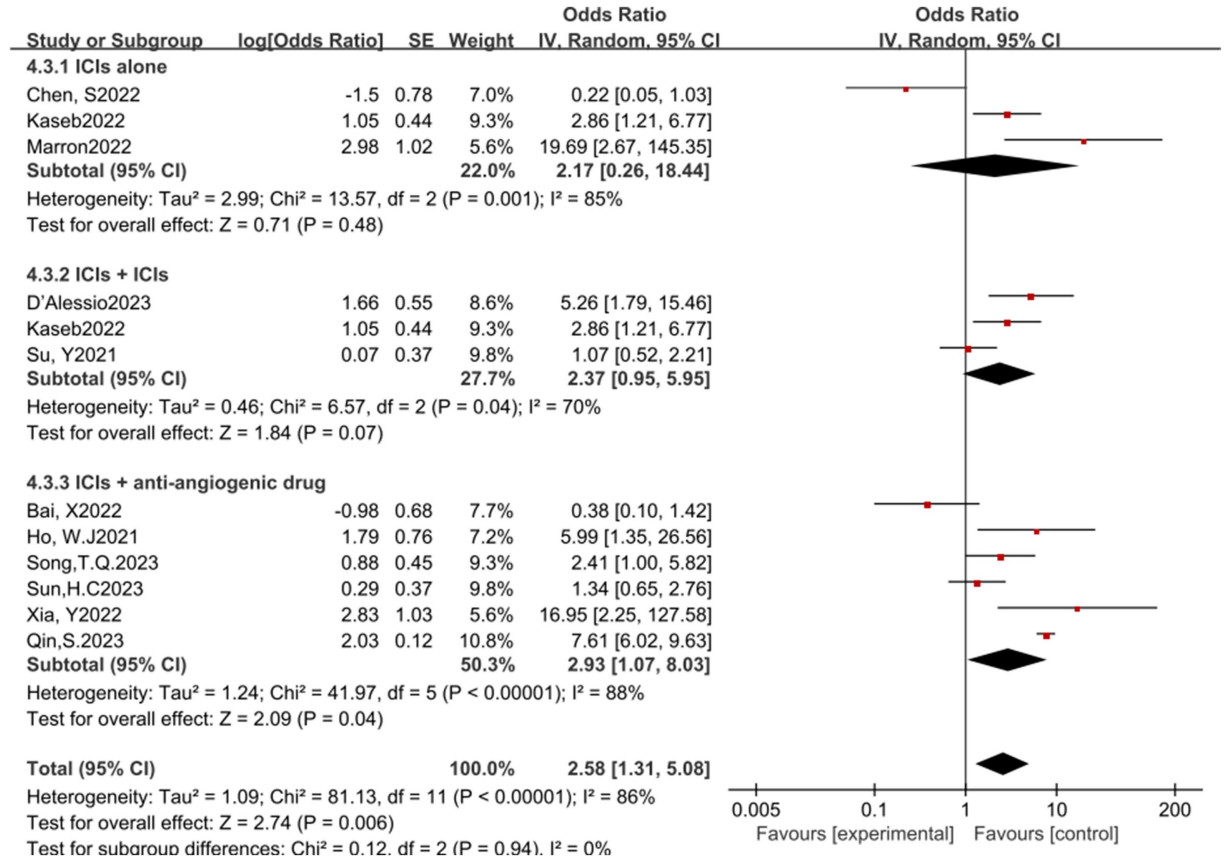

FIGURE 12
Subgroup analyses based on neoadjuvant immune checkpoint inhibitor combinations for Resection Rate.

Despite observing positive pathological and radiological responses in some patients, which are associated with improved survival outcomes, the incidence of grade 3–4 adverse events is low. Future research needs to further validate these results to provide a stronger evidence base for the application of neoadjuvant immunotherapy in the treatment of hepatocellular carcinoma.

Author contributions

AT: Formal analysis, Methodology, Software, Validation, Writing – original draft, Writing – review & editing. MM: Conceptualization, Supervision, Validation, Writing – review & editing. GH: Software, Validation, Writing – review & editing. GC: Formal analysis, Software, Writing – original draft, Writing – review & editing.

Funding

The author(s) declare that no financial support was received for the research, authorship, and/or publication of this article.

Acknowledgments

We acknowledge all past and present members who participated in this study.

Conflict of interest

The authors declare that the research was conducted in the absence of any commercial or financial relationships that could be construed as a potential conflict of interest.

Correction note

A correction has been made to this article. Details can be found at: 10.3389/fmed.2025.1682417.

Generative AI statement

The authors declare that no Gen AI was used in the creation of this manuscript.

Publisher's note

References

1. Sung H, Ferlay J, Siegel RL, Laversanne M, Soerjomataram I, Jemal A, et al. Global cancer statistics 2020: globocan estimates of incidence and mortality worldwide for 36 cancers in 185 countries. *CA Cancer J Clin*. (2021) 71:209–49. doi: 10.3322/caac.21660

2. Petrowsky H, Fritsch R, Guckenberger M, de Oliveira ML, Dutkowski P, Clavien PA. Modern therapeutic approaches for the treatment of malignant liver tumours. *Nat Rev Gastroenterol Hepatol*. (2020) 17:755–72. doi: 10.1038/s41575-020-0314-8

3. Carlino MS, Larkin J, Long GV. Immune checkpoint inhibitors in melanoma. *Lancet*. (2021) 398:1002–14. doi: 10.1016/S0140-6736(21)01206-X

4. Burnet FM. Immunological aspects of malignant disease. *Lancet*. (1967) 1:1171–4. doi: 10.1016/S0140-6736(67)92837-1

5. Ladányi A, Tímár J. Immunologic and immunogenomic aspects of tumor progression. *Semin Cancer Biol*. (2020) 60:249–61. doi: 10.1016/j.semcancer.2019.08.011

6. Kaseb AO, Hasanov E, Cao HST, Xiao L, Vauthey JN, Lee SS, et al. Perioperative nivolumab monotherapy versus nivolumab plus ipilimumab in resectable hepatocellular carcinoma: a randomised, open-label, phase 2 trial. *Lancet Gastroenterol Hepatol*. (2022) 7:208–18. doi: 10.1016/S2468-1253(21)00427-1

7. Pinato DJ, Cortellini A, Sukumaran A, Cole T, Pai M, Habib N, et al. Prime-Hcc: phase Ib study of neoadjuvant ipilimumab and nivolumab prior to liver resection for hepatocellular carcinoma. *BMC Cancer*. (2021) 21:301. doi: 10.1186/s12885-021-08033-x

8. Marron TU, Fiel MI, Hamon P, Fiaschi N, Kim E, Ward SC, et al. Neoadjuvant cemiplimab for resectable hepatocellular carcinoma: a single-arm, open-label, phase 2 trial. *Lancet Gastroenterol Hepatol*. (2022) 7:219–29. doi: 10.1016/S2468-1253(21)00385-X

9. Page MJ, McKenzie J, Bossuyt PM, Boutron I, Hoffmann TC, Mulrow CD, et al. The Prisma 2020 statement: an updated guideline for reporting systematic reviews. *BMJ*. (2021) 372:n71. doi: 10.1136/bmj.n71

10. el-Khoueiry A, Sangro B, Yau T, Crocenzi T, Kudo M, Hsu C, et al. Nivolumab in patients with advanced hepatocellular carcinoma (CheckMate 040): an open-label, non-comparative, phase 1/2 dose escalation and expansion trial. *Lancet*. (2017) 389:2492–502. doi: 10.1016/S0140-6736(17)31046-2

11. Johnson BT, Huedo-Medina TB eds. Ahrq methods for effective health care In: Meta-analytic statistical inferences for continuous measure outcomes as a function of effect size metric and other assumptions. The book was prepared by the University of Connecticut–Hartford Hospital Evidence-Based Practice Center and published by the Agency for Healthcare Research and Quality (AHRQ). Rockville: Agency for Healthcare Research and Quality (2013)

12. Shi Y-H, Ji Y, Liu W-R, Pang YR, Ding ZB, Fu XT, et al. Abstract 486: a phase Ib/ii, open-label study evaluating the efficacy and safety of Toripalimab injection (Js001) or combination with Lenvatinib as a neoadjuvant therapy for patients with resectable hepatocellular carcinoma (Hcc). *Cancer Res*. (2021) 81:486. doi: 10.1158/1538-7445.AM2021-486

13. Su Y, Lin Y, Hsiao C, Ou D, Chen S, Wu Y, et al. P-124 Nivolumab plus ipilimumab as neoadjuvant therapy for potentially resectable hepatocellular carcinoma. *Ann Oncol*. (2021) 32:S141. doi: 10.1016/j.annonc.2021.05.179

14. Ho WJ, Zhu Q, Durham J, Popovic A, Xavier S, Leatherman J, et al. Neoadjuvant Cabozantinib and Nivolumab converts locally advanced Hcc into Resectable disease with enhanced antitumor immunity. *Nat. Cancer*. (2021) 2:891–903. doi: 10.1038/s43018-021-00234-4

15. Xia Y, Tang W, Qian X, Li X, Cheng F, Wang K, et al. Efficacy and safety of camrelizumab plus apatinib during the perioperative period in resectable hepatocellular carcinoma: a single-arm, open label, phase ii clinical trial. *J Immunother Cancer*. (2022) 10:e004656. doi: 10.1136/jitc-2022-004656

16. Chen S, Wang Y, Xie W, Shen S, Peng S, Kuang M. 710P neoadjuvant tislelizumab for resectable recurrent hepatocellular carcinoma: a non-randomized control, phase ii trial (talent). *Ann Oncol*. (2022) 33:S867. doi: 10.1016/j.annonc.2022.07.834

17. Bai X, Chen Y, Zhang X, Zhang F, Liang X, Zhang C, et al. 712P Capt: a multicenter randomized controlled trial of perioperative versus postoperative camrelizumab plus apatinib for resectable hepatocellular carcinoma. *Ann Oncol*. (2022) 33:S868. doi: 10.1016/j.annonc.2022.07.836

18. Song T. A prospective, single-arm, phase ii clinical study of tislelizumab in combination with lenvatinib for perioperative treatment of resectable primary hepatocellular carcinoma with high risk of recurrence. *J Clin Oncol*. (2023) 41:e16218-e. doi: 10.1200/JCO.2023.41.16_suppl.e16218

19. D'Alessio A, Pai M, Spalding D, Goldin R, Scheiner B, Korolewicz J, et al. Neoadjuvant immunotherapy with ipilimumab plus nivolumab and radiologically and pathologically quantifiable responses through modulation of the tumour microenvironment in resectable hepatocellular carcinoma. *J Clin Oncol*. (2023) 41:4129. doi: 10.1200/JCO.2023.41.16_suppl.4129

20. Sun H, Zhu X, Gao Q, Qiu SJ, Shi YH, Wang XY, et al. Sintilimab combined with bevacizumab biosimilar as a conversion therapy in potentially resectable intermediate-stage hepatocellular carcinoma (Hcc): updated results of a phase ii trial. *J Clin Oncol*. (2023) 41:e16220-e. doi: 10.1200/JCO.2023.41.16_suppl.e16220

21. Wang K, Xiang YJ, Yu HM, Cheng YQ, Liu ZH, Qin YY, et al. Adjuvant sintilimab in resected high-risk hepatocellular carcinoma: a randomized, controlled, phase 2 trial. *Nat Med*. (2024) 30:708–15. doi: 10.1038/s41591-023-02786-7

22. Qin S, Chen M, Cheng AL, Kaseb AO, Kudo M, Lee HC, et al. Atezolizumab plus bevacizumab versus active surveillance in patients with resected or ablated high-risk hepatocellular carcinoma (Imbrave050): a randomised, open-label, multicentre, phase 3 trial. *Lancet*. (2023) 402:1835–47. doi: 10.1016/S0140-6736(23)01796-8

23. Kaseb A, Duda DG, Tran Cao HS, Abugabal YI, Vence LM, Rashid A, et al. Randomized, open-label, perioperative phase ii study evaluating nivolumab alone versus nivolumab plus ipilimumab in patients with resectable Hcc. *Ann Oncol*. (2019) 30:v880. doi: 10.1093/annonc/mdz394.038

24. Li Z, Wu X, Zhao Y, Xiao Y, Zhao Y, Zhang T, et al. Clinical benefit of neoadjuvant anti-Pd-1/Pd-L1 utilization among different tumors. *MedComm*. (2021) 2:60–8. doi: 10.1002/mco2.61

25. Hellmann MD, Chaft JE, William WN Jr, Rusch V, Pisters KM, Kalhor N, et al. Pathological response after neoadjuvant chemotherapy in resectable non-small-cell lung cancers: proposal for the use of major pathological response as a surrogate endpoint. *Lancet Oncol*. (2014) 15:e42–50. doi: 10.1016/S1470-2045(13)70334-6

26. Kou L, Wen Q, Xie X, Chen X, Li J, Li Y. Adverse events of immune checkpoint inhibitors for patients with digestive system cancers: a systematic review and meta-analysis. *Front Immunol*. (2022) 13:1013186. doi: 10.3389/fimmu.2022.1013186

27. Finn RS, Qin S, Ikeda M, Galle PR, Ducreux M, Kim TY, et al. Atezolizumab plus Bevacizumab in Unresectable Hepatocellular Carcinoma. *N Engl J Med*. (2020) 382:1894–905. doi: 10.1056/NEJMoa1915745

28. Cammarota A, Zanuso V, D'alessio A, Pressiani T, Personeni N, Rimassa L. Cabozantinib plus atezolizumab for the treatment of advanced hepatocellular carcinoma: shedding light on the preclinical rationale and clinical trials. *Expert Opin Investig Drugs*. (2022) 31:401–13. doi: 10.1080/13543784.2022.2032641

29. Xu J, Zhang Y, Jia R, Yue C, Chang L, Liu R, et al. Anti-Pd-1 antibody Shr-1210 combined with Apatinib for advanced hepatocellular carcinoma, gastric, or Esophagogastric junction cancer: an open-label, dose escalation and expansion study. *Clin Cancer Res*. (2019) 25:515–23. doi: 10.1158/1078-0432.CCR-18-2484

30. Ren Z, Xu J, Bai Y, Xu A, Cang S, du C, et al. Sintilimab plus a bevacizumab biosimilar (Ibi305) versus sorafenib in unresectable hepatocellular carcinoma (Orient-32): a randomised, open-label, phase 2-3 study. *Lancet Oncol*. (2021) 22:977–90. doi: 10.1016/S1470-2045(21)00252-7

31. Makker V, Rasco D, Vogelzang NJ, Brose MS, Cohn AL, Mier J, et al. Lenvatinib plus pembrolizumab in patients with advanced endometrial cancer: an interim analysis of a multicentre, open-label, single-arm, phase 2 trial. *Lancet Oncol*. (2019) 20:711–8. doi: 10.1016/S1470-2045(19)30020-8

32. Llovet JM, Castet F, Heikenwalder M, Maini MK, Mazzaferro V, Pinato DJ, et al. Immunotherapies for hepatocellular carcinoma. *Nat Rev Clin Oncol*. (2022) 19:151–72. doi: 10.1038/s41571-021-00573-2

33. Shigeta K, Datta M, Hato T, Kitahara S, Chen IX, Matsui A, et al. Dual programmed death Receptor-1 and vascular endothelial growth factor Receptor-2 blockade promotes vascular normalization and enhances antitumor immune responses in hepatocellular carcinoma. *Hepatology*. (2020) 71:1247–61. doi: 10.1002/hep.30889

34. Sperandio RC, Pestana RC, Miyamura BV, Kaseb AO. Hepatocellular carcinoma immunotherapy. *Annu Rev Med*. (2022) 73:267–78. doi: 10.1146/annurev-med-042220-021121

35. Yau T, Park JW, Finn RS, Cheng AL, Mathurin P, Edeline J, et al. Nivolumab versus sorafenib in advanced hepatocellular carcinoma (CheckMate 459): a randomised, multicentre, open-label, phase 3 trial. *Lancet Oncol*. (2022) 23:77–90. doi: 10.1016/S1470-2045(21)00604-5

36. Zhu AX, Finn RS, Edeline J, Cattan S, Ogasawara S, Palmer D, et al. Pembrolizumab in patients with advanced hepatocellular carcinoma previously treated with sorafenib (Keynote-224): a non-randomised, open-label phase 2 trial. *Lancet Oncol*. (2018) 19:940–52. doi: 10.1016/S1470-2045(18)30351-6

37. Peng Z, Cheng S, Kou Y, Wang Z, Jin R, Hu H, et al. The gut microbiome is associated with clinical response to anti-Pd-1/Pd-L1 immunotherapy in gastrointestinal cancer. *Cancer Immunol Res*. (2020) 8:1251–61. doi: 10.1158/2326-6066.CIR-19-1014

38. Merk C, Martling A, Lindberg J, Benhaim L, Taieb J, Lind P. Circulating tumor Dna (ctdna) in adjuvant therapy of early stage colon cancer: current status and future perspectives. *Acta Oncol*. (2022) 61:523–30. doi: 10.1080/0284186X.2022.2033831

frontiers | Frontiers in Medicine

TYPE Systematic Review
PUBLISHED 07 February 2025
DOI 10.3389/fmed.2024.1522292

OPEN ACCESS

EDITED BY
Pradeep Kumar Shukla,
University of Tennessee Health Science Center (UTHSC), United States

REVIEWED BY
Zheng Liu,
National Cancer Center of China, China
Daming Zhang,
First Affiliated Hospital of Harbin Medical University, China

*CORRESPONDENCE
Suyu He
✉ 13890893057@163.com

†These authors have contributed equally to this work

RECEIVED 04 November 2024
ACCEPTED 30 December 2024
PUBLISHED 07 February 2025

CITATION
Yan G, Li Y, He S, Li H, McClure MA, Li Q, Yang J, Wang H, Zhao L, Fan X, Yan J, Wu S and Guo W (2025) Prevalence and clinical implications of the rare arc of Bühler using computed tomography angiography and digital subtraction angiography: a systematic review and meta-analysis. *Front. Med.* 11:1522292. doi: 10.3389/fmed.2024.1522292

Prevalence and clinical implications of the rare arc of Bühler using computed tomography angiography and digital subtraction angiography: a systematic review and meta-analysis

Gaowu Yan[1,2†], Yong Li[1†], Suyu He[3*], Hongwei Li[4], Morgan A. McClure[5], Qiang Li[2], Jifang Yang[2], Hu Wang[2], Linwei Zhao[1], Xiaoping Fan[1], Jing Yan[1†], Siyi Wu[1] and Wenwen Guo[1]

[1]Department of Radiology, Suining Central Hospital, Suining, China, [2]Department of Radiology, Shehong Municipal Hospital of Traditional Chinese Medicine, Shehong, China, [3]Department of Gastroenterology, Suining Central Hospital, Suining, China, [4]Department of Radiology, The Third Hospital of Mianyang and Sichuan Mental Health Center, Mianyang, China, [5]Department of Radiology and Imaging, Institute of Rehabilitation and Development of Brain Function, The Second Clinical Medical College of North Sichuan Medical College, Nanchong Central Hospital, Nanchong, China

Background: Knowledge of the rare arc of Bühler (AOB) is limited but clinically important. At present, there is no publication of systematic review and meta-analysis on AOB in computed tomography angiography (CTA) and digital subtraction angiography (DSA) examinations.

Objective: The objective of this study was to evaluate the pooled prevalence and clinical implications of the AOB by using CTA and DSA examinations.

Methods: The PubMed, Web of Science, Scopus, Embase, Google Scholar, CBM, CNKI, WanFang, VIP, and Baidu Scholar databases were comprehensively searched for AOB-related literature. Stata 17.0 software was used to conduct the meta-analysis.

Results: Eleven publications with 3,837 patients and 65 AOB cases were included. The pooled prevalence of AOB was 1.9% (95% confidence interval: 0.8–3.2%). CTA showed a pooled prevalence of AOB of 2.0% (95% confidence interval: 0.5–4.3%) and DSA showed a pooled prevalence of AOB of 1.8% (95% confidence interval: 0.5–3.9%).

Conclusion: AOB is a rare anatomical variant, with a pooled prevalence of 1.9% in the general population. General surgeons, vascular surgeons, and interventional radiologists should consider its existence when performing relevant abdominal procedures to avoid intraoperative difficulties, visceral organ ischemia or bleeding, and other complications.

KEYWORDS

arc of Bühler, computed tomography angiography, digital subtraction angiography, meta-analysis, systematic review

Introduction

The arc of Bühler (AOB) was first described by Bühler in 1904, and it is currently defined as the anastomotic artery between the superior mesenteric artery and the celiac trunk or its branches (1). AOB is a rare anatomical variation that may affect various interventional radiological operations (e.g., interventional embolization of aneurysms) and abdominal surgeries (e.g., pancreaticoduodenectomy) (2, 3). However, most general surgeons, vascular surgeons, and interventional radiologists do not have a sufficient understanding of the anatomy and function of AOB, which may lead to a lack of awareness of potential adverse outcomes (such as iatrogenic injuries) during or after surgeries (4, 5). Therefore, when performing abdominal related surgeries, it is important to keep in mind the existence of AOB.

Computed tomography angiography (CTA) can noninvasively evaluate vascular diseases and anatomical variations in various parts of the body, and digital subtraction angiography (DSA) is currently considered the reference standard to diagnose vascular diseases in all parts of the body (6, 7). As a result, both CTA and DSA are clinically valuable to evaluate the prevalence and clinical implications of AOB.

With the rapid development of evidence-based medicine (EBM), the theory and concept of evidence-based anatomy (EBA) came into being. EBA applies the basic principles and research methods of EBM to the field of anatomy (8, 9). The actual prevalence of AOB remains unclear, with estimates in the literature suggesting it to be less than 3% (1). Thus, this study aimed to use a systematic review and meta-analysis (i.e., EBA) to review and analyse the literature on AOB and evaluate its reported prevalence and clinical implications based on CTA and DSA to guide the diagnosis and treatment of clinically related diseases.

Materials and methods

Inclusion and exclusion criteria

Studies of the general population who underwent abdominal CTA or DSA to evaluate the presence of anatomical variations in the abdominal vasculature were included in this systematic review and meta-analysis. The outcome index was the prevalence of AOB. In this present study, AOB was defined as the anastomotic artery between the superior mesenteric artery and the celiac trunk or its branches (1). The exclusion criteria were: (I) reviews, case reports, editorials, comments, and conference abstracts; (II) autopsies of animal or human cadavers; (III) duplicate publications; and (IV) an inability to obtain the full text, incomplete literature data, or data that could not be used to calculate the prevalence of AOB.

According to our previous experience in systematic review and meta-analysis, there are two common types of duplicate publications. The first type is multiple publication of the same research data in different languages. The second type is that some time following the publication of a study, a second study by the same author(s) on the same topic, with a larger sample size, was published. In the second situation, we will exclude the earlier study and only include the latest study with the largest sample size.

Literature retrieval strategy

The English databases of PubMed, Web of Science, Embase, Scopus, and Google Scholar; and the Chinese databases of CBM (China Biology Medicine Disc), CNKI (China National Knowledge Infrastructure), WanFang, VIP, and Baidu Scholar were all comprehensively searched. All cross-sectional studies on the prevalence of AOB were collected. The time frame for retrieval was from the establishment of each database to September 30, 2024. A combination of subject and free words that were modified based on the characteristics of each database was used for retrieval. Simultaneously, the references included in the study were searched to supplement and obtain relevant data. The searched words included in this study were Bühler, Buhler, arc, Bühler arc, Buhler arc, coeliac, coeliac trunk, celiac, celiac trunk, coeliac artery, celiac artery, celiac axis, celiac axis, trunk, axis, and superior mesenteric artery.

Literature screening and data extraction

Two researchers (with eight and 10 years of experience in abdominal radiology) independently examined the literature, extracted the data, and cross-checked it. If there were disagreements, they were resolved by discussion or consultation with a third researcher (with 15 years of experience in abdominal radiology). The title of the article was reviewed first throughout the literature screening procedure. Upon eliminating studies that were clearly irrelevant, the abstract and complete text were examined to decide whether or not to incorporate the study into the analysis. If necessary, the authors of the original study were contacted by e-mail or telephone to obtain data that were not reported but were important for this study. First author, publication time (year), country, research type (CTA or DSA), total sample size, number and prevalence of AOB (%), and AOB type were all included in the data.

Bias risk assessment

The same two researchers who performed the literature screening and data extraction procedures independently evaluated the risk of bias and cross-checked the results. Bias risk assessment was performed by using the "Anatomical Quality Assessment Tool" recommended by the International Evidence-Based Anatomy Working Group (10). The tool consisted of a series of questions in five domains: (I) research objectives and characteristics of research subjects, (II) research design, (III) methodology characterization, (IV) descriptive anatomy, and (V) reporting of results. If all questions in a particular domain were answered 'yes', then the risk of bias in that domain was determined to be 'low'; if any question in a particular domain was answered 'no' or 'unclear', the risk of bias in this domain was, respectively, determined to be 'high' or 'unclear'.

Statistical analysis

Data were collected and collated by using an Excel (Microsoft Corp., Redmond, WA, USA) table, and a single-group meta-analysis was performed using the metaprop module of Stata software (version 17.0; StataCorp, College Station, TX, USA). The prevalence of AOB was used

as the statistic for effect analysis, and a 95% confidence interval (CI) was provided. Heterogeneity between studies was evaluated using χ^2 tests and I^2 statistics. χ^2 tests ($p < 0.10$) indicated statistical heterogeneity. An I^2 value of 0–40% was considered "might not be important," that of 30–60% was considered "may represent moderate heterogeneity," that of 50–90% was considered "may represent substantial heterogeneity," and that of 75–100% was considered "considerable heterogeneity" (8). For the meta-analysis, the fixed-effects model was to be applied if there was no statistical heterogeneity among the outcomes. In cases where there was statistical heterogeneity in the data, the source of the heterogeneity was investigated further, and after ruling out the impact of clear clinical heterogeneity, a random-effects model was employed for the meta-analysis. The level of the meta-analysis was set as $\alpha = 0.05$. A subgroup analysis was conducted according to the type of study (CTA or DSA) to further explore the possible factors affecting the AOB prevalence.

Results

Literature screening procedures and results

On the basis of the preliminary screening, 1,168 pertinent studies were included. Eleven cross-sectional studies were eventually included following layer-by-layer screening (11–21). These included 3,837 participants (with 65 cases of AOB), of which 1769 were examined using CTA and 2068 were examined using DSA. The literature screening procedure and the results are shown in Figure 1.

Basic features and bias risk assessment results

The basic characteristics of the included studies and the results of the bias risk evaluation are presented in Tables 1, 2, respectively. The bias risk of eight studies in terms of "research objectives and characteristics of research subjects" was determined to be 'high', as the method of subject selection introduced bias into the study to some extent ($n = 8$), and that of seven studies in "methodology characterization" was determined to be 'high' due to the absence of appropriate measures for reducing inter- and intra-observer variability ($n = 7$). The bias risk in the remaining domains was determined to be 'low' (Figure 2).

Results of the meta-analysis

Pooled prevalence

Eleven studies were included (11–21). The χ^2 test identified a p value of less than 0.10, and the I^2 statistic was 82.80%. Both of the

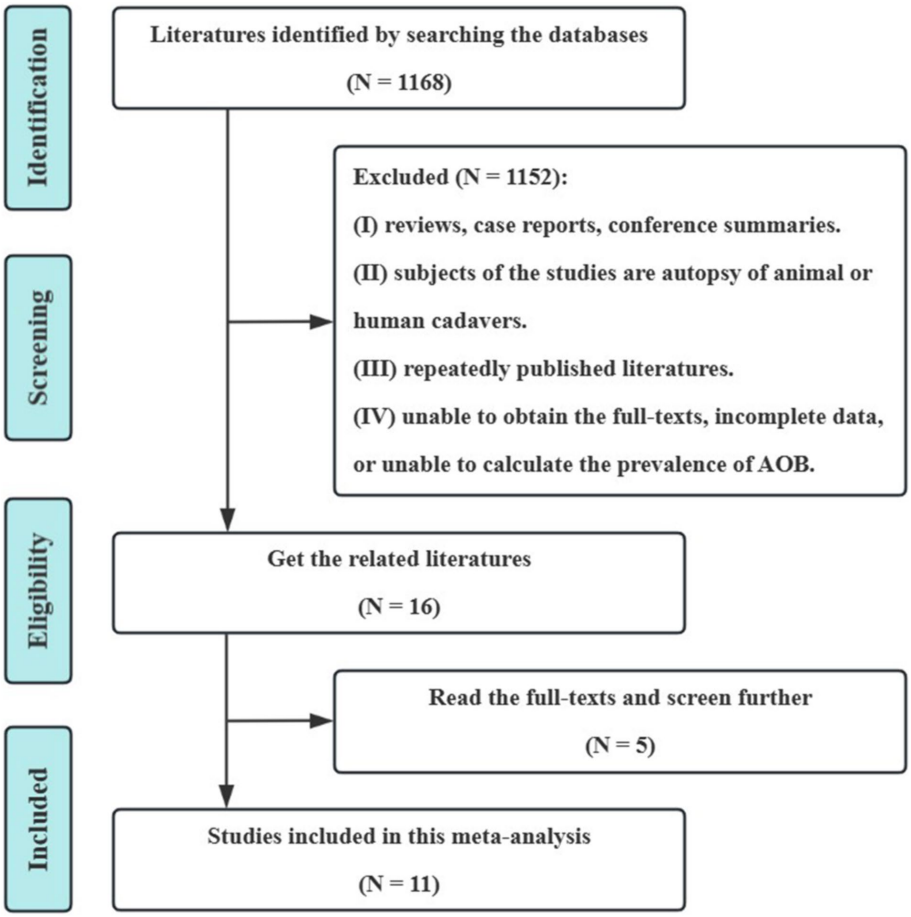

FIGURE 1
Screening process and literature review results. AOB, the arc of Bühler.

TABLE 1 Basic features and prevalence of AOB in included studies.

Author	Year of publication	Country	Study type	Sample size	AOB (%)	AOB composition
Wicke et al. (11)	1977	Austria	DSA	80	1 (1.25)	Celiac trunk-superior mesenteric artery
Grabbe et al. (12)	1980	Germany	DSA	340	14 (4.12)	Celiac trunk-superior mesenteric artery
Bertelli et al. (13)	1991	Italy	DSA	1,000	3 (0.30)	Celiac trunk-superior mesenteric artery
McNulty et al. (14)	2001	Ireland	DSA	300	3 (1.00)	Celiac trunk-superior mesenteric artery
Saad et al. (15)	2005	America	DSA	120	4 (3.33)	Celiac trunk-superior mesenteric artery
Ferrari et al. (16)	2007	Italy	CTA	60	2 (3.33)	Celiac trunk-superior mesenteric artery, Celiac trunk-splenetic artery
Sureka et al. (17)	2013	India	CTA	600	8 (1.33)	Celiac trunk-superior mesenteric artery
van Petersen et al. (18)	2014	Netherlands	DSA	228	7 (3.07)	Celiac trunk-superior mesenteric artery
Ognjanović et al. (19)	2014	Serbia	CTA	150	4 (2.67)	Celiac trunk-superior mesenteric artery
Farghadani et al. (20)	2016	Iran	CTA	607	2 (0.33)	Celiac trunk-superior mesenteric artery
Lin et al. (21)	2022	China	CTA	352	17 (4.8)	Celiac trunk-superior mesenteric artery and its branches*

CTA, computed tomography angiography, DSA, digital subtraction angiography, and AOB, Arc of Bühler. *Celiac trunk-superior mesenteric artery (n = 6), splenetic artery-superior mesenteric artery (n = 4), common hepatic artery-superior mesenteric artery (n = 3), celiac trunk-inferior pancreaticoduodenal artery (n = 1), dorsal pancreatic artery-inferior pancreaticoduodenal artery (n = 1), celiac trunk-ectopic origin of right hepatic artery (n = 1), and common hepatic artery-middle colonic artery (n = 1).

TABLE 2 Basic characteristics of included studies and AQUA quality evaluation.

Author	Objectives and subject characteristics	Study design	Methodology characterization	Descriptive anatomy	Reporting of results
Wicke et al. (11)	High	Low	High	Low	Low
Grabbe et al. (12)	High	Low	High	Low	Low
Bertelli et al. (13)	High	Low	High	Low	Low
McNulty et al. (14)	High	Low	High	Low	Low
Saad et al. (15)	High	Low	High	Low	Low
Ferrari et al. (16)	High	Low	Low	Low	Low
Sureka et al. (17)	Low	Low	Low	Low	Low
van Petersen et al. (18)	Low	Low	High	Low	Low
Ognjanović et al. (19)	High	Low	High	Low	Low
Farghadani et al. (20)	High	Low	Low	Low	Low
Lin et al. (21)	Low	Low	Low	Low	Low

AQUA, anatomical quality assessment tool.

results indicated statistically significant heterogeneity between the eleven included studies. The results of the random effect model meta-analysis (Table 3 and Figure 3) showed that the pooled prevalence of AOB was 1.9% (95% CI: 0.8–3.2%).

Subgroup analysis

Five CTA and six DSA studies were included into the subgroup analysis (Table 3). The χ^2 tests identified both of the p values were less than 0.10, and the I^2 statistics were 84.56 and 84.13%, respectively. All the results indicated statistically significant heterogeneity between the studies included into the subgroup analysis. According to the subgroup analysis of the included studies with the random effect models, the pooled prevalence of the AOB using CTA was 2.0% (95% CI: 0.5–4.3%), and that using DSA was 1.8% (95% CI: 0.5–3.9%).

Sensitivity analysis and publication bias test

Sensitivity analysis was performed by eliminating individual studies; the results showed no significant change in the combined estimates, suggesting that the results of this study are relatively stable. The publishing bias of the included studies was assessed by using funnel plots, Begg's test, and Egger's test (Figure 4). The findings indicated no significant publication bias ($p > 0.05$).

Discussion

Definition, prevalence, and anatomical types of the AOB

AOB is a rare anatomical variation. Bühler was the first to describe AOB as "the anastomotic artery between the celiac artery and the middle

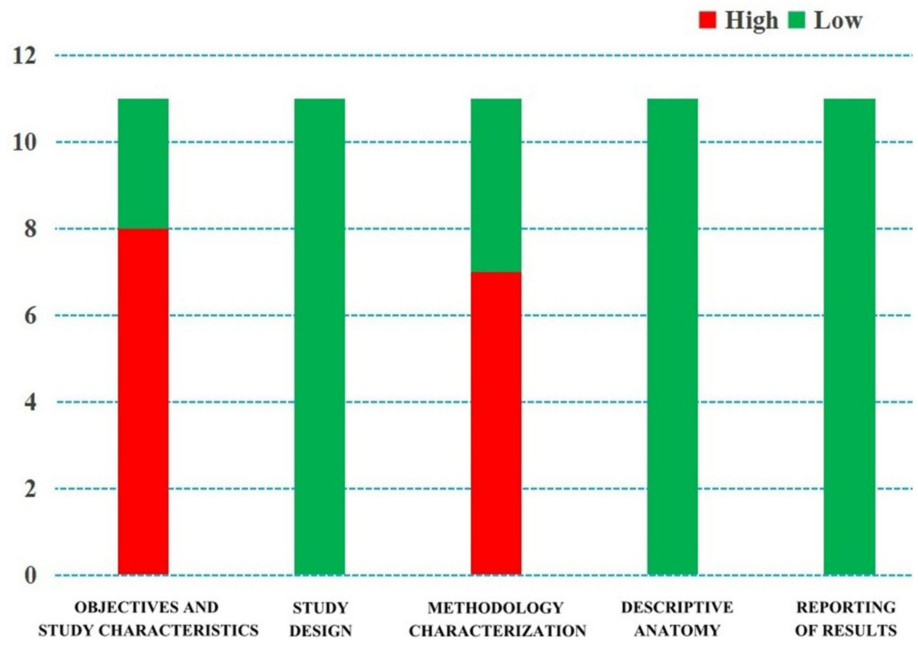

FIGURE 2
Quality evaluation by the "Anatomical Quality Assessment (AQUA) Tool" for the included studies.

colonic artery, usually as an additional collateral circulation between the celiac artery and the superior mesenteric artery" (1). With the increase in subsequent reports and a deepening of understanding, current studies have found that such anastomotic vessels can also occur in multiple branches of the celiac trunk and superior mesenteric artery including the following: celiac trunk and superior mesenteric artery, celiac trunk and inferior pancreaticoduodenal artery, celiac trunk and middle colonic artery, celiac trunk and first jejunal artery, celiac trunk and ectopic origin of right hepatic artery, splenetic artery and superior mesenteric artery, common hepatic artery and superior mesenteric artery, common hepatic artery and middle colonic artery, proper hepatic artery and first jejunal artery, gastroduodenal artery and pancreaticoduodenal artery, and pancreatic integument artery and anterior/posterior/inferior pancreaticoduodenal artery (1, 11–21). At present, AOB has been redefined as the anastomotic artery between the superior mesenteric artery and the celiac trunk or its branches (1).

In this meta-analysis, the AOB included in the study was primarily found between the celiac trunk and superior mesenteric artery (11–20), while Li and colleagues (21) reported many other types of AOB (Table 1). The author believes that the reasons may be as follows. First, in the early literature, researchers had insufficient understanding of the AOB, which was only defined as "the anastomotic artery between the celiac artery and the superior mesenteric artery"; thus, the reported frequency of AOB type is fairly low. Second, in subsequent studies, researchers had a deeper understanding of the AOB, which was redefined as "the anastomotic artery between the superior mesenteric artery and the celiac trunk or its branches"; thus the reporting frequency of AOB type was improved.

In this present meta-analysis, the overall prevalence of AOB was 1.9% (0.8–3.2%). For the subgroup analysis according to the type of inclusion study (Table 3), the pooled prevalence of AOB detected by CTA was 2.0% (95% CI: 0.5–4.3%) and that detected by DSA was 1.8% (95% CI: 0.5–3.9%). This is consistent with previous reports by Dubel et al. (22) and Xiao et al. (23) who demonstrated that the prevalence of AOB in the general population is less than 4.0% (Figure 5) (24).

Embryological mechanism of AOB

The MacKay arch theory and Handler's longitudinal anastomosis are two commonly used models to explain anatomical variation in abdominal aortic branches (25). According to the aforementioned model (25), the 10th–13th ventral segmental arteries (which develop into the left gastric artery, splenetic artery, common hepatic artery, and superior mesenteric artery, respectively) originate from the dorsal aorta in the initial stages of embryonic development. They communicate temporarily through ventral longitudinal anastomoses (Figure 6a). Under normal circumstances, the 11th and 12th ventral segmental arteries and ventral longitudinal anastomotic arteries degenerate and disappear, while the 10th and 13th ventral segmental arteries remain, finally forming the celiac trunk and the superior mesenteric arteries. Thus, both the celiac trunk and superior mesenteric artery originate separately from the abdominal aorta (Figure 6b). If the 13th ventral segmental artery and ventral longitudinal anastomotic artery persist and the 10th–12th ventral segmental arteries degenerate, the celiac trunk and superior mesenteric artery are formed. An AOB may form when the ventral longitudinal anastomotic artery persists (Figure 6c). These embryological mechanisms were further clarified in later studies (26–28).

Physiological function and clinical symptoms of AOB

The main physiological function of AOB is to act as a collateral circulation between the celiac trunk and the superior mesenteric artery. Saad et al. (15) used a 1.67 mm ductus arteriosus as a reference and

TABLE 3 Subgroup analysis according to the type of included studies.

Subgroup	Number of studies	Number of patients	Pooled prevalence of AOB: % (95% CI)	I^2 statistics (%)	*P* value
Overall	11	3,837	1.9 (0.8–3.2)	82.799	< 0.001
CTA	5	1769	2.0 (0.5–4.3)	84.561	< 0.001
DSA	6	2068	1.8 (0.5–3.9)	84.129	< 0.001

CTA, computed tomography angiography, DSA, digital subtraction angiography, and AOB, Arc of Bühler.

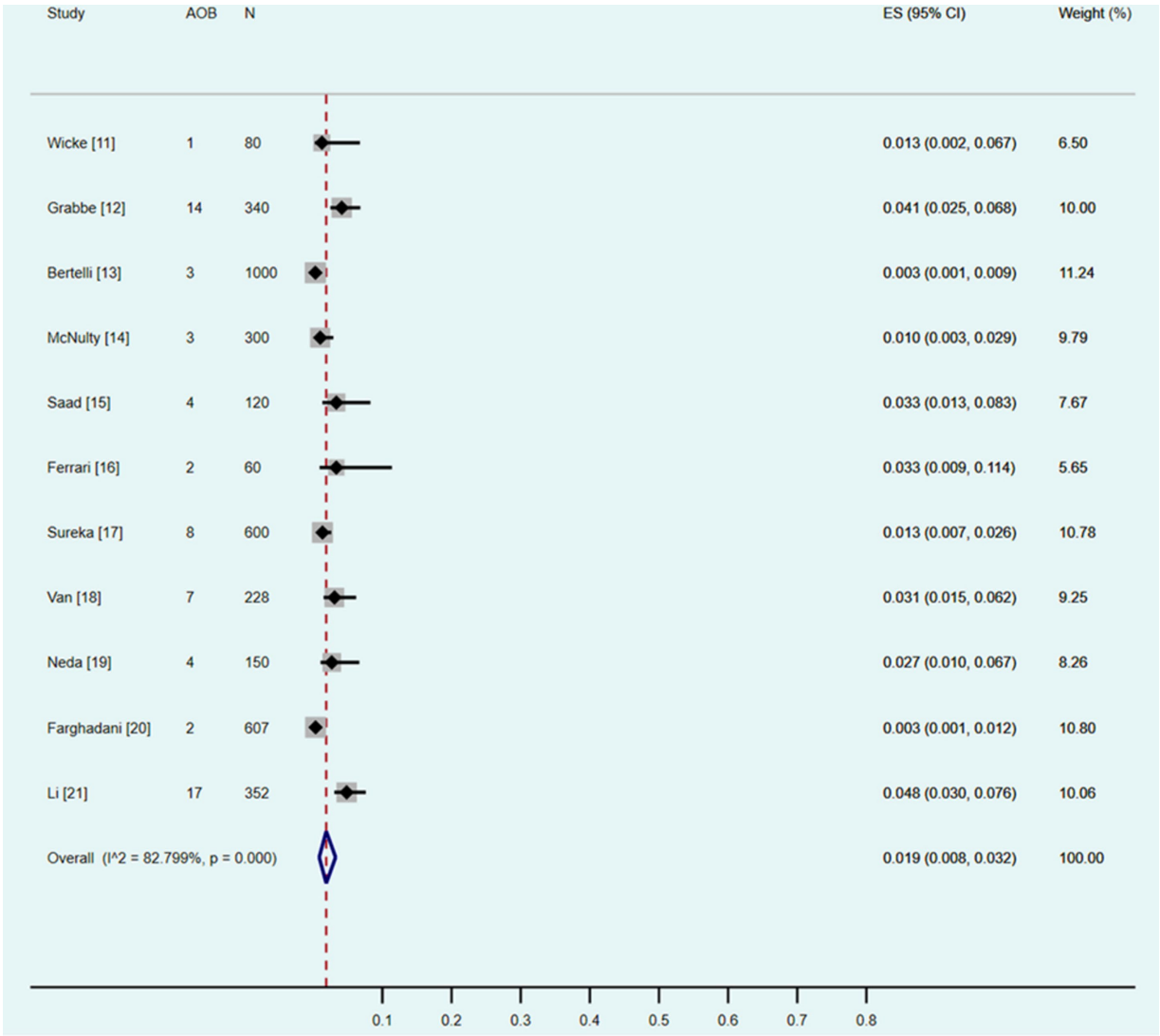

FIGURE 3
Forest plot showing a pooled incidence of the arc of Bühler (AOB) of 1.9% (95% confidence interval, 0.8–3.2%).

estimated the AOB diameter to be 1.5–2.5 mm. In another study, Grabbe and Bühler (12) estimated that the AOB diameter was 2.0–7.0 mm. Therefore, the AOB is usually very small, and the blood flow may be negligible under normal conditions; however, the hemodynamic behavior of the AOB may change in cases of stenosis or occlusion of the celiac trunk or superior mesenteric artery. In such cases, blood circulates through the collateral circulation of the AOB, ensuring blood circulation to the abdominal organs. However, this collateral circulation mechanism may also lead to the formation of AOB aneurysms because increased local blood flow may lead to increased arterial pressure, thickening of local arterial walls, and the formation of true aneurysms (29). AOB can also form an arterial shunt between the celiac trunk and superior mesenteric artery, resulting in decreased blood flow through the common hepatic artery (30).

The vast majority of patients with AOB did not have any clinical symptoms (86.79%), with it being incidentally detected on CTA or DSA. A few patients (13.21%) may have had epigastric discomfort, postprandial pain, gastrointestinal bleeding, obstructive jaundice,

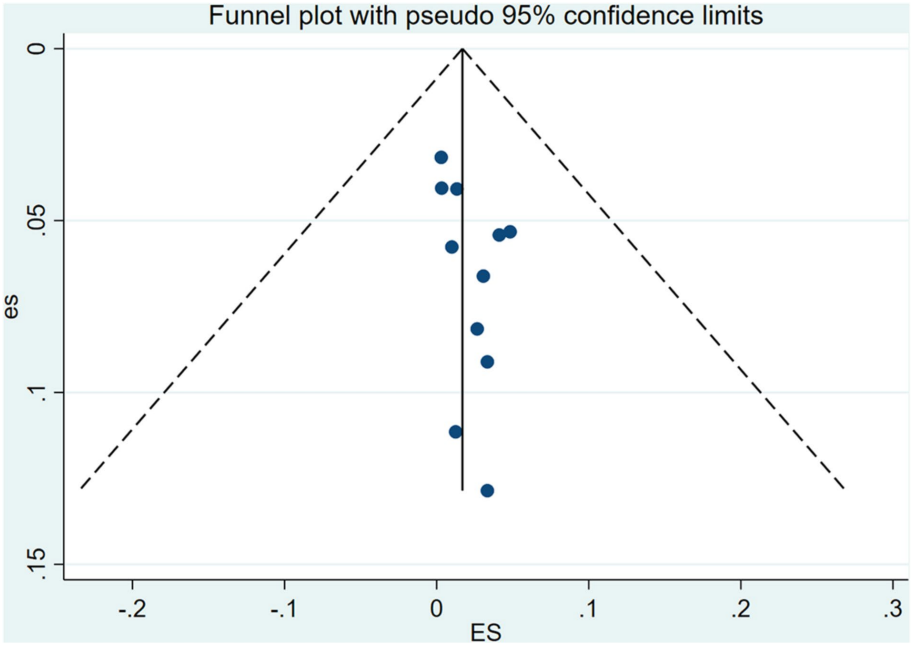

FIGURE 4
Funnel plot showing no publication bias in this study.

bleeding after endoscopic retrograde cholangiopancreatography, intraabdominal or retroperitoneal bleeding due to pressure phenomena, endovascular hemorrhage, or ruptured aneurysms (1, 23, 31–34).

Clinical correlation of AOB

The anatomy of the retropancreatic space is important during pancreaticoduodenectomy. The tissue structures in this area include the celiac trunk, superior mesenteric artery, portal vein, lymph nodes, and nerves. During pancreaticoduodenectomy, accidental injury to the AOB may lead to iatrogenic damage, such as abdominal organ ischemia or bleeding (35, 36). For interventional radiologists, in some cases (e.g., abdominal trunk occlusion), an unobstructed AOB can also become an alternative route for some abdominal surgeries, or even "an anatomical variation that saves patients' lives" (37, 38). Shah et al. (37) reported a patient who underwent AOB intubation chemoembolization for hepatocellular carcinoma due to abdominal trunk occlusion.

In another study, Nikolaos et al. (38) reported a patient with complex type B aortic dissection, whose abdominal trunk was almost completely occluded due to the involvement of the dissection, and faced a huge risk of abdominal organ malperfusion syndrome. However, after careful examination by the physicians, it was discovered that there was an AOB anatomical variation between the common hepatic artery and the superior mesenteric artery in the patient, which allowed for the maintenance of blood supply to the abdominal organs. As a result, the patient ultimately underwent endovascular repair surgery for aortic dissection to save his life.

Using PubMed for a literature retrieval with the keywords "arc of Bühler," "arc of Buhler," "Bühler," and "Buhler" (December 20, 2024), we identified a few publications on AOB in some clinical scenarios. For example, Quaretti et al. (39) reported a case of large Buhler aneurysm in the context of chronic celiac trunk occlusion, which was successfully treated by means of covered stent assisted coil embolization; Abouzaid et al. (40) presented a unique AOB variant that connecting the arteries of the foregut, midgut, and hindgut, which was more complex than what had previously been reported; and in another study, Ehemann and Kim (41) reviewed an extremely rare vascular complication of extracorporeal shock wave lithotripsy (ESWL) pseudoaneurysm of AOB, with only one other case recorded in the literature. Publications regarding AOB indexed in the PubMed from 2020 to 2024 have been summarized in Table 4 ($n = 10$).

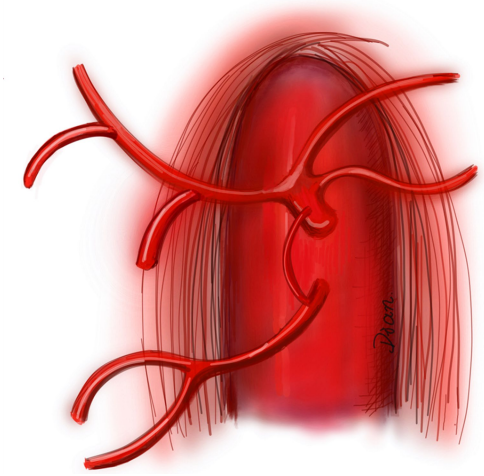

FIGURE 5
Diagram of the arc of Bühler (24). The arc of Bühler (AOB) is shown as an anastomotic artery between the celiac trunk and the superior mesenteric artery.

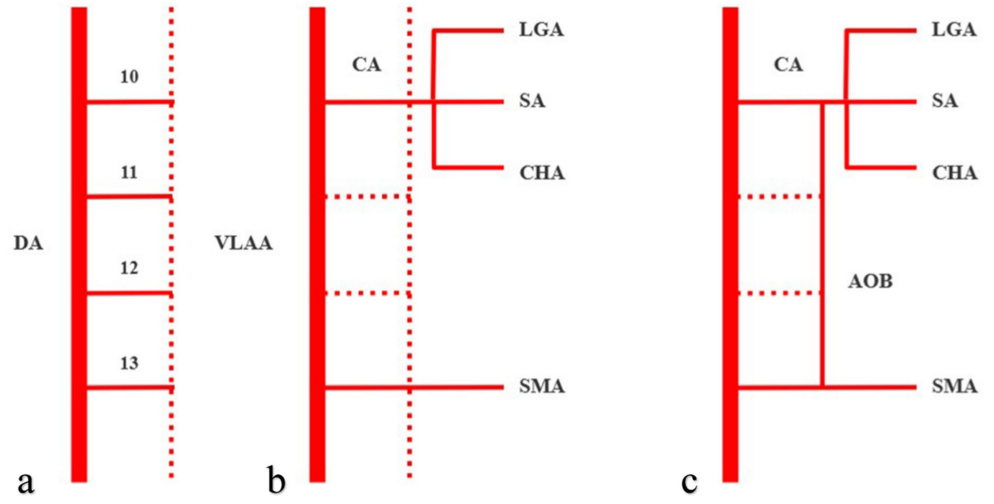

FIGURE 6
Arc of Bühler (AOB) schematic diagram of the embryological mechanism, with solid lines representing persistent blood vessels and dotted lines representing degenerated blood vessels. The 10th–13th ventral segmental arteries communicate temporarily through ventral longitudinal anastomoses **(a)**. When the 10th and 13th ventral segmental arteries remain, then the celiac trunk and superior mesenteric artery will originate separately from the abdominal aorta **(b)**. An AOB may form when the ventral longitudinal anastomotic artery persists **(c)**. DA, dorsal aorta, VLAA, ventral longitudinal anastomoses artery, CA, celiac axis, LGA, left gastric artery, SA, splenetic artery, CHA, common hepatic artery, and SMA, superior mesenteric artery.

Limitations and future directions

According to the guideline on conducting a systematic review and meta-analysis of anatomical study published by Henry et al., the heterogeneity in anatomical meta-analysis is almost always high (8). As such, due to the intrinsic heterogeneity in anatomical studies and for the purpose of maximizing the validity of the results, we used a random-effects model in our study. In our study, the χ^2 test identified a p value of less than 0.10, and the I^2 statistic was 82.80% for the eleven included studies. Both of the results indicated statistically significant heterogeneity between the studies.

The sources of heterogeneity in anatomical meta-analysis studies should always be explored. To probe them, according to the guideline published by Henry et al., subgroup analysis and sensitivity analysis can be performed (8). In our study, the subgroup analysis was performed by the modalities of the included studies (i.e., CTA *vs.* DSA). Other subgroup analyses, such as by geographical distribution of the studies (seven studies were performed in Europe, while the other four studies were performed in America, India, Iran, and China, respectively), or by gender, age, laterality, and side (left *vs.* right) were not conducted because the data were not applicable. Using confidence intervals (CIs) to assess for statistically significant differences between the CTA and DSA subgroups, an overlap between the two CIs (Table 3) was present. We may consider that the differences between the two groups were statistically insignificant. We also performed a sensitivity analysis to help explore the sources of heterogeneity in our study. The findings of the sensitivity analysis were robust to decisions made in the process of performing the meta-analysis. As a result, we may attribute the heterogeneity of our study to the inherent factors related to the complexity of the human body and diversity.

For methodology characterization and reporting among the included studies, since the concept of evidence-based anatomy was introduced by Henry et al. (8) and Yammine (9) it has emphasized the need for original anatomical studies with high clarity, transparency, and comprehensiveness in reporting. In our study, we used the "Anatomical Quality Assessment (AQUA) Tool" to evaluate the quality of the eleven included studies. The results showed that eight studies had high risk of bias in "objective (s) and subject characteristics" and seven studies had high risk of bias in "methodology characterization." Tomaszewski et al. (42) and Ottone et al. (43) introduced a checklist of reporting items that should be addressed by authors of original anatomical studies (i.e., the "Anatomical Quality Assurance (AQUA) Checklist"). In this checklist, twenty-nine items, crucial for reporting anatomical studies, have been designed and arranged. The items consist of eight sections, which include title (one item), abstract (one item), introduction (two items), methodology (twelve items), results (five items), discussion (four items), conclusions (one item), and other information (three items). For studies reporting anatomical findings in the future, we would highly recommend using this checklist as a reference.

For future directions, the number and quality of the currently included eleven studies are limited. This indicates the necessity for more investigations involving a large number of subjects, so as to provide a more precise evaluation of the prevalence of AOB, and improve consciousness among general surgeons, vascular surgeons, and interventional radiologists. When preparing to report anatomical findings in the future, we would also highly recommend the researchers involved to use the AQUA checklist as a reference.

Conclusion

AOB is a rare anatomical variation, with a pooled prevalence of approximately 1.9% in the general population. Although rare, such cases may play a significant role in general surgery, vascular surgery, and interventional radiology. General surgeons, vascular surgeons, and interventional radiologists should consider the existence of AOB when performing associated abdominal operations to avoid complications such as difficulty in the operation, abdominal organ ischemia, or bleeding. Higher-quality, larger-sample studies are required to corroborate the

TABLE 4 Publications regarding arc of Bühler or Buhler indexed in the PubMed from 2020 to 2024 (n = 10).

Author/ References	Year	Gender	Age (years)	Clinical presentations	AOB composition	Main highlights	Result
Huang et al. (2)	2024	Female	62	Two months of recurrent abdominal distension and postprandial pain	Celiac trunk-superior mesenteric artery	Revascularization of a superior mesenteric artery ostial occlusion via the arc of Buhler	Resolution
Quaretti et al. (39)	2024	Male	47	During rehabilitation following motorcycle trauma and vertebral surgery	Celiac trunk-superior mesenteric artery	Covered stent assisted coil embolization of large Buhler aneurysm in setting of chronic celiac trunk occlusion	Resolution
Abouzaid et al. (40)	2023	Male	76	Cadaveric donor	Celiac trunk-superior mesenteric artery	A unique arc of Bühler variant connecting the arteries of the foregut, midgut, and hindgut	NA
Ehemann and Kim (41)	2023	Male	70	Right mid-pole renal calculus	Celiac trunk-superior mesenteric artery	Rare vascular complication of ESWL pseudoaneurysm of arc of Buhler	Resolution
Padar et al. (31)	2023	Female	77	Sudden onset of pleuritic chest pain	Gastroduodenal artery and the first branch of the superior mesenteric artery	Unexpected finding of arc of Buhler with celiac artery stenosis during workup for a suspected pancreatic lesion	Resolution
Rathod et al. (29)	2022	Male	79	Cadaveric donor	Celiac trunk-superior mesenteric artery	A case of abnormally dilated and tortuous arc of Buhler and pancreaticoduodenal arteries in the absence of celiac trunk stenosis	NA
Schumacher et al. (35)	2022	NA	66	Painless jaundice and pathologic elevated cholestasis parameters	Common hepatic artery-superior mesenteric artery	A significant vascular variant in oncologic pancreaticoduodenectomy	Resolution
Manta et al. (44)	2022	Male	60	NA	Celiac trunk-the third jejunal artery	Hexafurcated coeliac trunks, trifurcated common hepatic artery, and a new variant of the arc of Bühler	NA
Incarbone et al. (45)	2021	Female	71	An ischemic stroke caused brain death	Celiac trunk-superior mesenteric artery	Discovery of a rare variant of the arc of Bühler during liver procurement	NA
Nikolaos et al. (38)	2020	Male	54	Sudden, severe, and generalized abdominal pain	Common hepatic artery-superior mesenteric artery	Arc of Buhler can be a lifesaving anatomic variation	Resolution

AOB, arc of Bühler or Buhler; ESWL, extracorporeal shock wave lithotripsy; NA, not available.

above conclusions because of the restricted number and quality of the included studies in this meta-analysis.

Data availability statement

The datasets presented in this article are not readily available because the raw data supporting the conclusions of this article will be made available by the authors, without undue reservation. Requests to access the datasets should be directed to yangaowu1989@163.com.

Author contributions

GY: Supervision, Writing – original draft, Writing – review & editing, Conceptualization, Funding acquisition. YL: Conceptualization, Supervision, Writing – original draft, Writing – review & editing. SH: Conceptualization, Supervision, Writing – original draft, Writing – review & editing. HL: Conceptualization, Supervision, Writing – original draft, Writing – review & editing. MM: Writing – original draft, Writing – review & editing. QL: Investigation, Software, Writing – review & editing, Data curation, Writing – original draft, Formal analysis. JY: Investigation, Software, Writing – review & editing, Data curation, Writing – original draft, Formal analysis. HW: Data curation, Formal analysis, Investigation, Software, Writing – original draft, Writing – review & editing. LZ: Data curation, Formal analysis, Investigation, Software, Writing – original draft, Writing – review & editing. XF: Data curation, Formal analysis, Investigation, Software, Writing – original draft, Writing – review & editing. JY: Data curation, Formal analysis, Investigation, Software, Writing – original draft, Writing – review & editing. SW: Data curation, Formal analysis, Investigation, Software, Writing – original draft, Writing – review & editing. WG: Data curation, Formal analysis, Investigation, Software, Writing – original draft, Writing – review & editing.

Funding

The author(s) declare that financial support was received for the research, authorship, and/or publication of this article. The present

study was supported by grants from the Sichuan Provincial Commission of Health (No. 19PJ284), Sichuan Medical Association (2024HR125), Sichuan Medical and Health Care Promotion Institute (KY2023QN0065), Science and Technology Association of Suining City (No. 6), and Suining Central Hospital (Nos. 2021y09 and 2022ypj01).

Conflict of interest

The authors declare that the research was conducted in the absence of any commercial or financial relationships that could be construed as a potential conflict of interest.

Generative AI statement

The authors declare that no Gen AI was used in the creation of this manuscript.

Publisher's note

All claims expressed in this article are solely those of the authors and do not necessarily represent those of their affiliated organizations, or those of the publisher, the editors and the reviewers. Any product that may be evaluated in this article, or claim that may be made by its manufacturer, is not guaranteed or endorsed by the publisher.

References

1. Michalinos A, Schizas D, Ntourakis D, Filippou D, Troupis T. Arc of Bühler: the surgical significance of a rare anatomical variation. *Surg Radiol Anat*. (2019) 41:575–81. doi: 10.1007/s00276-018-2168-0

2. Huang W, Wang K, Liu Y, Wang QQ, Wei HJ, He CS. Revascularization of superior mesenteric artery occlusion via the arc of Buhler: a case report and literature review. *Vascular*. (2024) 27:17085381241289485. doi: 10.1177/17085381241289485

3. Sugihara F, Murata S, Uchiyama F, Watari J, Tajima H, Kumita SI. Successful coil embolization of an aneurysm in the arc of Bühler. *J Nippon Med Sch*. (2016) 83:196–8. doi: 10.1272/jnms.83.196

4. Kowalczyk KA, Majewski A, Wysocki W, Tomaszewski K. Anatomy is the key to mastery in cancer and general surgery: the results of a survey on anatomical knowledge among surgeons. *J Oncol*. (2022) 72:226–30. doi: 10.5603/NJO.a2022.0033

5. Kowalczyk KA, Majewski A. Analysis of surgical errors associated with anatomical variations clinically relevant in general surgery: review of the literature. *Trans Res Anat*. (2021) 23:100107. doi: 10.1016/j.tria.2020.100107

6. Deng J, Ma T, Yan J, Wu S, Yan G, Li H, et al. Effect of low tube voltage (100 kV) combined with ASIR-V on the visualization and image quality of the Adamkiewicz artery: a comparison with 120 kV protocol. *Diagnostics*. (2023) 13:2495. doi: 10.3390/diagnostics13152495

7. Yan GW, Li HW, Yang GQ, Bhetuwal A, Liu JP, Li Y, et al. Iatrogenic arteriovenous fistula of the iliac artery after lumbar discectomy surgery: a systematic review of the last 18 years. *Quant Imaging Med Surg*. (2019) 9:1163–75. doi: 10.21037/qims.2019.05.12

8. Henry BM, Tomaszewski KA, Walocha JA. Methods of evidence-based anatomy: a guide to conducting systematic reviews and meta-analysis of anatomical studies. *Ann Anat*. (2016) 205:16–21. doi: 10.1016/j.aanat.2015.12.002

9. Yammine K. Evidence-based anatomy. *Clin Anat*. (2014) 27:847–52. doi: 10.1002/ca.22397

10. Henry BM, Tomaszewski KA, Ramakrishnan PK, Roy J, Vikse J, Loukas M, et al. Development of the anatomical quality assessment (AQUA) tool for the quality assessment of anatomical studies included in meta-analyses and systematic reviews. *Clin Anat*. (2017) 30:6–13. doi: 10.1002/ca.22799

11. Wicke L, Feigl W, Firbas W, Sinzinger H, Olbert F. Anastomoses between the coeliac and the superior mesenteric artery in radiological and anatomical material. *Radiol Clin*. (1977) 46:11–7.

12. Grabbe E, Bücheler E. Bühler's anastomosis. *Rofo*. (1980) 132:541–6. doi: 10.1055/s-2008-1056615

13. Bertelli E, Di Gregorio F, Civeli L. Various cases of direct connections between the celiac artery and the superior mesenteric. *Arch Ital Anat Embriol*. (1991) 96:281–9.

14. McNulty JG, Hickey N, Khosa F, O'Brien P, O'Callaghan J. Surgical and radiological significance of variants of Bühler's anastomotic artery: a report of three cases. *Surg Radiol Anat*. (2001) 23:277–80. doi: 10.1007/s00276-001-0277-6

15. Saad WE, Davies MG, Sahler L, Lee D, Patel N, Kitanosono T, et al. Arc of Buhler: incidence and diameter in asymptomatic individuals. *Vasc Endovasc Surg*. (2005) 39:347–9. doi: 10.1177/153857440503900407

16. Ferrari R, De Cecco CN, Iafrate F, Paolantonio P, Rengo M, Laghi A. Anatomical variations of the coeliac trunk and the mesenteric arteries evaluated with 64-row CT angiography. *Radiol Med*. (2007) 112:988–98. doi: 10.1007/s11547-007-0200-2

17. Sureka B, Mittal MK, Mittal A, Sinha M, Bhambri NK, Thukral BB. Variations of celiac axis, common hepatic artery and its branches in 600 patients. *Indian J Radiol Imaging*. (2013) 23:223–33. doi: 10.4103/0971-3026.120273

18. van Petersen AS, Kolkman JJ, Meerwaldt R, Huisman AB, van der Palen J, Zeebregts CJ, et al. Mesenteric stenosis, collaterals, and compensatory blood flow. *J Vasc Surg*. (2014) 60:111–119.e2. doi: 10.1016/j.jvs.2014.01.063

19. Ognjanović N, Jeremić D, Živanović-mačužić I, Sazdanović M, Sazdanović P, Tanasković I, et al. MDCT: angiography of anatomical variations of the celiac trunk and superior mesenteric artery. *Arch Biol Sci*. (2014) 66:233–40. doi: 10.2298/ABS1401233O

20. Farghadani M, Momeni M, Hekmatnia A, Momeni F, Baradaran Mahdavi MM. Anatomical variation of celiac axis, superior mesenteric artery, and hepatic artery: evaluation with multidetector computed tomography angiography. *J Res Med Sci*. (2016) 21:129. doi: 10.4103/1735-1995.196611

21. Lin B, Wang FW, Qiu ZQ, Zhang JX, Miu YN, Zhang HQ, et al. Imaging anatomy of celiac trunk-superior mesenteric artery system and its clinical significance in 352 cases of biliary tract disease. *Chin J Pract Surg*. (2022) 42:179–86. doi: 10.19538/j.cjps.issn1005-2208.2022.02.11

22. Dubel GJ, Ahn SH, Saeed MA. Interventional management of arc of Buhler aneurysm. *Semin Intervent Radiol*. (2007) 24:076–81. doi: 10.1055/s-2007-971193

23. Xiao N, Ahuja A, Patel R, Desai SS, Nemcek A Jr, Resnick S. Median arcuate ligament compression associated with flow-related visceral aneurysms. *J Vasc Interv Radiol*. (2023) 34:1176–82. doi: 10.1016/j.jvir.2023.03.026

24. McCracken E, Turley R, Cox M, Suhocki P, Blazer DG III. Leveraging aberrant vasculature in celiac artery stenosis: the arc of Buhler in Pancreaticoduodenectomy. *J Pancreat Cancer*. (2018) 4:4–6. doi: 10.1089/pancan.2017.0020

25. Douard R, Chevallier JM, Delmas V, Cugnenc PH. Clinical interest of digestive arterial trunk anastomoses. *Surg Radiol Anat*. (2006) 28:219–27. doi: 10.1007/s00276-006-0098-8

26. Mao Y, Yao Y, Li X, Zhang C, Chen X, Wang Y. Absence of the celiac trunk: definition, classification, multidetector computed tomography angiographic findings, and their probable embryological mechanisms. *Vascular*. (2023) 31:1214–21. doi: 10.1177/17085381221106318

27. Tang W, Shi J, Kuang LQ, Tang SY, Wang Y. Celiomesenteric trunk: new classification based on multidetector computed tomography angiographic findings and probable embryological mechanisms. *World J Clin Cases*. (2019) 7:3980–9. doi: 10.12998/wjcc.v7.i23.3980

28. Wang Y, Cheng C, Wang L, Li R, Chen JH, Gong SG. Anatomical variations in the origins of the celiac axis and the superior mesenteric artery: MDCT angiographic findings and their probable embryological mechanisms. *Eur Radiol*. (2014) 24:1777–84. doi: 10.1007/s00330-014-3215-9

29. Rathod S, Kolus R, Kim B, Gurnani S, Kim A, Kim E, et al. A case of abnormally dilated and tortuous arc of Buhler and pancreaticoduodenal arteries in the absence of celiac trunk stenosis. *Surg Radiol Anat*. (2022) 44:1343–7. doi: 10.1007/s00276-022-03018-2

30. Tokura M, Kawasaki S. A case of pancreaticoduodenal artery aneurysm without stenosis or obstruction of celiac artery. *Nihon Rinshō Geka Igakkai Zasshi*. (2002) 63:1203–7. doi: 10.3919/jjsa.63.1203

31. Padar M, Rieseberg A, Ratnayake S. Unexpected finding of arc of Buhler with celiac artery stenosis during workup for a suspected pancreatic lesion. *J Surg Case Rep*. (2023) 2023:rjad178. doi: 10.1093/jscr/rjad178

32. Ong DY, Pua U. Coil embolization of arc of Buhler aneurysm rupture. *Case Rep Radiol*. (2020) 2020:8855946. doi: 10.1155/2020/8855946

33. Baz RO, Scheau C, Baz RA, Niscoveanu C. Buhler's arc: an unexpected finding in a case of chronic abdominal pain. *J Gastrointestin Liver Dis*. (2020) 29:304. doi: 10.15403/jgld-2639

34. Biswas S, Gogna S. Arc of Buhler Pseudoaneurysm causing fatal retroperitoneal Hemorrhage; a rare case report and discussion of relevant literature. *Bull Emerg Trauma*. (2019) 7:183–6. doi: 10.29252/beat-070215

35. Schumacher L, Albrecht HC, Gretschel S. A significant vascular variant in oncologic pancreaticoduodenectomy: the arc of Buhler. *Surg Case Rep*. (2022) 8:37. doi: 10.1186/s40792-022-01387-9

36. Kageyama Y, Kokudo T, Amikura K, Miyazaki Y, Takahashi A, Sakamoto H. The arc of Buhler: special considerations when performing pancreaticoduodenectomy. *Surg Case Rep*. (2016) 2:21. doi: 10.1186/s40792-016-0149-2

37. Shah N, Chen O, Cohen GS. Arc of Buhler catheterization for tumor therapy: case report. *J Interv Radiol*. (2010) 3:28–30. doi: 10.2310/6650.2010.060003

38. Nikolaos S, Vasilios P, Niki L, Argyriou EO, Theodoros K, Mihalis A. Arc of Buhler: a lifesaving anatomic variation. A case report. *J Vasc Bras*. (2020) 19:e20200045. doi: 10.1590/1677-5449.200045

39. Quaretti P, Corti R, D'Agostino AM, Bozzani A, Moramarco LP, Cionfoli N. Covered stent assisted coil embolization of large Buhler aneurysm in setting of chronic celiac trunk occlusion. *CVIR Endovasc*. (2024) 7:9. doi: 10.1186/s42155-023-00416-4

40. Abouzaid KA, Lichtenberg AB, Karim AY, Stack ER, Algoul M, Imam A, et al. A unique arc of Bühler variant connecting the arteries of the foregut, Midgut, and hindgut and its surgical significance. *Cureus*. (2023) 15:e42611. doi: 10.7759/cureus.42611

41. Ehemann J, Kim JJY. Rare vascular complication of ESWL pseudoaneurysm of arc of Buhler. *BMJ Case Rep*. (2023) 16:e256089. doi: 10.1136/bcr-2023-256089

42. Tomaszewski KA, Henry BM, Kumar Ramakrishnan P, Roy J, Vikse J, Loukas M, et al. Development of the anatomical quality assurance (AQUA) checklist: guidelines for reporting original anatomical studies. *Clin Anat*. (2017) 30:14–20. doi: 10.1002/ca.22800

43. Ottone NE, Sandoval C, Cid-Gutierrez P, Vásquez-Balboa ML, Tubbs RS, Fuentes R. Systematic review and meta-analysis of the anatomy of the maxillary artery using the anatomical quality assurance (AQUA) checklist. *Surg Radiol Anat*. (2021) 43:1875–86. doi: 10.1007/s00276-021-02825-3

44. Manta BA, Rusu MC, Jianu AM, Ilie AC. Hexafurcated coeliac trunks, trifurcated common hepatic artery, and a new variant of the arc of Bühler. *Folia Morphol (Warsz)*. (2022) 81:365–71. doi: 10.5603/FM.a2021.0025

45. Incarbone N, De Carlis R, Centonze L, Lauterio A, De Carlis L. Discovery of a rare variant of the arc of Bühler during liver procurement. *Exp Clin Transplant*. (2021) 19:1345–7. doi: 10.6002/ect.2021.0302

frontiers | Frontiers in Medicine

TYPE Original Research
PUBLISHED 12 March 2025
DOI 10.3389/fmed.2025.1518540

OPEN ACCESS

EDITED BY
Pradeep Kumar Shukla,
University of Tennessee Health Science Center (UTHSC), United States

REVIEWED BY
Rentao Yu,
First Affiliated Hospital of Chongqing Medical University, China
Ricardo Adrian Nugraha,
Airlangga University, Indonesia

*CORRESPONDENCE
Dejian Li
lidejian880820@163.com
Aiguo Liu
doctorlag@163.com

†These authors have contributed equally to this work

RECEIVED 28 October 2024
ACCEPTED 25 February 2025
PUBLISHED 12 March 2025

CITATION
Bai N, Ying T, Li D and Liu A (2025) Relationship between albumin-corrected anion gap and non-alcoholic fatty liver disease: a cross-sectional analysis of NHANES 2017–2018.
Front. Med. 12:1518540.
doi: 10.3389/fmed.2025.1518540

Relationship between albumin-corrected anion gap and non-alcoholic fatty liver disease: a cross-sectional analysis of NHANES 2017–2018

Ning Bai[1†], Ting Ying[2†], Dejian Li[2*] and Aiguo Liu[2,3*]

[1]Department of Gastroenterology, Huaihe Hospital of Henan University, Kaifeng, China, [2]Research Institute of Digital and Intelligent Orthopedics, Shanghai Pudong Hospital, Fudan University Pudong Medical Center, Shanghai, China, [3]Department of Orthopedics, The First Affiliated Hospital of Henan University, Kaifeng, China

Objectives: The objective of this study was to examine the correlation between the albumin-corrected anion gap (ACAG) and non-alcoholic fatty liver disease (NAFLD) using data from the National Health and Nutrition Examination Survey (NHANES) 2017–2018.

Methods: A cross-sectional analysis was conducted, comprising 4,379 participants, who were stratified into two groups: those with NAFLD and those without NAFLD. The baseline characteristics were compared using the most appropriate statistical tests. The relationship between ACAG levels and NAFLD was assessed using generalized linear models, with adjustments made for potential confounding factors. The analysis of threshold effects was conducted using piecewise regression. Furthermore, the relationship between ACAG and NAFLD was investigated in different age groups.

Results: The mean age of participants with non-alcoholic fatty liver disease (NAFLD) was significantly higher than that of non-NAFLD participants (48.88 vs. 43.46 years, $p < 0.001$). The presence of NAFLD was associated with higher levels of ACAG (18.80 $\pm$ 0.24 vs. 18.10 $\pm$ 0.19, $p < 0.001$). In fully adjusted models, each 1-unit increase in ACAG was associated with a significantly increased risk of NAFLD in participants under 60 years old (β: 0.87, 95% CI: 0.05, 1.69, $p < 0.05$). In younger participants, elevated NAFLD risk was observed in those with higher ACAG quartiles (P for trend <0.05). In contrast, no significant associations were identified in participants aged 60 years and older (P for trend >0.05), suggesting the presence of age-specific differences in the relationship between ACAG and NAFLD.

Conclusion: The impact of ACAG on NAFLD is significantly correlated, especially in the age group, where elevated levels of ACAG are associated with increased risk of NAFLD in young people. ACAG may be a potential and reliable biomarker for predicting NAFLD risk in clinical assessment, but its implementation should consider the patient's age factor.

KEYWORDS

non-alcoholic fatty liver disease, albumin-corrected anion gap, age-related differences, cross-sectional study, NHANES

Introduction

Non-alcoholic fatty liver disease (NAFLD) is a prevalent chronic liver condition, defined by the excessive accumulation of fat within the liver. It affects approximately 25% of the global adult population (1, 2). This condition encompasses a spectrum of liver disorders, ranging from simple steatosis to non-alcoholic steatohepatitis (NASH), which is characterized by inflammation, hepatocyte ballooning, and varying degrees of fibrosis (3). The progression from NAFLD to NASH markedly elevates the risk of developing advanced liver diseases, including cirrhosis and hepatocellular carcinoma (4). This poses a significant public health challenge (5, 6). NAFLD is closely associated with several metabolic disorders, including obesity, type 2 diabetes mellitus (T2DM), and cardiovascular diseases. These conditions share common pathophysiological mechanisms, including insulin resistance and systemic inflammation (7–9). Moreover, NAFLD is acknowledged as an independent risk factor for cardiovascular disease and chronic kidney disease, contributing to elevated morbidity and mortality rates in affected individuals (10, 11).

The progression of NAFLD is frequently associated with metabolic dysregulation, particularly the emergence of insulin resistance, which gives rise to lipotoxicity, mitochondrial dysfunction, and oxidative stress, thereby intensifying inflammation and fibrosis (12–15). Recent studies have indicated that alterations in the acid–base balance may also exert an influence on the progression of NAFLD and its associated complications, including liver fibrosis and cirrhosis. An acidic microenvironment has been demonstrated to augment inflammatory responses and facilitate fibrogenesis in hepatic tissues (16). Therefore, it is of great significance to identify an acid-related biomarker and to monitor its levels in order to prevent the escalation of NAFLD in a timely manner.

The anion gap (AG) is a crucial parameter that reflects the body's acid–base balance. Primarily, it is used to assess the type of metabolic acidosis and its potential causes. An elevated AG value is typically indicative of the accumulation of lactic acid, ketone bodies, or other organic acids, which frequently occurs in conjunction with various metabolic disorders (17). In recent years, there has been a notable increase in research activity concerning the relationship between AG and NAFLD. It has been demonstrated that AG values are frequently significantly abnormal in patients with NAFLD, which may be closely associated with metabolic abnormalities and oxidative stress within the body (18, 19). Moreover, since albumin is a pivotal element in the calculation of AG, the clinical interpretation of AG may be hindered in patients with hypoalbuminemia (20). Accordingly, the albumin-corrected anion gap (ACAG) has been put forth as a means of more accurately assessing the acid–base balance in patients with liver diseases. The research on the correlation between ACAG and NAFLD indicates that higher ACAG levels may be closely associated with the severity and progression of NAFLD, particularly in patients with concurrent hypoalbuminemia, where ACAG more accurately reflects the abnormalities in their acid–base balance (21). These findings indicate that ACAG plays an important role in the evaluation of acid–base disorders and may also serve as a potential marker for assessing disease progression and the risk of complications in NAFLD patients.

Therefore, a cross-sectional study was conducted based on the National Health and Nutrition Examination Survey (NHANES) (2017–2018) with the objective of determining the correlation between ACAG and NAFLD. Furthermore, we sought to ascertain whether age influenced the correlation between ACAG and NAFLD. The objective was to explore the relationship between ACAG and NAFLD and to investigate whether ACAG levels have potential value in predicting the risk of NAFLD or fibrosis.

Methods

Study design and population

The research data utilized in this study were obtained from the National Health and Nutrition Examination Survey (NHANES), covering the years 2017 to 2018. This survey is a project managed by the Centers for Disease Control and Prevention (CDC) in the United States,[1] aiming to evaluate the health and nutritional conditions of the American populace, with assessments conducted biennially. The protocol for NHANES has received approval from the Ethics Review Committee at the National Health Statistics Research Center, ensuring that all participants have given their written informed consent. Detailed information regarding the ethical aspects and the consent process can be found on the NHANES website.[2]

A total of 9,254 samples were included in this cycle. The exclusion criteria included the following: an ineligible, not performed, or partial elastography examination status (n = 3,762); missing sodium data (n = 358); missing potassium data (n = 4); missing chloride data (n = 3); serologic positivity for viral hepatitis (n = 124); excessive alcohol intake, defined as more than four or five standard drinks per day (n = 529); and missing data on covariates (n = 95). Subsequently, 4,379 samples were included in the analysis (Figure 1).

Definition of NAFLD and significant liver fibrosis (SLF)

The liver ultrasound transient elastography has become a widely adopted non-invasive method for assessing liver health, having received FDA approval. This study employed the FibroScan® model 502 V2 Touch (Echosens, Paris, France), equipped with medium or extra-large probes, to perform elastography examinations in NHANES Mobile Examination Centres with the objective of evaluating liver stiffness and steatosis. It was required that participants fast for a minimum of three hours, provide at least ten valid measurements, and have an interquartile range-to-median ratio of liver stiffness measurements (LSM) less than 30% for the examinations to be considered complete. A diagnosis of NAFLD was made when a controlled attenuation parameter (CAP) value of 263 dB/m or above was observed, while SLF was indicated by a median liver stiffness of 8.2 kPa or above (22–24).

Variable extraction and ACAG calculation

The demographic characteristics of the participants included age, sex, race, educational attainment, body mass index (BMI) and poverty

1 https://www.cdc.gov/nchs/nhanes/?CDC_AAref_Val=https://www.cdc.gov/nchs/nhanes/index.htm

2 https://wwwn.cdc.gov/nchs/nhanes/ContinuousNhanes/Documents.aspx?BeginYear=2017

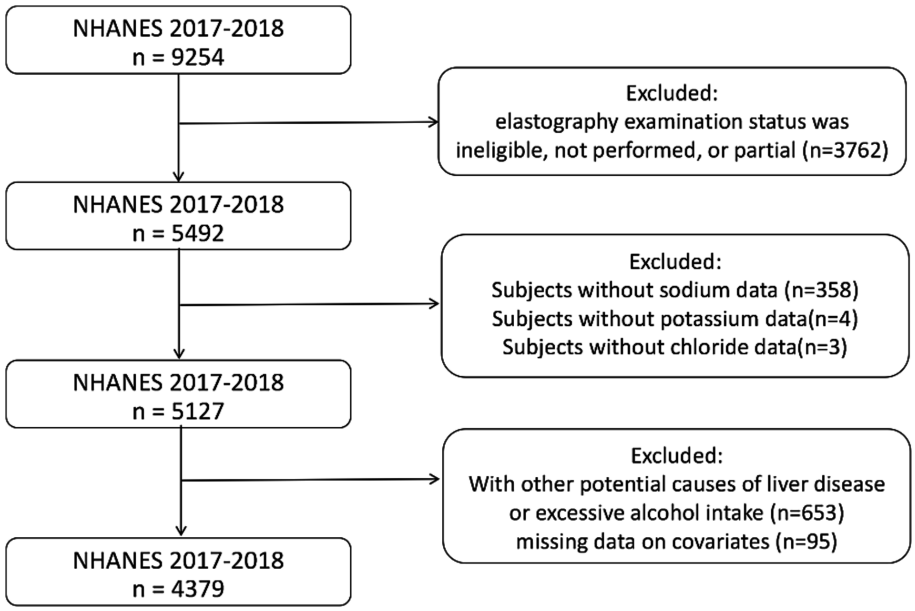

FIGURE 1
Flowchart of participants selection. NHANES, National Health and Nutrition Examination Survey.

income ratio (PIR). Information regarding smoking status was obtained from self-report questionnaires in the MECs. This included whether the participant was a former smoker (i.e., had smoked at least 100 cigarettes in their lifetime and still smoked cigarettes at the time of the survey) or a never smoker (i.e., had not smoked at least 100 cigarettes in their lifetime). Furthermore, data regarding diabetes were also collected via self-report questionnaires. Serum biochemistry profiles were obtained for the following parameters: total calcium, alanine aminotransferase (ALT), aspartate aminotransferase (AST), high-density lipoprotein (HDL) cholesterol, vitamin C, sodium, potassium, chloride, bicarbonate, and albumin. To avoid the potential for collinearity, sodium, potassium, chloride, bicarbonate, and albumin were employed exclusively for the calculation of ACAG and were subsequently excluded from further statistical analyses.

The AG was calculated in accordance with the following equation: AG (mmol/L) is calculated according to the following equation: AG (mmol/L) = (sodium + potassium) - (chloride + bicarbonate). The ACAG was calculated according to the following formula: ACAG (mmol/L) is calculated according to the following formula: ACAG (mmol/L) = [4.4 - albumin (g/dl)] * 2.5 + AG (25).

Statistical analysis

The baseline characteristics of participants were summarized using weighted analyses to account for the complex sampling design of NHANES. Continuous variables were expressed as weighted means ± standard error (SE) and categorical variables as weighted frequencies (percentages). Group comparisons for continuous variables were performed using weighted linear regression models for normally distributed data and weighted quantile regression for non-normally distributed data. Differences in categorical variables were evaluated with weighted chi-square tests. To explore the linear relationship between ACAG and NAFLD, we employed multivariate linear regression models, with subgroup analyses stratified by sex to identify variations across different populations. Non-linear relationships were investigated using smooth curve fittings and generalized additive models; if an inflection point was detected, it was calculated using two-piecewise linear regression models with a recursive algorithm. Association analyses utilized generalized linear models (GLMs) and logistic regression, while threshold effects were assessed through piecewise regression. Trend analyses were conducted to calculate *P*-trend values using quartile-based models, and subgroup analyses were adjusted for covariates in multivariable models. Statistical significance was defined as *p*-values less than 0.05, and all analyses were performed using R software (version 4.0.3[3]) and EmpowerStats (version 6.0[4]).

Results

Participant characteristics

Of the 4,379 participants, 2,409 were classified as non-NAFLD, while 1,970 exhibited NAFLD. Of these, 1,700 were found to have no SLF, while 270 exhibited SLF (Table 1). A statistically significant difference in age was observed between the groups, with participants diagnosed with NAFLD being older (mean age: 48.88 years) compared to those without the condition (mean age: 39.20 years; $p < 0.001$). The gender distribution revealed no significant difference between the groups, although a higher percentage of males were

3 https://www.R-project.org
4 https://www.empowerstats.net/analysis/install/index.php

TABLE 1 Baseline characteristics of participants in NHANES 2017–2018.

Variable	Overall (n = 4,379)	Non-NAFLD (n = 2,409)		NAFLD (n = 1970)			
			p value[b]	Total	Without SLF (n = 1700)	With SLF (n = 270)	p value[c]
Age (year)	43.46 ± 0.65	39.20 ± 0.66	<0.001	48.88 ± 0.80	48.57 ± 0.71	51.03 ± 1.93	0.141
Sex, n (%)[a]			<0.001				0.738
Male	2011 (46.26%)	1,018 (41.76%)		993 (51.99%)	850 (51.72%)	143 (53.84%)	
Female	2,368 (53.74%)	1,391 (58.24%)		977 (48.01%)	850 (48.28%)	127 (46.16%)	
Education level, n (%)[a]			<0.001				0.715
Under high school	1,500 (21.84%)	971 (26.42%)		529 (15.99%)	462 (16.12%)	67 (15.12%)	
High school or above high school	2,879 (78.16%)	1,438 (73.58%)		1,441 (84.01%)	1,238 (83.88%)	203 (84.88%)	
PIR, n (%)[a]			0.999				0.167
< 1	1,237 (21.16%)	679 (21.16%)		558 (21.15%)	486 (20.60%)	72 (24.98%)	
≥ 1	3,142 (78.84%)	1730 (78.84%)		1,412 (78.85%)	1,214 (79.40%)	198 (75.02%)	
Race/Ethnicity, n (%)[a]			<0.001				0.907
Non-hispanic white	660 (10.15%)	288 (7.92%)		372 (13.00%)	316 (12.92%)	56 (13.55%)	
Non-hispanic black	400 (7.05%)	220 (7.54%)		180 (6.41%)	155 (6.22%)	25 (7.73%)	
Mexican American	1,457 (61.28%)	797 (61.71%)		660 (60.73%)	570 (61.00%)	90 (58.91%)	
Other Hispanic	947 (10.67%)	580 (11.94%)		367 (9.04%)	319 (9.15%)	48 (8.31%)	
Other races	915 (10.85%)	524 (10.89%)		391 (10.82%)	340 (10.71%)	51 (11.50%)	
BMI, n (%)[a]			<0.001				<0.001
< 25 kg/m^2	1,472 (32.66%)	1,273 (52.15%)		199 (7.82%)	187 (8.59%)	12 (2.63%)	
25 ≤ BMI < 30 kg/m^2	1,328 (29.81%)	704 (29.91%)		624 (29.68%)	580 (32.09%)	44 (13.42%)	
≥ 30 kg/m^2	1,579 (37.53%)	432 (17.94%)		1,147 (62.50%)	933 (59.32%)	214 (83.95%)	
Smoke status, n (%)[a]			<0.001				0.361
Never	3,095 (68.00%)	1810 (71.97%)		1,285 (62.94%)	1,121 (63.31%)	164 (60.43%)	
Current	511 (11.70%)	273 (10.99%)		238 (12.60%)	209 (12.76%)	29 (11.49%)	
Former	773 (20.30%)	326 (17.04%)		447 (24.46%)	370 (23.93%)	77 (28.08%)	
Diabetes, n (%)[a]			<0.001				<0.001
Yes	529 (9.39%)	147 (3.55%)		382 (16.83%)	287 (14.31%)	95 (33.84%)	
No	3,850 (90.61%)	2,262 (96.45%)		1,588 (83.17%)	1,413 (85.69%)	175 (66.16%)	
AST (U/L)	21.40 ± 0.20	20.36 ± 0.34	0.002	22.72 ± 0.40	21.86 ± 0.40	28.51 ± 1.64	0.001
ALT (U/L)	21.76 ± 0.29	18.08 ± 0.32	<0.001	26.46 ± 0.72	25.34 ± 0.79	33.97 ± 1.80	<0.001
HDL cholesterol (mmol/L)	1.39 ± 0.01	1.48 ± 0.01	<0.001	1.27 ± 0.01	1.28 ± 0.01	1.20 ± 0.04	0.051
ACAG (mmol/L)	18.41 ± 0.21	18.10 ± 0.19	<0.001	18.80 ± 0.24	18.69 ± 0.23	19.57 ± 0.38	0.005
Serum vitamin C (umol/L)	52.58 ± 1.37	56.29 ± 1.37	<0.001	47.84 ± 1.92	48.90 ± 26.16	43.04 ± 25.55	0.002
Serum total calcium (mmol/L)	2.33 ± 0.02	2.34 ± 0.01	0.063	2.33 ± 0.01	2.33 ± 0.01	2.33 ± 0.01	0.832

Values are means ± SE for continuous variables. p Value was calculated by weighted linear regression model for continuous variables and weighted chi-square test was performed for categorical variables. [a]Unweighted frequency counts and weighted percentages are shown. [b]NAFLD vs. Non-NAFLD. [c]NAFLD without SLF vs. with SLF. NAFLD non-alcoholic fatty liver disease, SLF significant liver fibrosis, ACAG albumin-corrected anion gap, PIR poverty income ratio, BMI body mass index, HDL cholesterol high-density lipoprotein cholesterol, AST aspartate aminotransferase, ALT alanine aminotransferase.

present in the NAFLD group with SLF in comparison to their non-NAFLD counterparts (53.84% vs. 41.76%). There was a significant discrepancy in educational attainment, with a greater proportion of participants in the non-NAFLD group having attained a high school or higher level of education (84.01% vs. 73.58%, $p < 0.001$).

The prevalence of diabetes was notably higher in the NAFLD group (16.83% vs. 3.55%, $p < 0.001$). The BMI classifications revealed significant disparities between the two groups. A substantial proportion of the non-NAFLD participants had a BMI of less than 25 kg/m^2 (52.15%), while the majority of the NAFLD participants had a BMI of 30 kg/m^2 or greater (62.50%), with a statistically significant

difference between the two groups ($p < 0.001$). The prevalence of current smokers was similar across the groups. However, former smokers were more prevalent in the NAFLD group (24.46% vs. 17.04%, $p < 0.001$).

Biochemical parameters demonstrated notable discrepancies. Participants with NAFLD exhibited elevated levels of liver enzymes, with AST and ALT being higher in the NAFLD group (AST: 22.72 U/L; ALT: 26.46 U/L) compared to non-NAFLD participants (AST: 20.36 U/L; ALT: 18.08 U/L; both $p < 0.05$). Furthermore, participants with NAFLD exhibited lower HDL cholesterol levels (1.27 mmol/L) compared to those without NAFLD (1.48 mmol/L, $p < 0.001$). Additionally, serum vitamin C levels were significantly lower in the NAFLD group (47.84 umol/L vs. 56.29 umol/L, $p < 0.001$).

Association between ACAG and NAFLD

As demonstrated in Table 2, in Model 1, which remains unadjusted, each 1 unit increase in ACAG is associated with a β coefficient of 1.13 (95% CI: 0.46, 1.79), indicating a significant positive relationship with NAFLD ($p < 0.01$). Model 2, adjusted for age, sex, education level, PIR, and race/ethnicity, shows a similar trend with a β value of 1.20 (95% CI: 0.53, 1.87) ($p < 0.01$). However, in Model 3, which further includes adjustments for smoking status, diabetes, BMI, HDL cholesterol, AST, ALT, SLF, serum total calcium, and serum vitamin C, the association strengthens but becomes less pronounced, yielding a β coefficient of 0.72 (95% CI: 0.07, 1.36) ($p < 0.05$).

Regarding quartile analysis, participants in the second quartile (ACAG 17.05 to <18.45) exhibit a β of 5.64 (95% CI: 0.71, 10.58) in Model 1, indicating increased NAFLD risk, while Model 2 enhances this estimate to 6.15 (95% CI: 1.23, 11.08) ($p < 0.05$). In quartile 3 (ACAG 18.45 to <19.90), the association reaches 10.11 (95% CI: 5.19, 15.03) in Model 1 and 10.45 (95% CI: 5.52, 15.39) in Model 2, both statistically significant ($p < 0.001$). The highest quartile (≥19.90) reflects β coefficients of 9.33 (95% CI: 4.57, 14.09) and 10.32 (95% CI: 5.52, 15.12) in Models 1 and 2, respectively ($p < 0.001$). *P* for trend analyses across all models yield significant results ($p < 0.0001$ for Models 1 and 2, and $p = 0.0036$ for Model 3), indicating a robust relationship between ACAG levels and the prevalence of NAFLD.

TABLE 2 Association between ACAG and NAFLD.

ACAG	β (95% CI)		
	Model 1	Model 2	Model 3
Per 1 increment	1.13 (0.46, 1.79)**	1.20 (0.53, 1.87)**	0.72 (0.07, 1.36) *
Quartile			
Q1 (<17.05)	Reference	Reference	Reference
Q2 (17.05 to<18.45)	5.64 (0.71, 10.58)*	6.15 (1.23, 11.08)*	5.03 (0.40, 9.66)*
Q3 (18.45 to<19.90)	10.11 (5.19, 15.03)***	10.45 (5.52, 15.39) ***	6.87 (2.21, 11.53)**
Q4 (≥19.90)	9.33 (4.57, 14.09)***	10.32 (5.52, 15.12)***	7.04 (2.46, 11.62)**
P for trend	<0.0001	<0.0001	0.0036

Model 1 was adjusted for none. Model 2 was adjusted for Age, Sex, Education level, PIR, Race/Ethnicity. Model 3 was adjusted for Age, Sex, Education level, PIR, Race/Ethnicity, Smoke status, Diabetes, BMI, HDL cholesterol, AST, ALT, Serum total calcium, Serum vitamin C, SLF. β: CAP. *$p < 0.05$, **$p < 0.01$, ***$p < 0.001$. NAFLD non-alcoholic fatty liver disease, ACAG albumin-corrected anion gap, PIR poverty income ratio, BMI body mass index, HDL cholesterol high-density lipoprotein cholesterol, AST aspartate aminotransferase, ALT alanine aminotransferase, SLF significant liver fibrosis, CAP controlled attenuation parameter.

Identification of nonlinear relationship between ACAG and NAFLD

The threshold effect of ACAG on NAFLD, revealing a significant non-linear relationship that suggests an inverted U-shaped association (Table 3; Figure 2). In Model I, the linear analysis indicates a β coefficient of 0.39 (95% CI: −0.25, 1.02) with a *p*-value of 0.2349, suggesting no significant linear correlation between ACAG and the prevalence of NAFLD. However, upon further analysis in Model II, a turning point (K) of 23.05 is identified. For ACAG values below this threshold (ACAG < K), there is a positive association with NAFLD, reflected in a β of 0.86 (95% CI: 0.11, 1.60) and a statistically significant *p*-value of 0.0238. Conversely, for ACAG values at or above this turning point (ACAG ≥ K), the association shifts to negative, demonstrating a β of −3.16 (95% CI: −6.12, −0.21) with $p = 0.0360$. The logarithm likelihood ratio test (LRT) shows a *p*-value of 0.015, indicating that Model II significantly differs from Model I, strengthening the evidence for a non-linear relationship. The 95% confidence interval for the turning point ranges from 21.30 to 23.30, further substantiating the identified ACAG threshold.

Association between ACAG and NAFLD across different age groups

In individuals aged less than 60 years, there is a robust positive correlation between ACAG and NAFLD in all models (Table 4). Specifically, for each 1 increment in ACAG, the β coefficients are 1.86 (95% CI: 0.98, 2.75) in Model 1, 1.95 (95% CI: 1.06, 2.84) in Model 2, and 0.87 (95% CI: 0.05, 1.69) in Model 3, with the first two models achieving significance at $p < 0.001$. Quartile analyses in this age group show significant increases in β values across higher quartiles of ACAG, particularly notable in Q3 ($\beta = 11.55$, 95% CI: 5.37, 17.73; $p < 0.001$) and Q4 (β = 12.75, 95% CI: 6.67, 18.83; $p < 0.001$), with a clear trend ($p < 0.001$). In contrast, individuals aged 60 years and older demonstrate minimal associations between ACAG and NAFLD, with the β coefficients for each increment being non-significant across all models (0.08 to 0.19), indicating a lack of association. For the quartile analysis, the β values remain close to zero, with Q2, Q3, and Q4 demonstrating no significant increase in risk, and the *p*-values for trend do not reach significance ($p = 0.2959$ to 0.8515).

Discussion

The present study revealed the intricate relationship between ACAG and NAFLD through a comprehensive analysis of the results obtained from a variety of models. The results presented in Table 1 indicate that an increase in ACAG is significantly associated with an

TABLE 3 Threshold effect analysis of ACAG and NAFLD.

Model	β (95% CI)	*P* value
Model I		
One line effect	0.39 (−0.25, 1.02)	0.2349
Model II		
Turning point (K)	23.05	
ACAG<K	0.86 (0.11, 1.60)	0.0238
ACAG> = K	−3.16 (−6.12, −0.21)	0.0360
P value for LRT test*	0.015	
95% Cl for Turning point	21.30, 23.30	

Data were presented as β (95% CI) CAP *p* value; Model I, linear analysis; Model II, non-linear analysis. Adjusted for Age, Sex, Education level, PIR, Race/Ethnicity, Smoke status, Diabetes, BMI, HDL cholesterol, AST, ALT, Serum total calcium, Serum vitamin C. Restricted cubic spline smoothing were applied. *$p < 0.05$ indicates that Model II is significantly different from Model I. NAFLD non-alcoholic fatty liver disease, ACAG albumin-corrected anion gap, PIR poverty income ratio, BMI body mass index, HDL cholesterol high-density lipoprotein cholesterol, AST aspartate aminotransferase, ALT alanine aminotransferase, CAP controlled attenuation parameter, Cl confidence interval, LRT logarithm likelihood ratio test.

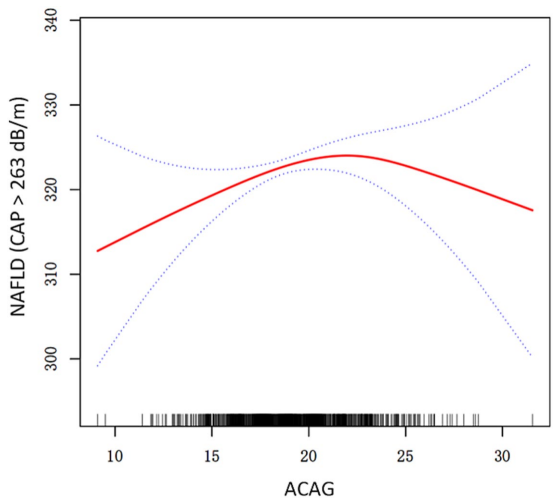

FIGURE 2
A threshold, nonlinear association between ACAG and NAFLD. Solid rad line represents the smooth curve fit between variables. Dashed line represent the 95% of confidence interval from the fit. All adjusted for Age, Sex, Education level, PIR, Race/Ethnicity, Smoke status, Diabetes, BMI, HDL cholesterol, AST, ALT, Serum total calcium, Serum vitamin C. NAFLD non-alcoholic fatty liver disease, ACAG albumin-corrected anion gap, PIR poverty income ratio, BMI body mass index, HDL cholesterol high-density lipoprotein cholesterol, AST aspartate aminotransferase, ALT alanine aminotransferase, CAP controlled attenuation parameter.

elevated risk of NAFLD, particularly in younger individuals, where this association is particularly pronounced. Table 2 provides further evidence of the effectiveness of ACAG as a potential biomarker, after adjustment for multiple confounding factors. Table 3 clearly demonstrates an inverse U-shaped relationship between ACAG and NAFLD risk. ACAG below a certain threshold is associated with a significant increase in risk, while above this threshold, there is a decrease in risk. This indicates that ACAG plays a dual role in NAFLD assessment. Finally, the age stratification analysis in Table 4 indicates that the effect of ACAG on NAFLD is significant in the population

TABLE 4 Association between ACAG and NAFLD in different models among age groups.

ACAG	β (95% CI)		
	Model 1	Model 2	Model 3
Aged <60 years			
Per 1 increment	1.86 (0.98, 2.75)***	1.95 (1.06, 2.84)***	0.87 (0.05, 1.69)*
Q1 (<16.80)	Reference	Reference	Reference
Q2 (16.80 to<18.20)	7.32 (1.11, 13.53)*	7.90 (1.70, 14.10)*	5.56 (−0.01, 11.13)
Q3 (18.20 to<19.55)	11.55 (5.37, 17.73)***	11.93 (5.75, 18.10)***	7.02 (1.44, 12.59)*
Q4 (≥19.55)	12.75 (6.67, 18.83)***	14.00 (7.88, 20.12)***	6.86 (1.25, 12.46)*
P for trend	<0.0001	<0.0001	0.0223
Aged ≥60 years			
Per 1 increment	0.08 (−0.93, 1.10)	0.19 (−0.83, 1.21)	−0.46 (−1.44, 0.53)
Q1 (<16.80)	Reference	Reference	Reference
Q2 (16.80 to<18.20)	2.41 (−5.73, 10.55)	2.72 (−5.43, 10.86)	−1.20 (−8.93, 6.53)
Q3 (18.20 to<19.55)	7.32 (−0.81, 15.45)	7.36 (−0.91, 15.62)	1.11 (−6.75, 8.97)
Q4 (≥19.55)	3.53 (−4.14, 11.21)	4.31 (−3.51, 12.14)	−1.32 (−8.85, 6.22)
P for trend	0.2959	0.2361	0.8515

Model 1 was adjusted for none. Model 2 was adjusted for Age, Sex, Education level, PIR, Race/Ethnicity. Model 3 was adjusted for Age, Sex, Education level, PIR, Race/Ethnicity, Smoke status, Diabetes, BMI, HDL cholesterol, AST, ALT, Serum total calcium, Serum vitamin C, SLF. β: CAP. *$p < 0.05$, **$p < 0.01$, ***$p < 0.001$. NAFLD non-alcoholic fatty liver disease, ACAG albumin-corrected anion gap, PIR poverty income ratio, BMI body mass index, HDL cholesterol high-density lipoprotein cholesterol, AST aspartate aminotransferase, ALT alanine aminotransferase, SLF significant liver fibrosis, CAP controlled attenuation parameter.

under 60 years of age, while no correlation is observed in the population aged 60 and above. These findings indicate that ACAG is not only an important indicator for assessing NAFLD risk, but also emphasize the moderating role of age in this relationship.

Our study shares similarities with Lu et al.'s research on the association between ACAG and NAFLD, while also demonstrating significant differences (21). Both studies confirm that ACAG is an independent risk factor for NAFLD and employ various statistical methods to assess the significance of this relationship. The published study emphasizes the role of waist circumference in moderating the relationship between ACAG and NAFLD across different populations, while our research explores the non-linear relationship between ACAG levels and NAFLD risk across different age groups, revealing an inverse U-shaped trend. These differences indicate that while both studies focus on the association between ACAG and NAFLD, our research further expands this field by providing a more comprehensive perspective on the effects of ACAG across diverse populations, offering new insights for clinical practice.

The association between ACAG and NAFLD involves multiple potential mechanisms that can be explained through metabolic

disorders and inflammatory responses. Firstly, an elevation in ACAG typically reflects an imbalance in the acid–base status of the body, particularly in the context of metabolic syndrome and insulin resistance. In such scenarios, the levels of lactate and ketone bodies tend to increase, which may exert direct toxic effects on the liver, thereby promoting lipid deposition and leading to the development of NAFLD (26). Furthermore, increased ACAG levels may also correlate with adipocyte dysfunction. Research indicates that metabolic abnormalities can lead to enhanced fat synthesis coupled with reduced fat oxidation, resulting in excessive fat accumulation in the liver and further promoting NAFLD progression (27). Secondly, the elevation of ACAG is closely associated with increased oxidative stress, which is recognized as a significant mechanism in the progression of NAFLD. Oxidative stress arises from the overproduction of free radicals, leading to lipid peroxidation and subsequent damage to liver cells, thereby triggering inflammatory responses (28). This chronic inflammatory state not only exacerbates hepatic steatosis but may also contribute to liver fibrosis and further hepatic injury (29, 30). The role of pro-inflammatory cytokines, such as TNF-α and IL-6, is particularly noteworthy, as they are extensively involved in the pathophysiology of NAFLD. Studies have shown that these cytokines are significantly elevated in NAFLD patients, and their presence correlates with the severity of liver inflammation and damage (31).

The observed inverted U-shaped relationship between ACAG and NAFLD risk may reflect dual biological mechanisms. At lower ACAG levels (<23.05 mmol/L), elevated AG likely signifies subclinical metabolic acidosis, promoting lipotoxicity, oxidative stress, and hepatic lipid accumulation. However, at higher ACAG levels (≥23.05 mmol/L), hypoalbuminemia (common in advanced liver disease) may dominate, reducing AG correction accuracy and masking acidosis effects. Additionally, compensatory mechanisms (e.g., renal bicarbonate retention) in chronic acidosis could mitigate hepatic damage, explaining the attenuated risk at higher ACAG (15, 25, 28).

This study examined the association between ACAG and significant fibrosis in NAFLD using a large sample study with nationally representative data and adjusted for potential confounders to improve the reliability of the results. However, this study has some limitations. Firstly, this is a cross-sectional study and cannot determine the causal relationship between ACAG and NAFLD. Second, including only individuals with complete data and excluding those with missing data may introduce bias for other potential confounders, affecting the accurate assessment of the true association. Third, the participants are based on the general population in the United States and may not be generalizable to other countries due to potential differences in genetics, language, culture and environmental factors between countries and regions. While weighted analyses were applied to baseline characteristics to reflect national estimates, subsequent multivariable models utilized unweighted data to prioritize biological inference. Future studies with larger samples should validate these associations using weighted approaches to ensure generalizability. Finally, there is currently no consensus regarding the critical value for the detection of steatosis and the evaluation of liver fibrosis using LSM. Consequently, the limitations of our research may be constrained by the identification of NAFLD with or without significant fibrosis.

In conclusion, the impact of ACAG on NAFLD is significantly correlated, especially in the age group, where elevated levels of ACAG are associated with increased risk of NAFLD in young people. ACAG may be a potential and reliable biomarker for predicting NAFLD risk in clinical assessment, but its implementation should consider the patient's age factor.

Data availability statement

The original contributions presented in the study are included in the article/supplementary material, further inquiries can be directed to the corresponding authors.

Ethics statement

The protocol for NHANES has received approval from the Ethics Review Committee at the National Health Statistics Research Center, ensuring that all participants have given their written informed consent. Detailed information regarding the ethical aspects and the consent process can be found on the NHANES website (https://wwwn.cdc.gov/nchs/nhanes/ContinuousNhanes/Documents.aspx?BeginYear=2017). The studies were conducted in accordance with the local legislation and institutional requirements. Written informed consent for participation was not required from the participants or the participants' legal guardians/next of kin because this survey is a project managed by the Centers for Disease Control and Prevention (CDC) in the United States (https://www.cdc.gov/nchs/nhanes/index.htm), aiming to evaluate the health and nutritional conditions of the American populace, with assessments conducted biennially. Written informed consent was obtained from the individual(s) for the publication of any potentially identifiable images or data included in this article.

Author contributions

NB: Conceptualization, Data curation, Investigation, Writing – original draft, Writing – review & editing. TY: Conceptualization, Data curation, Methodology, Writing – original draft, Writing – review & editing. DL: Conceptualization, Supervision, Writing – original draft, Writing – review & editing. AL: Conceptualization, Data curation, Methodology, Software, Writing – original draft, Writing – review & editing.

Funding

The author(s) declare that financial support was received for the research, authorship, and/or publication of this article. This work was supported by the Pudong New Area health talent training program (Grant No. 2025PDWSYCQN-06), the Health Industry Clinical Research Project of Shanghai Health Commission (Grant No. 20224Y0393), the Science and Technology Development Fund of Shanghai Pudong New Area (Grant No. PKJ2023-Y09), the Outstanding Leaders Training Program of Pudong Hospital affiliated to Fudan University (Grant No. LX202201), the Project of Key Medical Specialty and Treatment Center of Pudong Hospital of Fudan University (Grant No. Tszb2023-05), the New Quality Clinical Specialty Program of High-end Medical Disciplinary Construction in Shanghai Pudong New Area (2024-PWXZ-14), the Program of Key Medicine of

Shanghai Municipal Health Commission (2024ZDXK0031), the joint research project of Pudong Health Committee of Shanghai (Grant No. PW2021D-08), the Project of Key Medical Specialty and Treatment Center of Pudong Hospital of Fudan University (Zdxk2020-02, Zdzk2021-01), the Medical Science and Technology Tackling Program of Henan Province (Grant No. LHGJ20230441).

Conflict of interest

The authors declare that the research was conducted in the absence of any commercial or financial relationships that could be construed as a potential conflict of interest.

Generative AI statement

The authors declare that no Generative AI was used in the creation of this manuscript.

Publisher's note

All claims expressed in this article are solely those of the authors and do not necessarily represent those of their affiliated organizations, or those of the publisher, the editors and the reviewers. Any product that may be evaluated in this article, or claim that may be made by its manufacturer, is not guaranteed or endorsed by the publisher.

References

1. Martínez-Montoro JI, Cornejo-Pareja I, Gómez-Pérez AM, Tinahones FJ. Impact of genetic polymorphism on response to therapy in non-alcoholic fatty liver disease. *Nutrients*. (2021) 13:4077. doi: 10.3390/nu13114077

2. Manzano-Nunez R, Santana-Dominguez M, Rivera-Esteban J, Sabiote C, Sena E, Bañares J, et al. Non-alcoholic fatty liver disease in patients with polycystic ovary syndrome: a systematic review, meta-analysis, and meta-regression. *JCM*. (2023) 12:856. doi: 10.3390/jcm12030856

3. Bedossa P. Pathology of non-alcoholic fatty liver disease. *Liver Int*. (2017) 37:85–9. doi: 10.1111/liv.13301

4. Samy AM, Kandeil MA, Sabry D, Abdel-Ghany AA, Mahmoud MO. From NAFLD to NASH: understanding the spectrum of non-alcoholic liver diseases and their consequences. *Heliyon*. (2024) 10:e30387. doi: 10.1016/j.heliyon.2024.e30387

5. Younossi ZM, Koenig AB, Abdelatif D, Fazel Y, Henry L, Wymer M. Global epidemiology of nonalcoholic fatty liver disease—Meta-analytic assessment of prevalence, incidence, and outcomes. *Hepatology*. (2016) 64:73–84. doi: 10.1002/hep.28431

6. Chalasani N, Younossi Z, Lavine JE, Charlton M, Cusi K, Rinella M, et al. The diagnosis and management of nonalcoholic fatty liver disease: practice guidance from the American Association for the Study of Liver Diseases. *Hepatology*. (2018) 67:328–57. doi: 10.1002/hep.29367

7. Targher G, Byrne CD, Tilg H. NAFLD and increased risk of cardiovascular disease: clinical associations, pathophysiological mechanisms and pharmacological implications. *Gut*. (2020) 69:1691–705. doi: 10.1136/gutjnl-2020-320622

8. Mantovani A, Petracca G, Beatrice G, Csermely A, Lonardo A, Schattenberg JM, et al. Non-alcoholic fatty liver disease and risk of incident chronic kidney disease: an updated meta-analysis. *Gut*. (2022) 71:156–62. doi: 10.1136/gutjnl-2020-323082

9. Pirola CJ, Sookoian S. Non-alcoholic fatty liver disease mediates the effect of obesity on arterial hypertension. *Liver Int*. (2023) 43:2167–76. doi: 10.1111/liv.15643

10. Byrne CD, Targher G. NAFLD as a driver of chronic kidney disease. *J Hepatol*. (2020) 72:785–801. doi: 10.1016/j.jhep.2020.01.013

11. Targher G, Corey KE, Byrne CD. NAFLD, and cardiovascular and cardiac diseases: factors influencing risk, prediction and treatment. *Diabetes Metab*. (2021) 47:101215. doi: 10.1016/j.diabet.2020.101215

12. Wang C-H, Liu H-M, Chang Z-Y, Lee M, Hsu C-H, Lee T-Y. Antioxidants rich herbal formula Ger-gen-Chyn-Lian-tang protects lipotoxicity and ameliorates inflammation signaling through regulation of mitochondrial biogenesis and Mitophagy in nonalcoholic fatty liver disease mice. *Front Biosci*. (2022) 27:242. doi: 10.31083/j.fbl2708242

13. Albhaisi S, Sanyal AJ. Gene-environmental interactions as metabolic drivers of nonalcoholic steatohepatitis. *Front Endocrinol*. (2021) 12:665987. doi: 10.3389/fendo.2021.665987

14. Chen Y, Yang F, Chu Y, Yun Z, Yan Y, Jin J. Mitochondrial transplantation: opportunities and challenges in the treatment of obesity, diabetes, and nonalcoholic fatty liver disease. *J Transl Med*. (2022) 20:483. doi: 10.1186/s12967-022-03693-0

15. Lambert DC, Abramowitz MK. Obesity, Anion accumulation, and anion gap metabolic acidosis: a cohort study. *Kidney360*. (2021) 2:1706–15. doi: 10.34067/KID.0003562021

16. Jia Y, Li D, You Y, Yu J, Jiang W, Liu Y, et al. Multi-system diseases and death trajectory of metabolic dysfunction-associated fatty liver disease: findings from the UK biobank. *BMC Med*. (2023) 21:398. doi: 10.1186/s12916-023-03080-6

17. Sotiropoulou Z, Antonogiannaki EM, Koukaki E, Zaneli S, Bakakos A, Vontetsianos A, et al. Evaluation of the Acid–Base status in patients admitted to the ICU due to severe COVID-19: physicochemical versus traditional approaches. *JPM*. (2023) 13:1700. doi: 10.3390/jpm13121700

18. Jian L, Zhang Z, Zhou Q, Duan X, Xu H, Ge L. Association between albumin corrected anion gap and 30-day all-cause mortality of critically ill patients with acute myocardial infarction: a retrospective analysis based on the MIMIC-IV database. *BMC Cardiovasc Disord*. (2023) 23:211. doi: 10.1186/s12872-023-03200-3

19. Divatia JV, Pakavakis A, Paliwal R. Utility of Stewart's approach to diagnose missed complex acid–base disorders as compared to bicarbonate-anion gap-based methodology in critically ill patients: an observational study, Indian. *J Crit Care Med*. (2022) 26:23–32. doi: 10.5005/jp-journals-10071-24077

20. Li P, Shi L, Yan X, Wang L, Wan D, Zhang Z, et al. Albumin corrected anion gap and the risk of in-hospital mortality in patients with acute pancreatitis: a retrospective cohort study. *JIR*. (2023) 16:2415–22. doi: 10.2147/JIR.S412860

21. Lu Y, Zhan Y, Li W, Liao S. Relationship between albumin-corrected anion gap and non-alcoholic fatty liver disease varied in different waist circumference groups: a cross-sectional study. *Eur J Med Res*. (2024) 29:203. doi: 10.1186/s40001-024-01811-w

22. Castera L, Friedrich-Rust M, Loomba R. Noninvasive assessment of liver disease in patients with nonalcoholic fatty liver disease. *Gastroenterology*. (2019) 156:1264–1281.e4. doi: 10.1053/j.gastro.2018.12.036

23. Eddowes PJ, Sasso M, Allison M, Tsochatzis E, Anstee QM, Sheridan D, et al. Accuracy of FibroScan controlled attenuation parameter and liver stiffness measurement in assessing steatosis and fibrosis in patients with nonalcoholic fatty liver disease. *Gastroenterology*. (2019) 156:1717–30. doi: 10.1053/j.gastro.2019.01.042

24. Xiao G, Zhu S, Xiao X, Yan L, Yang J, Wu G. Comparison of laboratory tests, ultrasound, or magnetic resonance elastography to detect fibrosis in patients with nonalcoholic fatty liver disease: a meta-analysis. *Hepatology*. (2017) 66:1486–501. doi: 10.1002/hep.29302

25. Hatherill M. Correction of the anion gap for albumin in order to detect occult tissue anions in shock. *Arch Dis Child*. (2002) 87:526–9. doi: 10.1136/adc.87.6.526

26. Zhong H. Non-alcoholic fatty liver disease: pathogenesis and models. *Am J Transl Res*. (2024) 16:387–99. doi: 10.62347/KMSA5983

27. Yang C, Wu J, Yang L, Hu Q, Li L, Yang Y, et al. Altered gut microbial profile accompanied by abnormal short chain fatty acid metabolism exacerbates nonalcoholic fatty liver disease progression. *Sci Rep*. (2024) 14:22385. doi: 10.1038/s41598-024-72909-8

28. Hu Y, Yu Y. Dysregulation of miR-192-5p in acute pancreatitis patients with nonalcoholic fatty liver and its functional role in acute pancreatitis progression. *Biosci Rep*. (2020) 40:BSR20194345. doi: 10.1042/BSR20194345

29. Kong L, Wu Q, Zhao L, Ye J, Li N, Yang H. Effect of microRNA-27a-5p on apoptosis and inflammatory response of pancreatic acinar cells in acute pancreatitis by targeting PTEN. *J Cell Biochem*. (2019) 120:15844–50. doi: 10.1002/jcb.28855

30. Osorio-Conles Ó, Vega-Beyhart A, Ibarzabal A, Balibrea JM, Graupera I, Rimola J, et al. A distinctive NAFLD signature in adipose tissue from women with severe obesity. *IJMS*. (2021) 22:10541. doi: 10.3390/ijms221910541

31. Huang Y, Li S, Han Z, Du J, Liu X, Zhu Z, et al. Tyrosol ameliorates liver inflammatory response in a mouse model of nonalcoholic fatty liver disease (NFALD) by regulating JAK1/STAT3. *Nat Prod Commun*. (2022) 17:1934578X221111033. doi: 10.1177/1934578X221111033

Frontiers in Medicine

Translating medical research and innovation into improved patient care

A multidisciplinary journal which advances our medical knowledge. It supports the translation of scientific advances into new therapies and diagnostic tools that will improve patient care.

Discover the latest Research Topics

See more →

Frontiers

Avenue du Tribunal-Fédéral 34
1005 Lausanne, Switzerland
frontiersin.org

Contact us

+41 (0)21 510 17 00
frontiersin.org/about/contact